Synthesis and Optoelectronic Properties of Imidic *peri*- Xanthenoxanthene Derivatives

Andrea Sciutto

Thesis submitted in accordance with the requirements for the

degree of Doctor of Philosophy

Prof. Davide Bonifazi

School of Chemistry
Cardiff University

March 2018

To my family,
who always supported me

Table of Contents:

Acknowledgements

It is important at this moment to say how greatful I am to the people that throughout all these years they have been supporting me and encouraging me to continue with my dreams and goals.

Firstly, I would like to specially thank my supervisor, *Prof. Davide Bonifazi* for giving me the opportunity to start this PhD and work on interesting and challenging projects and for his constant guidance and support during these years.

Many thanks to *Prof. Krief* that even though he was not my supervisor he scientifically embraced me and enriched my love and knowledge for chemistry.

Sincere thanks should go to Cardiff University that provided home and support for my research.

I would also like to thank all the people from *Bonifazi group* for the warm and friendly environment they created and for their help, which was provided whenever it was needed. Special thanks to *Dr. Andrea Fermi* and *Dr. Andrey Berezin* with who I collaborated, as well as *Dr. Antoine Stopin* and *Dr. Tanja Miletic* and *Ms. Stavroula Sakellakou* for their support.

I would also like to thank my family, since without their constant support all these years I wouldn’t have managed to reach and surpass my goals.

List of abbreviations:

Å	Angstrom
Abs	Absorption
Ac	Acetyl
acac	Acetylacetone
AMOLED	Active-Matrix Organic Light-Emitting Diode
aq	Aqueous
B3LYP	Becke, 3-parameter, Lee-Yang-Parr
B_2pin_2	Bis(pinacolato)diboron
bpy	Bipyridine
Bu	Butyl
Bz	Benzoyl
^oC	Degree Celcius (0 ^oC = 273.16 K)
ca	Circa(latin)-approximately
calc	Calculated
CuCT	Copper(I)-thiophene-2-carboxylate
CV	Cyclic Volametry
Cy	Cyclohexyl
CW	Continious Wave
dba	Dibenzylideneacetone
DBU	1,8-Diazabicyclo(5.4.0)undec-7-ene
DCB	1,2 Dichlorobenzene
DCTB	*trans*-2-[3-(4-*tert*-Butylphenyl)-2-methyl-2-propenylidene]malononitrile
DEA	Diethylamine
DFT	Density Functional Theory
DIPEA	*N*,*N* - Diisopropylethylamine
DMA	*N*,*N*-Dimethylacetamide
DMF	*N*,*N'* - Dimethylformamide
DMSO	Dimethylsulfoxide
dppf	1,1'-Bis(diphenylphosphino)ferrocene
EI	Electron Ionization

E_g	Energy bandgap
E_{int}	Energy due to intermolecular interaction
E_m	Emission
EnT	Energy Transfer
EPR	Electron Paramagnetic Spectroscopy
E_{res}	Aromatic stabilization resonance energy
ESI	Electron Spray Ionisation
E_{sub}	Energy due to the substituents
ET	Electron Transfer
Et_3N	Triethylamine
Et_2O	Diethyl ether
EtOAc	Ethyl Acetate
EtOH	Ethanol
eq	Equivalents
eV	Electronvolt ($1eV= 1.602x10^{-19}$)
$E_{\delta r}$	Energy due to the conjugation length
E_θ	Energy due to the planarity
fac	facial
F_c	Ferrocene
FET	Field Effect Transistor
h	Hour
h	Planck's constant
HAT	Hydrogen Atom Transfer
HDI	Hexarylenebis(dicarboximide)
HOMO	Highest Occupied Molecular Orbital
HR	High Resolution
HRMS	High Resolution Mass Spectrometry
*i*Pr	Isopropyl
*i*PrOH	Isopropanol
IR	Infrared (spectroscopy)
K	Kelvin

LED	Light Emitting Diode
LR	Low Resolution
LUMO	Highest Occupied Molecular Orbital
M	Molar
MALDI	Matrix Assisted Laser Desorption/ Ionization
MCH	Methylcyclohexane
Me	Methyl
MeCN	Acetonitrile
MeOH	Methanol
MHz	Megahertz
min	Minute
M.p.	Melting point
MS	Mass Spectrometry
ms	millisecond
m/z	Mass-to-charge ratio
NDI	Naphtalene Diimide
NHE	Normal Hydrogen Electrode
NIR	Near Infrared
nm	Nanometer
NMA	Napthalenemonoanhydride
NMI	Napthalenemonoimide
NMP	N-Methyl-2-pyrrolidone
NMR	Nuclear Magnetic Resonance
ns	nanosecond
OFET	Organic Field Effect Transistor
OLED	Organic Light Emitting Diode
OPV	Organophotovoltaic
OTFT	Organic Thin Film Transistor
PAH	Polycyclic Aromatic Hydrocarbon
PBN	*N-tert*-Butyl-α-phenylnitrone
PDA	Perylenedianhydride

PDI	Perylene diimide
PET	Photoinduced Electron Transfer
Ph	Phenyl
PPh_3	Triphenylphosphine
PivOH	Pivalic acid
*p*TsOH	*p*Toluenesulfonic acid
ppm	Parts per million
ppy	Phenylpyridine
PXX	*peri*-Xanthenoxanthene
PXXDI	*peri*-Xanthenoxanthene diimide
PXXMI	*peri*-Xanthenoxanthene monoimide
QDI	Quaterrylenebis(dicarboximide)
Q-TOF	Quadrupole Time Of Flight
r	Radius
RT	Room Temperature
R_t	Retention time
SCE	Saturated Calomel Electrode
SET	Single Electron Transfer
t	Time
t	*tert*
T	Tesla
$TBAPF_6$	Tetrabutylammonium hexafluorophosphate
TCA	Trichloroacetic acid
TCQN	Tetracyanoquinodimethane
TDI	Terrylenebis(dicarboximide)
$TEAPF_6$	Tetraethylammonium hexafluorophosphate
TFA	Trifluoroacetic acid
THF	Tetrahydrofuran
TIPS	Triisopropylsilane
TLC	Thin Layer Chromatography
TMEDA	Tetramethylethylenediamine

TOF	Time Of Flight
UV-vis	Ultraviolet-visible
XRD	X-Ray Diffraction
ΔE	Energy Difference
ε	Molecular extinction coefficient
ε_d	Dielectric constant
θ	Dihedral angle
λ	Wavelength
μs	Microsecond
ν	Frequency
τ_f	Fluorescence life time
τ_{phos}	Phosphorescence life time
Φ	Fluorescence quantum yield
5DI	Pentarylenebis(dicarboximide)

Abstract

Nowadays polycyclic aromatic hydrocarbons (PAHs) have been the object of study in the search for novel semiconductor materials. Synthetic research in this field is ongoing since the beginning of the century, but it was only in recent years that technological development caused an increased interest for the optoelectronic properties of such systems. As a result, spectroscopic studies revealed interesting properties of *peri*-xanthenoxanthene (PXX) and its derivatives that will be extensively presented and discussed in this thesis. Concerning the tuning and tailoring of the optoelectronic properties of PAHs, many strategies can be applied in the quest for novel and better performing materials. One of the most common and efficient techniques is the atom doping that consists of a replacement of a carbon atom with a heavier one, such as oxygen or sulphur.

In Chapter 1, before addressing the detailed investigation of this thesis work, a brief introduction on the nature and applications of organic semiconductor materials is given. Optoelectronic properties of well-known perylene diimides (PDIs) are compared and the discussion eventually moves to PXX derivatives that are the core of this thesis.

In Chapter 2, a variety of synthetic pathways is explored in order to prepare PXX imide derivatives bearing electron-withdrawing groups in the *peri* position. The bottom-up approach is used to afford novel PXX systems. The synthesis of the desired systems is shown and discussed exploiting the key hydroxynaphthalene anhydride substrate.

As a conclusion of this thesis, Chapter 3 deals with the characterisation of the optoelectronic properties of PXX imide derivatives. Furthermore, PXX substrates have been screened as photoredox systems to perform dehalogenation reactions and the mechanism of the photo-triggered chemical transformation has been investigated.

Chapter 1. Introduction

1.1 Overview

This chapter will introduce the reader to dye molecules, their direct relationship with semiconductor behaviour and the tool-box to tune the electronic properties of these molecules by chemical modifications. Focusing on polycyclic aromatic hydrocarbons, and more specifically perylene diimide (PDI) derivatives, examples will be seen for performing these chemical modifications in order to tune their optical and redox properties. Subsequently, the application of dye molecules as semiconductors will be introduced and the application of PDIs and *peri*-xanthenoxanthene (PXX) derivatives as organic field effect transistor (OFET) devices will be highlighted. Eventually, the aim of this doctoral thesis will be presented.

1.2 Introduction

Human history is linked with pigments and dyes and from prehistoric times, humans have been using colours in their society.[1] At the beginning of the nineteenth century, only natural dyes and pigments were used such as indigo, alizarin and flavonol. In fact, only two synthetic dyes were known, picric acid and murexide.[2] In 1856, Perkin discovered Mauveine, which represents a milestone in human history as within 50 years from Perkin's first discovery,[3] synthetic dyes accounted for over 90% of the dyes used.[4]

A dye is constituted by a molecule that is able to absorb electromagnetic radiation in the UV and visible regions. The absorption of light promotes an electronic excitation from the lower energy level to a higher energy level (Figure 1). A chromophore is defined as the moiety in the molecule responsible for the absorption of the light in the UV or visible region. The energy of the photon absorbed is directly related to the frontier molecular orbital levels of the compound known as Highest-Occupied Molecular Orbital (HOMO) and Lowest Unoccupied Molecular Orbital (LUMO). After light absorption, the molecular chromophore in its excited state can relax to its ground state through different pathways: emission of a photon through luminescence or through non-radiative processes.

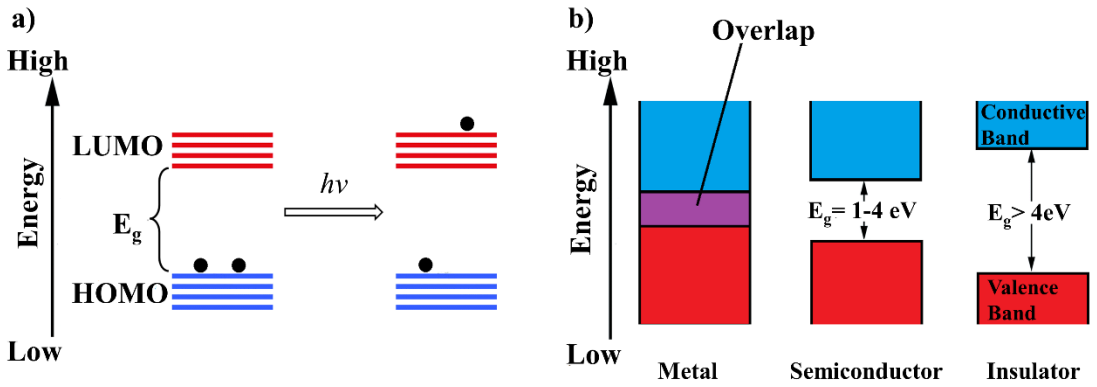

Figure 1: a) Schematic representation of electronic transition of a dye; **b)** Schematic representation of the valence and the conductive bands of a bulk material: metal, semiconductor and insulator.

Although the theory described before is valid for molecular chromophores, it is slightly different for bulk materials. In that case, the description of single discrete molecular orbitals cannot be used anymore and the band theory, representing a large number of discrete quantum states of the electrons, needs to be employed.[5] Based on the value of the energy gap between the valence and the conductive bands, the material can be defined as: *i)* conductor if the valence band partially overlaps with conductive band; *ii)* semiconductor if the difference of energy between the two bands ΔE is between 1 eV and 4 eV; *iii)* insulator if the band gap is higher than 4 eV.[6]

Typical semiconductors are based on gallium-,[7] aluminium-,[8] boron-[9] and silicon-based inorganic materials.[10] While they are very efficient, their general use in devices is affected by a major drawback, which is the high cost of preparation of semiconductors.[11] In this respect, organic materials show electrical properties spanning from insulator to conductor, including semiconductor.[12] However, several parameters, for instance, the morphology of semiconductor materials, need to be taken into account to prepare a device based on them. Organic semiconductors are promising because of the low cost preparation and purification of the semiconductor material and the easier processing from solution in comparison with the inorganic ones, which allows printing and therefore the preparation of large surface devices.[13] Moreover organic materials are appealing for the preparation of flexible devices.[14] Finally, the chemistry of organic molecules enables a fine tuning of the electronic properties by chemical modifications. Nevertheless, the performance of the devices based on organic semiconductors is lower in comparison with the one based on inorganic materials, and especially their lifetime is shorter.[15] The devices based on

organic semiconductors exploit conjugated polymers or small molecules. In contrast with the inorganic semiconductors, which are crystalline or polycrystalline, the structures of the organic semiconductor materials at the solid state are driven by weak interactions, principally van der Waals.[16] These interactions add to the material characteristic properties between conventional low mobility hopping transport in amorphous glass material[17] and high mobility band transport in covalently bonded single crystal.[18] The lifetime of the OFET is shorter in comparison to inorganic FET because the organic semiconductors show lower stability in working conditions. Extrinsic factors, such as oxidation and presence of moisture, can also affect the lifetime of the OFET.[19]

1.3. Tuning the color of molecules by tuning the HOMO-LUMO gap

Nowadays new dye molecules are studied for organic electronics such as organic light-emitting diodes (OLED),[20] organic photovoltaics (OPV)[21] and organic field-effect transistors (OFET).[22] In this regard, the tuning of the HOMO-LUMO gap and the magnitude of the HOMO and LUMO are essential requirements for the preparation of suitable materials.[23] In this context, the most important factors affecting the HOMO-LUMO gap (E_g) have been rationalised by Roncali[24] and are the following: *i*) conjugation length ($E_{\delta r}$), *ii*) resonance effect (E_{res}),[25] *iii*) planarity (E_θ),[26] *iv*) peripheral functionalisation (E_{Sub}),[27]and *v*) assembly effect (E_{int}).

The aforementioned factors can be summarised in the following empirical equation:

$$E_g = E_{\delta r} + E_{res} + E_\theta + E_{Sub} + E_{int}$$

The factors that affect the HOMO-LUMO gap tuning of single molecules are presented below (Figure 2).

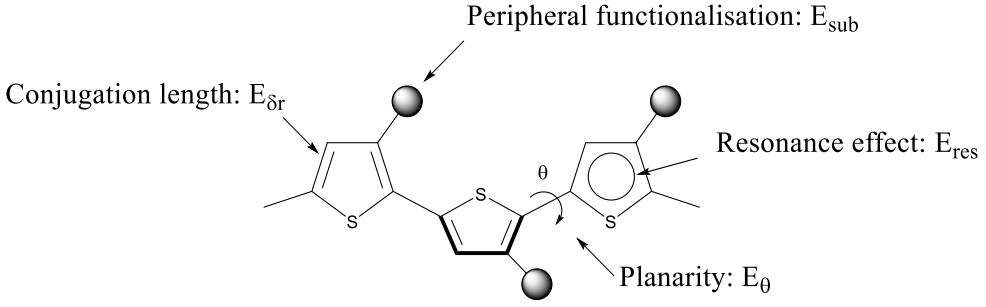

Figure 2: Representation of the structural factors that influence the HOMO-LUMO gap of π-conjugated systems.

1.3.1. Conjugation Length

Considering an extended linear π-conjugated system with degenerated mesomeric structures, such as polyenes, the π electrons are delocalized all over the backbone structure, which is an alternation of single and double carbon-carbon bonds. Applying a simple Hückel approximation the energy gap should be ideally zero with all the carbon-carbon bonds having the same length.[28] Nevertheless, such a mono-dimensional π-conjugated system has proved to be unstable, leading to a localization of the π-electrons entailing in a finite energy gap.[29] The degree of alternation of single and double bonds represents the major contribution to a finite band gap in the π-conjugated system.[30] Therefore, the bond length alternation in the conjugated system affects the E_g value, and its contribution is represented from $E_{\delta r}$. Typically, the extension of the conjugation length in a molecule induces a rise in energy of the HOMO and diminution in energy of the LUMO, with consequent shrinking of the HOMO-LUMO energy gap.[24a]

1.3.2 Resonance effect

Considering now an extended π-conjugated system such as poly(*p*-phenylene) or polythiophene, this system has a non-degenerate ground state, in fact the mesomeric structures, aromatic and quinoid forms, do not have the same energy (Scheme 1). Generally, the aromatic form is energetically more stable than the quinoid structure. The latter is higher in energy and it has a lower energy gap.[30a, 30d] The difference in energy between the aromatic and the quinoid form is the origin of the energy resonance effect. The π-electrons are localized in the aromatic ring, which is the most stable structure, preventing the delocalization of the π-electrons outside the ring along the chain and the conversion in the quinoid form. [24a]

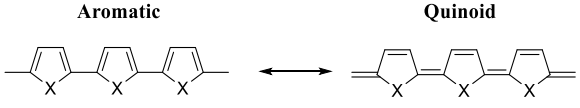

X= -CH=CH-, S, NH

Scheme 1: Mesomeric structures for: poly(*p*-phenylene); polythiophene and polypyrrole. On the left side the aromatic ground state is shown while on the right side the quinoid structure at higher energies is represented.[30a]

Therefore, the conversion of the aromatic form into a conjugated system with an enhanced quinoid character allows the decrease of the energy gap. In the case of the polythiophene one way to enhance the quinoid structures is based on the fusion of the thiophene ring with another aromatic ring which has higher resonance energy such as the benzene ring.[31] The aromatic sextet tends to delocalize in the system that has higher resonance energy. Therefore, due the difference of the resonance energy of the benzene and thiophene, the latter ring dearomatizes to a quinoid structure (Scheme 2).

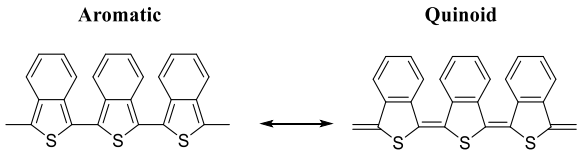

Scheme 2: Mesomeric structures of poly(benzo[c]thiophene). On the left side is depicted the thiophene in aromatic form while on the right side is represented the thiophene in quinoid structure.

The contribution of the energy resonance effect to E_g value is represented from E_{res}. By applying this strategy, it has been possible to tune the polythiophene energy gap.[32]

1.3.3 Planarity

Another parameter that affects the HOMO-LUMO gap of the π-conjugated system, such as polythiophene, is the planarity. The presence of single bond connecting the aromatic cycles allows the possibility to the ring to imply variations on the dihedral angle θ described by the two planes containing the adjacent ring. The loss of coplanarity leads to the increase of the dihedral angle θ, resulting in a decreased π electron delocalization (Figure 3).

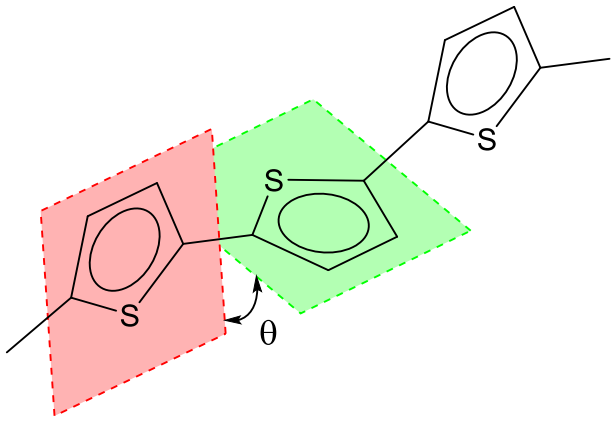

Figure 3: Representation of dihedral angle θ between two adjacent thiophene rings.

Thus, E_g is increased by a quantity E_θ.[24a] The effect of this parameter has been widely studied in poly (*p*-phenylene) and polythiophene systems.[24b, 33]

1.3.4 Peripheral Functionalisation

Introduction of electron donating or electron withdrawing substituent on a conjugated system engenders a tuning of the HOMO and LUMO energy levels. More specifically, the functionalization with electron donating groups results in a rising of the orbital energy affecting more the HOMO level, generally entailing a reduction of energy gap.[34] In other hand, the functionalisation with electron withdrawing groups, such as nitro-, cyano- and carboxy substituents, promotes a decrease of both HOMO and LUMO energy levels.[35] Additionally, when a conjugated molecule is functionalised with electron donor and electron acceptor moieties linearly conjugated, the formation of a charge transfer is observed.[36] This 'push-pull' system results in the formation of low energy molecular orbitals facilitating HOMO-LUMO transition.[37] Probably one of the most representative examples of fine HOMO-LUMO energy gap tuning is represented by the NDI derivatives.[38] Starting from the parent compound naphthalene diimide is possible to prepare a collection of colours by functionalisation of the aromatic core (Figure 4).[38] Starting from the unsubstituted NDI (molecule N Figure 4), upon introduction of electron donating groups a gradual shift of the frontier orbital energy is observed. [39] While a gradual shift for the LUMO energy is observed, a stronger effect is affecting the HOMO energy level (Figure 4). It is possible to observe a direct relationship between the electron donating properties of the substituents and the number of those substituents on the naphthalene core and the HOMO energy value which becomes more positive with the progressive electron donating ability of the substituent.[40] On the contrary, the introduction of electron withdrawing groups, such as cyano substituents, on the naphthalenic core promotes a decrease of both HOMO and LUMO energy levels (Figure 4).[38]

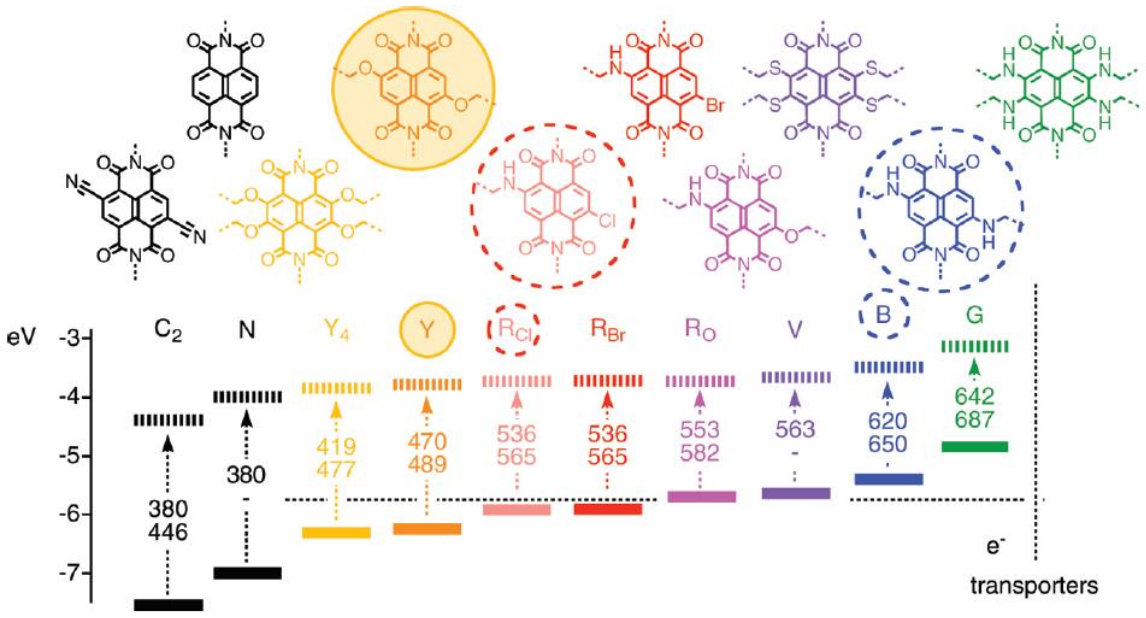

Figure 4: Frontier orbital energy levels of NDI derivatives, dashed arrows shows the absorption of light (*hv* in nm) of maximal absorption (top) and emission (bottom).[38]

1.3.5 Heteroatom doping

If even not mentioned in the Roncali equation, substitution of carbon atoms with heteroatoms is another approach to modify the electronic properties of the molecules, and it is particularly relevant to polycyclic aromatic hydrocarbons (PAH). The first atom doping has been performed by exploiting nitrogen. It relies on the well-established synthetic chemistry and stability of the *N*-containing systems.[41] Nevertheless, significant efforts have been made to prepare large heteroatomic systems containing boron,[42] phosphorous,[43] or chalcogen atoms.[44]

1.4 Polycyclic Aromatic Hydrocarbons

Polycyclic aromatic hydrocarbons (PAHs) are one the most relevant classes of compounds that are studied in organic electronics.[45] PAHs possess structures consisting of fused benzene rings whose core entity can be viewed as small aromatic sub-unit of graphene. Thus PAHs have promising semiconducting properties.[22] Moreover, the polycyclic aromatic hydrocarbons display higher solubility than graphene,[46] providing organic semiconductor solution-processable for OFET perparation.[47] In 1994, Haarer and co-workers investigated the electronic properties of a hexa-thiotriphenylene derivative **1** that provides semiconducting discotic columnar phases (Figure 5).[48]

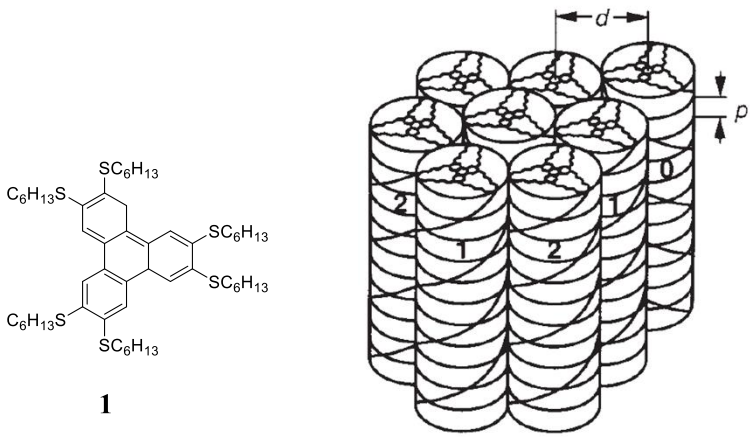

1

Figure 5: Molecular structure of 2,3,6,7,10,11-hexahexythiotriphenylene and a representation of the structure of its helical columnar phase.[48]

Hareer and co-workers reported a higher charge mobility along the columnar axis when the triphenylene units lie face to face with high degree of π-orbit overlap along the columns.[48] Since then, a wide range of PAHs has been studied for device applications, among them substituted hexabenzocoronenes have been the object of wide investigations.[49]

1.4.1 Rylene derivatives

Another two-dimensional extension of the benzene unit is represented by rylene chromophores. Rylene derivatives are based on the repetition of naphthalene units linked to each other in *peri*-position.[50] In general, rylene derivatives present chemical-, thermal- and photo-stability and also electron transport behaviour.[51] These derivatives are also called oligo-naphthalenes and follow the subsequent nomenclature: perylene (n = 2), terrylene (n = 3), quaterrylene (n = 4), pentarylene (n = 5) and hexarylene (n = 6). The extension of the aromatic scaffold results in a bathochromic shift in the absorption and emission properties. Rylenes can be functionalized in *peri*-positions and it was found that the introduction of imide moieties provides a further stabilization and a red-shift in absorption. One illustrative example provided by Müllen and co-workers is the synthesis and optical studies of rylene derivatives starting from perylene diimide to hexarylenediimide.[50-51, 52] The spectroscopic measurements show a bathochromic shift of about 100 nm per additional naphthalene unit (Figure 6).

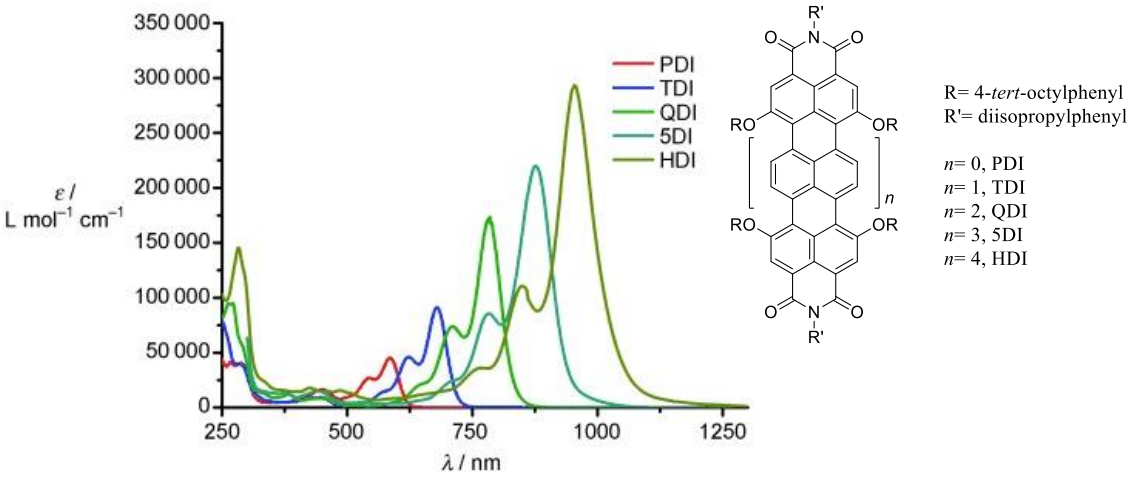

Figure 6: Absorption spectra of the entire tetraphenoxy-substituted rylene diimide series in $CHCl_3$ perylenebis(dicarboximide) (PDI), terrylenebis(dicarboximide) (TDI), quaterrylenebis(dicarboximide) (QDI), pentarylenebis(dicarboximide) (5DI), hexarylenebis(dicarboximide) (HDI).[50-51]

In this class of dyes, the most representatives are the perylene-3,4,9,10-tetracarboxydiimides, also known as perylene diimides (PDIs). PDIs are colorants that have been extensively studied and found application as industrial dyes and pigments, such as Pigment Red 179.[53] The parent compound, perylene dianhydride, has been known since 1913.[54] The physical properties of PDI derivatives can be modified by changing the substituents on the imide motifs or in the bay position of the aromatic core. Since 1913, several PDI derivatives have found applications as industrial dyes and pigments especially for carpet fibres and in the automotive industry.[54a, 55] Moreover, PDIs, apart from the already mentioned industrial applications, show high absorption in the visible with high quantum yield and photochemical stability. All these properties allow PDIs to be exploited for other applications, such as energy transfer.[56]

1.4.2 PDI derivatives

The general structure of perylene diimide and its functionalisation positions are presented in Figure 7.

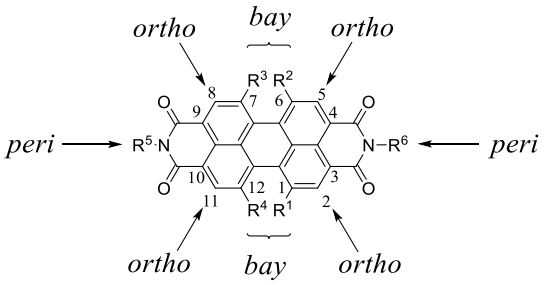

Figure 7: General structure of perylene diimide. The core positions are divided in three categories: *peri* (3, 4, 9, 10) *ortho* (2, 5, 8, 11) and *bay* (1, 6, 7, 12).

1.4.2.1 *Preparation of N-substituted A_2-type PDIs*

The synthesis of symmetrically *N*-substituted perylene diimides ($R^1 = R^2$) is achieved from the corresponding anhydride. The preparation of the perylene dianhydride starts from acenaphthene **2**, which is obtained from coal tar distillation,[57] acenaphthene **2** is oxidized to the 1,8-naphthalene anhydride **3**.[58] However, this one cannot be dimerised directly to perylene derivatives due the chemical incompatibility of anhydride with the reaction conditions for the coupling reaction. Therefore, 1,8-naphthalene anhydride **3** in the presence of ammonia is converted to naphthalene imide **4** and subsequently dimerised in the presence of KOH at 220 °C followed by air oxidation to yield derivative **5**. Finally, the perylene dianhydride **6** is obtained by acid hydrolysis of the perylene diimide **5** in hot concentrated sulfuric acid (Scheme 3).[59] The conversion of the perylene dianhydride **6** in the symmetric PDI **7** with primary aliphatic amines can be performed in organic solvents, such as benzene. While, for less reactive aliphatic and aromatic amines, the reactions are performed in high boiling point solvents, such as imidazole or quinoline, in the presence of $Zn(AcO)_2$.[60]

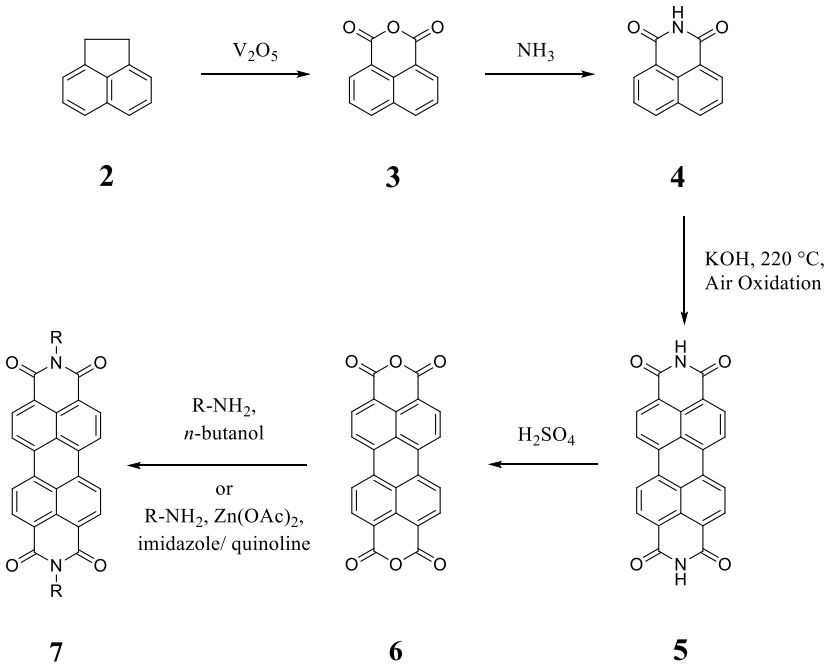

Scheme 3: Preparation of *N*-substituted A_2-type PDIs **7**.[59b]

The type of the imide substituent affects mainly the solubility and the morphology of the PDIs,[61] while the effect on the frontier orbital energies and optical properties is minimal.[60, 62] The HOMO and LUMO energy levels are not affected by the nature of the substituent since the nitrogen atoms of the imides is on the nodal plane of both HOMO and LUMO.[63] Insertion of long alkyl chains at the imide positions do not enhance the solubility, while branched chains and cyclic chains increase the solubility, because bulky substituents prevent the π-π stacking interaction of the perylene core.[64] In addition, the imide substituents can also strongly affect the crystal packing.[65]

1.4.2.2 *Preparation of N-substituted AB-type PDIs*

The synthesis of asymmetrical perylene diimides, bearing different substituents on each imide functionality has been reported.[66] The attempts for their synthesis revealed high difficulty in preparing them either in simultaneous presence of both amines in one-pot reaction or with sequential addition of two amines, because the difference in reactivity of the amines towards perylene dianhydride is low.[66a] The reaction provides the two undesired symmetrical derivatives A_2-type as main products, while the desired AB-type product is present in traces.[66a] A more convenient approach for the unsymmetrical PDIs is based on multistep methods.[66a] Two different synthetic pathways to achieve the

preparation of *N*-substituted AB-type PDIs are displayed in Scheme 4. The synthetic approach based on PATH A is based on the preparation of the A_2-type PDI **7** starting from perylene anhydride **6**. Subsequently, symmetrical PDI **7** is partially hydrolysed to perylene monoimide monoanhydride **8** in 50% yield.[66a] The desired unsymmetrical PDI **9** is formed after further imidization of perylene monoanhydride derivative with a second amine. The direct synthesis of perylene monoimide monoanhydride derivative from imidisation is performed with one equivalent of amine, probably due the enhanced solubility of the intermediate.[66a] The second synthetic method proceeds following PATH B, which relies on the formation of the perylene monoanhydride salt **10** from the hydrolysis of perylene dianhydride **6** and subsequently a stepwise imidisation and acid cyclization leading to the perylene monoimide monoanhydride **8** and eventually after a further imidisation reaction provides the unsymmetrical PDI **9**.[66b, 67] Despite the fact that both synthetic pathways provide the desired unsymmetrical PDIs, PATH A found a wider application because in general it provides the desired product in higher yield and the purification is easier.[68]

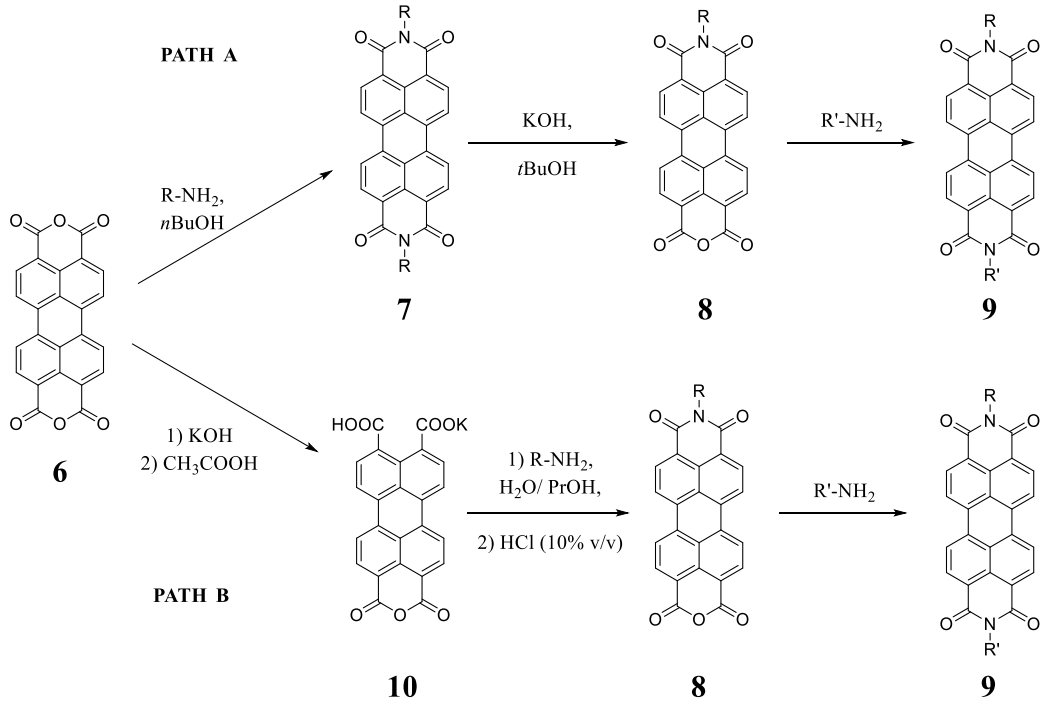

Scheme 4: The two methods for the preparation of *N*-substituted AB-Type PDIs.[66a]

The absorption and emission spectra of the AB-type PDI **9**, obtained from the aforementioned reactions, are usually indistinguishable from those of the respective symmetrical derivatives particularly in solution at low concentrations since the molecular

aggregation is limited. This can be explained by the nodes in the HOMO and LUMO at the imide positions of PDI that reduce the electronic coupling between the aromatic core of the molecule and its imide substituents (Figure 8).

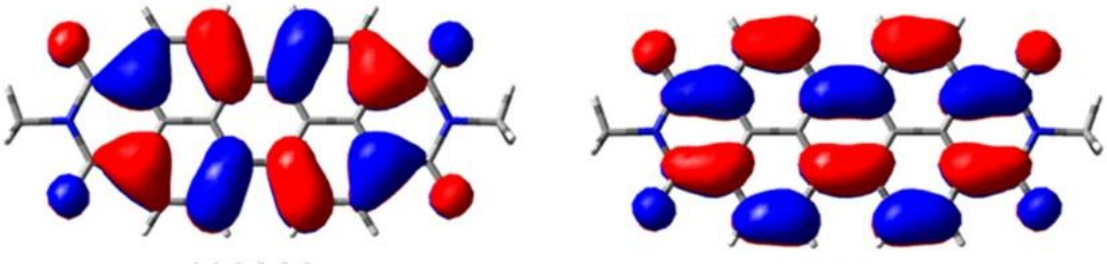

HOMO **LUMO**

Figure 8: The frontier orbitals (HOMO and LUMO) of perylene diimides.[69]

The major electronic effect from the imide group will always be inductive in nature. Therefore, the various imide substituents afford a small change in the electronic properties of perylene diimides.

1.4.2.3 *Preparation of bay-substituted PDIs*

The position of bay-functionalization plays a big role on the solubility of the compounds obtained. The introduction of aryl or aryloxy groups in the position 1, 6, 7 and 12 can be used to enhance the solubility of the perylene derivative **16** (Scheme 5) because the substituents are forced out of the plane of the molecule by steric interactions.[64] These substituents, as well as smaller groups such as bromine, induce a twisting of the molecule. This induces a decrease of the π-π stacking and improves the solubility of the compound. As already mentioned, the twisting of the molecule and the nature of the substituents on the bay position can affect the HOMO-LUMO energy gap of the PDIs.[55] Typically, in order to functionalise the bay positions, the perylene dianhydride needs, firstly, to be halogenated by chlorination or bromination, providing the related bromo derivative **11** in 90% yield [70] and chloro derivative **12** in 90% yield [71] and subsequently to be converted to the halogenated diimide derivative by reaction with a primary amine, because the halogenated dianhydride derivative is not soluble in most common organic solvents (Scheme 5). The soluble halo-diimide derivative either dibromo-PDI **13** or tetrachloro-PDI **14** can be functionalized by alkoxy, phenoxy, alkylthio and phenylthio-derivatives by

nucleophilic substitution.[55, 56b, 72] Substitution of the brominated derivative with secondary amines such as pyrrolidine has been achieved by reacting bromo-PDIs in the presence of an excess of amine leading the formation of the diamino substituted compound **17**.[72a, 72b, 73] The functionalisation of the bay position starting from the halo-PDI derivatives can also be performed by metal-catalysed cross coupling. Typically, Pd cross coupling such as Suzuki,[74] Sonogashira,[74b, 75] and Nigishi [76] have been used to introduce alkynyl **20**, aryl **18** and cyano **19** derivatives, respectively. Furthermore, the Sonogashira coupling provides acetylenic PDI **20** derivatives which could form coronene diimide **21** derivatives with an extension of the aromatic core.[75a, 77] Furthermore, several copper-mediated couplings have been reported for the introduction of perfluorinated[78] and cyano[56f] substituents in the bay positions. Apart from the enhancement of the solubility, substituents in these positions strongly affect the morphology in the solid state, with small substituents such as halogens or cyano groups **19** affording highly crystalline PDIs,[56f, 65] while aryl groups in the bay position provide amorphous materials.[74c] The bay substituents also affect the electronic properties. For instance, the presence of electron withdrawing groups, such as halides, induces the lowering of the HOMO and LUMO energy levels.[60] However, as both energy levels are affected, there is not a significant effect on the spectroscopic properties of the molecules, only 10 nm shift in the absorbance and emission properties in comparison with the unsubstituted PDI.[56f, 60, 79] On the contrary, electron donating substituents, such as phenoxy and pyrrolidinyl, promote a rise in energy of both, the HOMO and LUMO but in a different amount, with the HOMO energy, rising more than that of the LUMO.[60]

Therefore the energy gap decreases, which induces a bathochromic shift in absorption. A similar effect is observed for substituents that extend the π-conjugation of the aromatic core such as alkynyl and aryl groups.[74b, 74c, 75b]

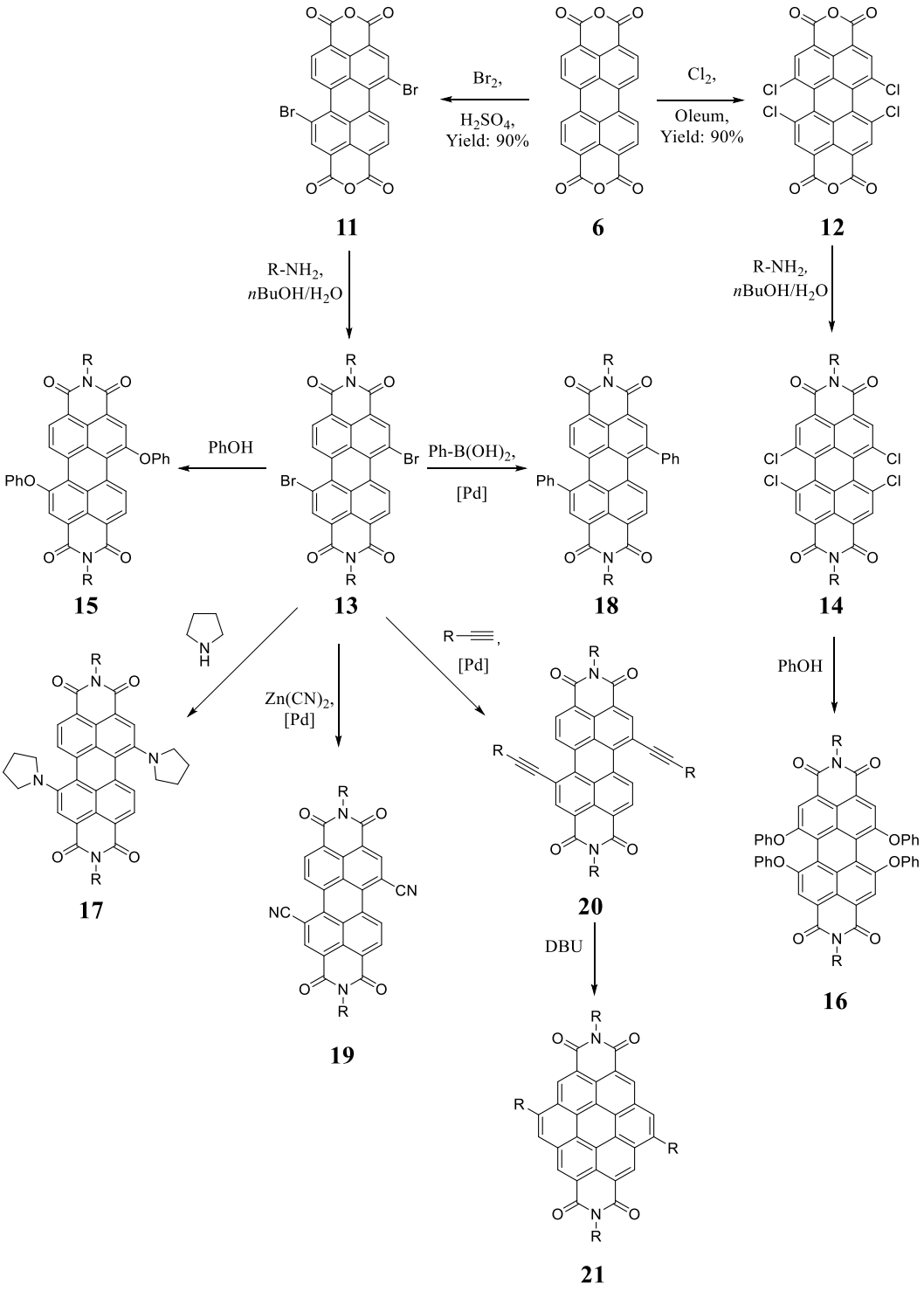

Scheme 5: PDIs functionalisation in bay position with different substituents.[55]

1.4.2.4 *Optical properties*

PDIs are considered to be excellent organic red dyes with high absorption extinction coefficients in the wavelength range of 400 to 600 nm and with almost unitary quantum yield. As described before, the absorption and emission maximum are not affected by changing the nature of the imides, while the substituents on the perylene core show a great influence on the absorption and emission spectra. Substituents such as two phenoxy groups in the bay position lead to a bathochromic shift of ≈ 20 nm in absorption and emission in comparison to the unsubtituted PDI.[55, 80] However, more pronounced spectral changes occur with electron donating substituent groups such as pyrrolidinyl groups, which result in a PDI with a dark-green colour in the solid state and in solution.[81] In addition, the optical properties of the PDIs are dependent on the concentration, temperature and solvent polarity. Typically, the aggregation driven by the aromatic core at high concentration (for example higher than 10^{-4} mol/L) induces a bathochromic shift and broader absorption and emission spectra.[55] As shown in Figure 9, the changes in the absorption spectrum due to the concentration-dependence are more significant in less polar solvents, where the strong aggregation driven by π-π interactions leads to a loss of the fine structure in the absorption spectra.

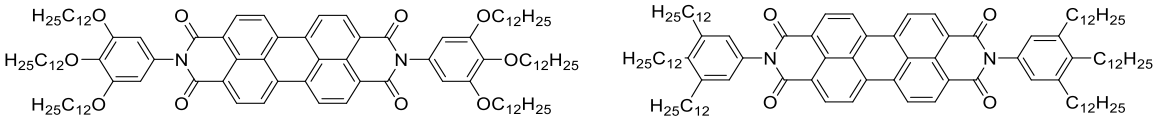

22 **23**

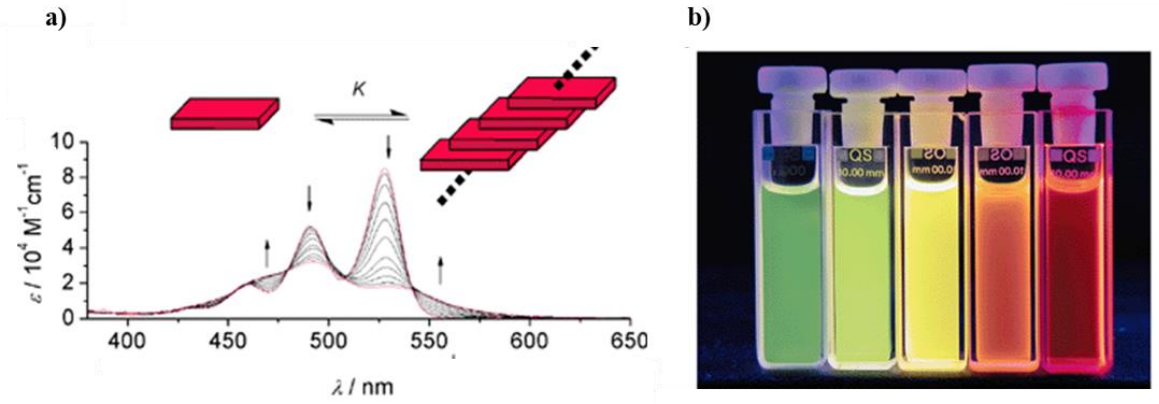

Figure 9: a) The concentration-dependent UV-vis absorption of the perylene diimide **22** in methylcyclohexane; **b)** and the concentration-dependent emission of the perylene diimide **23** in toluene .The concentrations from left to right are: 10^{-6}, 10^{-5}, 10^{-4}, 10^{-3} , and 10^{-2} M.[55]

In other solvents, such as $CHCl_3$, the PDI's aggregation is less influenced by the concentration and no aggregation phenomena are observed in the absorption spectrum with concentrations up to 10^{-5} mol/L.[55] Similar observations have been made for aggregation studies on PDI's emission spectra. PDIs have also been studied and used for supramolecular organisation. Spectro-electrochemical studies showed the high stability of both reduced species (anion and dianion) and of the oxidised species. Due to the high stability of the dianions,[82] the absorption spectra of the PDI radical anions can be easily identified (Figure 10).

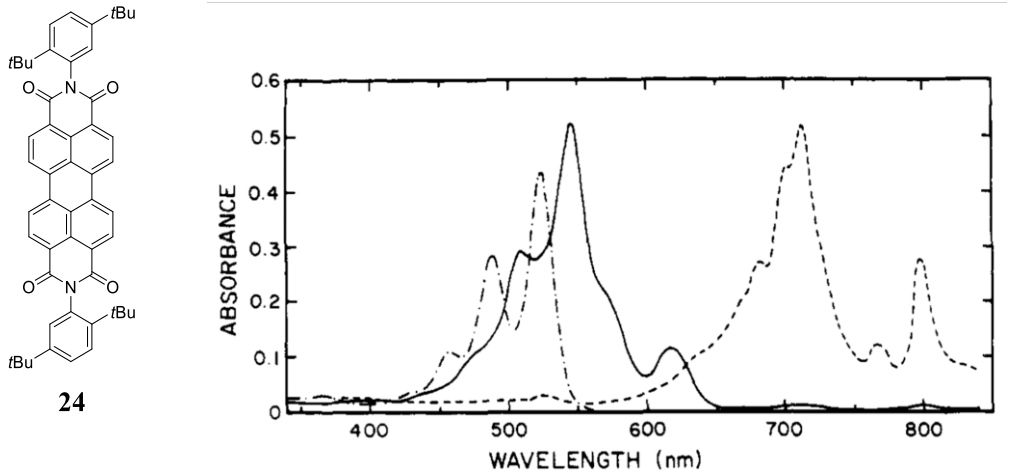

Figure 10: Absorption spectra of PDI **24** (−·−) PDI $\mathbf{24}^{\bullet-}$ (− −) and PDI $\mathbf{24}^{2-}$ (—) in ethanol (1×10^{-4} mol/L tetramethylammonium hydroxide) obtained by controlled reduction of PDI **24** with H_2 in the presence of Pt. The concentration for neutral PDI **24** was 5.4 μM.[82a]

Therefore, PDIs have been widely exploited in photoinduced charge-transfer studies. In general, they have been used to study photoinduced intermolecular charge-transfer between PDI systems as acceptors with electron donor such as polythiophenes or photoinduced intermolecular charge transfer in PDI systems.[83] These studies provide not only valuable information for the fundamental processes but are also relevant for technological applications, such as organic photovoltaics where the photophysical properties have a primary role.[84]

1.4.2.5 *Redox properties of PDIs*

The electrochemical properties of PDIs have been widely investigated. From these studies it emerged that perylene diimides are electron deficient systems and thus it is easier to reduce than to oxidise them. In general, perylene diimides display two reversible reductions and one reversible oxidation.[55] For instance, from electrochemical analysis, the PDI without substituent on the aromatic core shows two reversible reduction potentials (at ~ -1.0 and -1.2 V vs $F_c^{+/0}$) and one reversible oxidation potential (at ~ 1.2 V). Similarly to the optical properties, the effect on the redox properties of the substituents on the imides is moderate. This is due to the fact that the *N* atoms are on a nodal plane of the HOMO and LUMO and the orbital energy is affected by inductive effects via the imide *N* atoms. The substituents on the aromatic core have instead a great influence on the redox properties. For example, PDIs bearing electron-withdrawing substituents at the bay positions, such as cyano groups, are easily reduced and less readily oxidised in comparison to the unsubstituted derivatives. On the other hand, derivatives with π donating substituents, such as pyrrolidinyl, in the bay positions are less easily reduced and more easily oxidised, in comparison with the unsubstituted PDIs. PDIs bearing arylethynyl substituent in the bay position are more easily reduced in comparison with the parent PDI.[85]

1.5 Dye molecules as organic semiconductors

In the last decades, organic electronics became one of the most attractive fields in chemistry and material science.[86] This development has originated from the attractive role that organic materials could play in solar cells, [21b, 87] organic field effect transistors (OFET)[88] and organic light emitting displays.[89] In this regard, chemists have developed a wide number of systems with π-conjugated scaffolds. Polycyclic aromatic hydrocarbons such as acenes,[45] conjugated polymers, such as polythiophenes, fullerenes[90] and triphenylamines[91] are part of the molecules that have been investigated. Apart from the already mentioned structures, other molecules that are used in industry were tested as organic semiconductors, among them also two important pigments: phthalocyanine[92] and PDI[51b, 93] have been studied. In 1986, Tang reported for the first time the fabrication of a thin-film, two-layer organic heterojunction photovoltaic cell based on copper phthalocyanine and a perylene tetracarboxylic derivative.[94] The most promising

application for the dye-based organic semiconductors is represented by the solar cell due to the absorption of the visible light. Nowadays one of the most relevant challenges for the electronics industry is the fabrication of flexible and lightweight devices. In this respect PDI derivatives have been widely studied.[95]

1.5.1 Application of PDIs in OFET

Organic field-effect transistors (OFETs), using π-conjugated systems as the active semiconducting layer have attracted attention for printed and flexible electronic devices. The most important parameters that determine the efficiency of the OFET devices are the semiconducting properties and the charge mobility. These are related to the electronic properties as well as the molecular packing of the semiconductor material.[96] Therefore, the molecular packing of the organic semiconductors becomes very important for the charge transport between molecules.[86a] There are four different kinds of packing motifs: (1) herringbone packing (face-to-edge) without π-π overlap (face-to-face) between adjacent molecules (Figure 11a); (2) herringbone packing with π-π overlap between adjacent molecules, also called slipped π-stacking in some literature reports (Figure 11b); (3) lamellar packing, one-dimension (1-D) π-stacking (Figure 11c); and (4) lamellar packing, two-dimension (2-D) π-stacking (Figure 11d). Of the four kinds of packing motifs, lamellar packing (2-D π-stacking) is believed to be the most efficient for charge transport because it enhances the charge transport through an almost straight line (namely, the shortest route).[86a] However, the morphology also plays a crucial role in the charge carrier mobility.

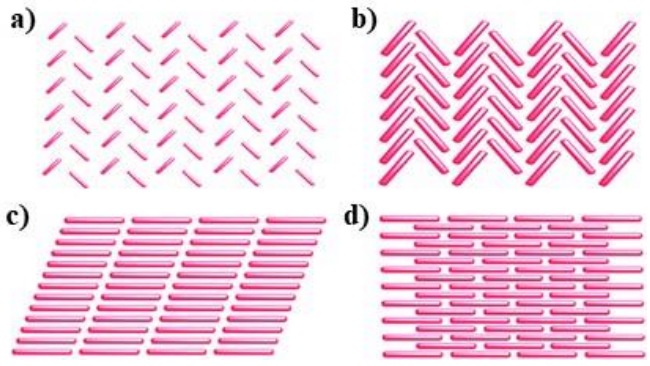

Figure 11: Molecular packing motifs in crystals. **a)** Herringbone packing (face-to-edge) without π–π overlap (face-to-face) between adjacent molecules; **b)** herringbone packing with π–π overlap between adjacent molecules; **c)** lamellar motif, 1D π-stacking; **d)** lamellar motif, 2D π-stacking.[97]

1.5.2 *Peri*-Xanthenoxanthene

In 2011, Sony released the first rollable AMOLED display that can be wrapped around a pen. This unprecedented result was achieved by fabricating an OTFT-driven flexible OLED display (Figure 12).[98] The presented device was prepared using an organic semiconductor, based on *peri*-xanthenoxanthene (PXX).

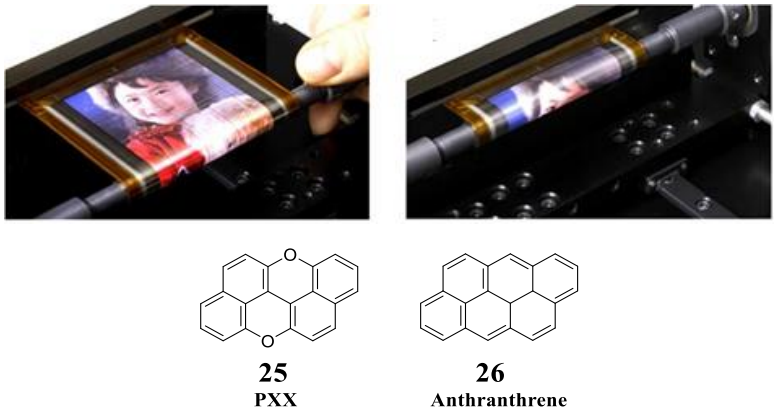

Figure 12: In the top is represented the Sony's rollable OTFT-driven OLED display in a flat condition and in a rolled-up condition with r = 4 mm. In the bottom are depicted the structures of anthranthrene **26** and the congener O-doped PXX **25** are shown.

Peri-xanthenoxanthene **25**, that is also called dinaphthalene dioxide or 6,12-dioxaanthanthrene, can be envisaged as the O-doped version of the parent anthanthrene **26** in 6 and 12 position. The PXX system is known since 1905, when Bünzly and Decker prepared the PXX by oxidation of binaphthol in the presence of $K_4[Fe(CN)_6]$.[99] However, PXX **25** did not receive great attention. In fact its physical and chemical properties started to be investigated at the end of the 70's, when Inabe and co-workers, while studying the electric resistivity of iodine complex of aromatic hydrocarbons, compared the electrical properties of the iodine complex of anthanthrene **26** and the iodine complex with PXX **25**.[100] The authors reported the formation of two different charged salts, $(PXX)_3^{2+}(I_3^-)_2$ and $(PXX)^+I_3^-$. Subsequently, in 1994, Hjort and co-workers, studying the charged complex as organic semiconductor, reported the crystal structure of the charge transfer complex of PXX with tetracyanoquinone (TCQN).[101] The crystal structure of the PXX-TCQN charge transfer complex shows the composition ratio of PXX **25** and TCQN of 1:1 and alternate stacks of PXX **25** and TCQN. More recently, the charge transfer complex of PXX with TCQN derivatives has been investigated as organic semiconductor for OFET fabrication.[102] In the same period, Inabe and co-workers prepared a highly conductive

charge transfer complex from PXX with dicyano(phthalocyaninato)cobalt(III).[103] In 2009, Kobayashi and co-workers reported the preparation of OTFT based on PXX derivatives.[104] The unfunctionalised PXX **25** does not form highly ordered films, this represents a disadvantage for the OTFT preparation. In order to overcome this problem, 3,9-diphenyl-PXX **27**, and 3,9-bis(4-propylphenyl)-PXX **28** (Figure 13) were synthesized.

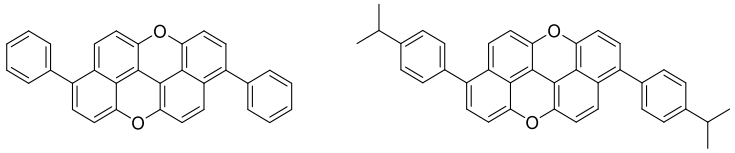

27 **28**

Figure 13: Stable structures of 3,9-diphenyl-PXX **27** and 3,9-bis(4-propylphenyl)-PXX **28** exploited for the preparation of stable OTFT.[104]

The first afforded uniform films by vacuum deposition, while the 4-propylphenyl derivative was suitable for a solution processing OTFT preparation. The diphenyl-PXX derivative has shown high mobility and great thermal stability under air. In 2013, Cui and co-workers reported the preparation of three dialkylated PXX derivatives **29**, **30** and **31**, bearing the octyl chains in different positions.[105] The optoelectronic investigation showed that their absorption and emission spectra were not significantly affected by the difference in the position of the substituents. When OFET devices were prepared with those three molecules, the 1,7-bis-octyl-PXX **30** derivative appeared as the most efficient. The authors have shown that 2,8 bis-octyl-PXX **29** and 5,11 bis-octyl-PXX **31** derivatives had a herringbone arrangement, while for the derivative **30** the authors assumed a lamellar type structure (Figure 14).[105]

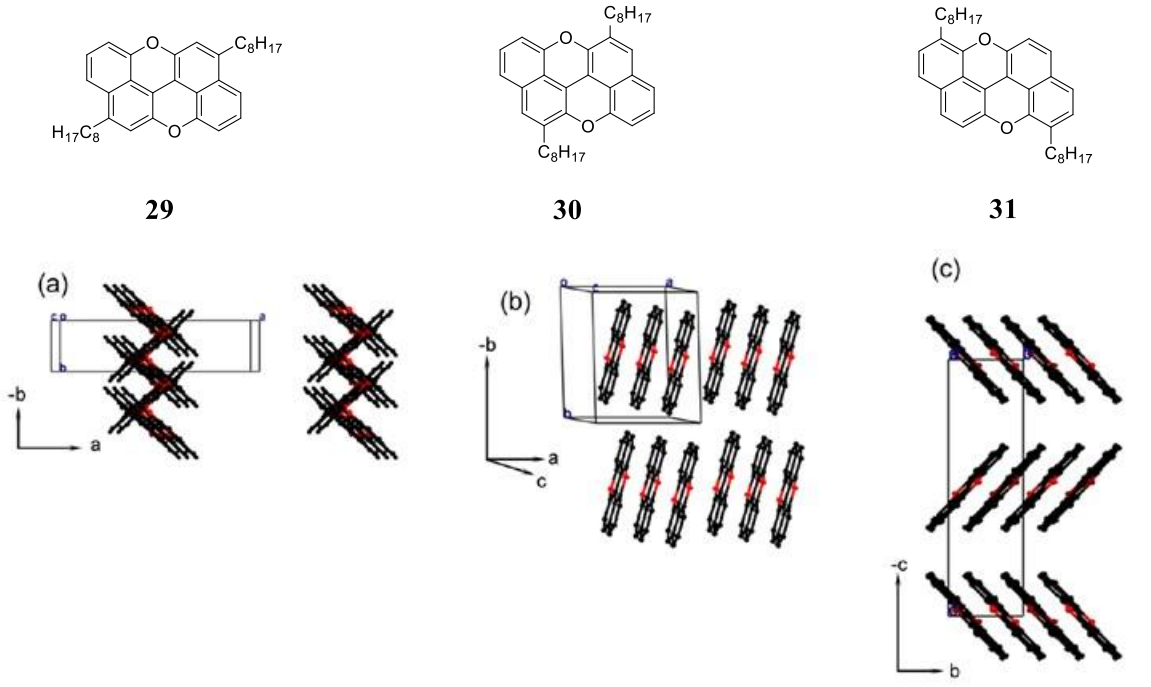

Figure 14: Influence of substituents' position on PXX scaffold on the crystal packing.[105]

However, all the investigations mentioned have been focused on the simple PXX **25**, and no larger congeners have been prepared and studied. The control over the O-doping and the understanding of the substituents effect on the optoelectronic properties can allow us to prepare novel organic semiconductors. Hence our group started to focus the attention on oxygen-doped π-extended PXX systems. In 2016, Stassen et al. reported the preparation of O-doped benzorylenes, pentaphenopentaphene derivatives **33**, **34** and naphotetraphenopyrarnthrene derivatives **35**, **36** presenting armchair-type edge (Figure 15).[106]

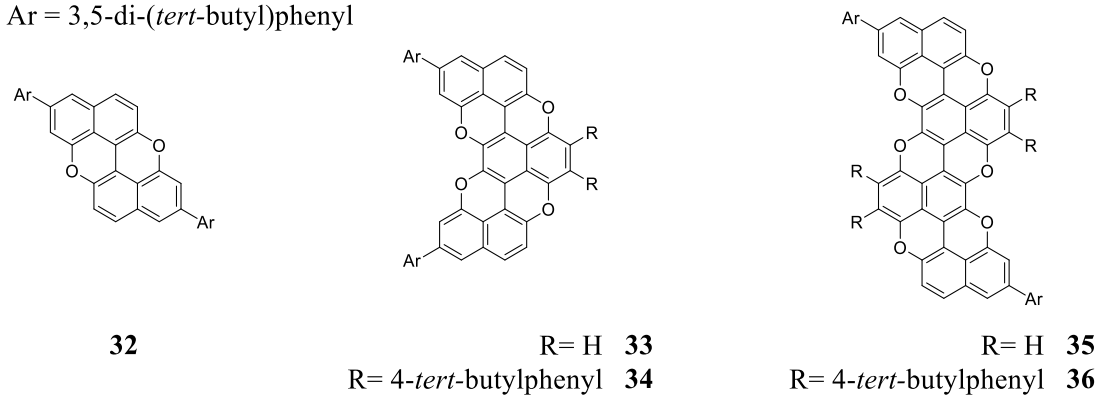

Figure 15: Heteroatom-doped benzorylenes developed by Stassen et al.[106]

These five new derivatives are functionalised with cumbersome substituents such as 3,5-di-*tert*-butylphenyl and 4-*tert*-butylphenyl to prevent the strong π-π interactions and increase the solubility. The ^{1}H NMR of derivatives **33**, **34**, **35** and **36** displays broad signals. Nevertheless, the ^{1}H NMR of molecule **34** upon treatment with hydrazine has shown a better resolution. This behaviour suggests that a fraction of the molecule **34** is present as radical cation, which is paramagnetic. The paramagnetic species are known to lead to a broad NMR spectrum,[107] while, the treatment with hydrazine reduces the radical cation leading to a diamagnetic species and therefore providing a better resolution of ^{1}H NMR spectrum. Conversely, in the case of **33**, **35** and **36**, the addition of hydrazine did not provide any improvement in the ^{1}H NMR resolution. The absorption and emission spectra of derivative **33**, **34** and **35**, **36** present the same electronic transition pattern of parent compound **32**, but with broader peaks. The absorption spectra of derivatives **33** and **34** show a bathochromic shift, in accordance with the increase of the conjugation length and shrinking of the HOMO-LUMO gap. A similar trend was observed for derivatives **35** and **36**, but with a broader signal arising from aggregation. The persistence of aggregation also at elevated temperature and the ^{1}H NMR results suggest that the aggregation takes place between the neutral molecule and a radical cation. The X-ray diffraction of **33** shows that the molecule undergoes a strong π-stacking at the solid state forming lamellar-like microstructures. Subsequently in 2017, in our group, Miletić et al. reported the π-extension of PXX, reporting the preparation of benzo-(**37**), naphtho- (**38**) and binaphtho-PXX (**39**) derivatives (Figure 16).[108]

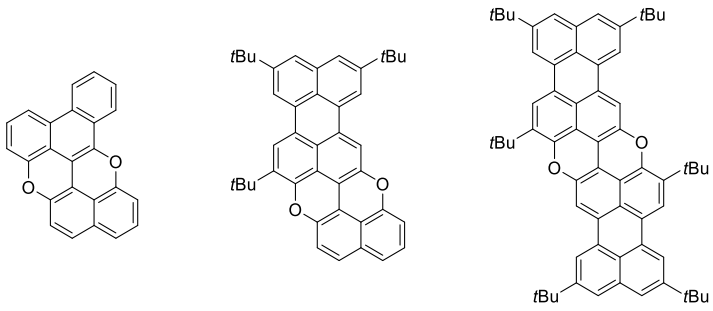

37 **38** **39**

Figure 16: π-Extended PXX derivatives prepared by Miletić et al.[108]

The progressive π-extension of the PXX core from derivative **37** to derivative **39** leads to a consequent bathochromic shift of the absorption maximum corresponding to a shrinking of the HOMO-LUMO gap and a decrease of the fluorescence lifetime.[108]

1.6 Aim

The work described in this doctoral thesis aims at the design of the synthesis and the study of novel organic semiconductors. Based on the intriguing properties of the PXX described so far, a novel class O-doped π-extended PAH was designed. The tuning of the electronic properties is achieved by peripheral functionalization. In particular, electron withdrawing substituents where chosen in analogy with the well known PDI substrate and one or two imide motifs were introduced to the PXX scaffold to afford the *peri*-xanthenoxanthene monoimide **40** and *peri*-xanthenoxanthene diimide **41** (Figure 17).

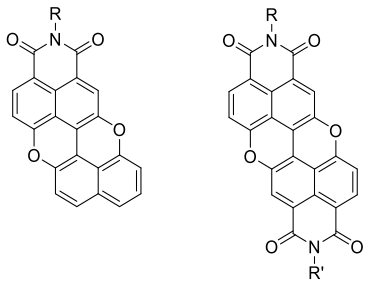

PXXMI **40** **PXXDI** **41**

Figure 17: General chemical structure of *N*-functionalised PXXMIs and PXXDIs (R = alkyl or aryl substituents.

Objective 1

To this end, two novel families of PXX will be prepared, namely PXXMI **40** and PXXDI **41**. The preparation of the two novel derivatives will be achieved via a bottom up approach relying on intramolecular metal catalyzed C-O bond formation. Moreover, due to the versatility of the functionalization at the imide group, in an analogy with *N*-substituted AB type PDI, we will also develop the synthesis of *N*-substituted AB type PXXDI (R ≠ R'). Eventually, we will develop a general synthesis for the preparation of PXXMI and PXXDI derivatives.

Objective 2

The spectroscopic properties of the two PXX families will be investigated. Absorption and emission spectroscopy, transient spectroscopy and cyclic voltammetry will be the tools employed to elucidate the spectroscopic and redox properties of the new dyes. Eventually, we intend to study the photoredox properties of the systems so as to trigger photoredox transformations investigating the mechanism of the dehalogenation reaction as a model reaction (Figure 18).

Figure 18: PXX derivatives as photoredox catalysts.

Chapter 2. O-Doped Polycyclic Aromatic Hydrocarbons

2.1 Overview

This chapter describes the synthetic strategies adopted for the preparation of a new series of PXX derivatives bearing electron withdrawing groups (EWGs) at the *peri*-positions. Molecules in which a PXX exposes either one (PXXMI) or two (PXXDI) functionalised imide groups (Figure 19) were prepared capitalizing on two main key reactions, namely C-C bond formation and C-O cyclisation.

The chapter is divided into four main sections: *i) section 2.1* addresses the general retrosynthetic analysis which is employed for the synthesis of *N*-functionalised PXXMIs and PXXDIs; *ii*) *section 2.2* gives a general account on aryl-aryl bond formation, while *iii) section 2.3* introduces the transition metal catalysed C-O cyclisation and *iv) section 2.4* collects the results obtained for the preparation of *N*-substituted PXXMIs and PXXDIs in a *N*-substituted A_2- or AB-type fashion following two main synthetic routes.

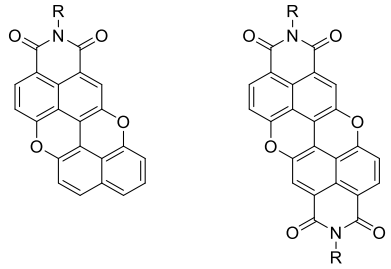

PXXMI **40**

PXXDI **41**

Figure 19: General chemical structure of *N*-functionalised PXXMIs and PXXDIs (R = alkyl or aryl substituents).

The results reported in this chapter regarding the synthesis *N*-Substituted AB-Type PXXDI are obtained in collaboration with *Dr. Andrey Berezin*, from *Cardiff University*.

Part of the results reported in this chapter have been published in *Chemistry A European Journal.* **2018**, *24*, 4382-4389.[109]

2.2 Retrosynthetic Analysis of PXXDIs and PXXMIs

2.2.1 *N*-Substituted A_2-Type PXXDIs

The synthesis of the substituted target *peri*-xanthenoxanthene-diimide (PXXDI) molecules could be approached by same synthetic strategies (Scheme 6).

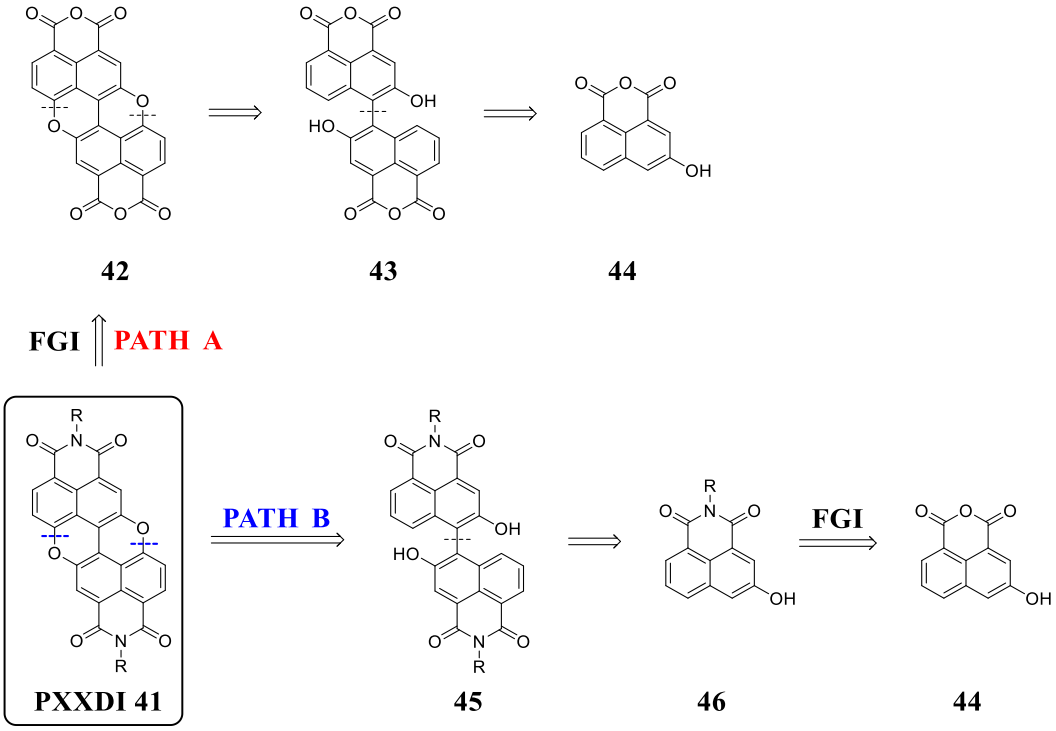

Scheme 6: Retrosynthetic analysis of *N*-substituted A_2-type PXXDIs.

The first retrosynthetic approach (Scheme 6, PATH A) is based on functional group interconversion of the dianhydride PXX (PXXDA) **42**, which represents the key intermediate. This can be prepared by double C-O cyclisation from binaphthol derivatives **43**, which, in turn, could be obtained from the dimerization of commercially available 3-hydroxy naphthalene anhydride **44** *via* C-C bond formation. This strategy is based on the preparation of PXXDA **42**, which could be converted in any PXXDIs. Following the second strategy (Scheme 6, PATH B), the synthesis of PXXDIs could be achieved by double C-O bond formation from the relative substituted binaphthols **45**, which could be obtained from the dimerization of monoimide derivatives **46**, prepared by functional group interconversion from the commercially available 3-hydroxy naphthalene anhydride **44**. This approach is based on a functional group conversion of the anhydride motif to imide in the early stage of the synthesis. This will improve the solubility of the intermediate, but

on the other hand, the applicability of the synthesis is limited. Both synthetic strategies rely on two key steps: C-C bond formation and subsequent double C-O cyclization.

2.2.2 Retrosynthesis of PXXMI

The synthesis of the target *peri*-xanthenoxanthene-monoimide (PXXMI) molecules could be approached by two different synthetic strategies (Scheme 7):

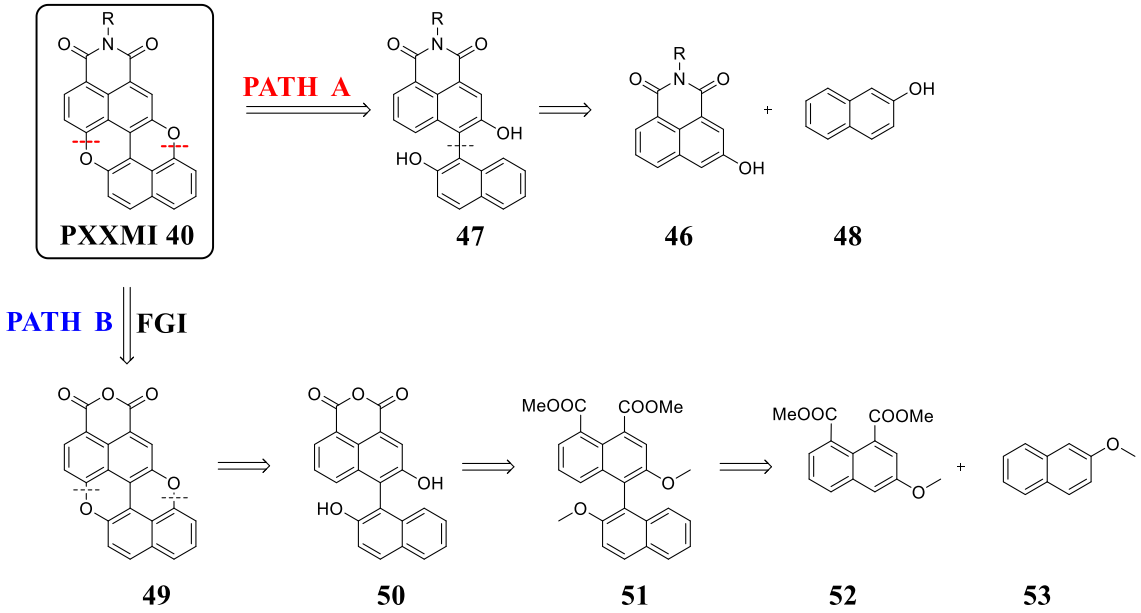

Scheme 7: Retrosynthetic analysis of **PXXMI**.

According to the first retrosynthetic approach (Scheme 7, PATH A), the target PXXMI molecules could be obtained by double C-O bond formation from the parent binaphthols **47**. These key intermediates could be prepared by C-C bond formation *via* cross coupling of the corresponding hydroxyl-naphthalene imides **46** or hydroxyl-naphthalene anhydride **44** with naphthol **48**. This approach is based on a functional group conversion of the anhydride motif to imide derivative in the early stage of the synthesis. The second retrosynthetic approach (Scheme 7, PATH B) is based on functional group interconversion of the monoanhydride PXX (PXXMA) **49**, which represents the key intermediate. Derivative **49** can be prepared by double C-O cyclization from binaphthol derivative **50**, which could be obtained from the diester binaphthyl **51** via methoxy cleavage and conversion of the ester groups to the anhydride. The synthesis of derivative **51** could be envisaged as cross coupling of methoxynaphthalene diester **52** with methoxynaphthalene **53**.

2.2.3 *N*-Substituted AB-Type PXXDI

Subsequently, we focused our attention on the preparation of AB-type *N*-substituted PXXDIs, in analogy to reported PDIs and NDIs.[110]

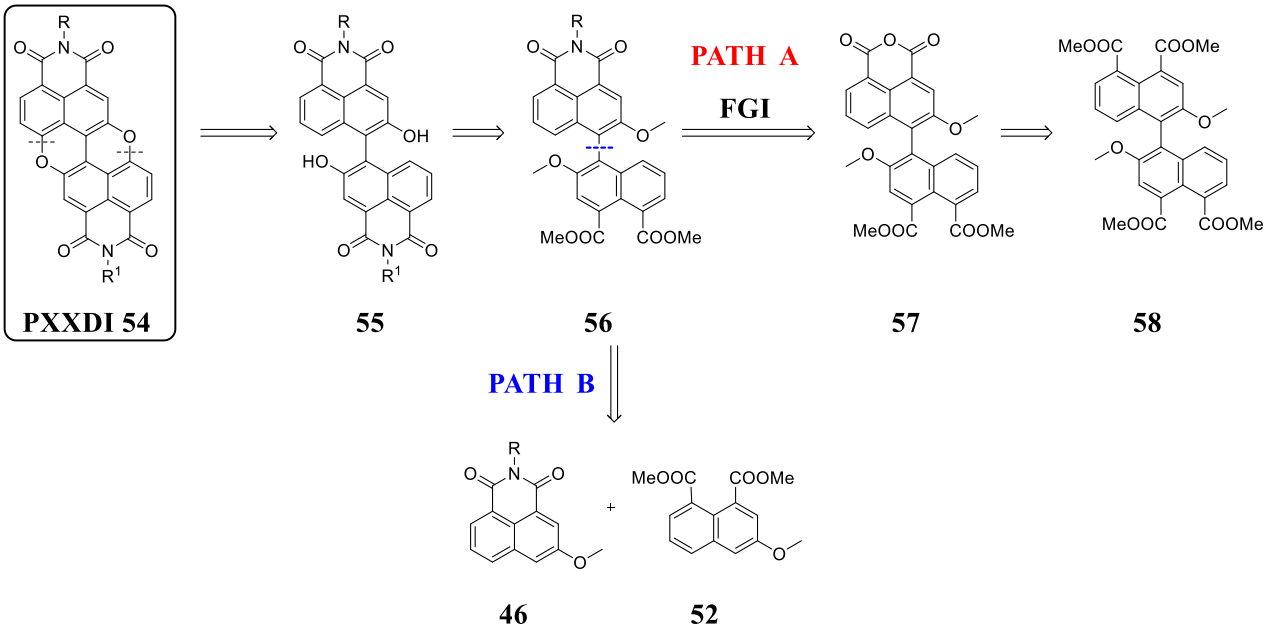

Scheme 8: Retrosynthetic analysis of *N*-substituted AB-type PXXDIs.

The target molecules can be prepared by double cyclization of the corresponding *N,N'*-bisimide binaphthols **55**, which can be obtained by dimethyl ester functional group conversion into the imide group of derivatives **56**. Two different retrosynthetic pathways, PATH A and PATH B, (Scheme 8) could be envisaged for the synthesis of these key intermediates. In the synthetic approach based on PATH A, derivatives **56** could be synthetized from the dimethyl ester monoanhydride **57**. The anhydride moiety, which could be prepared by selective ester hydrolysis followed by cyclization of tetramethyl ester **58**, can undergo a chemoselective functional group transformation to be easily converted into the imide derivative. With an alternative strategy, the imide key intermediates **56** could be obtained *via* cross coupling between **46** and derivative **52** (Scheme 8, PATH B).

2.3. General account on aryl-aryl bond formation

Biaryl systems are largely found in natural products such as alkaloids, lignans,[111] flavonoids,[112] tannins[113] just to mention a few. Moreover, biaryl motifs found wide applications in material science due to their redox, semiconductor and non-linear optical properties.[114] The formation of new carbon-carbon bonds between two aromatic units is one of the most important reactions in modern organic chemistry. Therefore, many studies have been performed to develop new synthetic methods to access biaryl scaffolds. Among them, it is possible to mention: *i)* oxidative coupling; *ii)* reductive coupling; *iii)* radical coupling; *iv)* metal-catalysed cross coupling; *v)* nucleophilic aromatic substitution; *vi)* direct arylation through C-H activation.

2.3.1 Oxidative coupling

The oxidative coupling achieves the formation of a carbon-carbon bond through an oxidative reaction, usually in the presence of a transition metal.[115] The first example of oxidative coupling of an aromatic core is represented by the synthesis of ellagic acid **60** by reaction of gallic acid **59** with H_3AsO_4 or AgO (Scheme 9), which was reported by Löwe in 1868.[116]

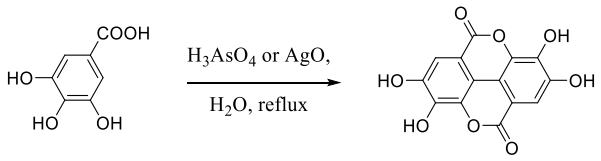

59 **60**

Scheme 9: Synthesis of ellagic acid **60**.

A few years later, the synthesis of 1,1'-bi-2-naphthol **61** by oxidation of 2-naphthol **48** was accomplished by Dianin, using $FeCl_3$ as single electron oxidant (Scheme 10).[117]

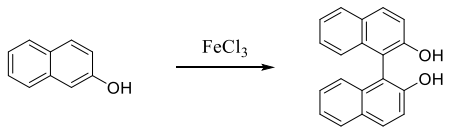

48 **61**

Scheme 10: Synthesis of binaphthol **61**.

At the same time, a wide range of phenols have been used in oxidative coupling to prepare biphenol derivatives.[118] This strategy allows the formation of carbon-carbon bond in the *ortho*- or *para*- position to the hydroxyl group. Indeed, the oxidative coupling of substituted 2-naphthols represents one of the most important synthetic applications of this approach. A wide range of oxidants has been investigated such as $FeCl_3$,[119] $Mn(acac)_3$[120] and Cu(II)-amine.[121] In particular, the Cu(II)amine complexes were found to be very effective. In this respect, in an early work, Brussee described the preparation of enantiomerically pure binaphthyls.[122] This involved the synthesis of symmetric systems by homocoupling and also asymmetric derivatives through heterocoupling reactions. Many efforts have been made to understand the mechanism of the oxidative coupling. It has been found that its basis relies on the oxidation of the phenolic residue through a single electron transfer, allowing the formation of a radical species, whose existence was demonstrated by EPR spectroscopy (Scheme 11).[123]

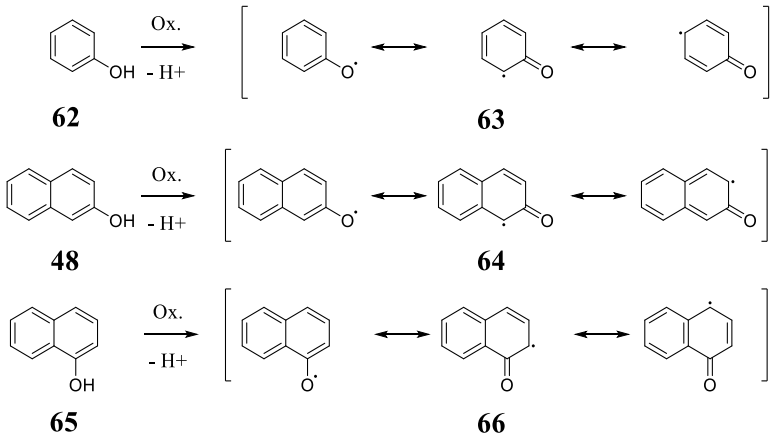

Scheme 11: Single electron oxidation of phenol **62**, 2-naphthol **48** and 1-naphthol **65**.

Considering 2-naphthol **48**, the mechanism proposed by Toda and co-worker suggests that the deprotonation and oxidation of two molecules of starting 2-naphthol **48** yields the formation of two radicals **64**. These undergo radical coupling to give keto derivative **67** that, by keto-enol tautomerisation, leads to final binaphthol **61** (Scheme 12).[124]

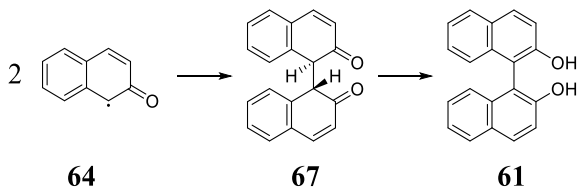

Scheme 12: Radical coupling mechanism proposed by Toda and co-workers.[124]

However, this mechanism could not explain the selective oxidative cross-coupling of 2-naphthol derivatives reported by Zavada and co-workers.[125] The authors reported on the oxidative cross-coupling of 2-naphthol **48** with electron-poor 2-naphthol **68** (Scheme 13).

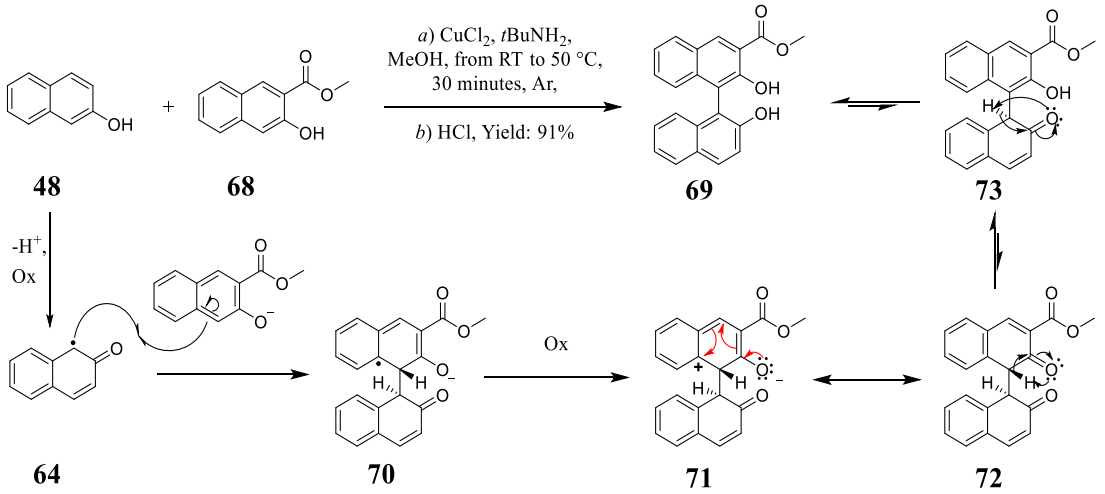

Scheme 13: Selective oxidative cross-coupling.[125]

Zavada's procedure allows to obtain the product of cross-coupling **69** in high yield, with a small amount of homo-coupling products. In order to explain the selectivity of the reaction, the authors proposed a mechanism based on the deprotonation and oxidation of 2-naphthol **48**. This suggests the formation of radical **64** that, through a radical insertion mechanism, reacts with the deprotonated derivative of 2-naphthol **68**. This yields the formation of radical intermediate **70** that readily oxidizes to zwitterionic derivative **71** in equilibrium with its neutral mesomeric form **72** (red arrows). Finally, keto-enol tautomerisation leads to final binaphthol **69** (black arrows) (Scheme 13).

2.3.2 Reductive coupling of aromatic halide

The reductive coupling of aryl halides is one of the oldest methods for the preparation of symmetrical biaryl derivatives **75**. This strategy consists of the coupling of two molecules of aryl halide **74** in the presence of a metal, with the elimination of a metal halide (Scheme 14).

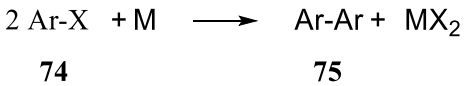

Scheme 14: Biaryl synthesis by reductive coupling of aryl-halide.

In 1901, Ullmann observed that copper metal is particularly effective in the condensation of two molecules of aryl halide to yield the relative biaryl with the elimination of copper(I)halide and this reaction is now known as Ullmann reaction.[126] This approach is particularly effective in this type of carbon-carbon bond formation. Due to its versatility, the Ullmann reaction has been employed to prepare a wide class of biaryl and poly-aryl scaffolds.[127] Albeit newer biaryl synthetic methods were developed, the Ullmann reaction remains an important method for biaryl synthesis, in particular due to its efficiency and simplicity, making it very useful for the symmetrical biaryl formation. Typically, the original procedure involves the reaction of two aromatic halides in the presence of an excess of finely ground metallic copper at high temperature, which provides the biphenyl derivatives. The success of the reaction depends on the aryl halide, with the order of reactivity increasing with the halogen atom size (I > Br > Cl), while aromatic-fluoride has never been reported to be active in Ullmann reactions (Scheme 15).

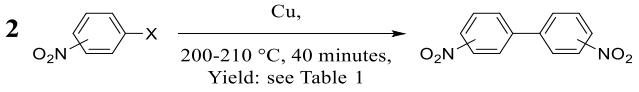

Scheme 15: Activated aryl-halide in Ullmann reaction.

Table 1: Reactivity of activated aryl-halide for Ullmann reaction in **Scheme 15**.

X	**Yield [%] of Dinitrobiphenyls from Nitrohalobenzene with**		
	ortho	*para*	*meta*
I	65	54	36
Br	64	36	15
Cl	40	0	0

In general, bromide and chloride aryl derivatives take part in coupling reaction only in the presence of activating agents on the aromatic core. [128] Electron-withdrawing substituents, particularly NO_2 groups, in *ortho*- position of the halogen atom, provide an activating effect on the aromatic core (Table 1).[129] As consequence of the activation effect, it is possible to achieve a regioselective process with respect to the relative position of the activating group. Due to the influence of the NO_2 functional group on the reactivity of the two bromide substituents, the synthesis of 4,4'-dibromo-2,2'-dinitro-1,1'-biphenyl **77** from 2,5-dibromo nitrobenzene **76** could be achieved in 70% yield (Scheme 16).[129-130]

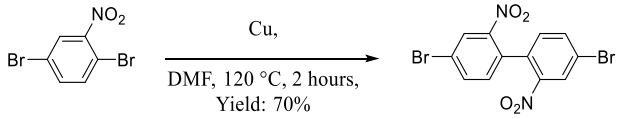

76 **77**

Scheme 16: Regioselective Ullmann reaction.

Conversely, substituents such as hydroxyl, amine and carboxylic acid do not favour the coupling because they take part in the reaction and promote the formation of side products,[131] such as aryl ethers[132] and aryl amine.[133] Due to the synthetic importance of the process, some research has been devoted to improve the reaction conditions, such as lowering the temperature, and to extend the reaction to the synthesis of unsymmetrical biaryls. The use of highly activated copper or copper(I)-thiophene-2-carboxylate appears to promote an Ullmann-like reaction at lower temperature.[134] Moreover, it has been noted that introducing DMF as solvent allows to perform the reaction at lower temperature and with less amount of copper.[135] Several strategies have been developed to extend the reaction to the preparation of unsymmetric biaryl systems. The first is based on the selection of aryl halides of nearly equal reactivity, which limits the self-condensation and subsequent formation of the symmetric biaryls, thus increasing the yield of the desired product.[131] An alternative approach to prepare hetero-biaryl systems is to perform templated reactions.[136] This approach is based on linking two different aryl halides to a bidentate tether, which increases their proximity promoting the hetero-biaryl formation. In 1992, following this approach, Iwasaki and collaborators achieved the synthesis of highly functionalised unsymmetrical biphenyl derivative **81** starting from the diacylated salicyl alcohol, which has been prepared by selective acylations of salicyl alcohol **80**. The templated derivative **78** has been coupled by intramolecular Ullmann reaction forming the intermediate **79**, which after basic hydrolysis provides target binaphthol **81** (Scheme 17).[136]

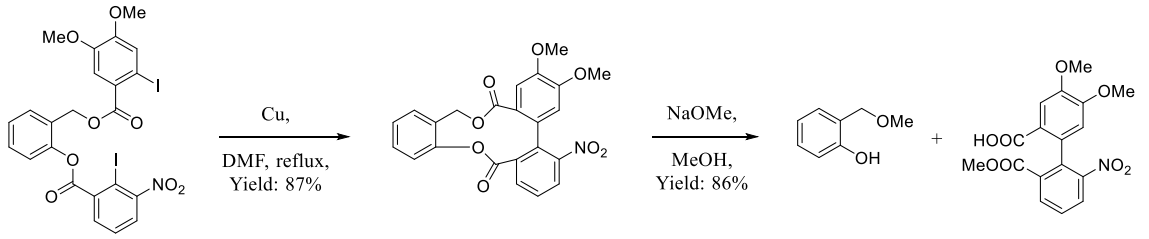

78 **79** **80** **81**

Scheme 17: Synthesis of hetero biphenyl by intramolecular Ullmann.

Similarly, Miyano and collaborators achieved the asymmetric synthesis of axially chiral diphenic acid derivative.[137] They accomplished the chiral induction using **61** as chiral template, which by stepwise esterification with two different benzoic acid derivatives provided diaryl ester **82**. Then they performed an Ullmann reaction on chiral di-aryl ester **82**, obtaining derivative **83** in good yield. The subsequent ester hydrolysis yielded enantiomerically pure derivative **84** (Scheme 18).[137]

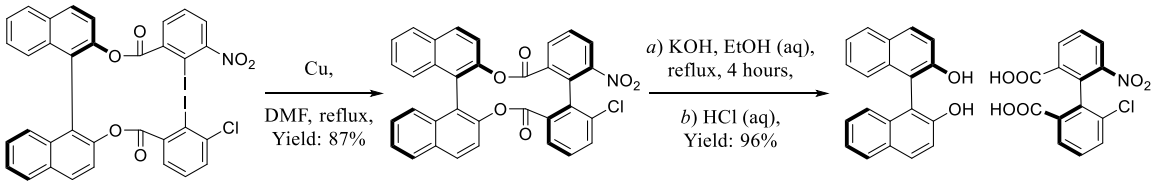

82 **83** **61** **84**

Scheme 18: Chiral induction by a chiral template in Ullmann reaction.

2.3.3 Palladium cross coupling

Palladium cross coupling represents a big advance in the development of synthetic chemistry and introduction of palladium chemistry can be considered as a revolution in organic synthesis. In this respect palladium catalyses the carbon-carbon bond formation between aryl- or vinyl-halides and triflates with another hydrocarbon. The latter usually are organo-metal derivatives such us organo-lithium, organo-magnesium, organo-zinc, organo-tin, organo-cuprate or as well non-metal derivatives such as organo-boron and organo-silane (Scheme 19).[138]

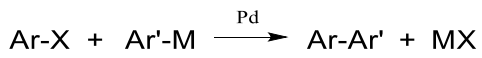

74 **85** **86**

Scheme 19: General scheme of palladium cross coupling reaction.

The fundamental steps of palladium catalysis are: oxidative addition of the aryl- or vinyl-halide or triflate to Pd(0), followed by transmetallation process, which consists in the transfer of the organo residue from the organo-metal to the palladium intermediate. Finally the disubstituted palladium undergoes a reductive elimination providing the new carbon bond and restoring the catalytically active species Pd(0) (Scheme 20).[139]

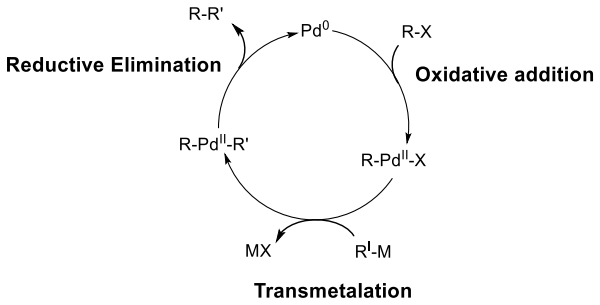

Scheme 20: General scheme of palladium catalysis.

In the context of biaryl synthesis the most important reactions are: *i)* the Stille cross coupling involving organo-tin derivatives and *ii)* the Suzuki cross coupling involving organo-boron derivatives.[139-140] In particular, the Suzuki reaction became the most important palladium catalysed cross coupling reaction due to its wide application in the synthesis.[141] For this reason, in the next paragraph, we will give an in-depth overview of the development of the Suzuki cross coupling reaction.

2.3.3.1 Suzuki cross coupling

Since the early 80's, the introduction of the Suzuki-Miyaura cross coupling represents the major improvement in the synthesis of carbon-carbon bond for biaryl preparation. The reaction is based on the use of boronic acid or boronic ester derivatives which are nucleophile. The boron derivatives showed several advantages compared with other organo-metal derivatives.[101] The main advantage is represented by the tolerance of a wide range of functional groups. Moreover, the boron derivatives are featured with a good stability that allows them to be handled in air, heated and tolerant to protic solvents such as water and alcohol from where they can be purified by crystallization. The origin of these properties can be explained by the electronegativity of the boron (*ca* 2.0), which is relatively close to the value of the carbon one (*ca* 2.5). It is considerably higher if compared with the one of lithium and magnesium and also to other transition metals that typically

span from 0.86 to 1.75. Because of the small difference in electronegativity between boron and carbon, without the presence of a catalyst organo-boron does not generally react with organo-halides or carbonyl groups. This low reactivity towards other functionalities has made the boron derivatives one of the most attractive nucleophile for the palladium cross coupling. If even this chemical stability and tolerance is also owned by the organo-tin derivatives employable in the Still cross coupling, boron reagents and by-products, in opposition to tin, are characterized by a lower toxicity.[140a] Typically Suzuki cross coupling proceeds with a good yield and for all these reasons it became a general tool for the carbon-carbon bond formation, not only for the biaryl preparation.[139] The mechanism of the Suzuki cross coupling, as well as the other palladium catalysed reactions, is involving in first instance an oxidative addition followed by a transmetallation and afterwards a reductive elimination (Scheme 21).[142] In this case, the oxidative addition is the rate determining step of the catalytic process. The reactivity of the aryl halide follows the order I > Br > Cl.[143] However, this general trend is highly affected by the presence of electron-withdrawing groups or electron-donating groups in position 2 or 4 of the aryl halide. Indeed, electron-withdrawing groups have an activating role inducing a positive charge on the carbon bonding to the halide via mesomeric effect, whereas electron donating groups have a deactivating effect.

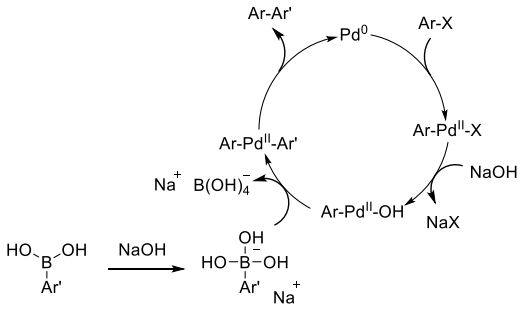

Scheme 21: General scheme of Suzuki cross coupling.

On the other hand, the boron derivatives acting as nucleophiles, are activated with electron-donating substituents that enhance the electron-richness of the organo-metal by mesomeric effect. The effect of the substituent should be taken into account when a retrosynthetic analysis is planned. Despite all the advances, the Suzuki cross coupling is affected by one major drawback: the preparation of boronic derivatives. Although many organo-boron

derivatives are commercially available, they undergo easy decomposition over time, and generally most of them are employed in excess. Consequently, organo-boron derivatives have to be prepared, which means that additional synthetic steps are required. The preparation of such compounds generally requires a halide derivative to be transformed in organo-metal, typically organo-lithium or organo-magnesium, followed by borylation.[144] An alternative procedure to prepare the organo-boron is the Miyaura borylation based on palladium catalysis.[145] The main synthetic importance of the Suzuki reaction is represented by high yielding preparation of dissymmetrical biaryl, however homo biaryl can be prepared as well. [146] One of the main challenges of the Suzuki coupling is the cross coupling of cumbersome substrates, in particular substrates bearing substituents in *ortho* position to the halide moiety or on the organo-boron derivative.[147] Infact the steric hindrance in the *ortho* position of the aryl halide derivatives prevents the oxidative addition addition of the Pd catalyst, leading to recover unreacted starting material.[148] Similarly, organo-boron derivatives bearing substituents in *ortho* positions undergo the transmetallation process more difficult, generally providing not satisfactory yield and yielding the hydrolytic deborylation of the organo-boron derivatives.[149] For this reason cross coupling of *ortho* substituted naphthalene halide with *ortho* substituted naphthalene boron derivative can be considered as a difficult task.[150] An evidence of the difficulties is the limited number of protocols reported to prepare 2,2'-dimethoxy-1,1'-binaphthalene.

2.3.3.2 Phosphine ligands

In the palladium catalytic cycle the ligands can modulate and enhance the catalytic activity, especially electon-rich ligands result particularly efficient towards chloride derivatives and as well electron rich substrates that do not undergo efficiently in oxidative addition process.[151] In order to improve the efficiency of the oxidative addition, several research groups developed electron-rich ligands that can be divided in five categories: bis(diphenylphosphino)alkyl,[147b, 152] trialkylphospine,[153] palladacycle,[154] *N*-heterocyclic carbene[155] and aryl-dialkylphosphine.[147a, 156] It is commonly agreed that the *in situ* formation of the catalytic species using a source of Pd(II) and a sterically hindered ligand, is based on the reduction of the Pd(II) to Pd(0) allowing the formation of unsaturated coordinated complexes such as 16 e^- PdL_3, 14 e^- PdL_2 and 12 e^- PdL, which are the actual catalytic species.[157] In 1998, Buchwald and co-worker achived the catalytic

amination of aryl chloride derivatives by exploiting electron rich aryl-dialkylphosphine ligands in order to improve the oxidative addition.[156c] Subsequently, these new phosphine ligands were successfully applied also in Suzuki cross coupling reactions. Starting from the studies on 2,2'-bis(dicyclohexylphosphino)-1-1'-binaphthyl **88**, the authors discovered that this ligand was active for the coupling of pyrrolidine with 4-chlorotoluene **85**.[156g] They designed and prepared a new bidentate ligand aminophosphine **89** (Davephos).[156c] They performed a catalytic amination on 4-chlorotoluene **85** with di-*n*-butylamine **86** in the presence of $[Pd_2(dba)_3]$ Davephos **89** and NaO*t*Bu in toluene at 100 °C for 20 hours, which yielded the *N*,*N*-dibutyl-4-methylaniline **87** in 98% yield (Scheme 22).

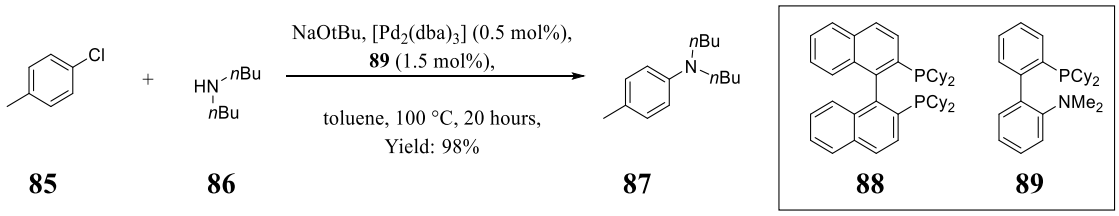

Scheme 22: Catalytic amination of 4-chlorotoluene.

In comparison to **88**, the use of the new ligand **89** was more efficient and extended the scope of the Pd-catalysed transformation to electron-rich and electron-deficient aryl chloride substrates and also allowed to perform Suzuki cross coupling reactions at room temperature. However, the catalyst **89**/Pd was inefficient in the amination reaction of inactivated substrates at room temperature. Indeed the reactivity has been improved by replacing of the cyclohexyl moiety with the more hindered di-*tert*-butyl, derivative **90**. (Scheme 23).

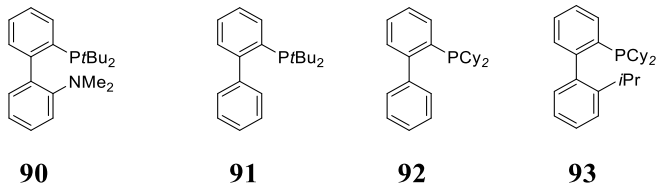

Scheme 23: Electron rich aryl-dialkylphosphine ligands.

The improvement of the reaction with the use of bulkier ligand **90** is presumably due to its ability of increasing the rate of the reductive elimination.[156e] Further investigation to prove the role of the amino group on the ligand in the amination process was studied with the ligand **91** without amine substituent (Scheme 23). From this study it emerged that the

catalyst **91**/Pd was also active in the amination process. Afterwards, the ligands **91** and **92** were successfully applied in the Suzuki cross coupling of aryl-chloride compounds with low catalyst loading. From this study it emerged that ligand **91** provides better results for room temperature Suzuki coupling reactions with hindered substrates. A further enhancement in oxidative addition was obtained by introducing an isopropyl group in the 2' position of **92**, to produce ligand **93** (Scheme 23). Indeed, **93** presents the advantages provided by the electron-richness, for the oxidative addition, and by the steric hindrance for the rate of the reductive elimination and maximises the quantity of L_1Pd complexes increasing the transmetalation rate.[156f] In this respect, catalyst **93**/Pd was very active also with sterically demanding substrates. As an example, 2-chloro-1,3-dimethylbenzene **94** was reacted with 2-methylphenylboronic acid **95** in the presence of K_3PO_4 and **93**/Pd in toluene at 100 °C, for 3 hours providing the biphenyl **96** in 92% yield. Remarkably, the same reaction performed with phosphine **92** provides biphenyl **96** in similar yield but with considerably longer reaction time (Scheme 24).[156f]

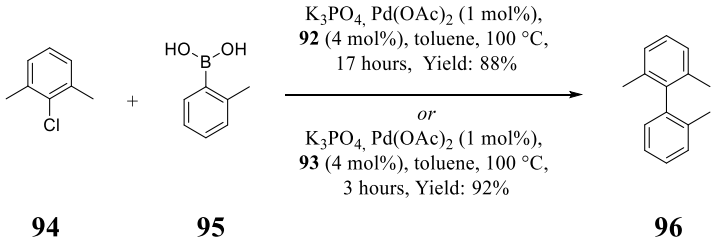

94 **95** **96**

Scheme 24: Suzuki cross coupling of sterically cumbersome substrates.

Nevertheless, despite all the development of ligands to overcome oxidative addition issues, the Suzuki-Miyaura cross coupling on sterically hindered substrates still remains difficult.[150] In 2001, Buchwald and co-workers reported a highly active catalyst for the synthesis of sterically hindered biaryls exploiting the phenanthrene based ligand **100**.[147a] In particular, 1-bromo-2-acetoxymethylnaphthalene **97** reacted with 2-methyl-1-naphthyl boronic acid **98** in the presence of K_3PO_4, $[Pd_2(dba)_3]$ and ligand **100** in toluene under reflux for 24 hours, yielding desired product **99** in 98% yield (Scheme 25).

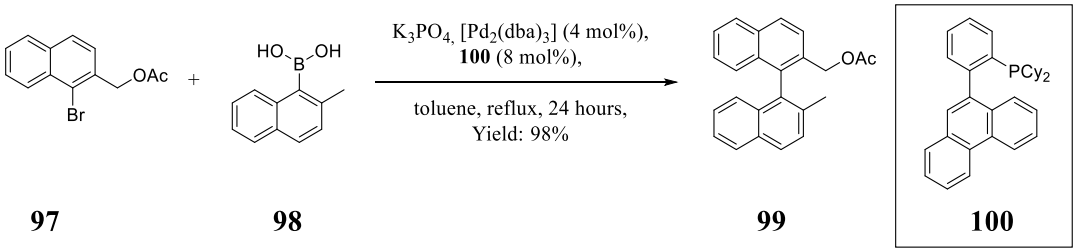

97 **98** **99** **100**

Scheme 25: Suzuki cross coupling of sterically hindered substrates.

Phosphine **100**, on the contrary to the other aryl-dialkylphosphines developed by Buchwald, is not commercially available. Based on the results on their ligands' studies, Buchwald and co-workers rationalized the effects of the ligands' substituents[156b] and, in 2004, they designed 2-(2',6'-dimethoxybiphenyl)dicyclohexylphosphine (SPhos) ligand **104**, which showed a comparable activity to phosphine **100**.[156d] Exploiting the potentiality of phosphine **104**, 2-bromo-1,3,5-trimethylbenzene **101** took part in the reaction with 2,6-dimethylphenylboronic acid **102** in the presence of K_3PO_4, [Pd (dba)$_2$] and SPhos **104** in toluene under reflux for 18 hours providing biphenyl **103** in 82% yield (Scheme 26).

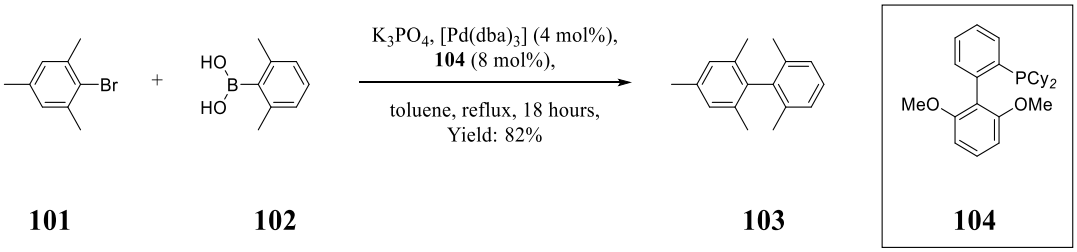

101 **102** **103** **104**

Scheme 26: Suzuki cross coupling of sterically hindered reagents.

SPhos **104** showed unprecedented activity in coupling extremely hindered aryl boronic acid and aryl halide providing a catalytic system with a wide application range in Suzuki cross coupling.[156a] From the broad investigation performed by Buchwald and his collaborators emerged that the efficiency of the ligand depends primarly on the electron donating ability of the phosphine and secondly on the steric hindrance of the ligand.[156a]

2.3.3.3 Synthesis of aryl-boron derivatives

The synthesis of aryl-boronic acids or esters can be achieved by several methods. One of the most common synthesis is based on the conversion of aryl-halides (aryl-chloride, -bromide and -iodide), such as bromobenzene **105**, into highly reactive aryl-metal derivatives, such as aryl-magnesium-halides or aryl-lithium **106**. Typically, the aryl-magnesium-halides are prepared by reacting the aryl-halide **105** with metallic Mg, in ethereal solvent. While the aryl-lithium derivatives are usually prepared by lithium halogen exchange by reaction of aryl-halide **105** with *n*BuLi or *t*BuLi in ethereal solvent. The resulting aryl-metal derivative **106** reacts with trialkyl borates, generally trimethyl borate or triisopropyl borate, forming a boronate intermediate that affords boronic acid **107** after acidic hydrolysis (Scheme 27 A).[144, 158]

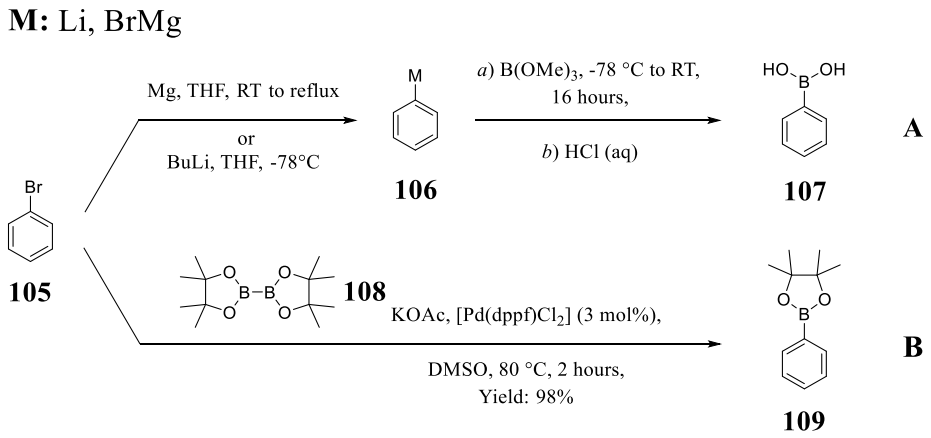

Scheme 27: Preparation of aryl-boron derivatives.

This strategy is an efficient method to prepare relatively simple organoboron compounds in large quantities. The main drawback is the low compatibility with a wide range of functional groups due to the high reactivity of the organo-lithium or organo-magnesium-halide. A milder approach for the preparation of aryl boronic esters is the synthetic protocol developed by Miyaura and co-workers in 1995 which allows the preparation of the aryl borate through Pd cross-coupling reaction on aryl-iodide or bromide with alkyloxy di-boron derivatives.[145] This method was the first one step procedure to prepare aryl boronic ester from aryl halide. Miyaura and co-workers reported the borylation of bromobenzene **105** with bis(pinacolato)diboron **108** in the presence of KOAc and [Pd(dppf)Cl_2] in DMSO for 2 hours at 80 °C, yielding phenyl boronic ester **109** in 98% yield (Scheme 27 B). This protocol, contrary to the cross coupling of aryl-halide with an aryl-boronic acid or ester in

the presence of a base such as K_2CO_3 or K_3PO_4, proceeds by promoting the borylation process in the presence of KOAc.[145] Because of the weakness of the base, further cross coupling between the aryl-halide and the organo-borate does not take place. However, if the synthetic protocol is carried out in the presence of K_2CO_3 or K_3PO_4, cross-coupling with formation of the biaryl can also occur. The rate of the reaction increases with solvent polarity: e.g. DMSO ≥ DMF > dioxane > toluene.[145] In a similar manner, the rate of the Suzuki cross coupling reaction of electron rich aryl halides is lower than that observed for the electron-poor derivatives. Contrary to the method based on the use of aryl-lithium or aryl-magnesium-halide derivatives, the Miyaura reaction displays the main advantage of compatibility with -CO_2Me, -COMe and -CN groups. In order to overcome the limitation of applicability of the borylation protocol to aryl-iodide -bromide and -triflate, and to extend the scope of the reaction to inactivated aryl chloride, other phosphines were tested. In 2007, Buchwald and co-workers achieved the borylation of inactivated aryl chloride derivatives using SPhos **104** and XPhos **112** phosphines.[159] The latter one permitted conversion of the inactivated 1-chloro-4-methoxybenzene **110** by reaction with bis(pinacolato)diboron **108** in the presence of KOAc, [$Pd_2(dba)_3$] and XPhos **112** as ligand in dioxane under reflux in 10 minutes, affording phenyl boronic ester **111** in 97% yield (Scheme 28).

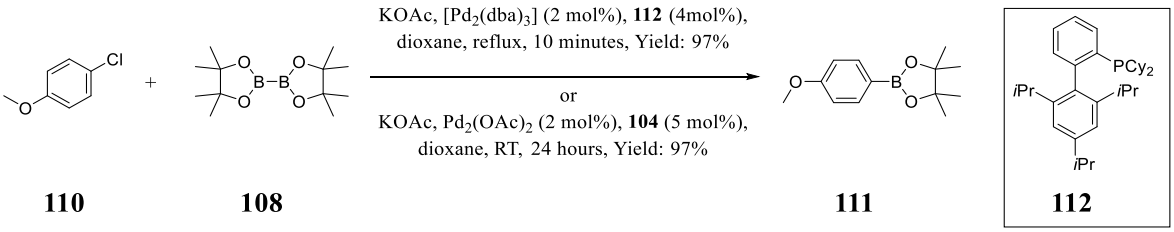

110 **108** **111** **112**

Scheme 28: Miyaura borylation on deactivated aryl-chloride.

Thanks to the efficiency of the protocol, Buchwald and co-workers aimed at achieving the Miyaura borylation at lower temperature.[159] When trying to apply this protocol at room temperature, the process was unsuccessful. Nevertheless, when $Pd(OAc)_2$/XPhos **112** was used as catalyst in the presence of K_3PO_4 *in lieu* of [$Pd_2(dba)_3$]/XPhos **112** and KOAc, the reaction proceeded efficiently at room temperature. Moreover, the room temperature protocol was further improved by replacing the ligand XPhos **112** with SPhos **104**, which provided better results. In fact, SPhos ligand allowed the Miyaura borylation also on the sterically hindered substrates. In particular, inactivated 1-chloro-4-methoxybenzene **110**

reacted with bis(pinacolato)diboron **108**, in the presence of K_3PO_4, $Pd(OAc)_2$ and SPhos **104** in dioxane at room temperature for 24 hours, yielding phenyl boronic ester **111** in 97% yield (Scheme 28). Aryl-boronates found many applications in Suzuki-Miyaura cross coupling reaction. However, the aryl-boronic ester is usually prepared and purified before being used in cross-coupling reactions. As a further extension of the synthetic scope, a one-pot protocol was developed, where the Miyaura borylation is followed by Suzuki coupling to form biaryl derivatives starting from an aryl chloride. As an example, 1-chloro-2-methoxybenzene **113** in the presence of bis(pinacolato)diboron **108**, K_3PO_4, $[Pd_2(dba)_3]$ and SPhos **104** in dioxane under reflux for 15 hours, yields biphenyl **114** in 70% yield (Scheme 29).[159]

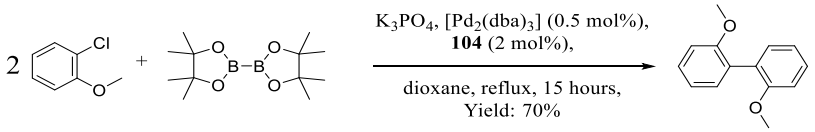

113 **108** **114**

Scheme 29: One-pot reaction involving a Miyaura borylation followed by Suzuki coupling on aryl chloride.

Following the same approach, the synthesis of unsymmetrical biaryls was achieved.[159] In the first step, boronic ester **116** was formed by the borylation of 1-bromo-3,5-dimethoxybenzene **115** in the presence of $[Pd_2(dba)_3]$, XPhos **112** and KOAc in dioxane under reflux for 3 hours. Then 2-chloro-1,3-dimethylbenzene **94** and aqueous K_3PO_4 were added into the reaction, and, after 15 hours under reflux, biphenyl **117** was obtained in 95% yield (Scheme 30).

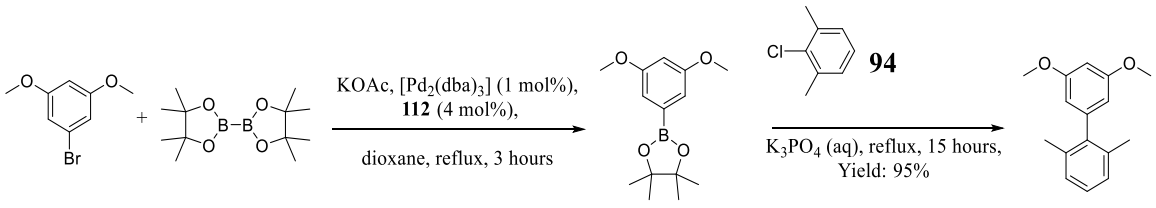

115 **108** **116** **117**

Scheme 30: Synthesis of unsymmetrical biaryl by Miyaura borylation followed by Suzuki coupling.

In 2017, Hawker and co-workers described the modular synthesis of asymmetric rylene derivatives,[160] which is based on a Suzuki –Miyuara coupling and cyclodehydrogenation reactions. The authors reported the cross coupling between the 4-bromo-3-methoxy naphthalene imide **118** and the boronic ester **119** in the presence of aqueous K_2CO_3,

[$Pd(PPh_3)_4$] in toluene at 100 °C for 12 hours. The reaction affords the desired binaphthyl derivative **120** in 63% yield (Scheme 31).[160]

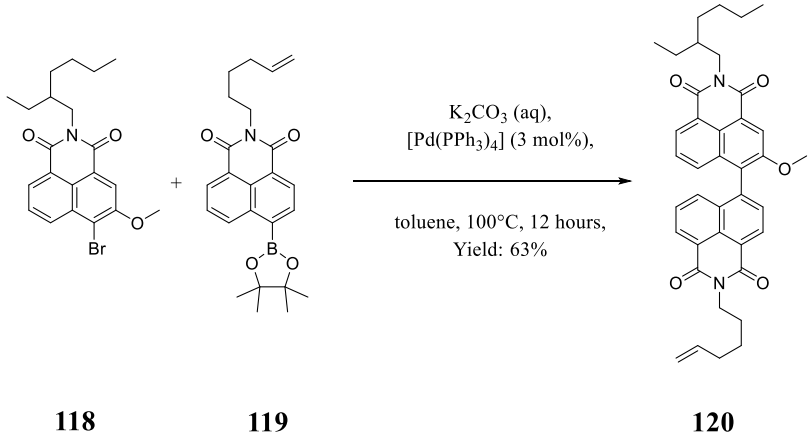

118 **119** **120**

Scheme 31: Synthesis of unsymmetrical binaphthyl derivative **120** through Suzuki cross-coupling.[160]

2.4 General account on cyclic diaryl ether formation by oxidative transition metal catalysis

Diaryl ethers are an interesting class of molecules, not only are they are present in nature,[161] but also display biological activity and they have been investigated as anticancer agents.[162] Moreover the diaryl derivative displays appealing properties in material science.[163] Due to their importance the synthesis of diaryl ethers has been widely investigated. Typically, the most common strategies to prepare intramolecular diaryl ethers are based on: *i)* acid catalyzed condensation of phenols, *ii)* nucleophilic aromatic substitution and *iii)* transition metal coupling, such as Cu-catalysed Ullmann diaryl ether coupling and Pd-catalysed Buchwald-Hartwig reaction. Ullmann and Buchwald-Hartwig reactions, which provide the coupling of aryl halides and phenols, in the presence of Cu and Pd complexes respectively, are the most studied synthetic pathways. A broad scope of ligands, solvents and bases has been investigated. Ullmann and Buchwald-Hartwig reactions, despite their great applicability and robustness, have a main drawback: the pre-functionalisation of one of the two reactants. However, Pd catalysts such as $Pd(OAc)_2$ are known to promote reactions on unfunctionalized substrates, mediating C-H activation.[164] Thus, the C-H activation has been an object of great interest. Recently, direct cyclisation of substrates bearing heteroatoms close to the C-H bond resulted in a versatile and efficient pathway to prepare heterocyclic structures.[165] In this field, azaheterocycle preparations received great attention, as the amine-direct C-H activation could be exploited and a vast

number of protocols based on metal mediated C-N bond formation has been developed.[166] While the progress in the azaheterocycle synthesis through C-H activation has been studied and reported, development of similar strategies for C-O bond formation mediating C-H activation has proven to be less efficient, leading only to a limited number of achievements in the field. [167]

2.4.1 Intramolecular C-O formation yielding furanyl ring

In 2011, Liu and collaborators reported the synthesis of dibenzofurans via intramolecular diaryl ether formation by coupling *ortho*-phenol derivatives, through C-H activation/C-O cyclisation promoted by Pd(0)/Pd(II) catalysis using air as oxidant, where the rate-determining step of the reaction is the reductive elimination (Scheme 32).[168]

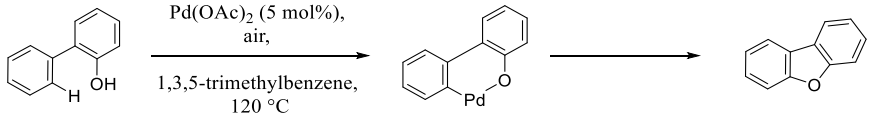

121 **122** **123**

Scheme 32: Synhtesis of dibenzofuran by C-O bond formation.

Also in this case, the reaction conditions are compatible with the presence of a large number of functional groups, demonstrating the wide scope of the synthesis for substituted dibenzofurans. In a first attempt, Liu and co-workers used $PhI(OAc)_2$ as external oxidant,[169] but only degradation was observed. Subsequently by screening for a milder oxidant, they found out that the catalytic cycle took place in the presence of O_2. A further improvement was achieved by introducing an anionic species that coordinates Pd(II) and promotes the C-H activation by acting as a proton shuttle. The process is temperature dependent, with an improvement of the yield at higher temperatures, underlining that the reductive elimination is the turnover-limiting step instead of the C-H activation. Finally, different ligands were tested in order to improve the reductive eliminations and 4,5-diazafluoren-9-one was the best candidate to help the aerobic oxidation of Pd(0) to Pd(II).[168] As an example, the biphenyl **121** underwent intramolecular cyclization in the presence of $Pd(OAc)_2$, under aerobic conditions, in 1,3,5-trimethylbenzene at 120 °C for 24 hours, affording dibenzofuran **123** in 90% yield (Scheme 33). The broad tolerance towards functional groups and the use of air as oxidant made this methodology highly attractive.

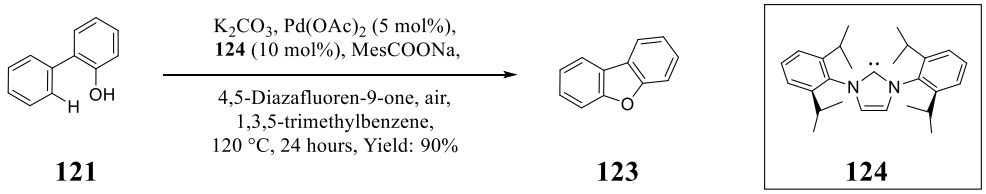

Scheme 33: Synthesis of dibenzofuran by C-O bond formation based on a Pd(0)/Pd(II) catalytic cycle.

In the same year, Yoshikai and collaborators reported a new protocol that allows the achievement of a similar transformation. Biphenyl **121** in the presence of $Pd(OAc)_2$, 3-nitropyridine and *tert*-butyl peroxybenzoate (BzOO*t*Bu) as oxidant, in C_6F_6/1,3-dimethyl-2-imidazolidinone (DMI), heated at 90 °C for 24 hours formed dibenzofuran **123** in 72% yield (Scheme 34).[170]

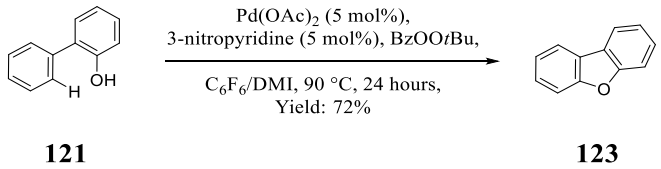

Scheme 34: Synthesis of dibenzofuran by C-O bond formation based on Pd(II)/Pd(IV) catalytic cycle.

This new protocol enables to have access to a large number of dibenzofurans, exhibiting tolerance towards different functionalities and employing a simpler catalytic system, in opposition with the one proposed by Liu.[168] In the latter reaction the rate determining step is the reductive elimination and the reaction involves a Pd(0)/Pd(II) catalytic cycle. Whereas the reaction proposed by Yoshikai is the C-H cleavage is the rate determining step, suggesting that the reaction proceeds through a Pd(II)/Pd(IV) catalytic cycle. Nevertheless, Pd is a rare and expensive metal and therefore other more abundant metals have been investigated in order to replace it. To this end, in the last decades, Cu has been investigated as catalyst to promote C-H activation, and, nowadays, copper catalysts find a large number of applications in heterocycle synthesis.[167] In particular, Zhu and co-workers, developed a procedure based on inexpensive copper (I) halide catalysts for the preparation of dibenzofurans, starting from electron-poor 2-arylphenols.[171] Nitrobiphenyl **125** underwent cyclic ether formation in the presence of Cs_2CO_3, CuBr and PivOH in DMSO at 140 °C for 24 hours, providing nitro-dibenzofuran **126** in 72% yield (Scheme 35).

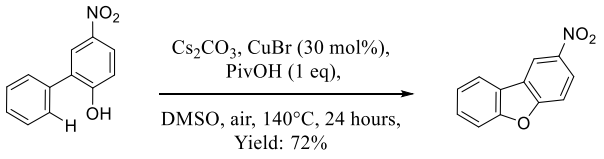

125 **126**

Scheme 35: Synthesis of dibenzofuran by copper promoted C-O bond formation.

The reaction occurs in the presence of an additive, such as PivOH, and under aerobic conditions similarly to Liu's procedure.[168] The reaction efficiency depends on the presence of the atmospheric oxygen, which plays a crucial role, as demonstrated by the fact that the reaction performed under argon atmosphere was considerably less efficient. From preliminary studies, the C-H activation resulted to be the rate determining step. Despite the fact that the procedure requires electron deficient substrates, the methodology is really attractive because it is based on a relatively simple catalytic system.

2.4.2 Intramolecular C-O formation yielding pyranyl ring

Among the polycyclic aromatic hydrocarbons containing pyranyl moieties, one of the most relevant derivatives is *peri*-xanthenoxanthene (**PXX**) **25**, which has been synthesised from 1,1'-bi-2-naphthol **61** through oxidation (Scheme 36).

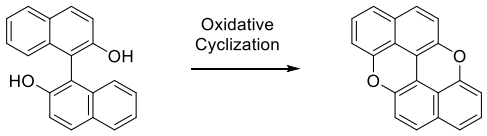

61 **25**

Scheme 36: General synthesis of *peri*-xanthenoxanthene by oxidative cyclisation**.**

The double oxidative cyclization has been achieved by using a wide number of oxidants. The first synthesis relying on this approach exploited $K_4[Fe(CN)_6]$ as oxidant. Afterwards, several protocols based on the use of metal salts, such as $Cu(OAc)_2$,[105, 172] or metal oxides, such as MnO_2 or CuO,[173] were described. Those processes took place under air at high temperature. In 2007, Wetherby and collaborators reported the synthesis of PXX following a different approach. The synthesis was achieved reacting 1,1'-bi-2-naphthol with a stoichiometric amount of hindered Hg(II)amide complex such as $Hg[N(SiMe_3)_2]_2$.[174] The reaction mechanism proceeds *via* an intramolecular electrophilic substitution. An

alternative synthetic approach to access double C-O bond formation is an electrochemical process that was exploited for the preparation of thiophene PXX-doped polymer.[175] In 2013, Cui and co-workers reported the synthesis of substituted PXX *via* oxidative cyclization using $Cu(OAc)_2$, in 1,2-dichlorobenzene at 190 °C by microwave irradiation.[105] However, the procedures described are affected by some limitations like compatibility to the reaction conditions with the substrates or low yield. Therefore, a general protocol for preparation of pyran rings in high yield was desirable. Thus our group started to investigate possible reaction conditions for the preparation of PXX. Starting from Pummerer's protocol based on oxidative cyclization of binaphthol using CuO as oxidant, other transition metal derivatives were employed.[106] Among the various tests performed, the protocol reported by Zhu and collaborators[105] provided the best result allowing us to convert the binaphthol **127** to PXX derivative **32** in 94% yield (Scheme 37).[106, 171] Based on this protocol unprecedented O-doped benzorylenes were prepared by Stassen et al. and this methodology was further exploited to prepare PXX derivatives with extended aromatic core, showing the robustness of the protocol.[108]

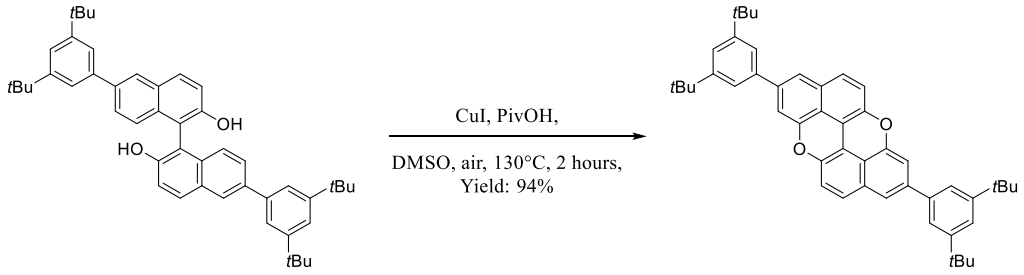

127 **32**

Scheme 37: Synthesis of *peri*-xanthenoxanthene promoted by CuI/PivOH.

More recently, Shimada and co-workers reported a high yielding reaction for the synthesis of PXX derivatives. Starting from binaphthol derivative **128** in the presence of CuCl/1-methylimidazole (NMI) as catalyst and K_2CO_3 in 1,3-dimethylbenzene at 120 °C under aerobic condition for 20 hours, they obtained derivative **129** in 55% yield (Scheme 38).[176]

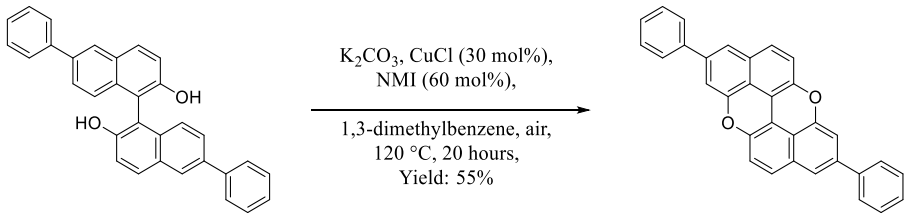

128 **129**

Scheme 38: Synthesis of *peri*-xanthenoxanthene promoted by CuCl/NMI.

2.5 Synthetic pathways toward *N*-Substituted PXXMIs and PXXDIs

2.5.1 Synthesis of PXXDI A_2-Type PATH B

To start we approached the synthesis of homo bis-substituted PXXDI (A_2-type PXXDI) following the path A of the retrosynthetic analysis, Scheme 6, p. 28.

2.5.1.1 *Results and discussion of oxidative coupling (PATH A and B)*

In a first approach of achieving carbon-carbon bond formation for the synthesis of target system **PXXDI**, we employed some conditions reported in the literature.[120, 177] We tried to prepare the binaphthol bisanhydride **43** (Scheme 6) through oxidative coupling of commercial anhydride **44**. Several attempts have been performed to achieve the C–C bond formation in the presence of an oxidizing agent. Numerous oxidising agents have been screened, such as: CuCl(OH)TMEDA,[177a] $Cu(OAc)_2$, $Mn(acac)_3$,[120] $K_2S_2O_8$,[177b] $FeCl_3{\cdot}6H_2O$[177c] and $Fe_2(SO_4)_3{\cdot}5H_2O$[177d] (Scheme 39, Table 2). The oxidizing agents screened did not allow the formation of desired derivative **43**, and only unreacted starting material was recovered. Remarkably, the attempt performed using $FeCl_3{\cdot}6H_2O$ (entry 4, Table 2) instead of providing the binaphthol dianhydride **43**,[178] provided the 4-chloro-3-hydroxyl-naphthalene monoanhydride **132** in 83% yield (Scheme 40).[178] Considering that naphthalene anhydride **44** is not soluble in most common solvents, we considered to prepare a soluble imide derivative following the PATH B of the retrosynthetic analysis (Scheme 6). To this end, molecule **44** was converted into imide derivative **130** (Scheme 39). The functional group conversion from anhydride to imide was performed following base-assisted reaction. In particular, derivative **44** was reacted with *n*-octylamine in the presence of DIPEA, in dioxane under reflux, for 16 hours providing derivative **130** in 75% yield (Scheme 39).[110b] Subsequently we tried to prepare derivative **131** by performing the oxidative coupling on soluble derivative **130** in the presence of $CuCl_2$/α-methylbenzylamine.[179] This attempt did not provide binaphthyl derivative **131** (entries 7 and 8, Table 2).

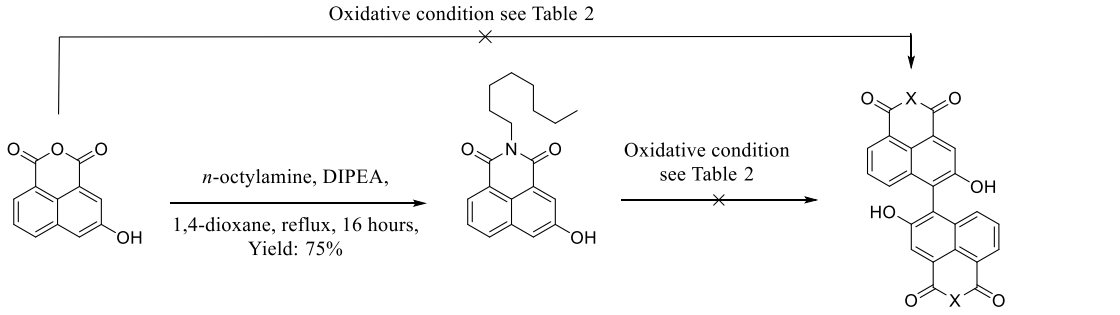

44 **130** **43**: X= O
131: X= *N*-octyl

Scheme 39: Attempts of oxidative coupling.

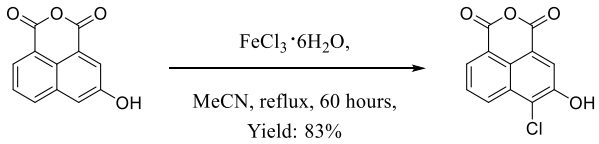

44 **132**

Scheme 40: Attempt of oxidative coupling with $FeCl_3 \cdot 6H_2O$.

Table 2: Oxidative conditions tested.

Entry	Substrate	Coupling Agent	Solvent	T [°C]	Time [h]	Outcome
1	**44**	CuCl(OH)TMEDA (0.2 eq)	CH_2Cl_2	RT	1	No Conversion
2	**44**	$Cu(OAc)_2$ (1.2 eq)	MeCN	82	20	No Conversion
3	**44**	$Mn(acac)_3$	MeCN	82	5	No Conversion
4	**44**	$FeCl_3 \cdot 6H_2O$ (12 eq)	MeCN	82	60	**132** 83% yield
5	**44**	$Fe_2(SO_4)_3 \cdot 5H_2O$ (1.2 eq)	MeCN	82	24	No Conversion
6	**44**	$K_2S_2O_8$ (1 eq), Bu_4NHSO_3 (1 eq)	TFA	72	18	No Conversion
7	**130**	$CuCl_2$, α-methylbenzylamine (2 eq)	MeOH / CH_2Cl_2	RT	16	No Conversion
8	**130**	$CuCl_2$, α-methylbenzylamine (2 eq)	MeOH / $CHCl_3$	RT	16	No Conversion

The oxidation potential of molecules is directly dependant from the electron density of the aromatic system.[180] The molecules that have a higher electron density undergo more easily in oxidative coupling.[115] Moreover, differences of electron density induce differences in the shielding of the nuclear magnetic moment,[181] which imply differences in the resonant frequency.[182] Electron density shields the proton and as consequence the nucleus have differents nuclear resonance frequency, corresponding to different chemical shifts on the nuclear magnetic resonance.[183] Stronger is the shielding effect on the nuclei, weaker will be the effective magnetic field on it and the chemical shift will decrease.[184] Conversely, a deshielding effect due to the removal of electron density corresponds to an increases of the chemical shift of the nuclei, since the effective magnetic field on the nuclei is higher. Nevertheless, the electron density depends on the electron donating or electron withdrawing properties of nearby atoms.[185] Therefore, the electron densities of two different molecules could be estimated comparing the difference in chemical shift of ^{1}H NMR. In the light of this, from the analysis of ^{1}H NMR spectra of 3-hydroxy naphthalene anhydride **44** and *N*-octyl-imide derivative **130** in DMSO-d6 (Figure 20) emerged that the proton in position 6 (*H) in derivative **44** displays a chemical shift of 7.78 ppm, while the proton in position 6 (*H) in derivative **130** shows a chemical shift of 7.72 ppm (Figure 20). The negligible difference of chemical shift reveals similar electron densities of the derivative **44** and derivative **130**.[186]

This result underlines how functional group interconversion from anhydride to imide does not provide any significant variation in the electron density of derivatives **44** and **130**, as consequence it could be assumed that the redox potentials of derivative **44** and derivative **130** are comparable. The failure of the oxidative coupling reactions on derivatives **44** and **130** is observed probably due to the fact that oxidising agents are not efficient enough to oxidize derivatives **44** and **130** in the tested conditions.

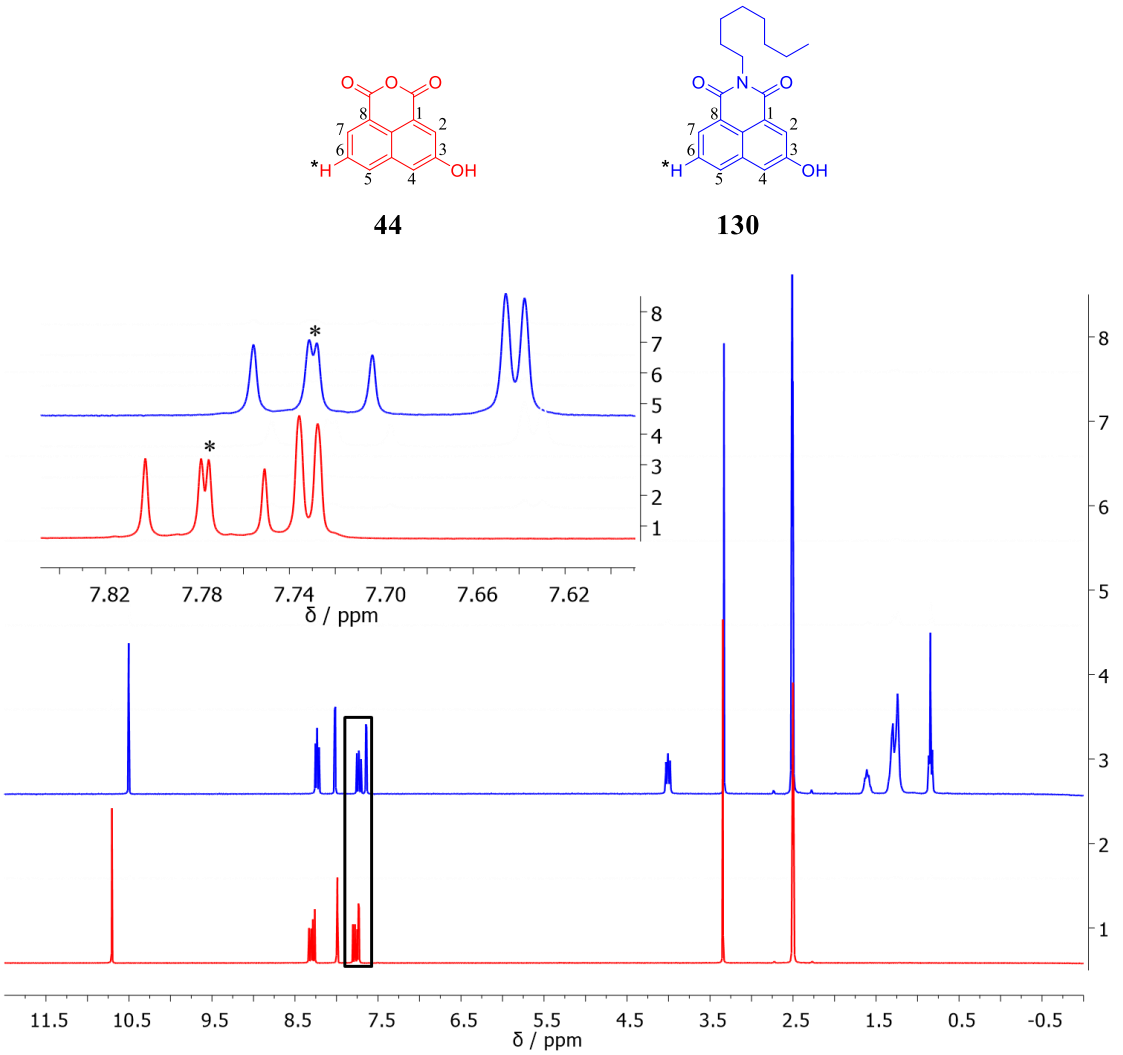

Figure 20: 300 MHz ^{1}H NMR spectra of derivative **44** in red and derivative **130** in blu in C_2D_6SO.

2.5.1.2 Results and discussion of reductive coupling of aromatic halide

Subsequently, to achieve the carbon-carbon bond formation and obtain binaphthyl derivatives **131**, an Ullmann-type strategy was investigated. To this end, a soluble bromo-derivative **134** was prepared. 3-Hydroxy-naphthalene anhydride **44** was treated with Br_2 in dioxane under reflux to obtain 4-bromo-3-hydroxy naphthalene anhydride **133** in 95% yield. Compound **133** was then reacted with *n*-octylamine in the presence of DIPEA to afford imide derivative **134** in 97% yield, which exhibits a good solubility in most of the common organic solvents.[110b, 187] As mentioned before, the free hydroxy group on the aromatic ring prevents the Ullmann process, therefore derivative **134** was submitted to

methylation in the presence of MeI and K_2CO_3 to yield quantitatively derivative **135** (Scheme 41).

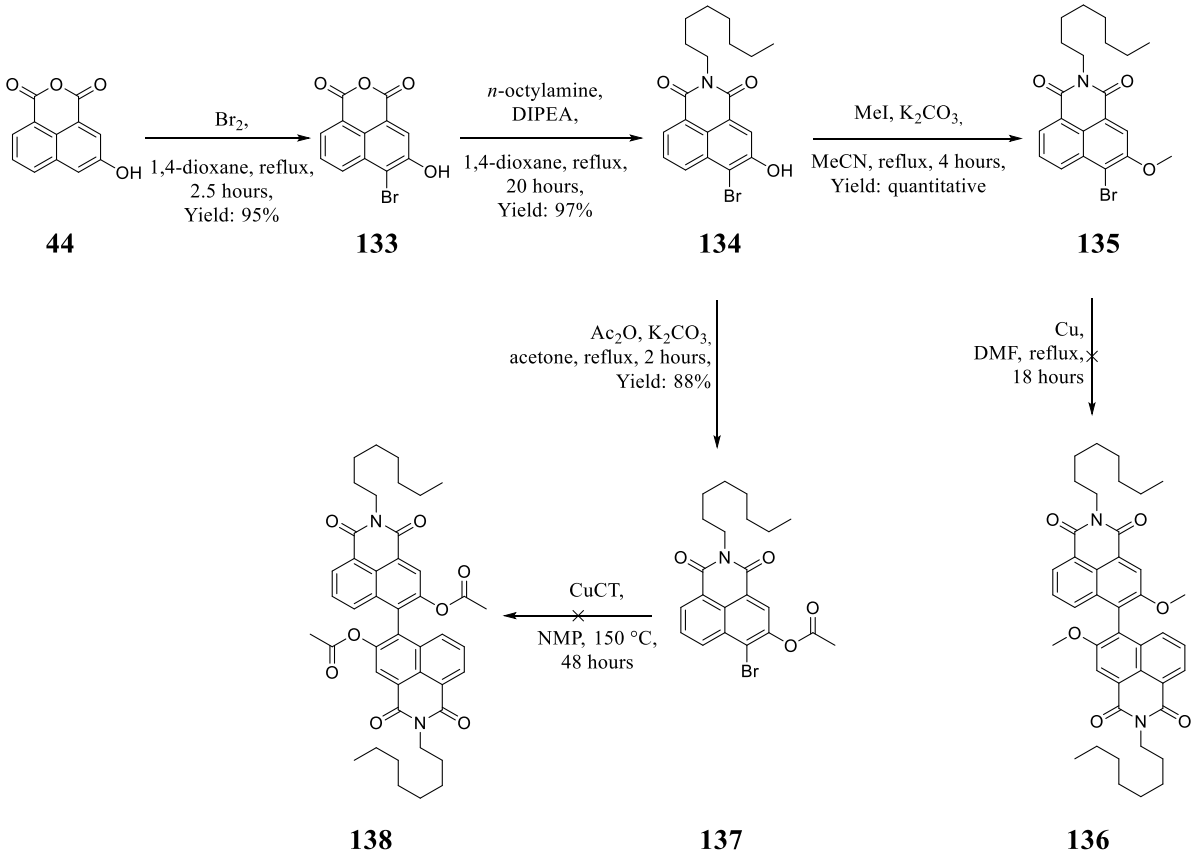

Scheme 41: Reductive coupling.

Prepared derivative **135** was submitted to Ullmann coupling in the presence of copper in DMF at reflux. However, desired binaphthyl **136** was not obtained (Scheme 41) and only the formation of the dehalogenated derivative was observed. When performing the same reaction at lower temperature, only starting material **135** was recovered without any conversion. In a second attempt, hydroxyl derivative **134** was protected with an acetyl group in order to decrease the electron-donating effect of the hydroxyl group and improve the reactivity towards Ullmann coupling. Compound **134** was treated with acetic anhydride, Ac_2O, in the presence of K_2CO_3 in acetone for 2 hours under reflux to yield derivative **137** in 88% yield. The latter underwent reaction with copper thiocarboxylate, CuCT, as coupling agent to attempt the C-C bond formation to yield derivative **138**. CuCT is known to be an active coupling agent for bi-aryl synthesis. However, applied on system **138** in classical conditions, at room temperature in NMP, only starting material was

recovered.[134] By increasing the reaction temperature from room temperature to 150 °C and prolonging the reaction time until 48 hours, we did not observe any conversion and only starting material was recovered (Scheme 41).

2.5.1.3 Results and discussion of Suzuki cross coupling

In the respect of synthetic pathway B (Scheme 6) as alternative route to the oxidative and reductive couplings, a Suzuki cross coupling was exploited to synthesize derivative **136**. As already mentioned Suzuki reaction takes place between an aryl-halide and an organo-boron derivative, requiring the preparation of the latter. Initially, we attempted to synthesise boronic acid **139** starting from bromo derivative **135** through the preparation of an organo-metallic derivative highly nucleophile, such as organo-magnesium-halide or organo-lithium, followed by reaction with an electrophile, namely trimethyl borate and finally with an acidic treatment (Scheme 42). Different attempts of metalation reaction on substrate **135** are summarised in Scheme 42 Table 3.

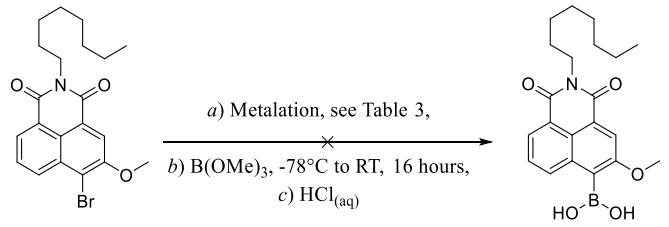

135 **139**

Scheme 42: Attemps to prepare boronic acid **139**.

Table 3: Attempts of metalation of derivative **135**.

Entry	Metalating Agent	Solvent	T[°C]	t [h]	Yield [%]
1	Mg	THF	RT	16	0 (No conversion)
2	Mg	THF	reflux	2	
3	Mg	THF	reflux	20	
4	*t*BuLi	THF	-84°C to RT	1	

As a first attempt, we tried to convert bromo-derivative **135** into organo-magnesium. However, reaction of derivative **135** in the presence of activated Mg in THF at room temperature did not provide desired organo-magnesium derivative **139** (Scheme 42, entry 1 Table 3). By increasing the reaction temperature from room temperature to refluxing THF and prolonging the reaction time until 20 hours(Scheme 42 entries 2 and 3 Table 3),

we did not observe any conversion and only starting material was recovered. Subsequently we tried to prepare the organo-lithium derivative through lithium halogen exchange on the bromo derivative. Compound **135** was treated with *tert*-butyllithium in THF at -84 °C (Scheme 42 entry 4 Table 3). The formation of the desired lithium halogen exchange product did not occur and only starting material was recovered, despite of a colour variation being observed and therefore assuming that a reaction took place. The inefficiency of the process could be explained by the competitive process of direct *ortho* metalation in position 2, which should be taken in consideration due to the presence of two *ortho* directing groups, namely the *N*-acyl of the imide moiety and the methoxy group, in positions 1 and 3, respectively. However, the boron derivative, resulting from this competitive process has not been isolated, allowing to suppose that the possible boronic derivative is not stable and decomposes through hydrolytic deborylation process. In order to prepare the naphthalene imide boronate, a different process more compatible with the functional groups present on the substrate was envisaged. In fact, we tried to prepare the organo-boron derivative **140** by Miyaura borylation promoted by palladium catalysis (Scheme 43). For this purpose, bromo derivative **135** was treated with bis(pinacolato)diboron **108**, in the presence of [Pd(dppf)Cl_2] as catalyst and KOAc as base in DMSO at 80 °C.[145] After 20 h of reaction, only dehalogenated derivative was isolated by silica gel permeation (Scheme 43 entry 1 Table 4). Due to such result, we investigated the role of the solvent and DMSO was replaced with a less polar solvent, DMF, as well suitable for the Miyaura borylation (Scheme 43 entry 2 Table 4). From this experiment, traces of product **140** were isolated. Furthermore, continuing to reduce the polarity of the solvent and performing the reaction in dioxane, the desired product **140** was isolated in a higher yield (22%) but still not satisfactory (Scheme 43 entry 3 Table 4). By reducing the reaction time, no particular improvement of the yield was observed (Scheme 43 entry 4 Table 4). The employment of [Pd(PPh_3)$_2Cl_2$] instead of [Pd(dppf)Cl_2] afforded a similar yield. Indeed, from the ^{1}H-NMR analysis of the crude only filtered on celite, it was possible to estimate the desired product **140** in *ca*. 60% yield (Scheme 43 entry 5 Table 4). However, after the purification by silica gel permeation, only a low amount of product was isolated. This last experiment suggested that the desired boronic ester has a low stability in the reaction conditions thanks to the presence of a notable amount of dehalogenation by-product. Moreover, the desired product also undergoes degradation on silica and attempts

to purify the product with other techniques such as precipitation or crystallization did not afford pure material.

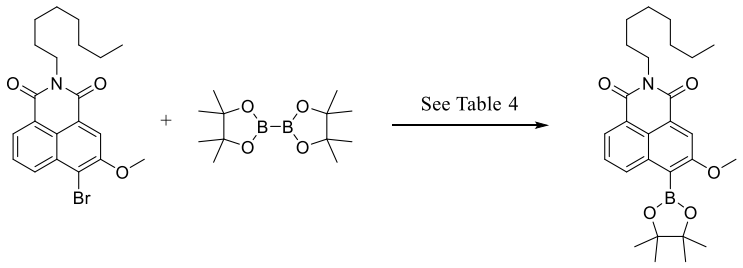

135 **108** **140**

Scheme 43: Miyaura borylation on derivative **135**.

Table 4: Tested conditions to perform Miyaura borylation.

Entry	Pd	Solvent	T[°C]	t[h]	Yield [%]
1	[Pd(dppf)Cl_2] (0.05 eq)	DMSO	80	20	0
2	[Pd(dppf)Cl_2] (0.05 eq)	DMF	60	4	12
3	[Pd(dppf)Cl_2] (0.05 eq)	1,4-dioxane*****	reflux	16	22
4	[Pd(dppf)Cl_2] (0.05 eq)	1,4-dioxane*****	reflux	8	18
5	[Pd(PPh_3)$_2Cl_2$] (0.05 eq)	1,4-dioxane*****	reflux	16	60******

***:** ACS grade 99%.
****:** estimated by ^{1}H NMR.

Considering the low stability and purification issue of boronic ester derivative **140**, we decided to use directly the reaction crude of **140** in the Suzuki cross coupling without purification. Therefore, the crude of the Miyaura borylation (after filtration on celite in order to remove the palladium catalyst) was reacted with bromo naphthyl imide derivative **135** in the presence of Pd catalyst (Scheme 44). Different reaction conditions were screened and the main results are gathered in Table 5.

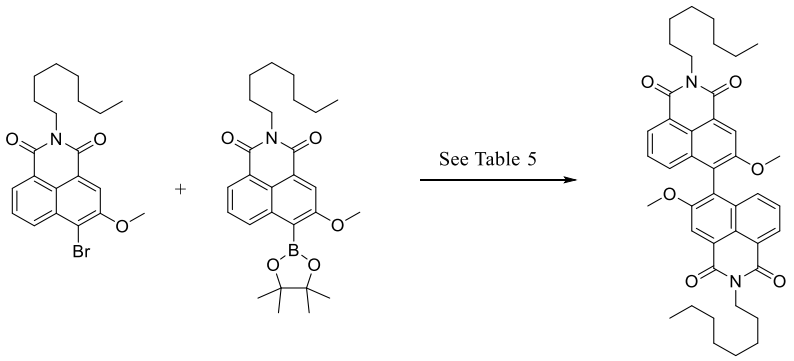

135 **140** **136**

Scheme 44: Synthesis of derivative **136** by Suzuki cross coupling.

Table 5: Tested reaction conditions to prepare derivative **136**

Entry	Pd	Base	Solvent	T [°C]	t [h]	Yield %
1	$[Pd(PPh_3)_2Cl_2]$ (0.06 eq)	K_2CO_3 (3 eq)	1,4-dioxane*	reflux	16	25
2	$[Pd(dppf)Cl_2 \cdot CH_2Cl_2]$ (0.06 eq)	K_2CO_3 (3 eq)	DMF	100	20	0
3	$[Pd(dppf)Cl_2 \cdot CH_2Cl_2]$ (0.05 eq)	Cs_2CO_3 (3 eq)	1,4-dioxane*	reflux	16	30
4	$[Pd(dba)_2]$/Sphos (0.05 /0.1 eq)	Cs_2CO_3 (3 eq)	1,4-dioxane*	reflux	18	41

*: ACS grade 99%.

In this respect, to prepare the desired binaphthyl system **136**, we decided to perform a Suzuki cross coupling between bromo derivative **135** and boron derivative **140** (Scheme 44), exploiting the conditions that provided the best result in the Miyaura borylation using $[Pd(PPh_3)_2Cl_2]$ in dioxane under reflux in the presence of K_2CO_3 as base. After 16 hours of reaction desired product **136** was isolated in 25% yield (Scheme 44 entry 1 Table 5). Subsequently, we tried to replace both, dioxane with a more polar solvent, namely DMF, and the catalytic system ($[Pd(PPh_3)_2Cl_2]$) with $[Pd(dppf)Cl_2 \cdot CH_2Cl_2]$, being featured with a bidentate ligand, which helps to promote the reductive elimination.[151] Therefore, we performed the reaction between bromo-derivative **135** and boron-derivative **140** in the presence of $[Pd(dppf)Cl_2 \cdot CH_2Cl_2]$ with K_2CO_3 as base, heated at 100 °C for 20 hours, (Scheme 44 entry 2 Table 5). This resulted in the isolation of derivative dehalogenated by product instead of target product **136**. Consequently, we tried to replace K_2CO_3 with more soluble Cs_2CO_3 and we performed the Suzuki cross coupling of **135** and **140** in the presence of $[Pd(dppf)Cl_2 \cdot CH_2Cl_2]$ in dioxane under reflux for 16 hours yielding the desired product bis imide binaphthyl **136** in 30% yield (Scheme 44 entry 3 Table 5). From these three experiments emerged that, for the coupling between molecules **135** and **140**, dioxane seems to be the best solvent for the process. Finally, considering the nature of the ligand of the palladium complex, PPh_3 and dppf are both electron poor phosphine ligands, while

the first is monodentate, the latter is bidentate, feature which should improve the reductive elimination in the catalytic process.[156c] However, we did not observe any significant difference in the yield for the two different ligands. This result highlights that the reductive elimination does not represent the critical step in the catalytic process. Therefore, trying to optimize the reaction conditions, we investigated the oxidative addition process to determine if it is the crucial step. Electron-poor phosphines are known to promote the transmetallation process, on the other hand electron rich phosphines enhance the oxidative addition process. Nevertheless, as molecules **135** and **140** are sterically demanding reagents, we tried to replace the electron-poor ligand of Pd, with an electron rich ligand bidentate, namely SPhos **104**. Eventually, we performed the coupling of bromo imide **135** and boron derivative **140** in the presence of the highly active catalytic system [$Pd(dba)_2$]/Sphos **104** with Cs_2CO_3 as base in dioxane under reflux for 18 hours affording the desired product in 41 % yield with the full conversion of the bromo derivative **135** (Scheme 44 entry 4 Table 5). The electron-rich phosphine did not dramatically affect the yield. Accordingly to these results, we can exclude the supposition that the oxidative addition mainly affects the yield of the process. Based on these results, we concluded that the yield of the Suzuki cross coupling between derivatives **135** and **140** is affected mainly by the stability of the boron derivative **140** in the reaction conditions. In the end, inspired by the work of Buchwald, a one-pot reaction approach involving a simultaneous Miyaura borylation and Suzuki cross coupling, was tried.[159] This strategy was exploited in order to overcome the low stability of organo-boron **140**. In such reaction conditions, **135** was treated with bis(pinacolato)diboron **108** in the presence of Pd-catalyst. The readily formed organo-boron **140** undergoes immediately in carbon-carbon coupling reacting with the excess of bromo-derivative **135**. This is possible employing a strong base that promotes not only the borylation but also the Suzuki coupling.[159] We first decided to perform the one-pot reaction exploiting the already optimised conditions and investigating the influence of the stoichiometry of bis(pinacolato)diboron **108** on the overall yield of the process (Scheme 45). Therefore bromo-derivative **135** took part in a reaction in the

presence of Cs_2CO_3 and [Pd(dba)$_2$]/SPhos in dioxane under reflux in the presence of different stoichiometry of bis(pinacolato)diboron **108**, Table 6.

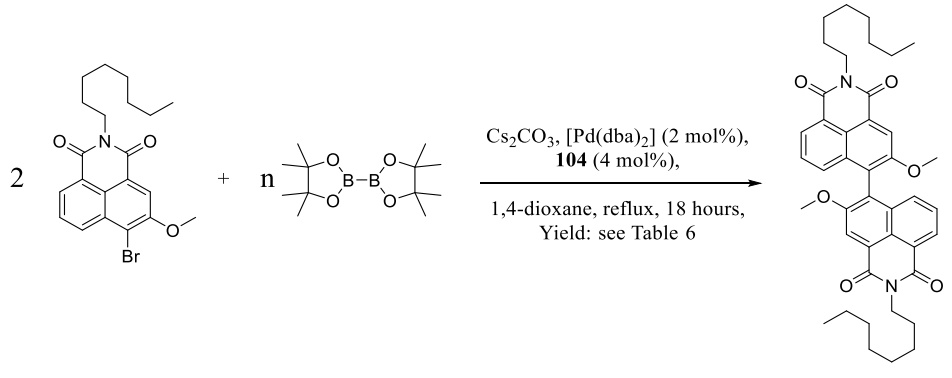

135 **108** **136**

Scheme 45: One-pot procedure to prepare derivative **136**.

Table 6: Influence of the stoichiometry of bis(pinacolato)diboron on the yield of **124** in one-pot process.

Entry	n [eq]	Yield [%]
1	1	20
2	2.0	37
3	3.0	49

Derivative **135** first took part in a reaction in the presence of a stoichiometric amount of bis(pinacolato)diboron **108**, Cs_2CO_3 and [Pd(dba)$_2$]/SPhos in dioxane for 18 hours, under reflux to yield binaphthyl product **136** in 20% yield, entry 1 Table 6. This condition should promote the formation of a stoichiometric quantity of boron derivative **140**, which can react with bromo derivative **135**. In this context, the yield is calculated in respect to bis(pinacolato)diboron **108** which can be considered the limiting reagent.[150] Nevertheless, in a typical Suzuki cross coupling protocol of cumbersome substrates organo-boron are employed in excess. Subsequently, we tried to increase the amount of in situ generated boron derivative **140**, by employing higher quantity of **108**. When we employed an equimolar amount of bis(pinacolato)diboron **108**, that corresponds to an over stoichiometric amount in respect to bromo derivative **135**, the process provided product **140** in 37% yield, (entry 2 Table 6). In this case the yield of the process is calculate in respect to half of the moles of bromo imide **135** that is the limiting reagent. Despite the over stoichiometry of derivative **108**, the yield of the product **136** is higher than entry 1 Table 6, where derivative **108** is used in stoichiometric ratio. Afterwards we tried to increase the proportion of bis(pinacolato)diboron **108** till 3 equivalents (entry 3 Table 6), yielding bis-octyl imide binaphthyl **136** in 49% yield, corresponding to half of the moles

of the bromo derivative **135**. So far this condition is the best one to perform the homo coupling of bromo imide **135** in a one pot process. From this experiment emerged that the yield of compound **136** increases with the use of an over stoichiometric amount of bis(pinacolato)diboron **108**, a trend that is in agreement with the previous supposition of degradation on the boronate ester **140** in reaction media. Subsequently, in order to perform the last step (i.e. the two oxidative cyclizations) and to obtain target systems **141**, a cleavage of the two methoxy ethers of **136** is necessary. The methyl-ether cleavage process relies on a broad number of procedures that have been developed, in order to achieve selectively the methoxy ethers cleavage.[188] The reaction was carried out in classical conditions employing BBr_3, as Lewis acid. Diimide-dimethoxy derivative **136** was treated with an excess of BBr_3 in CH_2Cl_2, yielding diimide-binaphthol **131** in a quantitative yield. Finally, we applied the reaction conditions developed in our group for C-O cyclization on newly prepared imide systems. In particular, diimide-binaphthol **131** was cyclized in the presence of CuI and PivOH in DMSO under air at 120 °C for 5 hours leading to the formation of the first target system bis-octyl-PXXDI **141** in 77% yield (Scheme 46).

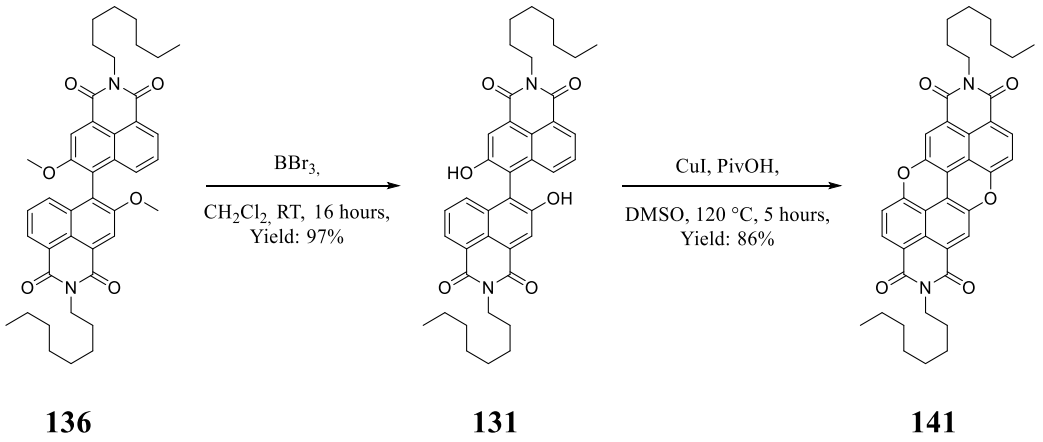

Scheme 46: Oxidative cyclization**.**

Remarkably, the CuI/PivOH protocol tolerates the imide functional group. In conclusion, following the synthetic pathway B, the final target system bis-octyl-PXXDI **141** was prepared with an overall yield of 34% starting from the commercially available 3-hydroxy-naphthalene anhydride **44**. Although the synthesis of **PXXDI** has been successfully achieved, this synthetic strategy is affected from one major drawback which is the imide synthesis as the second step. Indeed, it implicates that the functionalization on the imide

motifs has to be established at the beginning of the synthesis, which represents a big limitation in general application of the synthetic pathways, and especially for the preparation of a library of PXX imide derivatives, as each desired product requires different steps.

2.5.2 Synthesis of PXXDI A_2- Type PATH A

After the successful achievement of the target system **PXXDI 141** we focused our attention to develop a new synthetic strategy that avoids the imide synthesis in the early stage of the synthetic pathway. Based on this principle, we revised the retrosynthetic analysis Path A Scheme 6, planning the imide formation in the last stage of the synthesis by functional group conversion. We envisaged the revised synthesis on the preparation of a soluble bromo methoxy di ester naphthalene, which could undergo to homo coupling with already optimized Suzuki-Miyaura condition. To this end, 4-bromo-3-methoxy-dimethyl-esters naphthalene **142** was prepared by complete methylation of 4-bromo-3-hydroxynaphthalene anhydride **133** by reaction with MeI and DBU as a base in MeOH under reflux for 18 hours, yielding desired product **142** in 81% yield (Scheme 47).[189] Subsequently, dimethyl ester **142** was used in a homo-coupling Suzuki cross coupling reaction in a one-pot process, in the presence of K_3PO_4 as base, bis(pinacolato)diboron **108** and [$Pd(dba)_2$]/SPhos **104** as catalytic system, in dioxane under reflux for 20 hours yielding dimethoxy-tetramethyl-ester-binaphthyl **58** in 22% yield (Scheme 47, entry 1 Table 7). However, full conversion of starting material **142** was observed, implying an efficient oxidative addition process, similarly to what is reported for the preparation of the binaphthyl derivative **136**. The latter was mainly affected by the low stability of the boron derivative **140** in reaction conditions. The low yield of the coupling can be attributed to a problem during transmetallation in the Suzuki process, which might be affected from the stability of the boron derivative **143** formed in situ. Therefore, we investigated the role of the base as a possible responsible cause of low yielding process. In order to exclude methyl esters hydrolysis as parasite reaction, K_3PO_4 was replaced with MeONa (Scheme 47,entry 2 Table 7). In these conditions, the reaction yielded product **58** in a similar yield to entry 1 (i.e. K_3PO_4 used as base). As a third attempt, *t*BuONa was employed as less nucleophilic base leading the formation of only traces of product **58** (Scheme 47, entry 3 Table 7). Due

to the low influence of the base, we considered that the low yield of the process can be affected by the stability of the boronic ester intermediate.

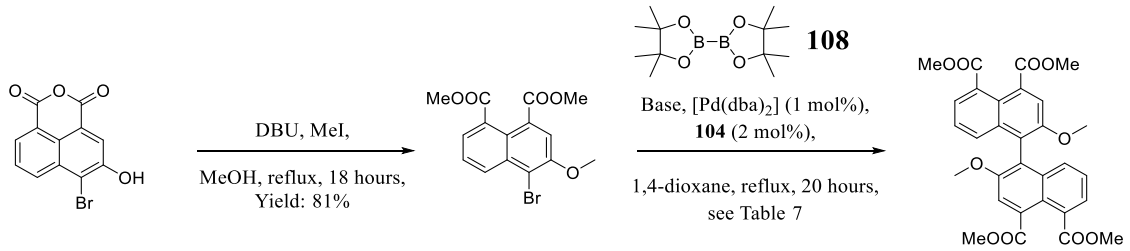

133 **142** **58**

Scheme 47: Synthesis of dimethoxy-tetramethyl-ester-binaphthyl **58** one-pot procedure.

Table 7: Reaction conditions tested to prepare derivative **58**.

Entry	Base [3 eq]	Yield [%]
1	K_3PO_4	22
2	MeONa	20
3	*t*BuONa	trace

In order to study the stability of the boronic ester **143**, Miyaura borylation on dimethyl ester derivatives **142** has been investigated (Scheme 48). We first applied the best condition previously found for the borylation of naphthalene monoimide **135** (Scheme 43, entry 5 Table 4). Performing the reaction on dimethyl ester **142** in the presence of KOAc, bis(pinacolato)diboron **108** and $[Pd(PPh_3)_2Cl_2]$ in dioxane under reflux for 16 hours, we noted the formation of the related boronic ester **143** which was surprisingly isolated by precipitation in 78% yield (Scheme 48). Nevertheless, boronic ester derivative **143** also exhibits a low stability on silica, feature which did not allow to follow the evolution of reaction by TLC, as only bromo dimethyl ester derivative and relative dehalogenated derivatives are detectable by TLC analysis. The achievement of boronic ester naphthalene derivative **143** synthesis offers the opportunity to optimize the synthesis of the tetramethyl ester derivative **58**. To perform the Suzuki cross coupling between bromo dimethyl ester **142** and boron derivative **143**, the optimised conditions of the dimethyl ester binaphthyl derivative **51** were applied (Scheme 53). Derivative **142** and **143** were reacted in the presence of K_3PO_4 as base and $[Pd(dba)_2]$/SPhos **104** as catalytic system in dry dioxane under reflux for 16 hours affording tetramethyl ester derivative **58** in 22% yield (Scheme 48, entry 1 Table 8). These Suzuki conditions allow us to afford desired product **58** in low yield, comparable with the one-pot process, Scheme 47.

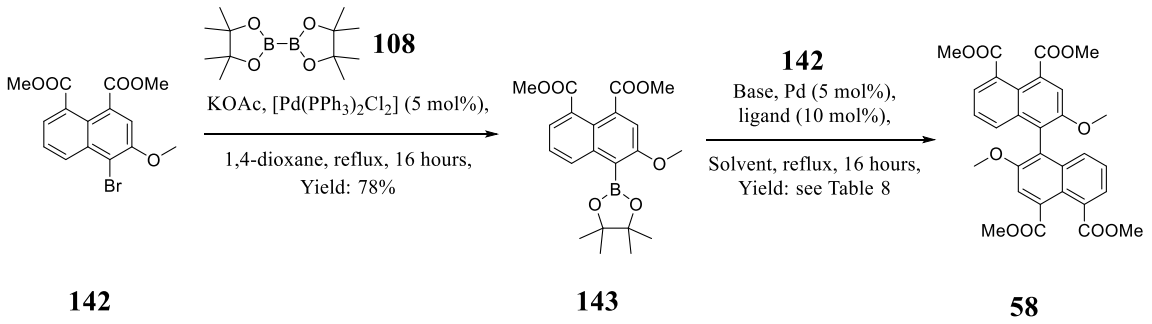

142 **143** **58**

Scheme 48: Synthesis of dimethoxy-tetramethyl-ester-binaphthyl **58** by Suzuki reaction.

Table 8: Reaction conditions tested to prepare compound **58** through Suzuki reaction.

Entry	Base	Pd/ Ligand	Solvent	Yield [%]
1	K_3PO_4	$[Pd(dba)_2]$/Sphos	1,4-dioxane (dry)	22
2	K_3PO_4	$[Pd(PPh_3)_2Cl_2]$	1,4-dioxane (dry)	trace
3	CsF	$[Pd(dba)_2]$/Sphos	1,4-dioxane*/H_2O (2/1)	44
4	MeONa	$[Pd(dba)_2]$/Sphos	1,4-dioxane (dry)	11
5	K_3PO_4	$[Pd(dba)_2]$/Sphos	1,4-dioxane*	58
6	K_3PO_4	$[Pd(dba)_2]$/Sphos	1,4-dioxane*/H_2O (5/1)	81

*: ACS grade 99%.

As a second attempt we replaced the electron-rich system $[Pd(dba)_2]$/SPhos **104** with the more electron-poor $[Pd(PPh_3)_2Cl_2]$, with the aim to improve the transmetallation process. Thus, the coupling between derivatives **142** and **143** was performed in the presence of K_3PO_4 as base $[Pd(PPh_3)_2Cl_2]$ in dry dioxane under reflux for 16 hours. Contrary to the expectations, the reaction yielded tetramethyl ester derivative **58** only in traces (entry 2 Table 8). Therefore, several reaction conditions have been screened in order to optimise the transmetallation step in the catalytic process and consequently improve the reaction yield. We performed the coupling between **142** and **143** in the presence of CsF and $[Pd(dba)_2]$/SPhos **104** in a solvent mixture dioxane/H_2O (2/1) under reflux for 16 hours which yielded the desired product **58** in 44% yield (entry 3 Table 8).[190] In a further attempt we used NaOMe as base, with $[Pd(dba)_2]$/SPhos **104**, in dry dioxane under reflux for 16 hours, providing the desired product in 11% yield (entry 4 Table 8). On the base of these three attempts emerged that the best reaction yield was obtained using CsF as base in a solvent mixture of dioxane/H_2O (2/1). Furthermore, the reaction between **142** and **143** was performed in the presence of K_3PO_4 as base and $[Pd(dba)_2]$/SPhos **104** as catalytic system in dioxane (ACS grade 99%) under reflux for 16 hours yielding tetramethyl ester derivative **58** in 58% (yield, entry 5 Table 8). Finally, the reaction between **142** and **143** performed

in the presence of K_3PO_4 and [Pd(dba)$_2$]/SPhos **104** in a solvent mixture of dioxane/H_2O (5/1) under reflux for 16 hours yielding the tetramethyl ester binaphthyl **58** in 81% yield, (entry 6 Table 8).[159] From these experiment is possible to observe the influence of the water on the yield of the reaction, as it is known that the presence of the water enhances the concentration of OH- ions which improve the formation of the hydroxyl palladium and the borate (Scheme 21). The enhanchment of the concentration of these species, which are involved in the transmetallation process leads to an improvement of the rate.[191] Subsequently, tetramethyl ester binaphthyl **58** was converted in anhydride **144** by saponification with KOH in *i*PrOH under reflux for 13 hours. The carboxylate intermediate was subsequently cyclised by acid condensation with aqueous HCl in AcOH, under reflux for 24 hours, yielding dimethoxy binaphthy bisanhydride **144** in 81% yield (Scheme 49). The resulting binaphthyl bis anhydride **144** showed a low solubility, which did not allow us to proceed with the following methyl ether cleavage in the previous developed conditions, BBr_3 in CH_2Cl_2. In order to perform the ether cleavage, derivative **144** was reacted with aqueous HBr in AcOH at 126 °C for 24 hours yielding dianhydride binaphthol **43** (Scheme 49).[188]

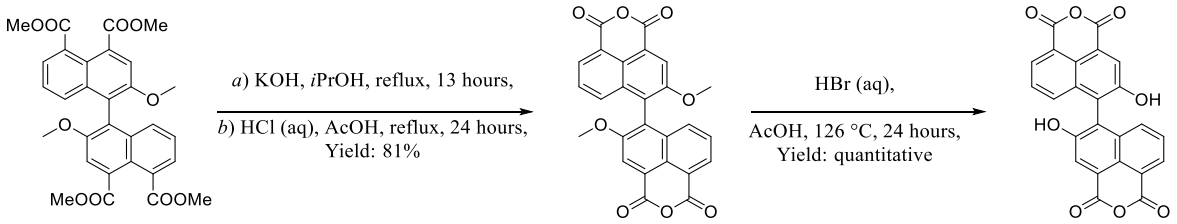

58 **144** **43**

Scheme 49: Synthesis of dianhydride binaphthol **43**.

2.5.3 Synthesis of PXXMI PATH A

To start we approached the synthesis of **PXXMI** following the path A of the retrosynthetic analysis (Scheme 7, p. 29). Having optimized the coupling procedure for the formation of binaphthol diimide **135**, to prepare the key intermediate **146**, we applied the previously used Suzuki cross-coupling conditions, in which bromo-imide compound **135** reacts with 2-methoxy-1-naphthaleneboronic acid **145** in the presence of [Pd(dba)$_2$]/Sphos **104** with Cs_2CO_3 as base in dioxane under reflux for 16 hours. The reaction yields binaphthyl-monoimide **146** in 96% yield (Scheme 50).

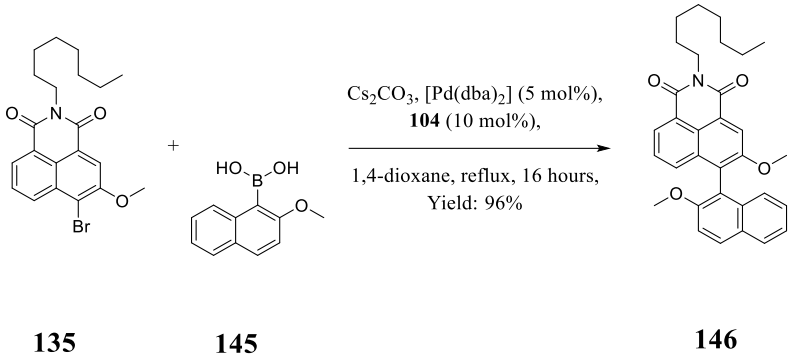

135 **145** **146**

Scheme 50: Synthesis of monoimide-binaphthyl **146**.

Subsequently, methoxy cleavage on monoimide binaphthyl **146** was achieved in similar fashion to diimide-dimethoxy derivative **136**, the reaction on binaphthyl derivative **146** was performed in the presence of excess of BBr_3 in CH_2Cl_2, providing monoimide-binaphthol **147** in 97% yield. Eventually, mono-imide- binaphthol **147** was treated with CuI and PivOH in DMSO under air at 120 °C for 5 hours affording target system octyl-PXXMI **148** in 86% yield (Scheme 51).

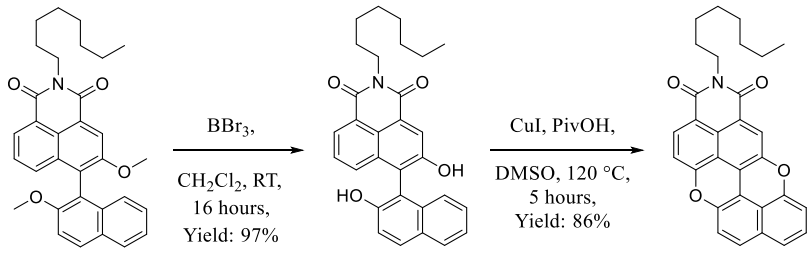

146 **147** **148**

Scheme 51: Oxidative cyclization.

In conclusion, the target systems **PXXMI 148** was prepared with an overall yield of 72% over six steps starting from the commercially available 3-hydroxy naphthalene anhydride **44**. This synthetic pathway, similarly to the synthetic pathway B of **PXXDI**, is affected by the imide synthesis in the early stage of the synthesis. Therefore, the functionalization on the imide motifs has to be established at the beginning of the synthesis, which represents a big limitation in a general application of the synthetic pathways.

2.5.4 Synthesis of PXXMI PATH B

Subsequently to the achievement of the target system following the synthetic PATH A, we focused our attention on the achievement of the **PXXMI** system following the synthetic PATH B depicted in Scheme 7. To start we tried to perform the C-C bond formation towards the Suzuki cross coupling, between bromo methoxy naphthalene anhydride derivative **149** and naphthyl boronic acid derivative **145**. 4-Bromo, 3-hydroxynaphthalene anhydride **133** was methylated in the presence of K_2CO_3 as base and MeI as alkylating agent in DMF at 40 °C. During the reaction, hydrolysis of the anhydride occurred, providing the formation of the methyl ester derivative. Therefore, to restore the anhydride moiety from the dimethyl ester functionality, it was necessary to perform a basic hydrolysis to yield the di-carboxylate, followed by an acidic treatment to promote the cyclization to anhydride, affording the desired product **149** in quantitative yield (Scheme 52). Subsequently, to prepare monoanhydride dimethyl binaphthol **150**, we tried to perform a Suzuki cross coupling, between methoxy derivative **149** and 2-methoxy-1-naphthaleneboronic acid **145** in the presence of [Pd(dba)$_2$]/Sphos **104** and Cs_2CO_3 as base in dioxane under reflux for 16 hours. Despite applying the already optimized conditions to prepare binaphthyl monoimide **146**, the reaction with anhydride **149** did not yield the desired product **150** but only the dehalogenated derivative (Scheme 52).

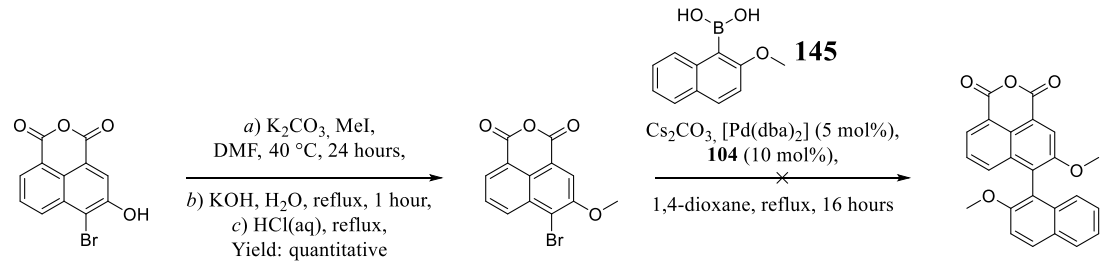

Scheme 52: Attempt to prepare monoanhydride dimethyl binaphthol **150**.

The formation of desired product **150** was not achieved due to probable hydrolysis of the anhydride interfering with the palladium catalysed reaction. In fact, in the early stage of the reaction the formation of black suspension has been observed, probably metallic Pd. Subsequently, in order to perform the Suzuki coupling, 4-bromo-3-methoxy-dimethyl-esters naphthalene **142** was used *in lieu* of 4-bromo-3-methoxynaphthalene anhydride **149**

(Scheme 53). When dimethyl ester derivative **142** was submitted to Suzuki reaction with 2-methoxy-1-naphthaleneboronic acid **145** in the presence of [Pd(dba)$_2$]/Sphos **104** and Cs_2CO_3 as base in dioxane under reflux for 16 hours, desired binaphthyl system **51** was not isolated. The synthesis of binaphthyl derivative **51** has been achieved by performing the coupling reaction replacing Cs_2CO_3 by K_3PO_4 and using dry dioxane. The modified procedure afforded the dimethyl 2,2'-dimethoxy-1,1'-binaphthalene-4,5-dicarboxylate **51** in quantitative yield (Scheme 53).

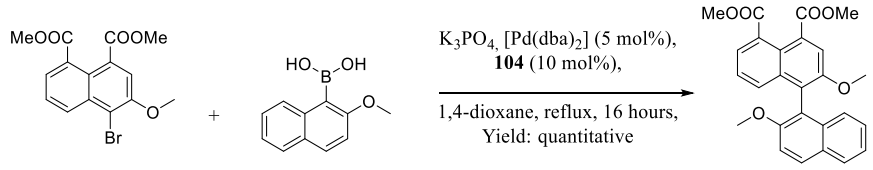

142 **145** **51**

Scheme 53: Synthesis of dimethyl 2,2'-dimethoxy-1,1'-binaphthalene-4,5-dicarboxylate **51**.

Subsequently dimethyl ester derivative **51** was converted in dimethoxybinaphthyl monoanhydride **150** in 86% yield by basic saponification and following acid condensation. Afterwards, derivative **150** was submitted to methyl ether cleavage with BBr_3 in CH_2Cl_2 at RT for 16 hours, affording binaphthol monoanhydride **49** in quantitative yield.[188] To prepare **PXXMA 49** we applied the C-O bond formation protocol on binaphthol **50**, which underwent reaction in the presence of CuI and PivOH in DMSO heated at 120 °C for 5 hours yielding a deep dark red solid of very low solubility (Scheme 54).[106, 108]

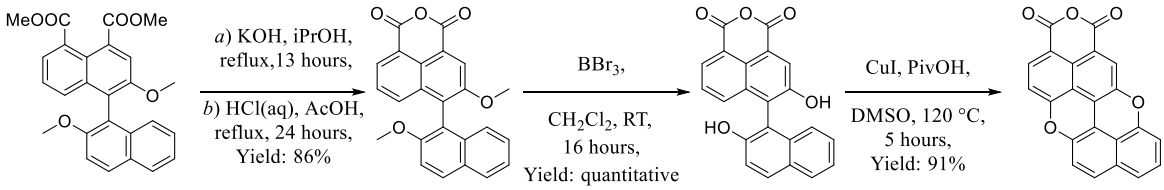

51 **150** **50** **49**

Scheme 54: Attempt to prepare **PXXMA 49**.

In order to prove the formation of pyranopyranyl derivative **49**, it was converted in octyl PXXMI **148**, with octylamine using DIPEA in dioxane under reflux for 16 hours.[110b] The process afforded alkyl-PXXMI, **148** in only 12% of yield (Scheme 55). Alternatively, a similar result was obtained treating PXX monoanhydride **49** with of *n*-octylamine in AcOH under reflux for 24 hours (Scheme 55).

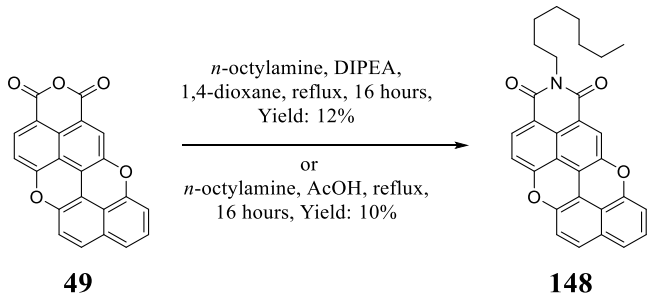

49 **148**

Scheme 55: Synthesis of octyl-PXXMI from **PXXMA**.

The low overall yield of the octyl-**PXXMI 148** starting from binaphthol monoanhydride **50** through the formation of **PXXMA 49** can be explained by the incompatibility of the anhydride moiety in the C-O bonds formation copper promoted reaction. Despite the fact that the reaction failed on the anhydride derivatives, it has already been demonstrated that the copper promoted C-O bond formation is active on imide derivative. Therefore, the binaphthol monoanhydride derivative **50**, in the presence of *n*-octylamine and DIPEA in dioxane under reflux for 20 hours, was converted quantitatively into the last intermediate of the first synthetic approach, derivative **147**. Which in the presence of CuI and PivOH in DMSO under air heated at 120 °C for 5 hours, afforded the desired octyl-PXXMI **148** in 86% yield (Scheme 56).

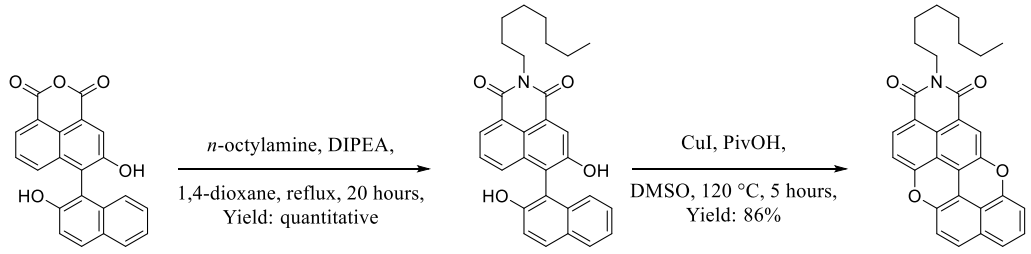

50 **147** **148**

Scheme 56: Synthesis of **octyl-PXXMI** from monoanhydride dimethyl binaphthol **148**.

To conclude, the synthesis of the desired scaffold **PXXMA 49** was not achieved using the proposed strategy because of the incompatibility of anhydride moiety in C-O bond formation process. Therefore, an alternative synthetic pathway for the preparation of **148** was developed. This involves seven steps with an overall yield of 56% starting from the commercially available 3-hydroxynaphthalene anhydride, **44**. Remarkably, the new synthetic pathway, even if it is one step longer compared to the original one, affords a more general synthesis and allows to differentiate the imide substituent in the second to last step

followed by the cyclization in the last step affording the desired **PXXMI**. Notably the overall yield of the new strategy is comparable with the original one. Despite this achievement, the synthesis still requires the involvement of a boronic acid pre-synthesized, which is a limitation in the coupling with other naphthalene derivatives, due to the preparation of the boronic acid derivatives. This problem could be solved with the preparation of an organo-boron starting from 4-bromo-3-methoxydimethyl-esters naphthalene **142**. Subsequently, the new Suzuki reaction conditions were applied to perform the cross coupling on 1-bromo-2-methoxynaphthalene **151** with dimethyl ester naphthalic boronic ester derivative **143** in the presence of K_3PO_4 and [Pd(dba)$_2$]/SPhos **104** in a solvent mixture dioxane/H_2O (5/1) yielding the dimethyl ester binaphthyl **51** in 96% yield (Scheme 57).

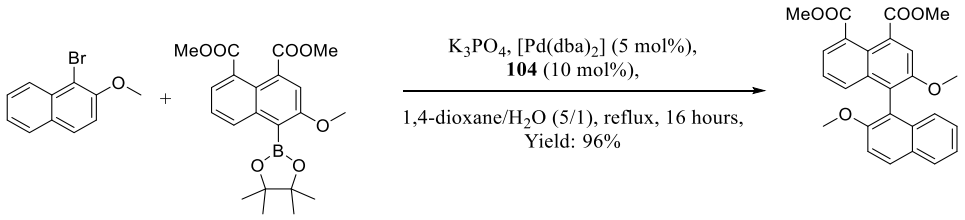

151 **143** **51**

Scheme 57: Synthesis of dimethyl 2,2'-dimethoxy-1,1'-binaphthalene-4,5-dicarboxylate **51**, by Suzuki reaction between **151** and **143**.

In conclusion, with the achievement of the boronic ester **143** it was possible to extend the scope of the of the general **PXXMI** synthesis. In fact, derivative **143** is a versatile building block that could be exploited to prepare other PXX derivatives, through Suzuki cross-coupling with aryl halide derivatives avoiding the preparation of the relative boron derivative.

2.5.5 Synthesis *N*-Substituted AB-Type PXXDI

In order to start preparing the AB-Type *N*-substituted PXXDI we approach the synthesis following the synthetic pathway depicted in Scheme 8, p. 30. This strategy relies on the preparation of the mono anhydride dimethyl ester derivative **57** by hydrolysis of the tetramethyl ester derivative **58**.

In principle, the preparation of mono anhydride derivative **57** starting from the tetramethyl ester binaphthyl derivative **58** could be performed either in basic or acid hydrolysis

(Scheme 58). Nevertheless, derivatives **57** can undergo a further ester-hydrolysis providing the bisanhydride derivative **144**.

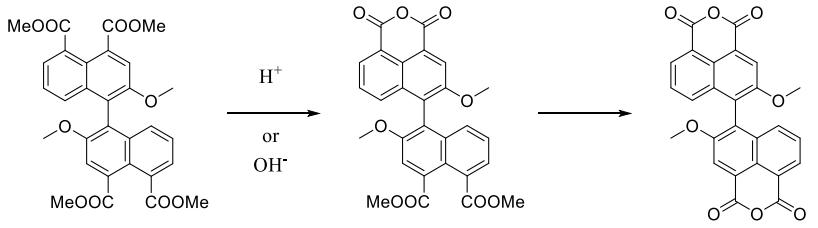

58 **57** **144**

Scheme 58: Hydrolysis of tetramethyl ester dimethylbinaphthol **58** to dimethyl ester anhydride dimethylbinaphthol **57**.

The yield of the anhydride formation is strictly correlated to a one-side ester hydrolysis: in fact, the intramolecular cyclization can occur only if the carboxylic residues are adjacent. Therefore, the acid hydrolysis, which is an equilibrium process, should theoretically ensure a higher yield due to the possibility of esterification-hydrolysis equilibrium (Scheme 59). Moreover, once the cyclization to anhydride occurred, the intermediate is not involved anymore in the esterification-hydrolysis process.[110a]

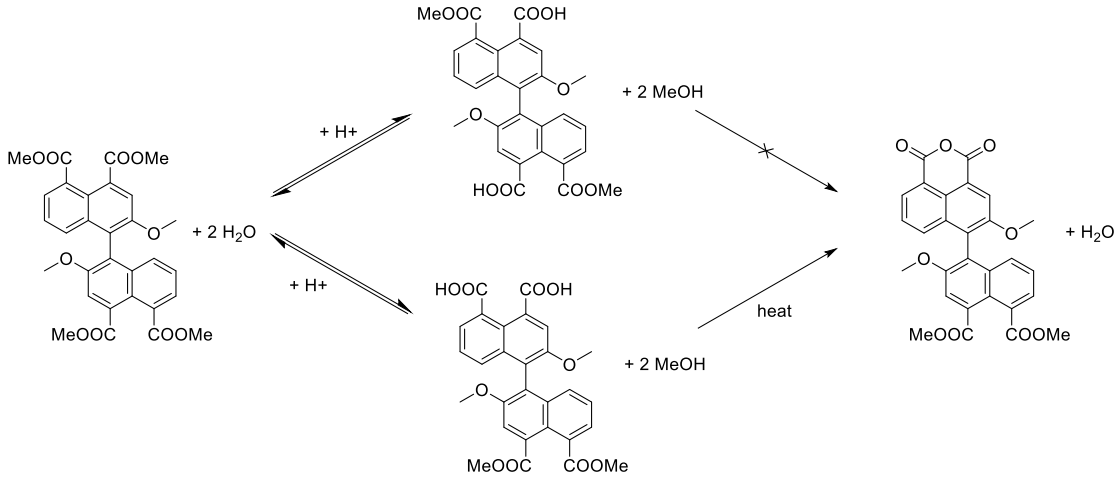

58 **57**

Scheme 59: Esterification-hydrolysis equilibrium of tetramethyl ester dimethylbinaphthol **58**.

A strategy to prepare selectively **57** and minimize the formation of derivative **144**, is based on performing acid hydrolysis reaction in a solvent that dissolves the tetramethyl ester **58**, but not the monohydride **57**. The precipitation of the monoanhydride **57** would decrease

the subsequent acid hydrolysis which promotes the formation of the dianhydride **144**. In order to selectively achieve the synthesis of **57**, several acids and solvents have been tested (Scheme 60, Table 9). As a first attempt, an acid hydrolysis of derivative **58**, was tried in the presence of *p*TsOH·H_2O in toluene under reflux for 16 hours yielding only **144** (Scheme 60 entry 1 Table 9). In a second attempt we submitted **58** to acid hydrolysis in a solvent where also the starting material is not soluble, in order to promote the precipitation of monoanhydride derivatives **57**. Therefore, tetramethyl ester **58** reacted in the presence of *p*TsOH·H_2O in hexane under reflux for 16 hours. This yielded a mixture of **57** and **144** together with unreacted starting material **53** (Scheme 60, entry 2 Table 9), determined by TLC analysis and mass analysis. Similarly, the same hydrolysis on tetramethyl ester **58** using cyclohexane under reflux for 22 hours provided a mixture of **57** and **144** in the presence of starting material as determined by TLC analysis (Scheme 60, entry 3 Table 9). We also tried to perform the reaction in a solvent that solubilizes the starting material **58**. Tetramethyl ester **58** in the presence of *p*TsOH·H_2O in $CHCl_3$ under reflux for 1 hour leads to a mixture of **57** and **144** (Scheme 60 entry 4 Table 9). Afterwards, tetramethyl ester **58** in the presence of a mixture of $HCl_{(aq)}$/ AcOH under reflux for 16 hours yielded the formation of traces **144**, in the presence of unreacted starting material **58** (Scheme 60 entry 5 Table 9). As a last attempt, we tried the acid hydrolysis of derivative **58** in the presence of CF_3SO_3H in toluene at room temperature yielding a mixture of derivative **57** and **144** (Scheme 60 entry 6 Table 9).

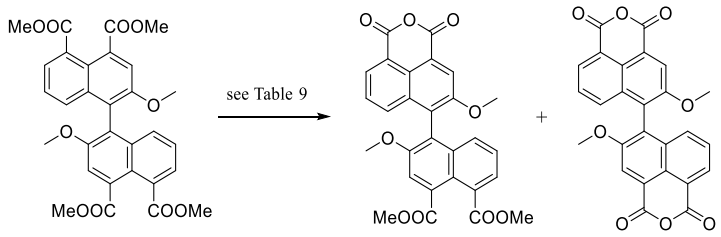

58 **57** **144**

Scheme 60: Attempts of acid hydrolysis of tetramethyl ester dimethylbinaphthol **53**.

Table 9: Tested reaction condition to perform acid hydrolysis.

Entry	Acid	Solvent	T [°C]	t [h]	Outcome*
1	*p*TsOH· H_2O	toluene	110	16	**144**
2		hexane	66	16	**57** and **144**
3		cyclohexane	81	22	**57** and **144**
4		chloroform	62	1	**57** and **144**
5	HCl(aq)	Acetic acid	118	16	**144**
6	CF_3SO_3H	toluene	RT	1	**57** and **144**

*** :** analysed by TLC.

Despite all attempts performed, no screened conditions allowed us to control the ester hydrolysis reaction; the first ester hydrolysis that allows the formation of mono anhydride diester-derivative **57** has always been followed by the subsequent acid ester hydrolysis that provides the dianhydride derivative **144**. The reason for the absence of selectivity in the hydrolysis process could be addressed by the comparable solubility of derivatives **58** and **57**. This feature prevents the selective precipitation of the desired derivative **57** in the solvents tested. (Scheme 60).

Subsequently, to achieve the synthesis of AB-type PXXDI the synthetic PATH B has been applied. Following this approach, a Suzuki cross-coupling has been performed between bromo derivative **135** and boron derivative **143** in the presence of K_3PO_4 and [$Pd(dba)_2$]/SPhos **104** in a solvent mixture dioxane/H_2O (5/1). The reaction afforded the key intermediate dimethyl ester-monoimide **143** in 59% yield (Scheme 61).

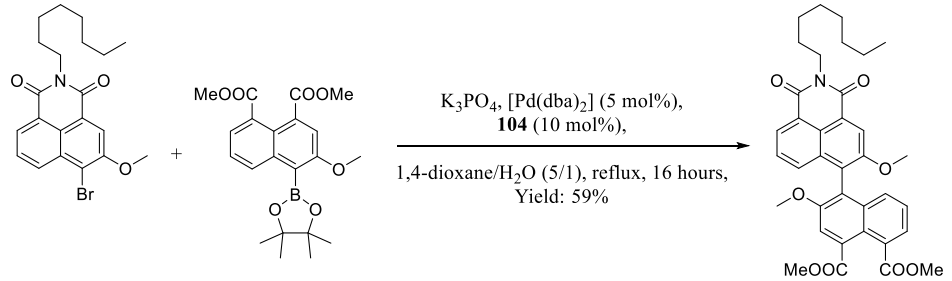

135 **143** **151**

Scheme 61: Synthesis of dimethyl ester-monoimide derivative **151** through Suzuki reaction**.**

Subsequently dimethyl ester-monoimide derivative **151** was transformed in dimethoxy monoimide monoanhydride **152**, by acid hydrolysis with TFA under reflux for 24 hours, in 87% yield. Afterwads, methoxy ether cleavages of derivative **152** in the presence of BBr_3 in CH_2Cl_2 afforded dihydroxy monoimide monoanhydride **153** in 99% yield (Scheme 62).[188]

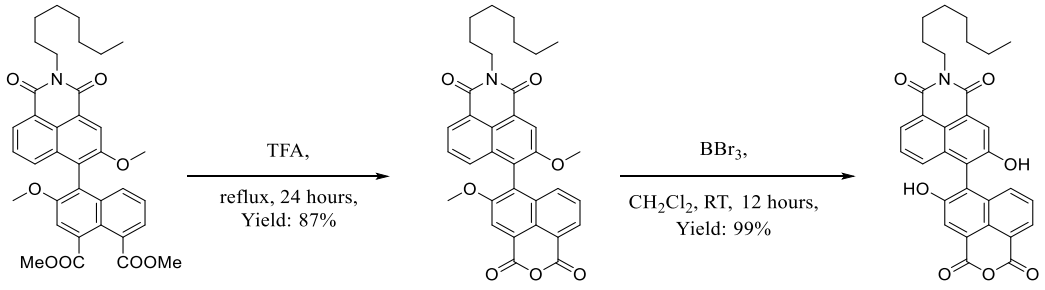

151 **152** **153**

Scheme 62: Synthesis of dihydroxy monoimide monoanhydride **153**.

Following, monoimide monoanhydride derivative **153** by imidisation reaction in the presence of 2,4,6-trimethylaniline, imidazole at 150 °C for 12 hours, afforded the AB-type *N*-subsistuted diimide **154** in 73% yield (Scheme 63). Eventually, final annulation of derivative **154** in the presence of CuI and PivOH in DMSO at 120 °C for 5 hours yielded. the AB-Type PXXDI **155** in 89% yield (Scheme 63).

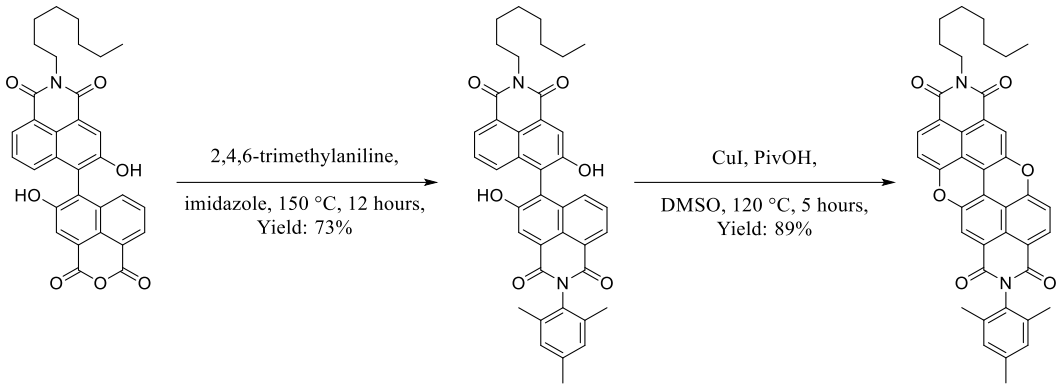

153 **154** **155**

Scheme 63: Synthesis of *N*-substituted AB-type PXXDI **155**.

2.6 Conclusion

Many attempts to prepare the PXXDI derivative starting from naphthalene hydroxy monoanhydride **44** were performed with different approaches for the C-C bond formation. The synthesis of the target molecules was achieved exploiting a Suzuki cross coupling reaction which was the only synthetic strategy that allowed us to obtain the key intermediate **136**. Reaction conditions were optimised, leading to the formation of the product in 49% yield. Applying the already developed protocol for cyclic diaryl ether formation based on transition metal catalysis, the formation of the desired perylene diimide was then successful.

In conclusion, the first derivative *N*-substituted A_2-type PXXDI has been prepared following the synthetic pathway B with an overall yield of 34%. After that, a more general synthesis for the preparation of PXXDI A_2-type **141** was performed. The main drawback of the first synthetic strategy was the preparation of the imide moiety in the early stage of the synthesis, which forced to perform all the synthetic steps for each desired PXXDI A_2-type. To overcome this issue, a new synthetic pathway where the imide formation takes place in the latest stage of the synthesis was developed. The synthesis of the key intermediated binaphthol bisanhydride **43**, which was obtained with PATH A could potentially be converted in binaphthol bisimide and eventually be cyclised to PXXDI. Despite the fact that this second strategy needs further optimization, it represents a more flexible synthetic pathway for the preparation of PXXDI A_2-type.

Subsequently, the synthesis of PXX monoimide has been achieved following the synthetic PATH A, performing a Suzuki coupling reaction that led to the formation of monoimide

binaphthol **146** in 96%, followed by methoxy group deprotection and final cyclic diaryl ether formation, providing the desired octyl PXXMI **148** with an overall yield of 72% over 6 steps, starting from the commercially available 3-hydroxy naphthalene monoanhydride **44**. Similarly, to the PATH B for the synthesis of PXXDI A_2-type, this strategy is also affected by the main drawback of the formation of the imide moiety in the early stage of the synthesis. With the aim to develop a higher yielding process that provides a more convenient synthetic pathway for the preparation of PXXMI library, a novel strategy based on Suzuki coupling on dimethyl ester methoxy bromo naphthalene **142** with methoxy naphthalene boronic acid **145** was developed, affording the dimethyl ester binapthalene **51**, which is then converted into the key intermediated binaphthol anhydride **150**. Several cyclization attempts were performed on binaphthol anhydride **50** to obtain PXXMI, which represents the most flexible scaffold for the PXXMI derivatives' preparation. Attempts to obtain PXXMI afforded insoluble derivatives as products, which after imide formation were converted to octyl PXXMI **144** with a yield of 10%. For this reason, binaphthol monoanhydride **50** has been conveniently converted by naphthol monoimide **147**. The latter can be further functionalised with a high yielding process into octyl PXXMI **148** with an overall yield of 56% over 6 steps. Moreover, Suzuki coupling reactions swapping the reacting partners were investigated performing the Suzuki cross coupling reaction on 1-bromomethoxy-2-naphthalene with the dimethyl ester naphthalic boronic ester derivative **143** affording the formation of dimethyl ester binaphthyl **51** in 96% yield.

Finally, the synthesis of *N*-functionalised AB type PXXDI by the preparation of dimethyl ester, dimethoxy monoanhydride dinaphthalene **57** was approached. However, all the screened conditions did not provide the selective formation of derivative **57**. For this reason, taking advantage from the already optimised Suzuki cross coupling conditions in the synthesis of PXXDI A_2-type path A, such reactions were performed on a bromomethoxy naphthalene imide **135** with the aforementioned dimethyl ester napthalic boronic ester derivative **143**, which provided the monoimide dimethyl ester binaphthyl derivative **151** in 59% yield. Afterwards dimethyl ester derivative **151** by stepwise acid hydrolysis afforded the key intermediates binaphthol **153**. This last imidisation and final cylcization provides the *N*-functionalised AB-type PXXDI **155**.

Chapter 3. Study of the photoredox properties

3.1 Overview

The chapter is divided into 4 sections: *i*) section 3.1. introduces the basic principles of photoredox catalysis; *ii*) section 3.2 studies the optoelectronic properties of PXX derivatives; *iii*) in section 3.3 the application of PXXs as photocatalytic agents are explored; *iv*) finally section 3.4 presents the investigation on the photocatalytic mechanism of PXX derivatives.

The results reported in this chapter are obtained in collaboration with *Dr. Andrea Fermi*, *Dr. Joseph M. Beames* and *Mr. Tommaso Battisti* from *Cardiff University* for UV/vis absorption and emission spectroscopy investigations, *Dr. Andrea Folli* and *Prof. Damien M. Murphy* from *Cardiff University* for EPR investigations.

Part of the results reported in this chapter have been published in *Chemistry A European Journal.* **2018**, *24*, 4382-4389.[109]

3.2 Excited states

An electronic state comprises of a set of closely spaced vibrational energy levels. In the electronic ground state as well as in the excited states, all molecules display a variety of nuclear geometries resulting from bond stretches or deformations, each of which corresponds to a unique vibrational frequency. The lowest vibrational frequency level, called the zero-point level, is normally populated. Photoexcited states are generally the result of a transition from the lowest vibrational level of the electronic ground state to a higher-energy electronic level *via* a vertical transition (*Franck-Condon* principle).

An excited state is rich in energy and corresponds to a reactive species. It can be defined as a singlet[a] (S_i) or triplet[b] (T_i) according to its spin multiplicity. After initial population of higher excited singlet states, the system often relaxes rapidly (10^{-11} – 10^{-13} s) to the lowest energy excited state, which is a "stable'' excited state that can undergo a photochemical reaction.

In view of the matters treated in this section, a concise discussion of the various possible relaxation pathways follows. Excited state relaxation pathways can be classified in two main categories, *i*) radiative (*i.e.*, transitions from higher-energy to lower-energy states with emission of light) and *ii*) non-radiative (*i.e.*, transitions from higher-energy to lower-energy states with release of translational, vibrational, and rotational energy). Fluorescence is a radiative relaxation pathway consisting of the emission of light related to a transition from the lowest vibrational level of an electronic excited singlet state to any of the vibrational levels of the electronic ground state. Phosphorescence is another radiative pathway that consists of an emission of a photon accompanying a transition between two states of different multiplicity, for example, between T_1 and S_0. Due to the fast relaxation of the vibrational excited states, both types of emission always originate from the lowest vibrational level of the excited states. Both emission processes are identified by a rate constant (k_i), by the energy of the released photons (hn_i), and by a quantum yield (f_i)

[a] A singlet state (S_i, with *i* indicating the labelling of the excited state) is, by definition, an electronic state in which the spins of the electrons are antiparallel or paired. "Singlet" designates the multiplicity of the state which is given in general by the well-known equation:

$m = 2S + 1$ (3.1)

where *m* is the multiplicity and *S* the total spin of all electrons. For example, for a molecule in the ground-state, with only paired electrons, S = 0 and m = 1.

[b] A triplet state (T_i) is an electronic state in which the spins of two electrons are parallel.

defined as the ratio between the number of photons emitted and the number of photons absorbed. If the ground state and excited state have identical multiplicity and if the vibrational levels of the two states are similar in energy, the fluorescence spectrum corresponds to the mirror image of the absorption spectrum. However, the emitted radiation is usually lower in energy than that of the excited state and, therefore, the emission spectra are slightly shifted towards lower energies in comparison to the absorption spectra. The difference between emission and absorption wavelength is called *Stokes shift* and it provides an indication for the structural distortion between the ground and the excited state. Phosphorescence spectra are further shifted in comparison to fluorescence spectra due to the fact that the energy of the triplet state is generally lower than that of the corresponding excited singlet state. The lifetimes are also quite different: the fluorescence lifetimes[c] are rather short (10^{-10}-10^{-6} s) whereas the phosphorescence lifetimes are comparatively long, ranging from 10^{-6} to 10 s.

3.2.1 Quenching pathways

In addition to the radiative and non-radiative transitions described in the previous section (**3.2**), the excited states can participate in numerous other inter- and intramolecular reactions. These processes include *i*) addition reactions in which the excited state species combine with a ground state molecule to form a stable product; *ii*) hydrogen abstraction; *iii*) energy transfer (EnT) whereby energy is transferred from the excited state to the ground state of another species; *iv*) electron transfer (ET) in which the excited state species act as an electron donor or acceptor in its interaction with species that are ground state.

Energy and electron transfer, generically called quenching mechanisms, are deactivation pathways taken by an excited species and involving an external component (quencher), which can be supramolecularly or covalently attached *via* a rigid or flexible spacer. The characteristics of the excited state and its decay pathways can be selectively tuned as a

[c] The lifetime τ of an excited state is, by definition, the time necessary for the concentration of the excited state species to diminish to $1/e$ of its initial value as a result of the deactivation process. The decrease of the concentration of the excited state (ES) species over time is given by equation *3.3*:

$$-\mathrm{d[ES]} / \mathrm{d}t = \Sigma k_i[\mathrm{ES}] \qquad (3.2)$$

where [ES] is the concentration of the ES species at time t and k_i is the first-order rate constant of the deactivation process i. The lifetime τ is thus given by equation *3.3*:

$$\tau = 1 / \Sigma k_i \qquad (3.3)$$

function of the environment, spacer, and molecular structure. Quenching mechanisms usually generate reactive intermediates that rapidly undergo transformation to more stable products. In the case of energy transfer, the quencher itself becomes excited and subsequently undergoes the same chemical and/or physical processes as if it had been excited directly by light. The energy transfer mechanism is schematically illustrated by the following equation (*5.3*):

$$\mathbf{D^*} + \mathbf{A} \xrightarrow{k_{EN}} \mathbf{D} + \mathbf{A^*} \qquad (5.3)$$

where k_{EN} is the rate constant of energy transfer and **D** and **A** are the energy donor and acceptor, respectively.

Similarly, in the photoinduced electron transfer process, the excited state species can act as energy donor (**D**) or acceptor (**A**). The photoinduced electron transfer mechanism can be illustrated by the following photoreaction schemes (*6.3* and *7.3*):

$$\mathbf{D}^n + \mathbf{A}^m + h\nu \longrightarrow \mathbf{D}^{n*} + \mathbf{A}^m \xrightarrow{k_{ET}} \mathbf{D}^{n+1} + \mathbf{A}^{m-1} \qquad (6.3)$$

or

$$\mathbf{D}^n + \mathbf{A}^m + h\nu \longrightarrow \mathbf{D}^n + \mathbf{A}^{m*} \xrightarrow{k_{ET}} \mathbf{D}^{n+1} + \mathbf{A}^{m-1} \qquad (7.3)$$

Where k_{ET} is the rate constant of electron transfer, $h\nu$ the energy necessary to excite the species, and m and n indicate the original charges of the molecules in their ground states. An electron transfer can also occur without photoexcitation; this case corresponds to a ground state electron transfer, *i.e.*, a standard redox reaction. A photoinduced electron transfer between two neutral reagents (n = m = 0) initially results in an ion pair of oxidized donor and reduced acceptor which is often called a charge-separation state. The ion pair is usually constituted of radical cation $\mathbf{D}^{\bullet+1}$ and anion $\mathbf{A}^{\bullet-1}$.

3.2.1.1 Classic Examples of Quenching

One of the most common examples of energy transfer process is the quenching of the excited state by O_2. The quenching of the excited singlet (S_i) and triplet (T_i) states has been investigated for a wide variety of compounds such as aliphatic hydrocarbons,[192] polycyclic aromatic hydrocarbons[193] and also charged aromatic compounds.[194] An example of the quenching of an electronically excited triplet state is represented by anthracene (^{3}**Ant**), which interacts with the ground state of $^3O_2$ leading to the formation of the excited state of singlet $^1O_2$* and regenerating the ground-state sensitizer.

$$^3\mathbf{Ant^*} + O_2(^3\textstyle\sum_g^-) \longrightarrow \mathbf{Ant} + O_2(^1\Delta_g)^*$$

Considering the photoinduced electron transfer where the fluorophore in the excited state acts as an electron donor an example is the quenching of the carbazole (**Carb**) fluorescence by trichloroacetic acid (**TCA**).[195] In 1980, Johnson studied the quenching of the fluorescence of carbazole derivatives in presence of electron deficient trichloromethyl quenchers.[195]

$$\mathbf{Carb}^* + \mathbf{TCA} \longrightarrow \mathbf{Carb}^{\bullet+1} + \mathbf{TCA}^{\bullet-1}$$

From this study emerged that the fluorescence quenching rate is depending on the electron acceptor strength of the quencher and on the ionization potential of the carbazole derivatives. Based on these experimental evidences, it has been postulated that the quenching mechanism relies on electron transfer from the excited state of the fluorophore to the quencher, resulting in the formation of a radical pair $\mathbf{Carb}^{\bullet+1}$and $\mathbf{TCA}^{\bullet-1}$.

Regarding the photoinduced electron transfer, a typical example is the quenching of anthracene (**Ant**) fluorescence by diethylaniline (**DEA**), where the fluorophore in the excited state is the electron acceptor.[196] In 1967, Weller and co-workers studied the quenching of anthracene fluorescence upon addition of diethylaniline in several solvents with different polarity.[196]

$$^3\mathbf{Ant} + \mathbf{DEA} \longrightarrow \mathbf{Ant}^{\bullet-1} + \mathbf{DEA}^{\bullet+1}$$

Transient absorption spectroscopy showed that in polar solvents occurs the formation of the radical pair **Ant**$^{\bullet-1}$ and **DEA**$^{\bullet+1}$. The authors postulated the formation of a solvent shared ion pair, in which the non-fluorescent radical ions are solvated. The solvation of the radical ion pair is strongly dependent on the solvent polarity; the increase of the dielectric constant of the solvent leads to an enhancement of the stabilisation of the radical ion pair.

3.2.2 Stern-Volmer equation

Fluorescence quenching refers to any process that decreases the intensity of fluorescence; typical molecular interactions that induce quenching are excited-state reactions, molecular rearrangements energy transfer, ground state complex interaction and collisional quenching. When a quenching occurs, the concentration of the excited state is reduced more rapidly than if the quencher Q was not present. Subsequently, the fluorescence, which depends on the concentration of the excited state, decreases. So, in addition to the intramolecular process of decay of the excited state M*, a bimolecular process between M* and the quencher Q has to be considered. The rates of the processes are described as:

		Rate
$M \longrightarrow {}^1M^*$		I_{abs}
${}^1M^* \longrightarrow M + h\nu_f,$		$k_f[{}^1M^*]$
${}^1M^* \longrightarrow {}^3M^* + \text{heat}$		$k_{isc}[{}^1M^*]$
${}^1M^* \longrightarrow M + \text{heat}$		$k_{ic}[{}^1M^*]$
$M^* + Q \longrightarrow M + Q$	quenching	$k_q[{}^1M^*]\,[Q]$

Among the quenching processes, we can mention the collisional quenching. This process takes place when a molecule in the excited state M* is deactivated by contact with another molecule in solution, which is called the quencher (Q). The deactivation of M* occurs during a diffusive encounter with the quencher.

The collisional quenching is described by the Stern Volmer equation:

$$\frac{F_0}{F} = 1 + K[Q] = 1 + k_q \tau_0 [Q]$$

where K is the Stern-Volmer quenching constant, k_q is the bimolecular quenching constant, τ_0 is the lifetime in absence of quencher and [Q] is the concentration of the quencher. F_0 is

the intensity of fluorescence in absence of the quencher and *F* is the intensity in presence of the quencher. The Stern Volmer constant *K* indicates the sensitivity of the molecule in its excited state M* towards the quencher Q. Considering the collision quenching, the quencher has to diffuse to interact with the molecule in its excited state during the lifetime of the excited state.

3.3 Application of photoredox system in organic transformations

Molecules in the excited state are reactive species, therefore the use of the light represents a convenient way to activate organic molecules to perform the organic transformations. This is possible because the light absorption promotes one electron from a lower energy orbital (HOMO) to a higher energy orbital (LUMO). As a consequence, the electron promoted to a higher energy orbital is easier to be removed. Therefore, a molecule in an electronically excited state has a smaller ionization potential and is more easily oxidized.[197] Nevertheless, the orbital lower in energy is half occupied and this electron vacancy can accept an electron, corresponding to a higher electron affinity regarding its ground state creating an easier reductive process. Based on this principle, a molecule can convert the energy of the light in chemical energy by single electron transfer to organic substrates, generating reactive intermediates.

3.3.1 Photoredox system in inorganic transformations

In the sixties, Crosby and co-workers reported the spectroscopic properties of Ir(III) and Ru(II) complexes with bipyridyl- type ligand.[198] In 1972, Gafney and Adamson mentioned the reductive electron transfer of $[Ru(bpy)_3]^{2+}$* to $[Co(NH_3)_5Cl]^{2+}$.[199]

$$[Ru(bpy)_3]^{2+}* + [Co(NH_3)_5Cl]^{2+} \longrightarrow [Ru(bpy)_3]^{3+} + [Co(NH_3)_5Cl]^{+}$$

This discovery was a milestone in modern photochemistry, because electron transfer from excited states were not common at this time. Several research groups started to study $[Ru(bpy)_3]^{2+}$* as a reactant and demonstrated the ability of this ruthenium complex to be used in visible light photocatalyst applications such as water splitting[200] and reduction of carbon dioxide to methane.[201] Furthermore, ruthenium complexes find application in dye-sensitized solar cells[202] and organic light emitting diodes.[203]

3.3.2 Photoredox system in organic transformations

The photoredox system is one of the most important process in photochemistry.[204] In particular, it received great interest in visible light induced photo-catalysis.[205] In fact, this approach envisages the catalytic activation of organic molecules exploiting the ability of a system in electronic excited state to perform a single electron transfer (SET) on organic substrates.[206] Among the metal complexes suitable to promote the photo electron transfer, the most commonly employed visible light photocatalysts are polypyridyl complexes of Ru(II) and Ir(III). In 2008, MacMillan and co-workers reported the direct asymmetric alkylation of aldehydes exploiting photoredox catalysis with organocatalysis.[207] The enantioselective catalytic α-alkylation of aldehydes has been achieved treating the aldehydes with an α-bromocarbonyl derivative in the presence of an amine as organocatalyst and $[Ru(bpy)_3]Cl_2$ as photoredox catalyst, upon irradiation, with white light (Scheme 64).

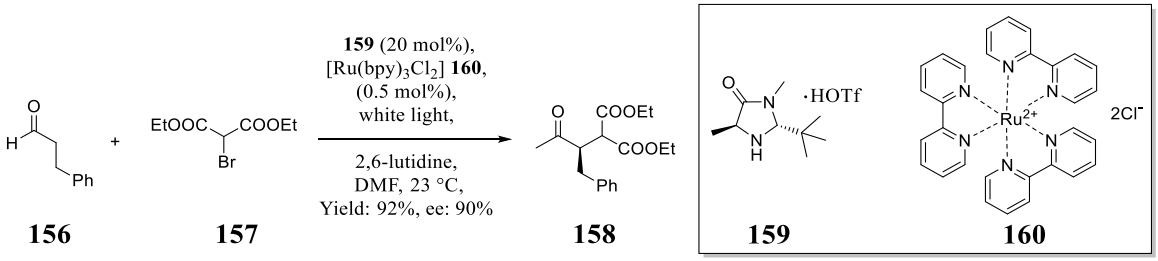

Scheme 64: Enantioselective catalytic α-alkylation of aldehydes

The reaction relies on dual-catalysis: the organocatalysis and the photoredox catalysis. The first is based on the formation of an electron rich enamine from the condensation of an aldehyde with an imidazoline catalyst. Although $[Ru(bpy)_3]^{2+}$* can behave as reductant and oxidant, the authors postulated that, as first step of the photocatalytic cycle, the excited state of Ru(II) is reduced by electron transfer to Ru(I) from a sacrificial quantity of enamine to initiate the catalytic cycle. The so-formed Ru(I) promotes the formation of the electron deficient alkyl radical through a SET to bromocarbonyl derivative, restoring the Ru(II) catalytic species.

The newly formed alkyl radical reacts with the electron rich enamine achieving the alkylation and affording the electron-rich α-amino radical, which *via* electron transfer can be oxidized by Ru(II)*, providing the formation of the iminium derivative and the reducing agent Ru(I) that can continue the catalytic cycle (Scheme 65).

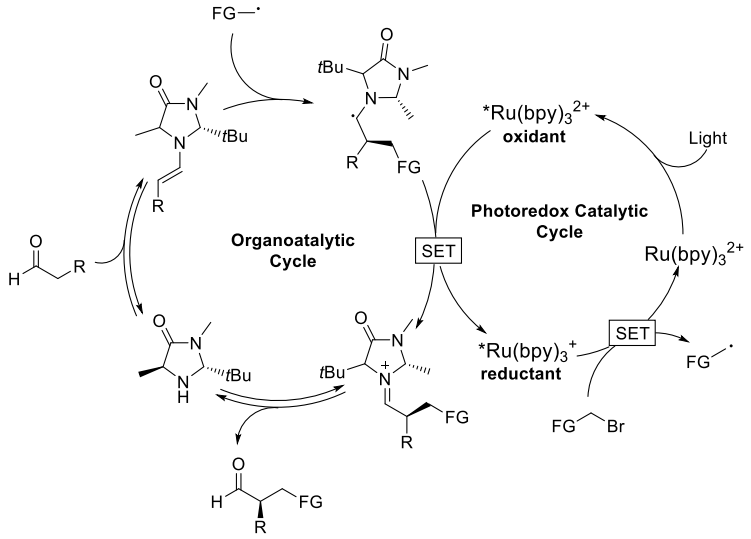

Scheme 65: Mechanism of enantioselective catalytic α-alkylation of aldehydes.

In 2011, MacMillan and co-workers reported a direct arylation of α-amino C-H bonds.[208] The reaction has been performed on 1-phenyl-pyrrolidine in presence of cyanoarenes, as arylating agent, with [Ir(ppy)$_3$] **164** as photocalyst and NaOAc as base in DMA, upon irradiation with white light. The reaction afforded α-arylamine (Scheme 66).

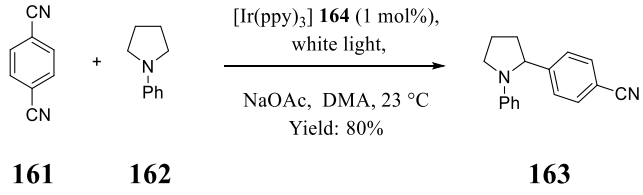

161 **162** **163**

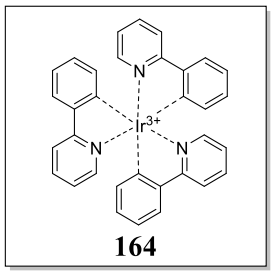

164

Scheme 66: Photoredox catalytic arylation of amine in α-position.

The proposed mechanism from the authors is based on the: initial reduction of the cyanoarene by the excited state of [Ir(ppy)$_3$] giving the aryl radical anion and the Ir(IV) state of the photocatalyst. The Ir(IV) species can readily oxidize 1-phenyl-pyrrolidine, and the resulting radical cation is deprotonated by NaOAc to generate the α-amino radical. The coupling between the aryl radical anion and α-amino radical followed by elimination of cyanide, generates the benzylic amine products. This protocol has been applied to a wide range of arenes and heteroarenes (Scheme 67).

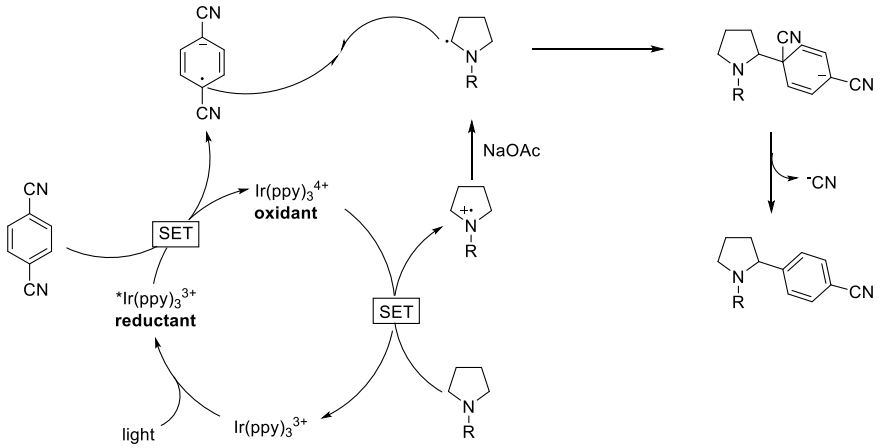

Scheme 67: Mechanism of photoredox catalytic arylation of amine in α-position.

Photoredox chemistry of transition metal complexes has been widely studied until today, with the most outstanding examples being Ru and Ir complexes. However, these complexes are based on rare and toxic metals so alternative photoinitiators have been explored. Consequently, organic chromophores have already been studied to promote photoinduced electron transfer (PET), but they have been exploited as photocatalytic agents only recently. The main advantage of organic photocatalysts over their transition metal counterparts is the variety of systems that can be exploited as photoredox catalysts, such as pyryliums, acridiniums, xanthenes, thiazenes and perylene diimide.[204a] Morever the chemical functionalization of those systems allows tuning of the redox properties of the photocatalyst.[209]

In 2015, König and co-workers reported the reductive photodehalogenation on activated aryl-halides (-I; -Br and -Cl) and also arylation of methylpyrrole in α-position exploiting commercially available perylene diimide (PDI) **168** as photocatalyst (Scheme 68).[210]

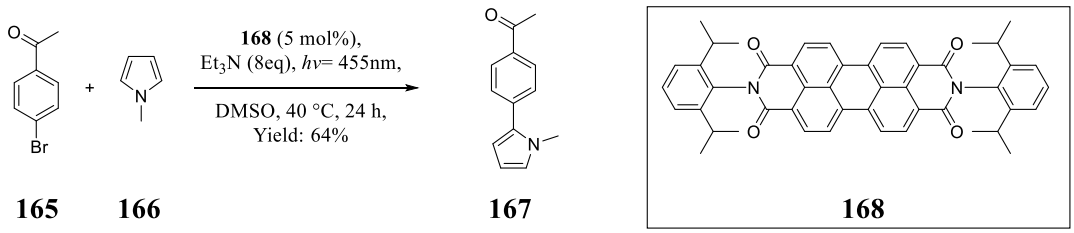

165 **166** **167** **168**

Scheme 68: Organo photoredox catalytic arylation of methyl pyrrole in α-position.

The proposed mechanism is based on two photoinduced electron transfers: the excited state of the PDI* **168** is at first reductively quenched by Et_3N yielding the formation of the

radical cation $Et_3N^{\bullet+}$ and radical anion $PDI^{\bullet-}$. The second excitation results in the formation of the excited state of radical anion ($PDI^{\bullet-*}$), which through single electron transfer to aryl-halides promotes the formation of aryl-halide radical ($Ar\text{-}X^{\bullet-}$) and restores the neutral PDI. Subsequently, the aryl radical anion leads to the formation of the aryl radical ($Ar^{\bullet}$) *via* fragmentation, which can react with methylpyrrole (Scheme 69).

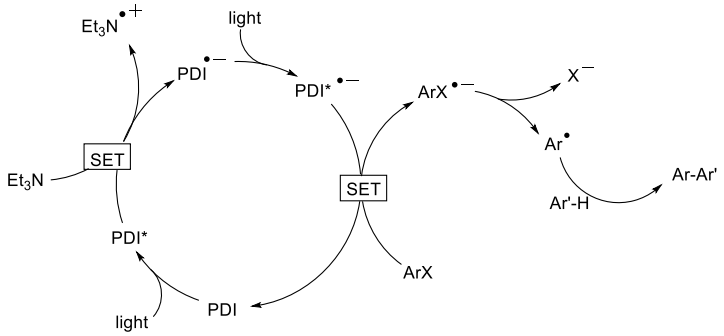

Scheme 69: Mechanism of organo photoredox catalytic arylation of amine in α-position**.**

In 2015, Read de Alaniz and co-workers reported the reductive photodehalogenation of aryl halide exploiting 10-phenylphenothiazine **172**, Scheme 70.[209] More recently, the same group described a chemoselective photoinduced dehalogenation (Scheme 70, Table 10). This result was achieved exploiting already mentioned 10-phenylphenothiazine **172** and tris-acetyl phenylphenothiazine **173**. The introduction of the three acetyl moieties affects the excited state reduction potential, tuning the redox properties of the two chromophores.[211]

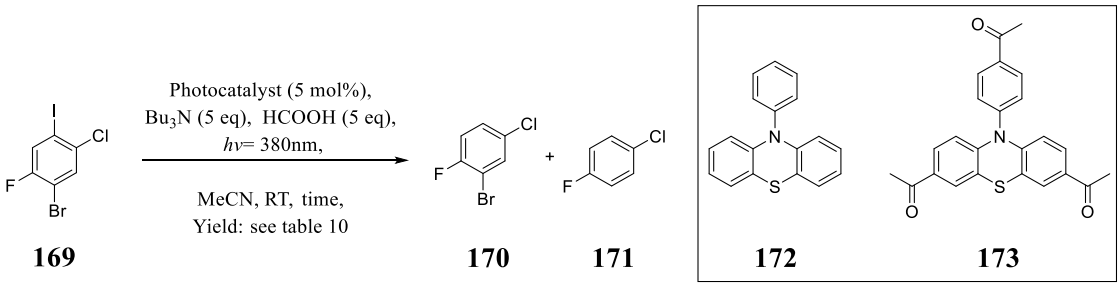

Scheme 70: Chemoselective photoinduced dehalogenation of **169**.

Table 10: Reaction condition for chemoselective dehalgenation of **169**.

Entry	Photocalyst	Time[h]	Yield of 170 [%]	Yield of 171 [%]
1	**172**	48	5	90
2	**173**	5	96	4

In 2016, König and co-workers reported a selective and sequential C-H arylation through light-colour regulation of redox potential of the photocalyst.[212] They reported the selective and sequential functionalization of 2,4,6-tribromopyrimidine **174** with 1,3,5-trimethoxybenzene and *N*-methylpyrrole. The reactions have been achieved in the presence of rhodamine-6G (Rh-6G) **177** as photocatalyst and DIPEA as sacrificial electron donor in DMSO as solvent, by changing the light source from green to blue (Scheme 71).

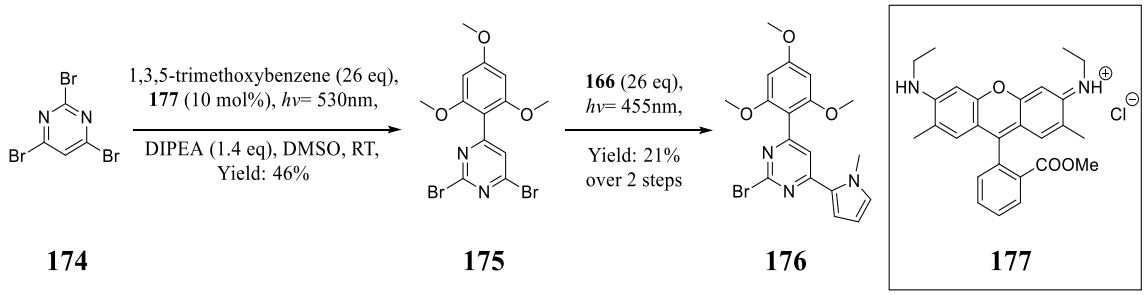

Scheme 71: Chromoselective organo photoredox reactions.

This sequential and selective reaction is possible because, upon irradiation with green light ($h\nu$=530 nm), Rh-6G **177** in the presence of DIPEA yields the formation of the radical anion of Rh-6G$^{\bullet-}$ in the ground state. Rh-6G$^{\bullet-}$, *via* electron transfer to 2,4,6-tribromopyrimidine **174**, promotes only the formation of dibromopyrimidyl radical which, reacting with 1,3,5-trimethoxybenzene, yields derivative **175**. Upon irradiation with blue light ($h\nu$=455 nm) the radical anion of Rh-6G is formed and excited. Rh-6G$^{\bullet-}$*, being a stronger reductant, can then promote the photoinduced electron transfer on pyrimidil derivatives **175**, yielding the formation of bromopyrimidyl radical. The latter reacts with methyl pyrrole affording derivative **176**. The sequential and selective arylation is based on the difference in the redox properties of Rh-6G$^{\bullet-}$ and Rh-6G$^{\bullet-}$* (Scheme 72).

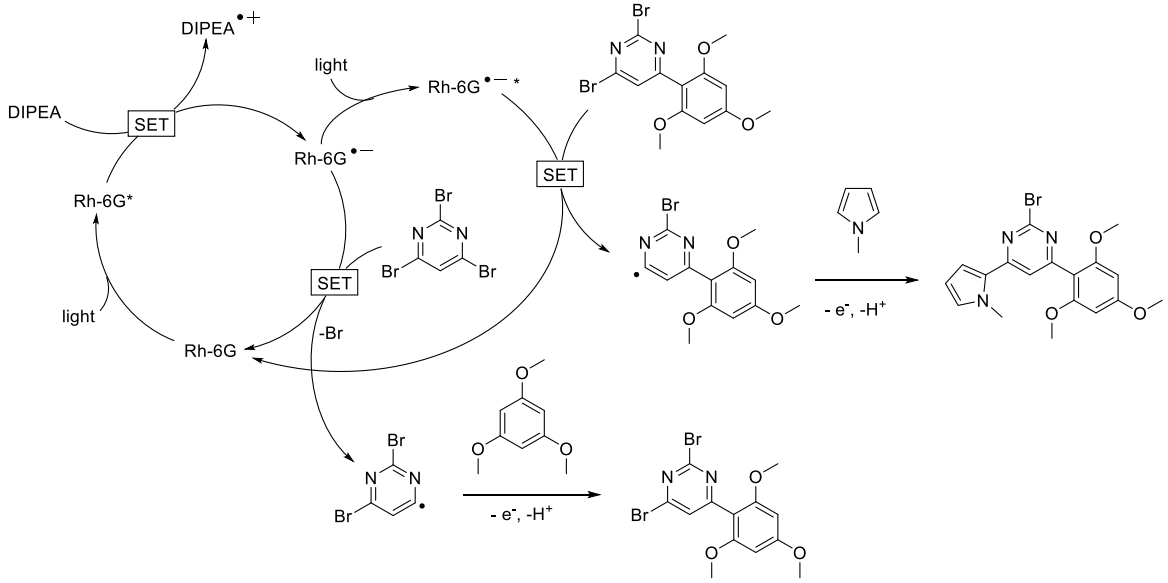

Scheme 72: Mechanism of selective and sequential of organo photocatalytic arylation.

In the last decade, the photoredox transformations have been demonstrated to be active in a wide range of organic transformations such as: *i*) carbon-carbon bond formation including three-,[213] four-,[214] five-,[215] and six member rings;[216] *ii*) carbon-heteroatom bond formation such as aromatic amination[217] and C-O bond formation;[218] *iii*) decarboxylative coupling reactions.[219]

Photoredox reactions have been successfully applied to $C(sp^3)$-$C(sp^3)$ bonds formation.[220] However also the $C(sp^2)$-$C(sp^3)$ bonds formation has been achieved. As example we can mention the Meerwein arylation,[221] which involves an aryl diazonium salt reduced by metal to aryl radical which reacts with an olefin yielding an alkyl radical which can give further reactions with a third reagent.[221] The photocatalytic reduction of the diazonium salts represents an alternative to redox-active metal. In 2012, König et al. reported photocatalysed α-arylation of enol acetates by reducing 4-nitrobenzenediazonium tetrafluoroborate **178** in presence of Ru photocatalyst (Scheme 73).[222]

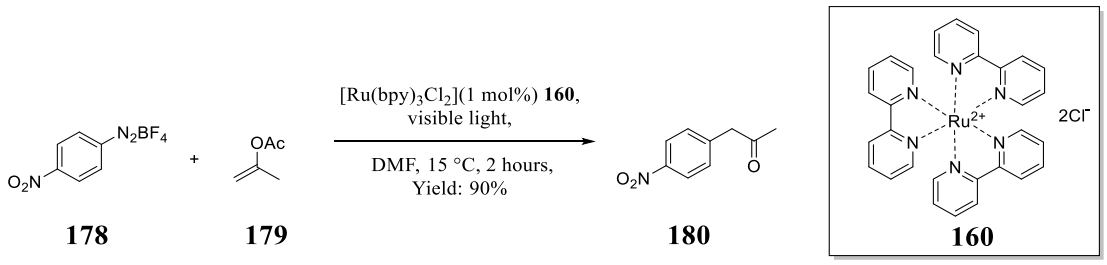

Scheme 73: Visible light α-arylation of enol acetates using 4-nitrobenzenediazonium salt **178**.[222]

The reduction of aryldiazonium salt **178** by $[Ru(bpy)_3]^{2+}$* generates the aryl radical and $[Ru(bpy)_3]^{3+}$. The addition of the aryl radical on the enol acetate **179**, affords a radical intermediate which is oxidized by $[Ru(bpy)_3]^{3+}$ to form an aryl carbocation intermediate. The aryl carbocation yields the product **180** through an acyl cation transfer to a nucleophile, e.g. solvent.[222]

Aryldiazonium salts have been used also for photocatalytic C(sp^2)-X cross-coupling reactions.[223] König and co-workers used aryldiazonium salts to perform C-H arylation on heteroarenes using eosin Y as photoredox catalyst irradiated with green light.[224] The protocol has been applied to couple 4-nitrobenzenediazonium tetrafluoroborate **178** with the furan **181** yielding the cross-coupling product derivative **182** in 85% yield (Scheme 74).[224]

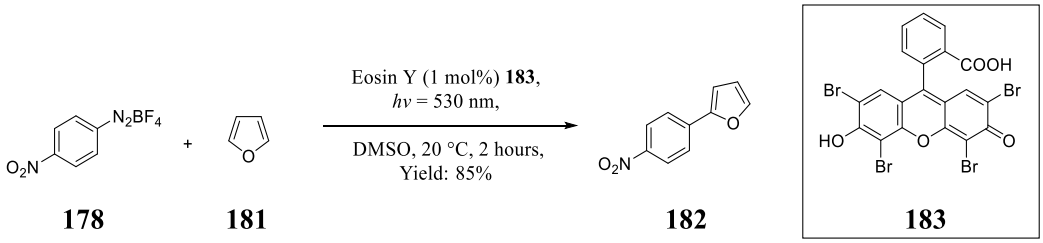

Scheme 74: Visible light C-H arylation on furan **181** 4-nitrobenzenediazonium salt **178**.[224]

Aside the already mentioned heteroarene derivatives, also unsaturated molecules such as the acetylenes are convenient trapping reagents for the aryl radical. König an co-workers applying a similar protocol to the aforementioned one, performed the photocatalytical radical annulation of 2-methylthioarendazonium salt derivative **184** with phenylacetylene **185** in the presence of eosin Y **183** as photocatalyst upon irradiation with green light providing the desired benzothiophenes **186** in good yield (Scheme 75).[225] The method is compatible with electron-donating or withdrawing groups on the arendiazonium salts and as well the mono- and disubstituted acetylenes, providing the desired benzothiophenes in moderate to good yield.[225]

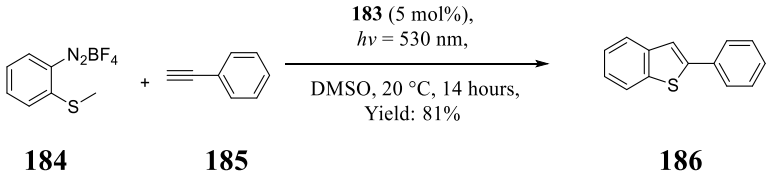

Scheme 75: Visible light photocatalytic synthesis of benzothiophene derivative **186**.

In addition, the photoredox catalysis has been applied to carbon-carbon bond formation to achieve the six-member ring formation. In 2013, Yu and co-workers reported the synthesis of polysubstituted naphthols by coupling 2-bromo-1,3-dicarbonyl derivatives with alkynes through photoredox reaction in the presence of iridium catalyst under irradiation (Scheme 76).[216]

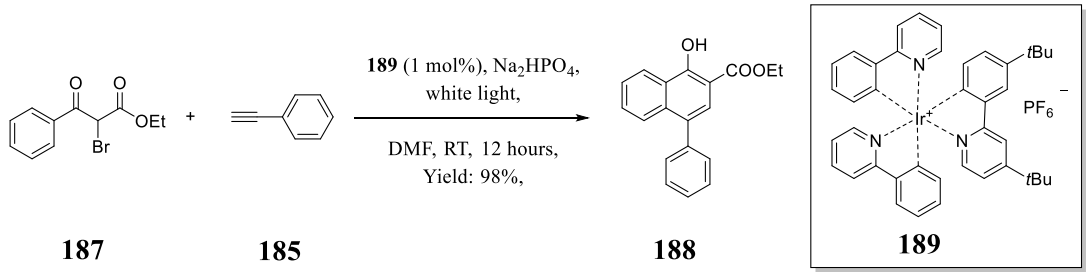

187 **185** **188** **189**

Scheme 76: Photoredox coupling of 2-bromo-1,3-dicarbonyl derivative **187** with phenylacetylene **185**.

The reaction is based on the Ir(III) phototriggered reductive dehalogenation of 2-bromo-1,3-dicarbonyl derivative **187** that yields a radical which reacts with the alkyne derivative **185** in a two steps radical process and subsequent oxidation mediated from Ir(IV) complex affords the naphthol derivative **188**. The authors report also a variation of the previous protocol that allows to prepare also polysubstituted furans, replacing the bromo-aryl ketones with a bromo-alkyl ketone such as ketone derivative **191**. The photoinduced radical reacts with alkyne **185** in a two-step radical process involving the oxygen of the carbonyl yielding the furan derivative **191** (Scheme 77).[216]

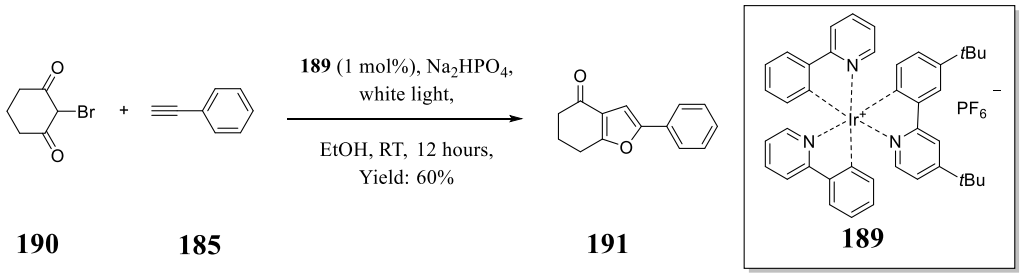

190 **185** **191** **189**

Scheme 77: Photoredox coupling of 2-bromo-1,3-dicarbonyl derivative **189** with phenylacetylene **185**.

An additional example of carbon-heteroatom bond formation is the C-S formation. The Stadler Ziegler reaction[226] relies on the conversion or arylamines into diazonium salt, which reacts with thiolates to yield aryl sulfides (Scheme 78a). In 2013, Wang, Cuny and Nöel developed the photocatalytic version of the Stadler Ziegler reaction (Scheme 78b).[227]

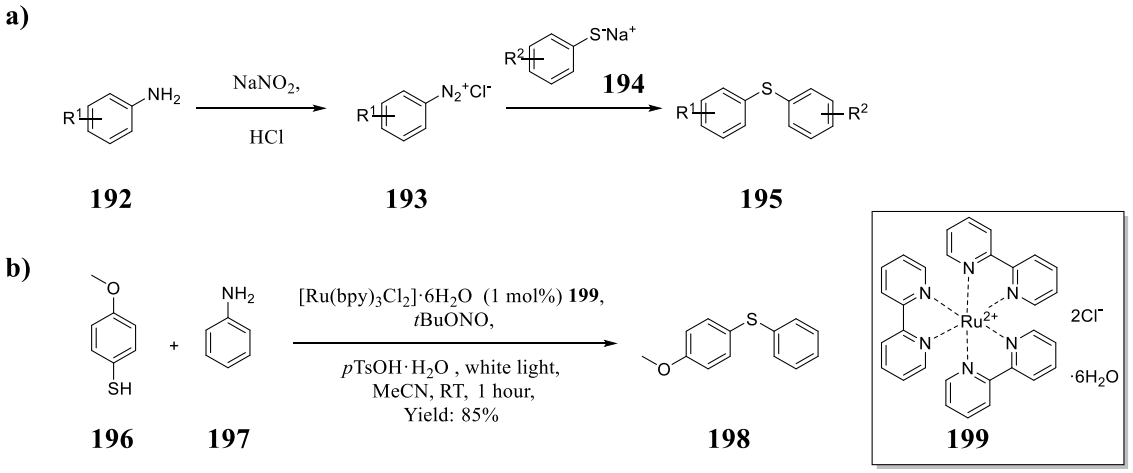

Scheme 78: a) Stedler-Ziegler reaction; b) Photoredox Stadler-Ziegler aryl sulfide synthesis.

The optimised process is one-pot reaction where the aniline **197** in presence of a *tert*-butyl nitrite is converted into aryldiazionium salt. Which upon irradiation in the presence of $[Ru(bpy)_3Cl_2]\cdot 6H_2O$ **199** is photoreduced to yield the aryl radical that is trapped by the 4-methoxybenzenethiol **196** affording the formation of the radical anion of diarylthioether. The latter is oxidised by $[Ru(bpy)_3]^{3+}$ to the diarylthioether **198**. In 2013, an additional approach has been reported by von Wangelin et al. reporting the photocatalytic formation of aryl methyl sulfide. In the developed protocol 4-methoxy aryldiazonium derivative **200** reacts with dimethylsulfide upon irradiation with green light in presence of eosin Y **183** as photoredox catalyst allowing to obtain 1-methoxy-4-(methylsulfanyl)benzene **201** in high yield (Scheme 79).[219]

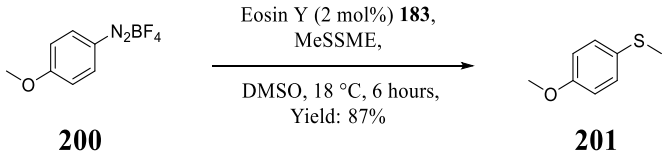

Scheme 79: Organo photoredox synthesis of aryl methyl sulfide **201**

The protocol has been effective also on the preparation of selenide derivatives.[219]

3.4. Steady State and Time Resolved Spectroscopies

3.4.1 UV-vis characterization

The key photophysical data of PXX **25**, octyl-PXXMI **148**, bis-octyl PXXDI **141** and PDI **202** (Figure 21) recorded in CH_2Cl_2 are gathered in Table 11, while the ground state absorption and emission spectra are shown in Figure 21.

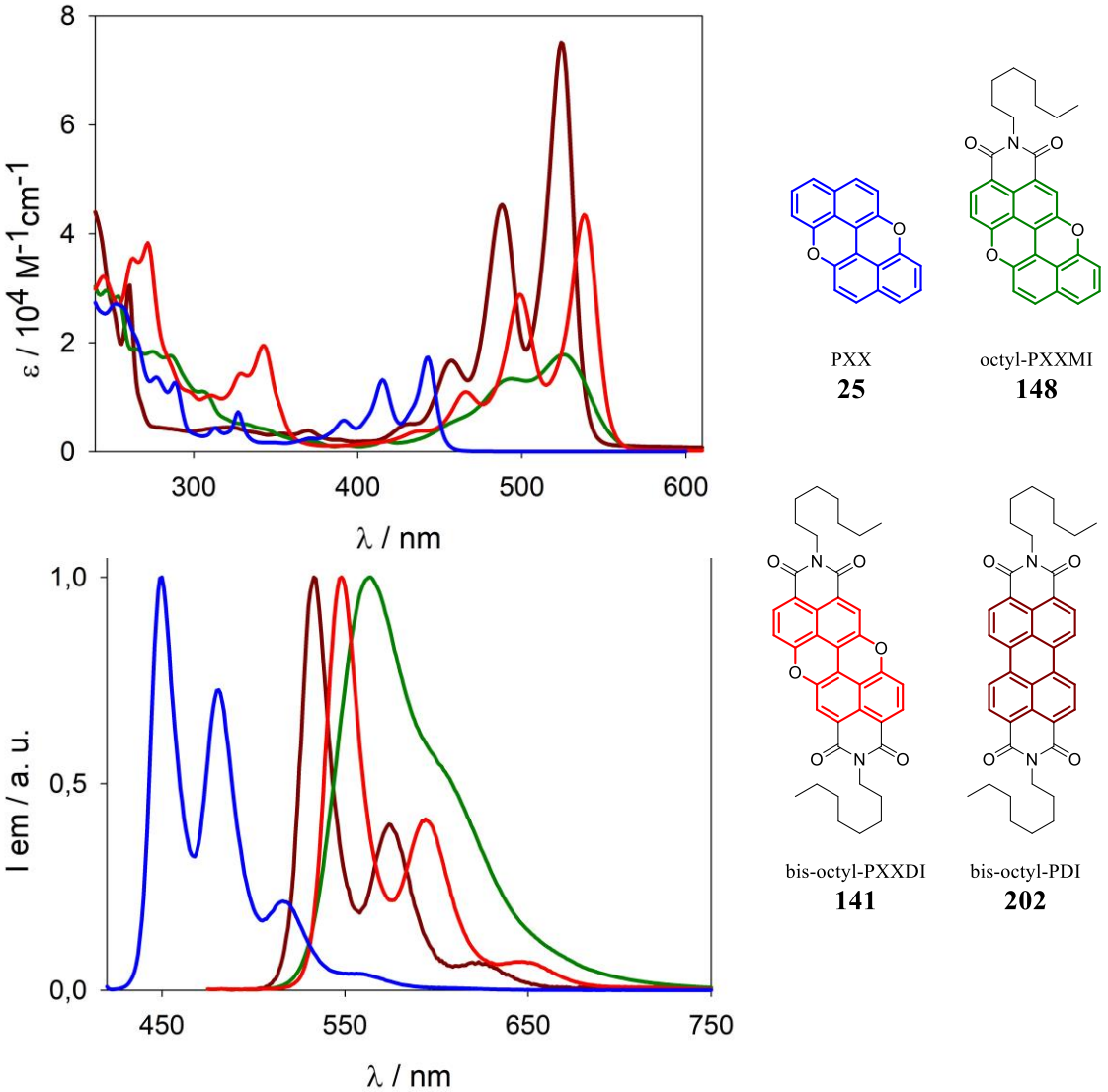

Figure 21: Absorption (top) spectra of PXX **25** (blue line, ~ $3.7 \cdot 10^{-5}$ M), bis-octyl-PDI **202** (dark red line, ~ $7.6 \cdot 10^{-6}$ M), octyl-PXXMI **148** (green line, ~ $4.1 \cdot 10^{-5}$ M) and bis-octyl-PXXDI **141** (red line, ~ $1.8 \cdot 10^{-5}$ M) in air equilibrated CH_2Cl_2 at room temperature and normalised emission (bottom) spectra of PXX **25** (blue line, ~ $4.0 \cdot 10^{-6}$ M, λ_{ex}= 415 nm), bis-octyl-PDI **202** (dark red line, ~ $6.6 \cdot 10^{-7}$ M, λ_{ex}= 480 nm), octyl-PXXMI **148** (green line, ~ $4.4 \cdot 10^{-6}$ M, λ_{ex}= 488 nm) and bis-octyl-PXXDI **141** (red line, ~ $1.4 \cdot 10^{-6}$ M, λ_{ex}= 466 nm) in air equilibrated CH_2Cl_2 at room temperature.

Reference compound PXX **25** displays, in CH_2Cl_2 solution at RT, the lowest energy electronic transition $S_0 \rightarrow S_1$ with absorption bands at 414 nm and maximum around 440 nm. Octyl-PXXMI **148** and bis-octyl-PXXDI **141** display a strong red-shifted band, octyl-PXXMI **148** is featured with a less structured electronic transition $S_0 \rightarrow S_1$ displaying vibronic bands at 490 nm and the maximum at 525 nm in CH_2Cl_2. The presence of the second imide motif on the PXX scaffold induces a further red shift, bis-octyl-PXXDI **141** reveals indeed, a structured electronic transition $S_0 \rightarrow S_1$, with absorption band at 498 nm and the maximum at 538 nm in CH_2Cl_2. Furthermore, bis-octyl-PXXDI **141** shows an absorption profile similar to the unsubstituted perylene diimides, in fact, the bis-octyl-PDI **202** displays the electronic transition $S_0 \rightarrow S_1$ with the (0,0) vibronic transition at ~ 524 nm and the (0,1) vibronic band at ~ 488 nm.[55] The red-shift observed in the PXX derivative could be explained as an effect of the presence of the electron-withdrawing imide moieties, which contribute to the stabilization of the $S_0 \rightarrow S_1$ transition. Moreover, symmetrical substitution with a second imide function on the periphery of the PXX core restores a vibrational structure and increases the intensity of the same band, similarly to other imide-substituted extended aromatics.[197] It is worth highlighting that in the compounds shown that the energy associated to these transitions is not dramatically modified (Figure 21), while the presence of a different number of imide-substituents on the periphery can affect the shape and the intensity of the absorption bands. In fact, while the introduction of the first imide on PXX **25**, giving octyl-PXXMI **148**, yields a significant bathochromic shift (82 nm), the following imide group introduction on octyl-PXXMI **148**, to afford bis-octyl-PXXDI **141**, promotes a further bathochromic shift of only 15 nm (data recorded in CH_2Cl_2). However, the absorption spectra of octyl-PXXMI **148** results in less structured bands in comparison with the one of the PXX **25** and bis-octyl-PXXDI **141**; the broadening of the absorption profile is probably a result of aggregation phenomena of octyl-PXXMI in solution. Similar behaviour has been observed from Bullock et al. in the study of photophysical properties of rylene imide and diimide.[228] Similarly to the PDI,[55] PXX derivatives show a fluorescence spectra as mirror image of the absorption profile (Figure 21). Both octyl-PXXMI **148** and bis-octyl-PXXDI **141** absorption bands cover the same visible region as bis-octyl-PDI **202**. However, the extinction coefficient of octyl-PXXMI

148 (ε = 17800) and bis-octyl-PXXDI **141** (ε = 43500) are considerably lower than the one of bis-octyl-PDI **202** (ε = 75000) in CH_2Cl_2 (Table 11).

The comparison between fluorescence spectra of PXX and octyl-PXXMI **136** and bis-octyl-PXXDI **141** (Figure 21) shows again a red-shift of the emission maxima from around 440 nm to 530 nm; while some differences in shape and vibrational substructure are evidenced, it is worth to underline that PXX-derivatives show very similar luminescence properties (Φ = 0.4–0.7; τ = 3–9 ns), with respect to bis-octyl-PDI **202**, with high quantum yields and lifetimes indicating a singlet deactivation in aerated solutions. Similar properties were also recorded in CH_3CN and C_6H_6 (Table 11).

Table 11: Photophysical data in aerated solvents at RT

		Absorption		Emission	
Compound	Solvent	λ, nm (ε, M^{-1} cm^{-1})	λ_{max} (nm)	τ (ns)[a][229]	Φ[b]
PXX	C_6H_6	444 (17500)	449	5.0	0.71[c]
PXXMI	C_6H_6	524 (17600)	546	7.6	0.71
PXXDI	C_6H_6	539 (35900)	549	3.3	0.39
PXX	CH_2Cl_2	443 (17300)	450	5.0	0.62[c]
PXXMI	CH_2Cl_2	525 (17800)	564	9.2	0.68
PXXDI	CH_2Cl_2	538 (43500)	548	3.2	0.39
PDI	CH_2Cl_2	524 (75000)	532	4.5	1.00
PXX	CH_3CN	439 (-)	447	5.1	0.60[c]
PXXMI	CH_3CN	519 (-)	570	9.8	0.61
PXXDI	CH_3CN	535 (-)	548	3.4	0.34

[a]λ_{ex} = 372 or 459 nm. [b]Standard: Rhodamine 6G in EtOH (Φ = 0.94). [c]Standard: coumarine 153 in EtOH (Φ = 0.53).

Phosphorescence, which was recorded in diluted solution in order to avoid aggregation, was not observed even in CH_2Cl_2/ MeOH at 77 K [104, 229-230] (Figure 22). Therefore, a precise determination of the triplet excited state was not possible. However, we observed an effective population of the excited triplet state for all the PXX derivatives by transient absorption spectroscopy (Figure 23) in deaerated C_6H_6 upon excitation at 355 nm (PXX **25**) and 532 nm (octyl-PXXMI **148** – bis-octyl-PXXDI **141**).

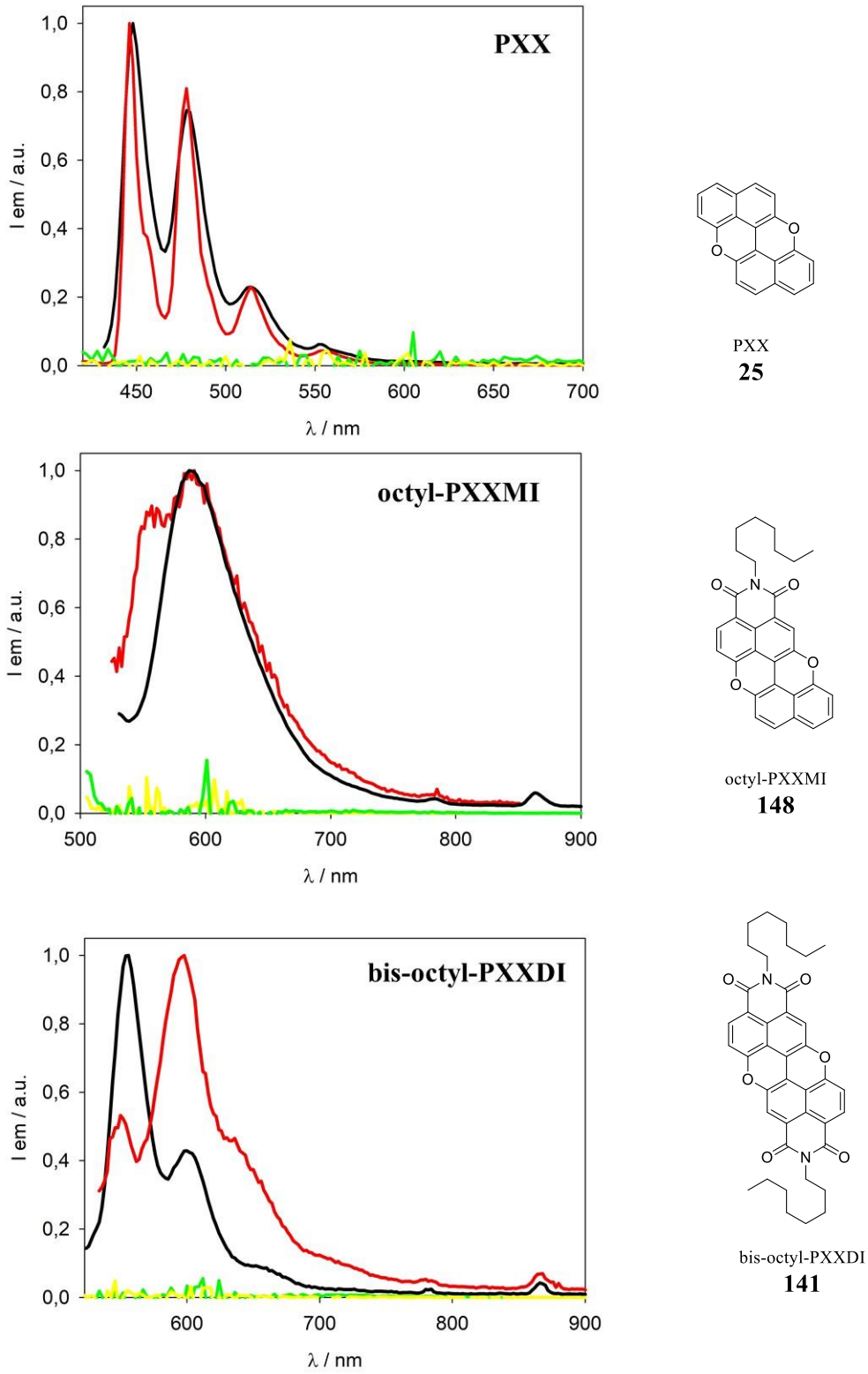

Figure 22: Fluorescence spectra at 77 K of PXX **25** (~ $6.0 \cdot 10^{-6}$ M) (top), octyl-PXXMI **148** (~ $6.0 \cdot 10^{-6}$ M) (middle) and bis-octyl-PXXDI **141** (~ $6.0 \cdot 10^{-6}$ M) (bottom) recorded in CH_2Cl_2:CH_3OH (1:1, v/v) rigid matrixes in liquid nitrogen (red lines). Fluorescence spectra at room temperature are showed as black lines. Phosphorescence spectra taken at 77 K (green lines: delay 0.1 ms, gate 50 ms; red lines: delay 0.1 ms, gate 300 ms). λ_{ex} = 405 (PXX **25**), 495 nm (octyl-PXXMI **148**, bis-octyl-PXXDI **141**).

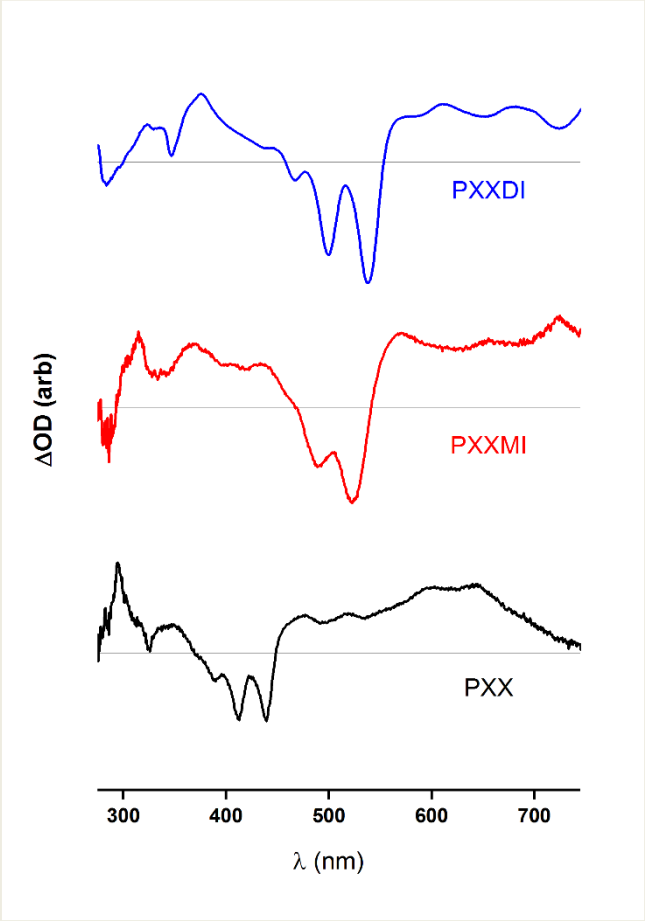

Figure 23: Normalised transient absorption spectra of bis-octyl-PXXDI **141** (top), octyl-PXXMI **148** (middle) and PXX **25** (bottom) solutions in deaerated C_6H_6 (~ $1.0 \cdot 10^{-5}$ M). The grey lines indicate ΔOD = 0 in each case. For bis-octyl-PXXDI and octyl-PXXMI: λ_{pump} = 532 nm; for PXX: λ_{pump} = 355 nm. Transient spectra recorded 500 ns after photoexcitation.

The nanosecond resolved temporal decay of the excited triplet states exhibits exponential kinetics (Figure 24, Figure 25), concomitant with the restoration of the respective photobleached ground states with averaged lifetimes of *ca.* 35 ms for PXX **25** and 50 ms for octyl-PXXMI **148** and bis-octyl-PXXDI **141**. No qualitative differences in spectra were observed when octyl-PXXMI **148** or bis-octyl-PXXDI **141** were pumped at λ_{ex}=355 nm. As expected, recovery times are heavily affected by the presence of O_2 in solution, with estimated quenching constants greater than $3 \cdot 10^8$ M^{-1} s^{-1} both for octyl-PXXMI **148** and bis-octyl-PXXDI **141** (Figure 26).

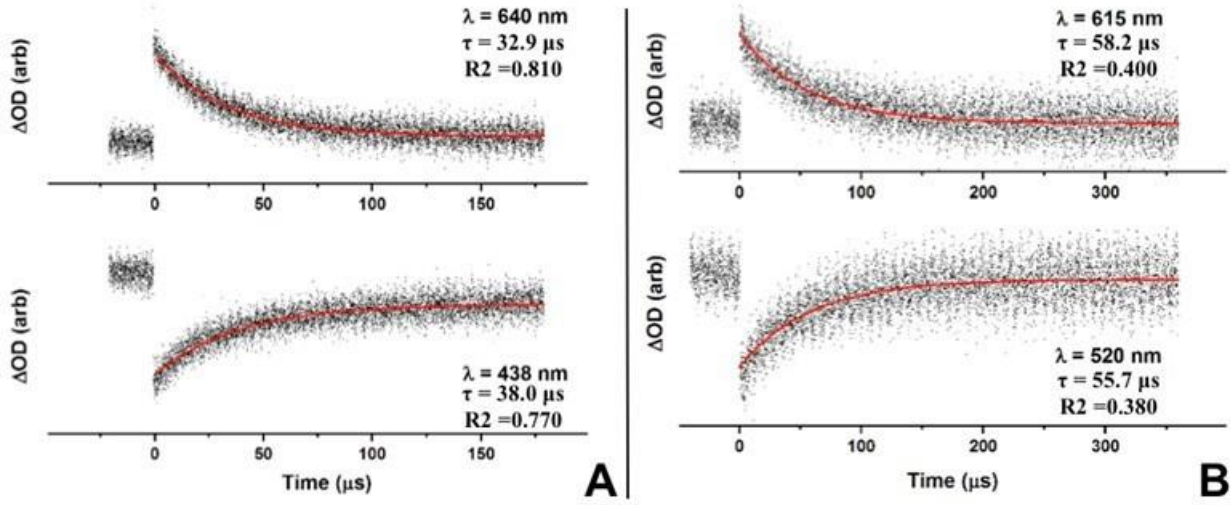

Figure 24: A) Time resolved transient absorption decay traces for PXX **25** solutions in deaerated C_6H_6 (~1.0x10^{-5} M, λ_{pump} = 355 nm). Monoexponential fits (λ_{abs} = 640 nm, top; λ_{abs} = 438 nm) are shown as solid red lines ($\tau \approx 35$ µs). **NOTE**: In the experimental conditions used, PXX **25** shows a certain degree of photosensitivity to pulsed laser excitation. B) Time resolved transient absorption decay traces for octyl-PXXMI **148** solutions in deaerated C_6H_6 (~ 1.0x10^{-5} M, λ_{pump} = 532 nm). Monoexponential fits (λ_{abs} = 615 nm, top; λ_{abs} = 520 nm) are shown as solid red lines ($\tau \approx 57$ µs).

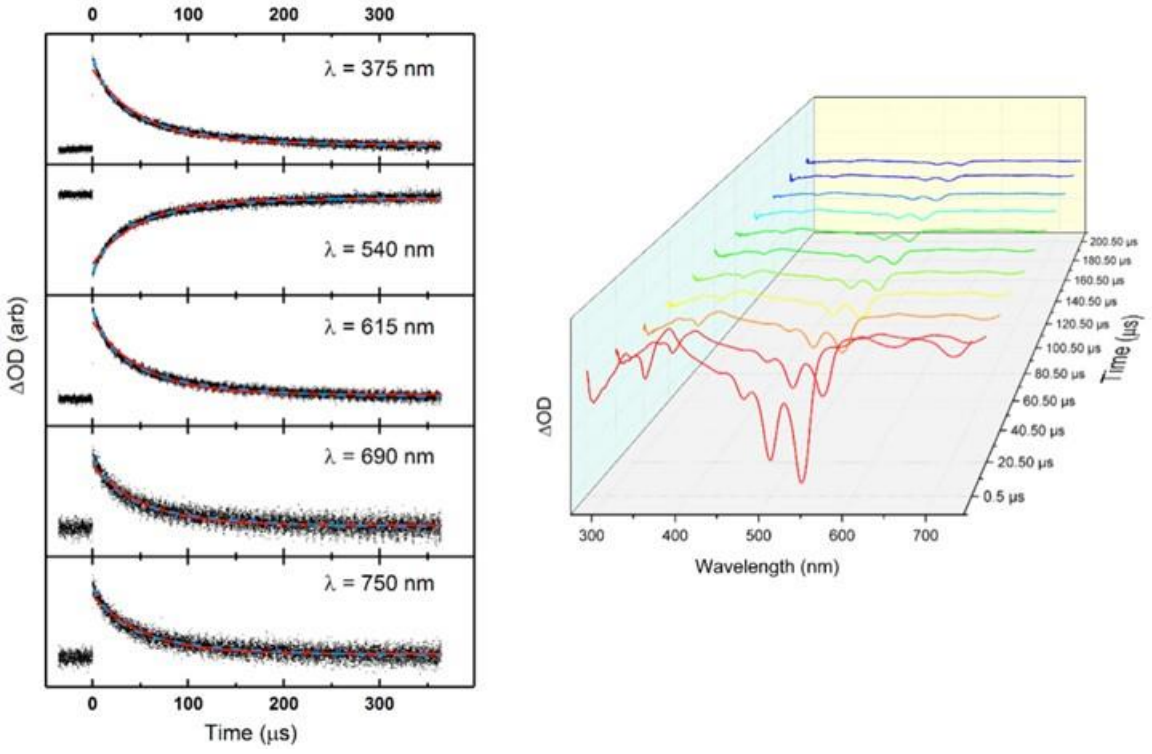

Figure 25: Transient absorption decay traces for a solution of bis-octyl-PXXDI **141** in deaerated C_6H_6 (~1.0x10^{-5} M) at various probe wavelengths. Solid (red) overlaid traces indicate mono-exponential fits to the data, dashed (blue) lines indicate bi-exponential fits. All traces are assigned to transient absorption features except λ = 540 nm which is a signal arising from ground state photobleaching. Right side: in the same experimental conditions, temporal decay of the bis-octyl-PXXDI **141** spectrum, shown in 20 ms intervals. Each spectral slice is generated by integrating for 2 ms, with a spectral resolution of: l = 2.05 nm.

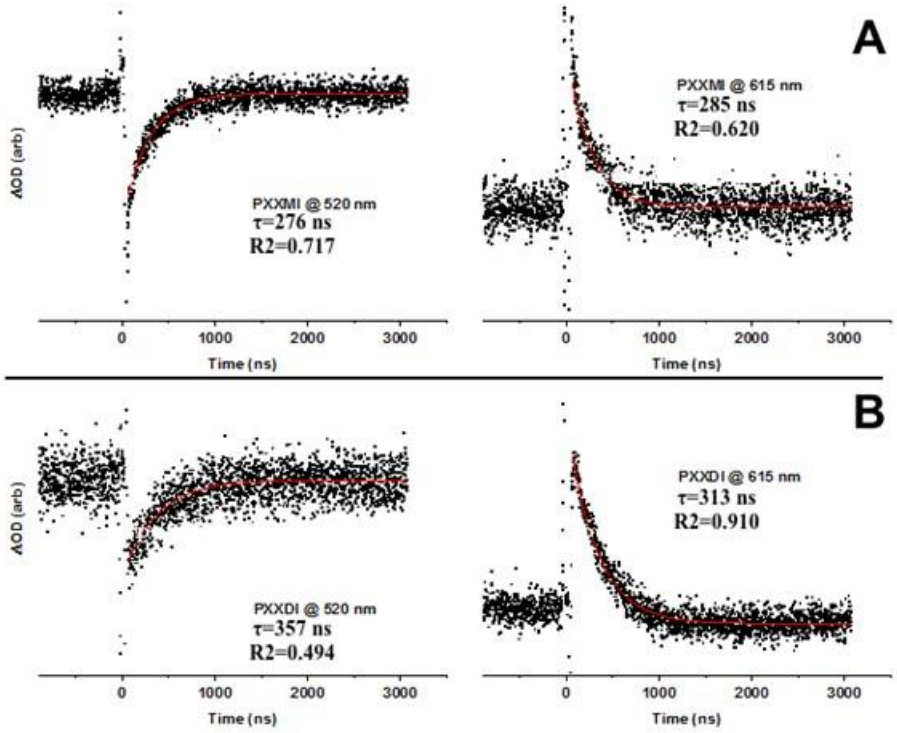

Figure 26: A) Time resolved transient absorption decay traces for octyl-PXXMI **148** solutions in air-equilibrated C_6H_6 (~$1.0x10^{-5}$ M, λ_{pump} = 532 nm). Monoexponential fits (λ_{abs} = 520 nm, left; λ_{abs} = 615 nm, right) are shown as solid red lines ($\tau \approx 280$ ns). B) Time resolved transient absorption decay traces for bis-octyl-PXXDI **141** solutions in air-equilibrated C_6H_6 (~$1.0x10^{-5}$ M, λ_{pump} = 532 nm). Monoexponential fits (λ_{abs} = 520 nm, left; λ_{abs} = 615 nm, right) are shown as solid red lines ($\tau \approx 335$ ns). Using 9.06 mM as the concentration of O_2 in C_6H_6, we can estimate the quenching constant k_{q_O2} for the quenching of the triplet excited states of octyl-PXXMI **148** and bis-octyl-PXXDI **141** as $3.9x10^8$ $M^{-1}s^{-1}$ and $3.3x10^8$ $M^{-1}s^{-1}$, respectively.

3.5. Electrochemical properties

Cyclic voltammetry (CV) was used to get further information about the frontier molecular orbital energies of the molecules in exam; halfwave redox potentials are reported in Table 12. PXX **25** is known to give a reversible oxidation wave at 0.30 V vs. ferrocene, while a reduction wave is usually not detected.[108] The oxidation potential reflects the electron-donating nature of the PXX moiety, whose oxygen-containing polyaromatic skeleton can more easily lead to a radical cation with respect to its full-carbon congener. Introduction of electron-depleting imide substituents on the PXX skeleton can efficiently deplete the aromatic core of electronic charge, making the two derivatives octyl-PXXMI **148** and bis-octyl-PXXDI **141** increasingly more difficult to be oxidized (reversible monoelectronic waves at E^1_{ox} = 0.63 and 0.92 V, respectively, in 1,2-dichlorobenzene, Figure 27 and Figure 28). At the same time, octyl-PXXMI **148** and bis-octyl-PXXDI **141** are easier to be reduced

in order to give the singly-charged radical anion compared with the model compound PXX **25** (reversible monoelectronic waves at E^1_{red} = -1.87 and -1.54 V, respectively, 1,2-dichlorobenzene, Figure 27 and Figure 28). In both cases, experimental evidence shows an increase in the oxidative character and a decrease in the reductive character. Each imide moiety promotes a shift of around +0.3V in reduction and oxidation halfwave potentials (Table 12). In agreement with the reported data, comparing bis-octyl-PXX **148** and bis-octyl-PDI **202**, the latter shows better oxidant character. Similar behaviour for the PXX derivatives has been observed in CH_2Cl_2 and MeCN (Figure 29 and Figure 30).

Table 12: CV data in 1,2-dichlorobenzene (DCB), CH_2Cl_2 and CH_3CN at RT.[a]

Compound	Solvent	$E^{1/2}_{ox,1}$	$E^{1/2}_{red,1}$	$E^{1/2}_{red,2}$	ΔE_{H-L}
PXX	DCB	0.30(111)	nd	Nd	nd
octyl-PXXMI	DCB	0.63(92)	-1.87(63)	Nd	2.40
bis-octyl-PXXDI	DCB	0.92(78)	-1.54(77)	-1.75(61)	2.46
bis-octyl-PDI	DCB	nd	-1.16(75)	-1.34(76)	nd
PXX	CH_2Cl_2	0.77(87)	nd	Nd	nd
octyl-PXXMI	CH_2Cl_2	1.10(67)	-1.31(60)	Nd	2.41
bis-octyl-PXXDI	CH_2Cl_2	1.41(80)	-1.01(110)	-1.19(92)	2.42
PXX	CH_3CN	0.77(87)	-2.16(75)	-2.40[b]	2.93
octyl-PXXMI	CH_3CN	1.04(74)	-1.25(65)	Nd	2.29

[a] Halfwave potentials in V vs. Fc^+/Fc (DCB); V vs. SCE (CH_2Cl_2 and CH_3CN); peak separations (in mV) are indicated in brackets. [b] Peak potential. "nd" stands for "not detected".

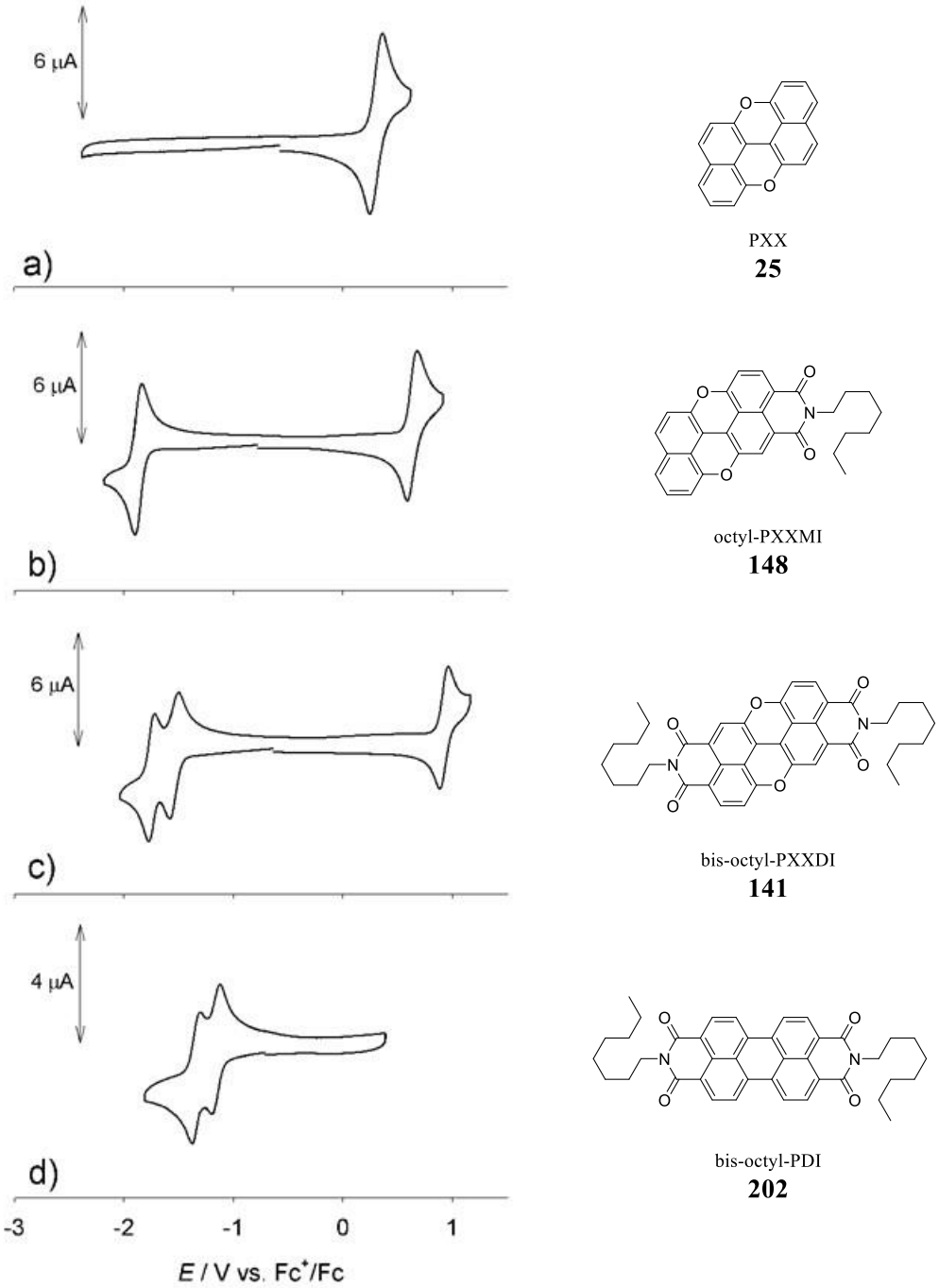

Figure 27: Cyclic voltammograms in 1,2-dichlorobenzene at RT of a) PXX **25** 0.67 mM, b) octyl-PXXMI **148** 0.67 mM, c) bis-octyl-PXXDI **141** 0.62 mM, d) bis-octyl-PDI **202** 0.60 mM. Scan rate: 50 mV/s. Electrolyte: $TBAPF_6$ (a-c: 0.063 M, d: 0.068 M). Ferrocene is used as internal reference standard.

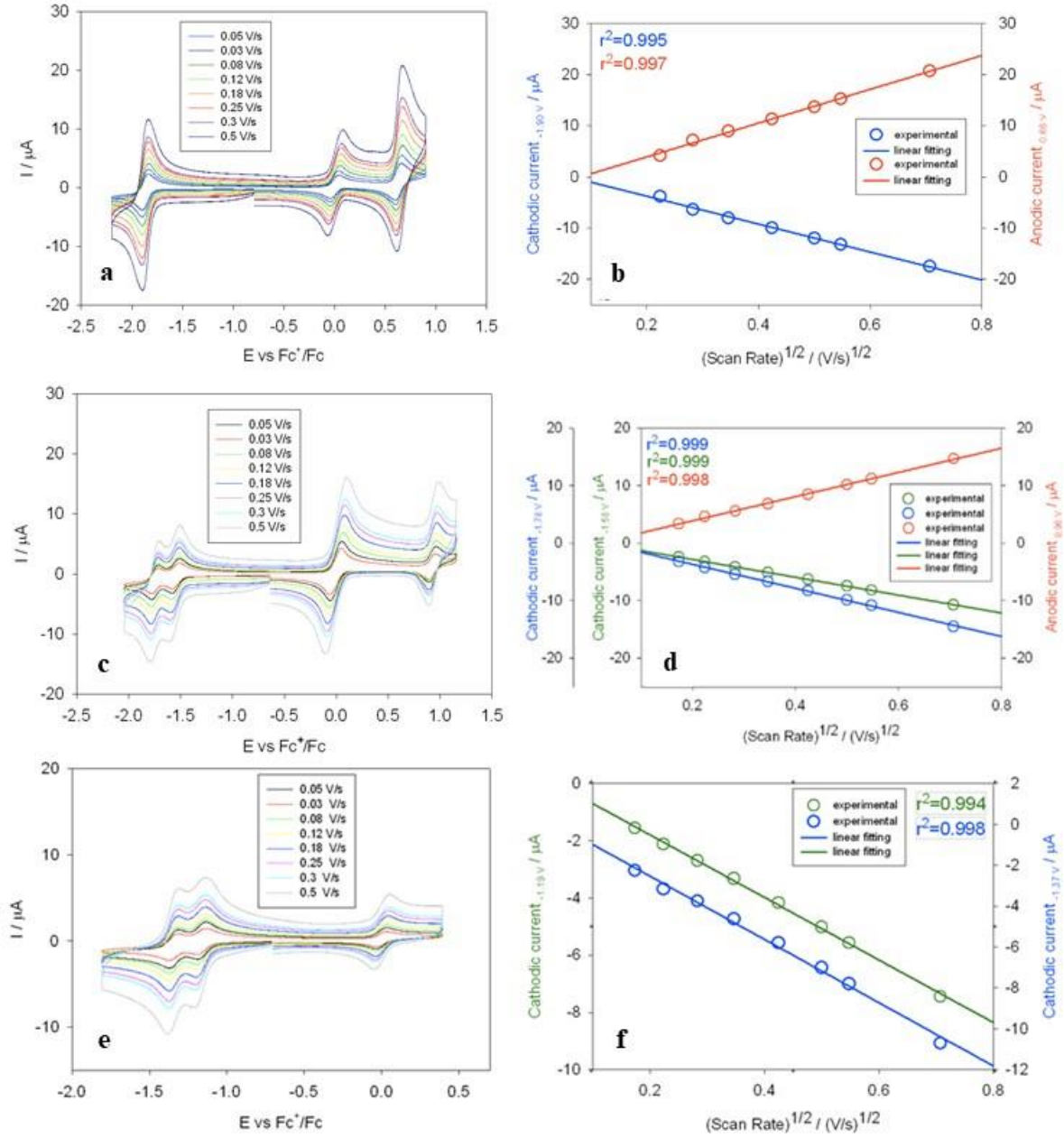

Figure 28: Cyclic voltammograms at variable scan rates and relative linear dependence between anodic or cathodic peak currents and scan rate$^{1/2}$ for compounds: a-b) octyl-PXXMI **148** (0.67 mM), c-d) bis-octyl-PXXDI **141** (0.70 mM), e-f) bis-octyl-PDI **202** (0.60 mM). For each calculated linear regression, the coefficient of determination r^2 is reported. Experimental conditions: 1,2-dichlorobenzene is used as solvent, supporting electrolyte: $TBAPF_6$ (0.063÷0.068 M for all experiments). Ferrocene is used as internal reference standard ($E_{Fc+/Fc}$ = 0.00 V).

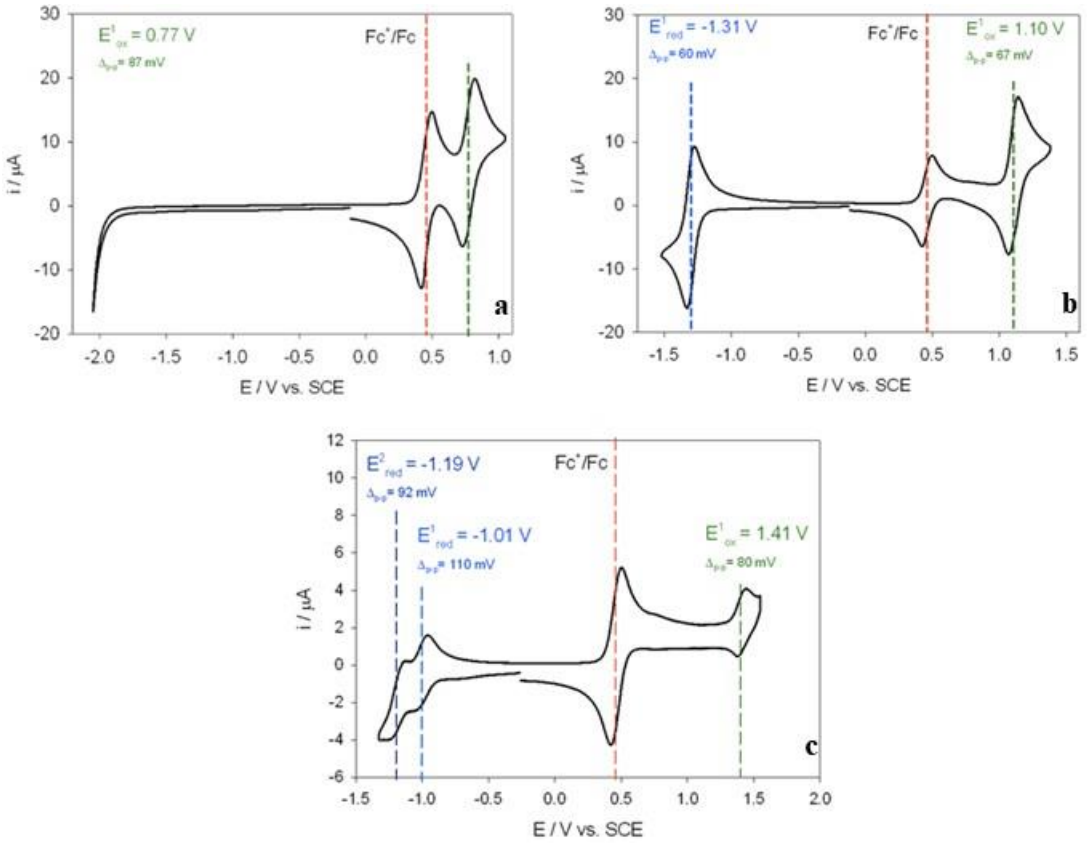

Figure 29: Cyclic voltammograms of a) PXX **25**, b) octyl-PXXMI **148** and c) bis-octyl-PXXDI **141** (0.90 mM, $TBAPF_6$ 0.10 M; 1.07 mM, $TBAPF_6$ 0.11 M; 0.67 mM, $TBAPF_6$ 0.11 M, respectively) in CH_2Cl_2 at RT, scan rate 0.05 V/s. Ferrocene is used as internal reference; $E_{Fc+/Fc}$ = 0.46 V *vs.* SCE.

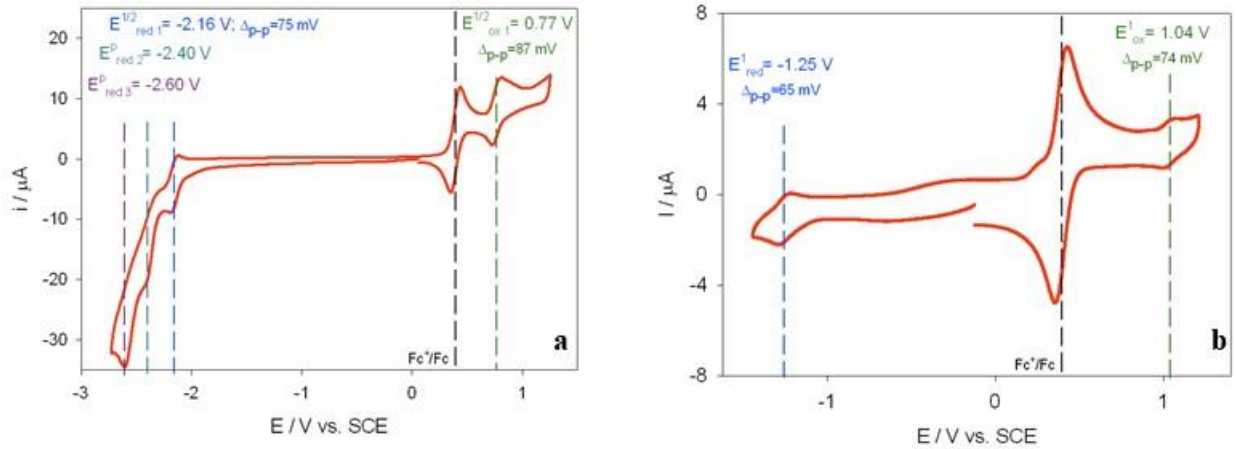

Figure 30: Cyclic voltammograms of a) PXX **25** and b) octyl-PXXMI **141** (0.60 mM and 0.52 mM, respectively; $TEAPF_6$ 0.11 M,) in MeCN at RT, scan rate 0.05 V/s. Ferrocene is used as internal reference; $E_{Fc+/Fc}$ = 0.395 V vs. SCE.

From the electrochemical and photophysical analysis we observe that the singlet excited states of PXX derivatives are progressively shifted by the introduction of the imide subunit in a rigid energy shift way. In other words, the redox potential changes but the HOMO-LUMO gap stays intact (Figure 31). This concept is better elucidated by taking into account the frontier orbital potentials diagram (Figure 32).

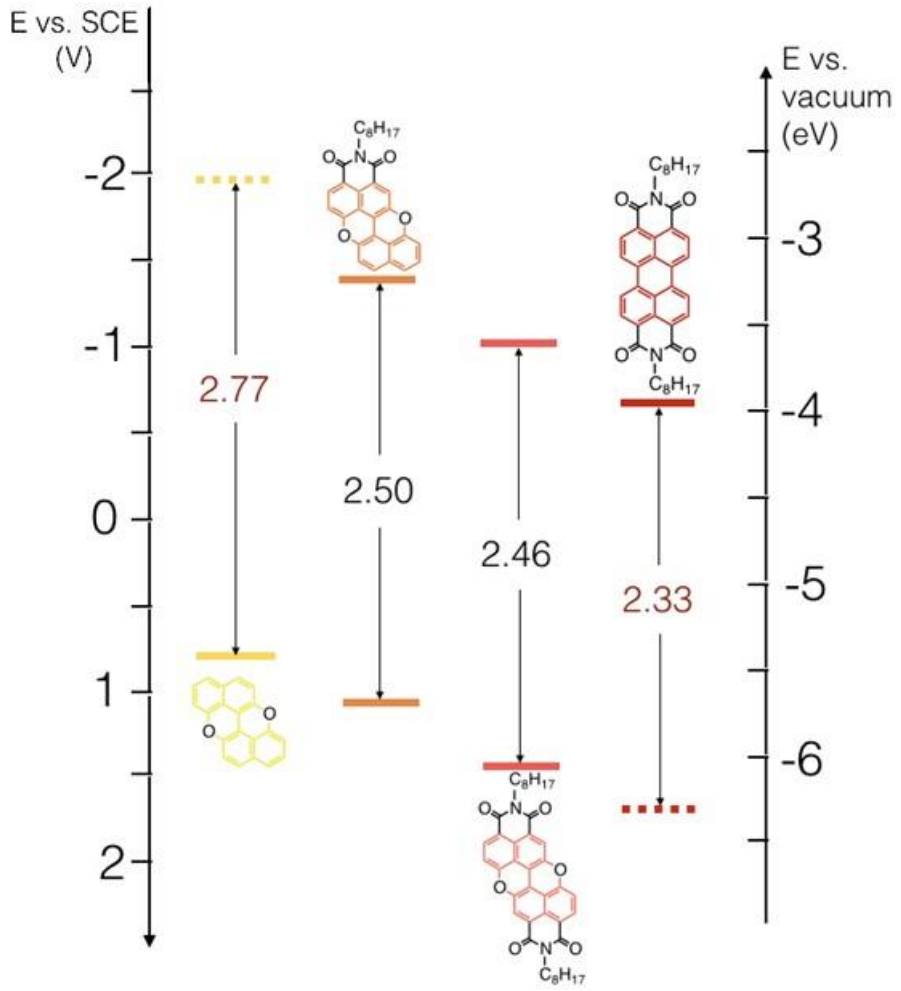

Figure 31: Frontier orbital energies and separations for the four molecules analysed by cyclic voltammetry in 1,2-dichlorobenzene (dashed lines corresponding to calculated energies using optical gap ΔE_{opt}). The formal potential of the ferrocene redox couple, taken as a reference, is assumed to be at -5.1 eV vs. vacuum, whereas the standard redox potential of ferrocene in 1,2-dichlorobenzene is 0.73V vs SHE,[231] which using the conversion factor of -0.24 V, corresponds to 0.49 V vs SCE.[232]

Both HOMO and LUMO levels are decreasing their potentials in stepwise fashion following the order of octyl-PXXMI **148** > bis-octyl-PXXDI **141** > bis-octyl-PDI **202**. Moreover octyl-PXXMI **148** and bis-octyl-PXXDI **141** are respectively stronger reducer and oxidizer in their singlet excited states compared to the triplet state of the extensively

employed $[Ru(bpy)_3]^{2+}$.[233] On the other hand, the singlet excited state of PXX is a greater reducer and oxidizer with respect to the triplet state of $[Ir(ppy)_3]$ (Figure 32).

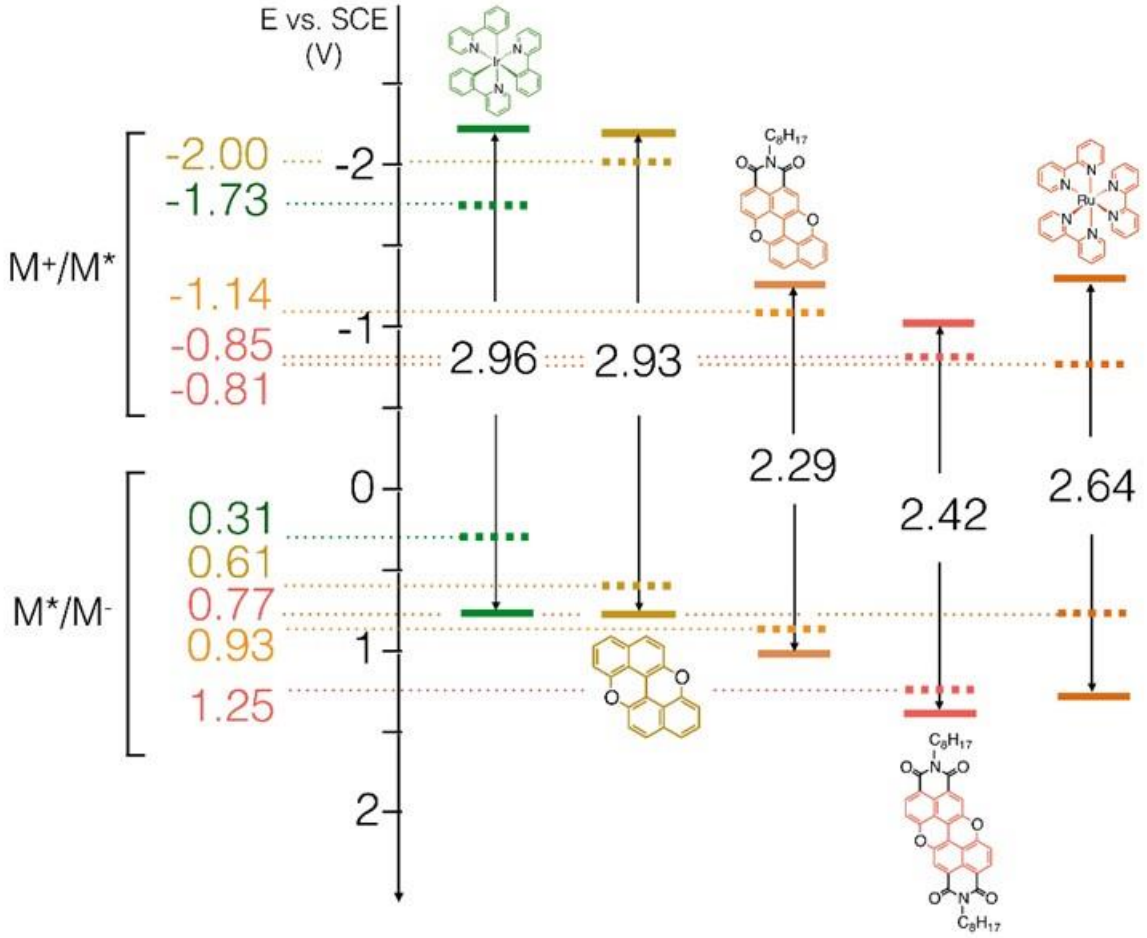

Figure 32: Comparison between redox potentials and electrochemical gaps of the three PXX derivatives, [*fac*-Ir(ppy)$_3$] and $[Ru(bpy)_3]^{2+}$ (in CH_3CN, except for bis-octyl-PXXDI, in CH_2Cl_2). Reduction (M^+/M^*) and oxidation (M^*/M^-) potentials of the respective excited states are evidenced by dashed lines, calculated taking into account emission maxima in the same solvents. Data for [*fac*-Ir(ppy)$_3$] and $[Ru(bpy)_3]^{2+}$ are taken from literature.[6]

From the experimental results it is possible to observe that E_g is solvent dependent. In fact, from cyclic voltammetry analysis the energy gap of the PXX derivatives results to be smaller in MeCN than 1,2-dichlorobenzene. This can be explained taking into account the principle of the analytical technique of the cyclic voltammetry. Cyclic voltammetry is a technique that allows to investigate the electrochemical behaviour of the molecules and also to estimate the HOMO and LUMO energies. The cyclic voltammetry provides a direct information of oxidation and reduction potential of the molecule under investigation. The oxidation process corresponds to the removal of one electron from the HOMO orbital with the formation of a cationic species with an electron hole. Conversely, the reduction process

corresponds to an addition of electron to LUMO orbital of the molecule leading the formation of an anionic species with an unpaired electron.[234] The potential of oxidation and reduction of a molecule can be correlated respectively to ionisation potential I_p and electron affinity E_a, which leads to the estimation of the energy gap E_g[235] of the frontier orbitals:

$$E_g = I_p - E_a$$

It has been demonstrated that E_{ox} value defers depending on the nature of the solvent, E_{ox} shifts to less positive potentials when increasing the polarity of the solvent:

$$DMSO < DMF < MeCN < CH_2Cl_2.$$

In other words, this indicates that the oxidation of the molecules to cationic species becomes more difficult when going from DMSO, the most polar solvent, to DCM, the least polar solvent.[236] The shift of the oxidation potential can be explained by donor-acceptor Lewis type interactions.[237] The newly formed cationic species M^+ in contrast to the neutral molecule is more prone to interact with the solvent. Therefore, this stronger interaction of M^+ - solvent molecule affects the oxidation process of the molecule and thus the E_{ox} value. Consequently, a strong electron contribution of the solvent molecule to the M^+ results in a diminution of the E_{ox}. Conversely, for the reduction process the opposite trend is observed: the reduction potential shifts over to more positive values when increasing the polarity of the solvent.[238] In other words, the anion M^- is more affected from the interaction with the solvent. Similarly, the stronger the interaction of M^- - solvent, the more is affected the E_{red} value; with a consequent increase of the E_{red} value. From all the above, it is concluded that it is easier to have an oxidation or reduction process in a more polar than in a less polar solvent and the energy gap is smaller in a more polar solvent. In this context, our experimental results are in agreement with the precedent statement since MeCN is the most polar solvent (ε_d = 35.9)[239] used in our analysis while CH_2Cl_2 and 1,2-dichlorobenzene that have similar dielectric constants (ε_d = 8.93 and ε_d = 9.93 respectively) are the least polar ones.[239] However, the energy gap determined by CV results to be bigger than the one determined by optical measurements. The optical band gap has been determined considering the maximum of emission (λ_{max}). The molecule in the excited state M* presents the HOMO and the LUMO half-filled. Upon irradiation of molecule M an electron promotion occurs from the HOMO to the LUMO. Therefore, the excited state, M* presents

the HOMO and the LUMO half-filled; the so-called electron hole pair which is characterized by a stronger interaction with the solvent in comparison with respective cation M^+ and anion M^-. This interaction with the solvent is stronger for a more polar solvent.[240] Thus, the more polar the solvent, the stronger the stabilization of M*- solvent. Due to this stabilization the emission is shifted to lower energy.[241] In general, M* has a bigger bipolar moment than M in the ground state. Therefore, upon excitation of M the molecules of solvent can reorient around M* and lower the energy of the excited state.[242] Thus, higher is the solvent polarity, larger is the stabilization effect, resulting in emission at lower energy. Typically, this effect is pronounced only from molecules that display a big bipolar moment, while non-polar molecules are less sensitive to the solvent polarity.[243] Typically, the fluorescence lifetime is in the order of 1-10 ns. This time is enough long to observe the solvent reorganization which takes place in 10-100 ps.[241] For this, the fluorescence spectra are affected by the solvent while the absorption spectra are not affected since the electronic transition promoted by light absorption is in the order of 10^{-15} sec, a time too short for the solvent reorganization.[243]

3.6 Investigation of the photoredox properties: Dehalogenation reactions

As mentioned in section 3.2.2, $[Ru(bpy)_3Cl_2]$[207] and $[Ir(ppy)_3]$[208] have been used to trigger photoredox reactions. However, simple organic molecules such us perylene diimide[210], phenylphenothiazine[209] and others dyes[204a] have also been applied to perform such organic photoredox transformations. Small molecular organic semiconductors that absorb visible light upon irradiation generate a charge transfer process, which could be used to trigger photoredox reactions.[244]

Based on the aforementioned results, PXX derivatives have been tested to trigger photochemical reactions. In order to evaluate the photo-triggering activity of the PXX derivatives, the photoinduced dehalogenation process has been taken in account as model transformation, similar to the work of König and co-workers, which has been achieved using PDI derivative **168** as photocatalyst.[210]

Firstly, the photoinduced dehalogenation of 2-bromoacetophenone **203** has been tested in the presence of DIPEA as sacrificial agent and either PXX **25**, octyl-PXXMI **148** or bis-octyl-PXXDI **141** in deaerated C_6H_6. Upon irradiation, we noted the complete conversion of starting material **203**, providing the dehalogenated product, acetophenone **204**, which was observed by GC-MS analysis (Scheme 80, entries 1, 4 and 7, Table 13, Figure 33).

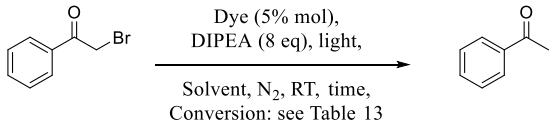

203 **204**

Scheme 80: Photoinduced dehalogenation of 2-bromoacetophenone **203** in presence of PXX derivatives.

Table 13: Conditions used to perform photoinduced dehalogenation of 2–bromoacetophenone **203**.

Entry	Dye	λ_{ex} (nm)	Solvent	Time [h]	Conversion
1	**PXXMI 148**	520	C_6H_6	24	100
2		520	CH_2Cl_2	24	95
3		520	MeCN	24	100
4	**PXXDI 141**	520	C_6H_6	29	100
5		520	CH_2Cl_2	24	100
6		520	MeCN	24	100
7	**PXX 25**	460	C_6H_6	24	100
8		460	CH_2Cl_2	24	100
9		460	MeCN	24	100

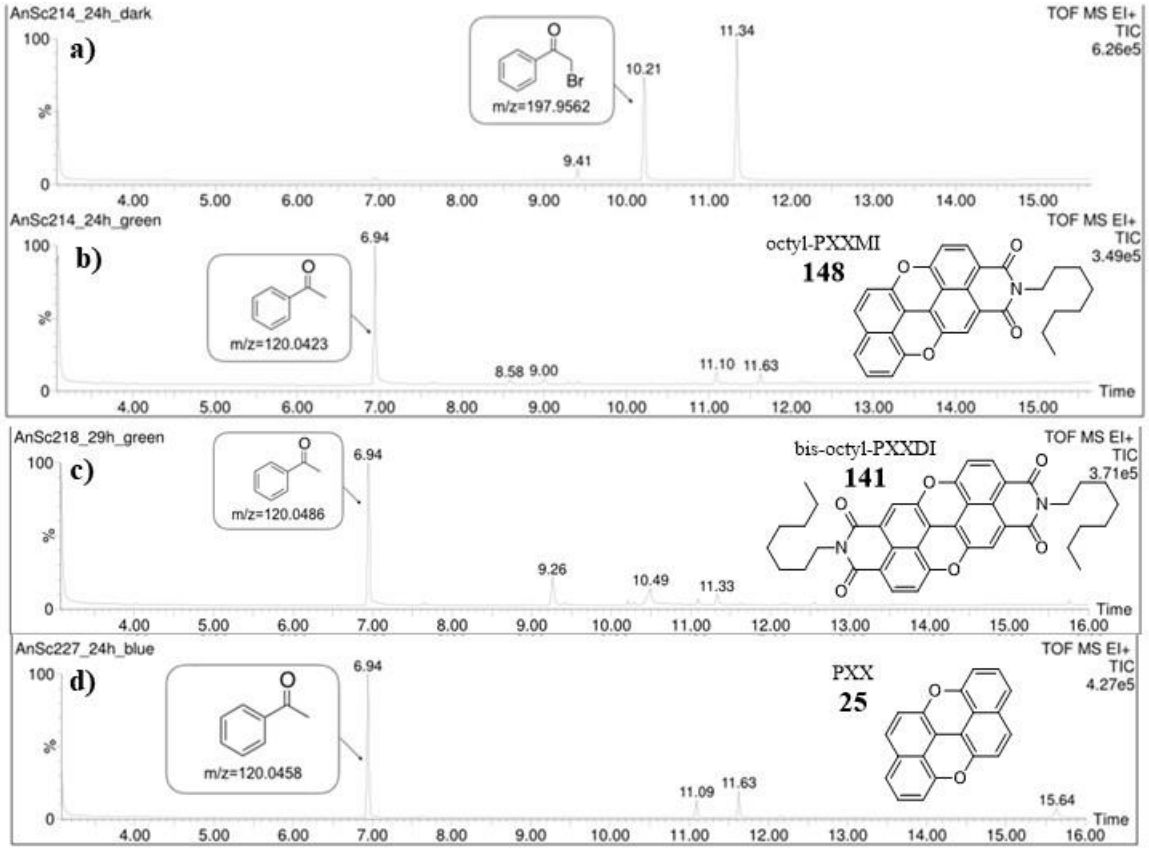

Figure 33: Photoinduced dehalogenation of 2-bromoacetophenone **203** (R_t = 10.21 min) to yield acetophenone **204** (R_t = 6.94 min), in C_6H_6: a) dark test, b) in the presence of octyl-PXXMI **148** upon irradiation, c) in the presence of bis-octyl-PXXDI **141** upon irradiation, c) in the presence of PXX **25** upon irradiation.

Subsequently, based on a photoinduced electron transfer and consequent formation of a radical pair intermediate, we decided to study the effect of the solvent polarity on the outcomes of the reaction. Therefore, C_6H_6 (ε_d = 2.28) was replaced by the more polar CH_2Cl_2 (ε_d = 8.93), and also by MeCN (ε_d = 35.9). Full conversion was achieved with all the three solvents screened, namely C_6H_6 (Figure 33), CH_2Cl_2 and MeCN (Figure 34), clearly indicating that the chemical nature of the intermediates is not sensitive to the polarity of the solvent (Table 13).

GC analysis of the phototriggered reactions show peaks corresponding to the formation of acetophenone **204** and also to some unidentified by-products. Nevertheless, the formation of this by-product also occurs when the reaction is kept in the dark. Those peaks were not taken in account for the determination of the conversion. The presence of by-products can be explained as consequence of the reactivity of nitroxides present in DIPEA towards the halogeno-substrate.

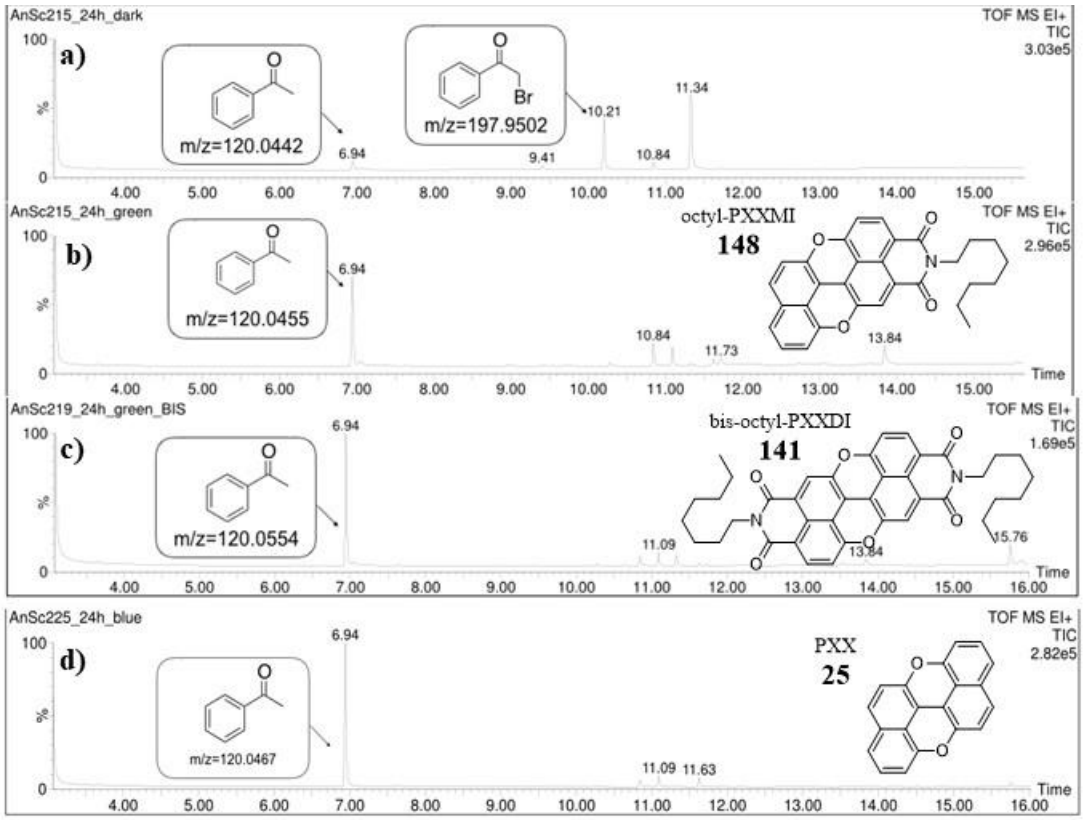

Figure 34: Photoinduced dehalogenation of 2-bromoacetophenone **203** (R_t = 10.21 min) to yield acetophenone **204** (R_t = 6.94 min), in MeCN,: a) dark test, b) in the presence of octyl-PXXMI **148** upon irradiation, c) in the presence of bis-octyl-PXXDI **141** upon irradiation, c) in the presence of PXX **25** upon irradiation.

Notably, performing the photoinduced dehalogenation reaction of α-bromoacetophenone in C_6H_6 tiny crystals' formation occurred. These crystals were identified as $[H_2NiPr_2]Br$ salt from X-ray analysis, (Figure 35).

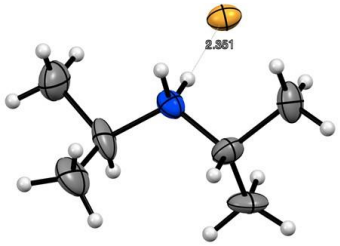

Figure 35: ORTEP representation of the crystal structure of diisopropylammonium bromide. Highlighted distance between Br atom and vicinal H atom is expressed in Å. Space group: P 21. Atom colors: grey C, white H, blue N, yellow Br.

After achievement of dehalogenation of 2-bromoacetophenone, we tried to perform the dehalogenation of an aromatic derivative. Therefore, we tried to perform the reaction on 4'-bromoacetophenone **205** in the presence of DIPEA and bis-octyl-PXXDI **141** in

dearated solvents, either C_6H_6, CH_2Cl_2 and MeCN (Scheme 81). Upon irradiation for 48 hours, no conversion of the starting material into acetophenone **204** was observed (entries 1, 2 and 3, Table 14). Subsequently, we tried to perform the reaction on 4'-bromoacetophenone in the presence of DIPEA and octyl-PXXMI **148** in dearated solvents, either C_6H_6, CH_2Cl_2 and MeCN. Upon irradiation for 48 hours, also in this case the conversion of the starting material **205** was not observed (entries 4, 5 and 6, Table 14). Eventually, performing the reaction in the presence of DIPEA and PXX **25** in C_6H_6, the formation of the desired product was not observed (entry 7, Table 14). For the reaction performed in CH_2Cl_2, a conversion of 6% was observed after 48 hours of irradiation (entry 8, Table 14). Eventually, upon performing the dehalogenation of 4'-bromoacetophenone **205** in the presence of DIPEA and PXX **25** in MeCN upon irradiation of 48 hours, full conversion was observed (entry 9, Table 14).

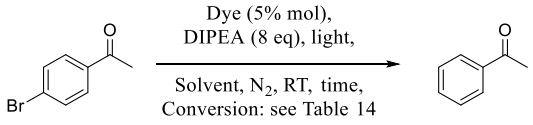

205 **204**

Scheme 81: Photoinduced dehalogenation of 4'-bromoacetophenone **205** in presence of a PXX derivative.

Table 14: Condition used to perform photoinduced dehalogenation of 4'-bromoacetophenone.

Entry	Dye	λ_{ex} (nm)	Solvent	Time [h]	Conversion
1	**PXXDI 141**	520	C_6H_6	48	0
2		520	CH_2Cl_2	48	0
3		520	MeCN	48	0
4	**PXXMI 148**	520	C_6H_6	48	0
5		520	CH_2Cl_2	48	0
6		520	MeCN	48	0
7	**PXX 25**	460	C_6H_6	48	0
8		460	CH_2Cl_2	48	6
9		460	MeCN	48	100

From these experiments, we demonstrated that the redox potential of the excited state of octyl-PXXMI **148** and bis-octyl-PXXDI **141** do not allow an efficient electron transfer to promote the photoinduced dehalogenation of 4'-bromoacetophenone **205**.

Subsequently, we used PXX **25** to promote photoinduced reduction of 4'-bromobenzaldehyde **206** in the presence of DIPEA, in dearated solvents under irradiation for 48 hours (Scheme 81). Similarly to 4'-bromoacetophenone **205**, the reaction does not proceed in C_6H_6 (entry 1, Table 15), whereas in CH_2Cl_2, the process provided low conversion (entry 2, Table 15) and in MeCN the full conversion of 4'-bromobenzaldehyde **206** in benzaldehyde **207** (entry 3, Table 15) was observed.

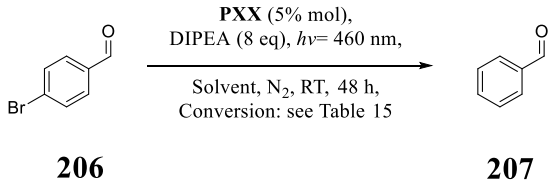

206 **207**

Scheme 82: Photoinduced dehalogenation of 4-bromobenzaldehyde **206** in presence of PXX **25**.

Table 15: Conditions used to perform photoinduced dehalogenation of 4-bromobenzaldehyde **206**.

Entry	Dye	λ_{ex} (nm)	Solvent	Time [h]	Conversion
1		460	C_6H_6	48	0
2	**PXX**	460	CH_2Cl_2	48	26
3		460	MeCN	48	100

These results suggest that for aromatic substrates, the formation of a key radical intermediate can occur, and it is better stabilized in polar solvent, such as MeCN. When the reaction is performed on 3'-bromoacetophenone **208**, in the presence of DIPEA and PXX in MeCN upon irradiation for 48 hours, the reaction proceeds with a good conversion (78%) providing the acetophenone **204** (Scheme 83). While, performing the reaction in similar reaction conditions on 2'-bromoacetophenone **209** the process provides a negligible conversion (Scheme 83).

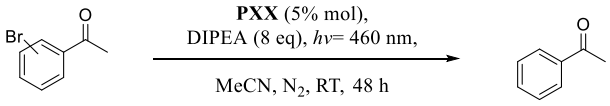

204

	Conversion [%]
3'-bromoacetophenone **208**	**73**
2'-bromoacetophenone **209**	**2**

Scheme 83: Photoinduced dehalogenation of bromoacetophenone derivative in presence of PXX **25**.

PXX **25** resulted active in the photoinduced dehalogenation of α-bromocinnamaldehyde **210**, in presence of DIPEA in MeCN upon irradiation for 48 hours. The reaction provides the mixture of stereoisomers E and Z of cinnamaldehyde **211** and **212** respectively, with a conversion of 58%, (Scheme 84).

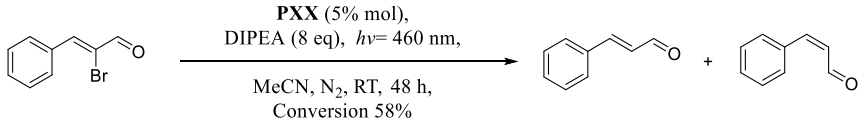

210 **211** **212**

Scheme 84: Photoinduced dehalogenation of α-bromocinnamaldehyde **210** in presence of PXX **25**.

Furthermore, both octyl-PXXMI and bis-octyl-PXXDI can induce the photoreduction of diethylbromomalonate **185** in the presence of DIPEA in MeCN under irradiation for 20 hours (Scheme 85). This reaction, affording diethylmalonate **187**, was obtained with a quantitative conversion (entries 1 and 2, Table 16). Performing the reaction on diethylchloromalonate **186** (Scheme 85) in the presence of DIPEA and octyl-PXXMI in MeCN, under irradiation for 96 hours, photodehalogenation was promoted, affording diethylmalonate **187** with a conversion of 75%, (entry 3, Table 16). While performing the reaction in the presence of DIPEA and bis-octyl-PXXDI in MeCN, under irradiation for 96 hours, traces of photo dehalogenation of diethylchloromalonate **186** were detected **(**entry 4, Table 16).

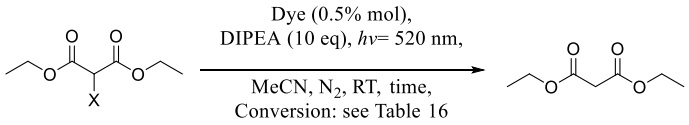

X: -Br **157**
-Cl **213**

214

Scheme 85: Photoinduced dehalogenation of diethyl-halomalonate in presence of octyl-PXXMI **148** or bis-octyl-PXXDI **141**.

Table 16: Conditions used to perform photoinduced dehalogenation of diethyl-halomalonate.

Entry	X	Dye	λ_{ex} (nm)	Solvent	Time [h]	Conversion
1	Br **(157)**	**PXXMI**	520	MeCN	20	100
2		**PXXDI**	520		20	100
3	Cl (**213**)	**PXXMI**	520	MeCN	96	75
4		**PXXDI**	520		96	*traces*

3.6.1 Mechanistic invenstigations

The difference in the photoreactivity of the PXX derivatives prompted us to go through a mechanistic study of the reactions. We tried to understand more in depth the chemical properties of the photoinduced radical intermediates produced during the reactions. The oxidation of the sacrificial reagent could occur at two different moments of the catalytic cycle, depending on whether the first stage of the catalytic cycle is oxidative or reductive quenching. Therefore, in order to determine which type of quenching occurs as first step, we performed a Stern-Volmer analysis of the PXX derivatives with DIPEA and the tested substrates in different solvents. For practical reasons, herein we report a selection of the most representative results to understand the study. All the spectroscopic data for the Stern-Volmer analysis are available in the experimental part (p.172). To begin, we studied the fluorescence quenching study of octyl-PXXMI **148** with DIPEA in MeCN (Figure 36) and octyl-PXXMI **148** with 2-bromoacetophenone ($PhCOCH_2Br$) **203** in MeCN (Figure 37). The quenching data are gathered in Table 17. We noted that the fluorescence of octyl-PXXMI **148** in MeCN is quenched faster by the DIPEA than 2-bromoacetophenone **203**. In fact, the first one follows a $k_q = 4.2 \cdot 10^9$ $M^{-1}s^{-1}$ (entry 1, Table 17) while the latter has a $k_q = 2.2 \cdot 10^8$ $M^{-1}s^{-1}$ (entry 2, Table 17).

In a similar way, bis-octyl-PXXDI **141** in MeCN in the presence of DIPEA resulted to a fluorescence quenching with a $k_q = 5.8 \cdot 10^9$ $M^{-1}s^{-1}$,(entry 3, Table 17) while bis-octyl-

PXXDI **141** in the presence of 2-bromoacetophenone **203** displayed a fluorescence quenching featured with a $k_q = 4.5 \cdot 10^8$ $M^{-1}s^{-1}$, (entry 4, Table 17).

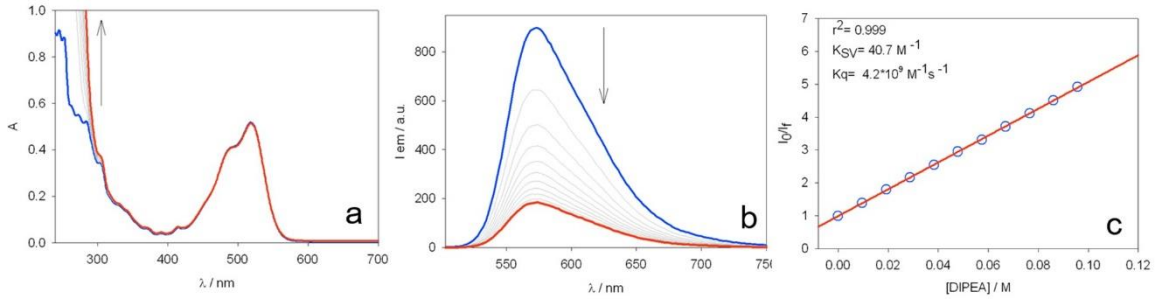

Figure 36: a) absorption and b) emission spectra of octyl-PXXMI **148** solution *ca.* $3 \cdot 10^{-5}$ M in MeCN in the presence of increasing amounts of DIPEA, from 0 to *ca.* 0.1 M; λ_{ex} = 495 nm. c) Stern-Volmer plot relative to the reductive quenching, considering emission maximum at λ_{em} = 575 nm.

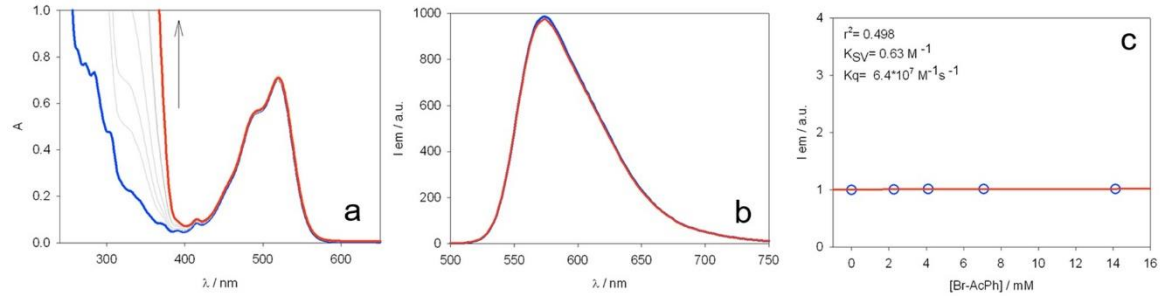

Figure 37: a) absorption and b) emission spectra of octyl-PXXMI **148** solution *ca.* $3 \cdot 10^{-5}$ M in MeCN in the presence of increasing amounts of 2-bromoacetophenone ($PhCOCH_2Br$), from 0 to *ca.* 14 mM; λ_{ex} = 495 nm. c) Stern-Volmer plot relative to the oxidative quenching, considering emission maximum at λ_{em} = 575 nm.

Table 17: Singlet quenching data for PXX derivatives.

Entry	Dye	Solvent	Quencher	Quencher E_{ox}/E_{red} [V vs SCE]	k_q [$M^{-1}s^{-1}$]
1	**PXXMI**	MeCN	DIPEA	0.52/ nd	$4.2 \cdot 10^9$
2	**PXXMI**	MeCN	$PhCOCH_2Br$	nd/-0.49	$2.2 \cdot 10^8$
3	**PXXDI**	MeCN/CH_2Cl_2	DIPEA	0.52/ nd	$5.8 \cdot 10^9$
4	**PXXDI**	MeCN/CH_2Cl_2	$PhCOCH_2Br$	nd/-0.49	$4.5 \cdot 10^8$
5	**PXX**	MeCN	DIPEA	0.52/ nd	$3.5 \cdot 10^7$
6	**PXX**	MeCN	$PhCOCH_2Br$	nd/-0.49	$2.7 \cdot 10^{10}$
7	**PXX**	MeCN	4Br-$ArCOCH_3$	nd	$1.3 \cdot 10^{10}$
8	**PXX**	CH_2Cl_2	4Br-$ArCOCH_3$	nd	$6.9 \cdot 10^9$
9	**PXX**	C_6H_6	4Br-$ArCOCH_3$	nd	$8.2 \cdot 10^8$
10	**PXX**	MeCN	4Br-ArCOH	nd/-1.76	$1.8 \cdot 10^{10}$

These results suggest that under irradiation, DIPEA is oxidised in the first step by octyl-PXXMI **148** and bis-octyl-PXXDI **141**, with the formation of respective radical anion octyl-PXXMI$^{\bullet -}$ and bis-octyl-PXXDI$^{\bullet -}$ and the radical cation DIPEA$^{\bullet +}$, (Scheme 86). Considering that the reactions also takes place in apolar solvents like C_6H_6, we can suppose that $PhCOCH_2Br$ reacts with either octyl-PXXMI$^{\bullet -}$ or bis-octyl-PXXDI$^{\bullet -}$, promoting the formation of the neutral phenacyl radical ($PhCOCH_2^{\bullet}$) and Br^- through a concerted dissociative mechanism.[245] $PhCOCH_2^{\bullet}$ successively reacts with DIPEA$^{\bullet +}$ *via* hydrogen-atom transfer (HAT)[246] providing desired product acetophenone **204** ($PhCOCH_3$) and the iminium bromide, which hydrolyses into $[H_2NiPr_2]Br$ and acetaldehyde. The formation of $[H_2NiPr_2]Br$ suggests that HAT took place only from the hydrogen of the methylene of DIPEA. Given the reactivity of $PhCOCH_2^{\bullet}$, the HAT could involve DIPEA providing as well the acetophenone **204** and $CH_3^{\bullet}CHNiPr_2$. Being a strong reducing species,[247] $CH_3^{\bullet}CHNiPr_2$ can in principle reduce $PhCOCH_2Br$ **203** leading to the formation of $PhCOCH_2^{\bullet}$ and the corresponding iminium, thereby self-propagating the reaction in a radical chain fashion (Scheme 86).[248]

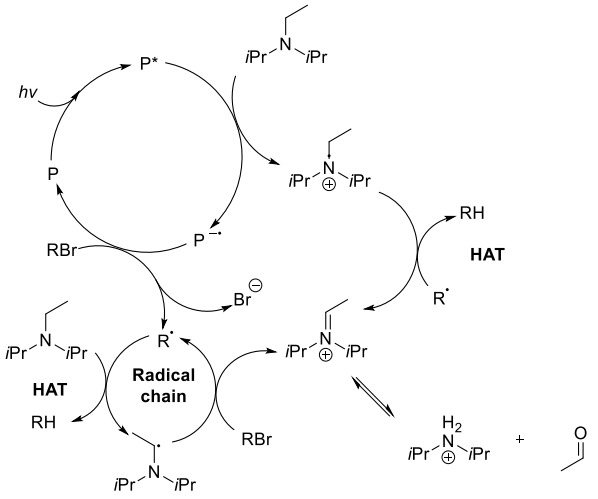

P = octyl-PXXMI,
bis-octyl-PXXDI

R = $PhCOCH_2$, EtOOC)CH

Scheme 86: Proposed photo-oxidative mechanism for octyl-PXXMI **148** /bis-octyl-PXXDI **141**.

Performing the reaction in aerated solutions did not yield any significant conversion to acetophenone **204** or other dehalogenated species, suggesting that the presence of O_2 probably inhibits the radical mechanism proposed. Moreover, we supposed that the triplet states of the octyl-PXXMI **148** and bis-octyl-PXXDI **141**, which shows a slow deactivation in deaerated solvent (~ 50 μs in C_6H_6), could have an active role in the photoinduced electron transfer process. Performing a preliminary triplet quenching analysis for octyl-

PXXMI **148** in the presence of DIPEA in C_6H_6 (Figure 38) provided a quenching constant ($k_{q\_T} = 2.5 \cdot 10^6$ $M^{-1}s^{-1}$) of two-order of magnitude lower compared with the singlet state quenching ($k_{q\_S} = 2.4 \cdot 10^8$ $M^{-1}s^{-1}$). Performing the triplet quenching analysis on the bis-octyl-PXXDI **141** resulted to no significant variation for the lifetime of the triplet (Figure 39). Therefore, taking into account all these information, the data suggest that actually in these conditions the triplet states of octyl-PXXMI **148** and bis-octyl-PXXDI **141** do not take part in the reaction mechanism.[197, 249]

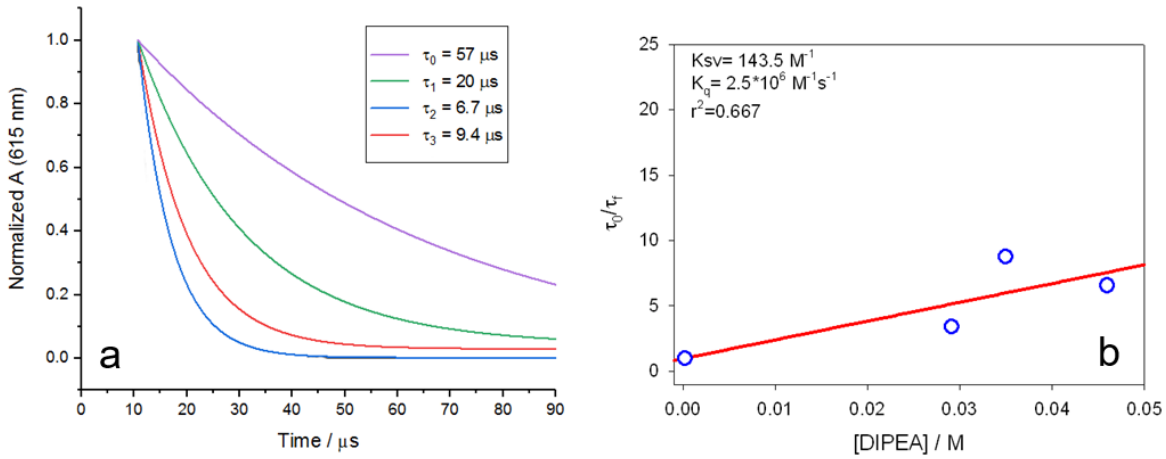

Figure 38: Time resolved transient absorption decay traces (only monoexponential fitting shown for clarity) of octyl-PXXMI **148** solution *ca.* $1.0 \cdot 10^{-5}$ M in deaerated C_6H_6 in the presence of increasing amounts of DIPEA, from 0 (purple line) to *ca.* 48 mM (black line); λ_{abs} = 615 nm; λ_{pump} = 532 nm. b) Stern-Volmer plot relative to the triplet excited state quenching by DIPEA, considering the decay times at λ_{abs} = 615 nm ($k_{q\_T} = 2.5 \cdot 10^6$ $M^{-1}s^{-1}$).

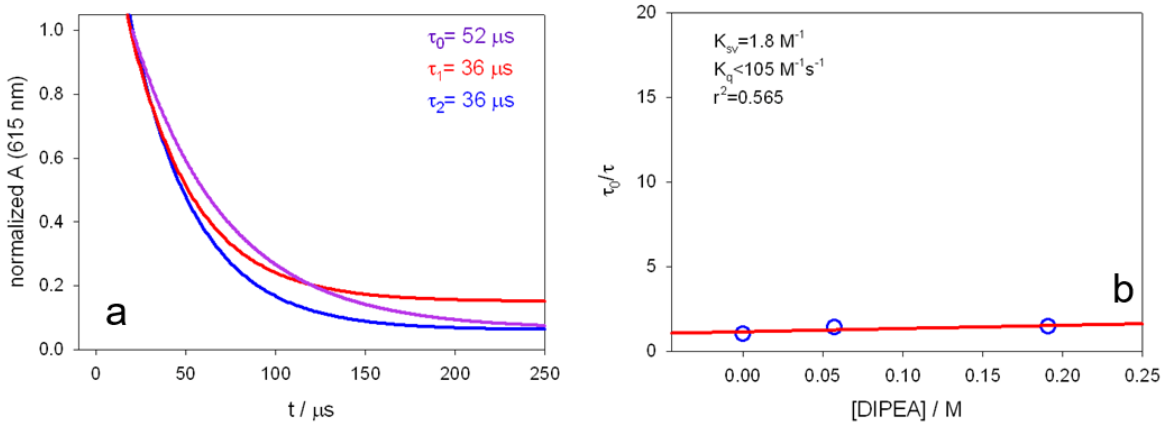

Figure 39: Time resolved transient absorption decay traces (only monoexponential fitting shown for clarity) of bis-octyl-PXXDI **141** solution *ca.* $1.0 \cdot 10^{-5}$M in deaerated C_6H_6 in the presence of increasing amounts of DIPEA, from 0 (purple line) to *ca.* 190 mM (blue line); λ_{abs} = 615 nm; λ_{pump} = 532 nm. b) Stern-Volmer plot relative to the triplet excited state quenching by DIPEA, considering the decay times at λ_{abs} = 615 nm ($k_{q\_T} < 105$ $M^{-1}s^{-1}$).

Regarding the PXX **25** Stern-Volmer studies (entries 5-10, Table 17), we observed that the quenching rate with 4Br-$ArCOCH_3$ (entry 7, Table 17) is considerably higher than the quenching rate observed with DIPEA (entry 5, Table 17) in MeCN. As expected, lower quenching constants are observed in less polar solvents such as CH_2Cl_2 (entry 8 Table 17) and C_6H_6 (entry 9 Table 17). In contrast to the imide derivatives, this evidence suggests that the formation of the radical cation $PXX^{\bullet+}$ with the simultaneous reduction of $4BrArCOCH_3$, into a ketyl radical anion derivative,[250] is stabilized in polar solvents (Scheme 87). The newly formed ketyl radical anion $4BrArCOCH_3^{\bullet-}$ undergoes fragmentation by dissociative electron transfer, providing the formation of aryl radical $^{\bullet}ArCOCH_3$ and Br^- anion.[251] In 1986, Andrieux et al. proposed that initially the unpaired electron is located in a π* orbital of the aromatic system.[251] As consequence of the C-Br stretching a three-electron bond is formed which afterwards cleaves in a unpaired electron located in the σ-HOMO orbital of the aryl radical $^{\bullet}ArCOCH_3$ and an electron pair is carried away in the p atomic orbital of the bromine atom. The stretching of the C-Br bond corresponds in stabilization of C-Br σ* orbital whereas the variation of energy π* orbital is small.[252] The crossing point of π* and a σ* energy levels can thus be considered the representation of the transition state.[251] Eventually in the proposed mechanism, $PXX^{\bullet+}$ reacts with DIPEA forming $DIPEA^{\bullet+}$. The latter is possibly reacting with $^{\bullet}ArCOCH_3$ through hydrogen atom transfer affording the $ArCOCH_3$ and the relevant iminium. Remarkably, the ketyl radical intermediate cannot be formed by reduction with $CH_3{}^{\bullet}CHNiPr_2$, otherwise it would have taken place in the photosystems involving octyl-PXXMI **148** and bis-octyl-PXXDI **141**.

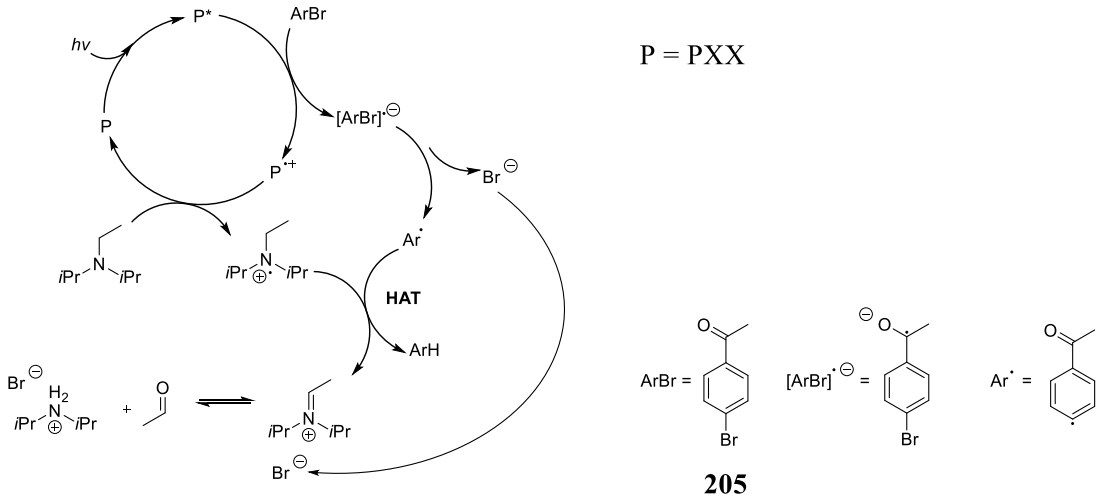

Scheme 87: Proposed photoreductive mechanism for PXX **25**.

Photodegradation upon laser excitation at 355 nm prevented the gathering of information of the activity of the excited triplet state of PXX **25**.

3.6.2 Electron Paramagnetic Resonance Investigations

To investigate the presence of the relevant radicals postulated in the mechanisms, electron paramagnetic resonance was performed. We started to investigate a deaerated solution of octyl-PXXMI **148**, DIPEA and 2-bromoacetophenone in CH_2Cl_2. This solution was analysed in the dark. From the CW X-band EPR spectra we observed the presence of nitroxyl radical **N1•** and **N2•**, both possibly derived from the dealkylation of trace DIPEA-N-oxide[253] (Figure 40).

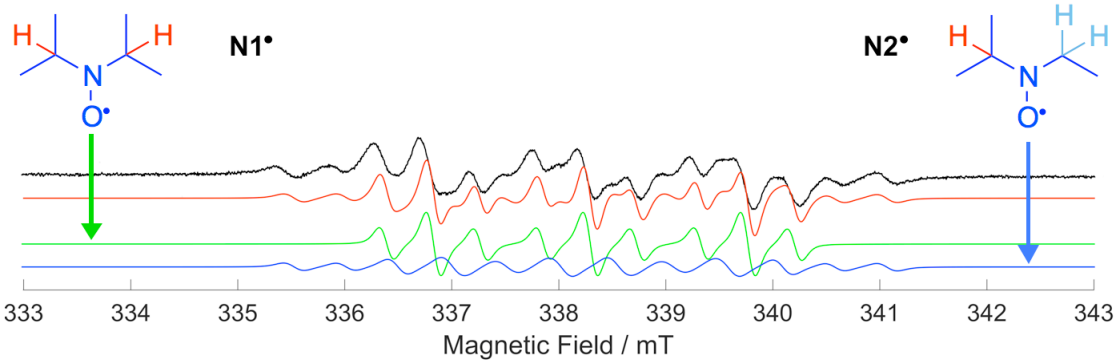

Figure 40: CW X-band EPR spectra (black traces) recorded at RT for CH_2Cl_2 solutions of $PhCOCH_2Br$ (0.05m), DIPEA (0.40m) and octyl-PXXMI (2.5 mm), before of irradiation in the absence PBN. EPR simulations are shown in red. The deconvoluted simulated spectra of diisopropylnitroxyl radical **N1•** and isopropylethylnitroxyl radical **N2•**, respectively are shown in green and blue.

Upon irradiation, the same signals display a steep increase in intensity, reaching a maximum which is possibly related to the consumption of the residual trace of O_2.[254] Then, a decrease in signal intensity is detected in a few seconds, possibly due to the scavenging of the paramagnetic **N1•** and **N2•** species by radical recombination and/or by quenching of the excited states of the dye. This suggests that the nitroxides could extinguish the photoinduced dehalogenation reaction (Figure 41).[255]

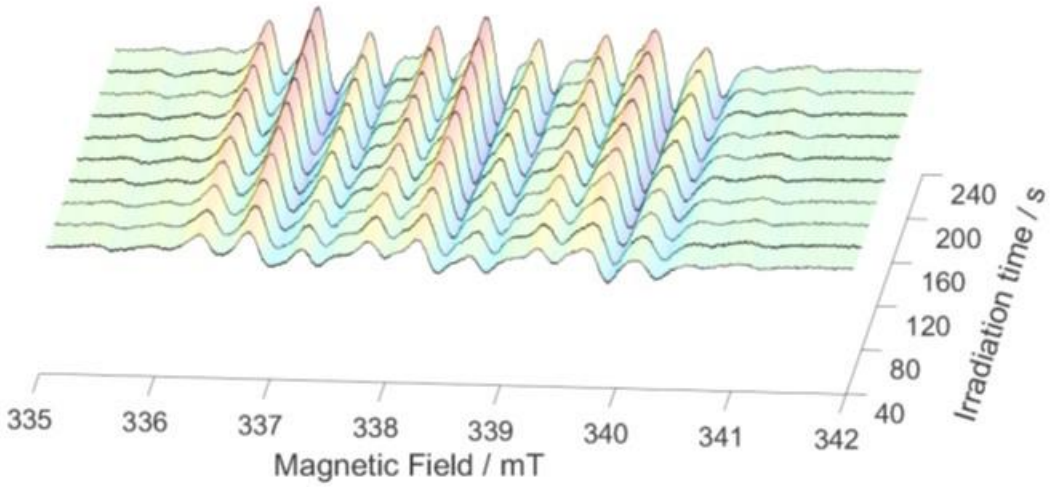

Figure 41: CW X-band EPR spectra revealing the kinetics of the first 240 s of irradiation using a 530 nm LED light source for the reaction system containing 2-bromoacetophenone, DIPEA and octyl-PXXMI **148** in CH_2Cl_2 at 298 K.

Upon prolonged irradiation of the reaction mixture, we gradually observed a new series of signals appearing in the EPR spectrum (Figure 42) that can be easily attributed to photoinduced radical **Ph-N2•**.

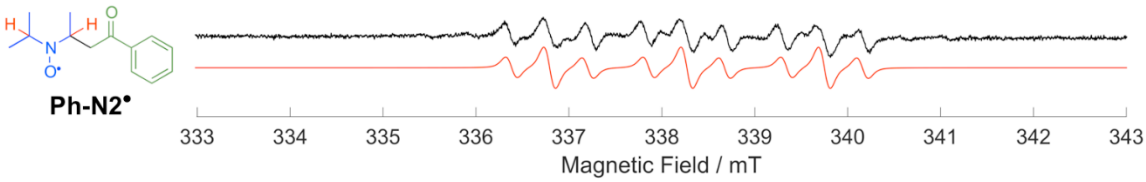

Figure 42: CW X-band EPR spectra of the reaction system containing 2-bromoacetophenone, DIPEA and octyl-PXXMI **148** after *ca.* 50 min irradiation (λ_{ex} = 530 nm) in CH_2Cl_2 at 298 K (black line). The EPR simulation is shown as the red line.

Performing the EPR experiment on the reaction mixture in the presence of *N-tert*-butyl-α-phenylnitrone (PBN) as a spin trap, which is a technique to determine the existence of short lived free radicals, under irradiation, in addition to the already described EPR signals of

Ph-N2•, we observed the formation of EPR signals that can be unambiguously assigned to the nitroxyl radical **Ph-ST•** which derived from the reaction of the photoinduced radical $PhCOCH_2^{\bullet}$ with PBN, (Figure 43).

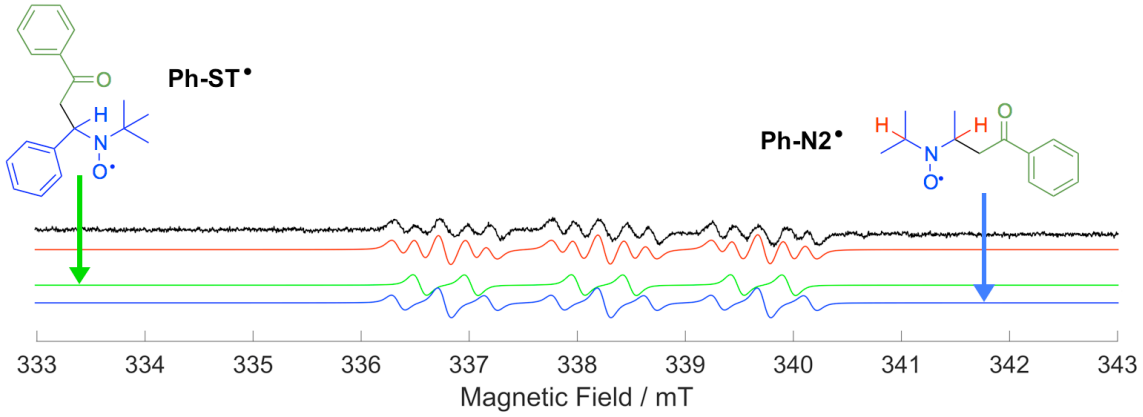

Figure 43: CW X-band EPR spectra of the reaction system containing 2-bromoacetophenone, DIPEA and octyl-PXXMI **148** after *ca.* 50 min irradiation (λ_{ex} = 530 nm) in CH_2Cl_2 at 298 K in the presence of *N-tert*-butyl-α-phenylnitrone (PBN) as a spin trap (black line). The EPR simulation is shown as the red line. The deconvoluted simulated spectra of the PBN-phenacyl radical adduct **Ph-ST•**.

Subsequently we studied a deaerated solution of PXX **25**, DIPEA and 4'-bromoacetophenone in CH_2Cl_2 in the dark. In solutions of octyl-PXXMI **148** kept in the dark we observed the presence of nitroxyl radical **N1•** and **N2•** (Figure 44-a); upon irradiation, their corresponding signals increase until a maximum and then decrease, (Figure 45-b). After this time-lapse, a new series of EPR signals, which are related to the formation of the photoinduced radical **Ar-N2•** (Figure 44-b) appear. When the reaction mixture is irradiated in presence of PBN, in addition to the signal of **Ar-N2•**, new EPR signals are present, which can be unambiguously assigned to the nitroxyl radical **Ar-ST•**, as product of the reaction between PBN with $^{\bullet}ArCOCH_3$ (Figure 44-c). The evolution of the signal corresponding to **Ar-ST•** as function of the irradiation time is depicted in Figure 45-A, showing a steady increase after 180 seconds of irradiation, suggesting the formation of **Ar•** and therefore the progression of the dehalogenation.

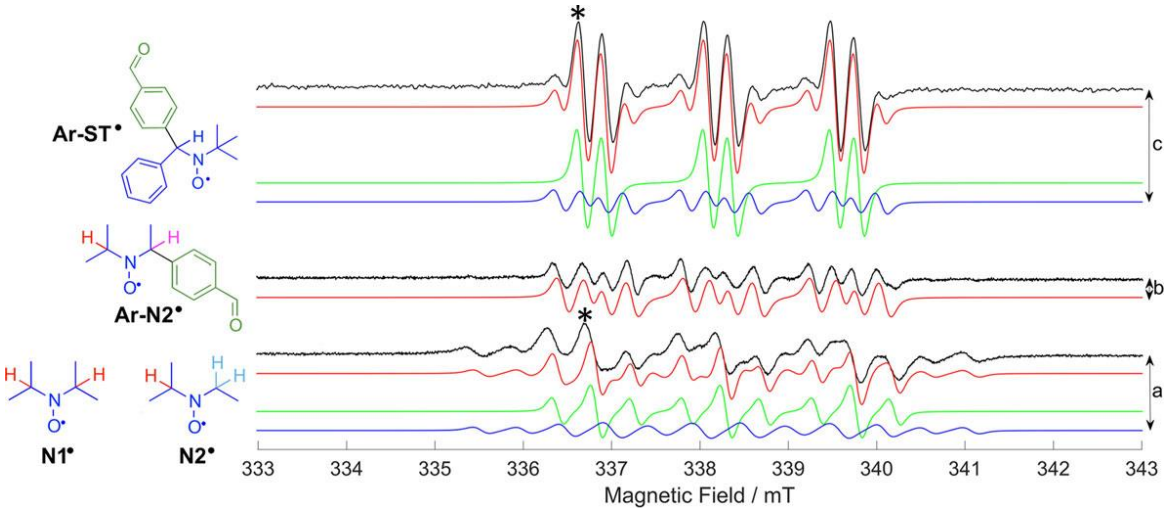

Figure 44: CW X-band EPR spectra (black traces) recorded at RT for CH_2Cl_2 solutions of 4Br-ArCOH (0.05 M), DIPEA (0.40 mM) and PXX (2.5 mM), before (a) and after (b) *ca.* 50 min of irradiation (λ_{ex} = 455 nm) both in the absence (b) and presence (c) of PBN. EPR simulations are shown in red. The deconvoluted simulated spectra of **N1•** and **N2•** are reported in green and blue, respectively in (a) whilst those of **Ar-ST•** and **Ar-N2•** are reported in green and blue, respectively in (c). Star indicates the magnetic field monitored during the kinetical analysis.

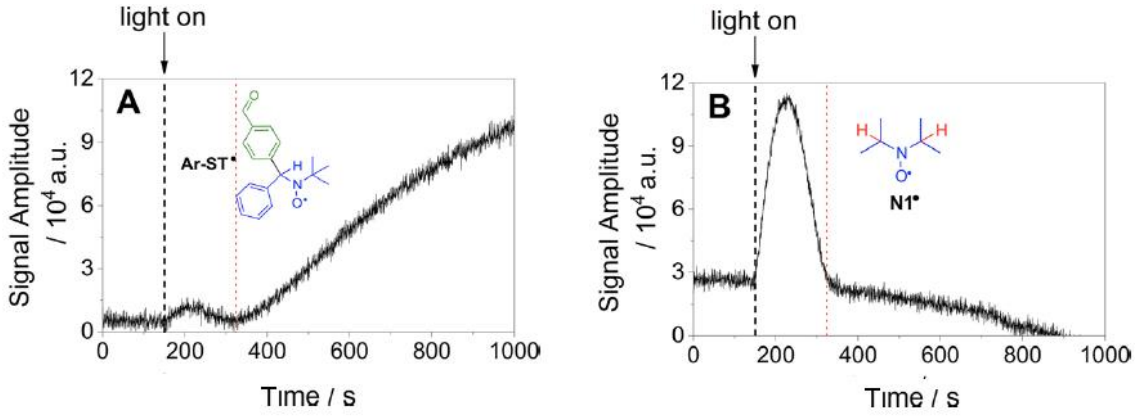

Figure 45: Evolution of the EPR signal intensity as a function of the irradiation time (λ_{ex} = 455 nm) taken at 336.6 mT in the presence of PBN (A) and at 336.7 mT in the absence of PBN (B) for a solution containing PXX **25**, DIPEA and 4-bromobenzaldehyde in CH_2Cl_2. Black line indicates the start of the irradiation; red line indicates the start of the production of the **Ar-ST•** radical.

3.6.3 Phototriggered chemoselective dehalogenation

Based on this mechanistic insight, we could envisage a phototriggered chemoselective dehalogenation of distinctive C-Br groups, sequentially irradiating with green and blue light. In principle, this would enable a chemoselective transformation on the same substrate. Chemoselectivity is a fundamental problem in multi-step and multicomponent reactions. As proof of concept, we decided to consider as substrate 2,4'-dibromoacetophenone, 4Br-ArCOCH$_2$Br, which is featured by two C-Br bonds having

different reactivities. A solution of 4Br-ArCOCH$_2$Br **215**, DIPEA, PXX and octyl-PXXMI in MeCN was irradiated with green light (λ_{irr} = 520 nm) for 30 hours providing selectively the α-dehalogenated product 4Br-ArCOCH$_3$ **205**. Subsequently, irradiation with blue light (λ_{irr} = 460 nm) for 44 hours afforded the complete conversion to PhCOCH$_3$, **204** (Scheme 88).

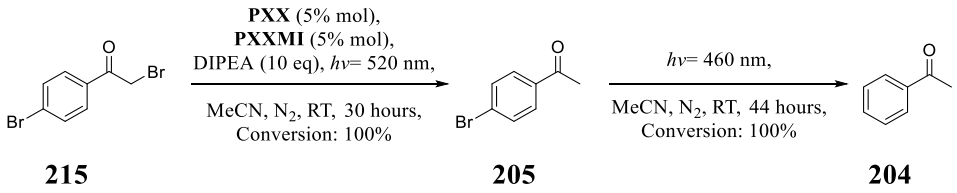

Scheme 88: Phototriggered chemoselective dehalogenation.

Taking into account the low concentration of the dyes (5% mol), we can consider that the two chromophores act orthogonally upon a selective irradiation, following the photoinduced mechanisms proposed (Scheme 86 and Scheme 87). Stern-Volmer analysis showed that the PXX **25** acts as a very effective quencher of the singlet excited state of the octyl-PXXMI **148** with a $k_q \approx 2.2 \cdot 10^{10}$ $M^{-1}s^{-1}$, suggesting the fast and efficient electron transfer to form the $PXX^{\bullet+}$/octyl-$PXXMI^{\bullet-}$ couple suggesting that PXX **25** is acting as quencher similar to DIPEA (Figure 46).

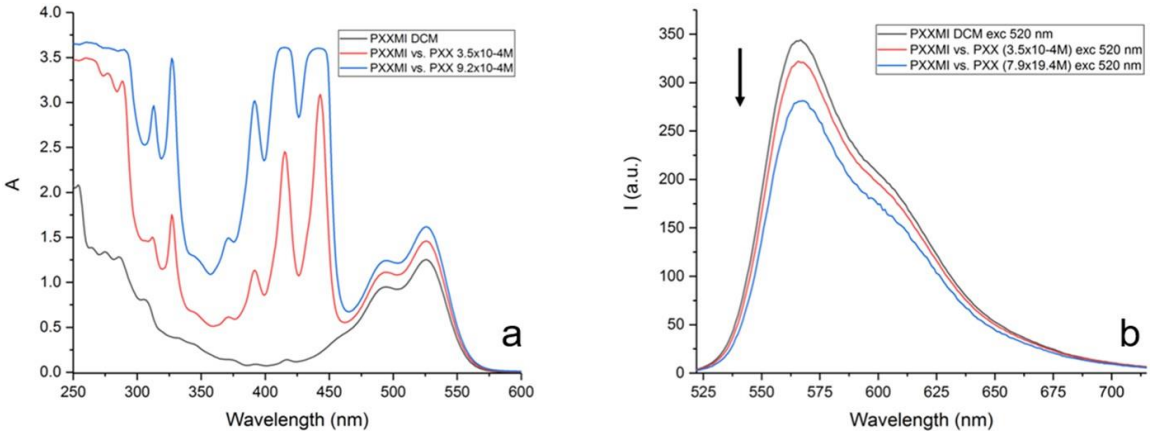

Figure 46: a) absorption and b) emission spectra of a octyl-PXXMI **148** solution *ca.*$1.4 \cdot 10^{-4}$ M in CH_2Cl_2 in the presence of increasing amounts of PXX **25**, from 0 to 0.92 mM; λ_{ex}=520 nm. By Stern-Volmer analysis, the estimated quenching constant kq_PXX relative to the reductive quenching of octyl-PXXMI **148** is ≈ $2.5 \cdot 10^{10}$ $M^{-1}s^{-1.}$

However, in the presence of an excess of DIPEA (≈ 0.25 M) only 3% of singlet excited states of octyl-PXXMI **148** can by quenched by PXX **25**. To corroborate these

assumptions, we performed the dehalogenation reactions under more diluted conditions. As expected the desired products were provided, although with a lower conversion.

3.7. Conclusion

Studying the spectroscopic properties of PXX derivatives using PXX **25** as a reference, the absorption spectra show a clear bathochromic shift for both octyl-PXXMI **148** and bis-octyl-PXXDI **141**. This is a consequence of the presence of the electron withdrawing imide group. As observed by comparing the spectra, the number of the imide moieties introduced on the PXX changes the shape and intensity of the absorption band. However, it is worth mentioning that, whereas in the case of octyl-PXXMI **148** we observe a strong shift of 82 nm, in the case of bis-octyl-PXXDI the further shift in the spectra is less than 15 nm in CH_2Cl_2. This implies that the second imide functionalization does not affect dramatically the energy associated to the transition. Similarly, the fluorescence spectra of PXX **25**, octyl-PXXMI **148** and bis-octyl-PXXDI **141** display a bathochromic shift highlighting the difference in shape and vibrational structure of the absorption profile. The PXX derivatives do not exhibit phosphorescence even at low temperature (77 K). However, a non-emissive triplet has been detected by transient spectroscopy. From cyclic voltammetry analysis we observe that the introduction of electron withdrawing imide substituents on the PXX induces an electron depletion on the aromatic core. Consequently, octyl-PXXMI **148** and bis-octyl-PXXDI **141** are increasingly more difficult to be oxidised and easier to be reduced. In both cases, the shift in the reduction and oxidation halfwave potential is 0.3V. Therefore, the spectroscopic and electrochemical results highlight a rigid energy shift of the frontier molecular orbitals. Comparing the redox potential of the singlet excited state of the PXX derivatives with the most well-known photoredox catalysts such as $[Ru(bpy)_3]^{2+}$ and $[Ir(ppy)_3]$ complexes, we observe that octyl-PXXMI **148** and bis-octyl-PXXDI **141** are stronger reducers and oxidisers than the triplet excited state of $[Ru(bpy)_3]^{2+}$. Additionally, the singlet excited state of the parent PXX **25** is a greater reducer and oxidiser compared to the triplet excited state of $[Ir(ppy)_3]$.

Capitalizing on these results, we employed the PXX derivatives in photoredox transformation as photocatalysts. We studied the photocatalytic dehalogenation of organic

halides as a model reaction, as well as the subsequent phototriggered mechanism. The fact that PXX derivatives have different photoredox properties results in a difference in their photocatalytic activity. Based on this difference of their photoredox properties, octyl-PXXMI **148** and bis-octyl-PXXDI **141** are catalytically active on dehalogenation of Csp^3, but not on aromatic substrates. On the other hand, PXX is active also on dehalogenation reactions involving bromo aromatic derivatives. Investigation of the mechanisms by Stern-Volmer analysis reveals that octyl-PXXMI **148** and bis-octyl-PXXDI **141** proceed through an oxidative mechanistic quenching. However, PXX photocatalytic cycle is based on a reductive quenching. Confirmation of the catalytic mechanism has been established by EPR analysis. Based on the difference in the absorption and photoredox properties, we were able to perform a chemoselective transformation by irradiating the reaction mixture, containing PXX **25** and octyl-PXXMI **148**, at two different wavelengths.

References:

[1] J. R. Barnett, S. Miller, E. Pearce, *Opt. Laser Technol.* **2006**, *38*, 445-453.

[2] R. D. Welham, *J. Soc. Dyers Colour*.**1963**, *79*, 98-105.

[3] W. H. Perkin, Patent *GB 1984*, **1856**.

[4] I. Holme, *Color. Technol.* **2006**, *122*, 235-251.

[5] S. Holgate, *Understanding Solid State Physics*, Boca Raton: CRC Press., **2009**.

[6] M. Pope, C. E. Swenberg, *Electronic Processes in Organic Crystals and Polymers*, Oxford University Press, **1999**.

[7] a) R. R. Moskalyk, *Miner. Eng.* **2003**, *16*, 921-929; b) J. S. Blakemore, *J. Appl. Phys.* **1982**, *53*, R123-R181.

[8] J. Whitaker, *Solid State Electron.***1965**, *8*, 649-652.

[9] a) G. Cassabois, P. Valvin, B. Gil, *Nat. Photonics*, **2016**, *10*, 262–266; b) G. K. Gaule, *Boron: Vol. 2: Preparation, Properties, and Applications*, Plenum Press, **1965**.

[10] a) M. Arif, M. Rahman, W. Y. San, *Int. J. Adv. Manuf. Technol.* **2012**, *63*, 481-504; b) G. L. Pearson, J. Bardeen, *Phys. Rev.* **1949**, *75*, 865-883.

[11] W. M. Holt, *Proc. IEEE Int'l Solid State Circuits Conf.*, **2016,** 8–13.

[12] K. P. Goetz, D. Vermeulen, M. E. Payne, C. Kloc, L. E. McNeil, O. D. Jurchescu, *J. Mater. Chem. C* **2014**, *2*, 3065-3076.

[13] a) A. C. Annis., *Dig. Tech. Pap.* **2017**, *48*, 1509-1511; b) H. E. Katz, *Chem. Mater.* **2004**, *16*, 4748-4756.

[14] S. E. Root, S. Savagatrup, A. D. Printz, D. Rodriquez, D. J. Lipomi, *Chem. Rev.* **2017**, *117*, 6467-6499.

[15] J. W. Ward, Z. A. Lamport, O. D. Jurchescu, *ChemPhysChem* **2015**, *16*, 1118-1132.

[16] H. Sirringhaus, *Adv. Mater.* **2014**, *26*, 1319-1335.

[17] E. A. Davis, N. F. Mott, *Philos. Mag.* **1970**, *22*, 903-922.

[18] V. Coropceanu, J. Cornil, D. A. da Silva Filho, Y. Olivier, R. Silbey, J. L. Brédas, *Chem. Rev.* **2007**, *107*, 926-952.

[19] H. Sirringhaus, *Adv. Mater.* **2009**, *21*, 3859-3873.

[20] a) A. A. Shoustikov, Y. Yujian, M. E. Thompson, *IEEE Journal of Selected Topics in Quantum Electronics* **1998**, *4*, 3-13; b) M. Jacob, *Electronics* **2014**, *3*, 594-597; c) C., Sekine, Y. Tsubata, T. Yamada, M. Kitano, S. Doi, *Sci. Technol. Adv. Mater.* **2014,** *15*, 034203; d) L. A. Duan, L. D. Hou, T. W. Lee, J. A. Qiao, D. Q. Zhang, G. F. Dong, L. D. Wang and Y. Qiu, *J. Mater. Chem.* **2010**, *20*, 6392-6407.

[21] a) J Roncali, P.Leriche, P. Blanchard, *Adv. Mater.***2014**, *26*, 3821-3838; b) Y. Lin, Y. Li, X. Zhan, *Chem. Soc. Rev.* **2012**, *41*, 4245-4272.

[22] A. Facchetti, *Mater. Today.* **2007**, *10*, 28-37.

[23] Y. Xu, H. Sun, Y. Y. Noh, *IEEE Trans. Electron Devices* **2017**, *64*, 1932-1943.

[24] a) J Roncali, *Macromol. Rapid Commun.* **2007**, *28*, 1761-1775; b) J. Roncali, *Chem. Rev.* **1997**, *97*, 173-206.

[25] a) H. A. M. van Mullekom, J. A. J. M. Vekemans, E. E. Havinga, E. W. Meijer, *Mater. Sci. Eng. R* 2001, *32*, 1-40; b) M. Stępień, E. Gońka, M. Żyła, N. Sprutta, *Chem. Rev.* **2017**, *117*, 3479-3716.

[26] S. Ito, S. Hiroto, S. Lee, M. Son, I. Hisaki, T. Yoshida, D. Kim, N. Kobayashi, H. Shinokubo, *J. Am. Chem. Soc.* **2015**, *137*, 142-145.

[27] a) P. M. Beaujuge, C. M. Amb, J. R. Reynolds, *Acc. Chem. Res.* **2010**, *43*, 1396-1407; b) D. P. Hagberg, T. Marinado, K. M. Karlsson, K. Nonomura, P. Qin, G. Boschloo, T. Brinck, A. Hagfeldt, L. Sun, *J. Org. Chem.* **2007**, *72*, 9550-9556.

[28] O. Wennerstroem, *Macromolecules* **1985**, *18*, 1977-1980.

[29] R. S. Peierls, *Quantum theory of solids*, Oxford: Oxford University Press, **2001**.

[30] a) J. L. Brédas, *J. Chem. Phys.* **1985**, *82*, 3808-3811; b) W. P. Su, J. R. Schrieffer, A. J. Heeger, *Phys. Rev. Lett.* **1979**, *42*, 1698-1701; c) J. P. Lowe, S. A. Kafafi, *J. Am. Chem. Soc.* **1984**, *106*, 5837-5841; d) Y. S. Lee, M. Kertesz, *J. Chem. Phys* **1988**, *88*, 2609-2617.

[31] F. Wudl, M. Kobayashi, A. J. Heeger, *J. Org. Chem.* **1984**, *49*, 3382-3384.

[32] a) M. Pomerantz, B. Chaloner-Gill, L. O. Harding, J. J. Tseng, W. J. Pomerantz, *J. Chem. Soc., Chem. Commun.* **1992**, *22*, 1672-1673; b) S. Y. Hong, D. S. Marynick, *Macromolecules* **1992**, *25*, 4652-4657; c) G. A. Sotzing, K. Lee, *Macromolecules* **2002**, *35*, 7281-7286.

[33] a) R. S. Mulliken, C. A. Rieke, W. G. Brown, *J. Am. Chem. Soc.* **1941**, *63*, 41-56; b) J. L. Brédas, G. B. Street, B. Thémans, J. M. André, *J. Chem. Phys* **1985**, *83*, 1323-1329.

[34] J. Roncali, R. Garreau, A. Yassar, P. Marque, F. Garnier, M. Lemaire, *J. Phys. Chem.* **1987**, *91*, 6706-6714.

[35] L. Zöphel, V. Enkelmann, K. Müllen, *Org. Lett.* **2013**, *15*, 804-807.

[36] E. E. Havinga, W. ten Hoeve, H. Wynberg, *Polym. Bull.* **1992**, *29*, 119-126.

[37] F. Würthner, S. Ahmed, C. Thalacker, T. Debaerdemaeker, *Chem. Eur. J.* **2002**, *8*, 4742-4750.

[38] R. S. K. Kishore, O. Kel, N. Banerji, D. Emery, G. Bollot, J. Mareda, A. Gomez-Casado, P. Jonkheijm, J. Huskens, P. Maroni, M. Borkovec, E. Vauthey, N. Sakai, S. Matile, *J. Am. Chem. Soc.* **2009**, *131*, 11106-11116.

[39] a) M. Licchelli, A. Orbelli Biroli, A. Poggi, *Org. Lett.* **2006**, *8*, 915-918; b) S. Alp, Ş. Erten, C. Karapire, B. Köz, A. O. Doroshenko, S. İçli, *J. Photochem. Photobiol. A Chem.* **2000**, *135*, 103-110.

[40] a) C. Thalacker, C. Röger, F. Würthner, *J. Org. Chem.* **2006**, *71*, 8098-8105; b) C. Röger, F. Würthner, *J. Org. Chem.* **2007**, *72*, 8070-8075.

[41] T. H. Vo, M. Shekhirev, D. A. Kunkel, F. Orange, M. J. F. Guinel, A. Enders, A. Sinitskii, *Chem. Commun.* **2014**, *50*, 4172-4174.

[42] A. Escande, M. J. Ingleson, *Chem. Commun.* **2015**, *51*, 6257-6274.

[43] a) T. Baumgartner, *Acc. Chem. Res.* **2014**, *47*, 1613-1622; b) Q. Miao, *Polycyclic Arenes and Heteroarenes*, Wiley-VCH Verlag, **2015**.

[44] L. Zhang, S. M. Fakhouri, F. Liu, J. C. Timmons, N. A. Ran, A. L. Briseno, *J. Mater. Chem.* **2011**, *21*, 1329-1337.

[45] J. E. Anthony, *Chem. Rev.* **2006**, *106*, 5028-5048.

[46] F. Dötz, J. D. Brand, S. Ito, L. Gherghel, K. Müllen, *J. Am. Chem. Soc.* **2000**, *122*, 7707-7717.

[47] S. Allard, M. Forster, B. Souharce, H. Thiem, U. Scherf, *Angew. Chem. Int. Ed.* **2008**, *47*, 4070-4098.

[48] D. Adam, P. Schuhmacher, J. Simmerer, L. Häussling, K. Siemensmeyer, K. H. Etzbachi, H. Ringsdorf, D. Haarer, *Nature* **1994**, *371*, 141-143.

[49] a) W. Pisula, A. Menon, M. Stepputat, I. Lieberwirth, U. Kolb, A. Tracz, H. Sirringhaus, T. Pakula, K. Müllen, *Adv. Mater*. **2005**, *17*, 684-689; b) A. M. van de Craats, J. M. Warman, A. Fechtenkötter, J. D. Brand, M. A. Harbison, K. Müllen, *Adv. Mater.* **1999**, *11*, 1469-1472; c) K. D. Harris, S. Xiao, C. Y. Lee, M. S. Strano, C. Nuckolls, G. B. Blanchet, *J. Phys. Chem. C* **2007**, *111*, 17947-17951.

[50] N. G. Pschirer, C. Kohl, F. Nolde, J. Qu, K. Müllen, *Angew. Chem. Int. Ed.* **2006**, *118*, 1429-1432.

[51] a) T. Weil, T. Vosch, J. Hofkens, K. Peneva, K. Müllen, *Angew. Chem. Int. Ed.* **2010**, *49*, 9068-9093; b) X. Zhan, A. Facchetti, S. Barlow, T. J. Marks, M. A. Ratner, M. R. Wasielewski, S. R. Marder, *Adv. Mater.* **2011**, *23*, 268-284.

[52] Y. Avlasevich, C. Li, K. Mullen, *J. Mater. Chem.* **2010**, *20*, 3814-3826.

[53] M. Kardos, Patent *DE 276956*, **1913**.

[54] a) W. Herbst, K. Hunger, *Industrial organic pigments: production, properties, applications*, John Wiley & Sons, **2006**; b) M. Kardos, Patent *DE 276357*, **1913**.

[55] F. Würthner, *Chem. Commun.* **2004**, *14*,1564-1579.

[56] a) W. E. Ford, P. V. Kamat, *J. Phys. Chem.* **1987**, *91*, 6373-6380; b) G. Seybold, G. Wagenblast, *Dyes and Pigm.* **1989**, *11*, 303-317; c) T. Weil, U. M. Wiesler, A. Herrmann, R. Bauer, J. Hofkens, F. C. De Schryver, K. Müllen, *J. Am. Chem. Soc.* **2001**, *123*, 8101-8108; d) R. Gronheid, J. Hofkens, F. Köhn, T. Weil, E. Reuther, K. Müllen, F. C. De Schryver, *J. Am. Chem. Soc.* **2002**, *124*, 2418-2419; e) J. M. Serin, D. W. Brousmiche, J. M. J. Fréchet, *Chem. Commun.* **2002**, 2605-2607; f) B. A. Jones, A. Facchetti, M. R. Wasielewski, T. J. Marks, *J. Am. Chem. Soc.* **2007**, *129*, 15259-15278.

[57] R. Schmidt, K. Griesbaum, A. Behr, D. Biedenkapp, H. Voges, D. Garbe, C. Paetz, G. Collin, D. Mayer, H. Höke, *Ullmann's Encyclopedia of Industrial Chemistry*, Vol. 18 Wiley-VCH Verlag, **2014**, 133-189.

[58] a) I. Farbenindustrie, Patent *DE 428 088*, **1921**; b) Selden, Patent *GB 318 617*, **1929**.

[59] H. Langhals, *Heterocycles* **1995**, *40*, 477-500.

[60] C. Huang, S. Barlow, S. R. Marder, *J. Org. Chem.* **2011**, *76*, 2386-2407.

[61] F. Würthner, C. Thalacker, S. Diele, C. Tschierske, *Chem. Eur. J.* **2001**, *7*, 2245-2253.

[62] M. Sadrai, L. Hadel, R. R. Sauers, S. Husain, K. Krogh-Jespersen, J. D. Westbrook, G. R. Bird, *J. Phys. Chem.* **1992**, *96*, 7988-7996.

[63] a) S. L. Oliveira, D. S. Corrêa, L. Misoguti, C. J. L. Constantino, R. F. Aroca, S. C. Zilio, C. R. Mendonça, *Adv. Mater.* **2005**, *17*, 1890-1893; b) D. S. Corrêa, S. L. Oliveira, L. Misoguti, S. C. Zilio, R. F. Aroca, C. J. L. Constantino, C. R. Mendonça, *J. Phys. Chem. A* **2006**, *110*, 6433-6438.

[64] F. Würthner, A. Sautter, J. Schilling, *J. Org. Chem.* **2002**, *67*, 3037-3044.

[65] R. Schmidt, J. H. Oh, Y. S. Sun, M. Deppisch, A. M. Krause, K. Radacki, H. Braunschweig, M. Könemann, P. Erk, Z. Bao, F. Würthner, *J. Am. Chem. Soc.* **2009**, 131, 6215-6228.

[66] a) Y. Nagao, *Prog. Org. Coat.* **1997**, *31*, 43-49; b) I. K. Iverson, S. W. Tam-Chang, *J. Am. Chem. Soc.* **1999**, *121*, 5801-5802.

[67] L. Ivan, L. Heinz, *Chem. Ber.* **1983**, *116*, 3524-3528.

[68] a) M. Sommer, S. M. Lindner, M. Thelakkat, *Adv. Funct. Mater.* **2007**, *17*, 1493-1500; b) S. Michael, L. A. S., T. Mukundan, *Angew. Chem. Int. Ed.* **2008**, *47*, 7901-7904; c) S. M. Lindner, S. Hüttner, A. Chiche, M. Thelakkat, G. Krausch, *Angew. Chem. Int. Ed.* **2006**, *45*, 3364-3368; d) S. Hóttner, M. Sommer, M. Thelakkat, *Appl. Phys. Lett.* **2008**, *92*, 093302.

[69] F. Würthner, C. R. Saha-Möller, B. Fimmel, S. Ogi, P. Leowanawat, D. Schmidt, *Chem. Rev.* **2016**, *116*, 962-1052.

[70] A. Boehm, H. Arms, G. Henning, P. Blaschka, Patent. *DE 19547209 A1*, **1997**.

[71] V. I. Rogovik, L. F. Gutnik, *Zh. Org. Khim.* **1988**, *24*, 635-639.

[72] a) C. Zhao, Y. Zhang, R. Li, X. Li, J. Jiang, *J. Org. Chem.* **2007**, *72*, 2402-2410; b) R. K. Dubey, A. Efimov, H. Lemmetyinen, *Chem. Mater.* **2011**, *23*, 778-788; c) L. Perrin, P. Hudhomme, *Eur. J. Org. Chem.* **2011**, *28*, 5427-5440.

[73] F. Würthner, V. Stepanenko, Z. Chen, C. R. Saha- Möller, N. Kocher, D. Stalke, *J. Org. Chem.* **2004**, *69*, 7933-7939.

[74] a) W. Qiu, S. Chen, X. Sun, Y. Liu, D. Zhu, *Org. Lett.* **2006**, *8*, 867-870; b) M. Queste, C. Cadiou, B. Pagoaga, L. Giraudet, N. Hoffmann, *New J. Chem.* **2010**, *34*, 2537-2545; c) V. Sivamurugan, K. Kazlauskas, S. Jursenas, A. Gruodis, J. Simokaitiene, J. V. Grazulevicius, S. Valiyaveettil, *J. Phys. Chem. B* **2010**, *114*,

1782-1789; d) S. Dey, A. Efimov, H. Lemmetyinen, *Eur. J. Org. Chem.* **2012**,*12*, 2367-2374.

[75] a) U. Rohr, P. Schlichting, A. Böhm, M. Gross, K. Meerholz, C. Bräuchle, K. Müllen, *Angew. Chem. Int. Ed.* **1998**, *37*, 1434-1437; b) N. V. Handa, K. D. Mendoza, L. D. Shirtcliff, *Org. Lett*. **2011**, *13*, 4724-4727; c) C. Lótke Eversloh, C. Li, K. Müllen, *Org. Lett.* **2011**, *13*, 4148-4150.

[76] a) M. J. Ahrens, M. J. Fuller, M. R. Wasielewski, *Chem. Mater*. **2003**, *15*, 2684-2686; b) B. A. Jones, M. J. Ahrens, M. H. Yoon, A. Facchetti, T. J. Marks, M. R. Wasielewski, *Angew. Chem. Int. Ed.* **2004**, *43*, 6363-6366; c) R. T. Weitz, K. Amsharov, U. Zschieschang, E. B. Villas, D. K. Goswami, M. Burghard, H. Dosch, M. Jansen, K. Kern, H. Klauk, *J. Am. Chem. Soc.* **2008**, *130*, 4637-4645.

[77] U. Rohr, C. Kohl, K. Müllen, A. van de Craats, J. Warman, *J. Mater. Chem.* **2001**, *11*, 1789-1799.

[78] a) Y. Li, L. Tan, Z. Wang, H. Qian, Y. Shi, W. Hu, *Org. Lett.* **2008**, *10*, 529-532; b) T. Schnitzler, C. Li, K. Müllen, *Helv. Chim. Acta* **2009**, *92*, 2525-2531.

[79] J. E. Anthony, A. Facchetti, M. Heeney, S. R. Marder, X. Zhan, *Adv. Mater.* **2010**, *22*, 3876-3892.

[80] F. Würthner, C. Thalacker, S. Diele, C. Tschierske, *Chem. Eur. J.* **2001**, *7*, 2245-2253.

[81] A. S. Lukas, Y. Zhao, S. E. Miller, M. R. Wasielewski, *J. Phys. Chem. B* **2002**, *106*, 1299-1306.

[82] a) W. E. Ford, H. Hiratsuka, P. V. Kamat, *J. Phys. Chem.* **1989**, *93*, 6692-6696; b) E. Shirman, A. Ustinov, N. Ben-Shitrit, H. Weissman, M. A. Iron, R. Cohen, B. Rybtchinski, *J. Phys. Chem. B* **2008**, *112*, 8855-8858.

[83] a) Á. J. Jiménez, F. Spänig, M. S. Rodríguez-Morgade, K. Ohkubo, S. Fukuzumi, D. M. Guldi, T. Torres, *Org. Lett*. **2007**, *9*, 2481-2484; b) M. P. O'Neil, M. P. Niemczyk, W. A. Svec, D. Gosztola, G. L. Gaines, M. R. Wasielewski, *Science* **1992**, *257*, 63-65.

[84] G. Yu, A. J. Heeger, *J. Appl. Phys.* **1995**, *78*, 4510-4515.

[85] Z. An, S. A. Odom, R. F. Kelley, C. Huang, X. Zhang, S. Barlow, L. A. Padilha, J. Fu, S. Webster, D. J. Hagan, E. W. Van Stryland, M. R. Wasielewski, S. R. Marder, *J. Phys. Chem. A* **2009**, *113*, 5585-5593.

[86] a) H. Dong, X. Fu, J. Liu, Z. Wang, W. Hu, *Adv. Mater*. **2013**, *25*, 6158-6183; b) L. Dou, J. You, Z. Hong, Z. Xu, G. Li, R. A. Street, Y. Yang, *Adv. Mater*. **2013**, *25*, 6642-6671; c) A. J. Heeger, *Adv. Mater*. **2014**, *26*, 10-28; d) H. Sirringhaus, *Adv. Mater*. **2014**, *26*, 1319-1335; e) Y. Zhao, Y. Guo, Y. Liu, *Adv. Mater*. **2013**, *25*, 5372-5391; f) G. Schweicher, Y. Olivier, V. Lemaur, Y. H. Geerts, *Isr. J. Chem.* **2014**, *54*, 595-620.

[87] a) Y. Lin, X. Zhan, *Acc. Chem. Res.* **2016**, *49*, 175-183; b) A. Mishra, P. Bäuerle, *Angew. Chem. Int. Ed.* **2012**, 51, 2020-2067; c) C. Li, M. Liu, N. G. Pschirer, M. Baumgarten, K. Müllen, *Chem. Rev.* **2010**, *110*, 6817-6855.

[88] H. Klauk, *Chem. Soc. Rev*. **2010**, *39*, 2643-2666.

[89] A. C. Grimsdale, K. Leok Chan, R. E. Martin, P. G. Jokisz, A. B. Holmes, *Chem. Rev.* **2009**, *109*, 897-1091.

[90] A. R. Murphy, J. M. J. Fréchet, *Chem. Rev.* **2007**, *107*, 1066-1096.

[91] Y. Shirota, H. Kageyama, *Chem. Rev.* **2007**, *107*, 953-1010.

[92] O. A. Melville, B. H. Lessard, T. P. Bender, *ACS Appl. Mater. Interfaces* **2015**, *7*, 13105-13118.

[93] S. R. Forrest, *Chem. Rev.* **1997**, *97*, 1793-1896.

[94] C. W. Tang, *Appl. Phys. Lett.* **1986**, *48*, 183-185.

[95] a) L. Ma, Y. Guo, Y. Wen, Y. Liu, X. Zhan, *Appl. Phys. Lett.* **2013**, *103*, 203303; b) L. E. Shoer, S. W. Eaton, E. A. Margulies, M. R. Wasielewski, *J. Phys. Chem. B* **2015**, *119*, 7635-7643.

[96] J. L. Brédas, J. P. Calbert, D. A. da Silva Filho, J. Cornil, *Proc. Natl. Acad. Sci. U.S.A* **2002**, *99*, 5804-5809.

[97] K. Zhou, H. Dong, H. Zhang, W. Hu, *Phys. Chem. Chem. Phys.* **2014**, *16*, 22448-22457.

[98] M. Noda, N. Kobayashi, M. Katsuhara, A. Yumoto, S. Ushikura, R. Yasuda, N. Hirai, G. Yukawa, I. Yagi, K. Nomoto, T. Urabe, *J. Soc. Inf. Disp.* **2011**, *19*, 316-322.

[99] H. Bünzly, H. Decker, *Ber. Dtsch. Chem. Ges.* **1905**, *38*, 3268-3273.

[100] D. Susumu, F. Akiyoshi, I. Shigeo, I. Tamotsu, M. Yoshio, *Bull. Chem. Soc. Jpn.* **1979**, *52*, 2494-2500.

[101] A. R. Martin, Y. Yang, *Acta Chem. Scand.* **1993**, *47*, 221-221.

[102] S. Yokokura, Y. Takahashi, H. Hasegawa, J. Harada, T. Inabe, M. M. Matsushita, K. Awaga, *J. Nanosci. Nanotechnol.* **2016**, *16*, 3355-3359.

[103] a) T. Susumu, N. Toshio, I. Tamotsu, *Chem. Lett.* **1998**, *27*, 1249-1250; b) A. Takehiro, N. Toshio, I. Tamotsu, M. Masaki, T. Hiroyuki, *Chem. Lett.* **2004**, *33*, 128-129; c) A. Takehiro, I. Manabu, N. Toshio, M. Masaki, T. Hiroyuki, I. Tamotsu, *Chem. Lett.* **2005**, *34*, 936-937.

[104] N. Kobayashi, M. Sasaki, K. Nomoto, *Chem. Mater*. **2009**, *21*, 552-556.

[105] N. Lv, M. Xie, W. Gu, H. Ruan, S. Qiu, C. Zhou, Z. Cui, *Org. Lett.* **2013**, *15*, 2382-2385.

[106] D. Stassen, N. Demitri, D. Bonifazi, *Angew. Chem. Int. Ed.* **2016**, *55*, 5947-5951.

[107] G. N. La Mar, W. D. Horrocks, R. H. Holm, *NMR of Paramagnetic Molecules*, Academic Press: New York, **1973**.

[108] T. Miletić, A. Fermi, I. Orfanos, A. Avramopoulos, F. D. Leo, N. Demitri, G. Bergamini, P. Ceroni, M. G. Papadopoulos, S. Couris, D. Bonifazi, *Chem. Eur. J*. **2017**, *23*, 2363-2378.

[109] A. Sciutto, A. Fermi, A. Folli, T. Battisti, J. M. Beames, D. M. Murphy, D. Bonifazi, *Chem. Eur. J.* **2018**, *24*, 4382-4389.

[110] a) C. Xue, R. Sun, R. Annab, D. Abadi, S. Jin, *Tetrahedron Lett.* **2009**, *50*, 853-856; b) A. Berezin, A. Sciutto, N. Demitri, D. Bonifazi, *Org. Lett.* **2015**, *17*, 1870-1873.

[111] R. B. Teponno, S. Kusari, M. Spiteller, *Nat. Prod. Rep.* **2016**, *33*, 1044-1092.

[112] N. E. Es-Safi, S. Ghidouche, P. Ducrot, *Molecules* **2007**, *12*, 2228-2258.

[113] B. Lochab, S. Shukla, I. K. Varma, *RSC Advances* **2014**, *4*, 21712-21752.

[114] T. Yamamoto, *Synlett* **2003**, *4*, 425-450.

[115] M. Grzybowski, K. Skonieczny, H. Butenschön, D. T. Gryko, *Angew. Chem. Int. Ed.* **2013**, *52*, 9900-9930.

[116] J. Löwe, *Z. Chemie* **1868**, 603-604.

[117] A. P. Dianin, *Zh. Russ. Fiz.-Khim. O-va.* **1874**, 183.

[118] A. I. Scott, *Q. Rev. Chem. Soc.* **1965**, *19*, 1-35.

[119] W. R. Roush, A. D. Palkowitz, *J. Org. Chem.* **1989**, *54*, 3009-3011.

[120] M. J. S. Dewar, T. Nakaya, *J. Am. Chem. Soc.* **1968**, *90*, 7134-7135.

[121] M. Smrcina, J. Polakova, S. Vyskocil, P. Kocovsky, *J. Org. Chem.* **1993**, *58*, 4534-4538.

[122] J. Brussee, J.L.G. Groenendijk, J.M. te Koppele, A.C.A. Jansen, *Tetrahedron* **1985**, *41*, 3313-3319.

[123] T. J. Stone, W. A. Waters, *J. Chem. Soc* **1964**, 213-218.

[124] F. Toda, K. Tanaka, S. Iwata, *J. Org. Chem*. **1989**, *54*, 3007-3009.

[125] M. Hovorka, J.Günterová, J. Závada, Tetrahedron Lett. **1990**, *31*, 413-416.

[126] F. Ullmann, J. Bielecki, *Ber. Dtsch. Chem. Ges.* **1901**, *34*, 2174-2185.

[127] a) P. E. Fanta, *Chem. Rev.* **1964**, *64*, 613-632; b) P. E. Fanta, *Synthesis* **1974**, *1*, 9-21.

[128] W. Davey, R. W. Latter, *J. Chem. Soc*. **1948**, 264-265.

[129] J. F. Corbett, P. F. Holt, *J. Chem. Soc.* **1960**, 3646-3653.

[130] T. Yamato, C. Hideshima, K. Suehiro, M. Tashiro, G. K. S. Prakash, G. A. Olah, *J. Org. Chem*. **1991**, *56*, 6248-6250.

[131] a) J. Forrest, *J. Chem. Soc.* **1960**, 566-573; b) J. Forrest, *J. Chem. Soc.* **1960**, 574-580; c) J. Forrest, *J. Chem. Soc.* **1960**, 581-588; d) J. Forrest, *J. Chem. Soc.* **1960**, 592-594; e) J. Forrest, *J. Chem. Soc.* **1960**, 589-592; f) J. Forrest, *J. Chem. Soc.* **1960**, 594-601.

[132] Y. Zhai, X. Chen, W. Zhou, M. Fan, Y. Lai, D. Ma, *J. Org. Chem.* **2017**, *82*, 4964-4969.

[133] J. Gao, S. Bhunia, K. Wang, L. Gan, S. Xia, D. Ma, *Org. Lett.* **2017**, *19*, 2809-2812.

[134] S. Zhang, D. Zhang, L. S. Liebeskind, *J. Org. Chem*. **1997**, *62*, 2312-2313.

[135] N. Kornblum, D. L. Kendall, *J. Am. Chem. Soc.* **1952**, *74*, 5782-5782.

[136] M. Takahashi, Y. Moritani, T. Ogiku, H. Ohmizu, K. Kondo, T. Iwasaki, *Tetrahedron Lett.* **1992**, *33*, 5103-5104.

[137] S. Miyano, H. Fukushima, S. Handa, H. Ito, H. Hashimoto, *Bull. Chem. Soc. Jpn.* **1988**, *61*, 3249-3254.

[138] S. P. Stanforth, *Tetrahedron* **1998**, *54*, 263-303.

[139] N. Miyaura, A. Suzuki, *Chem. Rev.* **1995**, *95*, 2457-2483.

[140] a) J. K. Stille, *Angew. Chem. Int. Ed. Engl.* **1986**, *25*, 508-524; b) S. P. H. Mee, V. Lee, J. E. Baldwin, *Angew. Chem. Int. Ed.* **2004**, *43*, 1132-1136; c) N. Miyaura, T. Yanagi, A. Suzuki, *Synth. Commun.* **1981**, *11*, 513-519.

[141] O. Navarro, R. A. Kelly, S. P. Nolan, *J. Am. Chem. Soc.* **2003**, *125*, 16194-16195.

[142] K. Matos, J. A. Soderquist, *J. Org. Chem.* **1998**, *63*, 461-470.

[143] P. Fitton, E. A. Rick, *J. Organomet. Chem.* **1971**, *28*, 287-291.

[144] H. C. Brown, T. E. Cole, *Organometallics* **1983**, *2*, 1316-1319.

[145] T. Ishiyama, M. Murata, N. Miyaura, *J. Org. Chem.* **1995**, *60*, 7508-7510.

[146] N. G. Andersen, S. P. Maddaford, B. A. Keay, *J. Org. Chem.* **1996**, *61*, 9556-9559.

[147] a) J. Yin, M. P. Rainka, X.-X. Zhang, S. L. Buchwald, J. Am. Chem. Soc. **2002**, *124*, 1162-1163; b) A. N. Cammidge, K. V. L. Crepy, *Chem. Commun.* **2000**, 18, 1723-1724.

[148] T. R. Hoye, M. Chen, *J. Org. Chem.* **1996**, *61*, 7940-7942.

[149] a) T. Watanabe, N. Miyaura, A. Suzuki, Synlett **1992**, *3*, 207-210; b) H. Chaumeil, S. Signorella, C. Le Drian, *Tetrahedron* **2000**, *56*, 9655-9662.

[150] G. Miroslav, A. Antonio, E. Pablo, *Chem. Eur. J.* **2006**, *12*, 9346-9352.

[151] C. A. Fleckenstein, H. Plenio, *Chem. Soc. Rev.* **2010**, *39*, 694-711.

[152] a) T. Hayashi, M. Konishi, M. Kumada, *Tetrahedron Lett.* **1979**, *20*, 1871-1874; b) W. J. Thompson, J. H. Jones, P. A. Lyle, J. E. Thies, *J. Org. Chem.* **1988**, *53*, 2052-2055.

[153] a) W. Shen, *Tetrahedron Lett.* **1997**, *38*, 5575-5578; b) A. F. Littke, C. Dai, G. C. Fu, *J. Am. Chem. Soc.* **2000**, *122*, 4020-4028; c) G. C. Fu, *Acc. Chem. Res.* **2008**, *41*, 1555-1564.

[154] a) D. A. Albisson, R. B. Bedford, P. Noelle Scully, S. E. Lawrence, *Chem. Commun.* **1998**, *19*, 2095-2096; b) H. Weissman, D. Milstein, *Chem. Commun.* **1999**, *18*, 1901-1902; c) D. A. Alonso, C. Nájera, M. C. Pacheco, *Org. Lett.* **2000**, *2*, 1823-1826; d) D. Zim, A. S. Gruber, G. Ebeling, J. Dupont, A. L. Monteiro, *Org. Lett.* **2000**, *2*, 2881-2884.

[155] a) W. A. Herrmann, M. Elison, J. Fischer, C. Köcher, G. R. J. Artus, Angew. Chem. Int. Ed. Engl. **1995**, *34*, 2371-2374; b) W. A. Herrmann, C. P. Reisinger, M. Spiegler, *J. Organomet. Chem.* **1998**, 557, 93-96; c) C. Zhang, J. Huang, M.

L. Trudell, S. P. Nolan, *J. Org. Chem.* **1999**, *64*, 3804-3805; d) M. Alcarazo, S. J. Roseblade, A. R. Cowley, R. Fernández, J. M. Brown, J. M. Lassaletta, *J. Am. Chem. Soc.* **2005**, *127*, 3290-3291.

[156] a) T. E. Barder, S. D. Walker, J. R. Martinelli, S. L. Buchwald, *J. Am. Chem. Soc.* **2005**, *127*, 4685-4696; b) R. Martin, S. L. Buchwald, *Acc. Chem. Res.* **2008**, *41*, 1461-1473; c) D. W. Old, J. P. Wolfe, S. L. Buchwald, *J. Am. Chem. Soc.* **1998**, *120*, 9722-9723; d) S. D. Walker, T. E. Barder, J. R. Martinelli, S. L. Buchwald, *Angew. Chem. Int. Ed.* **2004**, *43*, 1871-1876; e) J. P. Wolfe, S. L. Buchwald, *Angew. Chem. Int. Ed.* **1999**, *38*, 2413-2416; f) J. P. Wolfe, R. A. Singer, B. H. Yang, S. L. Buchwald, *J. Am. Chem. Soc.* **1999**, *121*, 9550-9561; g) X. Zhang, K. Mashima, K. Koyano, N. Sayo, H. Kumobayashi, S. Akutagawa, H. Takaya, *J. Chem. Soc., Perkin Trans. 1* **1994**, 2309-2322.

[157] C. Amatore, A. Jutand, *Acc. Chem. Res.* **2000**, *33*, 314-321.

[158] T. Leermann, F. R. Leroux, F. Colobert, *Org. Lett.* **2011**, *13*, 4479-4481.

[159] K. L. Billingsley, T. E. Barder, S. L. Buchwald, *Angew. Chem. Int. Ed.* **2007**, *46*, 5359-5363.

[160] C. S. Sample, E. Goto, N. V. Handa, Z. A. Page, Y. Luo, C. J. Hawker, *J. Mater. Chem. C* **2017**, *5*, 1052-1056.

[161] a) M. V. Sargent, P. O. Stransky, *J. Chem. Soc., Perkin Trans. 1* **1982**, 1605-1610; b) R. T. Scannell, R. Stevenson, *J. Chem. Soc., Perkin Trans. 1* **1983**, 2927-2931; c) M. Millot, A. Dieu, S. Tomasi, *Nat. Prod. Rep.* **2016**, *33*, 801-811; d) K. Paul, S. Jalal, S. Kundal, U. Jana, *J. Org. Chem.* **2016**, *81*, 1164-1174; e) T. Yempala, B. K. Cassels, *Synth. Commun.* **2016**, *46*, 1909-1915.

[162] F. Bedos-Belval, A. Rouch, C. Vanucci-Bacqué, M. Baltas, Med. Chem. Commum. **2012**, *3*, 1356-1372.

[163] Y. Shi, K. Hou, Y. Wang, K. Wang, H. Ren, M. Pang, F. Chen, S. Zhang, *J. Mat. Chem. A* **2016**, *4*, 5415-5422.

[164] X. Chen, K. M. Engle, D. H. Wang, J. Q. Yu, *Angew. Chem. Int. Ed.* **2009**, *48*, 5094-5115.

[165] T.S. Mei, L. Kou, S. Ma, K. M. Engle, J. Q. Yu, *Synthesis* **2012**, *44*, 1778-1791.

[166] P. Thansandote, M. Lautens, *Chem. Eur. J.* **2009**, *15*, 5874-5883.

[167] X.-X. Guo, D.-W. Gu, Z. Wu, W. Zhang, *Chem. Rev.* **2015**, *115*, 1622-1651.

[168] B. Xiao, T.-J. Gong, Z.-J. Liu, J.-H. Liu, D.-F. Luo, J. Xu, L. Liu, J. *Am. Chem. Soc.* **2011**, *133*, 9250-9253.

[169] X. Wang, Y. Lu, H.-X. Dai, J.-Q. Yu, *J. Am. Chem. Soc.* **2010**, *132*, 12203-12205.

[170] Y. Wei, N. Yoshikai, *Org. Lett.* **2011**, *13*, 5504-5507.

[171] a) J. Zhao, Y. Wang, Y. He, L. Liu, Q. Zhu, *Org. Lett.* **2012**, *14*, 1078-1081; b) J. Zhao, Q. Zhang, L. Liu, Y. He, J. Li, J. Li, Q. Zhu, *Org. Lett.* **2012**, *14*, 5362-5365.

[172] R. Pummerer, A. Rieche, *Ber. Dtsch. Chem. Ges.* **1926**, *59*, 2161-2175.

[173] R. Pummerer, E. Prell, A. Rieche, Ber. Dtsch. Chem. Ges. **1926**, *59*, 2159-2161.

[174] A. E. Wetherby, S. D. Benson, C. S. Weinert, *Inorg. Chim. Acta* **2007**, *360*, 1977-1986.

[175] C. Song, T. M. Swager, *Macromolecules* **2009**, *42*, 1472-1475.

[176] T. Kamei, M. Uryu, T. Shimada, *Org. Lett*. **2017**, *19*, 2714-2717.

[177] a) A. S. Hay, *J. Org. Chem.* **1962**, *27*, 3320-3321; b) N. Y. More, M. Jeganmohan, *Org. Lett*. **2015**, *17*, 3042-3045; c) T. Horiuchi, T. Ohta, M. Stephan, H. Takaya, *Tetrahedron: Asymmetry* **1994**, *5*, 325-328; d) K. Ding, W. Yang, L. Zhang, W. Yangjie, T. Matsuura, *Tetrahedron* **1996**, *52*, 1005-1010.

[178] Z. Zhang, Q. Zhou, R. Tang, H. Zai, Chemical Research and Application **2009**, *21*, 113-116.

[179] a) M. Smrcina, M. Lorenc, V. Hanus, P. Sedmera, P. Kocovský, *J. Org. Chem*. **1992**, *57*, 1917-1920; b) M. Smrcina, M. Lorenc, V. Hanuš, P. Kocovský, Synlett **1991**, *4*, 231-232.

[180] H. G. Roth, N. A. Romero, D. A. Nicewicz, Synlett **2016**, *27*, 714-723.

[181] J. T. Arnold, S. S. Dharmatti, M. E. Packard, *J. Chem. Phys.* **1951**, *19*, 507-507.

[182] W. G. Proctor, F. C. Yu, *Phys. Rev.* **1950**, *77*, 717-717.

[183] L. H. Meyer, A. Saika, H. S. Gutowsky, *J. Am. Chem. Soc.* **1953**, *75*, 4567-4573.

[184] H. S. Gutowsky, C. J. Hoffman, *J. Chem. Phys.***1951**, *19*, 1259-1267.

[185] a) L. Pauling, *J. Am. Chem. Soc.* **1932**, *54*, 3570-3582; b) M. I. Trofimov, E. A. Smolenskii, *Russ. Chem. Bull*. **2005**, *54*, 2235-2246.

[186] T. Schaefer, W. G. Schneider, *Can. J. Chem.* **1963**, *41*, 966-982.

[187] A. K. Amegadzie, M. E. Carey, J. M. Domagala, L. Huang, R. G. Micetich, R. Singh, M. A. Stier, A. Vaisburg, J. P. Sanchez, Patents *WO 9819648 A2*, **1998**.

[188] M. V. Bhatt, S. U. Kulkarni, *Synthesis* **1983**, *4*, 249-282.

[189] J. Kelber, M.-F. Achard, F. Durola, H. Bock, *Angew. Chem. Int. Ed.* **2012**, *51*, 5200-5203.

[190] S. W. Wright, D. L. Hageman, L. D. McClure, *J. Org. Chem.* **1994**, *59*, 6095-6097.

[191] A. A. Thomas, H. Wang, A. F. Zahrt, S. E. Denmark, *J. Am. Chem. Soc.* **2017**, *139*, 3805-3821.

[192] W. M. Nau, J. C. Scaiano, *J. Phys. Chem.* **1996**, *100*, 11360-11367.

[193] a) C. Wirp, H. D. Brauer, J. Bendig, *Ber. Bunsen-Ges. Phys.* **1997**, *101*, 961-967; b) C. Grewer, H. D. Brauer, *J. Phys. Chem.* **1993**, *97*, 5001-5006; c) A. F. Olea, F. Wilkinson, *J. Phys. Chem.* **1995**, *99*, 4518-4524; d) C. Sato, K. Kikuchi, K. Okamura, Y. Takahashi, T. Miyashi, *J. Phys. Chem.* **1995**, *99*, 16925-16931; e) M. Okamoto, F. Tanaka, *J. Phys. Chem. A* **2002**, *106*, 3982-3990; f) A. A. Gorman, I. Hamblett, M. A. J. Rodgers, *J. Am. Chem. Soc.* **1984**, *106*, 4679-4682; g) O. L. J. Gijzeman, F. Kaufman, G. Porter, J. Chem. Soc. Faraday Trans. 2 **1973**, *69*, 708-720.

[194] K. Kikuchi, C. Sato, M. Watabe, H. Ikeda, Y. Takahashi, T. Miyashi, *J. Am. Chem. Soc.* **1993**, *115*, 5180-5184.

[195] G. E. Johnson, *J. Phys. Chem.* **1980**, *84*, 2940-2946.

[196] H. Knibbe, K. Röllig, F. P. Schäfer, A. Weller, *J. Phys. Chem.* **1967**, *47*, 1184-1185.

[197] V. Balzani, G. Bergamini, P. Ceroni, *Angew. Chem. Int. Ed.* **2015**, *54*, 11320-11337.

[198] a) D. M. Klassen, G. A. Crosby, *J. Phys. Chem.***1968**, *48*, 1853-1858; b) G. A. Crosby, J. N. Demas, *J. Am. Chem. Soc.* **1970**, *92*, 7262-7270.

[199] H. D. Gafney, A. W. Adamson, *J. Am. Chem. Soc.* **1972**, *94*, 8238-8239.

[200] M. Graetzel, *Acc. Chem. Res.* **1981**, *14*, 376-384.

[201] H. Takeda, O. Ishitani, *Coord. Chem. Rev.* **2010**, *254*, 346-354.

[202] K. Kalyanasundaram, *Coord. Chem. Rev.* **1982,** *46*, 159-244.

[203] C. Ulbricht, B. Beyer, C. Friebe, A. Winter, U. S. Schubert, *Adv. Mater.* **2009**, *21*, 4418-4441.

[204] a) N. A. Romero, D. A. Nicewicz, *Chem. Rev.* **2016**, *116*, 10075-10166; b) C. K. Prier, D. A. Rankic, D. W. C. MacMillan, *Chem. Rev.* **2013**, *113*, 5322-5363.

[205] D. Ravelli, S. Protti, M. Fagnoni, *Chem. Rev.* **2016**, *116*, 9850-9913.

[206] M. H. Shaw, J. Twilton, D. W. C. MacMillan, *J. Org. Chem.* **2016**, *81*, 6898-6926.

[207] D. A. Nicewicz, D. W. C. MacMillan, *Science* **2008**, *322*, 77-80.

[208] A. McNally, C. K. Prier, D. W. C. MacMillan, *b* **2011**, *334*, 1114-1117.

[209] E. H. Discekici, N. J. Treat, S. O. Poelma, K. M. Mattson, Z. M. Hudson, Y. Luo, C. J. Hawker, J. R. de Alaniz, *Chem. Commun*. **2015**, *51*, 11705-11708.

[210] I. Ghosh, T. Ghosh, J. I. Bardagi, B. König, *Science* **2014**, *346*, 725-728.

[211] S. O. Poelma, G. L. Burnett, E. H. Discekici, K. M. Mattson, N. J. Treat, Y. Luo, Z. M. Hudson, S. L. Shankel, P. G. Clark, J. W. Kramer, C. J. Hawker, J. Read de Alaniz, *J. Org. Chem.* **2016**, *81*, 7155-7160.

[212] I. Ghosh, B. König, *Angew. Chem. Int. Ed.* **2016**, *55*, 7676-7679.

[213] Y. Zhang, R. Qian, X. Zheng, Y. Zeng, J. Sun, Y. Chen, A. Ding, H. Guo, *Chem. Commun.* **2015**, *51*, 54-57.

[214] J. Du, T. P. Yoon, *J. Am. Chem. Soc.* **2009**, *131*, 14604-14605.

[215] J. W. Tucker, J. D. Nguyen, J. M. R. Narayanam, S. W. Krabbe, C. R. J. Stephenson, *Chem. Commun.* **2010**, *46*, 4985-4987.

[216] H. Jiang, Y. Cheng, Y. Zhang, S. Yu, *Org. Lett.* **2013**, *15*, 4884-4887.

[217] N. A. Romero, K. A. Margrey, N. E. Tay, D. A. Nicewicz, *Science* **2015**, *349*, 1326-1330.

[218] J. A. Terrett, J. D. Cuthbertson, V. W. Shurtleff, D. W. C. MacMillan, *Nature* **2015**, *524*, 530-534.

[219] M. Majek, A. J. von Wangelin, *Chem. Commun.* **2013**, *49*, 5507-5509.

[220] a) K. T. Tarantino, P. Liu, R. R. Knowles, *J. Am. Chem. Soc.* **2013**, *135*, 10022-10025; b) E. C. Gentry, R. R. Knowles, *Acc. Chem. Res.* **2016**, *49*, 1546-1556; c) L. J. Rono, H. G. Yayla, D. Y. Wang, M. F. Armstrong, R. R. Knowles, *J. Am. Chem. Soc.* **2013**, *135*, 17735-17738.

[221] M. R. Heinrich, *Chem. Eur. J.* **2009**, *15*, 820-833.

[222] T. Hering, D. P. Hari, B. König, *J. Org. Chem.* **2012**, *77*, 10347-10352.

[223] P. H. Durga, H. Thea, K. Burkhard, *Angew. Chem. Int. Ed.* **2014**, *53*, 725-728.

[224] D. P. Hari, P. Schroll, B. König, *J. Am. Chem. Soc.* **2012**, *134*, 2958-2961.

[225] D. P. Hari, T. Hering, B. König, *Org. Lett.* **2012**, *14*, 5334-5337.

[226] a) S. Otto, *Ber. Dtsch. Chem. Ges.* **1884**, *17*, 2075-2081; b) J. H. Ziegler., *Ber. Dtsch. Chem. Ges.* **1890**, *23*, 2469-2472; c) G. E. Hilbert, T. B. Johnson, *J. Am. Chem. Soc.* **1929**, *51*, 1526-1536.

[227] W. Xiao, C. G. D., N. Timothy, *Angew. Chem. Int. Ed.* **2013**, *52*, 7860-7864.

[228] J. E. Bullock, M. T. Vagnini, C. Ramanan, D. T. Co, T. M. Wilson, J. W. Dicke, T. J. Marks, M. R. Wasielewski, *J. Phys. Chem. B* **2010**, *114*, 1794-1802.

[229] L. Wang, G. Duan, Y. Ji, H. Zhang, *J. Phys. Chem. C* **2012**, *116*, 22679-22686.

[230] a) R. Al-Aqar, A. C. Benniston, A. Harriman, T. Perks, *ChemPhotoChem* **2017**, *1*, 198-205; b) M. Noda, N. Kobayashi, M. Katsuhara, A. Yumoto, S. Ushikura, R. Yasuda, N. Hirai, G. Yukawa, I. Yagi, K. Nomoto, T. Urabe, *SID Symposium Digest* **2010**, *41*, 710-713.

[231] P. Peljo, T. Rauhala, L. Murtomaeki, T. Kallio, K. Kontturi, *Int. J. Hydrogen Energy* **2011**, *36*, 10033-10043.

[232] G. J. Janz, D. J. Ives, *Reference electrodes theory and practice*, Academic Press, **1961**.

[233] a) A. Juris, V. Balzani, F. Barigelletti, S. Campagna, P. Belser, A. von Zelewsky, *Coord. Chem. Rev.* **1988**, *84*, 85-277; b) B. Colasson, A. Credi, G. Ragazzon, *Coord. Chem. Rev.* **2016**, *325*, 125-134.

[234] N. Elgrishi, K. J. Rountree, B. D. McCarthy, E. S. Rountree, T. T. Eisenhart, J. L. Dempsey, *J. Chem. Educ.* **2018**, *95*, 197-206.

[235] J. L. Brédas, R. Silbey, D. S. Boudreaux, R. R. Chance, *J. Am. Chem. Soc.* **1983**, *105*, 6555-6559.

[236] S. M. Batterjee, M. I. Marzouk, M. E. Aazab, M. A. El-Hashash, *Appl. Organomet. Chem.* **2003**, *17*, 291-297.

[237] H. Svith, H. Jensen, J. Almstedt, P. Andersson, T. Lundbäck, K. Daasbjerg, M. Jonsson, *J. Phys. Chem. A* **2004**, *108*, 4805-4811.

[238] Y. Marcus, *J. Solution Chem.* **1984**, *13*, 599-624.

[239] W. M. Haynes, *CRC Handbook of Chemistry and Physics*, 94th Edition, CRC Press, **2013**.

[240] M. Noboru, K. Yozo, K. Masao, *Bull. Chem. Soc. Jpn.* **1956**, *29*, 465-470.

[241] C. Reichardt, *Chem. Rev.* **1994**, *94*, 2319-2358.

[242] E. Lippert, *Acc. Chem. Res.* **1970**, *3*, 74-80.

[243] J. R. Lakowicz, *Principles of fluorescence spectroscopy*, Second edition. New York: Kluwer Academic/Plenum, **1999**.

[244] L. Wang, W. Huang, R. Li, D. Gehrig, P. W. M. Blom, K. Landfester, K. A. I. Zhang, *Angew. Chem. Int. Ed.* **2016**, *55*, 9783-9787.

[245] C. P. Andrieux, J.-M. Savéant, A. Tallec, R. Tardivel, C. Tardy, *J. Am. Chem. Soc.* **1997**, *119*, 2420-2429.

[246] I. Ghosh, B. König, *Angew. Chem. Int. Ed.* **2016**, *55*, 7676-7679.

[247] D. D. M. Wayner, J. J. Dannenberg, D. Griller, Chem. *Phys. Lett.* **1986**, *131*, 189-191.

[248] A. Studer, D. P. Curran, *Angew. Chem. Int. Ed.* **2016**, *55*, 58-102.

[249] C. D. McTiernan, S. P. Pitre, J. C. Scaiano, *ACS Catalysis* **2014**, *4*, 4034-4039.

[250] D. D. Tanner, J. J. Chen, L. Chen, C. Luelo, *J. Am. Chem. Soc.* **1991**, *113*, 8074-8081.

[251] C. P. Andrieux, J. M. Savéant, K. B. Su, *J. Phys. Chem.* **1986**, *90*, 3815-3823.

[252] J. M. Savéant, C. P. Andrieux, D. Zann, *Nouv. J. Chim* **1984**, *8*, 107.

[253] A. Albini, *Synthesis* **1993**, *3*, 263-277.

[254] G. Nardi, I. Manet, S. Monti, M. A. Miranda, V. Lhiaubet-Vallet, *Free Rad. Biol. Med.* **2014**, 77, 64-70.

[255] A. Seret, E. Gandin, A. Van De Vorst, *J. Photochem.* **1987**, *38*, 145-155.

4. Experimental Part

4.1. Instrumentation

Melting points (M.p.) were measured on a Stuart SMP11 apparatus in open capillary tubes and have not been corrected. **Nuclear magnetic resonance** (NMR) ^{1}H, ^{13}C spectra were obtained on a 300 MHz NMR (Bruker Ultrashield 300), 400 MHz (Bruker Avance III 400 HD, BBFO Smartprobe) or 600 MHz (Bruker Avance III, Inverse QCI Cryoprobe) at RT, unless otherwise stated. Chemical shifts are reported in ppm with TMS δ = 0 ppm using the solvent residual signal as an internal reference ($CDCl_3$: δ_H = 7.26 ppm, δ_C = 77.16 ppm; $(CD_3)_2SO$: δ_H = 2.50 ppm, δ_C = 39.52 ppm; CD_2Cl_2: δ_H = 5.32 ppm, δ_C = 53.84; $(CD_3)_2CO$: δ_H = 2.05 ppm, δ_C = 29.84 ppm, 206.26 ppm). Coupling constants (*J*) are given in Hz. Resonance multiplicity is described as *s* (singlet), *d* (doublet), *t* (triplet), *dd* (doublet of doublets), *m* (multiplet) and *br* (broad signal). Carbon spectra were acquired with a complete decoupling for the proton. **Infrared spectra** were recorded on a Shimadzu IR-Affinity 1S FTIR spectrometer on small amounts of powders. **Mass spectrometry:** *i*) *High resolution electrospray mass spectrometry* (HRMS-ESI) was performed by the analytical service at School of Chemistry, Cardiff University on a Waters Synapt G2-Si Time of flight mass spectrometer coupled to a Waters H-class UPLC with the column removed. The data was acquired in positive ion mode. 1 µl of solution of a CH_2Cl_2 solution of approximately 2 mg/ml was injected using 50:50 Water: ACN as the carrier solvent with 0.1% Formic acid; *ii*) *High resolution matrix assisted laser desorption ionisation* (HRMS-MALDI) was performed using a Waters Synapt G2-Si time of flight mass spectrometer. The matrix used was DCTB. High resolution gas chromatography mass spectrometry was performed using a Waters GCT premier time of flight mass spectrometer coupled to a GC chromatograph. The column was purchased from Agilent, phase DB-5ms 30 m x 0.25 mm x 0.1 um. **XRD analysis**: single-crystal XRD data were collected on an Agilent SuperNova Dual Atlas diffractometer with a mirror monochromator [using either Cu (λ = 1.5418 Å) or Mo (λ = 0.7107 Å) radiation], equipped with an Oxford Cryosystems cooling apparatus. Crystal structures were solved and refined using SHELX.[S1] Non-hydrogen atoms were refined with anisotropic displacement parameters. Hydrogen atoms were inserted in idealized positions and a riding model was used with Uiso set at 1.2 or 1.5 times the value of Ueq

for the atom to which they are bonded. **EPR analysis*:*** the RT X-band CW-EPR spectra were recorded on a Bruker EMX Micro spectrometer equipped with a Bruker ER4123-D dielectric resonator, operating at 100 kHz field modulation. The spectra were recorded either in darkness or under in situ irradiation using a Labino Nova 530 nm LED green light source or a Labino Nova 455 nm LED blue light source. Both light sources have a 20 nm bandwidth centred around the main wavelength. The experimental EPR spectra were simulated using the EasySpin package[S2] operating within the Mathworks Matlab environment. **Electrochemical analysis**: Cyclic voltammetry experiments were carried out at RT in nitrogen-purged 1,2-dichlorobenzene (freshly filtered on alumina, 50-200 μm), dry CH_2Cl_2 or dry CH_3CN with a Model 800 potentiostat (CH Instruments). The working electrode consisted of a glassy carbon electrode (3 mm diameter), the counter electrode was a Pt spiral and a Ag wire was used as quasi-reference electrode (AgQRE). Working electrode and quasi-reference electrodes were polished on a felt pad with 0.05 or 0.3 μm alumina suspension and sonicated in deionized water for 1 minute before each experiment; the Pt wire was flame-cleaned. Tetrabutylammonium hexafluorophosphate ($TBAPF_6$) or tetraethylammonium hexafluorophosphate ($TEAPF_6$) were added to the solution as supporting electrolytes at concentrations typically 100 times higher than the electroactive analyte. Ferrocene (sublimed at reduced pressure) was used as an internal reference ($E_{Fc+/Fc}$ = 0.00 V for experiments in 1,2-dichlorobenzene; $E_{Fc+/Fc}$ = 0.46 V vs. SCE in CH_2Cl_2; $E_{Fc+/Fc}$ = 0.395 V *vs.* SCE in CH_3CN). HOMO and LUMO energies were calculated from the first formal redox potentials (half-wave potentials) using equations:[S3,S4]

$$E_{HOMO} = -(5.1\ eV + E^{1}_{ox}\ vs.\ Fc^{+}/Fc)$$

$$E_{LUMO} = -(5.1\ eV + E^{1}_{red}\ vs.\ Fc^{+}/Fc)$$

In the cases where oxidation or reduction waves were not detected by means of cyclic voltammetry, HOMO or LUMO levels are calculated using the optical gap ΔE_{opt}, considering the maximum of the emission band (λ_{max}) recorded in the same solvent, following equation:

$$\Delta E_{opt} = 1240 / \lambda_{max}\ (nm)$$

Redox potentials of the excited states of dyes in CH_3CN or CH_2Cl_2 are calculated following equations:

$$E^0_{(A+/A^*)} = E^0_{(A+/A)} - E_{00\ (A^*/A)}$$

$$E^0_{(A^*/A-)} = E^0_{(A/A-)} + E_{00\ (A^*/A)}$$

where $E^{0\text{-}0}_{(A^*/A)}$ indicates the one-electron potential associated to the electronic energy of the excited state, calculated from the maxima of the emission bands of the dyes either in CH_3CN or CH_2Cl_2.

Photophysical analysis. *Absorption* spectra of compounds were recorded in air equilibrated 1,2-dichlorobenzene, CH_2Cl_2, C_6H_6 or CH_3CN solutions at RT with an Agilent Cary 5000 UV-Vis spectrophotometer, using quartz cells with path length of 1.0 cm. *Emission* spectra were recorded on an Agilent Cary Eclipse fluorescence spectrofluorometer. Emission lifetime measurements were performed on a JobinYvon-Horiba FluoroHub single photon counting module, using Nano-LED pulsed source at 459 nm. Quantum yield values were calculated using quinine sulfate in air equilibrated 0.5 M H_2SO_4 (Φ = 0.546), Rhodamine 6G or coumarin153 in air equilibrated ethanol (Φ = 0.94 and 0.53, respectively), following the method of Demas and Crosby.[S5] Low temperature emission spectra were recorded on CH_2Cl_2:MeOH 1:1 (v/v) rigid matrixes immersed in liquid nitrogen contained in a quartz Dewar flask. *Transient absorption* (TA) measurements are performed utilizing an Edinburgh Instruments LP920 spectrometer. Spectra were collected using either the second (532 nm) or third (355 nm) harmonic of a Continuum Surelite Nd:YAG laser (power < 2 mJ/pulse, 10 Hz, bandwidth < 1 nm) as the pump light source. The probe beam intersects the sample normal to the Xe probe lamp, affording TA signals between *ca*. 250 < λ < 750 nm. Wavelength dependent spectral signatures were collected by dispersing the probe light on to an Andor ICCD camera, with a 2.05 nm resolution 250 < λ < 750 nm, integrated between 0.5 and 2.5 ms after the pump laser pulse. The spectra are presented as ΔOD signals, corresponding to the change in optical density of the sample upon irradiation with the Xe lamp, with and without the pump laser pulse. Lifetime data are also reported as ΔOD, collected using a Hamamatsu photomultiplier tube (PMT) for time resolved signals relative to the pump pulse (τ_0): data collected using the PMT have an identical 2.05 nm resolution. Lifetime data were fitted using the Origin 2017 software package. Uncertainties in lifetimes are taken directly from the Least-Squares fitting algorithm and are not indicative of fluctuations over multiple datasets. Lifetime traces have been corrected for pump laser induced fluorescence emission at time ≈ τ_0, using an active background subtraction scheme. All transient absorption

measurements are made using degassed samples by means of a freeze/pump/thaw procedure within a modified fluorescence quartz cuvette. Each pump step lasts approximately 15 minutes and the cycle are repeated 3 times, with the sample purged with nitrogen after each pump step. At the end of the procedure, the cell is re-filled to one atmosphere with nitrogen and sealed. Typical sample concentrations are 10^{-5} M in anhydrous 99.8% C_6H_6. **Photochemical reactions:** all reactions run under visible light were performed using a 5 meters long TINGKAM® RGB LED flexible stripe (LED type: 5050 PLCC-4 SMT SMD), equipped with a remote controller and placed on the inner surface of a metal cylinder (~ 20 cm diameter); estimated total output power: 36 W. **Calculations** and geometry optimizations were carried out using Gaussian 09 including the D01 revision[S6] at the B3LYP/6-31G* level of theory.[S7,S8]

4.2. Materials and methods

Thin layer chromatography (TLC) was conducted on pre-coated aluminum sheets with 0.20 mm Machevery-Nagel Alugram SIL G/UV254 with fluorescent indicator UV254. Column chromatography was carried out using Merck Gerduran silica gel 60 (particle size 63-200 μm). **Chemicals** were purchased from *Sigma Aldrich*, *Acros Organics*, *Fluorochem*, *TCI*, *Alfa Aesar* and *ABCR* and used as received. Solvents were purchased from *Sigma Aldrich*, *Fisher Scientific* and *VWR*, while deuterated solvents from *Sigma Aldrich*, *Fluorochem* and *Eurisotop*. Diethyl ether and THF were distilled from sodium-benzophenone-cetyl, toluene was refluxed over calcium hydride and dichloromethane was refluxed over phosphorous pentoxide. Anhydrous DMF was purchased from *Acros Organics*. Sulfuric acid and hydrochloric acid (HCl 32%) were purchased from *Fischer Scientific*. Pyridine was purchased from *Acros Organics*. MeOH, $CHCl_3$ and acetone were purchased as reagent-grade and used without further purification. Low temperature baths were prepared using different solvent mixtures depending on the desired temperature: -78°C with acetone/dry ice, -40 °C with CH_3CN/liquid N_2, -10 °C with ice-H_2O/NaCl and 0 °C with ice/H_2O. Anhydrous conditions were achieved by drying Schlenk tubes or 2-neck flasks by flaming with a heat gun under vacuum and then purging with Argon. The inert atmosphere was maintained using Argon-filled balloons equipped with a syringe and needle that was used to penetrate the silicon stoppers used to close the flasks' necks. Additions of liquid reagents were performed using dried plastic or glass syringes.

4.3 Synthesis and detailed experimental procedures

4.3.1. Synthesis of *N*-substituted A_2-type PXXDI: PATH B

Synthesis of 3-hydroxy-1,8-naphthalic(octyl)imide (130)

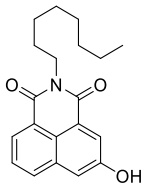

In a single-neck round bottom flask (250 ml), DIPEA (1.81 g, 14 mmol) was added to a suspension of compound **44** (1.5 g, 7.0 mmol) in dioxane (75 mL). The solution turned red and *n*-octylamine (1.36 g, 10.522 mmol) was added. The reaction mixture was stirred under reflux for 16 hours and a change in color (brown) was observed. The solvent was removed under reduced pressure and the solid residue suspended in HCl(aq) (100 ml, 10 % w/w) and extracted with $CHCl_3$ (150 ml, 3 times). The combined organic layers were dried over $MgSO_4$, filtered and evaporated under reduced pressure. The crude material was purified by silica gel chromatography (eluents: pentane/AcOEt, 2/1), affording **130** (1.71 g, 75 %) as a yellow solid. Rf = 0.50, pentane/AcOEt, 2/1. M.p.: 153-154 °C. ^{1}H NMR (300 MHz, $CDCl_3$) δ_H: 8.45 (*d*, *J* = 2.5 Hz, 1H), 8.42 (*dd*, *J* = 7.3, 1.1 Hz, 1H), 8.04 (*dd*, *J* = 8.3, 1.1 Hz, 1H), 7.67 (*dd*, *J* = 8.3, 7.3 Hz, 1H), 7.60 (*d*, *J* = 2.5 Hz, 1H), 6.87 (*s*, 1H), 4.25 – 4.11 (*m*, 2H), 1.82 – 1.68 (*m*, 2H), 1.51 – 1.16 (*m*, 10H), 0.86 (*t*, *J* = 6.9 Hz, 3H) ppm. ^{1}H NMR (300 MHz, C_2D_6SO) δ_H: 10.50 (*s*, 1H), 8.27 – 8.17 (*m*, 2H), 8.01 (*d*, *J* = 2.5 Hz, 1H), 7.72 (*dd*, *J* = 8.3, 7.3 Hz, 1H), 7.63 (*d*, *J* = 2.5 Hz, 1H), 4.10 – 3.90 (*m*, 2H), 1.70 – 1.50 (*m*, 2H), 1.38 – 1.17 (*m*, 10H), 0.84 (*t*, *J* = 6.9 Hz, 3H) ppm. ^{13}C NMR (75 MHz, $CDCl_3$) δ_C: 164.81, 164.42, 155.45, 133.50, 132.83, 128.99, 127.52, 123.63, 123.37, 122.64, 122.29, 116.80, 40.98, 31.94, 29.45, 29.36, 28.26, 27.31, 22.76, 14.22 ppm. FTIR (ATR) ν (cm^{-1}): 3371 (m), 2949 (m), 2918 (m), 2850 (m), 1695 (s), 1618 (s), 1516 (s), 1440 (s), 1352 (m), 1284 (s), 1134 (m), 1091 (m), 1062 (m), 1043 (m). HRMS-ESI-TOF (m/z): calcd. for $C_{20}H_{23}NO_3$ $[M+H]^+$ 326.1756; found 326.1740.

Synthesis of 4-Chloro-3-hydroxy-1,8-naphthalic anhydride (132)

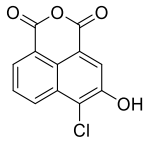

In a single-neck round bottom flask (25 mL), 3-hydroxy-1,8-naphthalenic anhydride **44** (214 mg, 1 mmol) was dissolved in MeCN (7 mL) and $FeCl_3 \cdot 6H_2O$ (3.24 g, 12 mmol) was added at RT. The resulting solution was heated under reflux for 60 hours, cooled down to RT and the solvent removed under reduced pressure. The solid residue was suspended in HCl (aq) (50 mL) and the precipitate filtered to give **132** (354 mg, 83 %) as an orange solid. M.p.: 187 °C (decompose). ^{1}H NMR (400 MHz, C_2D_6SO) δ_H: 11.55 (*s*, 1H), 8.51 (*d*, *J* = 8.5 Hz, 1H), 8.38 (*d*, *J* = 7.3 Hz, 1H), 8.18 (*s*, 1H), 7.94 (*brdd*, *J* = 7.9 Hz, 1H) ppm. ^{13}C NMR (101 MHz, C_2D_6SO) δ_C: 160.40, 159.99, 152.26, 130.40, 129.73, 129.66, 128.93, 124.92, 122.73, 120.80, 119.52, 118.72 ppm. FTIR (ATR) ν (cm^{-1}): 3365 (w), 3336 (w), 1772 (m), 1751 (m), 1722 (m), 1701 (m), 1685 (m), 1647 (m), 1570 (m), 1560 (m), 1533 (m), 1506 (m), 1419 (m), 1288 (m), 1236 (m), 1211 (m), 1176 (m), 1147 (m), 1033 (m), 1006 (m). HRMS-EI-TOF (m/z): calcd. for $C_{12}H_5O_4Cl$ $[M]^+$ 247.9876; found 247.9872.

Synthesis of 4-Bromo-3-hydroxy-1,8-naphthalic anhydride (133)

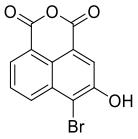

In a single-neck round bottom flask (250 mL), 3-hydroxy-1,8-naphthalenic anhydride **44** (2.0 g, 9.34 mmol) was dissolved in dioxane (50 mL) and Br_2 (3.88 g, 24.29 mmol) was added at RT. The resulting solution was heated under reflux for 2.5 hours, cooled down to RT and the solvent removed under reduced pressure. The solid residue was suspended in water (75 mL) and the precipitate filtered to give **133** (2.6 g, 95 %) as a yellow solid. M.p.: >220 °C. ^{1}H NMR (400 MHz, C_2D_6SO) δ_H: 11.58 (*s*, 1H), 8.47 (*dd*, *J* = 8.6, 0.9 Hz, 1H), 8.36 (*dd*, *J* = 7.3, 0.9 Hz, 1H), 8.14 (*s*, 1H), 7.92 (*dd*, *J* = 8.6, 7.3 Hz, 1H) ppm. ^{13}C NMR (126 MHz, C_2D_6SO) δ_C: 160.32, 160.08, 153.60, 132.19, 131.80, 129.69, 129.10, 124.93, 122.27, 119.42, 119.36, 113.25 ppm. FTIR (ATR) ν (cm^{-1}): 3375 (m),1762 (s), 1728 (s), 1280 (s), 1166, (s), 1143 (m), 1023 (s), 1004 (s). HRMS-EI-TOF (m/z): calcd. for $C_{12}H_5O_4Br$ $[M]^+$ 291.9371; found 291.9370.

Synthesis of 4-Bromo-3-hydroxy-1,8-naphthalic(octyl)imide (134)

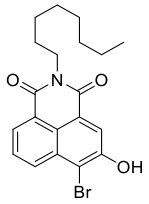

In a single-neck round bottom flask (250 mL), DIPEA (1.32 g, 10.24 mmol) was added to a suspension of bromo-derivative **133** (1.5 g, 5.14 mmol) in dioxane (75 mL). The solution turned red and *n*-octylamine (0.99 g, 7.68 mmol) was added. The reaction mixture was heated under reflux for 20 hours and a change in color (brown) was observed. Then solvent was evaporated under reduced pressure and the solid residue suspended in $HCl_{(aq)}$ (100 mL, 10 % w/w) and extracted with $CHCl_3$ (150 mL, 3 times). The combined organic layers were dried over $MgSO_4$, filtered and evaporated under reduced pressure. The crude material was purified by silica gel chromatography (eluents: pentane/AcOEt, 2/1) affording **134** (2.02 g, 97 %) as a yellow solid. *Rf* = 0.50, pentane/AcOEt 2/1. M.p.: 153-154°C. ^{1}H NMR (400 MHz, $CDCl_3$) δ_H: 8.50 (*dd*, *J* = 7.3, 1.1 Hz, 1H), 8.37 (*dd*, *J* = 8.5, 1.1 Hz, 1H), 8.33 (*s*, 1H), 7.81 (*dd*, *J* = 8.5, 7.3 Hz, 1H), 6.21 (*s*, 1H), 4.20 – 4.11 (*m*, 2H), 1.77 – 1.66 (*m*, 2H), 1.47 – 1.18 (*m*, 10H), 0.91 – 0.81 (*t*, *J* = 6.9 Hz, 3H) ppm. ^{13}C NMR (126 MHz, $CDCl_3$) δ: 163.86, 163.49, 151.98, 131.62, 131.57, 129.35, 128.75, 124.24, 123.61, 123.10, 121.70, 113.33, 40.88, 31.95, 29.47, 29.36, 28.22, 27.27, 22.78, 14.23 ppm. FTIR (ATR) ν (cm^{-1}): 3325 (m), 2925 (m), 2825 (m), 1695 (s), 1648 (s), 1612 (s), 1601 (s), 1574 (s), 1413 (s), 1350 (s), 1285 (s), 1264 (s), 1245 (s), 1235 (m), 1180 (m). HRMS-EI-TOF (m/z): calcd. for $C_{20}H_{22}NO_3Br$ $[M]^+$ 403.0783; found 403.0782.

Synthesis of 4-Bromo-3-methoxy-1,8-naphthalic(octyl)imide (135)

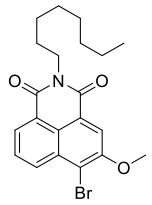

In a single-neck round bottom flask (500 mL), imide-derivative **134** (2.0 g, 4.96 mmol) was dissolved in boiling CH_3CN (155 mL). K_2CO_3 (0.68 g, 4.96 mmol) was added and the solution turned red. Subsequently, CH_3I (0.84 g, 5.93 mmol) was added and the reaction mixture stirred under reflux for 4 hours. During this period the reaction mixture turned from red to yellow. After cooling down to RT, the solvent was evaporated under reduced pressure and the solid residue suspended in water and extracted with $CHCl_3$ (100 mL, 3 times). The combined organic layers were dried over $MgSO_4$, filtered and evaporated under reduced pressure. The crude material was purified by silica gel chromatography (eluents: pentane/AcOEt, 10/1) to afford **135** (2.06 g, 99%) as a yellow solid. *Rf* = 0.60, pentane/AcOEt, 2/1. M.p.: 114-115 °C. ^{1}H NMR (400 MHz, $CDCl_3$) δ_H: 8.53 (*dd*, *J* = 8.6, 1.1 Hz, 1H), 8.50 (*dd*, *J* = 7.3, 1.1 Hz, 1H), 8.31 (*s*, 1H), 7.79 (*dd*, *J* = 8.6, 7.3 Hz, 1H), 4.20 – 4.13 (*m*, 5H), 1.79 – 1.66 (*m*, 2H), 1.46 – 1.24 (*m*, 10H), 0.87 (*t*, *J* = 6.9 Hz, 3H) ppm. ^{13}C NMR (101 MHz, $CDCl_3$) δ_C: 163.86, 163.79, 154.98, 132.46, 132.27, 129.83, 128.60, 124.35, 123.19, 123.01, 116.86, 116.48, 57.45, 40.83, 31.97, 29.47, 29.35, 28.25, 27.27, 22.78, 14.23 ppm. FTIR (ATR) *v* (cm^{-1}): 2925 (m), 2853 (m),1697 (s), 1653 (s), 1613 (s), 1592 (s), 1566 (s), 1401 (s), 1354 (s), 1324 (s), 1281 (m), 1231 (m), 1088 (m), 1075 (m), 1041 (m). HRMS-ESI-TOF (m/z): calcd. for $C_{21}H_{25}BrNO_3$ $[M+H]^+$ 418.1018; found 418.1008.

Synthesis of 4-Bromo-3-acetoxy-1,8-naphthalic(octyl)imide (137)

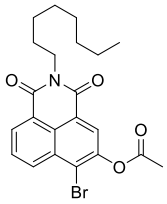

In a single-neck round bottom flask (500 mL), imide-derivative **134** (1.0 g, 4.96 mmol) was dissolved in boiling acetone (155 mL). K_2CO_3 (0.51 g, 3.70 mmol) and Ac_2O (0.50 g, 4.95 mmol) were added and the reaction mixture heated under reflux for 4 hours. The

solvent was evaporated under reduced pressure and the solid residue suspended in water. The obtained solid was filtered and dried in *vacuo* to afford **137** (0.97 g, 88%) as a pale yellow solid. ^{1}H NMR (300 MHz, $CDCl_3$) δ_H: 8.63 (*dd*, *J* = 7.3, 1.1 Hz, 1H), 8.58 (*dd*, *J* = 8.5, 1.1 Hz, 1H), 8.32 (*s*, 1H), 7.86 (*dd*, *J* = 8.5, 7.3 Hz, 1H), 4.23 – 4.08 (*m*, 2H), 2.47 (*s*, 3H), 1.76 – 1.66 (*m*, 2H), 1.47 – 1.17 (*m*, 10H), 0.87 (*t*, *J* = 6.7 Hz, 3H) ppm. ^{13}C NMR (75 MHz, $CDCl_3$) δ_C: 168.39, 163.51, 162.93, 147.61, 133.08, 131.91, 131.59, 128.81, 126.99, 126.68, 123.46, 123.25, 122.83, 40.83, 31.93, 29.44, 29.33, 28.18, 27.22, 22.76, 20.90, 14.21 ppm. FTIR (ATR) *v* (cm^{-1}): 2980 (m), 2920 (m), 2852 (m), 1768 (m), 1699 (m), 1653 (s), 1618 (m), 1571 (m), 1404 (m), 1328 (m), 1253 (m), 1193 (s), 1172 (m), 1136 (m), 1043 (m), 1020 (m). HRMS-ESI-TOF (m/z): calcd. for $C_{22}H_{25}BrNO_4$ $[M+H]^+$ 446.0967; found 446.0976.

Synthesis of Bis(octyl)-2,2'-dimethoxy-4,4',5,5'-(1,1'-binaphthalic)-diimide (136)

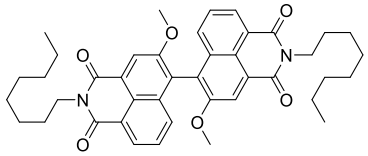

In a single-neck round bottom flask (100 mL), methoxy-imide-derivative **135** (1.0 g, 2.39 mmol) and Cs_2CO_3 (2.34 g, 7.17 mmol) were suspended in dioxane (40 mL) and water (0.5 mL). The resulting mixture was degassed for 20 minutes by bubbling N_2 and B_2Pin_2 (910 mg, 3.58 mmol), $Pd(dba)_2$ (27 mg, 0.047 mmol) and SPhos (39 mg, 0.095 mmol) were added to the reaction mixture. The resulting suspension was degassed for additional 20 minutes and stirred under reflux for 18 hours under N_2. After cooling down to RT the mixture was filtered over celite® and the solvent evaporated under reduced pressure. The crude material was purified by silica gel chromatography (eluents: hexane/AcOEt, 10/1) to obtain **136** as a yellow solid (400 mg, 49%). *Rf* = 0.30, hexane/AcOEt, 10/1. M.p.: 155-156 °C. ^{1}H NMR (300 MHz, $CDCl_3$) δ_H: 8.53 (*s*, 2H), 8.47 (*dd*, *J* = 7.2, 1.1 Hz, 2H), 7.50 (*dd*, *J* = 8.5, 7.2 Hz, 2H), 7.37 (*dd*, *J* = 8.5, 1.1 Hz, 2H), 4.34 – 4.15 (*m*, 4H), 3.90 (*s*, 6H), 1.86 – 1.67 (*m*, 4H), 1.52 – 1.19 (*m*, 20H), 0.89 (*t*, *J* = 6.9 Hz, 6H) ppm. ^{13}C NMR (75 MHz, $CDCl_3$) δ: 163.90, 163.78, 155.64, 132.26, 130.75, 129.08, 127.62, 124.49, 124.41, 123.77, 122.85, 116.86, 56.70, 56.64, 40.46, 31.75, 29.28, 29.16, 28.08, 27.08, 22.58, 14.03 ppm. FTIR (ATR) *v* (cm^{-1}): 2924 (m), 2852 (m), 1697 (s), 1655 (m), 1614 (m), 1589 (m), 1566 (m), 1402 (m), 1346 (m), 1327 (m), 1273 (m), 1232 (m), 1085 (m), 1053 (m),

1020 (m). HRMS-MALDI-TOF (m/z): calcd. for $C_{42}H_{49}N_2O_6$ $[M+H]^+$ 677.3591; found 677.3576.

Synthesis of Bis(octyl)-2,2'-dihydroxy-4,4',5,5'-(1,1'-binaphthalenic)-diimide (131)

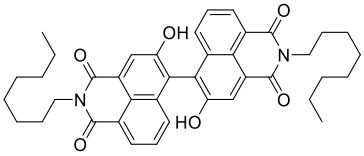

In an oven dried single-neck round bottom flask (100 mL), binaphthyl-diimide-derivative **136** (200 mg, 0.29 mmol) was dissolved in dry CH_2Cl_2 (20 mL). The solution was cooled down to 0 °C and BBr_3 (1 M in CH_2Cl_2, 2.95 mL, 2.95 mmol) added dropwise. The resulting solution was stirred overnight at RT. The reaction mixture was poured on crushed ice and extracted with AcOEt (60 mL, 3 times). The organic layers were dried over $MgSO_4$, filtered and evaporated under reduced pressure. The reaction crude was purified by precipitation from AcOEt/petroleum ether affording **131** as a yellow solid (190 mg, quantitative). *Rf* = 0.50, petroleum ether/AcOEt, 3/2. M.p.: >220 °C. ^{1}H NMR (300 MHz, C_2D_6SO) δ: 10.46 (*s*, 2H), 8.33 (*s*, 2H), 8.28 (*brdd*, *J* = 7.1 Hz, 2H), 7.58 (*brdd*, *J* = 7.9 Hz, 2H), 7.42 (*brdd*, *J* = 8.4 Hz, 2H), 4.07 (*brm*, 4H), 1.66 (*brm*, 4H), 1.30 (*brm*, Hz, 20H), 0.85 (*brt*, *J* = 6.6 Hz, 6H) ppm. ^{13}C NMR (75 MHz, C_2D_6SO) δ_C: 163.55, 163.20, 154.05, 132.46, 130.64, 127.64, 127.50, 123.35, 122.52, 122.36, 121.76, 121.63, 31.28, 28.77, 28.64, 27.53, 26.57, 22.11, 13.98 ppm, One peak is missing due to overlap. FTIR(ATR) *v* (cm^{-1}): 2924 (m), 2854 (m), 1697(m), 1614 (m), 1589 (m), 1436 (m), 1406 (m), 1363 (m), 1327 (m), 1273 (m), 1230 (m), 1083(m). HRMS-MALDI-TOF (m/z): calcd. for $C_{40}H_{45}N_2O_6$ $[M+H]^+$ 649.3278; found 649.3251.

Synthesis of *N,N'*-Bis(octyl)-3,4,8,10-*peri*-Xanthenoxanthene-tetracarboxylic-Diimide (141, PXXDI)

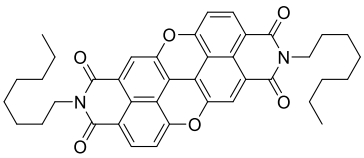

In a single-neck round bottom flask (25 mL), binaphthalyl-diimide-derivative **131** (150 mg, 0.23 mmol), pivalic acid (47 mg, 0.46 mmol) and CuI (132 mg, 0.69 mmol) were dissolved in DMSO (9 mL). The suspension was heated at 120 °C under air for 5 h. After

cooling down to RT, the reaction crude was poured into water and extracted with $CHCl_3$ (80 mL, 5 times). The combined organic layers were dried over $MgSO_4$, filtered and evaporated under reduced pressure. The crude material was purified by silica gel chromatography (eluent: CH_2Cl_2) affording **141** as a red solid (115 mg, 77%). *Rf* = 0.50, CH_2Cl_2. M.p.: >220 °C. ^{1}H NMR (300 MHz, $CDCl_3$) δ_H: 8.37 (*d*, *J* = 8.3 Hz, 2H), 8.21 (*s*, 2H), 7.15 (*d*, *J* = 8.3 Hz, 2H), 4.19 – 4.08 (*m*, 4H), 1.78 – 1.64 (*m*, 4H), 1.47 – 1.22 (*m*, 20H), 0.88 (*t*, *J* = 6.9 Hz, 6H) ppm. ^{13}C NMR (151 MHz, $CDCl_3$) δ_C: 163.03, 162.73, 156.73, 145.78, 134.28, 126.64, 123.86, 121.35, 119.06, 116.59, 116.56, 111.81, 41.00, 31.97, 29.49, 29.38, 28.16, 27.29, 22.80, 14.27 ppm. FTIR(ATR) ν (cm^{-1}): 2918 (w), 2848 (w), 1696 (m), 1658 (m), 1630 (m), 1596 (m), 1379 (m), 1364 (m), 1342 (m), 1269 (m), 1243 (m), 1122 (w), 1087 (w). HRMS-MALDI-TOF (m/z): calcd. for $C_{40}H_{40}N_2O_6$ $[M]^+$ 644.2886; found 644.2866.

4.3.2 Synthesis of *N*-substituted A_2-type PXXDI: PATH A

Synthesis of dimethyl 4-bromo-3-methoxynaphthalene-1,8-dicarboxylate (142)

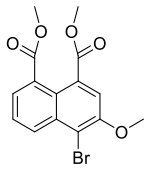

In a single-neck round bottom flask (250 mL), DBU (7.79 g, 51.18 mmol) was added to a suspension of bromo-derivative **133** (5.0 g, 17.06 mmol) in MeOH (100 mL) at 0 °C. The solution turned yellow and CH_3I (7.24 g, 51.18 mmol) was added. The reaction mixture was allowed to warm up at RT and heated under reflux for 16 hours. The volatiles were removed in *vacuo* and the residue taken in CH_2Cl_2. The solution was washed with HCl(aq) (100 mL,10 % w/w) and $Na_2S_2O_3$ (aq) (100 mL 4.4 M), dried over $MgSO_4$, filtered and evaporated under reduced pressure. The crude material was purified by crystallization from MeOH, affording **142** (4.88 g, 81 %) as a white solid. M.p.= 131 °C. ^{1}H NMR (300 MHz, $CDCl_3$) δ_H: 8.49 (*dd*, *J* = 8.7, 1.2 Hz, 1H), 7.93 (*dd*, *J* = 7.1, 1.2 Hz, 1H), 7.77 (*s*, 1H), 7.60 (*dd*, *J* = 8.7, 7.1 Hz, 1H), 4.08 (*s*, 3H), 3.92 (*s*, 3H), 3.91 (*s*, 3H) ppm.^{13}C NMR (75 MHz, $CDCl_3$) δ_C: 169.04, 168.60, 153.19, 134.22, 130.81, 130.61, 130.02, 128.77, 127.08, 123.87, 117.09, 113.23, 57.23, 52.50, 52.36 ppm. FTIR (ATR) *v* (cm^{-1}):3024 (w), 2993 (w), 2947 (m), 2846 (w), 1720 (s), 1560 (m), 1435 (m), 1354 (m), 1269 (m), 1074 (m). HRMS-EI-TOF (m/z): calcd. for $C_{15}H_{13}O_5Br$ $[M]^+$ 351.9946; found 341.9945.

Synthesis of dimethyl 4-pinacoloborate-3-methoxynaphthalenic-1,8-dicarboxylate (143)

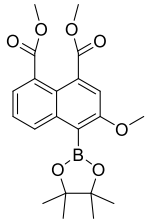

In a single-neck round bottom flask (500 mL), methoxy-bromo-derivative **142** (2.0 g, 5.66 mmol) and KOAc (1.66 g, 16.98 mmol) were suspended in dioxane (200 mL) and the resulting mixture degassed for 20 minutes by bubbling N_2. Subsequently, B_2Pin_2 (1.58 g, 6.22 mmol), $Pd(PPh_3)_2Cl_2$ (198 mg, 0.28 mmol) were added to the reaction mixture. The resulting suspension was degassed for other 20 minutes and heated under reflux for 16 hours under N_2. After cooling down to RT, the mixture was filtered over celite® and the solvent evaporated under reduced pressure. The crude material was suspended in CH_2Cl_2 and precipitated from petroleum ether, to give **143** as a white solid (1.79 g, 79 %). M.p.: 180 °C. ^{1}H NMR (300 MHz, $CDCl_3$) δ_H: 8.01 (*d*, *J* = 8.2 Hz, 1H), 7.85 (*d*, *J* = 6.9 Hz, 1H), 7.71 (s, 1H), 7.47 (*brdd*, *J* = 7.8 Hz, 1H), 3.96 (*s*, 3H), 3.90 (*s*, 3H), 3.89 (*s*, 3H), 1.47 (*s*, 12H) ppm. ^{13}C NMR (75 MHz, $CDCl_3$) δ: 169.56, 169.17, 160.30, 138.38, 132.87, 131.50, 129.90, 128.01, 125.86, 122.99, 116.51, 84.64, 56.78, 52.31, 52.15, 25.00 ppm; one peak is missing. FTIR (ATR) ν (cm^{-1}): 2978 (w), 2954 (w), 1726 (s), 1342 (m), 1309 (m), 1267 (m), 1138 (s), 1070 (m). HRMS-EI-TOF (m/z): calcd. for $C_{21}H_{25}O_7{}^{10}B$ $[M]^+$ 399.1730; found 399.1734.

Synthesis of tetramethyl 2,2'-dimethoxy-[1,1'-binaphthalene]-4,5, 4',5',-tetracarboxylatecarboxylate (58)

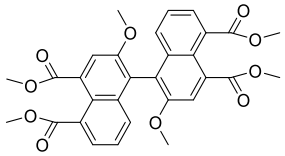

Method 1. In a single-neck round bottom flask (50 mL), bromo-derivative **142** (0.50 g, 1.41 mmol) and K_3PO_4 (3.075 g, 14.154 mmol) were suspended in dry dioxane (20 mL) and the resulting mixture degassed for 20 minutes by bubbling N_2. Subsequently, B_2Pin_2 (197 mg, 0.77 mmol), $Pd(dba)_2$ (9.7 mg, 0.017 mmol) and SPhos (13 mg, 0.033 mmol) were added to the reaction mixture. The resulting suspension was degassed for additional

20 minutes and heated under reflux for 20 hours under N_2. After cooling down to RT, the mixture was filtered over celite® and the solvent evaporated under reduced pressure. The crude material was purified by silica gel chromatography (eluents: petroleum ether/AcOEt, 1/1) affording **58** as a white solid (92 mg, 22%).

Method 2. In a single-neck round bottom flask (250 mL), methoxy-bromo-derivative **145** (1.0 g, 2.83 mmol) and K_3PO_4 (1.84 g, 8.49 mmol) were suspended in a mixture of dioxane/H_2O (5/1 v/v, 120 mL) and the resulting mixture degassed for 20 minutes by bubbling N_2. Subsequently, boron-derivative **143** (2.26 g, 5.66 mmol), $Pd(dba)_2$ (81 mg, 0.14 mmol) and SPhos (116 mg, 0.28 mmol) were added to the reaction mixture. The resulting suspension was degassed for additional 20 minutes and stirred under reflux for 20 hours under N_2. After cooling down to RT, the mixture was filtered over celite® and the solvent evaporated under reduced pressure. The crude material was purified by silica gel chromatography (eluents: petroleum ether/AcOEt, 1/1) affording **58** as a white solid (1.25 g, 81%).

Rf = 0.32, hexane/AcOEt, 10/1. M.p.: = 233 °C. ^{1}H NMR (400 MHz, $(CD_3)_2CO$) δ_H: 8.02 (*s*, 2H), 7.84 (*dd*, *J* = 7.0, 1.3 Hz, 2H), 7.39 (*dd*, *J* = 8.6, 7.0 Hz, 2H), 7.28 (*dd*, *J* = 8.6, 1.3 Hz, 2H), 3.93 (*s*, 6H), 3.91 (*s*, 6H), 3.84 (*s*, 6H) ppm. ^{13}C NMR (101 MHz, $(CD_3)_2CO$) δ_C: 169.69, 169.27, 155.18, 135.77, 133.04, 131.45, 129.84, 128.64, 127.01, 123.86, 123.16, 118.20, 56.98, 52.61, 52.43 ppm. FTIR (ATR) *v* (cm^{-1}): 2980 (m), 2889 (m), 1716 (s), 1508 (m), 1436 (m), 1340 (m), 1261 (m), 1166 (m), 1145 (s), 1066 (m), 1006 (m). HRMS-APCI-TOF (m/z): calcd. for $C_{30}H_{26}O_{10}$ $[M]^+$ 546.1526; found 546.1522.

2,2'-dimethoxy-[1,1'-binaphthalene]-dianhydride (144)

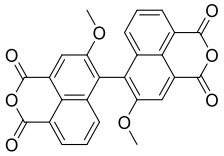

In a single-neck round bottom flask (250 mL), binaphthyl-tetramethyl ester **58** (1.0 g, 1.83 mmol) and KOH (513 mg, 9.14 mmol) were dissolved in *i*PrOH (50 mL) and stirred under reflux for 13 hours. The solvent was removed under reduced pressure and the solid residue suspended in a mixture of AcOH/$HCl_{(conc)}$ (1/1 v/v, 100 mL) and heated under reflux for additional 24 hours. The reaction mixture was poured on crushed ice and a dark precipitate was formed. The solid was filtered and dried in *vacuo* to give **144** as a brown solid (674

mg, 81%). M.p.: > 300 °C. ^{1}H NMR (300 MHz, C_2D_6SO) δ_H: 8.51 (*s*, 2H), 8.41 (*d*, *J* = 7.1 Hz, 2H), 7.69 (*brdd*, *J* = 7.9 Hz, 2H), 7.45 (*d*, *J* = 8.5 Hz, 2H), 3.91 (*s*, 6H) ppm. ^{13}C NMR (75 MHz, C_2D_6SO) δ_C: 160.60, 160.48, 155.54, 131.67, 131.33, 130.37, 128.65, 125.52, 124.53, 121.28, 119.66, 118.42, 56.92 ppm. FTIR (ATR) *v* (cm^{-1}): 2980 (m), 2889 (m), 1770 (m), 1730 (s), 1591 (m), 1570 (m), 1510 (m). 1460 (m), 1388 (m), 1344 (m), 1263 (s), 1149 (m), 1014 (s). HRMS-APCI-TOF (m/z): calcd. for $C_{26}H_{15}O_5$ $[M+H]^+$ 455.0767; found 455.0765.

Synthesis of 2,2'-dihydroxy-[1,1'-binaphthalene]-dianhydride (43)

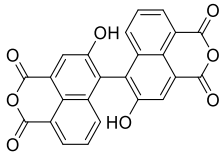

In a single-neck round bottom flask, (50 mL) binaphthyl-dianhydride **144** (200 mg, 0.44 mmol) was suspended in AcOH/HBr (48% w/w aq.) (1/1 v/v, 20 mL) and heated at 126 °C for 24 hours. After cooling down to RT, the volatiles were removed. The solid residue was suspended in H_2O and filtered to give **43** (185 mg, quantitative) as a dark solid. ^{1}H NMR (300 MHz, C_2D_6SO) δ_H: 10.77 (*s*, 2H), 8.33 (*d*, *J* = 6.2 Hz, 4H), 7.66 (*brdd*, *J* = 7.8 Hz, 2H), 7.47 (*d*, *J* = 8.5 Hz, 2H) ppm. ^{13}C NMR (75 MHz, C_2D_6SO) δ_C: 160.74, 160.49, 154.16, 132.33, 131.40, 129.25, 128.09, 124.82, 123.09, 122.38, 120.35, 119.33 ppm. FTIR (ATR) *v* (cm^{-1}): 3055 (w), 2980 (m), 2889 (m), 2260 (w), 1768 (m), 1728 (s), 1585 (m), 1508 (m), 1402 (s), 1257 (m), 1178 (m), 1145 (m),1085 (m), 1018 (m). HRMS-EI-TOF (m/z): calcd. for $C_{24}H_{10}O_8$ $[M]^+$ 426.0376; found 426.0381.

4.3.3 Synthesis of *N*-substituted PXXMI: PATH A

Synthesis of 2,2'-dimethoxy-(1,1'-binaphthalene)-4,5-(octyl)-Imide (146)

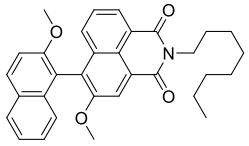

In a single-neck round bottom flask (100 mL), methoxy-imide-derivative **138** (500 mg, 1.2 mmol) and Cs_2CO_3 (1.16 g, 3.57 mmol) were suspended in dioxane (50 mL) and H_2O (0.5 mL) and the resulting mixture degassed for 20 minutes by bubbling N_2. Subsequently, 2-methoxy-naphthaleneboronic acid **145** (482 mg, 2.39 mmol), $Pd(dba)_2$ (34 mg, 0.059

mmol) and SPhos (49 mg, 0.12 mmol) were added and the resulting suspension degassed for additional 20 minutes. The reaction mixture was thus stirred under reflux for 16 hours under N_2. After cooling down to RT, the reaction crude was filtered over celite® and the residue concentrated in *vacuo*. The crude was purified by silica gel chromatography (eluents: hexane/AcOEt, from 10/1 to 10/3) to give **146** as a yellow solid (556 mg, 94%). *Rf* = 0.35, hexane/AcOEt, 10/3. M.p.: 121-122 °C. ^{1}H NMR (300 MHz, CD_2Cl_2) δ_H: 8.51 (*s*, 1H), 8.40 (*dd*, *J* = 5.5, 2.8 Hz, 1H), 8.06 (*d*, *J* = 9.1 Hz, 1H), 7.91 (*brd*, *J* = 8.0 Hz, 1H), 7.53 – 7.42 (*m*, 3H), 7.39 – 7.31 (*m*, 1H), 7.28 – 7.20 (*m*, 1H), 6.99 (*brd*, *J* = 8.0 Hz, 1H), 4.26 – 4.13 (*m*, 2H), 3.90 (*s*, 3H), 3.77 (*s*, 3H), 1.84 – 1.67 (*m*, 2H), 1.48 – 1.23 (*m*, 10H), 0.89 (*t*, *J* = 6.8 Hz, 3H) ppm. ^{13}C NMR (101 MHz, CD_2Cl_2) δ_C: 164.68, 164.50, 156.55, 155.34, 133.90, 133.35, 131.96, 130.89, 129.56, 129.25, 128.69, 127.69, 127.50, 127.37, 124.97, 124.46, 124.33, 124.31, 123.49, 117.72, 117.56, 114.13, 57.34, 57.03, 40.93, 32.43, 29.97, 29.84, 28.71, 27.74, 23.24, 14.39 ppm. FTIR(ATR) *v* (cm^{-1}): 2926 (m), 2852 (m), 2358 (w),1697 (m), 1654 (s), 1614 (m), 1591 (m), 1508 (m), 1404 (m), 1348 (m), 1269 (s), 1251 (s), 1234 (m), 1085 (m), 1060 (m), 1020 (m). HRMS-MALDI-TOF (m/z): calcd. for $C_{32}H_{33}NO_4$ $[M]^+$ 495.2410; found 495.2379.

Synthesis of 2,2'-dihydroxy-(1,1'-binaphthalene)-4,5-dicarboxylic -(octyl)-Imide (147)

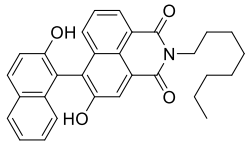

In an oven dried single-neck round bottom flask (250 mL), binaphthyl-imide-derivative **146** (1.0 g, 2.02 mmol) was dissolved in dry CH_2Cl_2 (50 mL). The solution was cooled down to 0 °C and BBr_3 (1 M in CH_2Cl_2, 21 mL, 21 mmol) added. The resulting solution was stirred overnight at RT. Afterwards, the reaction mixture was poured on crushed ice and extracted with AcOEt (100 mL, 3 times). The organic layers were dried over $MgSO_4$, filtered and evaporated under reduced pressure. The crude was purified by silica gel chromatography (eluents: hexane/AcOEt, 5/2) to give **147** as a yellow solid (916 mg, 97%). *Rf* = 0.25, hexane/AcOEt, 5/2. M.p.: 166-167 °C. ^{1}H NMR (300 MHz, CD_2Cl_2) δ_H: 8.30 (*s*, 1H), 8.26 (*dd*, *J* = 4.6, 3.7 Hz, 1H), 8.05 (*brd*, *J* = 8.9 Hz, 1H), 7.94 (*brd*, *J* = 8.0 Hz, 1H), 7.51 (*s*, 1H), 7.49 (*brd*, *J* = 1.1 Hz, 1H), 7.39 (*brm*, 2H), 7.35 – 7.26 (*brm*, 1H), 7.02

(*brd*, *J* = 8.3 Hz, 1H), 5.98 (*brs*, 1H), 5.70 (*brs*, 1H), 4.06 – 3.92 (*m*, 2H), 1.70 – 1.60 (*brm*, 2H), 1.42 – 1.20 (*brm*, 10H), 0.88 (*brt*, *J* = 6.8 Hz, 3H) ppm. ^{13}C NMR (75 MHz, CD_2Cl_2) δ_C: 164.46, 163.86, 154.10, 153.48, 133.67, 133.22, 132.61, 131.27, 129.95, 129.13, 128.56, 128.23, 125.30, 125.27, 124.75, 124.45, 124.21, 123.35, 122.40, 120.52, 118.89, 110.31, 40.93, 32.38, 29.86, 29.79, 28.49, 27.63, 23.20, 14.41 ppm. FTIR(ATR) *v* (cm^{-1}): 3357 (m), 2926 (m), 2854 (m), 2358 (w), 1697 (m), 1647 (m), 1614 (m), 1597 (m), 1508 (m), 1404 (s), 1271 (s), 1228 (w), 1217 (w), 1143 (w). HRMS-MALDI-TOF (m/z): calcd. for $C_{30}H_{30}NO_4$ $[M+H]^+$ 468.2175; found 468.2180.

Synthesis of N-octyl-3,4-*peri*-Xanthenoxanthene-tetracarboxylic-Imide (148, PXXMI)

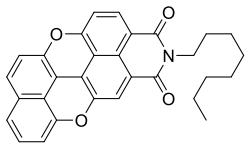

In a single-neck round bottom flask (25 mL), binaphthalyl-imide-derivative **147** (120 mg, 0.25 mmol), pivalic acid (52 mg, 0.51 mmol) and CuI (146 mg, 0.767 mmol) were dissolved in DMSO (4 mL). The reaction mixture was heated at 120 °C under air for 5 hours. The resulting mixture was poured into H_2O and extracted with $CHCl_3$ (50 mL, 5 times). The combined organic layers were dried over $MgSO_4$, filtered and evaporated under reduced pressure. The crude material was purified by silica gel chromatography (eluent: CH_2Cl_2) affording **148** as a red solid (102 mg, 86%). *Rf* = 0.70, CH_2Cl_2. M.p.: >220 °C. ^{1}H NMR (300 MHz, $CDCl_3$) δ_H: 8.12 (*d*, *J* = 8.3 Hz, 1H), 7.76 (*s*, 1H), 7.38 (*d*, *J* = 9.2 Hz, 1H), 7.16 – 7.06 (*m*, 2H), 6.96 (*d*, *J* = 9.2 Hz, 1H), 6.83 (*d*, *J* = 8.3 Hz, 1H), 6.64 (*dd*, *J* = 7.3, 1.1 Hz, 1H), 4.09 – 4.04 (*m*, 2H), 1.72 – 1.64 (*m*, 2H), 1.44 – 1.25 (*m*, 10H), 0.88 (*t*, *J* = 6.7 Hz, 3H) ppm. ^{13}C NMR (151 MHz, CD_2Cl_2) δ_C: 163.38, 163.10, 157.24, 152.60, 145.58, 145.45, 133.49, 131.90, 129.73, 128.75, 126.61, 121.71, 121.17, 121.12, 120.63, 119.16, 118.60, 117.73, 116.21, 110.59, 110.55, 40.96, 32.44, 29.97, 29.87, 28.58, 27.80, 23.25, 14.45 ppm; one peak is missing due to overlap. FTIR(ATR) *v* (cm^{-1}): 2922 (m), 2852 (m), 1696 (s), 1660 (s), 1647 (m), 1599 (m), 1373 (m), 1344 (m), 1315 (m), 1273 (m), 1247 (w), 1124 (m), 1089 (w). HRMS-MALDI-TOF (m/z): calcd. for $C_{30}H_{25}NO_4$ $[M]^+$ 463.1783; found 463.1765.

4.3.4 Synthesis of *N*-substituted PXXMI: PATH B

Synthesis of dimethyl 2,2'-dimethoxy-[1,1'-binaphthalene]-4,5-dicarboxylate (51)

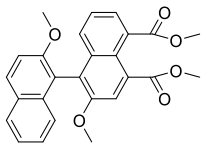

Method 1. In a single-neck round bottom flask (100 mL), methoxy-bromo-derivative **142** (1.66 g, 4.72 mmol) and K_3PO_4 (3.08 g, 14.15 mmol) were suspended in dry dioxane (55 mL) and the resulting mixture degassed for 20 minutes by bubbling N_2. Subsequently, 2-methoxy-naphthaleneboronic acid **145** (1.91 g, 9.43 mmol), $Pd(dba)_2$ (135 mg, 0.23 mmol) and SPhos (193 mg, 0.47 mmol) were added to the reaction mixture. The resulting suspension was degassed for additional 20 minutes and heated under reflux for 24 hours under N_2. After cooling down to RT, the reaction mixture was filtered over celite® and the solvent evaporated under reduced pressure. The crude material was purified by silica gel chromatography (eluents: petroleum ether/AcOEt, 3/1) to give **51** as a white solid (2.01 g, **quantitative**).

Method 2. In a single-neck round bottom flask (50 mL), 1-bromo-2-methoxynaphthalene **151** (100 mg, 0.42 mmol) and K_3PO_4 (276 mg, 1.27 mmol) were suspended in dioxane/H_2O (5/1 v/v, 12 mL) and the resulting mixture degassed for 20 minutes bubbling N_2. Subsequently, boron-derivative **143** (339 mg, 0.84 mmol), $Pd(dba)_2$ (12 mg, 0.02 mmol) and SPhos (17 mg, 0.04 mmol) were added to the reaction mixture. The resulting suspension was degassed for other 20 minutes and stirred under reflux for 16 hours under N_2. After cooling down to RT, the reaction mixture was filtered over celite® and the solvent evaporated under reduced pressure. The crude material was purified by silica gel chromatography (eluents: petroleum ether/AcOEt, 3/1) to give **51** as a white solid (2.01 g, **quantitative**).

Rf = 0.44, petroleum ether/AcOEt, 3/2. M.p.: 201 °C. ^{1}H NMR (300 MHz, CD_2Cl_2) δ_H: 8.03 (*d*, *J* = 9.1 Hz, 1H), 7.94 (*s*, 1H), 7.89 (*d*, *J* = 8.1 Hz, 1H), 7.80 (*dd*, *J* = 6.5, 1.9 Hz, 1H), 7.48 (*d*, *J* = 9.1 Hz, 1H), 7.39 – 7.17 (*m*, 4H), 7.05 – 6.97 (*m*, 1H), 3.95 (*s*, 3H), 3.91 (*s*, 3H), 3.82 (*s*, 3H), 3.77 (*s*, 3H) ppm.^{13}C NMR (101 MHz, CD_2Cl_2) δ_C: 169.85, 169.46, 155.38, 154.75, 135.76, 134.06, 131.52, 130.56, 130.41, 130.12, 129.56, 128.59, 128.41, 127.22, 126.15, 125.15, 124.41, 124.22, 123.52, 118.41, 118.09, 114.19, 57.20, 56.97, 52.73, 52.57 ppm. FTIR (ATR) *v* (cm^{-1}): 3066 (w), 2947 (m), 2843 (w), 1708 (s), 1583

(m), 1508 (m), 1431 (s), 1267 (s), 1242 (m), 1139 (m), 1112 (m), 1085 (m), 1058 (m). HRMS-EI-TOF (m/z): calcd. for $C_{26}H_{22}O_6$ $[M^+]$ 430.1416; found 430.1423.

Synthesis of 2,2'-dimethoxy-[1,1'-binaphthalene]-anhydride (150)

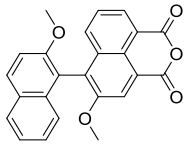

In a single-neck round bottom flask (100 mL), binaphthyl-dimethyl ester-derivative **51** (910 mg, 2.11 mmol) and KOH (237 mg, 4.22 mmol) were dissolved in *i*PrOH (20 mL) and stirred under reflux for 13 hours. After cooling down to RT, the solvent was removed in *vacuo* and the solid residue suspended in a mixture of AcOH/HCl(conc) (4/1 v/v, 25 mL) and stirred under reflux for 24 hours. The solvent was evaporated under reduced pressure. The crude material was purified by silica gel chromatography (eluents: petroleum ether/AcOEt, 3/2) to give **150** as a yellow solid (788 mg, 86%). *Rf* = 0.65, petroleum ether/AcOEt, 3/2. M.p.: 234 °C. ^{1}H NMR (400 MHz, CD_2Cl_2) δ_H: 8.51 (*s*, 1H), 8.45 (*dd*, *J* = 6.8, 1.3 Hz, 1H), 8.08 (*d*, *J* = 9.0 Hz, 1H), 7.92 (*d*, *J* = 8.2 Hz, 1H), 7.61 – 7.47 (*m*, 3H), 7.36 (*ddd*, *J* = 8.2, 6.8, 1.3 Hz, 1H), 7.26 (*ddd*, *J* = 8.2, 6.8, 1.3 Hz, 1H), 6.96 (*m*, 1H), 3.92 (*s*, 3H), 3.77 (*s*, 3H) ppm. ^{13}C NMR (101 MHz, CD_2Cl_2) δ_C: 161.34, 161.31, 156.82, 155.25, 133.69, 133.60, 133.57, 131.66, 131.25, 129.79, 129.49, 128.77, 128.14, 127.55, 126.60, 124.67, 124.39, 119.94, 119.41, 119.29, 116.79, 113.97, 57.40, 56.93 ppm. FTIR(ATR) *v* (cm^{-1}): 3057 (w), 2916 (m), 2916 (m), 2846 (m), 1766 (s), 1728 (s), 1591 (m) , 1506 (m), 1406 (m), 1346 (m), 1267 (s), 1141 (m), 1078 (m), 1058 (m), 1001 (s). HRMS-EI-TOF (m/z): calcd. for $C_{24}H_{16}O_5$ $[M]^+$ 384.0998; found 384.0992.

Synthesis of 2,2'-dihydroxy-[1,1'-binaphthalene]-anhydride (50)

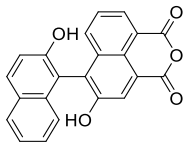

In an oven dried single-neck round bottom flask (100 mL), binaphthyl-anhydride-derivative **150** (1.0 g, 2.60 mmol) was dissolved in dry CH_2Cl_2 (30 mL). The solution was cooled down to 0 °C and BBr_3 (1 M in CH_2Cl_2, 26.0 mL, 26.0 mmol) added. The resulting solution was stirred overnight at RT for 30 hours. The reaction mixture was poured on

crushed ice and extracted with AcOEt (60 mL, 5 times). The organic layers were dried over $MgSO_4$, filtered and evaporated under reduced pressure. The reaction gave **50** as a yellow solid (903 mg, quantitative). *Rf* = 0.20, petroleum ether/AcOEt, 3/2. M.p.: 239 °C. ^{1}H NMR (300 MHz, CD_2Cl_2) δ_H: 8.46 (*dd*, *J* = 4.9, 3.5 Hz, 1H), 8.43 (*s*, 1H), 8.07 (*d*, *J* = 8.9 Hz, 1H), 7.96 (*d*, *J* = 7.9 Hz, 1H), 7.62 (*s*, 1H), 7.61 (*d*, *J* = 1.4 Hz, 1H), 7.47 – 7.23 (*m*, 3H), 7.03 (*d*, *J* = 8.5 Hz, 1H), 5.65 (*s*, 1H), 5.28 (*s*, 1H) ppm. ^{13}C NMR (101 MHz, $(CD_3)_2CO$) δ_C: 161.43, 161.17, 155.40, 154.06, 134.47, 134.30, 133.06, 131.31, 130.20, 129.51, 128.90, 128.27, 127.41, 126.35, 125.60, 124.54, 124.46, 123.79, 120.57, 119.88, 119.13, 113.05 ppm. FTIR (ATR) *v* (cm^{-1}): 3402 (m), 2980 (m), 2920 (m), 2850 (w), 1776 (m), 1705 (s), 1593 (m), 1510 (m), 1406 (m), 1375 (m), 1269 (m), 1217 (m), 1134 (m), 1062 (s). HRMS-EI-TOF (m/z): calcd. for $C_{22}H_{12}O_5$ $[M]^+$ 356.0685; found 356.0671.

Synthesis of 2,2'-dihydroxy-(1,1'-binaphthalene)-4,5-dicarboxylic -(octyl)-Imide (147)

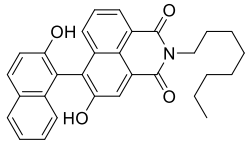

In a single-neck round bottom flask (250 mL), DIPEA (144 mg, 0.84 mmol) was added to a suspension of dihydroxy-binaphthyl-anhydride **50** (200 mg, 0.56 mmol) and *n*-octylamine (108 mg, 0.84 mmol) in dioxane (75 mL). The reaction mixture was stirred under reflux for 20 hours. After cooling down to RT, the solvent was evaporated under reduced pressure and the solid residue suspended in HCl(aq) (10 % w/w) and extracted with $CHCl_3$ (50 mL, 3 times). The combined organic layers were dried over $MgSO_4$, filtered and evaporated under reduced pressure. The crude was purified by silica gel chromatography (eluents: hexane/AcOEt, 5/2) to give **147** as a yellow solid (256 mg, 97%). Characterization in accordance with data reported for PXXMI following PATH A.

Dimethyl 3-methoxy-4-(5-methoxy-2-octyl-1,3-dioxo-2,3-dihydro-1*H*-benzo[*de*]isoquinolin-6-yl)naphthalene-1,8-dicarboxylate (151)

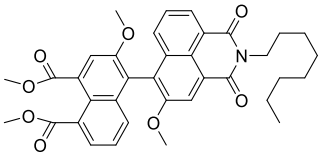

In a single-neck round bottom flask (100 mL), methoxy-imide-derivative **138** (0.50 g, 1.20 mmol) and K_3PO_4 (0.76 g, 3.59 mmol) were suspended in a mixture of 1,4-dioxane/H_2O (5/1 v/v, 60 mL) and the resulting mixture degassed for 20 minutes by bubbling N_2 under sonication. Subsequently, dimethyl 4-pinacoloborate-3-methoxynaphthalenic-1,8-dicarboxylate **143** (0.96 g, 2.39 mmol), [Pd(dba)$_2$] (34.0 mg, 0.06 mmol) and SPhos (49.0 mg, 0.12 mmol) were added to the reaction mixture. The resulting suspension was stirred under reflux for 24 hours under inert atmosphere. The reaction mixture was cooled down to RT and the volatiles removed in *vacuo*. The crude material was dissolved in CH_2Cl_2 (20 mL) and chromatographed on SiO_2 (eluents: CH_2Cl_2 to CH_2Cl_2/MeOH 10:1) to give crude product which was recrystallised from MeOH affording compound **151** as beige prisms (431mg, 59%). M.p.: 122 - 128 °C (from MeOH). ^{1}H NMR ($CDCl_3$, 300 MHz) δ_H: 8.51 (*s*, 1H), 8.44 (*dd*, 1H, *J* = 7.1, 1.3 Hz), 7.95 (*s*, 1H), 7.86 (*dd*, *J* = 6.9, 1.4 Hz, 1H), 7.48 (*dd*, *J* = 8.5, 7.1 Hz, 1H), 7.39 (*dd*, *J* = 8.5, 1.3 Hz, 1H), 7.30 – 7.15 (*m*, 2H), 4.26 – 4.19 (*m*, 2H), 3.99 (*s*, 3H), 3.97 (*s*, 3H), 3.87 (*s*, 3H), 3.81 (*s*, 3H), 1.77 (*quint*, *J* = 7.6 Hz, 2H), 1.51-1.24 (*m*, 10H), 0.88 (*t*, *J*= 6.8 Hz, 3H) ppm. ^{13}C NMR (APT, $CDCl_3$, 75 MHz) δ_C:169.41 (*s*), 169.00 (*s*), 164.21 (*s*), 164.07 (*s*), 155.86 (*s*), 153.99 (*s*), 134.80 (*s*), 132.55 (*s*), 131.86 (*s*), 131.18 (*d*), 129.98 (*s*), 129.18 (*d*), 129.08 (*d*), 128.22 (*d*), 127.58 (*d*), 126.15 (*d*), 125.63 (*s*), 124.21 (*s*), 123.90 (*s*), 123.12 (*s*), 122.89 (*s*), 121.72 (*s*), 117.37 (*d*), 117.06 (*d*), 56.73 (*C*H$_3$), 56.68(*C*H$_3$), 52.42 (*C*H$_3$), 52.26 (*C*H$_3$), 40.60 (*C*H$_2$), 31.86 (*C*H$_2$), 29.39 (*C*H$_2$), 29.26 (*C*H$_2$), 28.21 (*C*H$_2$), 27.19 (*C*H$_2$), 22.68 (*C*H$_2$), 14.13 (*C*H$_3$) ppm. FTIR (ATR) *v* (cm^{-1}): 2951 (m), 2926 (m) 2849 (m), 1728 (s), 1697 (s), 1655 (s), 1614 (m), 1589 (m), 1508 (m), 1460 (m), 1437 (m), 1396 (m), 1342 (s), 1265 (s), 1229 (s), 1217 (s), 1196 (s), 1173 (s), 1138 (s), 1128 (s), 1086 (s), 1069 (s), 1053 (m), 1024 (m), 978 (m), 962 (m), 928 (m), 891 (m), 876 (m), 841 (m), 824 (m), 781 (s), 766 (s), 746 (m), 737 (m), 714 (m), 696 (m), 671 (m), 608 (m), 584 (m), 554 (w), 490 (w), 447 (w), 430 (w), 403 (m). (ASAP-TOF): m/z [M+H]$^+$ calcd for ($C_{36}H_{37}NO_8$+H$^+$): 612.2597; found: 612.2597.

5-methoxy-6-(5-methoxy-1,3-dioxo-1*H*,3*H*-benzo[*de*]isochromen-6-yl)-2-octyl-1*H*-benzo[*de*]isoquinoline-1,3(2*H*)-dione (152)

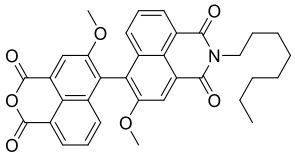

In a single-neck round bottom flask (25 mL), a solution of compound **151** (250 mg, 0.41 mmol) in TFA (6 mL) was stirred at *ca.* 73 °C for 12 hours. After cooling down to RT, the volatiles were removed *in vacuo*, the solid residue was dissolved in CH_2Cl_2 (20 mL) and chromatographed on silica (eluents: hexane/EtOAc 1:1) to give derivative **152** as pale yellow powder (202 mg, 87%). M.p.: 210 - 215 °C (from EtOH). ^{1}H NMR ($CDCl_3$, 300 MHz) δ_H: 8.54 (*s*, 1H), 8.53 (*s*, 1H), 8.52 – 8.45 (*m*, 2H), 7.60-7.45 (*m*, 3H), 7.34 (*dd*, *J* = 8.5, 1.1 Hz, 1H), 4.26 – 4.20 (*m*, 2H), 3.91 (*s*, 3H), 3.90 (*s*, 3H), 1.77 (*quint*, *J* = 7.6 Hz, 2H), 1.50 – 1.23 (*m*, 10H), 0.89 (*t*, *J* = 6.7 Hz, 3H) ppm. ^{13}C NMR (APT, $CDCl_3$, 75 MHz) δ_C: 164.16 (*s*), 164.00 (*s*), 160.71 (*s*), 160.54 (*s*), 156.14 (*s*), 155.72 (s), 132.72 (*s*), 132.47 (*d*), 132.21 (*s*), 131.60 (*d*), 130.55 (*d*), 129.42 (*d*), 128.31 (*d*), 128.09 (*d*), 126.80 (*s*), 126.12 (*s*), 124.96 (*s*), 123.97 (*s*), 123.61 (*s*), 123.17 (*s*), 120.49 (*s*), 119.14 (*s*), 118.87 (*d*), 116.95 (*d*), 57.04 (*C*H_3), 56.89 (*C*H_3), 40.79 (*C*H_2), 31.96 (*C*H_2), 29.48 (*C*H_2), 29.36 (*C*H_2), 28.31 (*C*H_2), 27.29 (*C*H_2), 22.79 (*C*H_2), 14.23 (*C*H_3) ppm. FTIR (ATR) ν (cm^{-1}): 3123 (w), 3080 (w), 2955 (w), 2926 (m), 2853 (m), 1778 (m), 1736 (s), 1697 (s), 1659 (s), 1616 (m), 1591 (s), 1576 (m), 1514 (m), 1464 (m), 1441 (m), 1400 (s), 1346 (s), 1331 (s), 1292 (m), 1263 (s), 1238 (m), 1215 (m), 1190 (m), 1180 (m), 1142 (m), 1107 (w), 1086 (m), 1051 (m), 1030 (s), 1011 (s), 970m, 949 (m), 895 (m), 883 (m), 854 (m), 831 (w), 779 (s), 743 (s), 708 (m), 696 (m), 675 (m), 660(w), 590 (m), 577 (m), 554 (m), 528 (w), 484 (m), 444(w), 436 (w), 430 (w), 420 (w). HRMS (APCI-TOF): m/z $[M+H]^+$ calcd for ($C_{34}H_{31}NO_7$+H^+): 566.2179; found: 566.2186.

5-hydroxy-6-(5-hydroxy-1,3-dioxo-1*H*,3*H*-benzo[*de*]isochromen-6-yl)-2-octyl-1*H*-benzo[*de*]isoquinoline-1,3(2*H*)-dione (153)

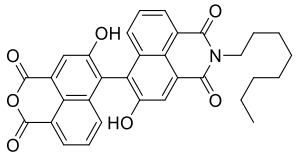

In a single-neck round bottom flask (25 mL), to a solution of compound **153** (224 mg, 0.40 mmol) in CH_2Cl_2 (5 mL) BBr_3 (1M solution in CH_2Cl_2, 2 mL, 2.0 mmol) was added at *ca.* 0 °C. The reaction mixture was allowed to warm up to RT and stirred for 12 hours. The reaction mixture was cooled down to *ca.* 0 °C and quenched with crushed ice. The solidified reaction mixture was dispersed in petroleum ether (10 mL) and the solid material collected by filtration. The crude solid product was dissolved in EtOAc (20 mL), passed through a thin pad of silica (EtOAc) and the volatiles were removed *in vacuo* to give product **154** as yellow powder (212 mg, 99%). M.p.: 278 - 293 °C (from EtOH). ^{1}H NMR ($(CD_3)_2SO$, 300 MHz) δ_H: 10.61 (*brs*, 2H), 8.39-8.23 (*m*, 4H), 7.69-7.55 (*m*, 2H), 7.51 (*d*, , *J* = 8.4 Hz 1H), 7.38 (*d*, , *J* = 8.4 Hz 1H), 4.14 – 4.00 (*m*, 2H), 1.73 – 1.58 (*m*, 2H), 1.42-1.17 (*m*, 10H), 0.86 (*t*, *J*= 6.3 Hz, 3H) ppm. ^{13}CNMR (APT, $(CD_3)_2CO$, 75 MHz) δ_C: 164.52 (*s*), 164.15 (*s*), 161.50 (*s*), 161.28 (*s*), 155.32 (*s*), 155.13 (*s*), 134.11 (*s*), 133.81 (*s*), 132.97 (*d*), 131.23 (*d*), 130.66 (*d*), 128.97 (*d*), 128.68 (*d*), 128.66 (*d*), 126.53 (*s*), 125.62 (*s*), 124.53 (*d*), 124.34 (*s*), 123.97 (*s*), 123.97 (*s*), 122.74 (*d*), 121.66 (*s*), 121.32 (*s*), 120.32 (*s*), 40.85 (CH_2), 32.59 (CH_2), 30.00 (CH_2), 28.82 (CH_2), 27.86 (CH_2), 23.32 (CH_2), 14.37 (CH_3) ppm 1 CH_2 missing. FTIR (ATR) *v* (cm^{-1}): 3246 (m), 2949 (m), 2924 (m), 2855 (m), 1769 (s), 1736 (s), 1701 (w), 1680 (s), 1639 (s), 1611 (m), 1593 (s), 1582 (s), 1535 (w), 1512 (m), 1466 (m), 1452 (m), 1408 (s), 1385 (m), 1368 (s), 1341 (m), 1321 (m), 1287 (m), 1265 (s), 1221 (s), 1188s, 1167 (m), 1134 (s), 1099 (m), 1082 (m), 1063 (m), 1043 (m), 1001 (s), 934 (m), 912 (m), 901 (m), 883 (m), 866 (m), 856 (m), 831 (m), 783 (s), 754 (m), 743 (m), 718 (m), 704 (m), 692 (m), 664 (m), 638 (m), 598s, 584 (m), 563 (m), 554 (m), 540 (m), 530 (m), 500 (m), 482 (m), 465 (m), 449 (m), 444 (m), 432 (m), 420 (m), 403 (m).HRMS (APCI-TOF): m/z $[M+H]^+$ calcd for ($C_{32}H_{27}NO_7+H^+$): 538.1866; found: 538.1867.

5,5'-dihydroxy-2-mesityl-2'-octyl-1*H*,1'*H*-[6,6'-bibenzo[*de*]isoquinoline]-1,1',3,3'(2*H*,2'*H*)-tetraone (154)

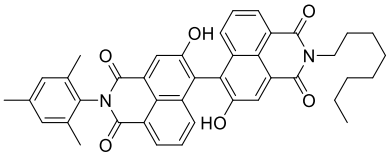

In a single-neck round bottom flask (50 mL), 2,4,6-Trimethylaniline (50.0 mg, 0.37 mmol), compound **153** (100 mg, 0.19 mmol) and imidazole (1.00 g) were stirred at *ca.* 150 °C for 12 hours under inert atmosphere. After cooling down to RT, the reaction mixture was suspended in $HCl_{(aq)}$ (10 % w/w, 10 mL). The solid material was collected by filtration, washed with $HCl_{(aq)}$ (10 % w/w, 10 mL), H_2O (10 mL) and dried. The crude material was chromatographed on silica (eluent: CH_2Cl_2) to give derivative **154** as orange powder (89.0 mg, 73%). M.p.: 215 - 218 °C. ^{1}H NMR ($CDCl_3$, 300 MHz) δ_H: 8.54 (*s*, 1H), 8.50 (*dd*, *J* = 7.1, 1.1 Hz, 1H), 8.41 (*s*, 1H), 8.38 – 8.31 (*m*, 1H), 7.61 – 7.42 (*m*, 4H), 6.96 (*d*, *J* = 2.6 Hz, 2H), 3.97 – 3.83 (*m*, 2H), 2.25 (*s*, 3H), 2.12 (*s*, 3H), 2.04 (*s*, 3H), 1.57 (*quint*, *J* = 7.0 Hz, 2H), 1.35 – 1.14 (*m*, 10H), 0.83 (*t*, *J* = 6.8 Hz, 3H) ppm, two O*H* signals are missing. ^{13}C NMR ($CDCl_3$, 75 MHz) δ_C: 163.97 (*s*), 163.79 (*s*), 163.67 (*s*), 163.55 (*s*), 153.93 (*s*), 153.79 (*s*), 138.83 (*s*), 135.16 (*s*), 132.74 (*s*), 132.68 (*s*), 131.07 (*d*), 131.01 (*s*), 130.91 (*d*), 129.58 (*d*), 129.31 (*d*), 128.44 (*d*), 128.30 (*d*), 125.02 (*s*), 124.57 (*s*), 123.79 (*s*), 123.54 (*d*), 123.08 (*s*), 122.95 (*d*), 122.74 (*s*), 120.09 (*s*), 119.86 (*s*), 40.74 (*C*H_2), 31.93 (*C*H_2), 29.37 (*C*H_2), 29.32 (*C*H_2), 28.09 (*C*H_2), 27.17 (*C*H_2), 22.75 (*C*H_2), 21.28 (*C*H_3), 17.89 (*C*H_3), 17.89 (*C*H_3), 14.22 (*C*H_3) ppm, 1 C_q and 1 C_{tert} missing. FTIR (ATR) ν (cm^{-1}): 3310 (m), 2953 (m), 2924 (m), 2855 (m), 1699 (s), 1649 (s), 1612 (s), 1587 (s), 1512 (m), 1483 (w), 1458 (m), 1437 (m), 1404 (s), 1369 (s), 1339 (s), 1306 (m), 1271 (s), 1233 (s), 1211 (s), 1173 (m), 1152 (m), 1096 (m), 1063 (m), 1032 (m), 1011 (m), 988 (w), 955 (w), 907 (w), 887 (m), 849 (m), 824 (m), 783 (s), 758 (m), 745 (m), 718 (m), 706 (m), 694 (m), 671 (m), 662 (m), 646 (w), 629 (w), 590 (m), 571 (m), 559 (m), 530 (m), 509 (m), 484 (m), 473 (m), 447 (m), 413 (m), 405 (m).HRMS (APCI-TOF): m/z $[M+H]^+$ calcd for ($C_{41}H_{38}N_2O_6+H^+$): 655.2808; found: 655.2807.

***N*-mesityl, *N'*-octyl-3,4,8,10-*peri*-xanthenoxanthenetetracarboxylic-diimide (155)**

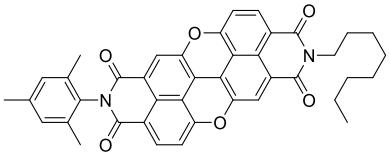

In a single-neck round bottom flask (25 mL) derivative **154** (70.0 mg, 0.11 mmol), pivalic acid (22.0 mg, 0.21 mmol) and CuI (60.0 mg, 0.32 mmol) were dissolved in DMSO (10 mL). The reaction mixture was heated at 120 °C under air for 12 hours and then diluted with H_2O (10 mL). The precipitated solid material was collected by filtration, washed with H_2O (10 mL), MeOH (2 mL) and then dissolved in CH_2Cl_2 (5 mL). The dissolved product was chromatographed on silica (eluents: CH_2Cl_2/EtOH 10:0.5) to give derivative **155** as red powder (62.0 mg, 89%). M.p.: 265 - 293 °C. ^{1}H NMR ($CDCl_3$, 300 MHz) δ_H: 8.44 (*d*, *J* = 8.3 Hz, 1H), 8.34 (d, *J* = 8.3 Hz, 1H), 8.27 (*s*, 1H), 8.19 (*s*, 1H), 7.18 (*d*, *J* = 8.3 Hz, 1H), 7.13 (*d*, *J* = 8.3 Hz, 1H), 7.04 (*s*, 2H), 4.16 – 4.07 (*m*, 2H), 2.36 (*s*, 3H), 2.10 (*s*, 6H), 1.68 (*quint*, *J* = 7.3 Hz, 2H), 1.43 – 1.22 (*m*, 10H), 0.88 (*t*, *J* = 6.7 Hz, 3H). ^{13}C NMR (APT, $CDCl_3$, 75 MHz) δ_C: 162.88 (s), 162.59 (*s*), 162.46 (*s*), 162.13 (*s*), 157.00 (*s*), 156.63 (*s*), 145.832(*s*), 145.80 (*s*), 138.81 (*s*), 135.10 (*s*), 134.74 (*d*), 134.26 (*d*), 131.27 (*s*), 129.63 (*d*), 127.45 (*s*), 126.65 (*s*), 124.00 (*s*), 123.96 (*s*), 121.76 (*d*), 121.36 (*d*), 119.32 (*s*), 119.03 (*s*), 116.82 (*s*), 116.70 (*s*), 116.64 (*s*), 116.44 (*s*), 111.87 (*d*), 111.83 (*d*), 40.97 (*C*H_2), 31.96 (*C*H_2), 29.47 (*C*H_2), 29.36 (*C*H_2), 28.16 (*C*H_2), 27.27 (*C*H_2), 22.78 (*C*H_2), 21.33 (*C*H_3), 17.90 (*C*H_3), 14.24 (*C*H_3) ppm. FTIR (ATR) ν (cm^{-1}): 3080 (w), 3051 (w), 2953 (m), 2924 (m), 2855 (m), 1707 (m), 1694 (s), 1659(s), 1630(s), 1597(s), 1582 (m), 1560 (m), 1506 (m), 1485 (w), 1466 (w), 1458 (w), 1410(s), 1360(s), 1346(s), 1314 (m), 1298(s), 1267(s), 1242(s), 1204 (m), 1194 (m), 1179(s), 1171(s), 1119 (m), 1088 (m), 1053 (m), 1036 (m), 1015 (m), 959 (w), 945 (m), 907 (m), 870 (m), 853 (m), 839(s), 808(s), 758 (m), 741(s), 731 (m), 718 (m), 694 (m), 677 (m), 656 (m), 623 (m), 613 (m), 600 (m), 571 (m), 561 (m), 534 (m), 523 (m), 509 (m), 488 (m), 434 (s) .HRMS (APCI-TOF): m/z $[M+H]^+$ calcd for ($C_{41}H_{34}N_2O_6$+H^+): 651.2495; found: 651.2491.

4.4. Photophysical characterization

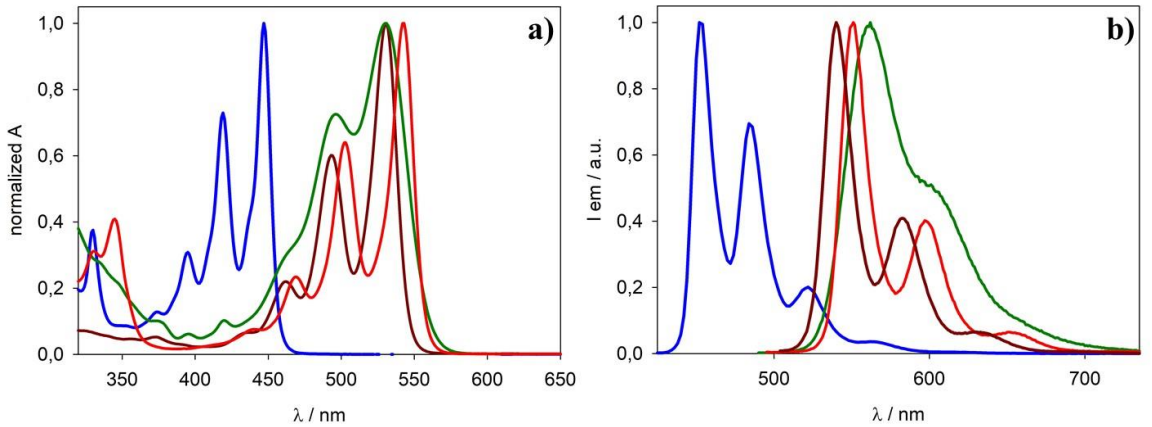

Figure 47: a) Normalized absorption spectra of PXX **25** (blue line), bis-octyl-PDI **202** (dark red line**)**, octyl-PXXMI **148 (**green line) and bis-octyl-PXXDI **141** (red line) in 1,2-dichlorobenzene at RT (arbitrary concentrations). b) normalized emission spectra of molecules in the same solvent at RT PXX **25** (blue line, λ_{ex} = 415 nm), bis-octyl-PDI **202** (dark red line, λ_{ex} = 485 nm), octyl-PXXMI **148 (**green line, λ_{ex} = 485 nm) and bis-octyl-PXXDI **141** (red line, λ_{ex} = 485 nm).

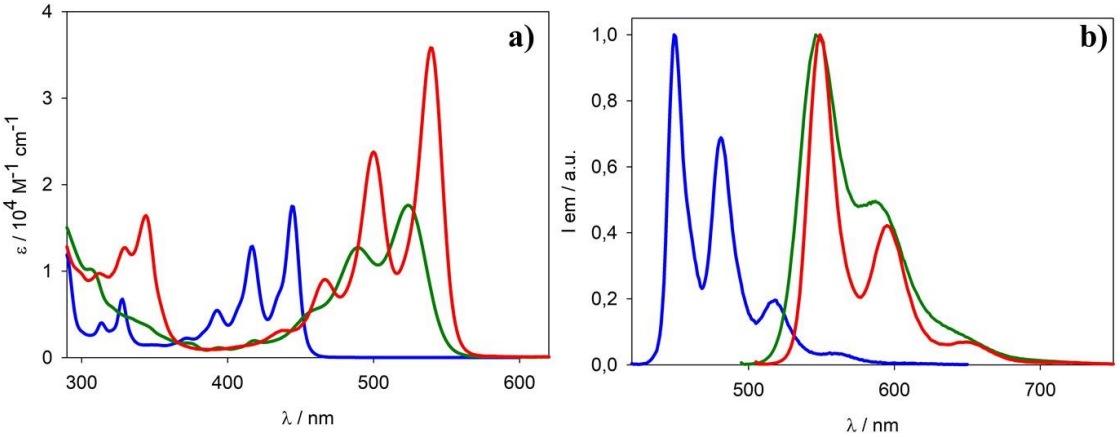

Figure 48:a) Absorption spectra of PXX **25** (blue line, ~ $4.1 \cdot 10^{-5}$ M), octyl-PXXMI **148** (green line, ~ $4.7 \cdot 10^{-5}$ M) and bis-octyl-PXXDI **141** (red line, ~ $2.2 \cdot 10^{-5}$ M) in air equilibrated C_6H_6 at room temperature and b) normalised emission spectra of PXX **25** (blue line, ~ $4.0 \cdot 10^{-6}$ M, λ_{ex} = 415 nm), octyl-PXXMI **148** (green line, ~ $4.6 \cdot 10^{-6}$ M, λ_{ex} = 488 nm) and bis-octyl-PXXDI **141** (red line, ~ $2.0 \cdot 10^{-6}$ M, λ_{ex} = 466 nm) in air equilibrated C_6H_6 at room temperature.

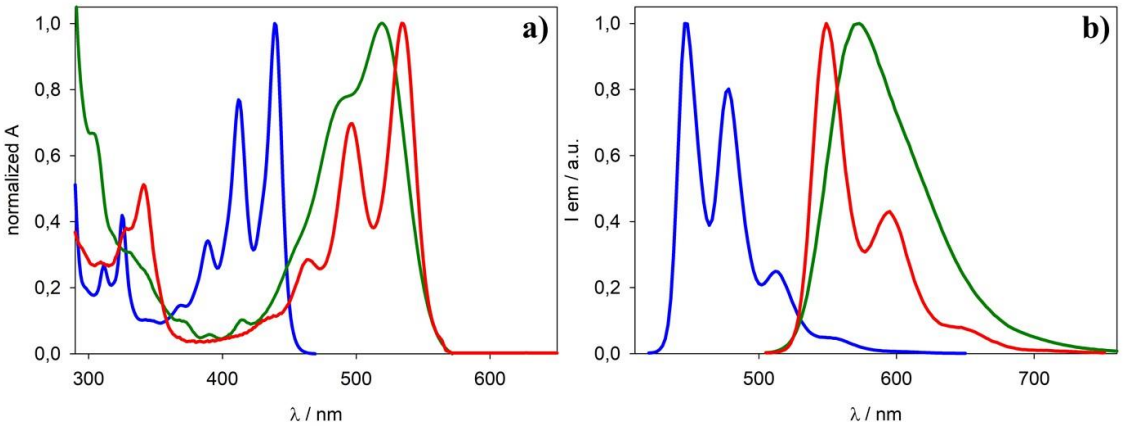

Figure 49: a) Normalized absorption spectra of PXX **25** (blue line), octyl-PXXMI **148 (**green line) and bis-octyl-PXXDI **141** (red line**)** in air equilibrated CH_3CN at RT. (arbitrary concentrations). b) Normalized emission spectra of molecules in the same solvent at RT PXX **25** (blue line, λ_{ex} = 41**0** nm), octyl-PXXMI **148** (green line, λ_{ex} = 490 nm) and bis-octyl-PXXDI **141** (red line, λ_{ex} = 470 nm) in air equilibrated CH_3CN at RT.

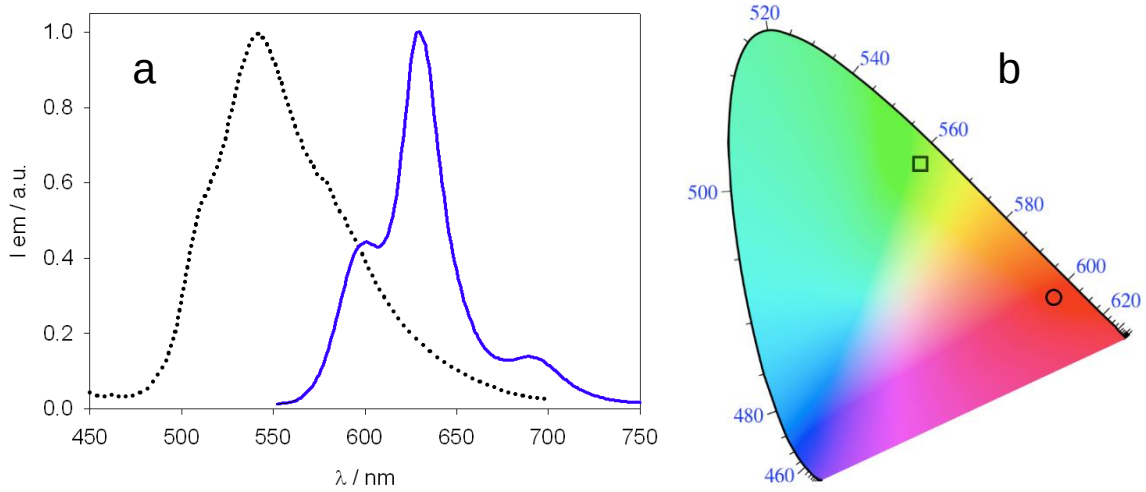

Figure 50: a) solid state emission spectra of molecules PXX **25** (dotted line) and bis-octyl-PXXDI **141** (solid blue line). λ_{ex} = 450 nm and 530 nm, respectively. b) calculated CIE diagram for the two solid state emitters (PXX **25**, square; bis-octyl-PXXDI **141**, circle).

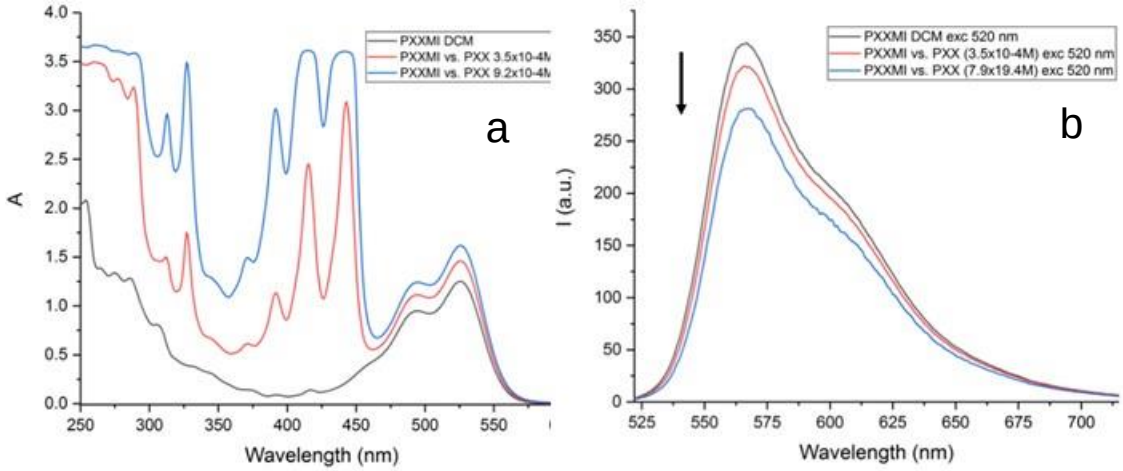

Figure 51: . a) Absorption and b) emission spectra of a octyl-PXXMI **148** solution *ca*. 1.4*10^{-4} M in CH_2Cl_2 in presence of increasing amounts of PXX **25**, from 0 to 0.92 mM; λ_{ex} = 520 nm. By Stern-Volmer analysis, the estimated quenching constant k_{q_PXX} relative to the reductive quenching of octyl-PXXMI **148** is ~2.5x10^{10} $M^{-1}s^{-1}$.

NOTE: the quenching constant k_{q_PXX} between PXX **25** and the excited state of octyl-PXXMI **148** suggests fast and efficient electron transfer to form the **PXX**$^{\bullet+}$/**PXXMI**$^{\bullet-}$ couple, suggesting that in double-dye photoinduced transformation PXX **25** is acting as a quencher, similarly to the DIPEA. Nevertheless, from these data we can calculate the ratio ρ_{PXX} of octyl-PXXMI* quenched by PXX in the experimental conditions used for photoinduced transformations on 2-4'-dibromoacetophenone, as:

$$\rho_{PXX} = 100 \bullet (k_{q\_PXX} * [\mathbf{PXX}]) / (1/\tau_{0\_PXXMI} + k_{q\_PXX} * [\mathbf{PXX}] + k_{q\_DIPEA} * [DIPEA]) \approx 3.2\%$$

While, considering the quenching from DIPEA, in the same conditions used for photoinduced dehalogenations, the ratio ρ_{DIPEA} is around 80%. Therefore, PXX **25** likely gives a small contribution to the production of octyl-PXXMI$^{\bullet-}$; this contribution becomes negligible as long as the concentrations of the two dyes decrease.

The dual experiment, monitoring quenching of PXX **25** in presence of increasing amounts of octyl-PXXMI **148** cannot give any useful information due to inner filter effect caused by octyl-PXXMI **148** at high concentrations, which would lead to an overestimation of the quenching constant.

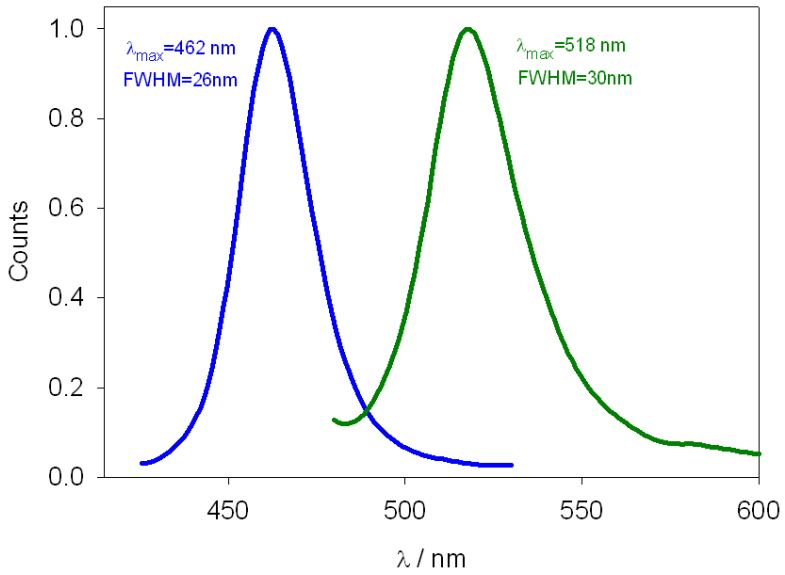

Figure 52: Normalized emission profiles of the blue and green LEDs used to irradiate solutions of PXX **25** and octyl-PXXMI **148/b**is-octyl-PXXDI **141**, respectively.

Table 18: Lifetimes for bis-octyl-PXXDI 141 transient absorption features in deaerated C_6H_6 (~1.0×10^{-5} M, λ_{pump} = 532 nm), showing comparative mono-exponential and bi-exponential parameters.

λ_{abs}	τ (µs)[a]	R^2 [a]	τ_A (µs)[b]	τ_B (µs)[b]	R^2 [b]
375 nm	51.5 (1)	0.974	19.3 (3)	93 (1)	0.986
540 nm	50.1 (2)	0.962	18.5 (4)	91 (2)	0.974
615 nm	52.2 (2)	0.966	18.5 (4)	92 (2)	0.978
690 nm	53.1 (5)	0.852	19.0 (11)	96 (5)	0.862
750 nm	52.4 (5)	0.867	20.1 (11)	98 (5)	0.877

[a] Monoexponential fitting. [b] Biexponential fitting.

NOTE: decay traces of air-equilibrated solutions of **PXX** are not reported since the molecule shows photoinstability upon excitation with pulsed laser sources (λ_{pump} = 355 nm).

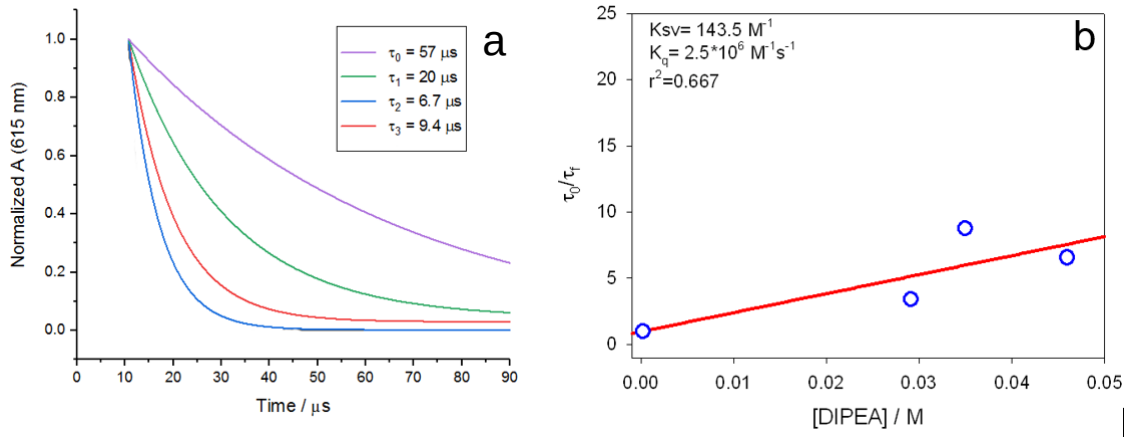

Figure 53: Time resolved transient absorption decay traces (only monoexponential fitting shown for clarity) of a octyl-PXXMI **148** solution *ca.* 1.0*10^{-5} M in deaerated C_6H_6 in presence of increasing amounts of DIPEA, from 0 (purple line) to *ca.* 48 mM (black line); λ_{abs} = 615 nm; λ_{pump} = 532 nm. b) Stern-Volmer plot relative to the triplet excited state quenching by DIPEA, considering the decay times at λ_{abs} = 615 nm (k_{q_T} = 2.5x10^6 $M^{-1}s^{-1}$).

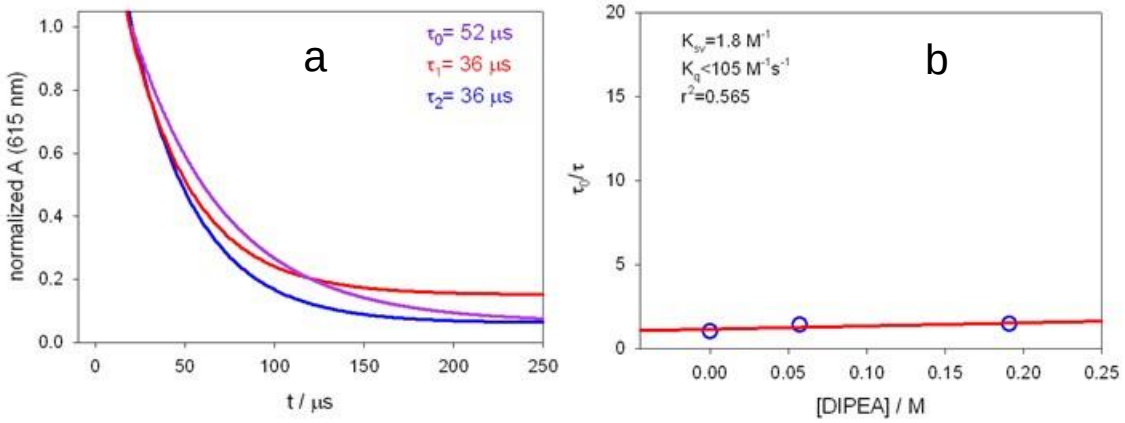

Figure 54: Time resolved transient absorption decay traces (only monoexponential fitting shown for clarity) of a bis-octyl-PXXDI **148** solution *ca.* 1.0*10^{-5} M in deaerated C_6H_6 in presence of increasing amounts of DIPEA, from 0 (purple line) to *ca.* 190 mM (blue line); λ_{abs} = 615 nm; λ_{pump} = 532 nm. b) Stern-Volmer plot relative to the triplet excited state quenching by DIPEA, considering the decay times at λ_{abs} = 615 nm (k_{q_T} < 10^5 $M^{-1}s^{-1}$).

4.5. Stern-Volmer analysis

Table 19: Fluorescence quenching constants for the fluorescence quenching of PXX **25** and octyl-PXXMI **148** measured in CH_2Cl_2 or CH_3CN; values in italics are qualitatively estimated.

Dye (solvent)	**Quencher**	**Quencher E_{ox}/E_{red} (V vs. SCE)**	**k_q ($M^{-1}s^{-1}$)**
PXX (C_6H_6)	DIPEA	0.52/*nd* [a]	$2.9x10^7$
PXX (CH_2Cl_2)	DIPEA	0.52/*nd* [a]	$2.2x10^7$
PXX (CH_3CN)	DIPEA	0.52/*nd* [a]	$3.5x10^7$
PXXMI (C_6H_6)	DIPEA	0.52/*nd* [a]	$2.4x10^8$
PXXMI (CH_2Cl_2)	DIPEA	0.52/*nd* [a]	$1.9x10^9$
PXXMI (CH_3CN)	DIPEA	0.52/*nd* [a]	$4.2x10^9$
PXXDI (C_6H_6)	DIPEA	0.52/*nd* [a]	$5.7x10^9$
PXXDI (CH_3CN:CH_2Cl_2,1:1)	DIPEA	0.52/*nd* [a]	$5.8x10^9$
PXX (C_6H_6)	$PhCOCH_2Br$	*nd*/-0.49 [b]	$2.3x10^{10}$
PXX (CH_3CN)	$PhCOCH_2Br$	*nd*/-0.49 [b]	$2.7x10^{10}$
PXXMI (C_6H_6)	$PhCOCH_2Br$	*nd*/-0.49 [b]	$2.2x10^8$
PXXMI (CH_3CN)	$PhCOCH_2Br$	*nd*/-0.49 [b]	$2.2x10^8$
PXXDI (C_6H_6)	$PhCOCH_2Br$	*nd*/-0.49 [b]	$7.2x10^8$
PXXDI (CH_3CN:CH_2Cl_2,1:1)	$PhCOCH_2Br$	*nd*/-0.49 [b]	$4.5x10^8$
PXX (C_6H_6)	*p*Br-ArCOH	*nd*/-1.76 [c]	$7.0x10^9$
PXX (CH_2Cl_2)	*p*Br-ArCOH	*nd*/-1.76 [c]	$1.3x10^{10}$
PXX (CH_3CN)	*p*Br-ArCOH	*nd*/-1.76 [c]	$1.8x10^{10}$
PXX (C_6H_6)	*p*Br-$ArCOCH_3$	*nd*	$8.2x10^8$
PXX (CH_2Cl_2)	*p*Br-$ArCOCH_3$	*nd*	$6.9x10^9$
PXX (CH_3CN)	*p*Br-$ArCOCH_3$	*nd*	$1.3x10^{10}$
PXXMI (C_6H_6)	*p*Br-$ArCOCH_3$	*nd*	$<10^7$
PXXDI (C_6H_6)	*p*Br-$ArCOCH_3$	*nd*	$8.8x10^7$
PXXMI (CH_3CN)	diethylchloromalonate	*nd*	$9.0x10^6$
PXXDI (CH_3CN:CH_2Cl_2,1:1)	diethylchloromalonate	*nd*	$3.8x10^7$
PXXMI (CH_3CN)	diethylbromomalonate	*nd*	$2.1x10^7$
PXXDI (CH_3CN:CH_2Cl_2,1:1)	diethylbromomalonate	*nd*	$8.6x10^7$

[a]Taken from reference [S9]. Other reported values are 0.72 V *vs.* SCE in CH_3CN,[S10] 0.65 V *vs.* SCE in CH_3CN.[S11] [b]From reference [S12]. [c]Peak potential, from reference [S13].

Table 20: Estimated quenching of dye emissions (I_0/I_f), calculated by the Stern-Volmer relation ($I_0/I_f = 1+k_q*\tau_0*[Q]$) in presence of quenchers (at the same concentrations usually employed for photoinduced reactions); the percentage of quenched emission Q% is calculated as $Q\% = [1-1/(I_0/I_f)]*100$.

Dye (solvent)	**Quencher (M)**	k_q ($M^{-1}s^{-1}$)	I_0/I_f	Q%
PXX (C_6H_6)	*i*Pr_2NEt (0.13)	$2.9x10^7$	1.0	~0
PXX (CH_2Cl_2)	*i*Pr_2NEt (0.13)	$2.2x10^7$	1.0	~0
PXX (CH_3CN)	*i*Pr_2NEt (0.13)	$3.5x10^7$	1.0	~0
PXXMI (C_6H_6)	*i*Pr_2NEt (0.13)	$2.4x10^8$	1.2	17
PXXMI (CH_2Cl_2)	*i*Pr_2NEt (0.13)	$1.9x10^9$	3.3	70
PXXMI (CH_3CN)	*i*Pr_2NEt (0.13)	$4.2x10^9$	6.4	84
PXXDI (C_6H_6)	*i*Pr_2NEt (0.13)	$5.7x10^9$	3.4	71
PXXDI (CH_3CN:CH_2Cl_2,1:1)	*i*Pr_2NEt (0.13)	$5.8x10^9$	3.4	71
PXX (C_6H_6)	Br-Ac-Ph (0.016)	$2.3x10^{10}$	2.8	64
PXXMI (C_6H_6)	Br-Ac-Ph (0.017)	$2.2x10^8$	1.0	~0
PXXMI (CH_3CN)	Br-Ac-Ph (0.017)	$2.2x10^8$	1.0	~0
PXXDI (C_6H_6)	Br-Ac-Ph (0.017)	$7.2x10^8$	1.0	~0
PXXDI (CH_3CN:CH_2Cl_2,1:1)	Br-Ac-Ph (0.017)	$4.5x10^8$	1.0	~0
PXX (C_6H_6)	4-bromoacetophenone (0.017)	$8.2x10^8$	1.1	9
PXX (CH_2Cl_2)	4-bromoacetophenone (0.017)	$6.9x10^9$	1.6	37
PXX (CH_3CN)	4-bromoacetophenone (0.017)	$1.3x10^{10}$	2.1	52
PXXMI (C_6H_6)	4-bromoacetophenone (0.017)	$<10^7$	1.0	~0
PXXDI (C_6H_6)	4-bromoacetophenone (0.017)	$8.8x10^7$	1.0	~0
PXXMI (CH_3CN)	diethylchloromalonate (0.025)	$9.0x10^6$	1.0	~0
PXXDI (CH_3CN:CH_2Cl_2,1:1)	diethylchloromalonate (0.025)	$3.8x10^7$	1.0	~0
PXXMI (CH_3CN)	diethylbromomalonate (0.016)	$2.1x10^7$	1.0	~0
PXXDI (CH_3CN:CH_2Cl_2,1:1)	diethylbromomalonate (0.016)	$8.6x10^7$	1.0	~0

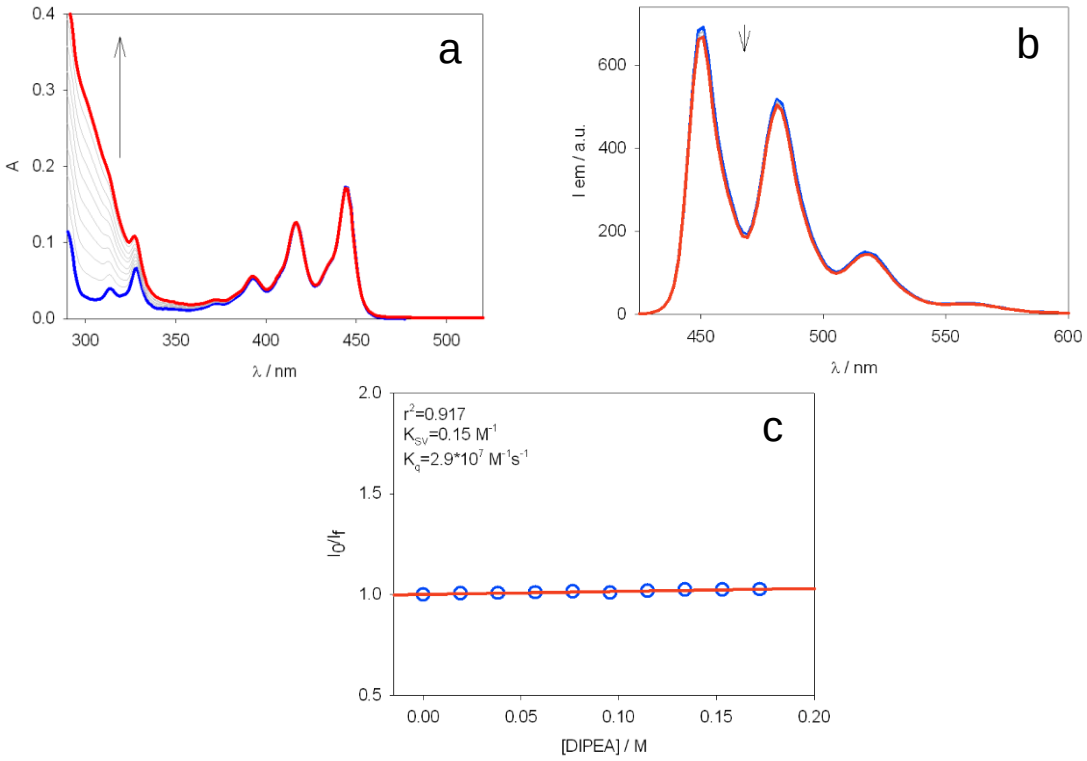

Figure 55: a) Absorption and b) emission spectra of a PXX 25 solution *ca*. 9.8*10^{-6} M in C_6H_6 in presence of increasing amounts of *N*,*N*-diisopropylethylamine (*i*Pr$_2$NEt, DIPEA), from 0 to *ca*. 0.18 M; λ_{ex} = 417 nm. c) Stern-Volmer plot relative to the oxidative quenching, considering emission maximum at λ_{em} = 482 nm.

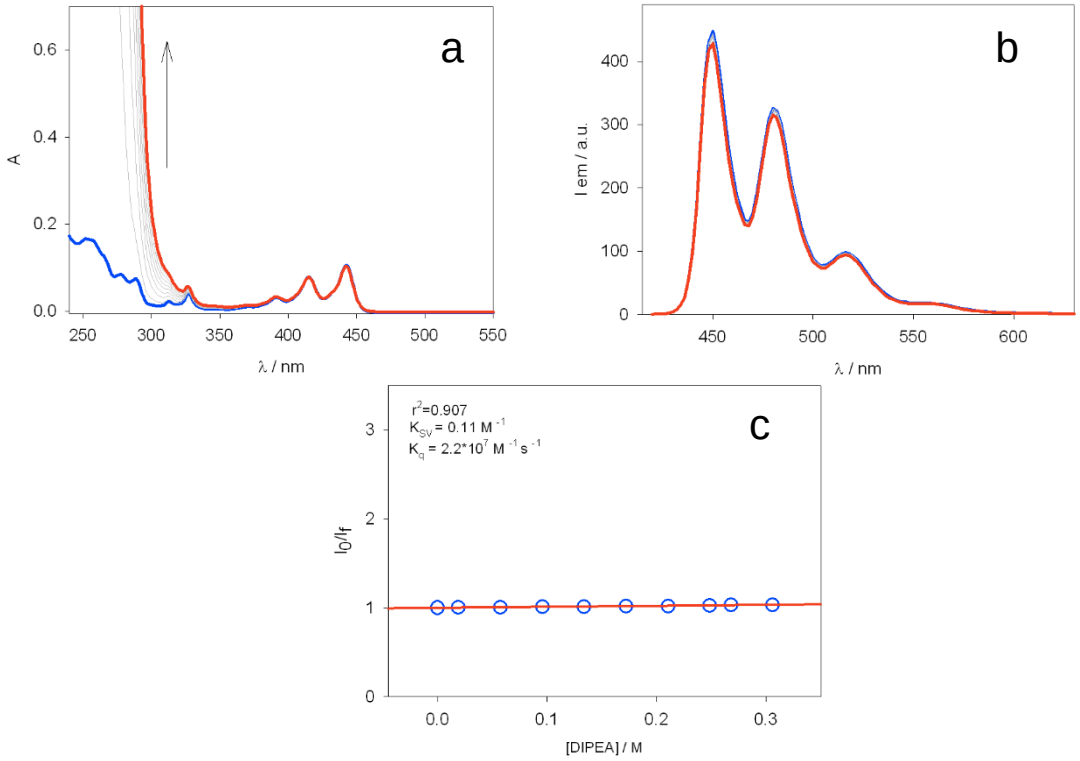

Figure 56: a) absorption and b) emission spectra of a PXX **25** solution *ca*. 6.0*10^{-6} M in CH_2Cl_2 in presence of increasing amounts of *N*,*N*-diisopropylethylamine (*i*Pr$_2$NEt, DIPEA), from 0 to *ca.* 0.3 M; λ_{ex} = 412 nm. c) Stern-Volmer plot relative to the oxidative quenching, considering emission maximum at λ_{em} = 482 nm.

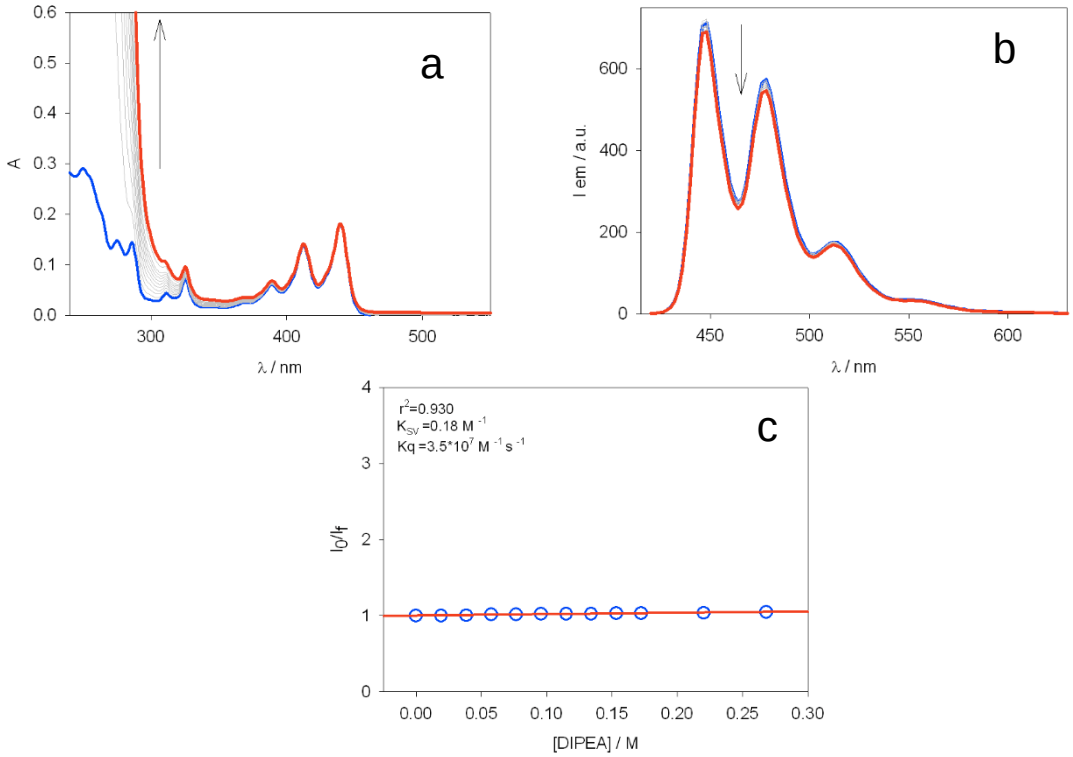

Figure 57: a) Absorption and b) emission spectra of a PXX solution *ca*. 1.0*10^{-5} M in MeCN in presence of increasing amounts of *N*,*N*-diisopropylethylamine (*i*Pr$_2$NEt, DIPEA), from 0 to *ca*. 0.28 M; λ_{ex} = 412 nm. c) Stern-Volmer plot relative to the oxidative quenching, considering the emission peak at λ_{em} = 480 nm.

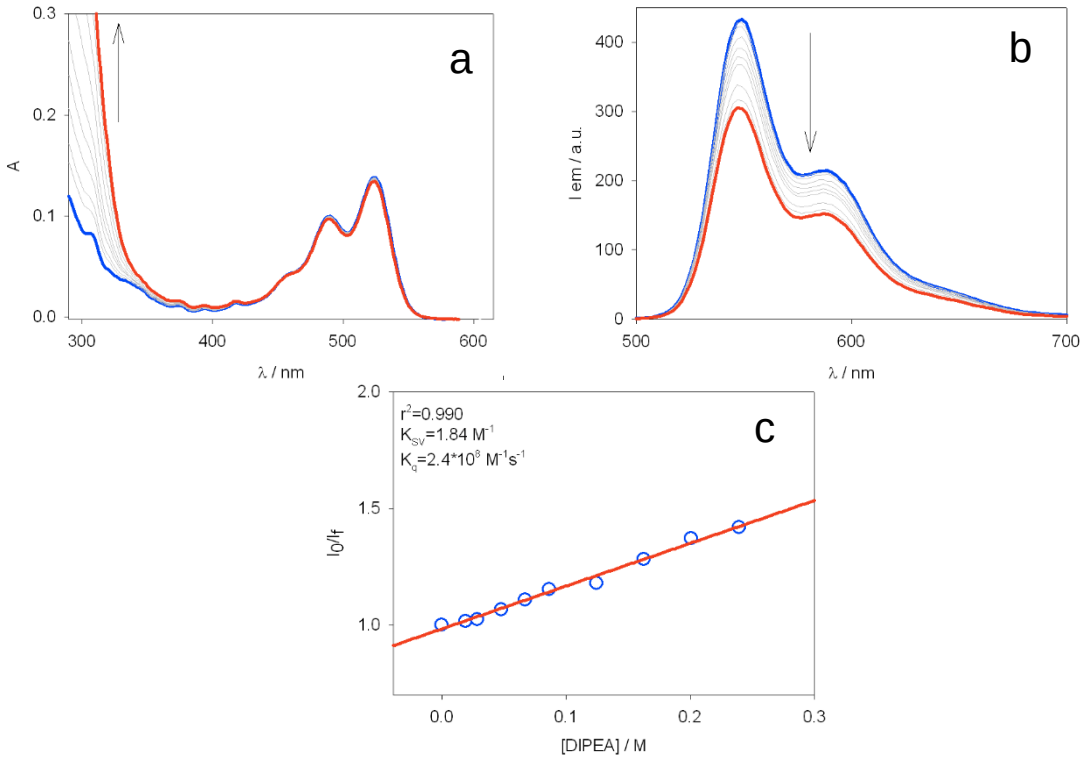

Figure 58: a) Absorption and b) emission spectra of a octyl PXXMI **148** solution *ca*. 7.8*10-6 M in C_6H_6 in presence of increasing amounts of *N*,*N*-diisopropylethylamine (*i*Pr_2NEt, DIPEA), from 0 to *ca*. 0.25 M; λ_{ex} = 490 nm. c) Stern-Volmer plot relative to the reductive quenching, considering the emission peak at λ_{em} = 590 nm.

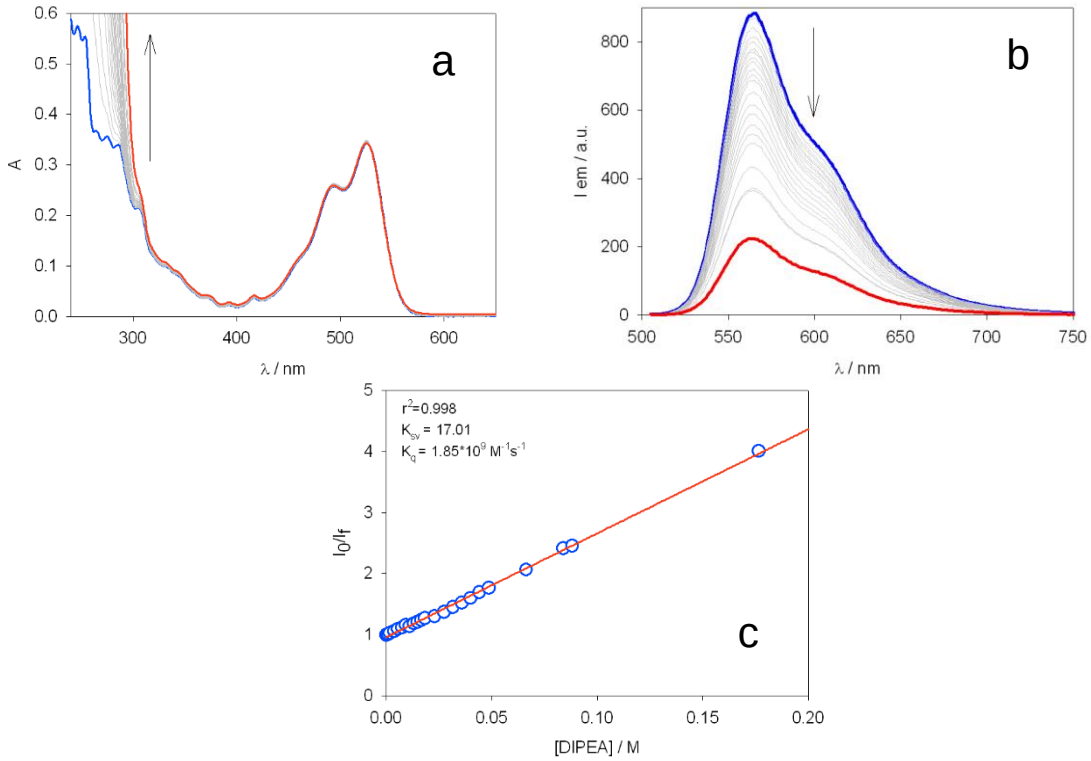

Figure 59: a) absorption and b) emission spectra of a octyl-PXXMI **148** solution *ca*. $1.9*10^{-5}$ M in CH_2Cl_2 in presence of increasing amounts of *N*,*N*-diisopropylethylamine (*i*Pr_2NEt, DIPEA), from 0 to *ca.* 0.18 M; λ_{ex} = 500 nm. c) Stern-Volmer plot relative to the reductive quenching, considering the emission peak at λ_{em} = 565 nm.

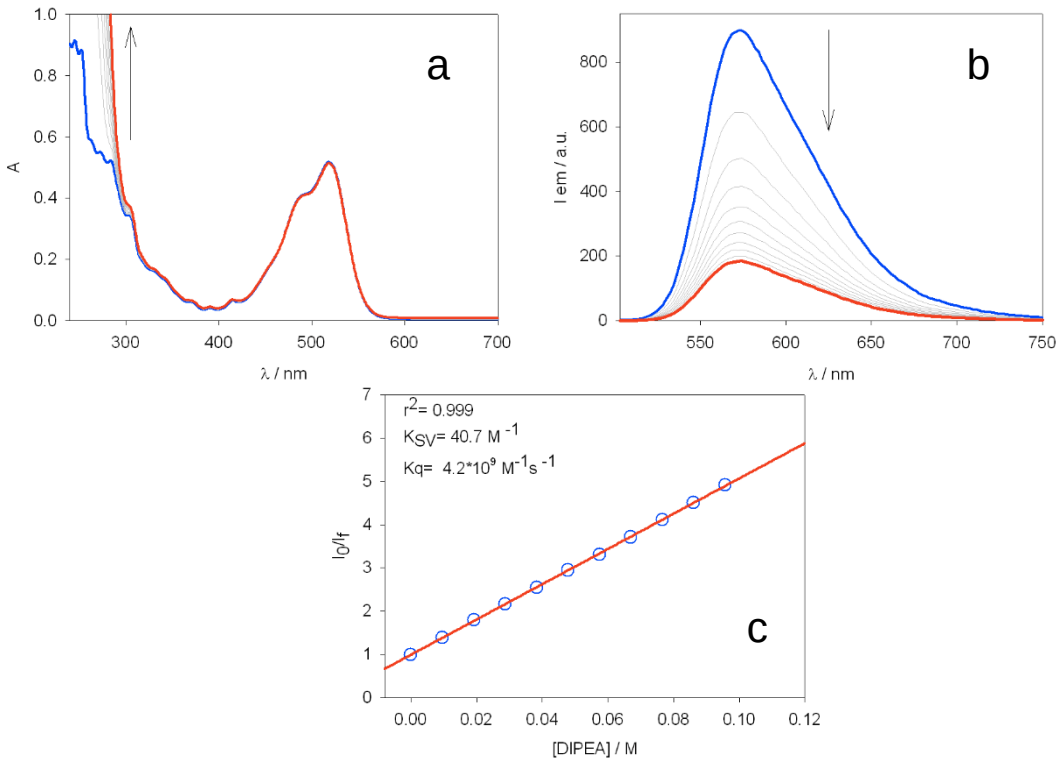

Figure 60: a) Absorption and b) emission spectra of a octyl-PXXMI **148** solution *ca.* $3*10^{-5}$ M in MeCN in presence of increasing amounts of *N*,*N*-diisopropylethylamine (*i*Pr$_2$NEt, DIPEA), from 0 to *ca.* 0.1 M; λ_{ex} = 495 nm. c) Stern-Volmer plot relative to the reductive quenching, considering emission maximum at λ_{em} = 575 nm.

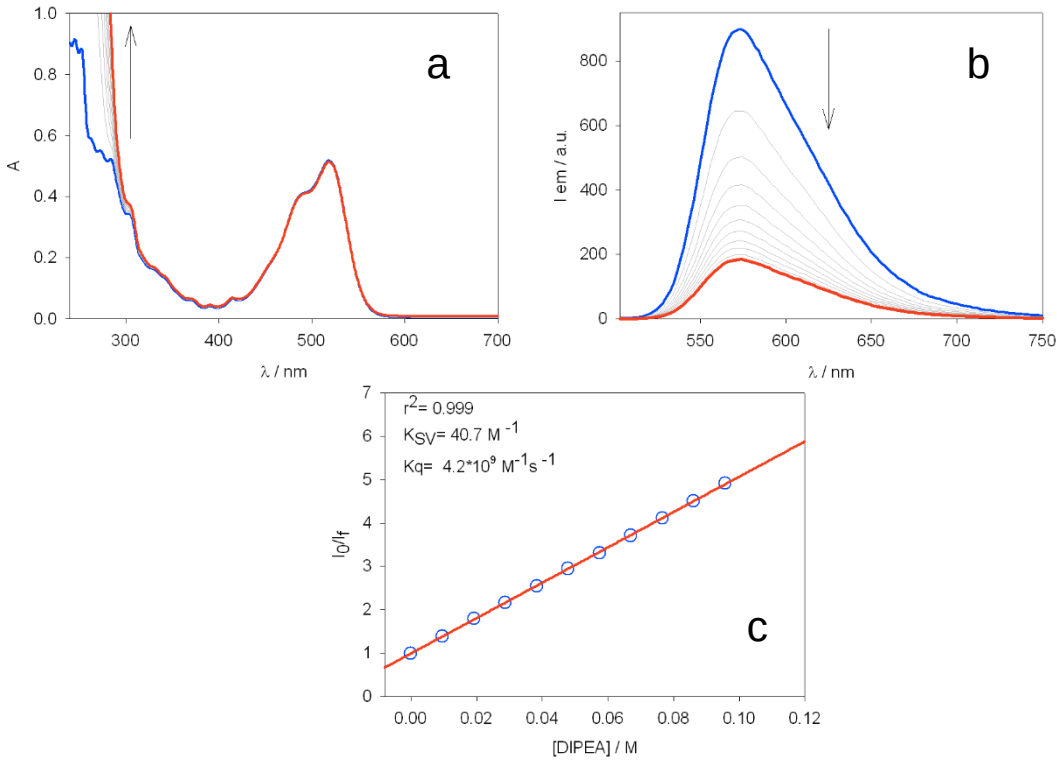

Figure 61: a) absorption and b) emission spectra of a octyl-PXXMI **148** solution *ca*. $3*10^{-5}$ M in MeCN in presence of increasing amounts of *N*,*N*-diisopropylethylamine (*i*Pr$_2$NEt, DIPEA), from 0 to *ca.* 0.1 M; λ_{ex} = 495 nm. c) Stern-Volmer plot relative to the reductive quenching, considering emission maximum at λ_{em} = 575 nm.

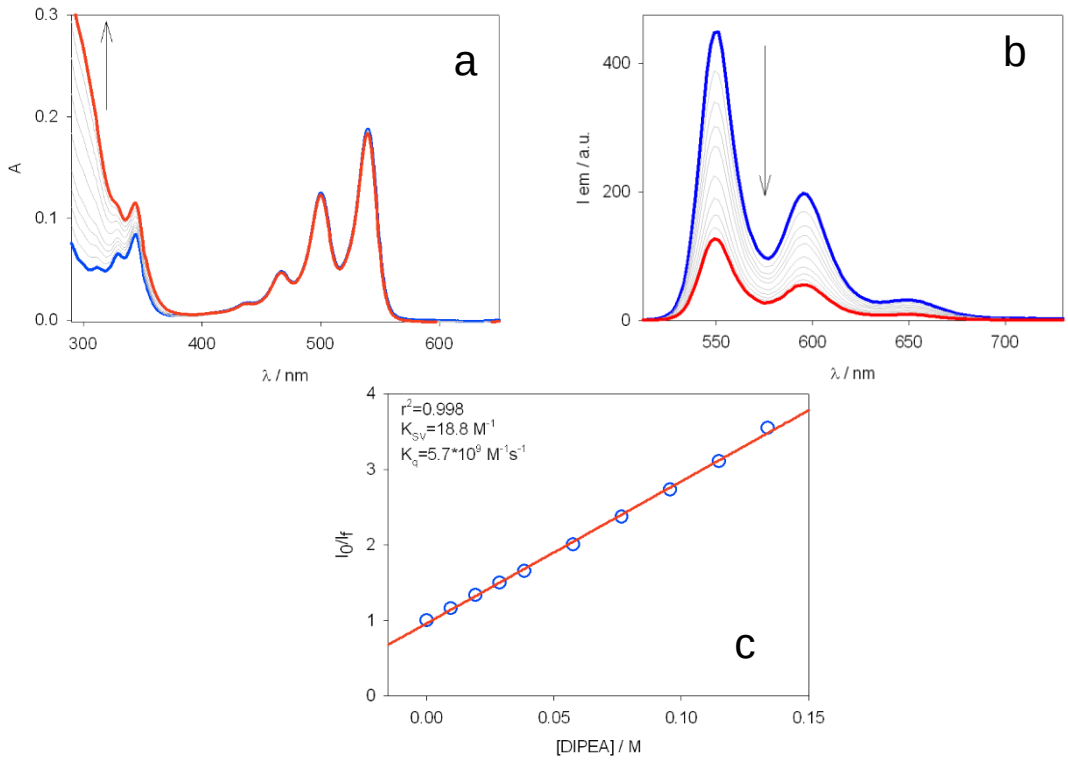

Figure 62: a) Absorption and b) emission spectra of a bis-octyl-PXXDI **141** solution *ca*. 5.2*10^{-6} M in C_6H_6 in presence of increasing amounts of *N*,*N*-diisopropylethylamine (*i*Pr_2NEt, DIPEA), from 0 to *ca.* 14 mM; λ_{ex} = 500 nm. c) Stern-Volmer plot relative to the oxidative quenching, considering emission maximum at λ_{em} =595 nm.

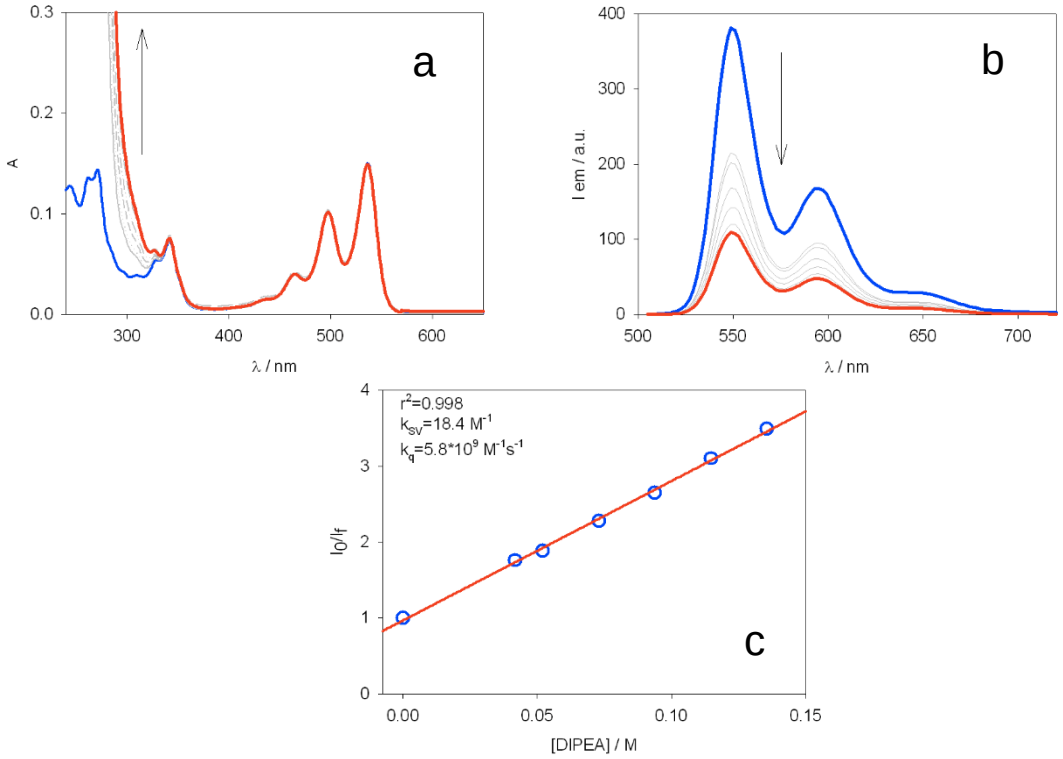

Figure 63: a) Absorption and b) emission spectra of a bis-octyl-PXXDI **141** solution *ca*. 3.4*10^{-6} M in CH_2Cl_2:MeCN 1:1 (v/v) in presence of increasing amounts of *N*,*N*-diisopropylethylamine (*i*Pr_2NEt, DIPEA), from 0 to *ca*. 0.15 M; λ_{ex} = 498 nm. c) Stern-Volmer plot relative to the reductive quenching, considering the emission peak at λ_{em} = 595 nm.

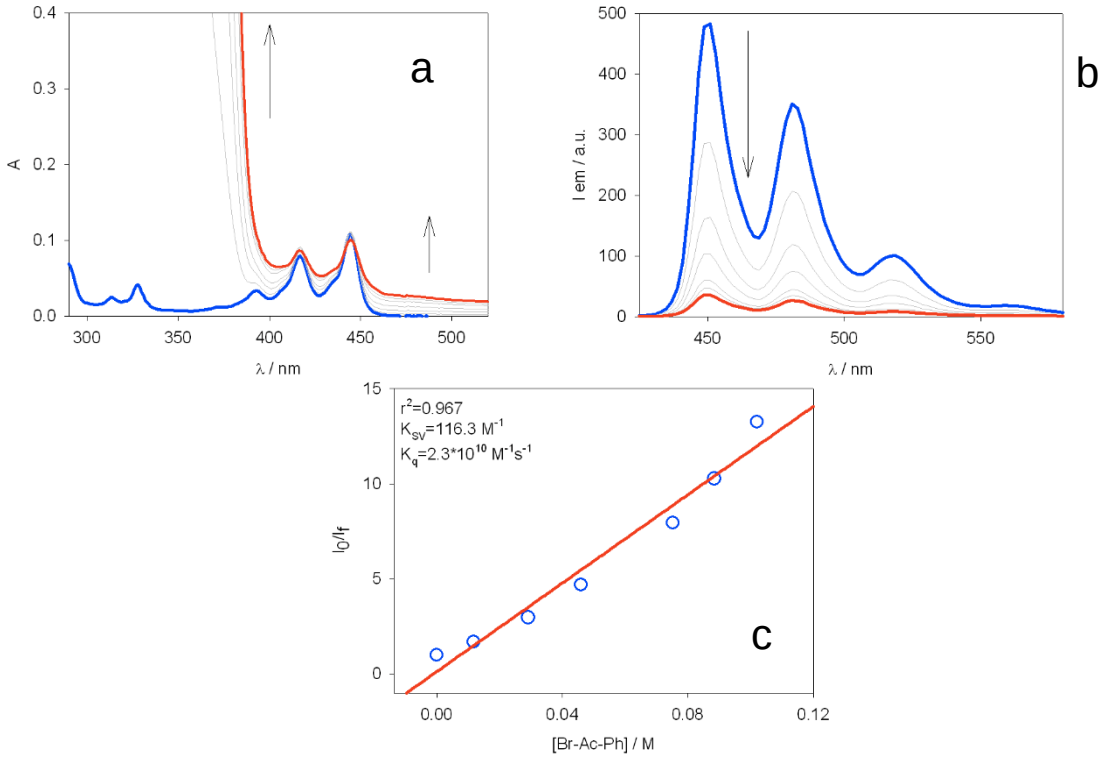

Figure 64: a) absorption and b) emission spectra of a PXX **25** solution *ca*. 6.2*10^{-6} M in C_6H_6 in presence of increasing amounts of 2-bromoacetophenone (Br-Ac-Ph), from 0 to *ca.* 0.1 M; λ_{ex} = 417 nm. c) Stern-Volmer plot relative to the oxidative quenching, considering emission maximum at λ_{em} = 481 nm.

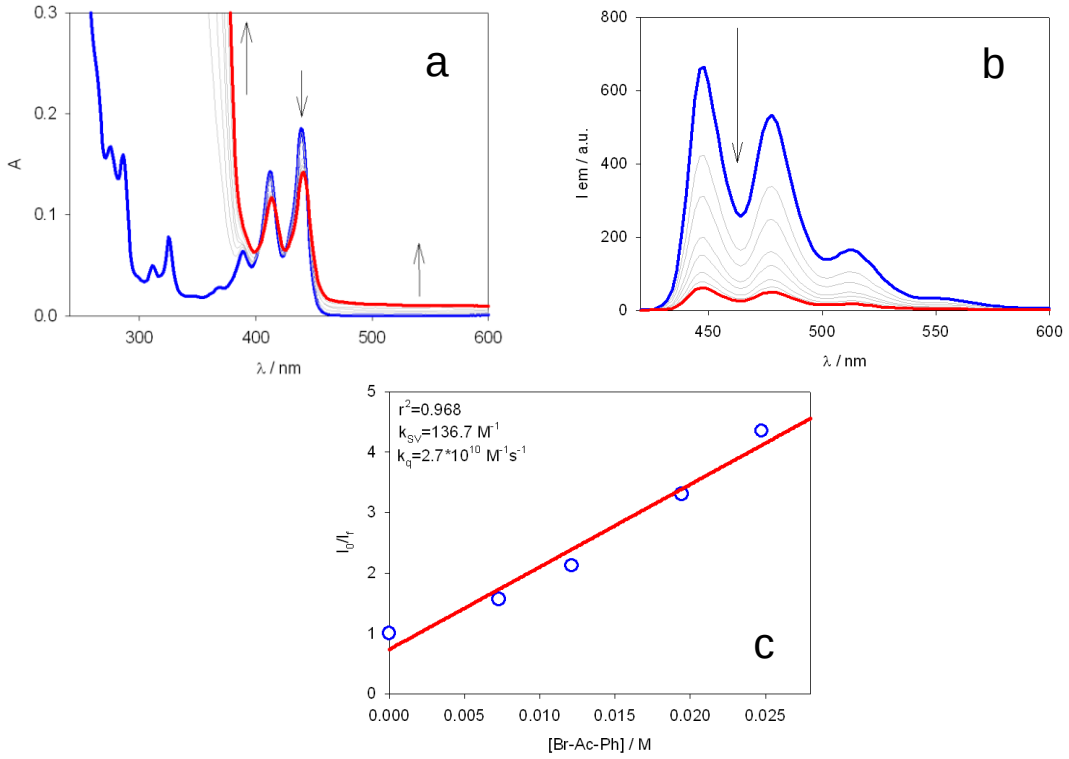

Figure 65: a) Absorption and b) emission spectra of a **PXX** solution *ca.* $1.0*10^{-5}$ M in CH_3CN in presence of increasing amounts of *2*-bromoacetophenone (Br-Ac-Ph), from 0 to *ca.* 0.25 M; λ_{ex} = 413 nm. c) Stern-Volmer plot relative to the oxidative quenching, considering emission maximum at λ_{em} = 477 nm.

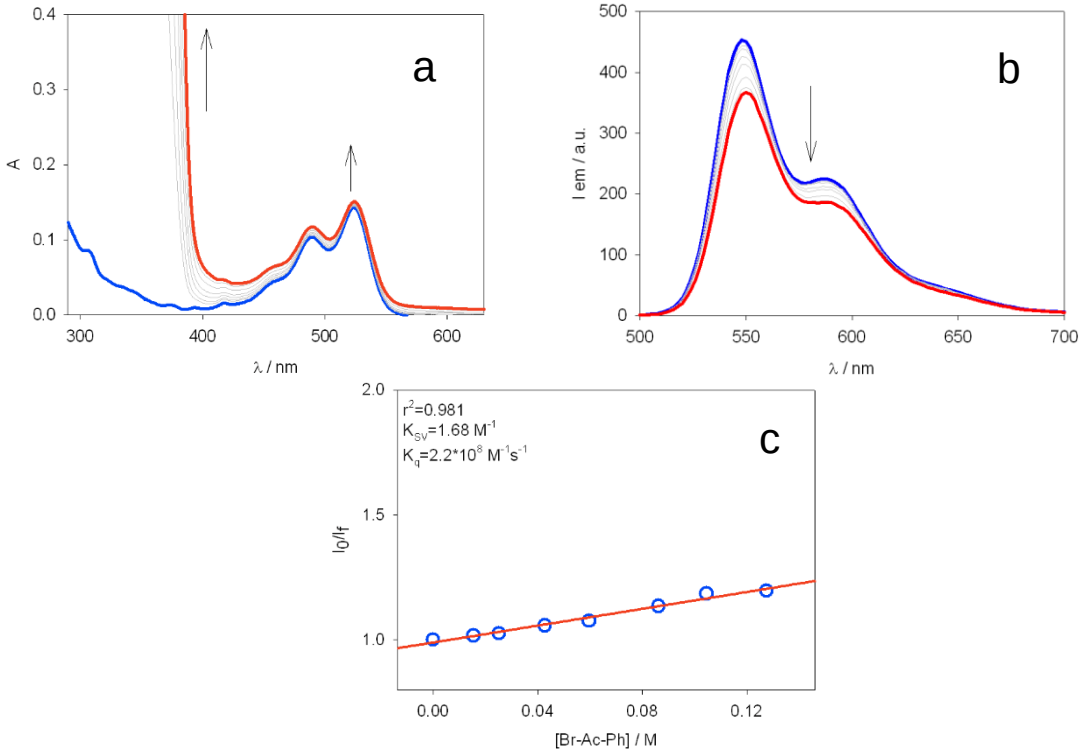

Figure 65: a) Absorption and b) emission spectra of a octyl-PXXMI **148** solution *ca.* $8.1*10^{-6}$ M in C_6H_6 in presence of increasing amounts of 2-bromoacetophenone (Br-Ac-Ph), from 0 to *ca.* 0.13 M; λ_{ex} = 490 nm. c) Stern-Volmer plot relative to the oxidative quenching, considering emission maximum at λ_{em} = 590 nm.

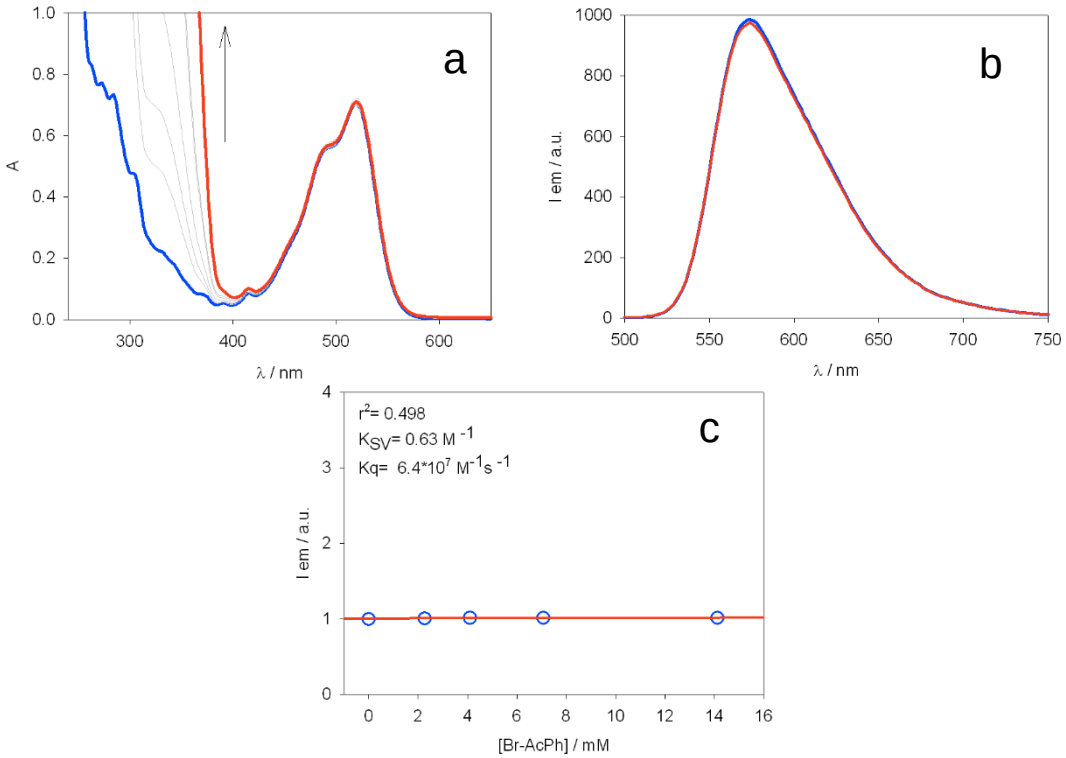

Figure 66: a) absorption and b) emission spectra of a octyl-PXXMI **148** solution *ca*. $3*10^{-5}$ M in MeCN in presence of increasing amounts of 2-bromoacetophenone (Br-Ac-Ph), from 0 to *ca*. 14 mM; λ_{ex} = 495 nm. c) Stern-Volmer plot relative to the oxidative quenching, considering emission maximum at λ_{em} = 575 nm.

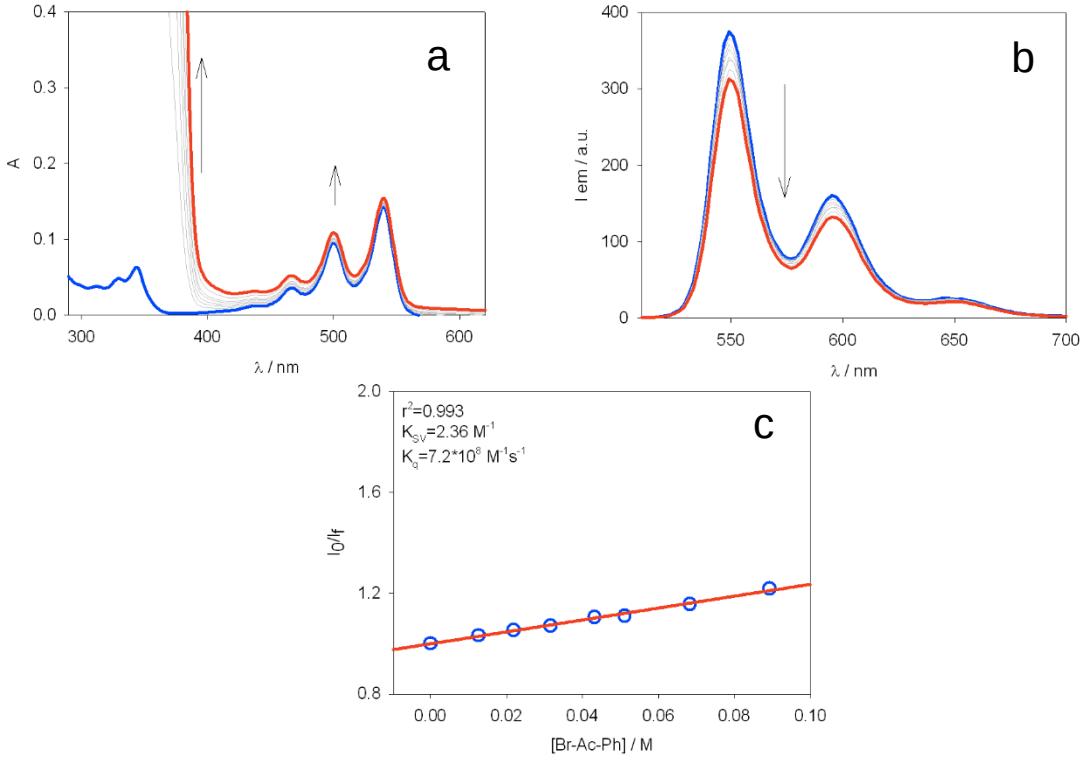

Figure 67: a) Absorption and b) emission spectra of a bis-octyl-PXXDI **141** solution *ca*. 4.0*10^{-6} M in C_6H_6 in presence of increasing amounts of 2-bromoacetophenone (Br-Ac-Ph), from 0 to *ca*. 90 mM; λ_{ex} = 500 nm. c) Stern-Volmer plot relative to the oxidative quenching, considering emission maximum at λ_{em} = 595 nm.

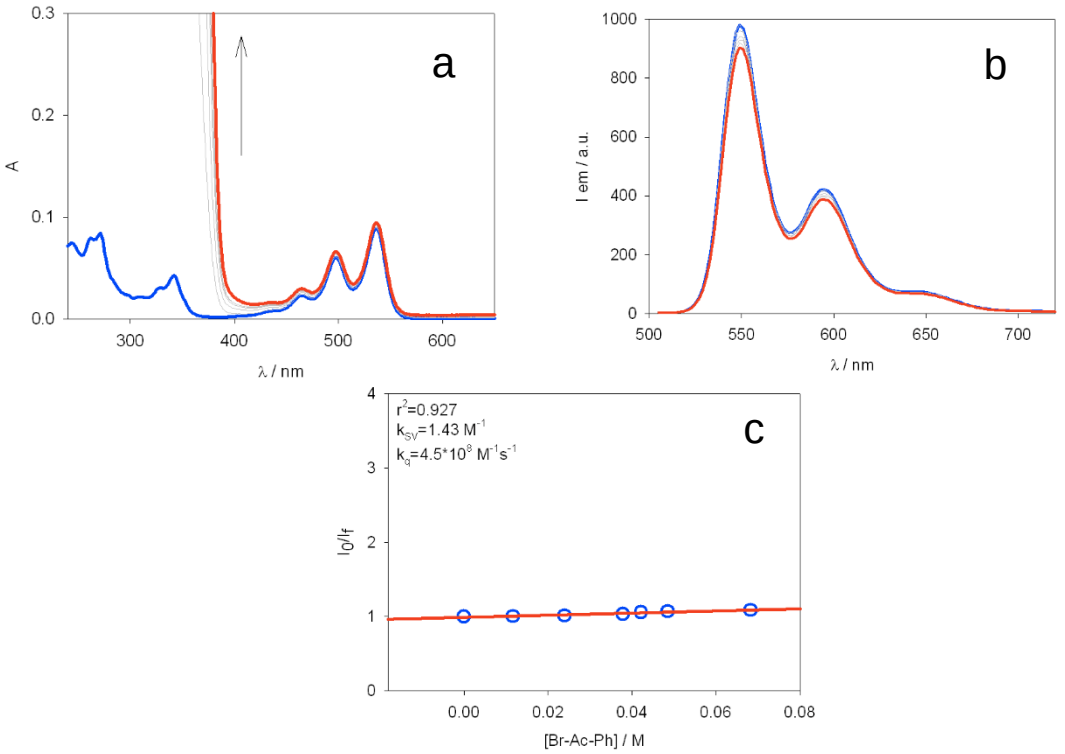

Figure 68: a) Absorption and b) emission spectra of a bis-octyl-PXXDI **141** solution *ca*. 2.0*10^{-6} M in CH_2Cl_2:MeCN 1:1 (v/v) in presence of increasing amounts of 2-bromoacetophenone (Br-Ac-Ph), from 0 to *ca*. 0.07 M; λ_{ex} = 498 nm. c) Stern-Volmer plot relative to the reductive quenching, considering the emission peak at λ_{em} = 594 nm.

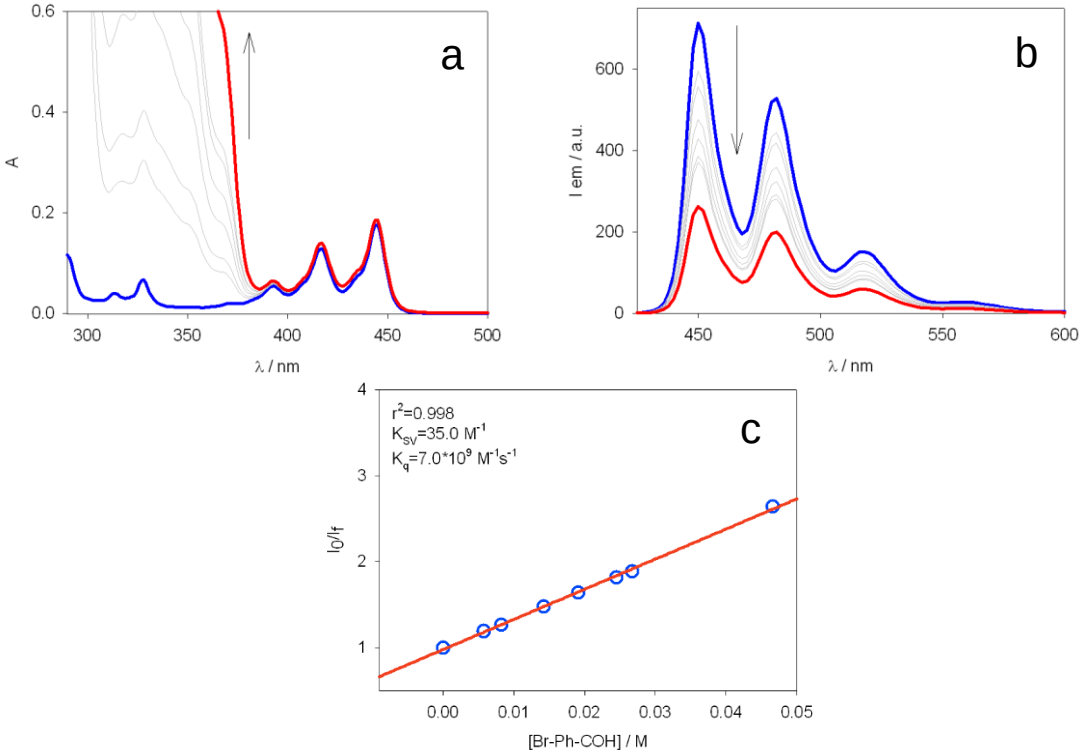

Figure 69: a) Absorption and b) emission spectra of a PXX **25** solution *ca.* $1.0*10^{-5}$ M in C_6H_6 in presence of increasing amounts of 4-bromobenzaldehyde (Br-Ph-COH), from 0 to *ca.* 45 mM; λ_{ex} = 417 nm. c) Stern-Volmer plot relative to the oxidative quenching, considering emission maximum at λ_{em} = 482 nm.

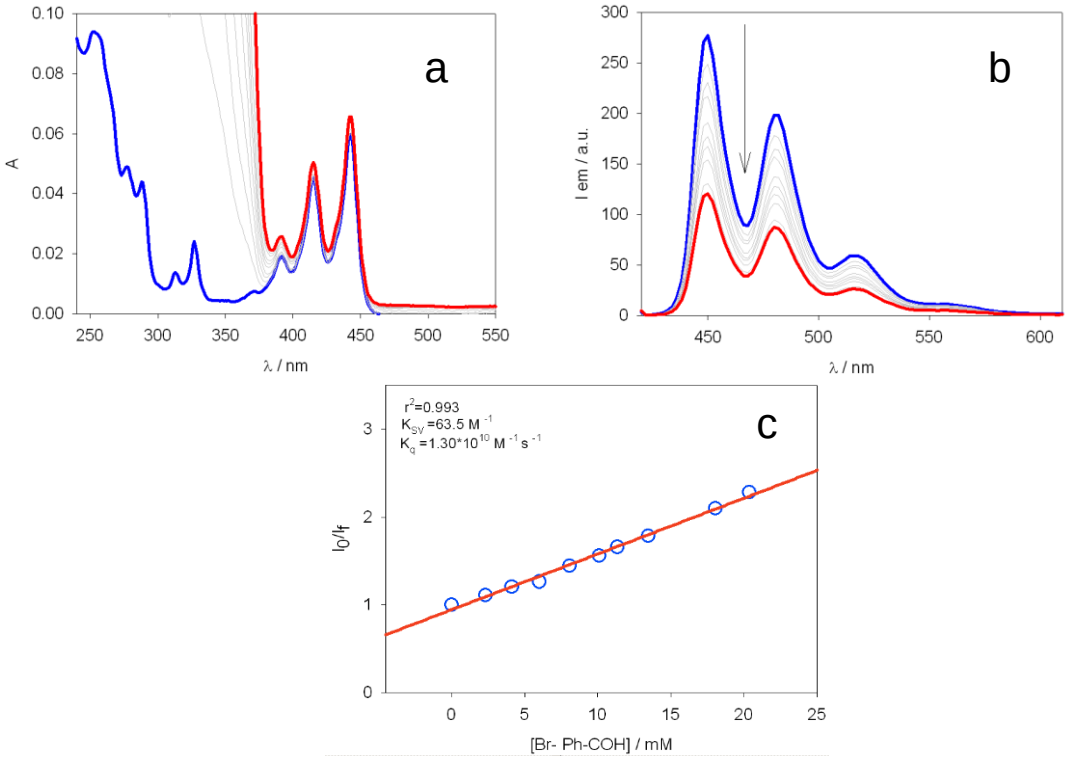

Figure 70: a) Absorption and b) emission spectra of a PXX **25** solution *ca*. 2.6*10^{-6} M in CH_2Cl_2 in presence of increasing amounts of 4-bromobenzaldehyde (Br-Ph-COH), from 0 to *ca*. 20 mM; λ_{ex} = 412 nm. c) Stern-Volmer plot relative to the oxidative quenching, considering emission maximum at λ_{em} = 481 nm.

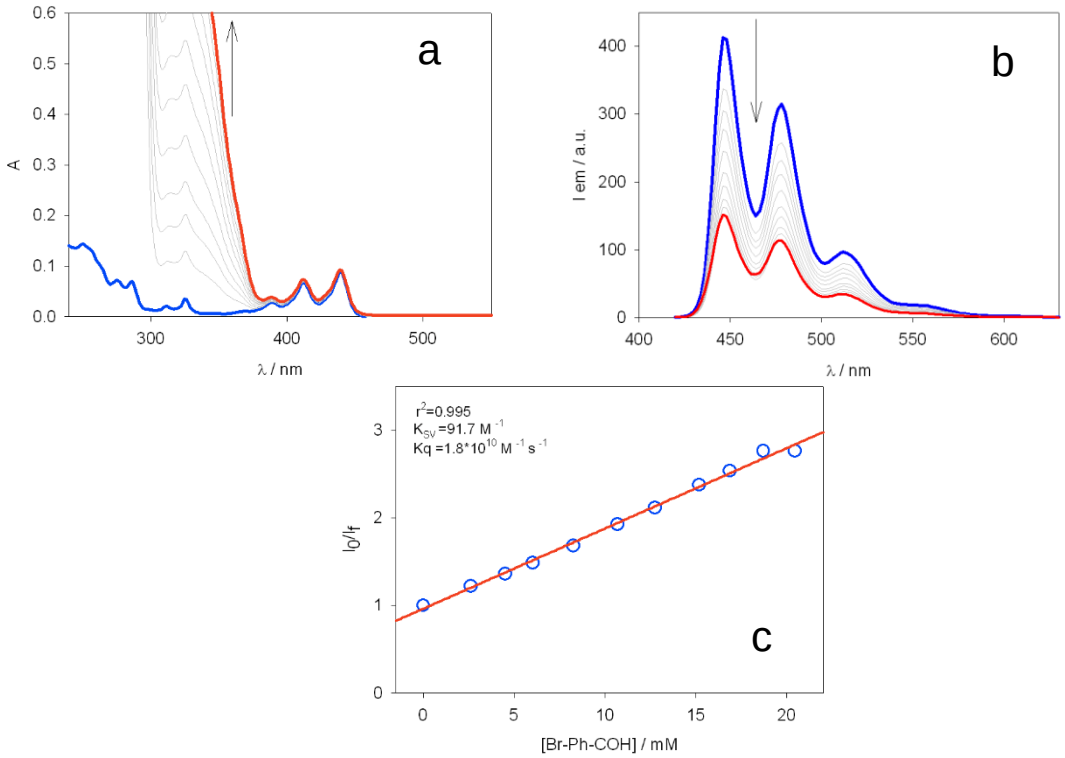

Figure 71: a) Absorption and b) emission spectra of a PXX **25** solution *ca*. 4.8*10^{-6} M in MeCN in presence of increasing amounts of 4-bromobenzaldehyde (Br-Ph-COH), from 0 to *ca.* 20 mM; λ_{ex} = 412 nm. c) Stern-Volmer plot relative to the oxidative quenching, considering the emission peak at λ_{em} = 480 nm.

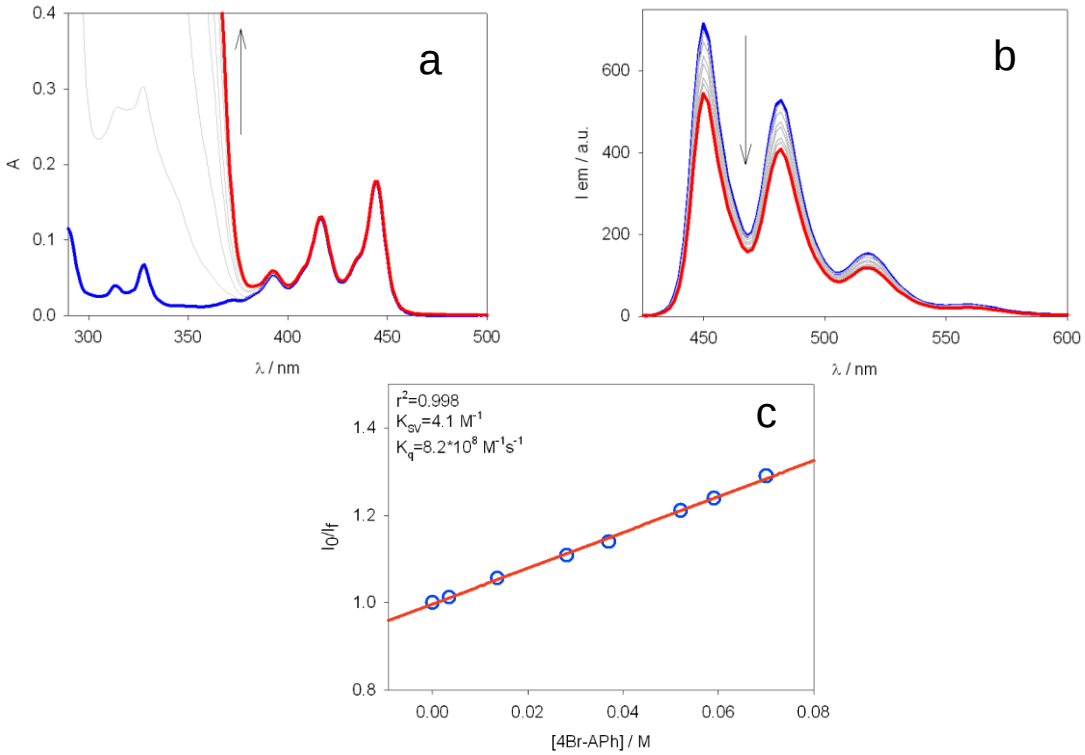

Figure 72: a) Absorption and b) emission spectra of a PXX **25** solution *ca.* $1.0*10^{-5}$ M in C_6H_6 in presence of increasing amounts of 4'-bromoacetophenone (4Br-APh), from 0 to *ca.* 70 mM; λ_{ex} = 417 nm. c) Stern-Volmer plot relative to the oxidative quenching, considering the emission peak at λ_{em} = 482 nm.

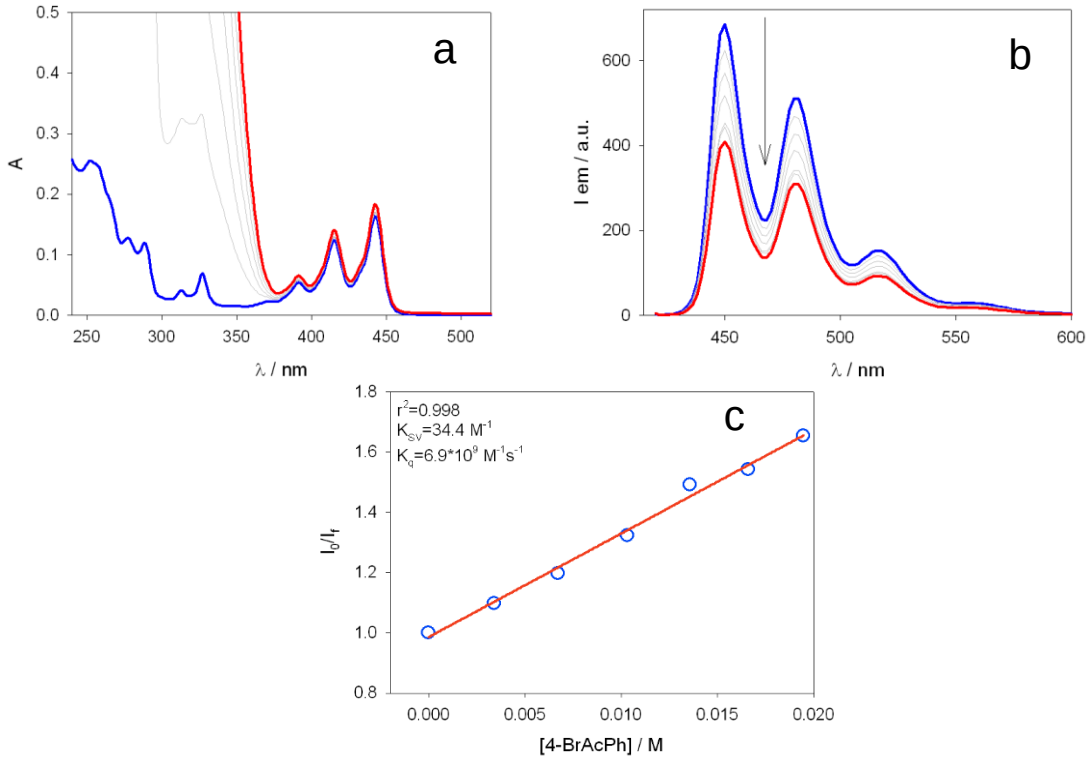

Figure 73: a) Absorption and b) emission spectra of a PXX **25** solution *ca*. $1.1*10^{-5}$ M in CH_2Cl_2 in presence of increasing amounts of 4'-bromoacetophenone (4Br-Ac-Ph), from 0 to *ca*. 20 mM; λ_{ex} = 415 nm. c) Stern-Volmer plot relative to the oxidative quenching, considering the emission peak at λ_{em} = 482 nm.

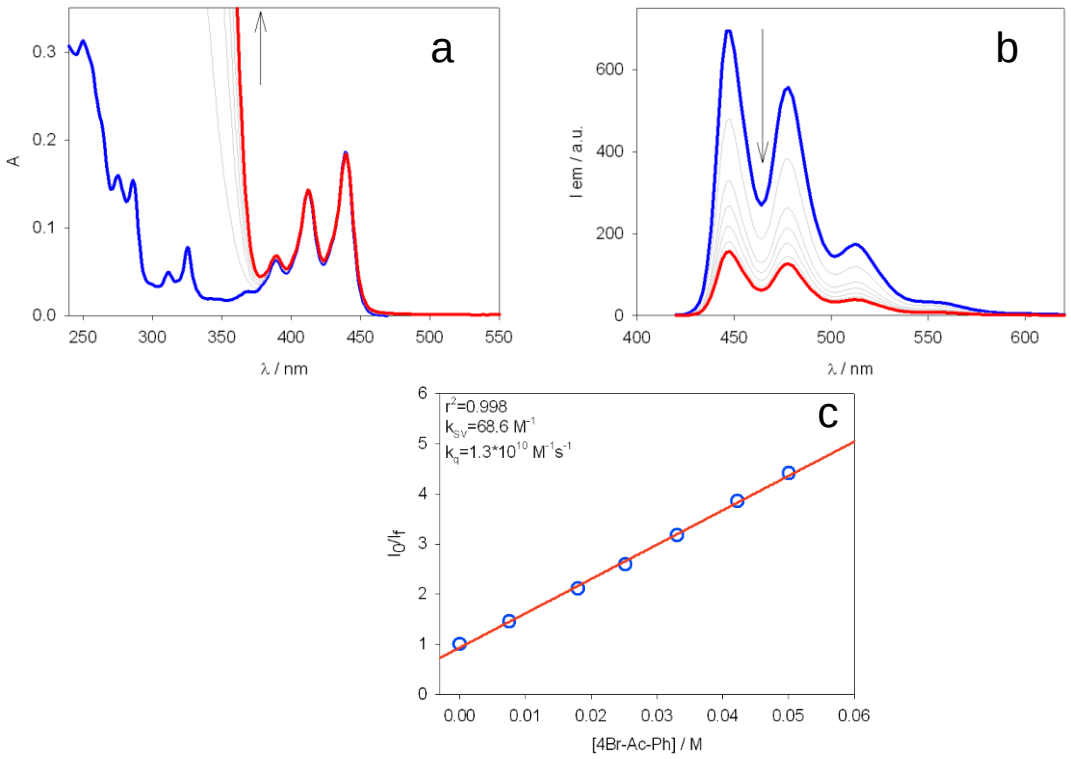

Figure 74: a) Absorption and b) emission spectra of a PXX **25** solution *ca*. 1.1*10^{-5} M in MeCN in presence of increasing amounts of 4'-bromoacetophenone (4Br-Ac-Ph), from 0 to *ca*. 50 mM; λ_{ex} = 412 nm. c) Stern-Volmer plot relative to the oxidative quenching, considering the emission peak at λ_{em} = 476 nm.

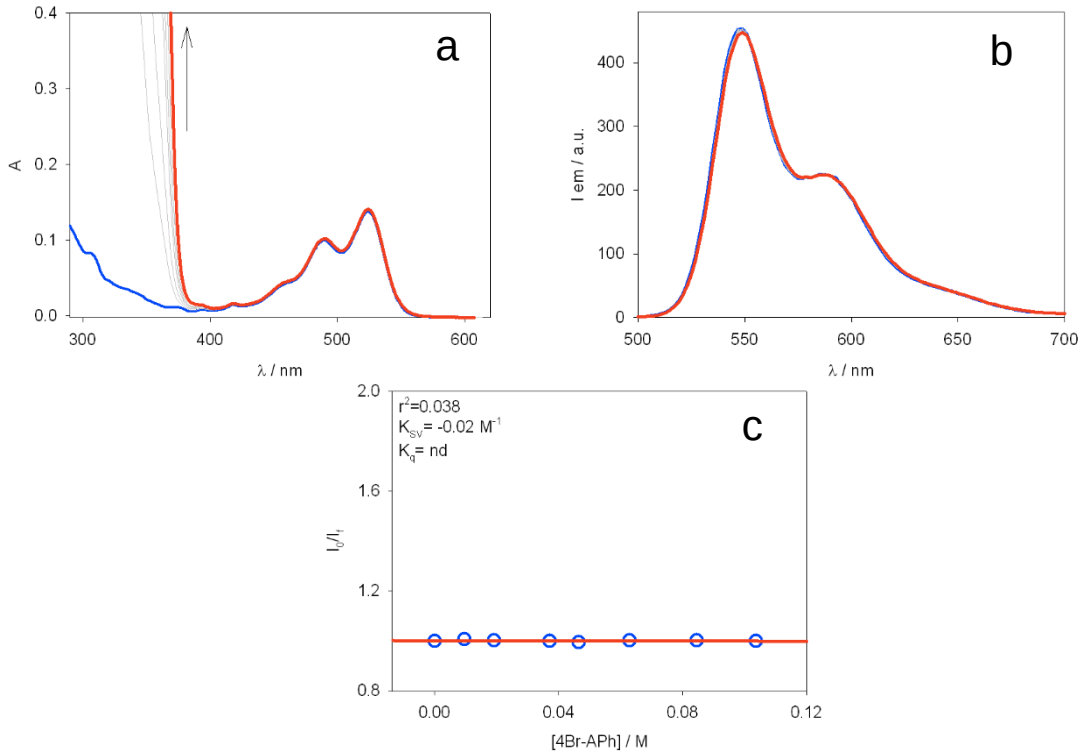

Figure 75: a) Absorption and b) emission spectra of a octyl-PXXMI 148 solution *ca.* $7.8*10^{-6}$ M in C_6H_6 in presence of increasing amounts of 4'-bromoacetophenone (4Br-APh), from 0 to *ca.* 0.1 M; λ_{ex} = 490 nm. c) Stern-Volmer plot relative to the oxidative quenching, considering the emission peak at λ_{em} = 590 nm.

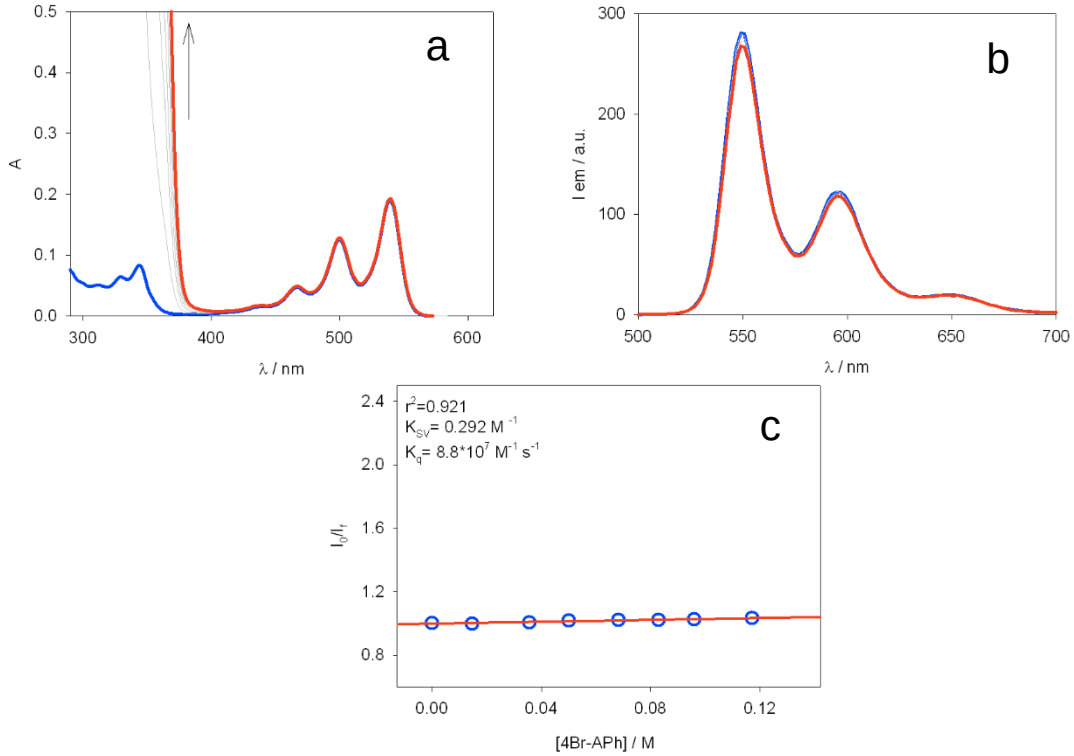

Figure 76: a) Absorption and b) emission spectra of a bis-octyl-PXXDI **141** solution *ca*. 5.2*10^{-6} M in C_6H_6 in presence of increasing amounts of 4'-bromoacetophenone (4Br-APh), from 0 to *ca*. 0.1 M; λ_{ex} = 499 nm. c) Stern-Volmer plot relative to the oxidative quenching, considering the emission peak at λ_{em} = 595 nm.

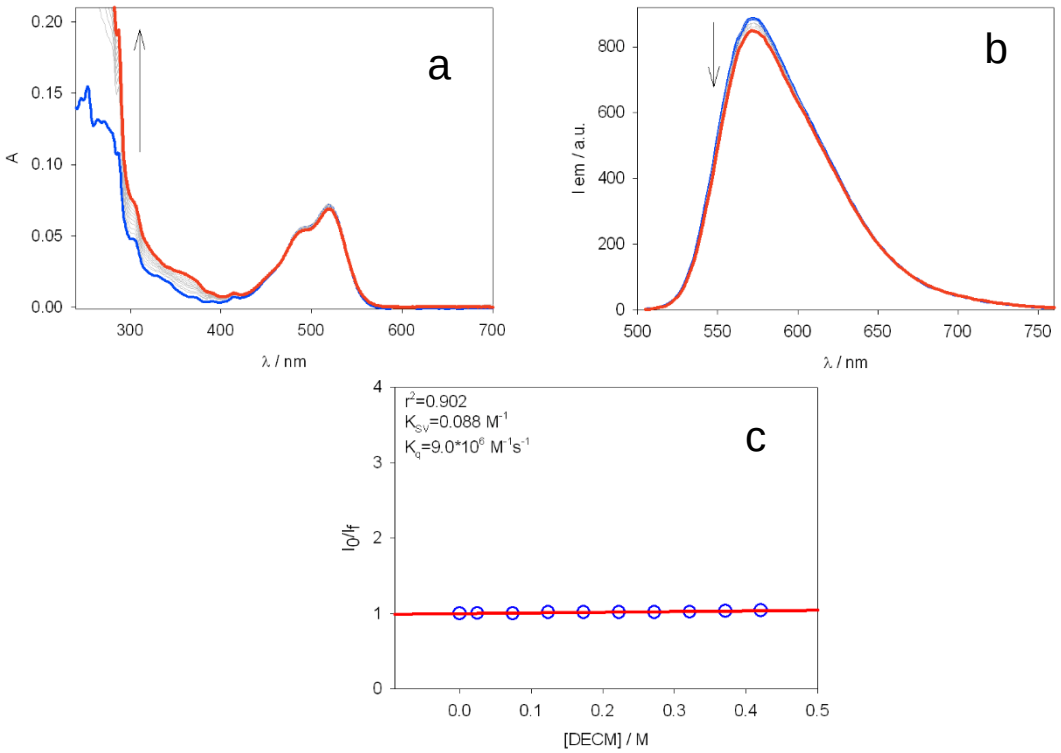

Figure 77: a) Absorption and b) emission spectra of a octyl-PXXMI **148** solution *ca*. 4.1*10^{-6} M in MeCN in presence of increasing amounts of diethylchloromalonate (DECM), from 0 to *ca*. 0.42 M; λ_{ex} = 497 nm. c) Stern-Volmer plot relative to the oxidative quenching, considering the emission peak at λ_{em} = 575 nm.

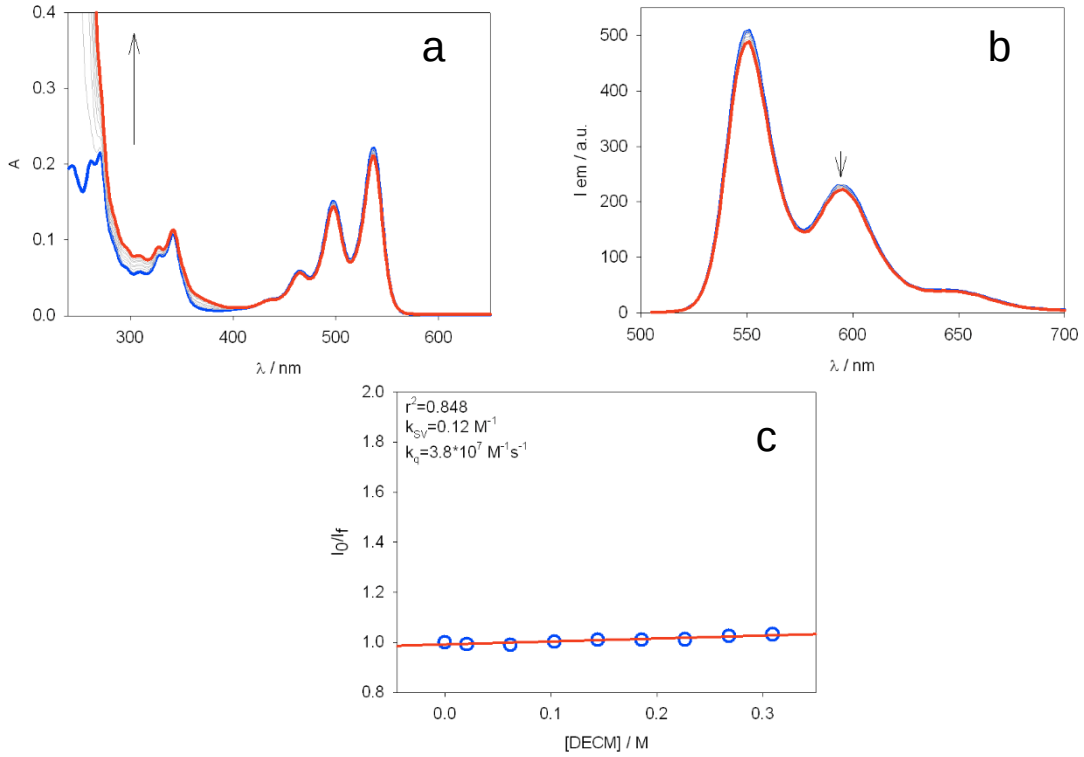

Figure 78: a) Absorption and b) emission spectra of a bis-octyl-PXXDI **141** solution *ca*. $5.1*10^{-6}$ M in CH_2Cl_2:MeCN 1:1 (v/v) in presence of increasing amounts of diethylchloromalonate (DECM), from 0 to *ca*. 0.2 M; λ_{ex} = 497 nm. c) Stern-Volmer plot relative to the oxidative quenching, considering the emission peak at λ_{em} = 595 nm.

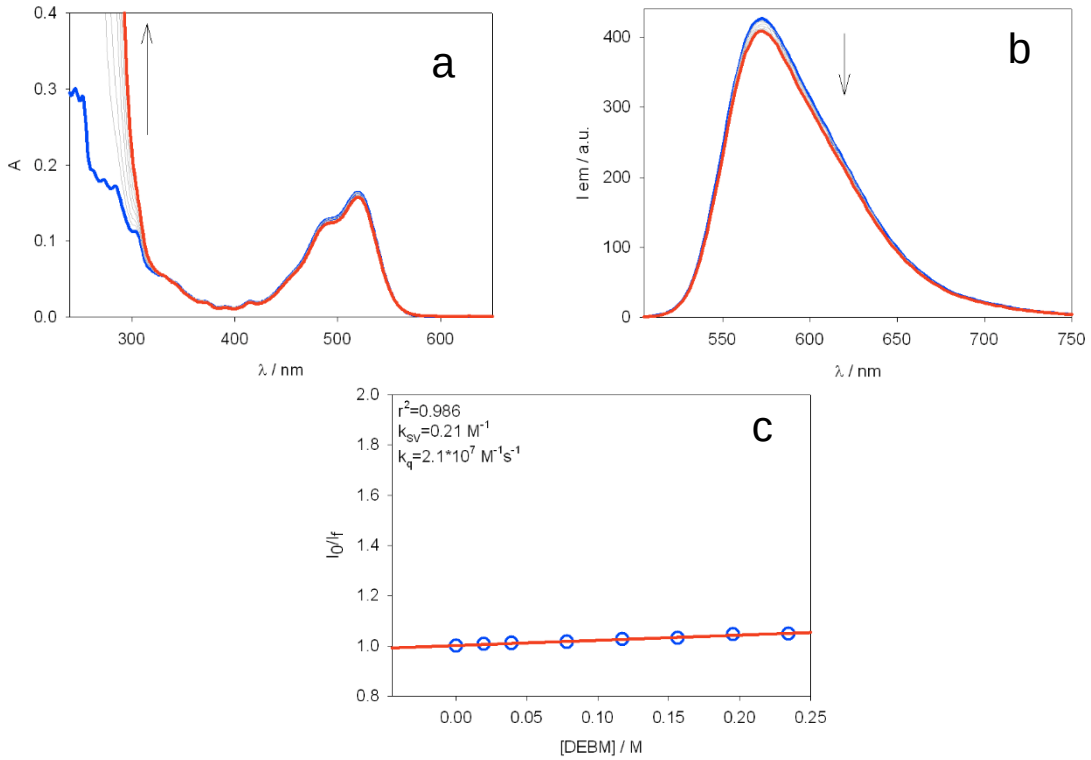

Figure 79: a) Absorption and b) emission spectra of a octyl-PXXMI **148** solution *ca*. 5.1*10^{-6} M in CH_3CN in presence of increasing amounts of diethylbromomalonate (DEBM), from 0 to *ca.* 0.23 M; λ_{ex} = 493 nm. c) Stern-Volmer plot relative to the oxidative quenching, considering the emission peak at λ_{em} = 575 nm.

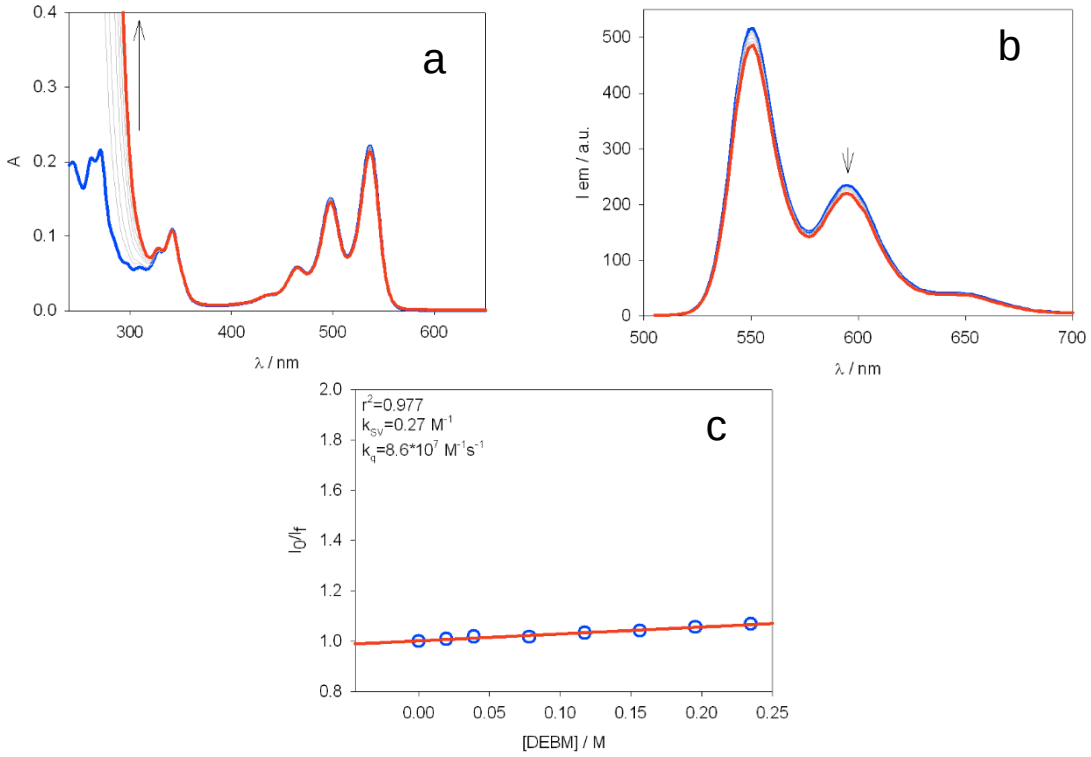

Figure 80: a) Absorption and b) emission spectra of a bis-octyl-PXXDI **141** solution *ca*. 5.1*10^{-6} M in CH_2Cl_2:MeCN 1:1 (v/v) in presence of increasing amounts of diethylbromomalonate (DEBM), from 0 to *ca*. 0.23 M; λ_{ex} = 497 nm. c) Stern-Volmer plot relative to the oxidative quenching, considering the emission peak at λ_{em} = 595 nm.

4.6. Photoactivated reactions and control experiments

All the photochemichal reactions run under visible light were performed using a 5 meters long TINGKAM® RGB LED flexible stripe (LED type: 5050 PLCC-4 SMT SMD), equipped with a remote controller and placed on the inner surface of a metal cylinder (~ 20 cm diameter); estimated total output power: 36 W.

4.6.1. General procedure for photodehalogenation reactions

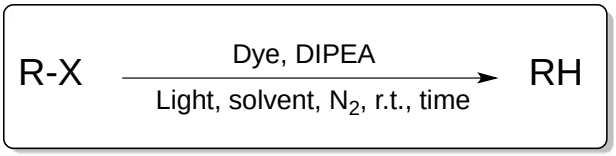

A screw cap vial was charged with halogen-derivative ($5.0 \cdot 10^{-2}$ mmol), DIPEA ($4.0 \cdot 10^{-1}$ mmol) and the dye (5 mol%, $2.5 \cdot 10^{-3}$ mmol, $8.3 \cdot 10^{-4}$ M), in solvent (3 mL).

For the experiments involving diethylbromo- or diethylchloromalonate, the vial was charged with halogen-derivative ($1.3 \cdot 10^{-1}$ mmol), DIPEA (1.3 mmol) and the dye (0.5 mol%, $6.7 \cdot 10^{-4}$ mmol, $1.3 \cdot 10^{-4}$ M), in solvent (5 mL).

For reactions on *α-para*-dibromoacetophenone, the experiments were carried out adding DIPEA 0.27 M ($7.5 \cdot 10^{-1}$ mmol in 3 mL) to the mixtures containing the dyes at 0.83 mM and 0.41 mM.

The reaction mixtures were readily degassed by freeze/pump/thaw (3 cycles). The vial was irradiated with a specified light source (see section 4.1), and cooled by compressed air in order to maintain ambient temperature.

Control experiments were carried out on solutions at the same concentrations of reactants kept in the dark for the same amount of time, depending on the reaction ("dark" experiments), and on irradiated solutions at the same concentrations of reactants in the absence of the photoactive species ("blank" experiments). Control experiments without DIPEA were carried out with the usual concentration of the other reactants.

Reaction conversion was estimated by considering the ratio between integrations of each product peak and the sum of product and starting material peaks, analysed by GC-MS.

4.6.2. GC-MS data

4.6.2.1 Dehalogenation of α-bromoacetophenone

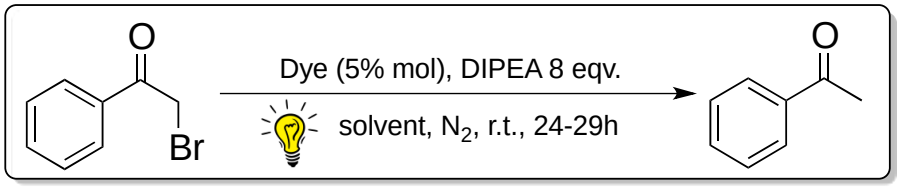

Table 21: Dehalogenation of 2-bromoacetophenone.

Entry	Dye	λ_{ex} [nm]	Solvent	Time [h]	Conversion [%]
1	**PXXMI 148**	520	benzene	24	100
		Dark			traces
2		520	CH_2Cl_2	24	95
		Dark			6
3		520	CH_3CN	24	100
		dark			15
4	**PXXDI 141**	520	benzene	29	100
		dark			traces
5		520	CH_2Cl_2	24	100
		dark			5
6		520	CH_3CN	24	100
		dark			20
7	**PXX 25**	460	benzene	24	100
		dark			traces
8		460	CH_2Cl_2	24	100
		dark			3
9		460	CH_3CN	24	100
		dark			10
10	blank	520	benzene	29	traces
		460			traces
11	blank	520	CH_2Cl_2	24	0
		460			2
12	blank	520	CH_3CN	24	15
		460			34
13	**PXXDI 141**, 0 eqv DIPEA	520	CH_3CN	24	traces

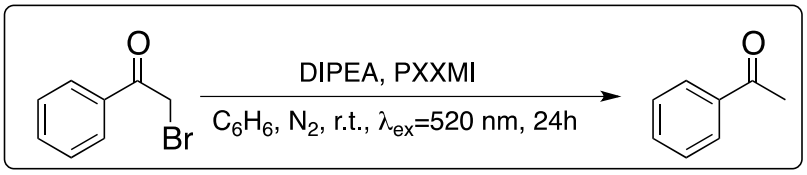

Table 21, entry 1

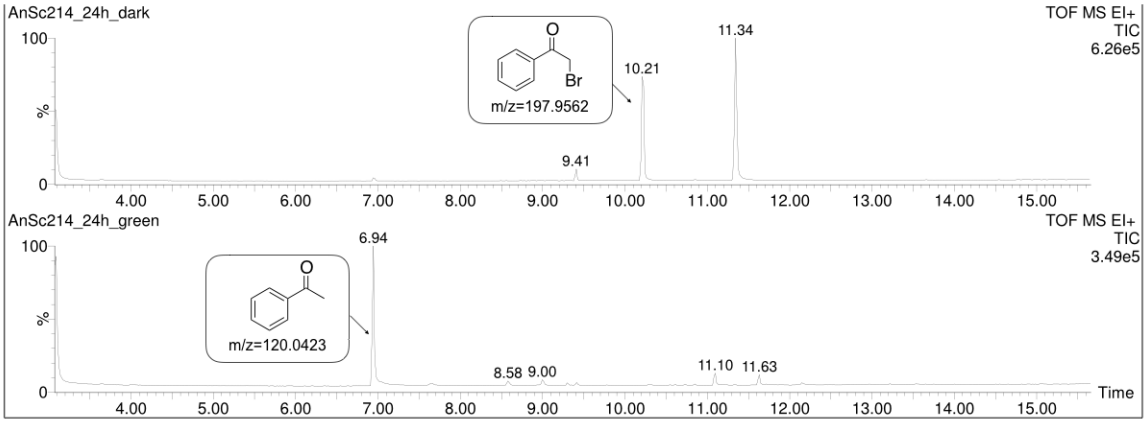

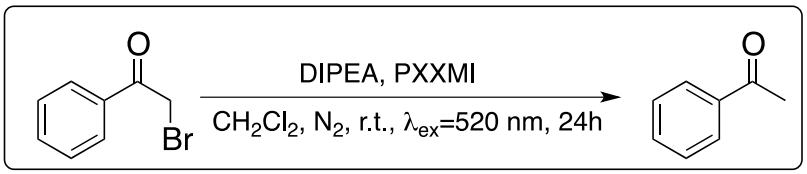

Table 21, entry 2

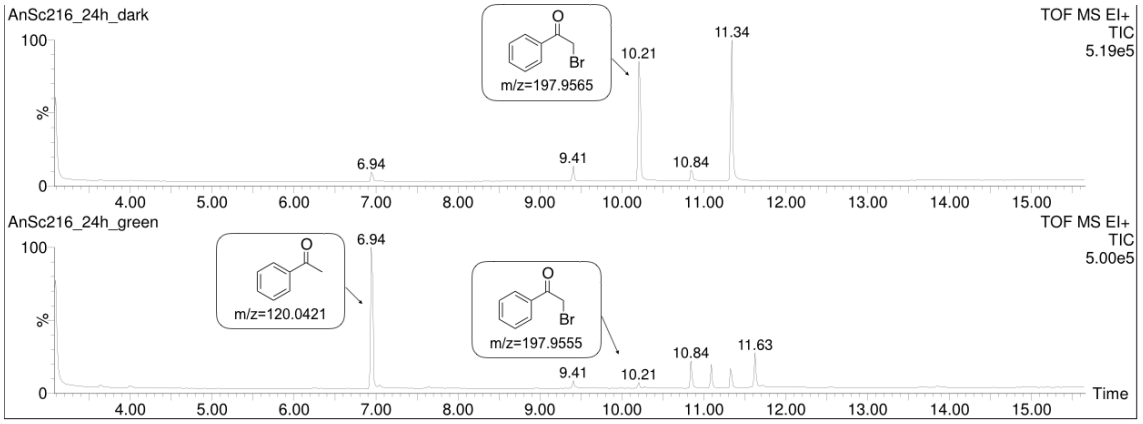

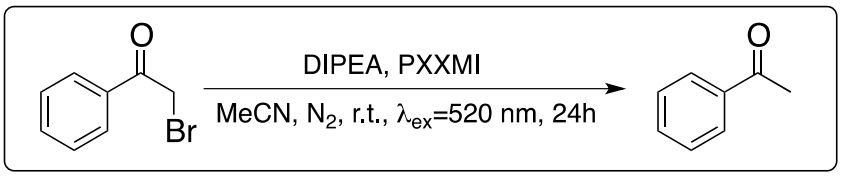

Table 21, entry 3

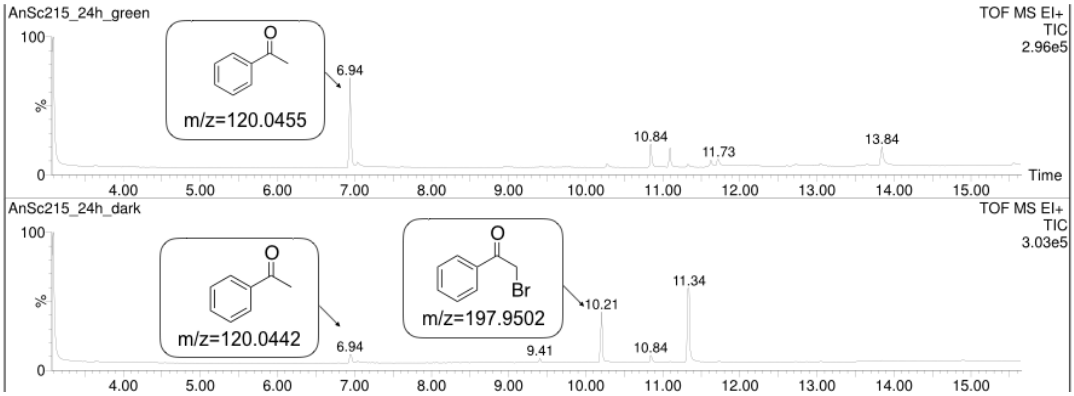

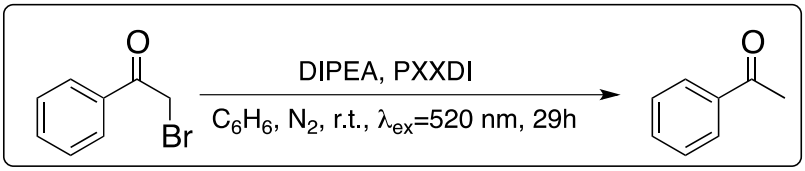

Table 21, entry 4

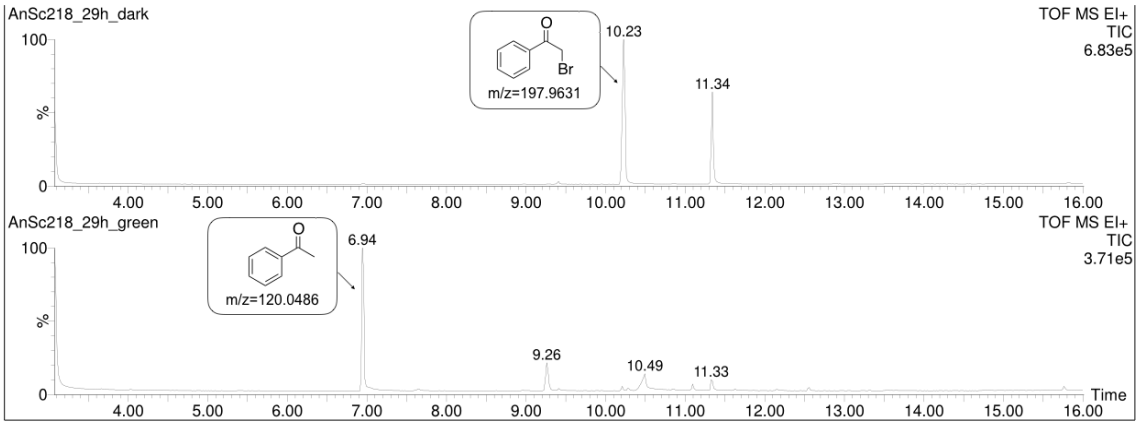

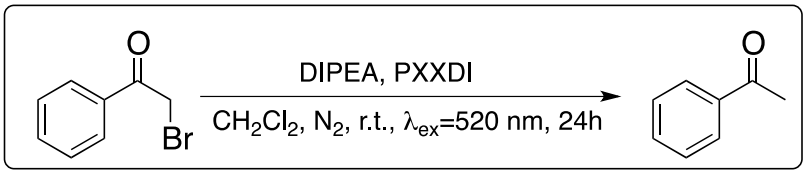

Table 21, entry 5

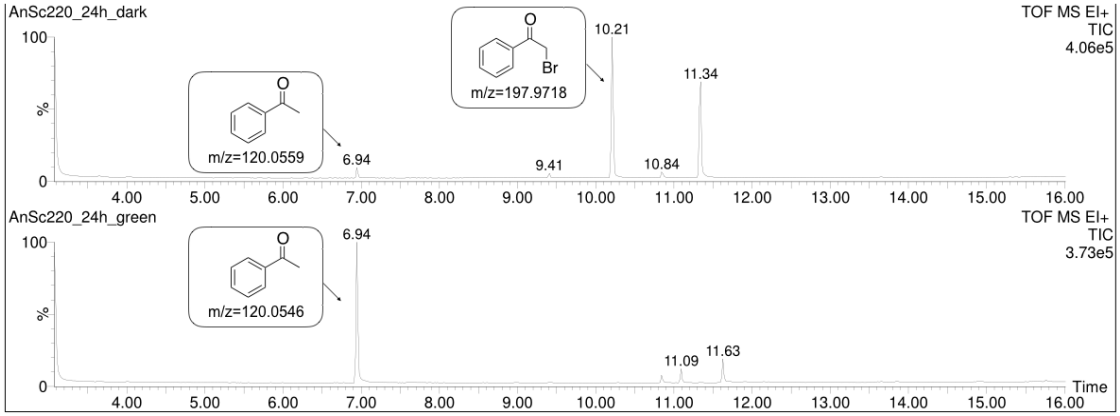

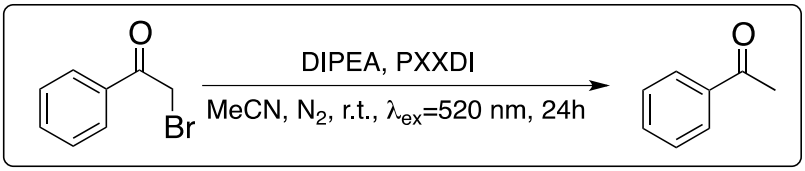

Table 21, entry 6

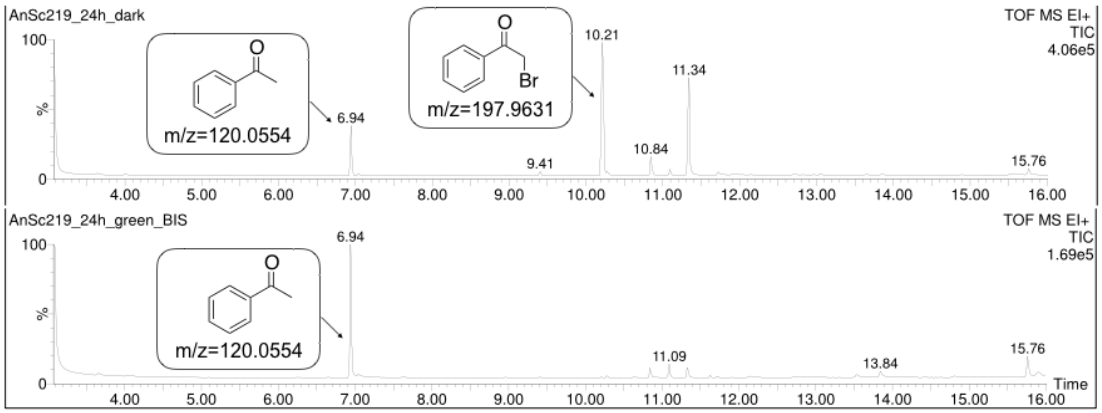

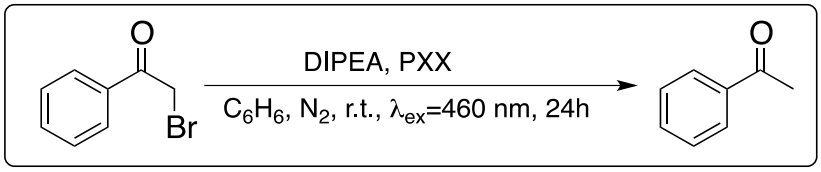

Table 21, entry 7

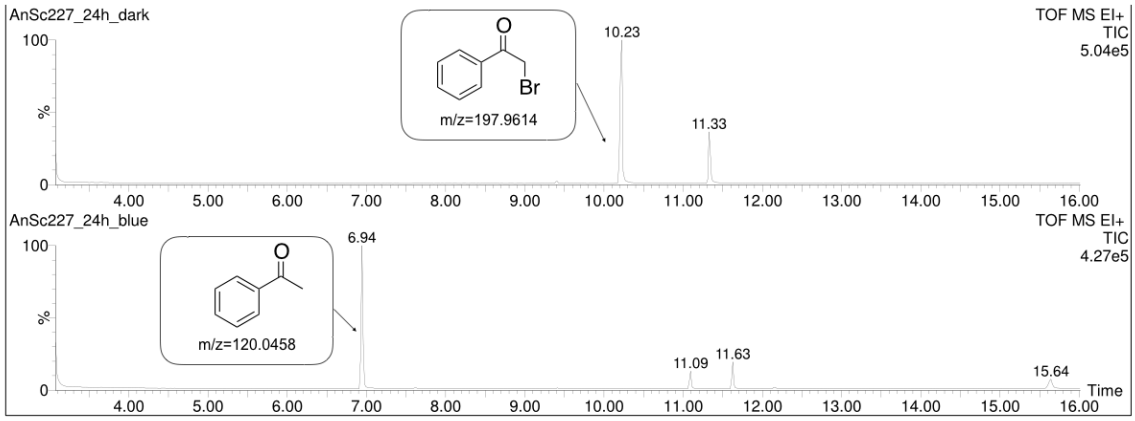

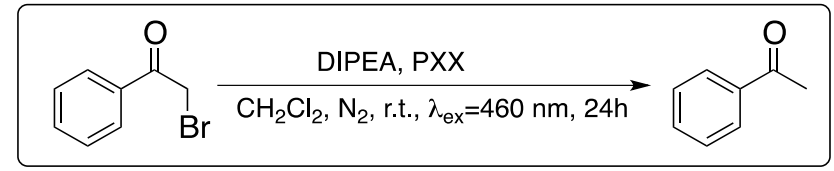

,

Table 21, entry 8

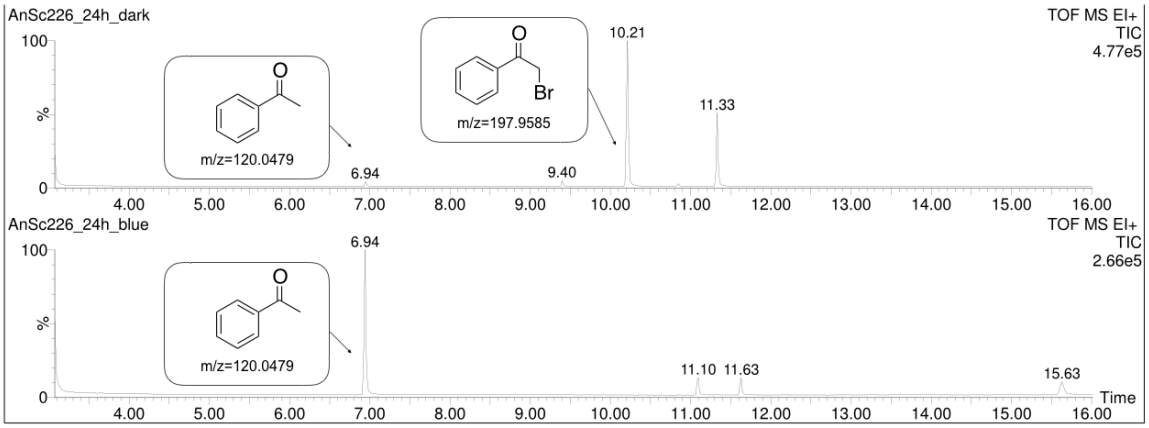

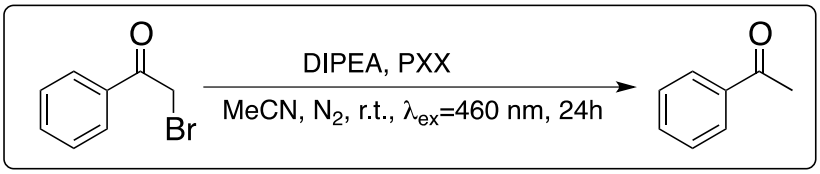

Table 21, entry 9

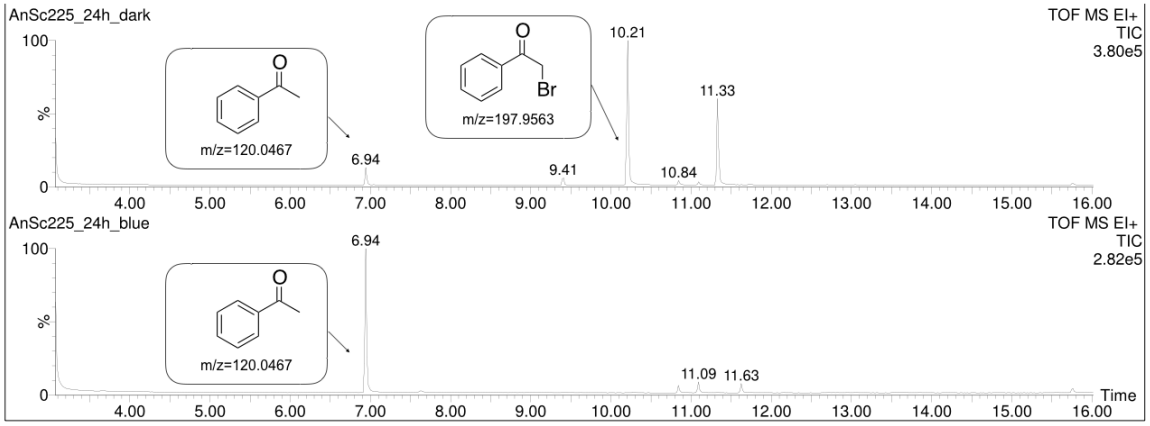

Table 21 entry 10

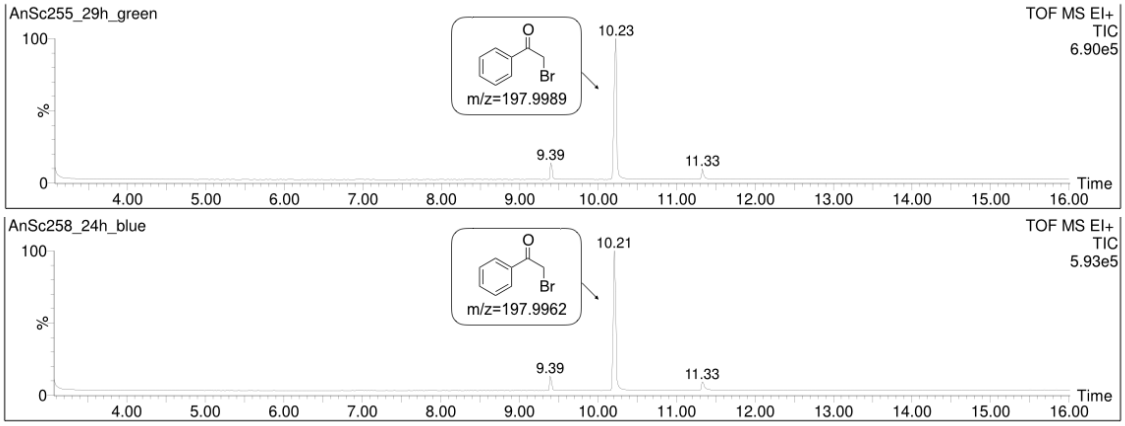

Table 21, entry 11

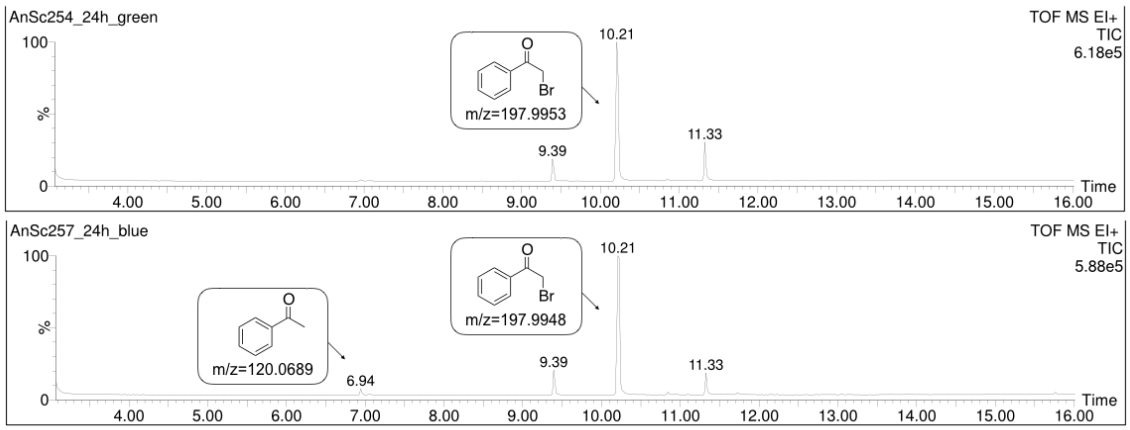

Table 21, entry 12

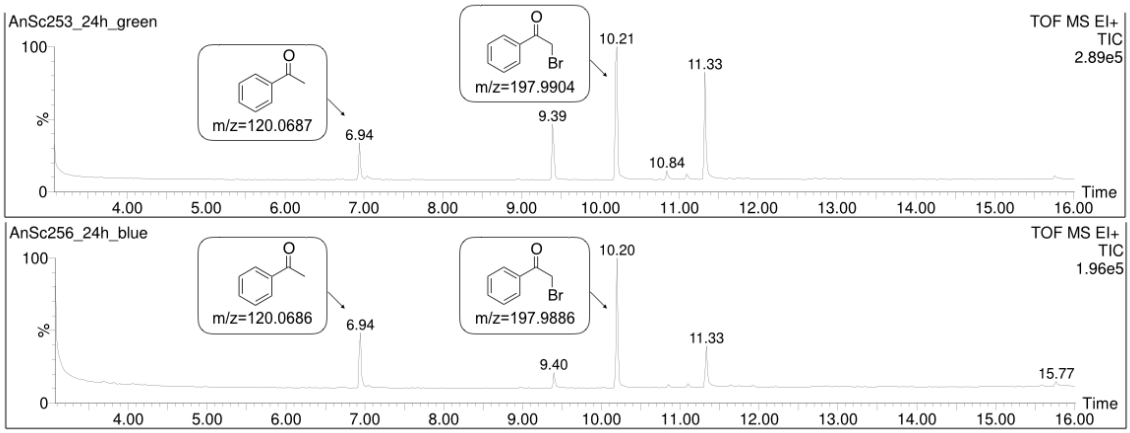

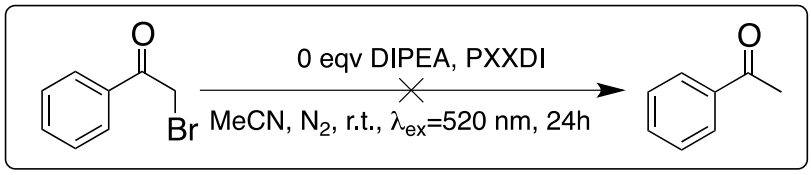

Table 21, entry 13

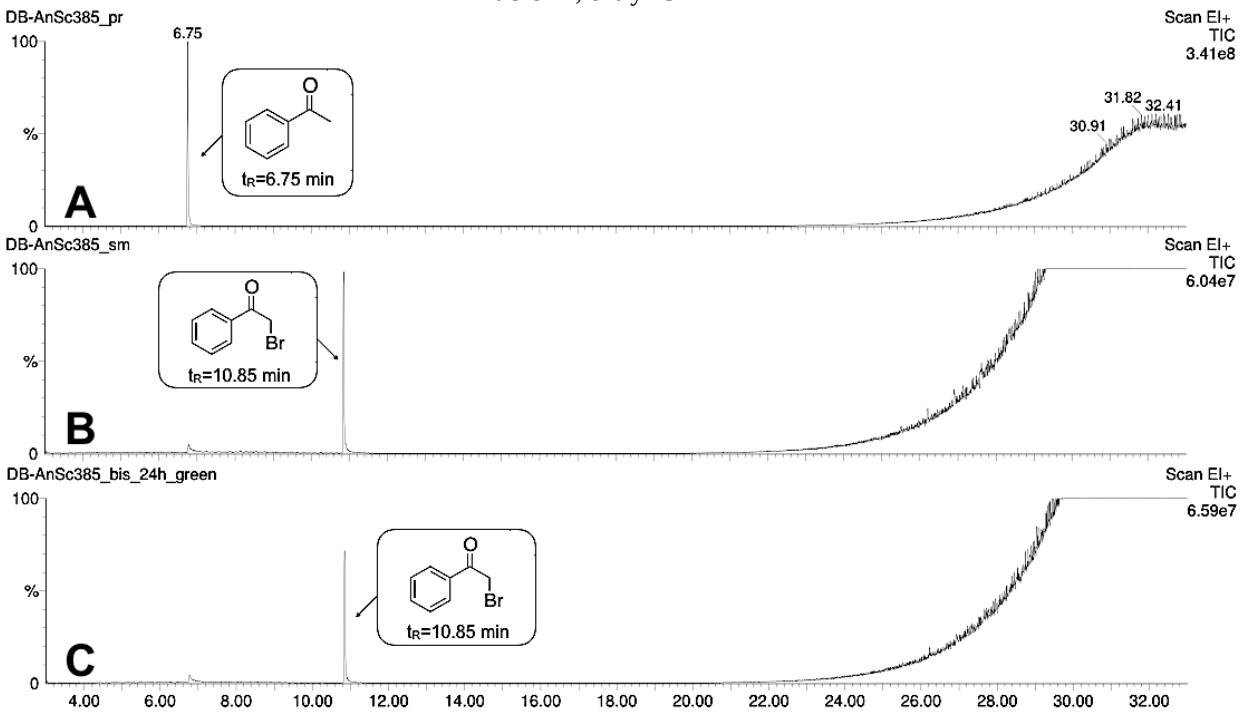

A: acetophenone; **B**: 2-bromoacetophenone; **C**: irradiated solution at 520 nm after 24h.

4.6.2.2 Dehalogenation of 2'-, 3'- and 4'-bromoacetophenones

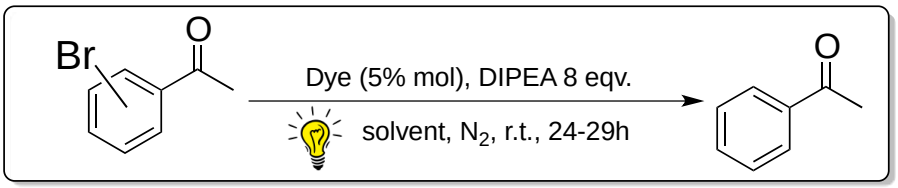

Table 22: Dehalogenation of 4'-bromoacetophenone.

Entry	Dye	λ_{ex} [nm]	Solvent	Time [h]	Conversion [%]
1	**PXXMI 148**	520	Benzene	48	0
		dark			0
2		520	CH_2Cl_2	48	0
		dark			0
3		520	CH_3CN	48	0
		dark			0
4	**PXXDI 141**	520	Benzene	48	0
		dark			0
5		520	CH_2Cl_2	48	0
		dark			0
6		520	CH_3CN	48	0
		dark			0
7	**PXX 25**	460	Benzene	48	0
		dark			0
8		460	CH_2Cl_2	48	6
		dark			0
9		460	CH_3CN	48	100
		dark			0
10	blank	520	Benzene	48	0
		460			0
11	blank	520	CH_2Cl_2	48	0
		460			0
12	blank	520	CH_3CN	48	0
		460			0
13	**PXX 25**, 0 eqv DIPEA	460	CH_3CN	48	traces

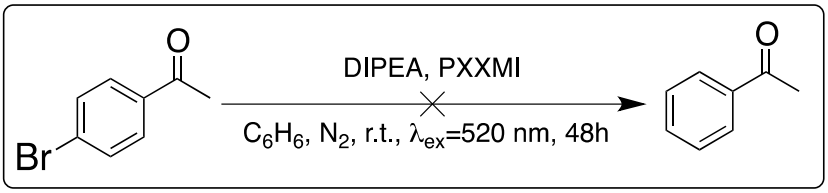

Table 22, entry 1

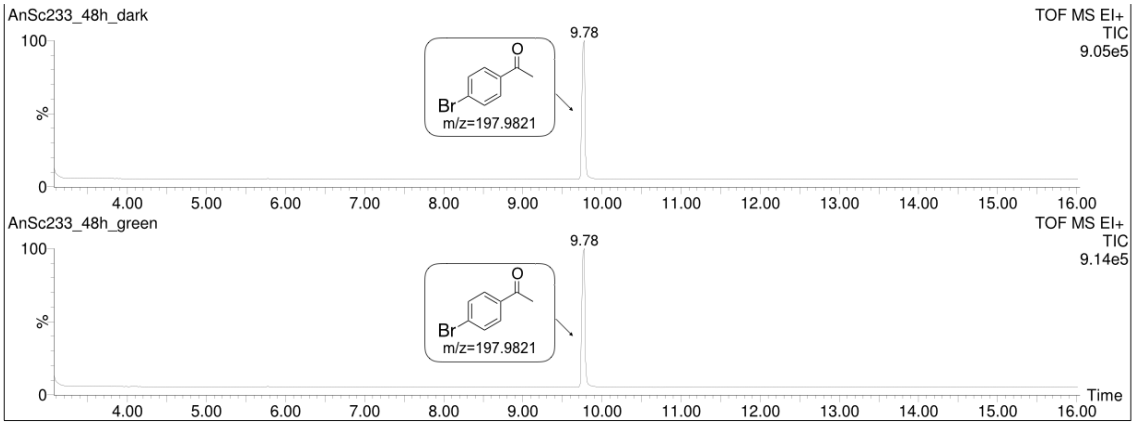

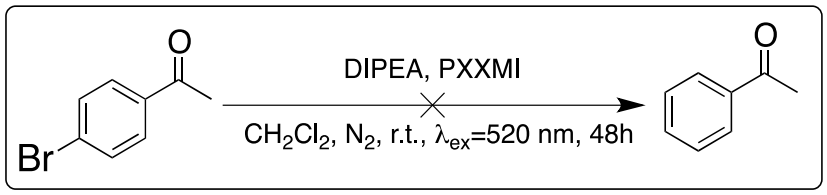

Table 22, entry 2

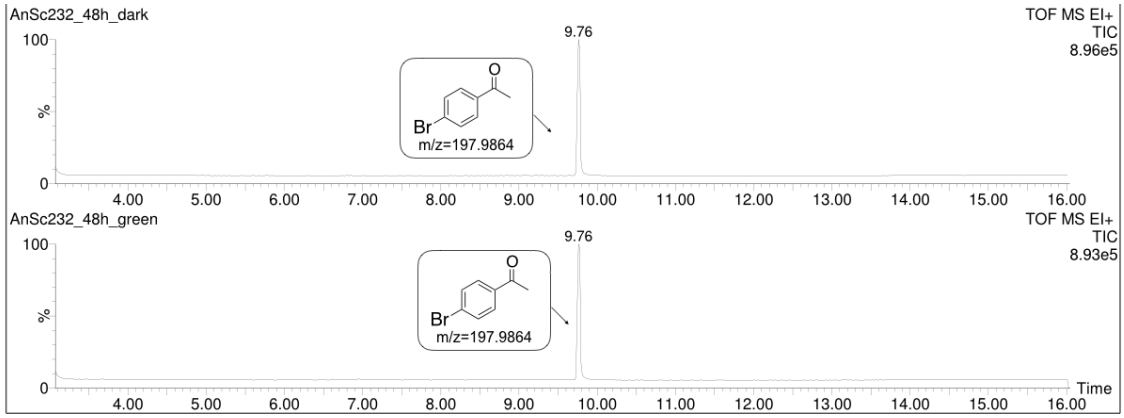

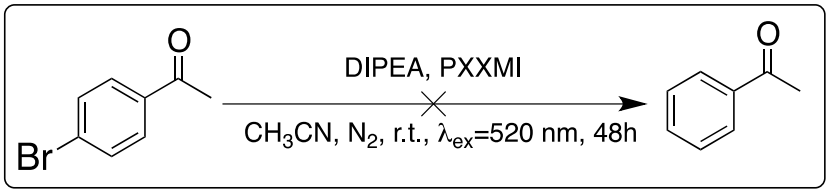

Table 22, entry 3

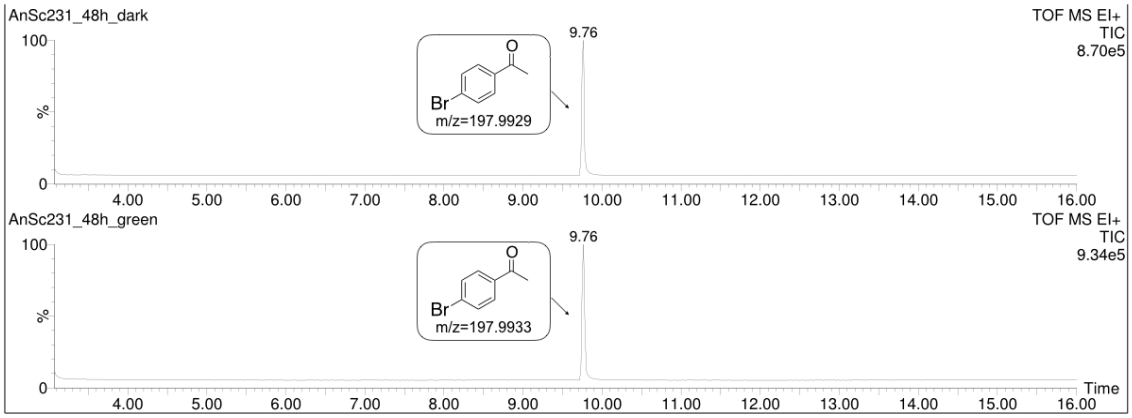

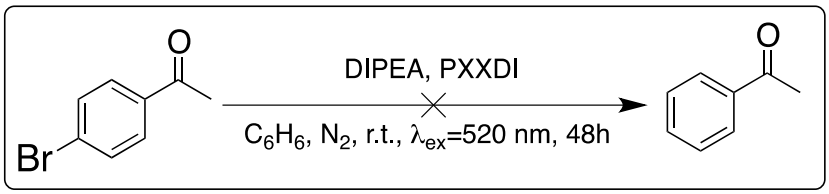

Table 22, entry 4

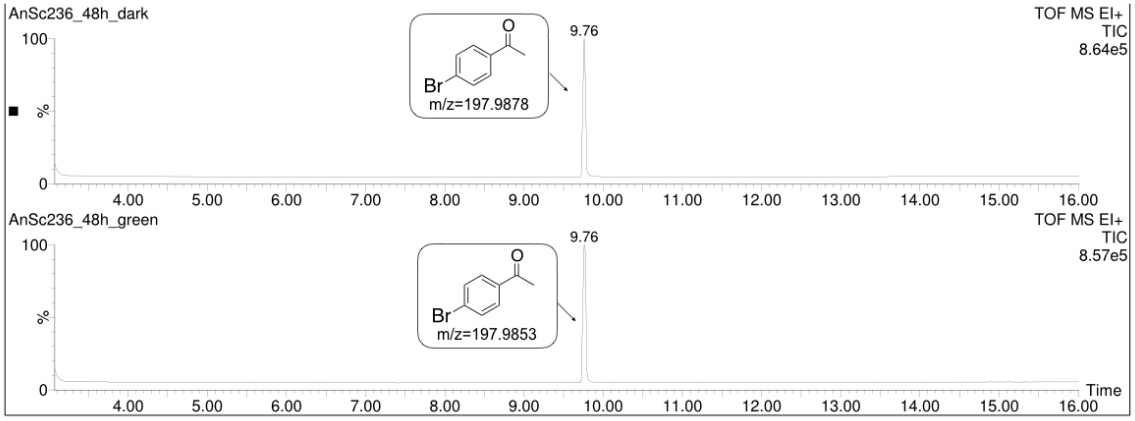

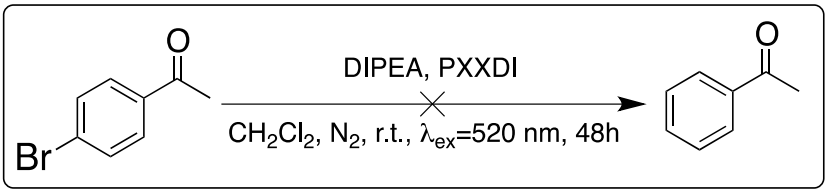

Table 22, entry 5

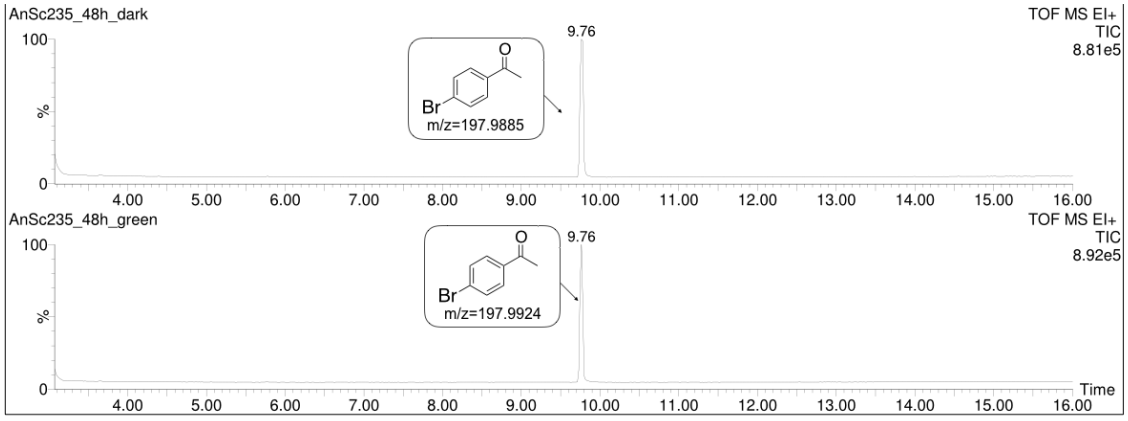

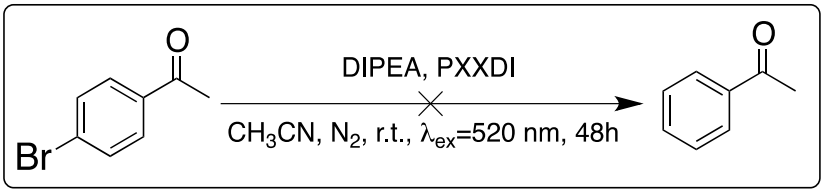

Table 22, entry 6

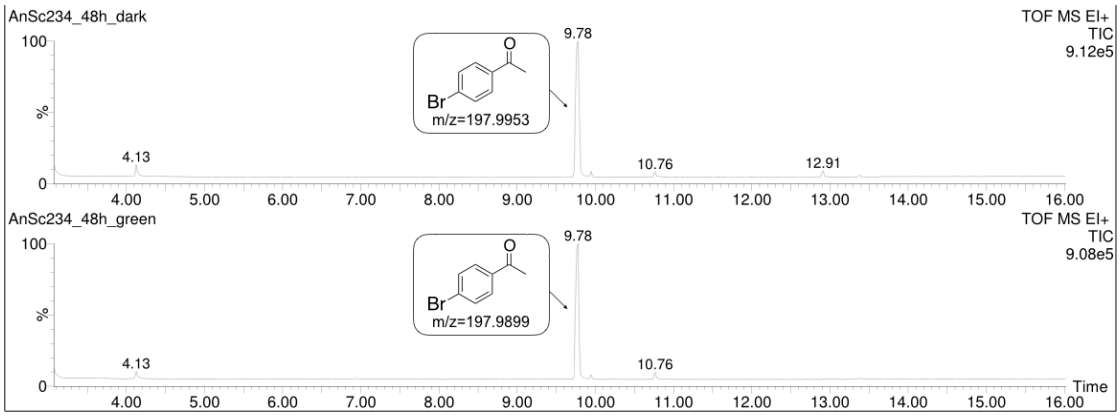

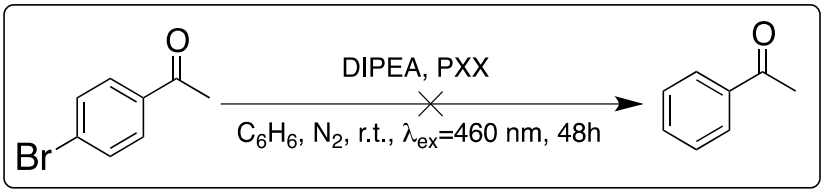

Table 22, entry 7

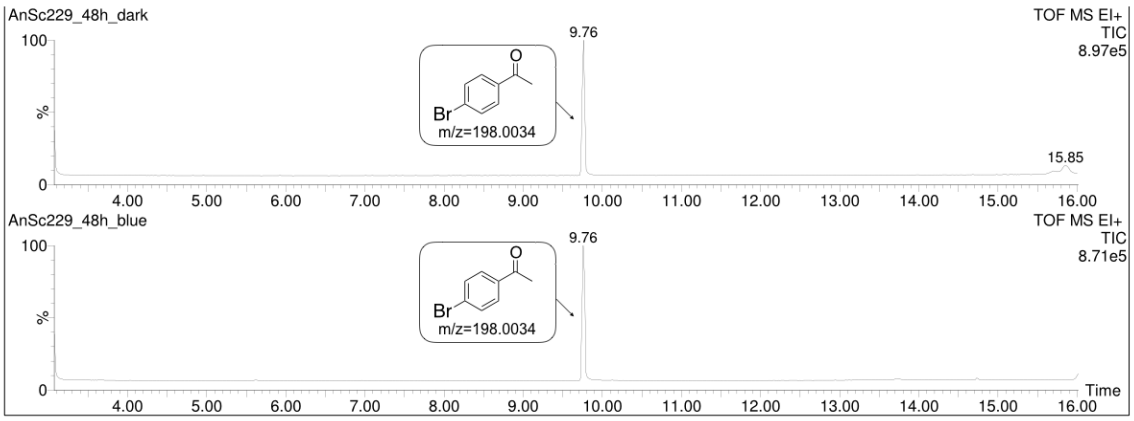

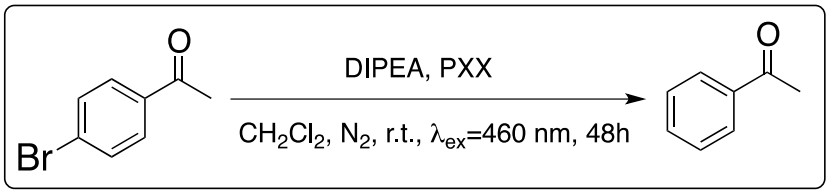

Table 22, entry 8

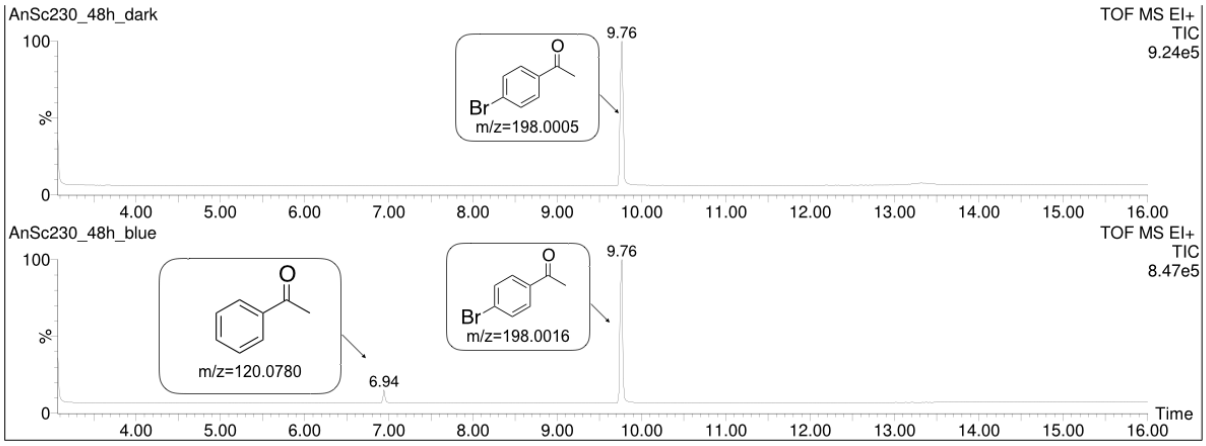

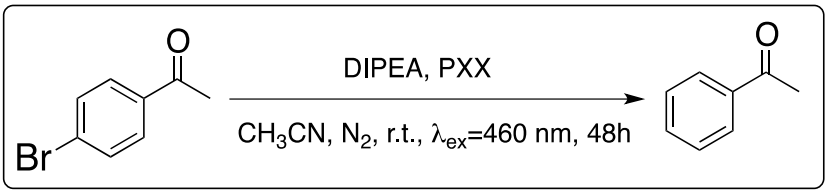

Table 22, entry 9

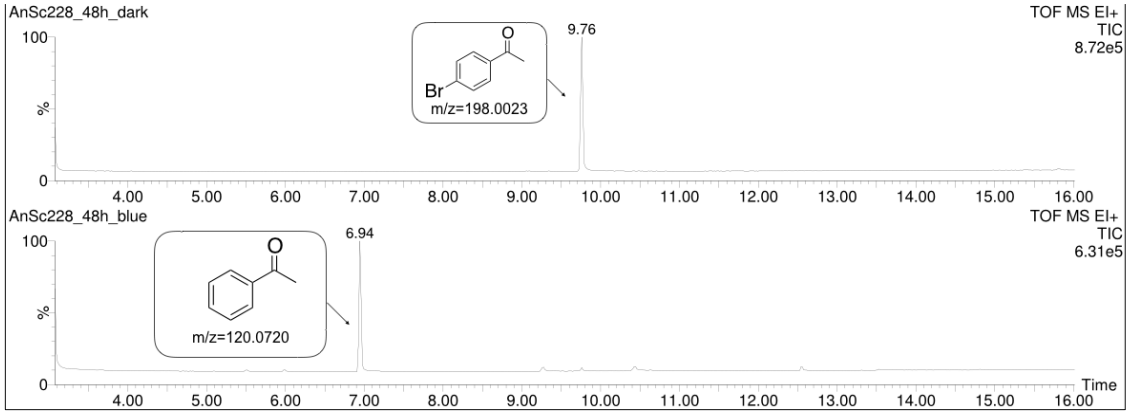

Table 22, entry 10

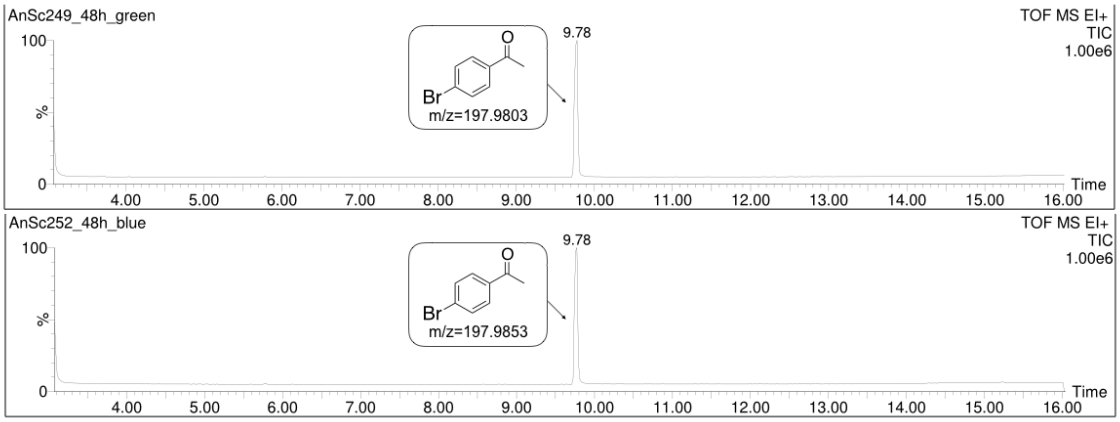

Table 22, entry 11

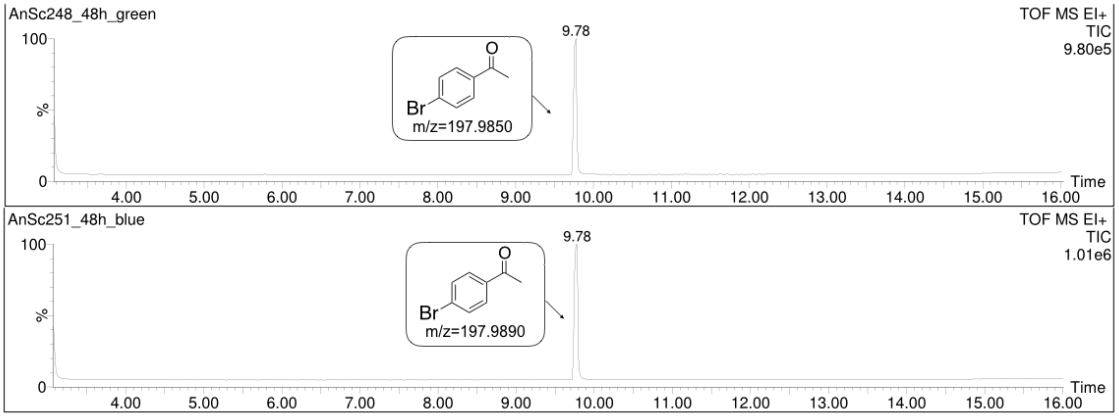

Table 22, entry 12

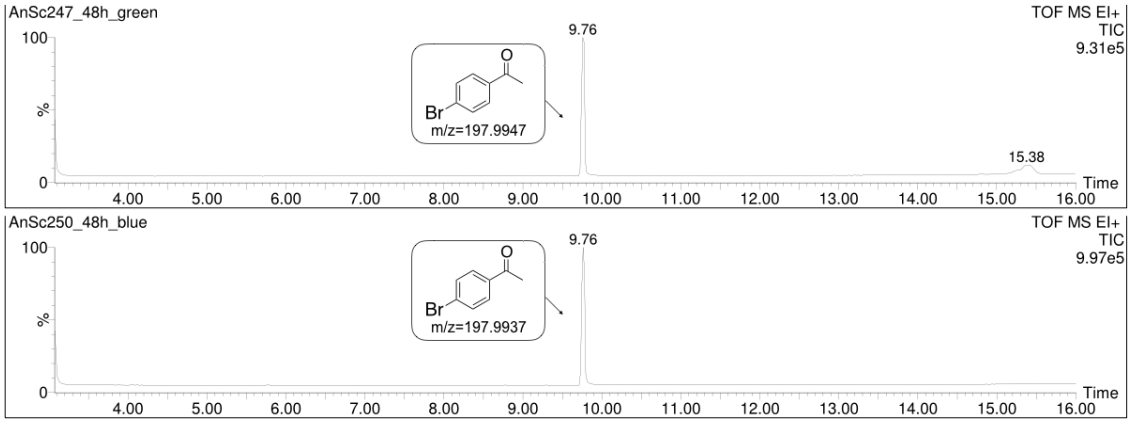

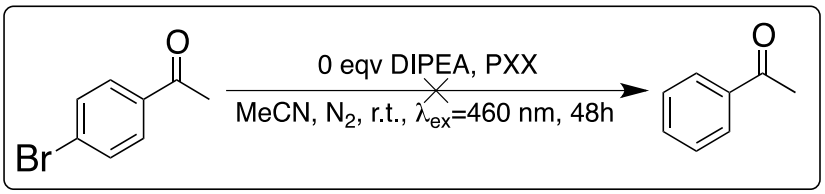

Table 22, entry 13

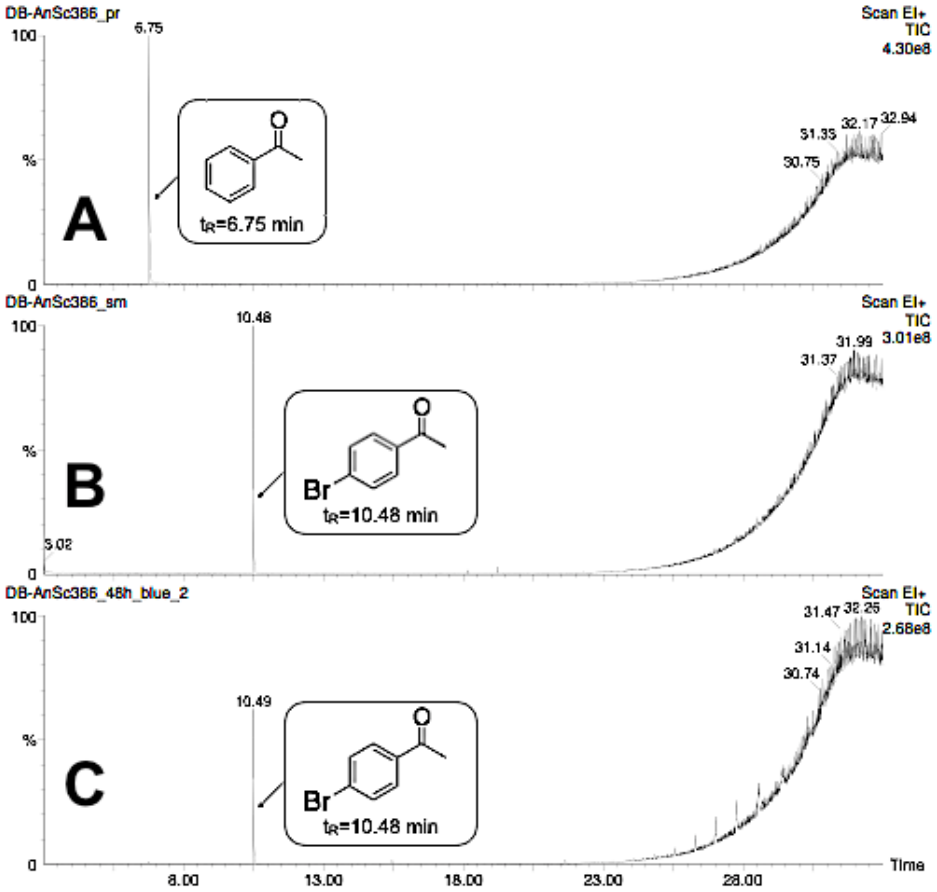

A: acetophenone; **B**: 4'-bromoacetophenone; **C**: irradiated solution at 460 nm after 24h.

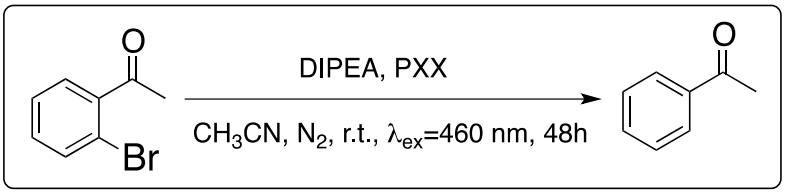

Table 23: Dehalogenation of 2'-bromoacetophenone.

Entry	Dye	λ_{ex} [nm]	Solvent	Time [h]	Conversion [%]
1	**PXX 22**	460	CH_3CN	48	2
		dark			0
2	blank	460		48	0

Table 23, entry 1

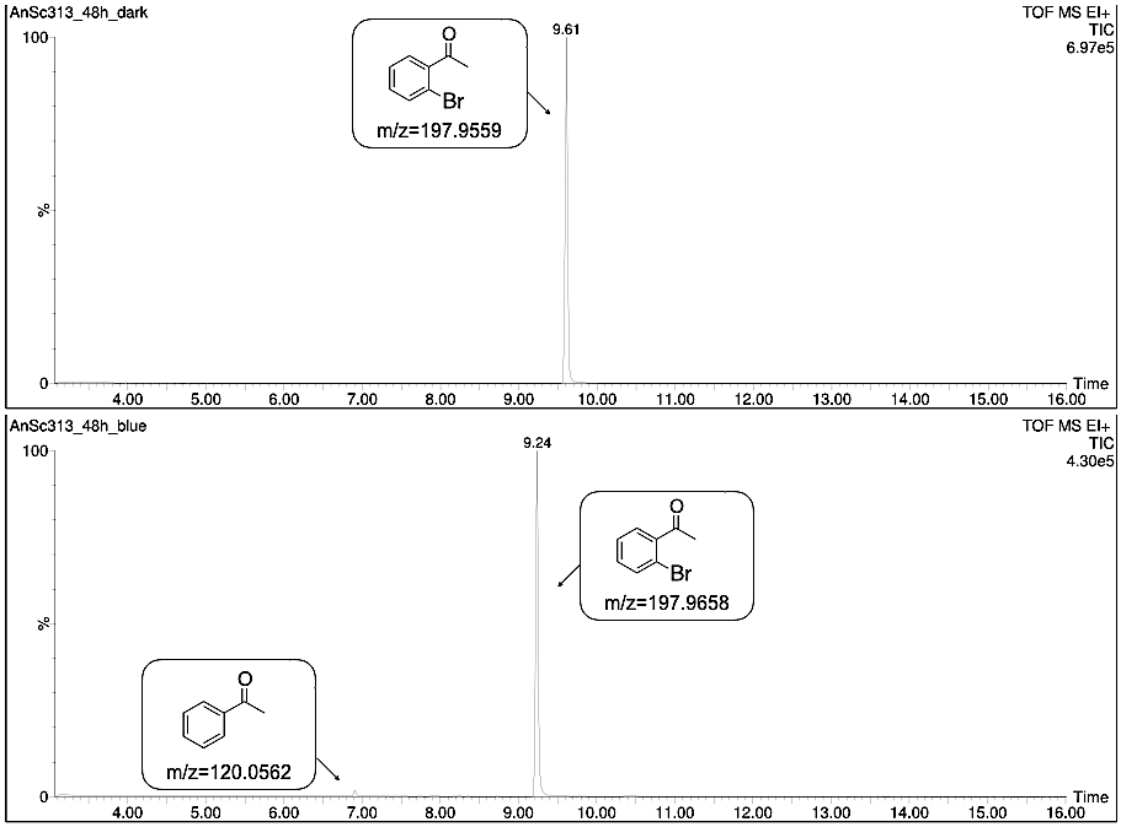

Table 23, entry 2

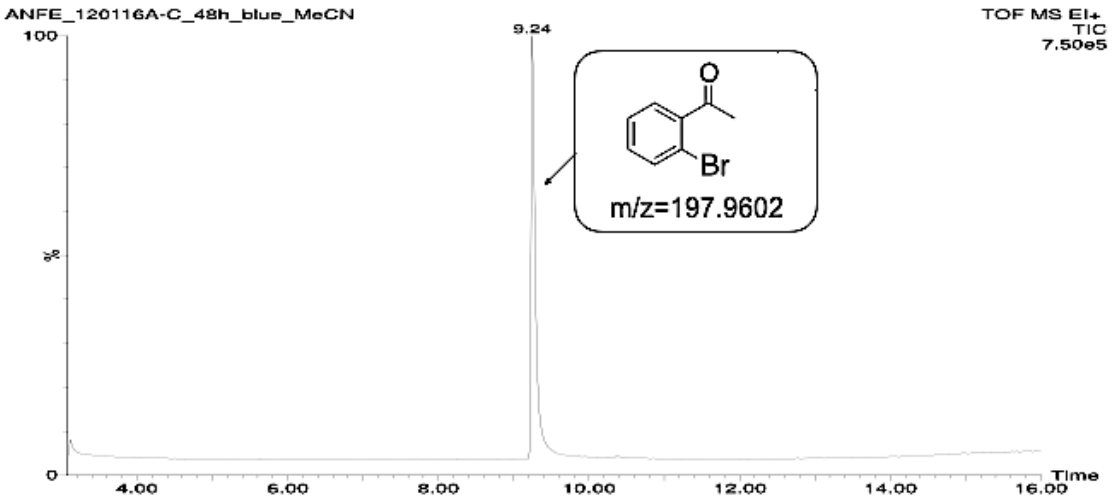

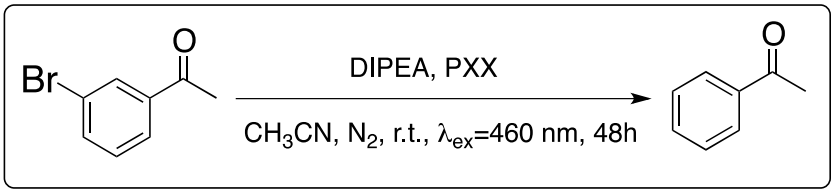

Table 24: Dehalogenation of 3'-bromoacetophenone.

Entry	Dye	λ_{ex} [nm]	Solvent	Time [h]	Conversion [%]
1	**PXX 25**	460	CH_3CN	48	73
		dark			0
2	blank	460		48	0

Table 24 entry 1

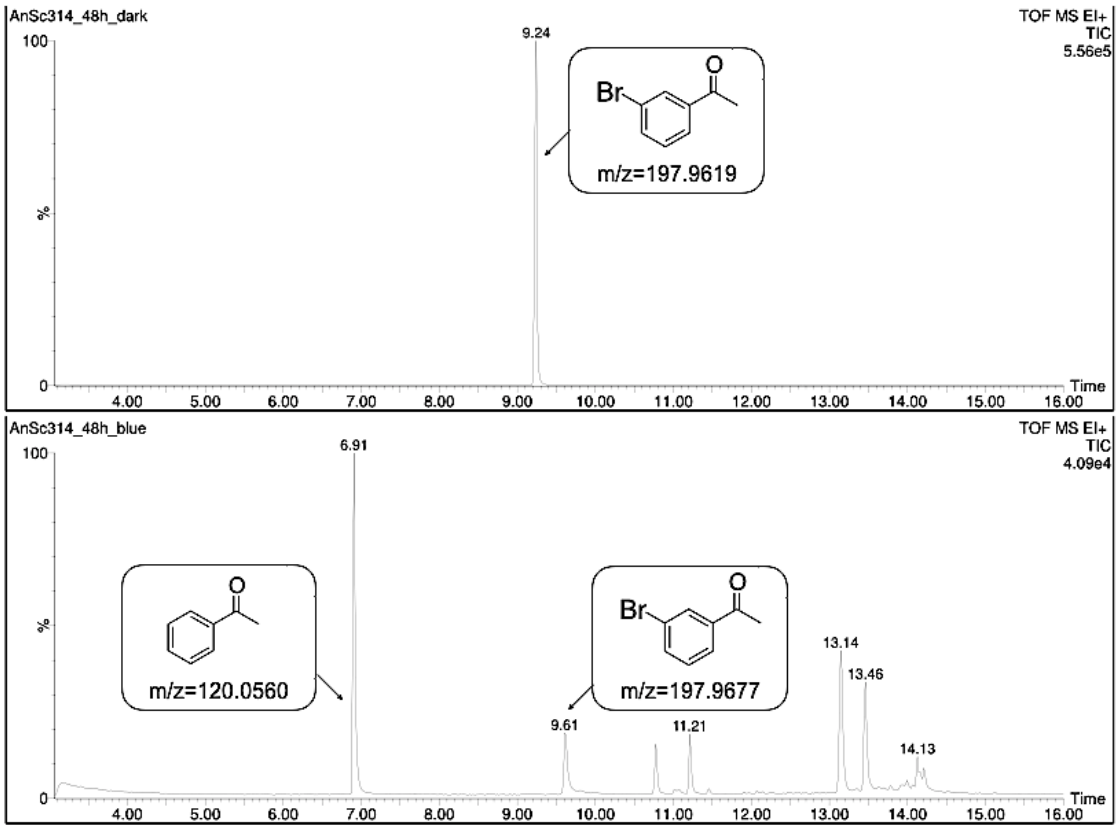

Table 24, entry 2

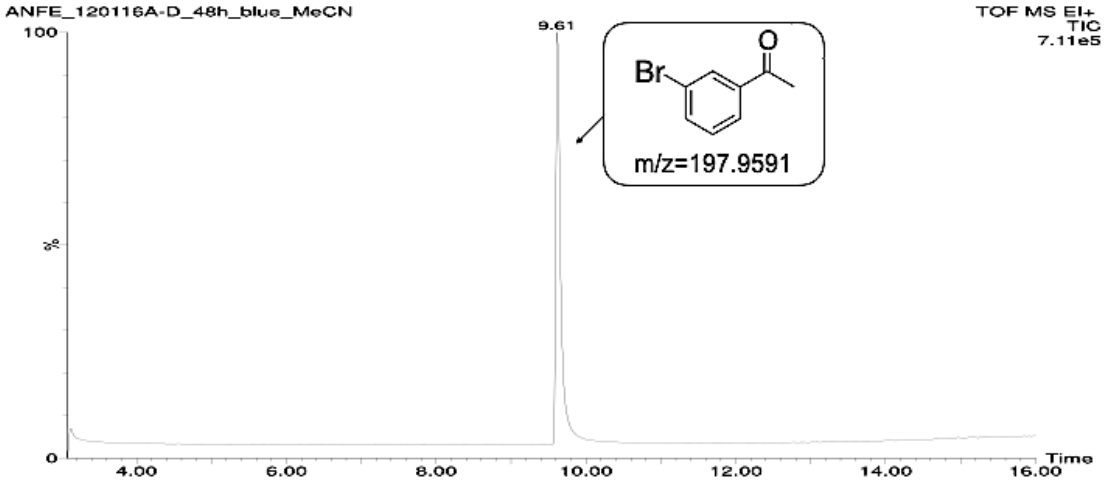

4.6.2.3 Dehalogenation of *p*-bromobenzaldehyde

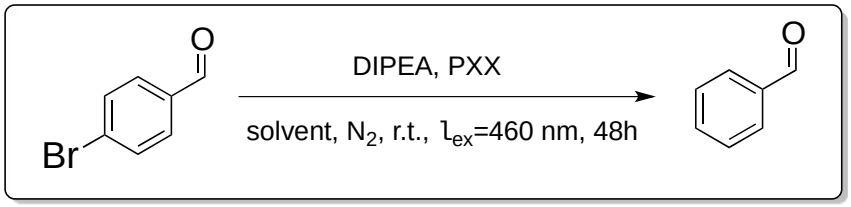

Table 25: Dehalogenation of 4-bromobenzaldehyde

Entry	Dye	λ_{ex} [nm]	Solvent	Time [h]	Conversion [%]
1	**PXX 25**	460	C_6H_6	48	0
		dark			0
2		460	CH_2Cl_2	48	26
		dark			0
3		460	CH_3CN	48	100
		dark			0
4	blank	460	C_6H_6	48	0
5			CH_2Cl_2		0
6			CH_3CN		*traces*

Table 25, entry 1

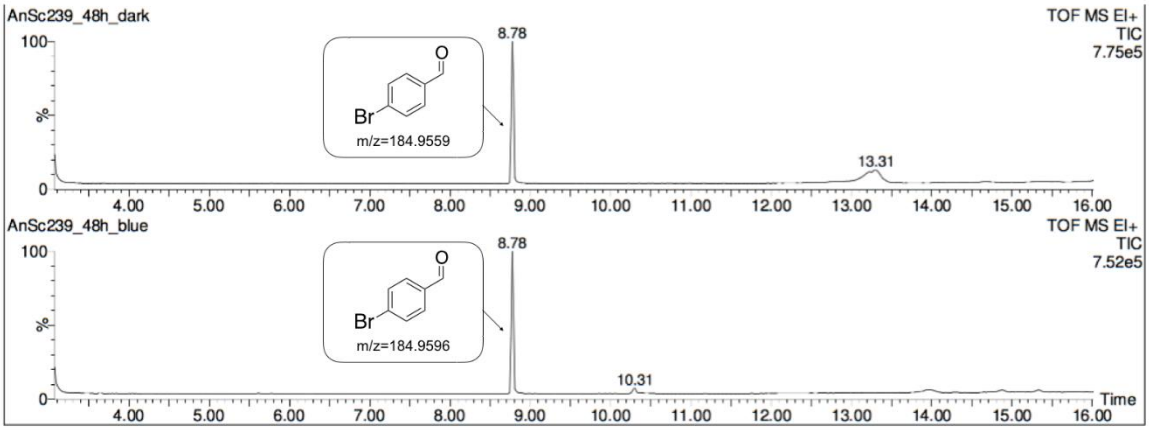

Table 25, entry 2

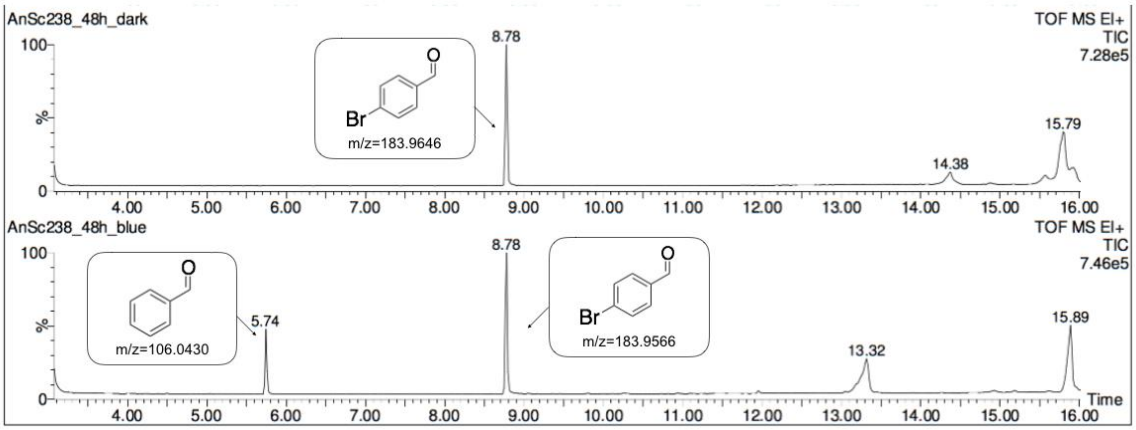

Table 25, entry 3

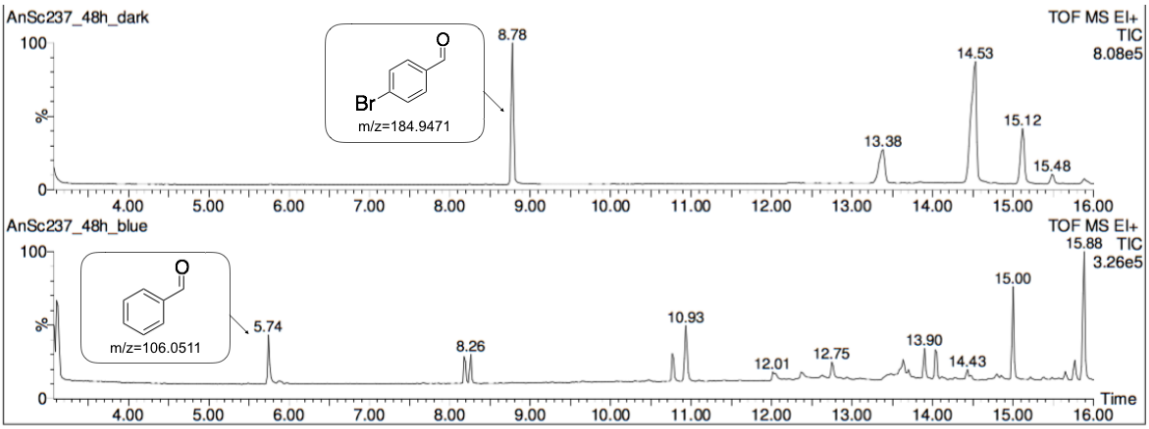

Table 25, entry 4

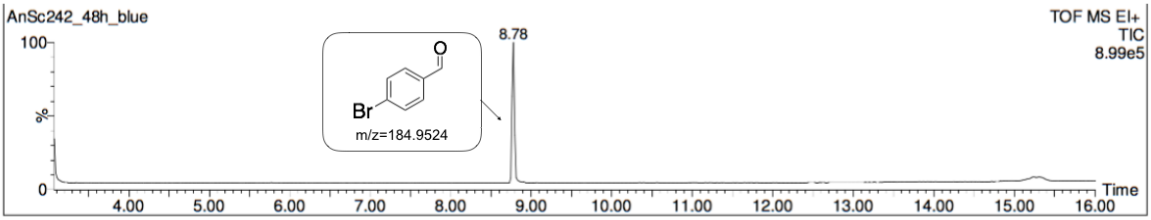

Table 25, entry 5

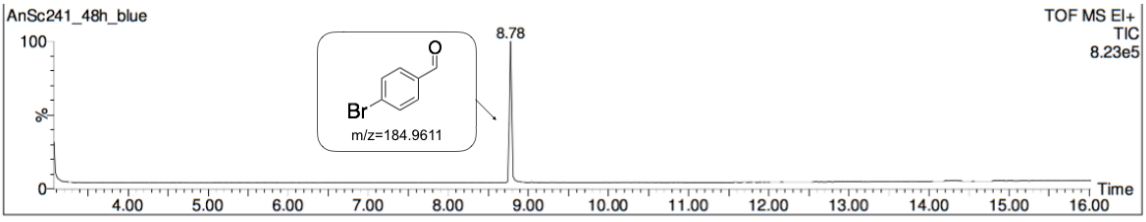

Table 25, entry 6

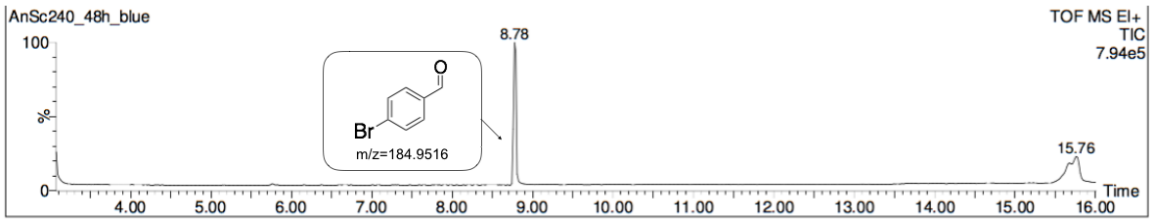

4.6.2.4 Dehalogenation of α-bromocinnamaldehyde

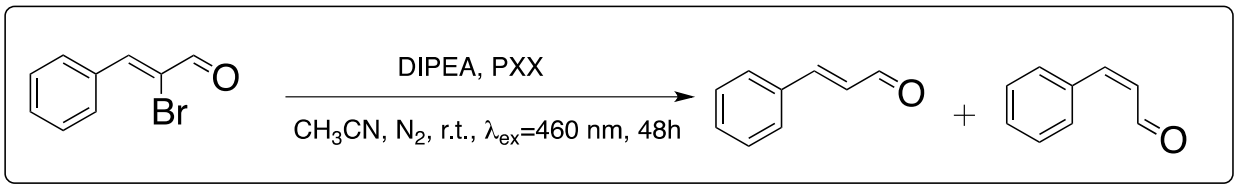

Table 26: Dehalogenation of *α*-bromocinnamaldehyde.

Entry	Dye	λ_{ex} [nm]	Solvent	Time [h]	Conversion [%]
1	**PXX 25**	460	CH_3CN	48	58 (*E*:*Z* 1:2.8)
		dark			0
2	blank	460		48	8

Table 26, entry 1

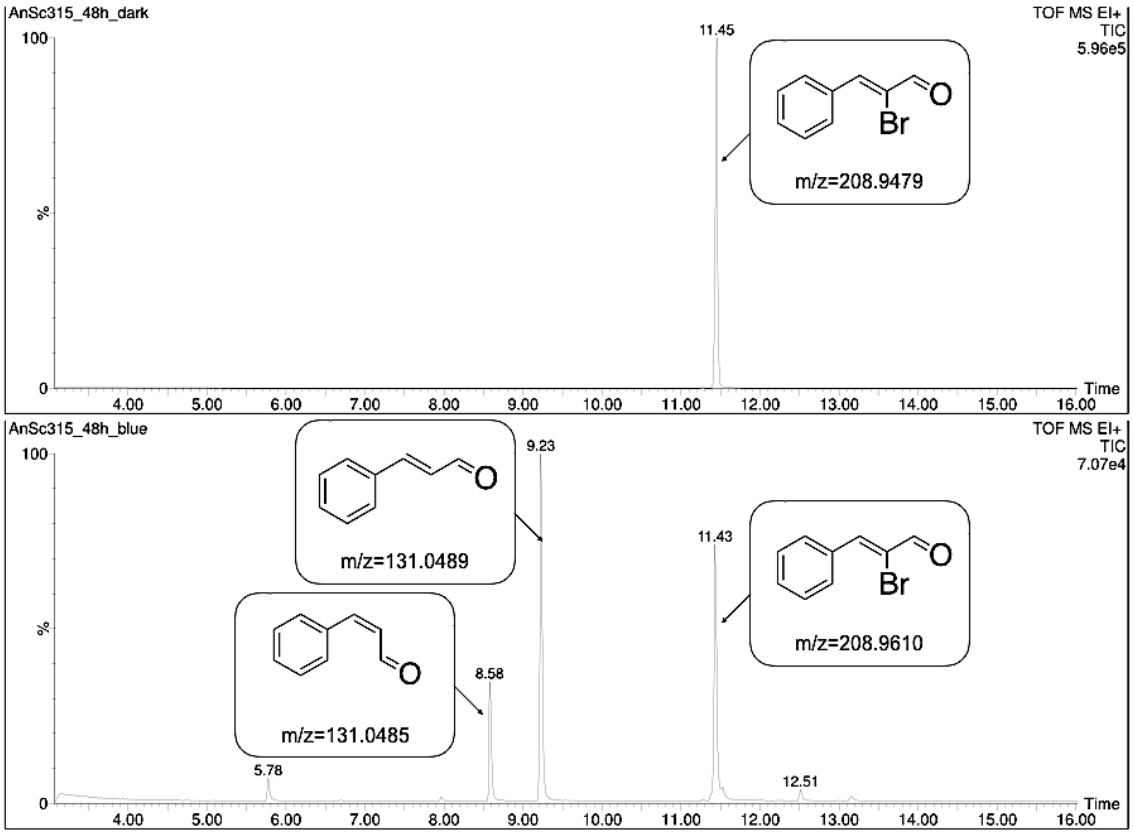

Table 26, entry 2

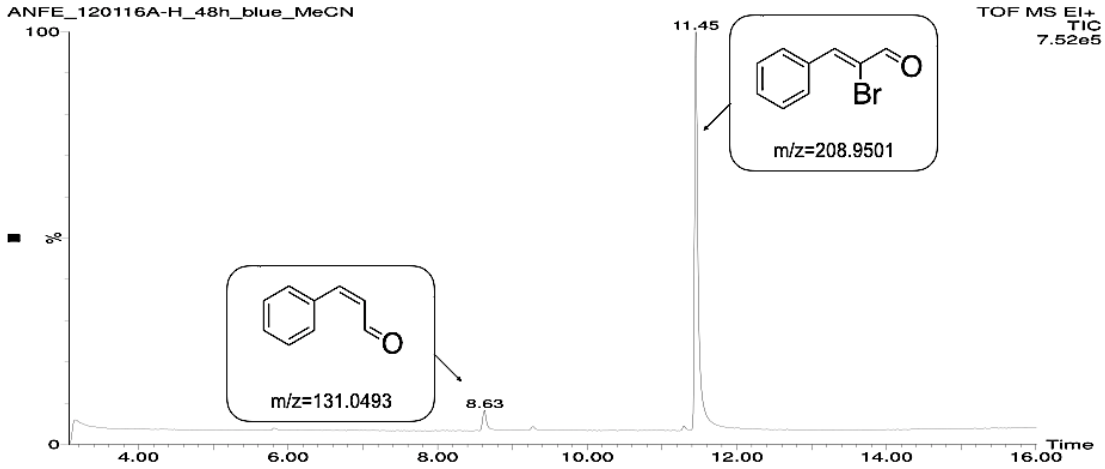

4.6.2.5 Dehalogenation of diethylbromomalonate

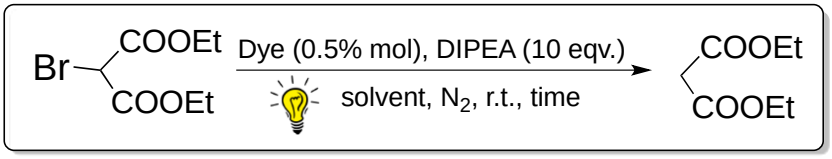

Table 27: Dehalogenation of diethylbromomalonate.

Entry	Dye	λ_{ex} [nm]	Solvent	Time [h]	Conversion [%]
1	**PXXMI 148**	520	CH_3CN	20	100
		dark			6
2	**PXXDI 141**	520		20	100
		dark			8
3	blank	520		20	5
4	**PXXMI 148**, 0 eqv DIPEA	520		20	traces

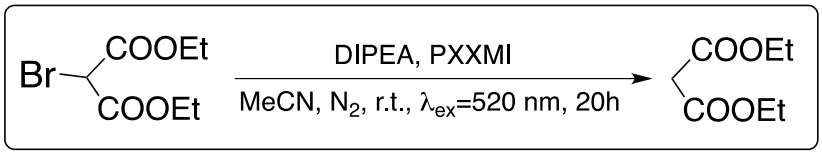

Table 27, entry 1

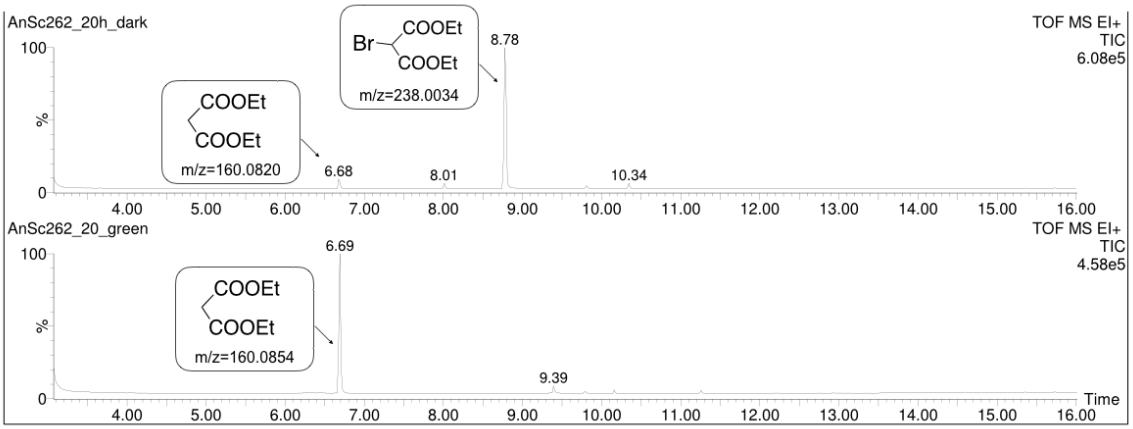

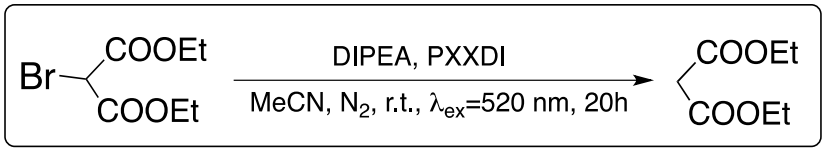

Table 27, entry 2

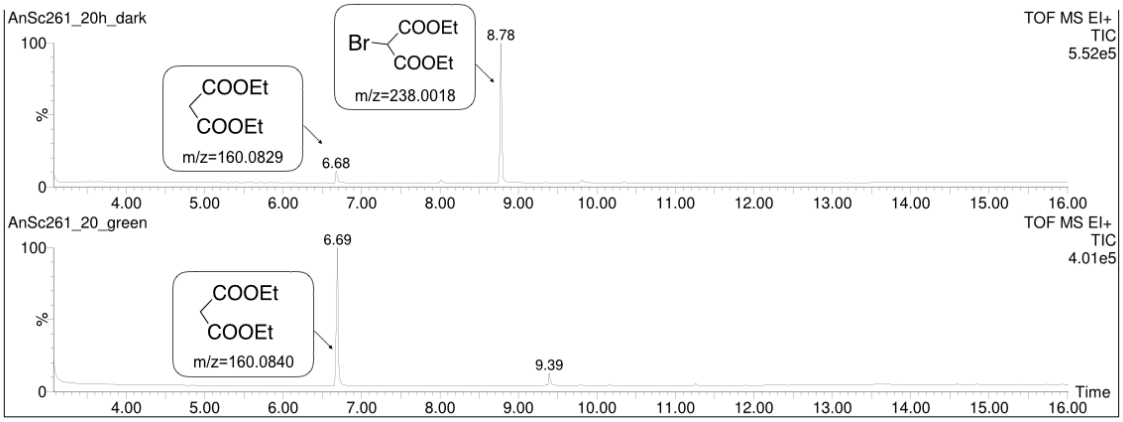

Table 27, entry 3

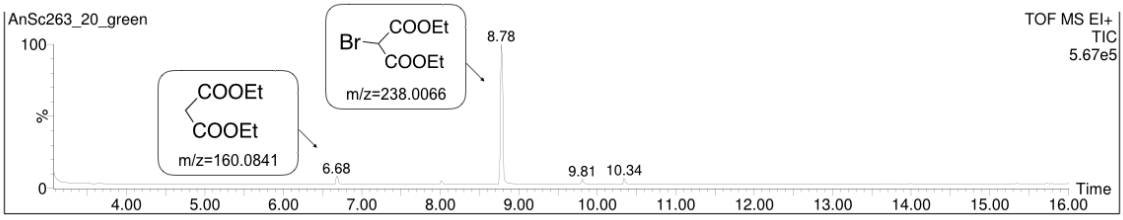

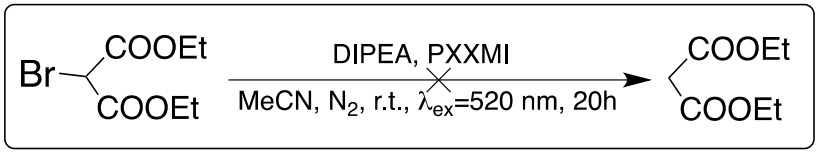

Table 27, entry 4

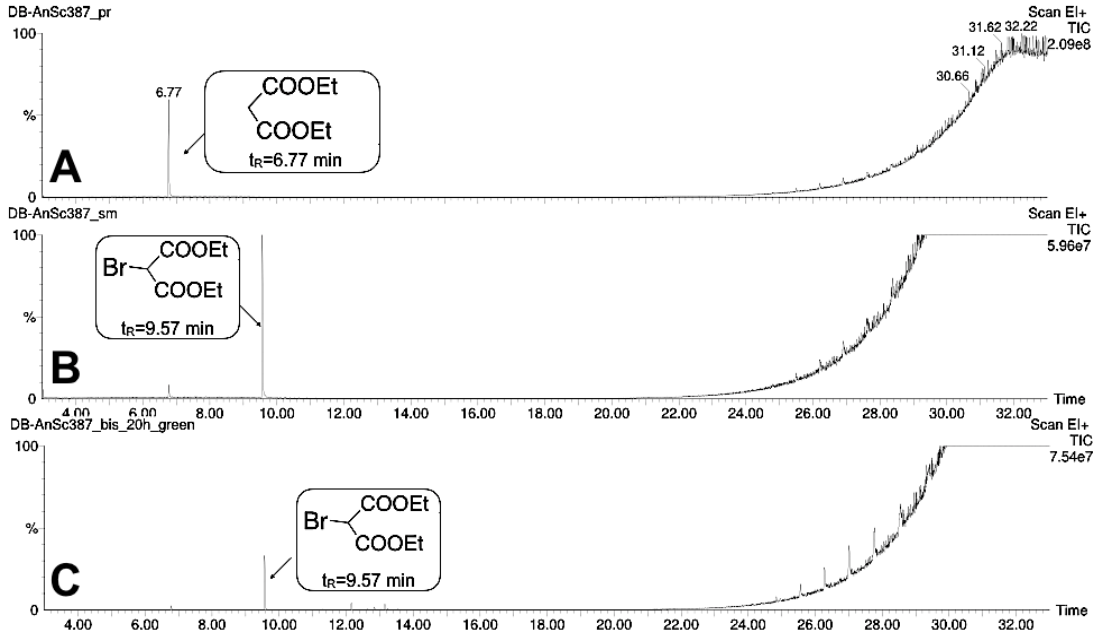

A: diethylmalonate; **B**: diethylbromomalonate; **C**: irradiated solution at 520 nm after 24h.

4.6.2.6 Dehalogenation of diethylchloromalonate

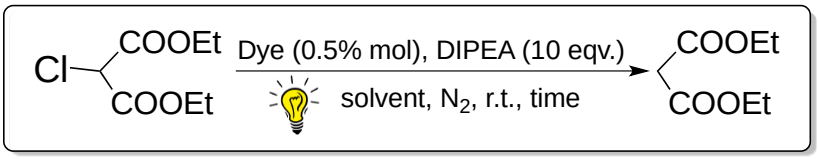

Table 28: Dehalogenation of diethylchloromalonate.

Entry	Dye	λ_{ex} [nm]	Solvent	Time [h]	Conversion [%]
1	**PXXMI**	520	CH_3CN	96	75
		dark		96	0
2	**PXXDI**	520		96	traces
		dark		96	0
3	blank	520		96	0

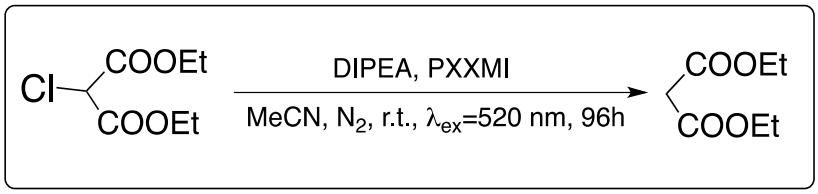

Table 28, entry 1

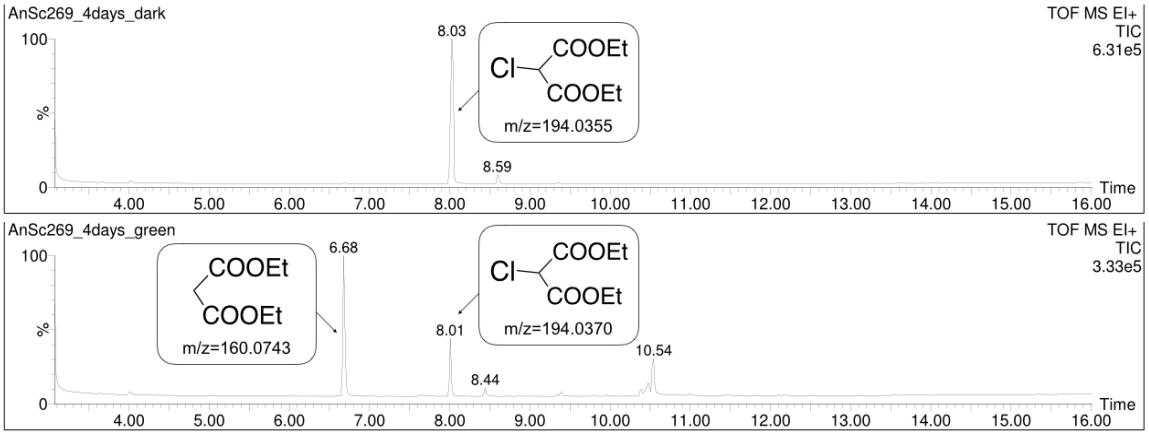

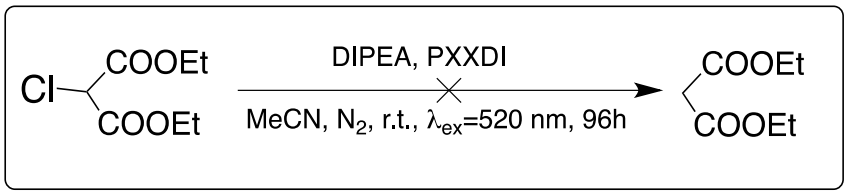

Table 28, entry 2

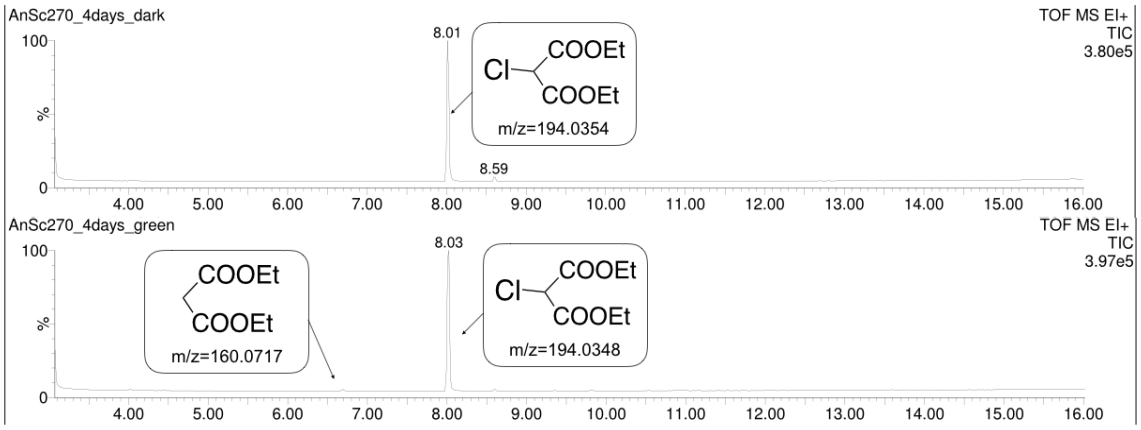

Table 28, entry 3

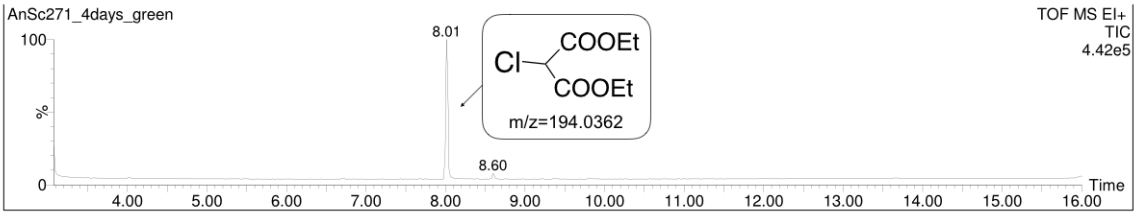

4.6.2.7 Sequential dehalogenation of 2-4'-dibromoacetophenone

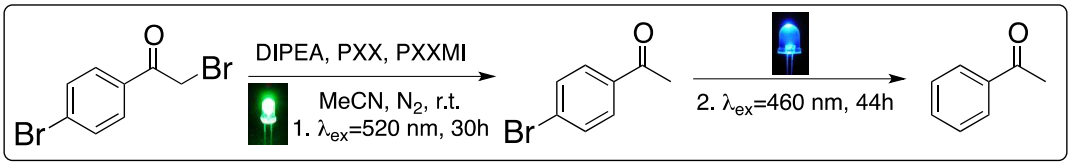

Table 29: Sequential dehalogenation on 2-4'-dibromoacetophenone.

Entry	Dye	λ_{ex} [nm]	Solvent	Time [h]	Conversion [%]
1	1. **PXXMI 148**	520	CH_3CN	30	100 (α)
		dark		30	48 (α)
	2. **PXX 25**	460		74	100 (para)
		dark		74	0 (para)
2	1. blank	520		30	42 (α)
	2. blank	460		72	0 (para)
3	1. **PXXMI 148** (0.41 mM)	520		30	100 (α)
		dark		-	-
	2. **PXX 25** (0.41 mM)	460		74	10 (para)
		dark		74	0 (para)

Table 29, entry 1

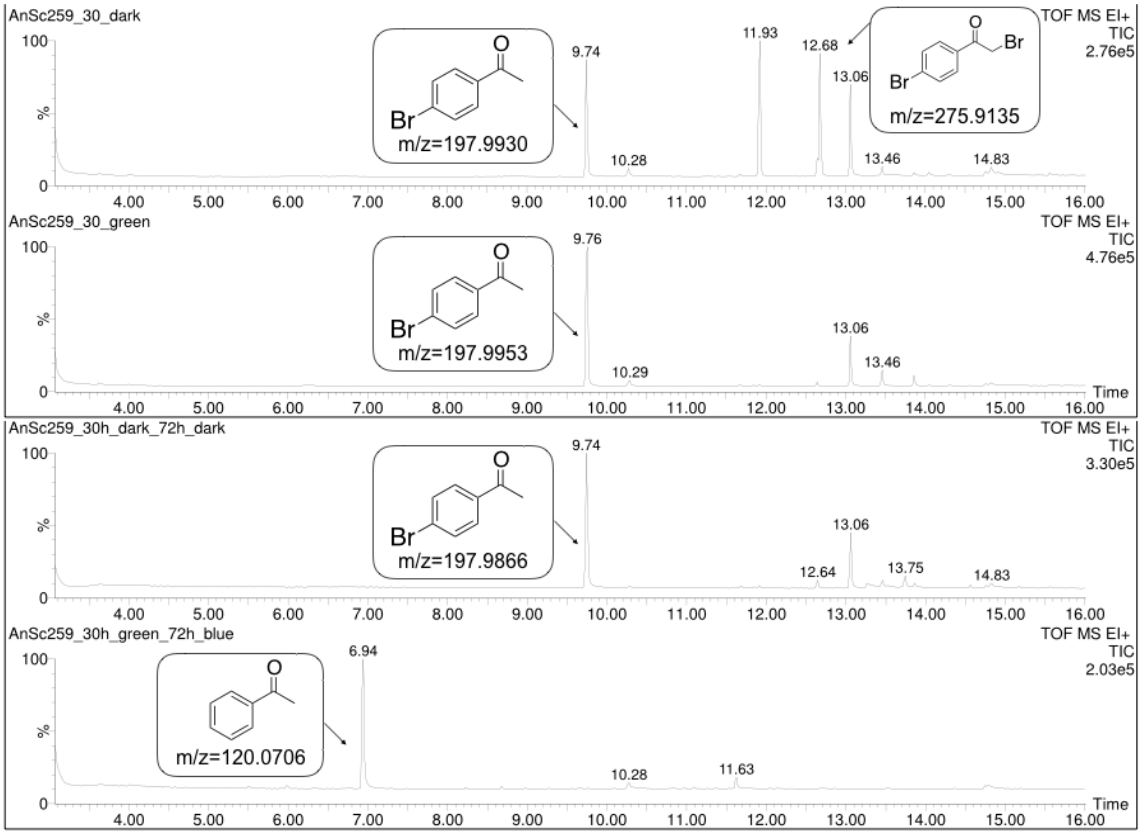

Table 29, entry 2

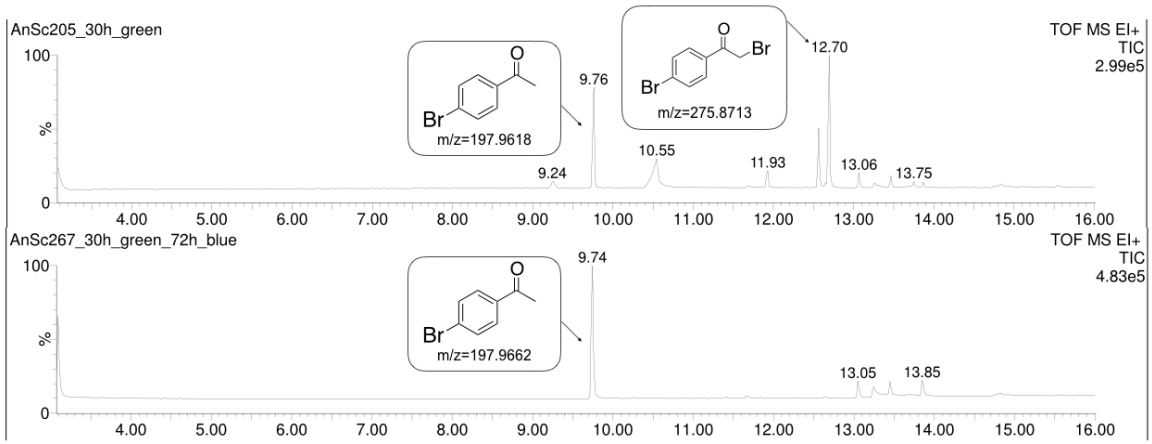

Table 29, entry 3

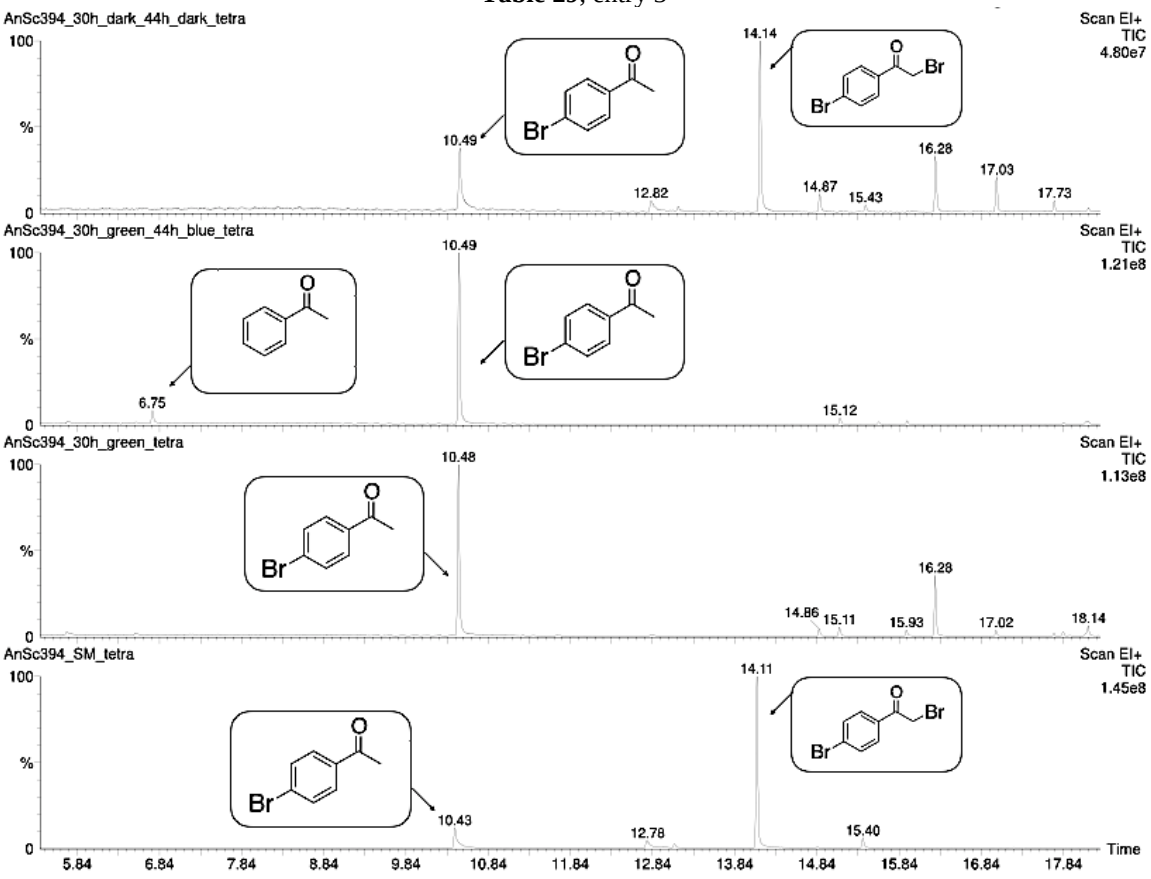

4.7. Theoretical calculations

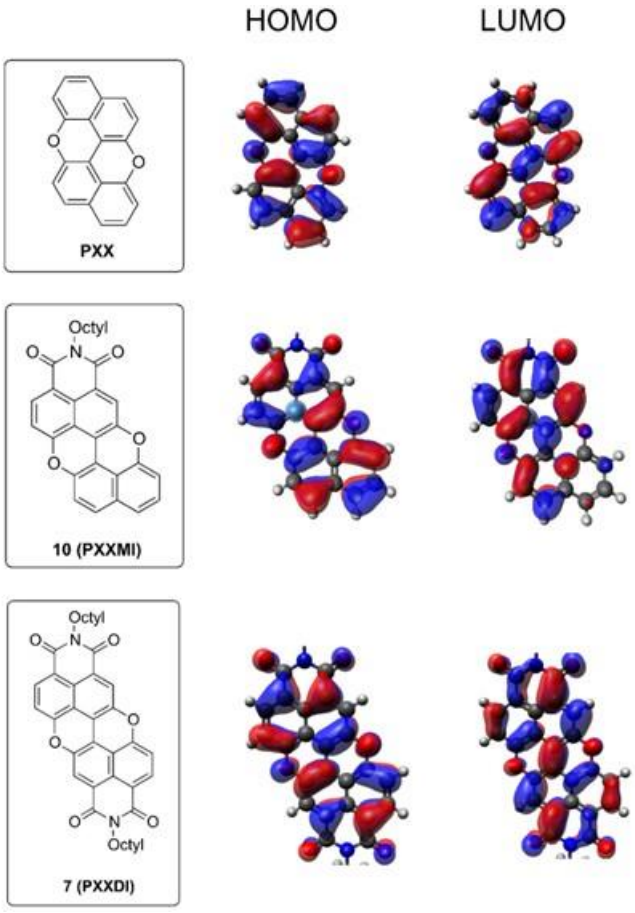

Figure 81: HOMO and LUMO orbitals calculated at the B3LYP/6-31G* level of theory.

Table 30: Calculated redox potentials of excited states and ground states of the different dyes in CH_3CN (in V *vs*. SCE), unless differently specified. Optical gaps (in eV) are calculated from the maxima of emission spectra in the same solvents at RT. Data for [*fac*-Ir(ppy)$_3$] and $[Ru(bpy)_3]^{2+}$ are taken from the literature.[S14]

Dye	E_{00} (eV)	$E^{1/2}$ (M^+/M^*)	$E^{1/2}$ (M^*/M^-)	$E^{1/2}$ (M^+/M)	$E^{1/2}$ (M/M^-)
[*fac*-Ir(ppy)$_3$]	2.51	-1.74	0.32	0.77	-2.19
PXX	2.77	-2.00	0.61	0.77	-2.16
PXXMI	2.18	-1.14	0.93	1.04	-1.25
PXXDI[a]	2.26	-0.85	1.25	1.41	-1.01
$[Ru(bpy)_3]^{2+}$	2.10	-0.81	0.77	1.29	-1.33

[a]Data in CH_2Cl_2.

4.8. XRD analysis

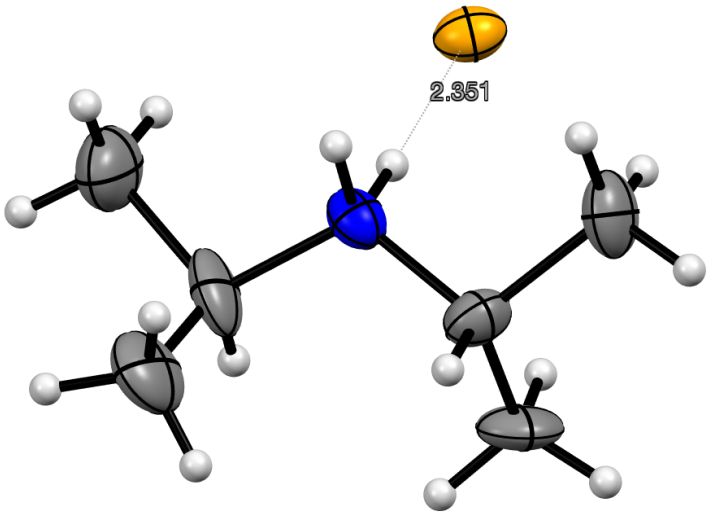

Figure 82: ORTEP representation of the crystal structure of diisopropylammonium bromide. Highlighted distance between Br atom and vicinal H atom is expressed in Å. Space group: P 2_1. Atom colors: grey C, white H, blue N, yellow Br.

Table 31: Crystal data and refinements for the structure of diisopropylethylammonium bromide.

Identification code	Shelx	
Empirical formula	$C_6 H_{16} Br N$	
Formula weight	182.11	
Temperature	150(2) K	
Wavelength	0.71073 Å	
Crystal system	Monoclinic	
Space group	$P 2_1$	
Unit cell dimensions	a = 7.7737(12) Å	α= 90°
	b = 7.9732(7) Å	β= 116.360(19)°
	c = 7.8452(12) Å	γ= 90°
Volume	435.70(12) $Å^3$	
Z	2	
Density (calculated)	1.388 Mg/m^3	
Absorption coefficient	4.636 mm^{-1}	
F(000)	188	
Crystal size	0.860 x 0.488 x 0.217 mm^3	
Theta range for data collection	3.865 to 29.250°	
Index ranges	-10<=h<=10, -10<=k<=10, -10<=l<=10	
Reflections collected	3544	
Independent reflections	2024 [R(int) = 0.0436]	
Completeness to theta = 25.242°	99.7%	
Refinement method	Full-matrix least-squares on F2	
Data / restraints / parameters	2024 / 1 / 73	
Goodness-of-fit on F^2	1.056	
Final R indices [I>2sigma(I)]	R1 = 0.0496, wR2 = 0.1107	
R indices (all data)	R1 = 0.0622, wR2 = 0.1227	
Absolute structure parameter	0.320(19)	
Extinction coefficient	n/a	
Largest diff. peak and hole	1.141 and -1.034 e.Å-3	

4.9. EPR experiments

Samples for EPR analysis were prepared by dissolving one of the dyes (PXX **25** or PXXMI **148**) in CH_2Cl_2 (c = 2.5*10^{-3} M) in presence of DIPEA (c = 0.40 M), bromo-derivative (c = 0.05 M) and, for the spin trap experiments, using *N-tert*-Butyl-α-phenylnitrone (PBN, *ca.* 6*10^{-3} M). The resulting solution was deoxygenated for 25 min by bubbling N_2. A capillary tube suitable for EPR experiments was thus filled with the oxygen-free solution under inert conditions and kept in the dark.

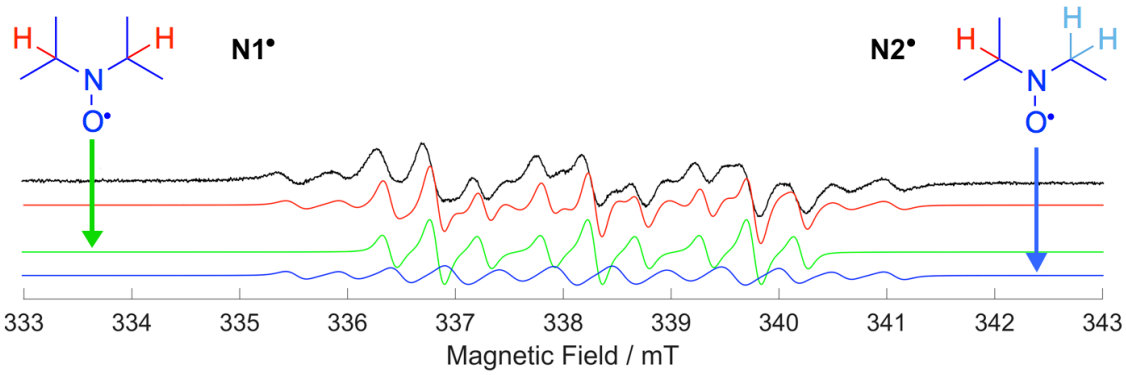

Figure 83: CW X-band EPR spectra recorded at 298 K of the reaction system containing 4-bromobenzaldehyde, DIPEA and PXX **25** in CH_2Cl_2 before irradiation (black line). The EPR simulation is shown as the red line. The green and blue lines correspond to the deconvoluted simulated spectra of diisopropylnitroxyl radical **N1**• and isopropylethylnitroxyl radical **N2**•, respectively.

Radical **N1**• shows a triplet of triplets due to the unpaired electron coupling with a ^{14}N nucleus (I = 1) and two equivalent ^{1}H (I = 1/2) in the β-position with respect to the N atom (highlighted in red in the inset Scheme). The radical is characterised by the spin Hamiltonian parameters of g_{iso} = 2.006, $a_{iso}(^{14}N)$ = 42.3±1.4 MHz and $a_{iso}(^{1}H)$ = 12.6±1.4 MHz, in agreement with results reported elsewhere.[S15]

Radical **N2**• shows eighteen lines corresponding to a triplet of 1:1:2:2:1:1 sextets, due to the unpaired electron coupling with a ^{14}N nucleus and three ^{1}H in the β-position with respect to the N atom, two of which are equivalent (highlighted in turquoise in the insert). The overlapping of some of the lines reduces the number of visible lines to twelve (blue line in Figure 4.45). The radical is characterised by the spin Hamiltonian parameters of g_{iso} = 2.006, $a_{iso}(^{14}N)$ = 44.8±1.4 MHz, $a_{iso}(^{1}H)$ = 28.0±1.4 MHz (x2), $a_{iso}(^{1}H)$ = 14.0±1.4 MHz, in agreement with what reported by Hudson and Hussein who found higher couplings for ^{14}N and the β-^{1}H with ethyl chains compared to isopropyl chains.[S15]

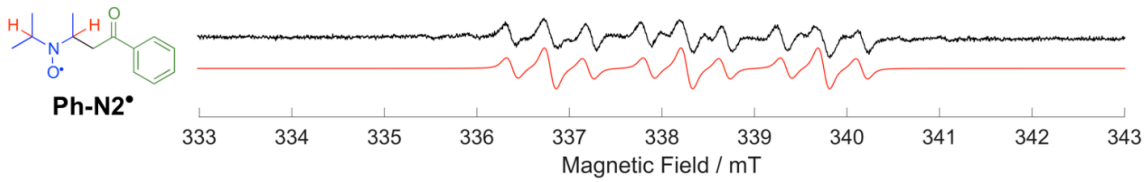

Figure 84: CW X-band EPR spectra of the reaction system containing 2-bromoacetophenone, DIPEA and PXXMI **148** after ca. 50 min irradiation (λ_{ex} = 530 nm) in CH_2Cl_2 at 298K (black line). The EPR simulation is shown as the red line. The presence of the adduct **Ph-N2•** is evidenced by the triplet of triplets pattern, given that the couplings detectable at X-band at 298 K are those originating from the ^{14}N nucleus and the two β-^1H's (highlighted in red in the Figure). Although these ^1H are not chemically equivalent, their couplings are so similar, they appear equivalent in the EPR spectrum. Adduct **Ph-N2•** is characterised by the spin Hamiltonian parameters of g_{iso} = 2.006, $a_{iso}(^{14}N)$ = 42.6±1.4 MHz, and $a_{iso}(^1H)$ = 11.8±1.4 MHz (x2).

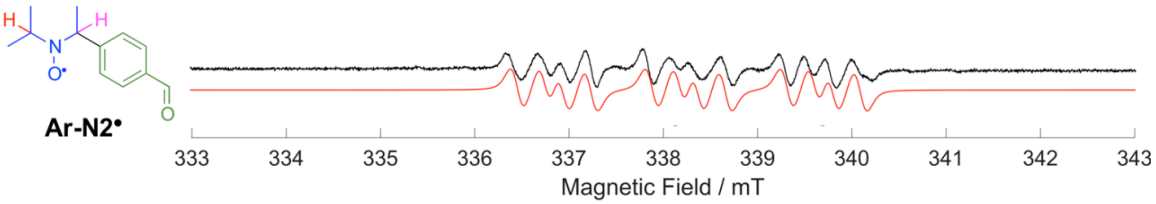

Figure 85: CW X-band EPR spectra of the reaction system containing 4-bromobenzaldehyde, DIPEA and PXX **25** after ca. 50 min irradiation (λ_{ex} = 455 nm) in CH_2Cl_2 at 298K (black line). The EPR simulation is shown as the red line. The presence of the adduct **Ar-N2•** is evidenced by the triplet of doublets of doublets pattern, as in this case the two β ^1H are significantly different due to a -C_6H_5COH substituent directly bound to the α C carrying the β-^1H (evidenced in pink in the inset Scheme). The spin Hamiltonian parameters for adduct **Ar-N2•** are g_{iso} = 2.006, $a_{iso}(^{14}N)$ = 41.2±1.4 MHz, and $a_{iso}(^1H)$ = 14.0±1.4 MHz for the β-^1H on the isopropyl chain, with $a_{iso}(^1H)$ = 8.4±1.4 MHz for the β- ^1H on the 1-(4'-formylphenyl)ethyl chain.

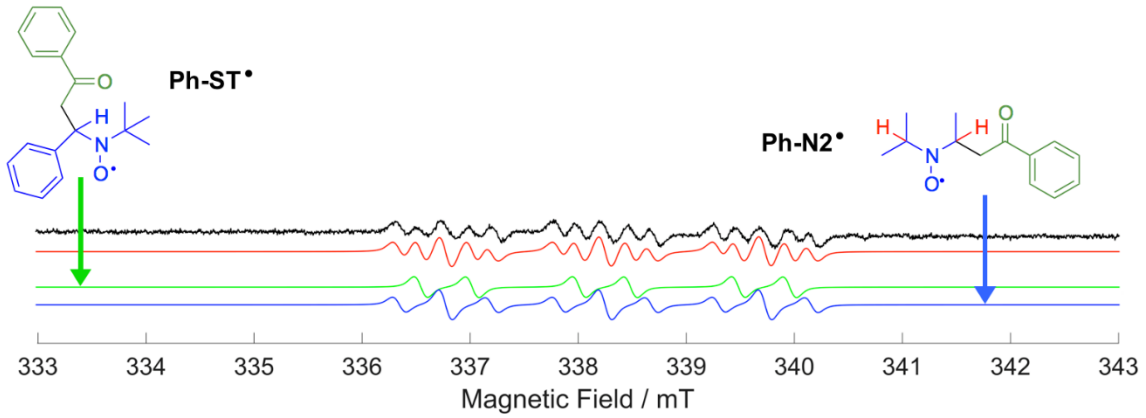

Figure 86: CW X-band EPR spectra of the reaction system containing 2-bromoacetophenone, DIPEA and **PXXMI** after ca. 50 min irradiation (λ_{ex} = 530 nm) in CH_2Cl_2 at 298K in presence of α-phenyl-N-*tert*-butylnitrone (PBN) as a spin trap (black line). The EPR simulation is shown as the red line. The deconvoluted simulated spectra of the PBN-phenacyl radical adduct **Ph-ST•** and radical **Ph-N2•** are shown as the green and blue lines respectively. The spin Hamiltonian parameters for the radical adduct **Ph-ST•** (top left) were $a_{iso}(^{14}N)$ = 42.3±1.4 MHz, $a_{iso}(^1H)$ = 13.7±1.4 MHz for the β-^1H (shown in blue). These values are in good agreement with the couplings reported by Barclay *et al.*[S16] for *m*- and *p*- substituted phenacyl radicals trapped by PBN.

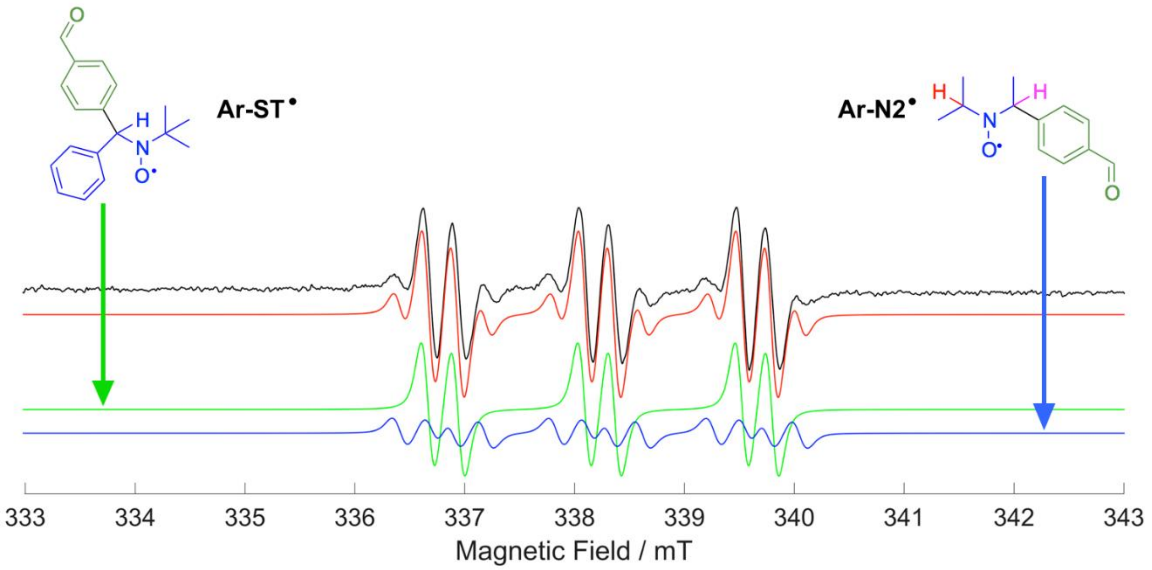

Figure 87: CW X-band EPR spectra of the reaction system containing 4-bromobenzaldehyde, DIPEA and PXX after ca. 50 min irradiation (λ_{ex} = 455 nm) in CH_2Cl_2 at 298 K in presence of *α*-phenyl-N-*tert*-butylnitrone (PBN) as the spin trap (black line). The EPR simulation is shown as the red line. The deconvoluted simulated spectra of the PBN-*p*-formylphenyl radical adduct Ar-ST• and radical Ar-N2• are shown as the green and blue lines respectively. Radical adduct Ar-ST• (top left) had the spin Hamiltonian parameters of $a_{iso}(^{14}N)$ = 41.2±1.4 MHz, $a_{iso}(^{1}H)$ = 7.8±1.4 MHz for the *β*-^{1}H (shown in blue), in good agreement with the values reported by Sankar *et al.*[S17] and Buettner.[S18]

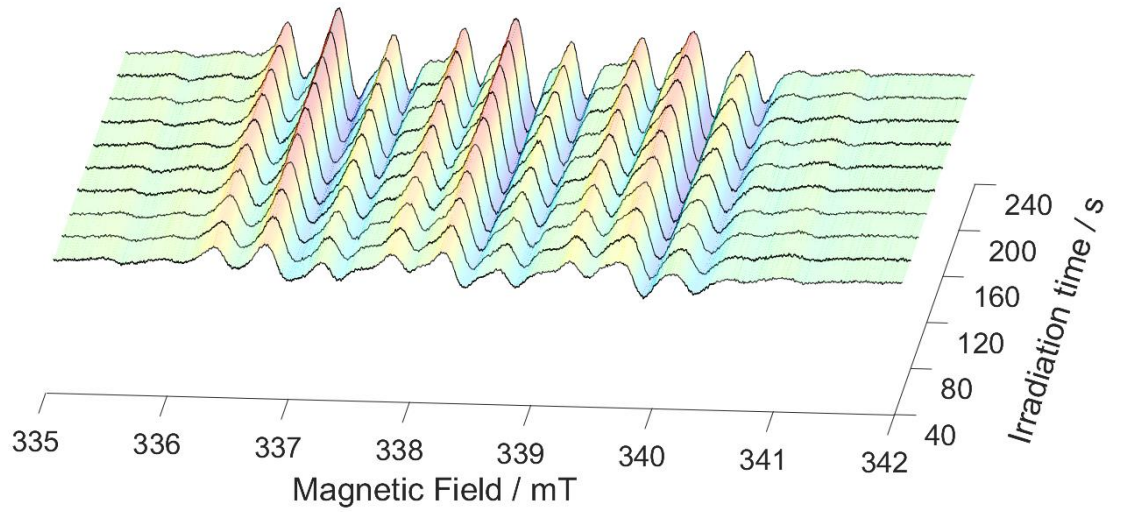

Figure 88: CW X-band EPR spectra revealing the kinetics of the first 240 s of irradiation using a 530 nm LED light source for the reaction system containing 2-bromoacetophenone, DIPEA and PXXMI **148** in CH_2Cl_2 at 298 K.

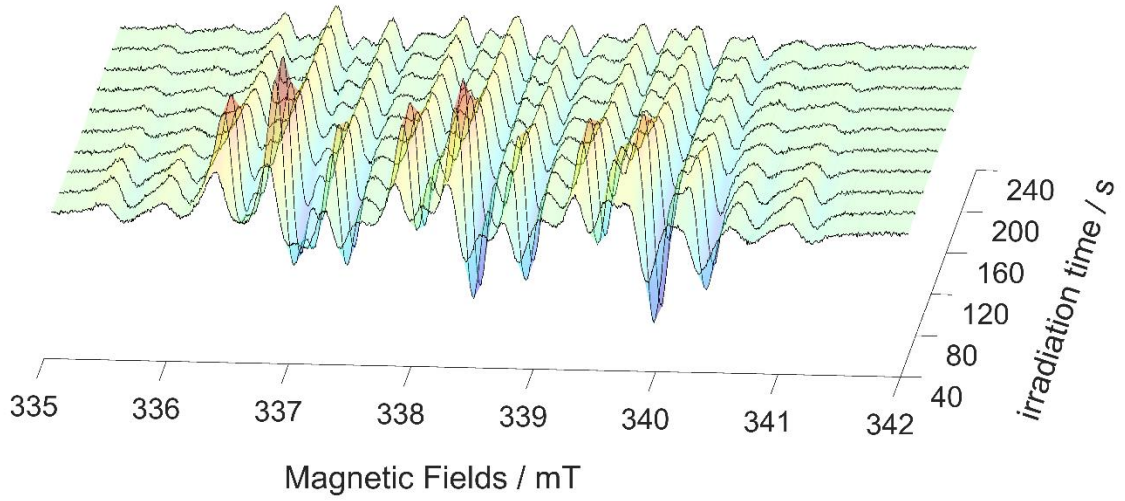

Figure 89: CW X-band EPR spectra revealing the kinetics of the first 240 s of irradiation using a 455 nm LED light source for the reaction system containing *p*-bromobenzaldehyde, DIPEA and PXX in CH_2Cl_2 at 298 K.

4.10. Miscellaneous information

Figure 90: Photographs taken on the setup used for the photoactivated reactions: switched off under ambient light (left); λ = 460 nm switched on (center); λ = 520 nm switched on (right). Reaction vials are illuminated concentrically from the inner side of the reactor.

4.11 References:

[S1] G. M. Sheldrick, *Acta Crystallogr. Sec. A* **2008**, *64*, 112–122.

[S2] S. Stoll, A. Schweiger, *J. Magn. Reson.* **2006**, *178*, 42–55.

[S3] C. M. Cardona, W. Li, A. E. Kaifer, D. Stockdale, G. C. Bazan, *Adv. Mater.* **2011**, *23*, 2367–2371.

[S4] A. Bolag, J. López-Andarias, S. Lascano, S. Soleimanpour, C. Atienza, N. Sakai, N. Martín, S. Matile, *Angew. Chem. Int. Ed.* **2014**, *53*, 4890–4895.

[S5] G. Crosby, J. Demas, *J. Phys. Chem.* **1971**, *75*, 991–1024.

[S6] M. Frisch, G. Trucks, H. Schlegel, G. Scuseria, M. Robb, J. Cheeseman, G. Scalmani, V. Barone, B. Mennucci, G. Petersson, et al., *GAUSSIAN 09 (Revision D.01), Gaussian Inc., Wallingford, CT* **2013**.

[S7] A. D. Becke, *J. Chem. Phys.* **1993**, *98*, 5648-5652.

[S8] C. Lee, W. Yang, R. Parr, *Phys. Rev. B* **1988**, *37*, 785–789.

[S9] L. Wang, W. Huang, R. Li, D. Gehrig, P. W. M. Blom, K. Landfester, K. A. I. Zhang, *Angew. Chem. Int. Ed.* **2016**, *55*, 9783–9787.

[S10] J. Schwarz, B. König, *Green Chem.* **2016**, *18*, 4743–4749.

[S11] J. Li, H. Tian, M. Jiang, H. Yang, Y. Zhao, H. Fu, *Chem. Commun.* **2016**, *52*, 8862–8864.

[S12] M. Neumann, S. Füldner, B. König, K. Zeitler, *Angew. Chem. Int. Ed.* **2011**, *50*, 951–954.

[S13] O. Amiri-Attou, T. Terme, M. Médebielle, P. Vanelle, *Tetrahedron Lett.* **2008**, *49*, 1016–1020.

[S14] C. K. Prier, D. A. Rankic, D. W. C. MacMillan, *Chem. Rev.* **2013**, *113*, 5322–5363.

[S15] A. Hudson, H. A. Hussain, *J. Chem. Soc. B Phys. Org.* **1967**, 1299-1300.

[S16] L. R. C. Barclay, G. R. Cromwell, J. W. Hilborn, *Can. J. Chem.* **1994**, *72*, 35–41.

[S17] M. Sankar, E. Nowicka, E. Carter, D. M. Murphy, D. W. Knight, D. Bethell, G. J. Hutchings, *Nat. Commun.* **2014**, *5*, 3332–3335.

[S18] G. R. Buettner, *Free Radic. Biol. Med.* **1987**, *3*, 259–303.

Appendix

A.1 Selected ^{1}H, ^{13}C NMR and HRMS spectra

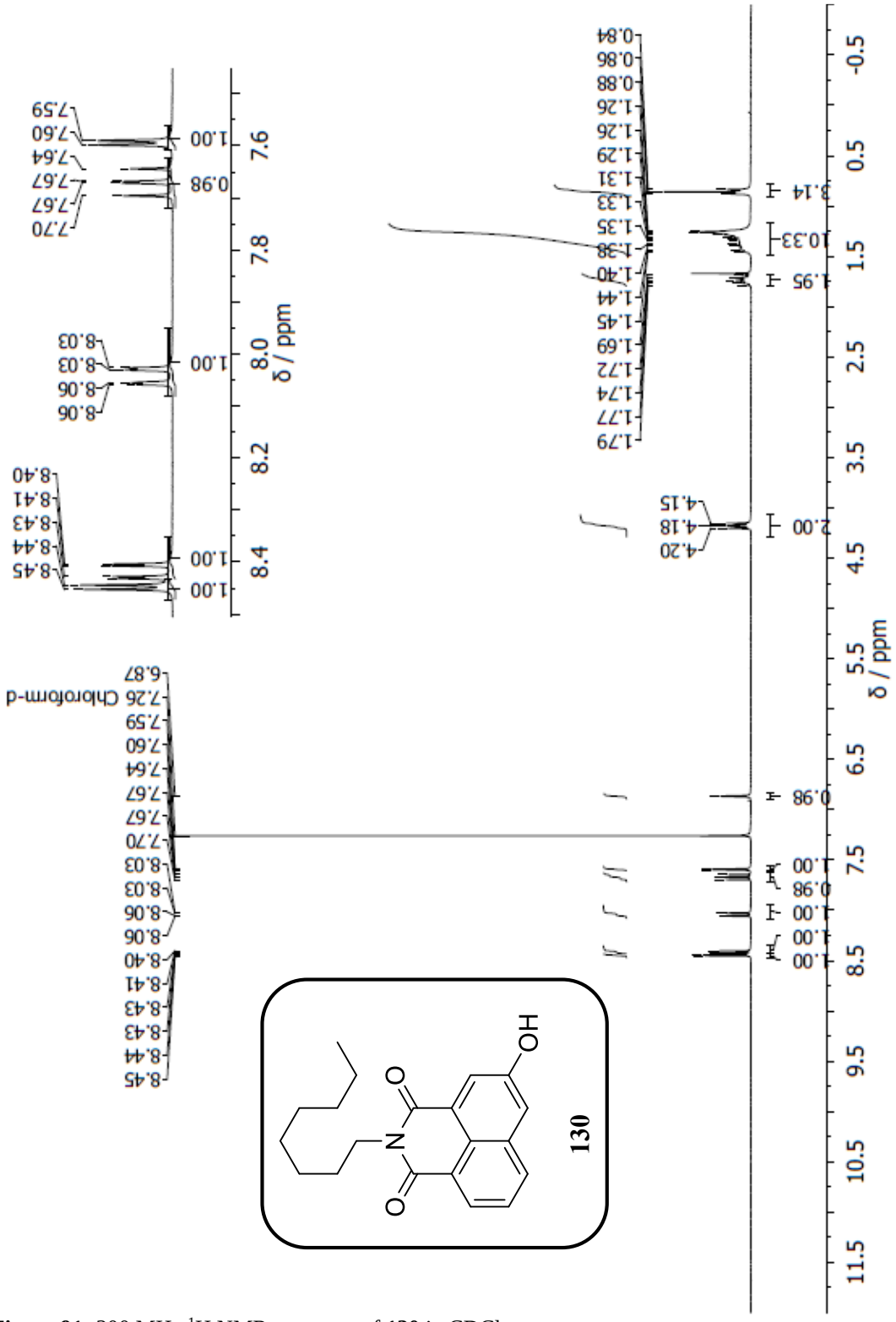

Figure 91: 300 MHz ^{1}H NMR spectrum of **130** in $CDCl_3$.

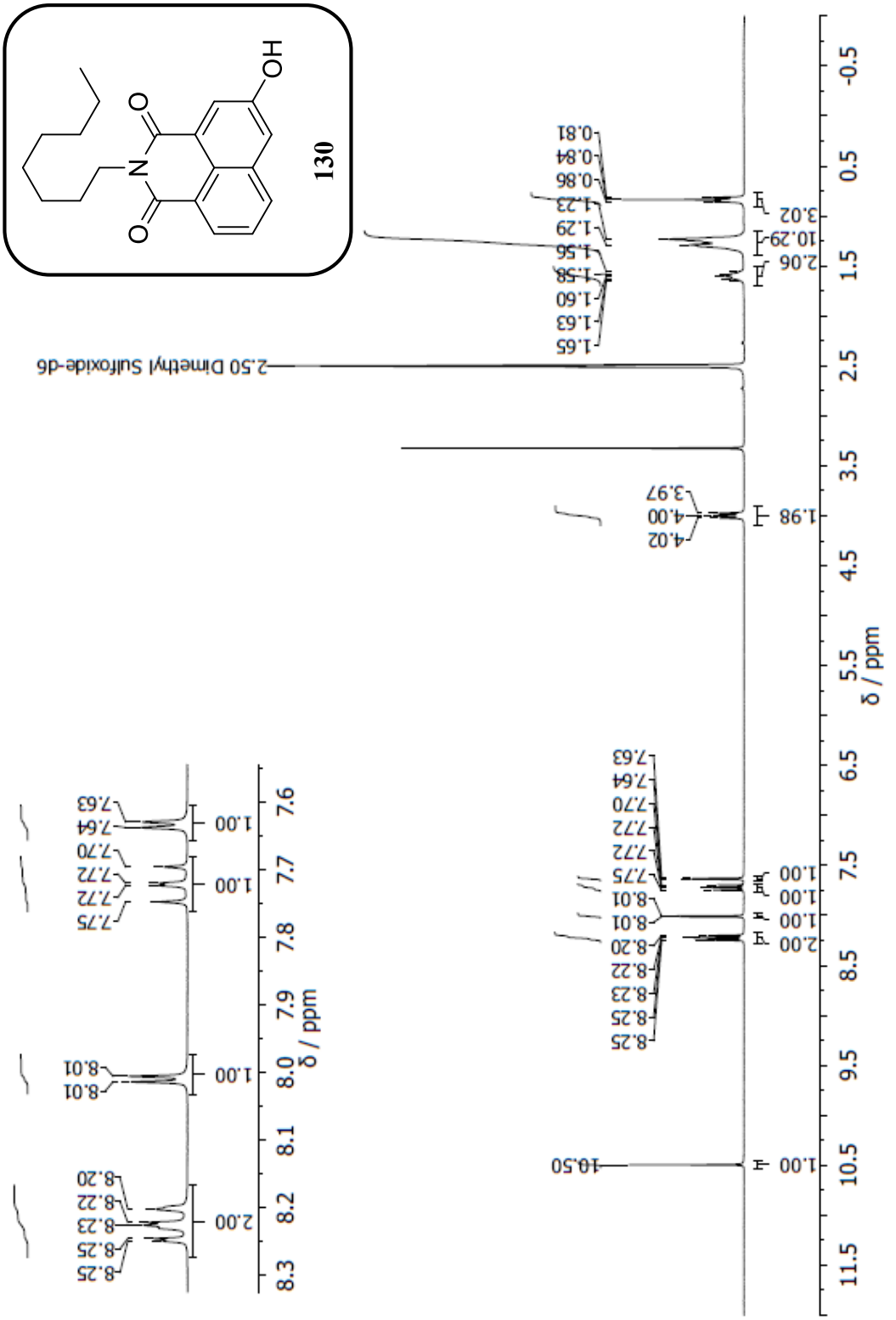

Figure 92: 300 MHz ^{1}H NMR spectrum of **130** in C_2D_6SO.

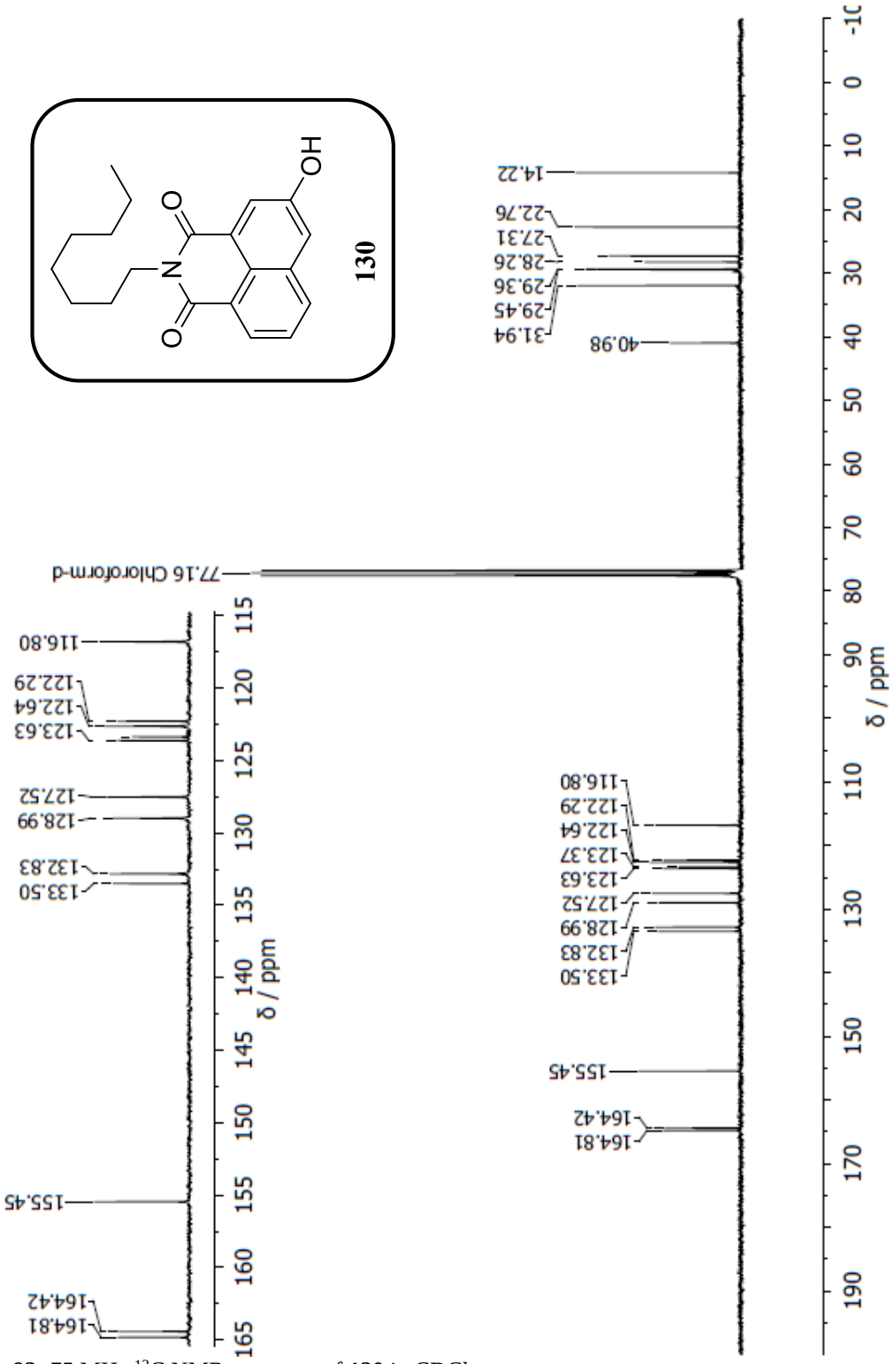

Figure 93: 75 MHz ^{13}C NMR spectrum of **130** in $CDCl_3$.

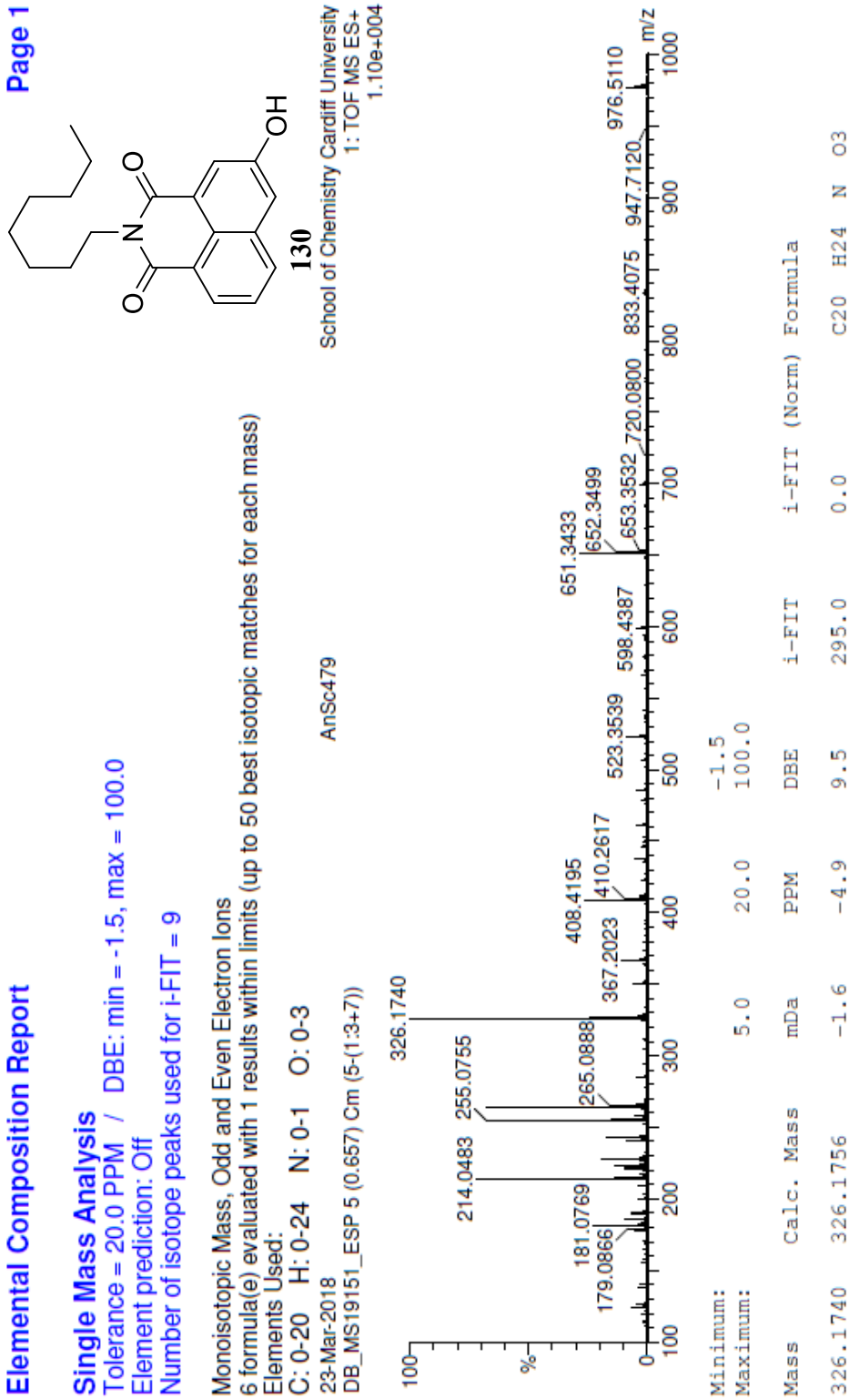

Figure 94: ESI-HRSM spectrum of **130**.

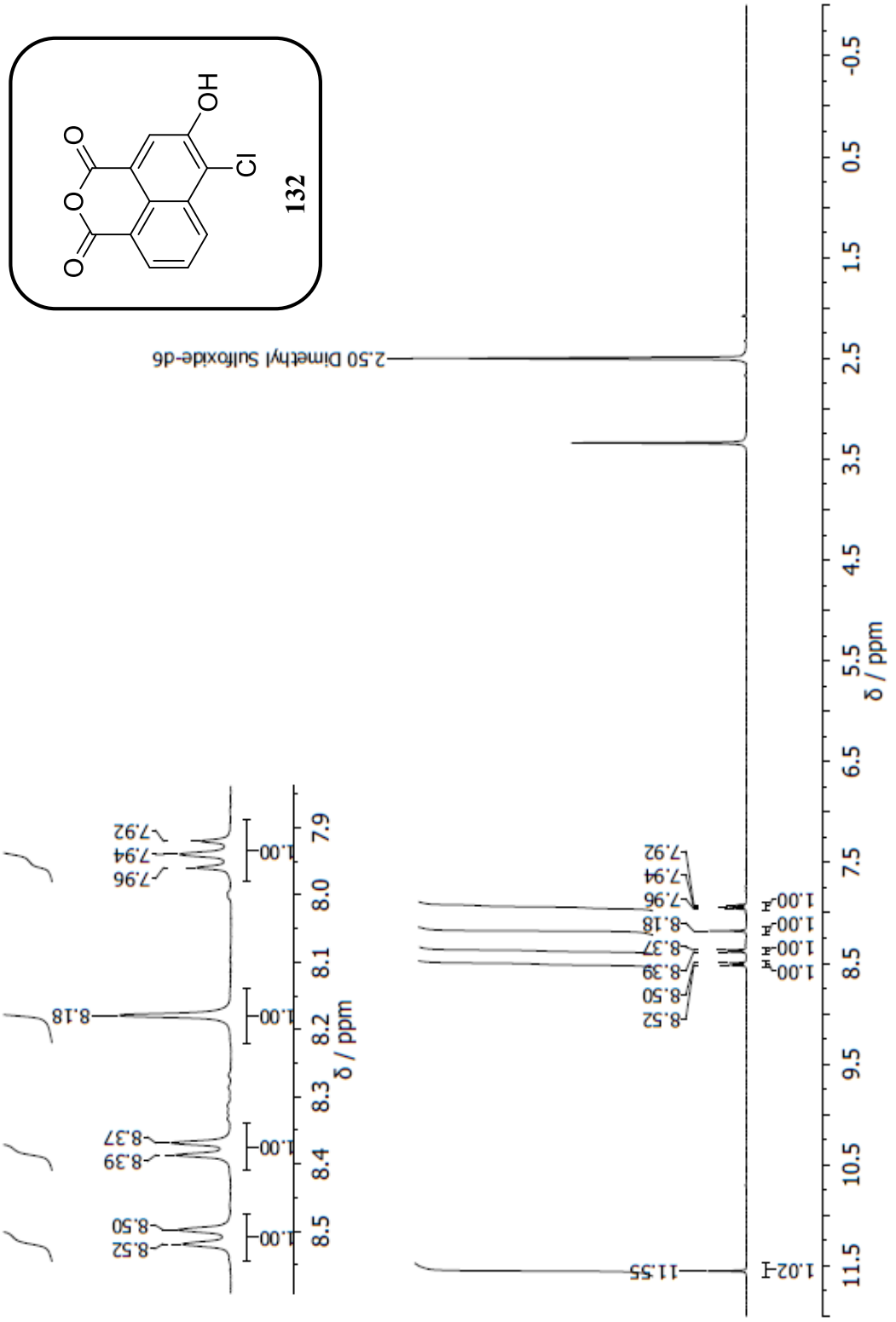

Figure 95: 400 MHz ^{1}H NMR spectrum of **132** in C_2D_6SO.

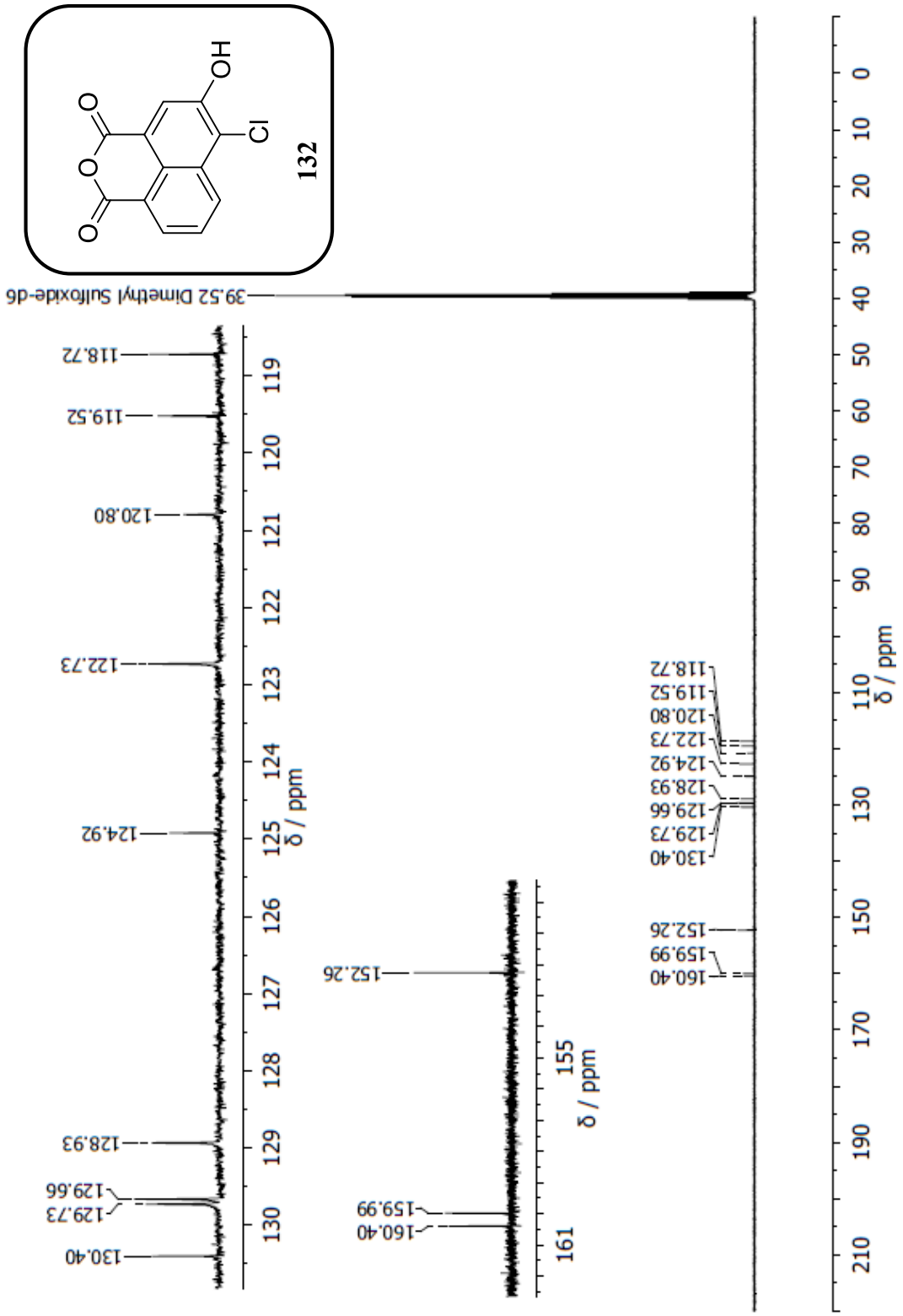

Figure 96: 101 MHz ^{13}C NMR spectrum of **132** in C_2D_6SO

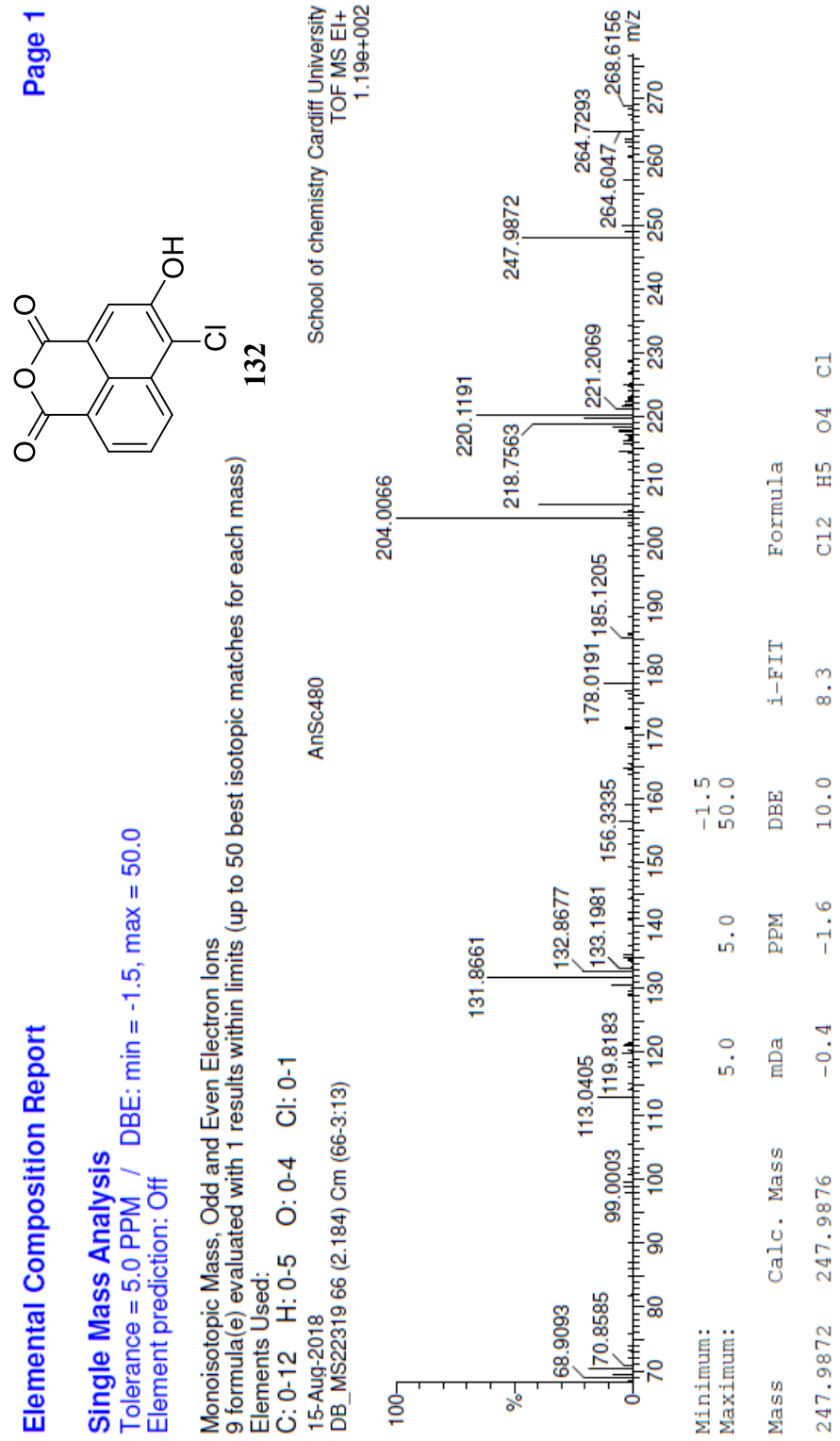

Figure 97: EI-HRSM spectrum of **132**.

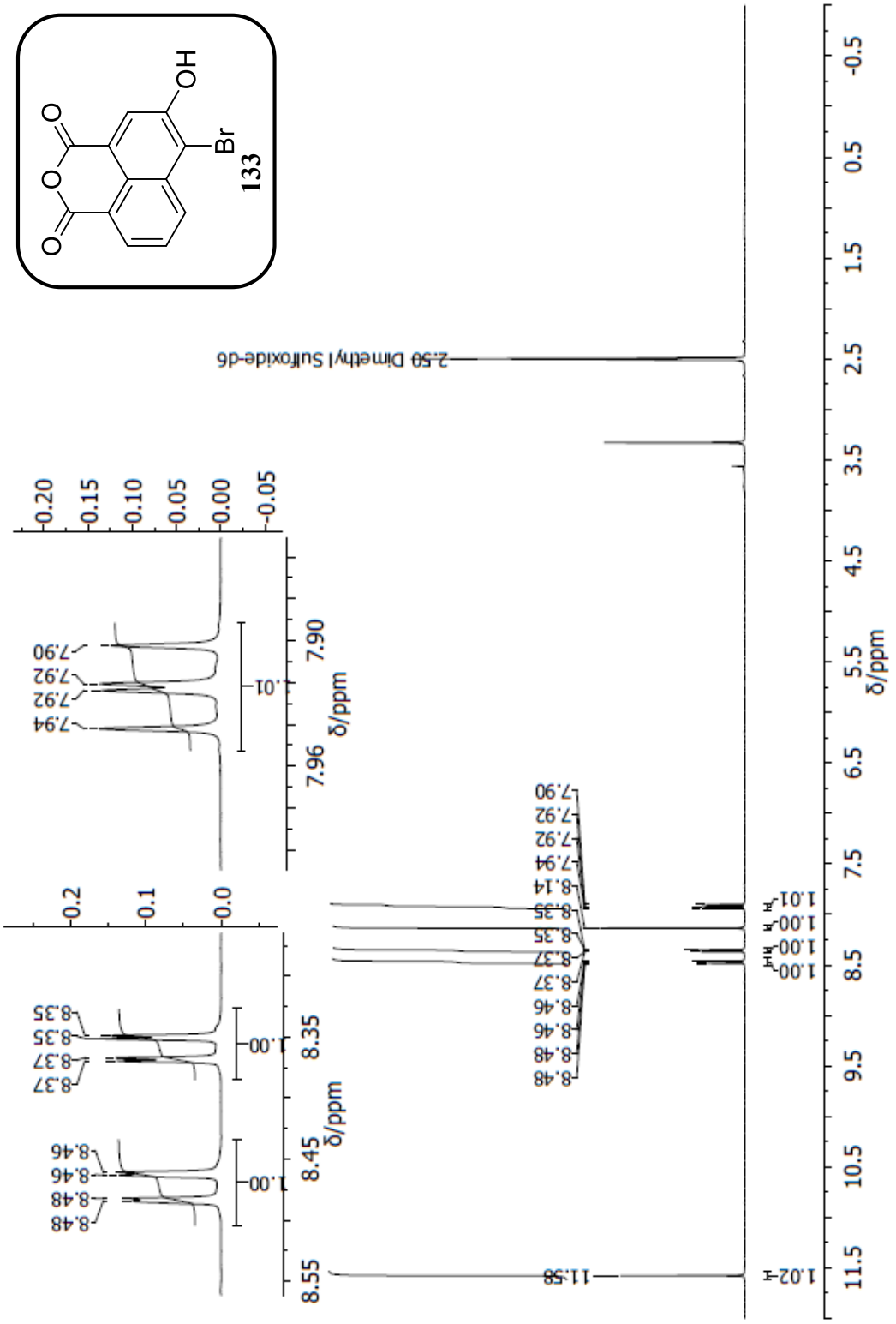

Figure 98: 400 MHz ^{1}H NMR spectrum of **133** in C_2D_6SO.

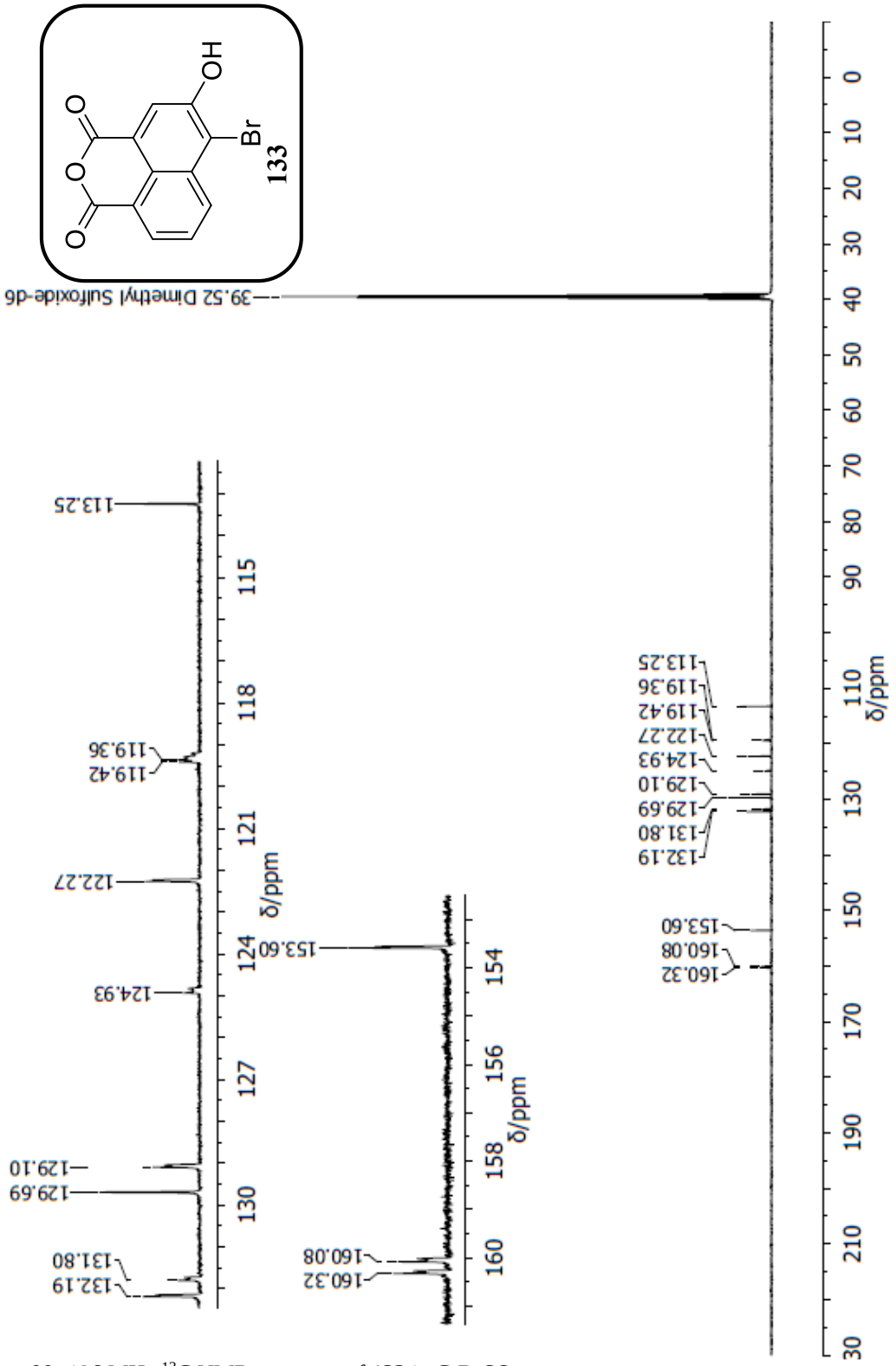

Figure 99: 126 MHz ^{13}C NMR spectrum of **133** in C_2D_6SO.

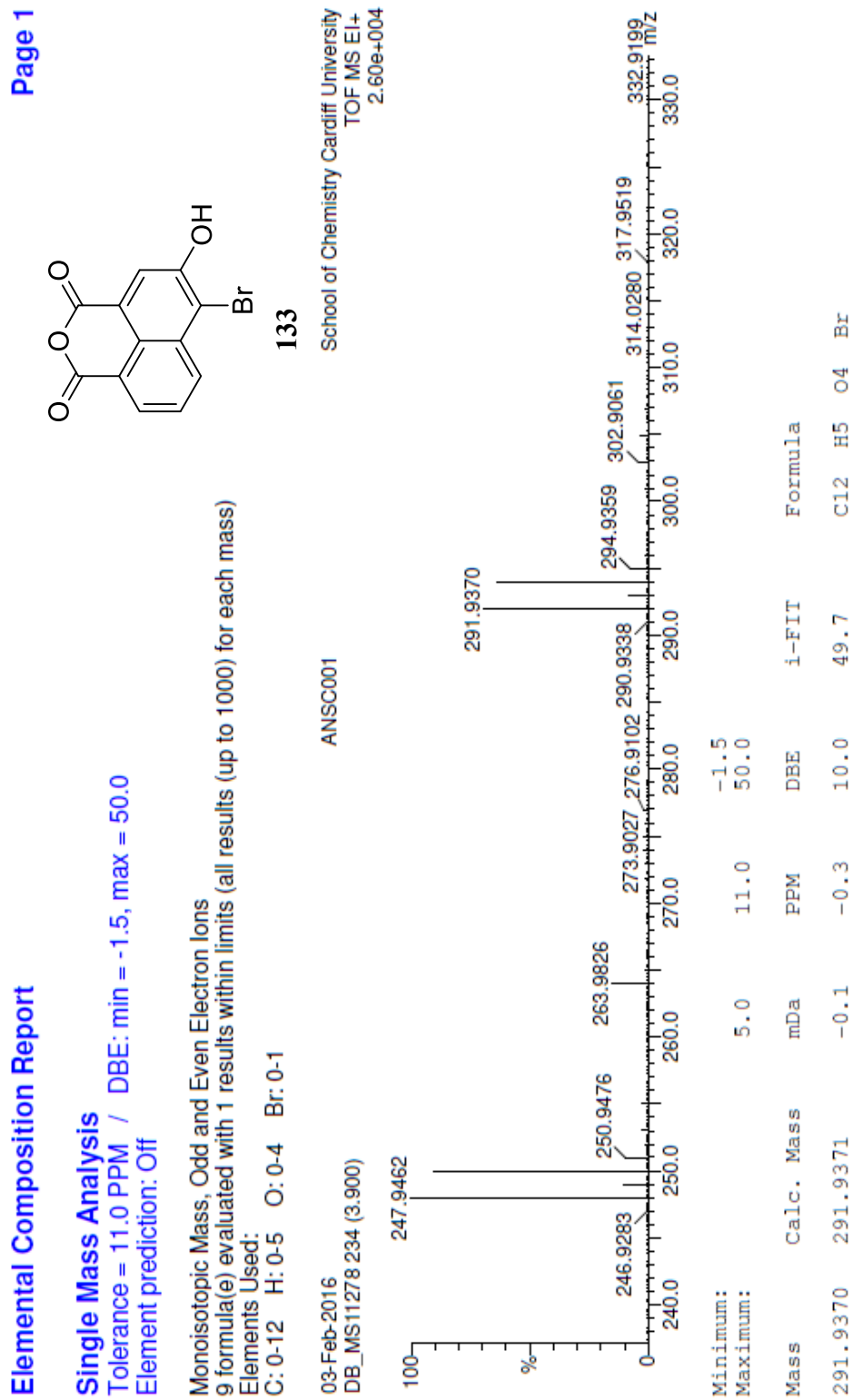

Figure 100: EI-HRSM spectrum of **133**.

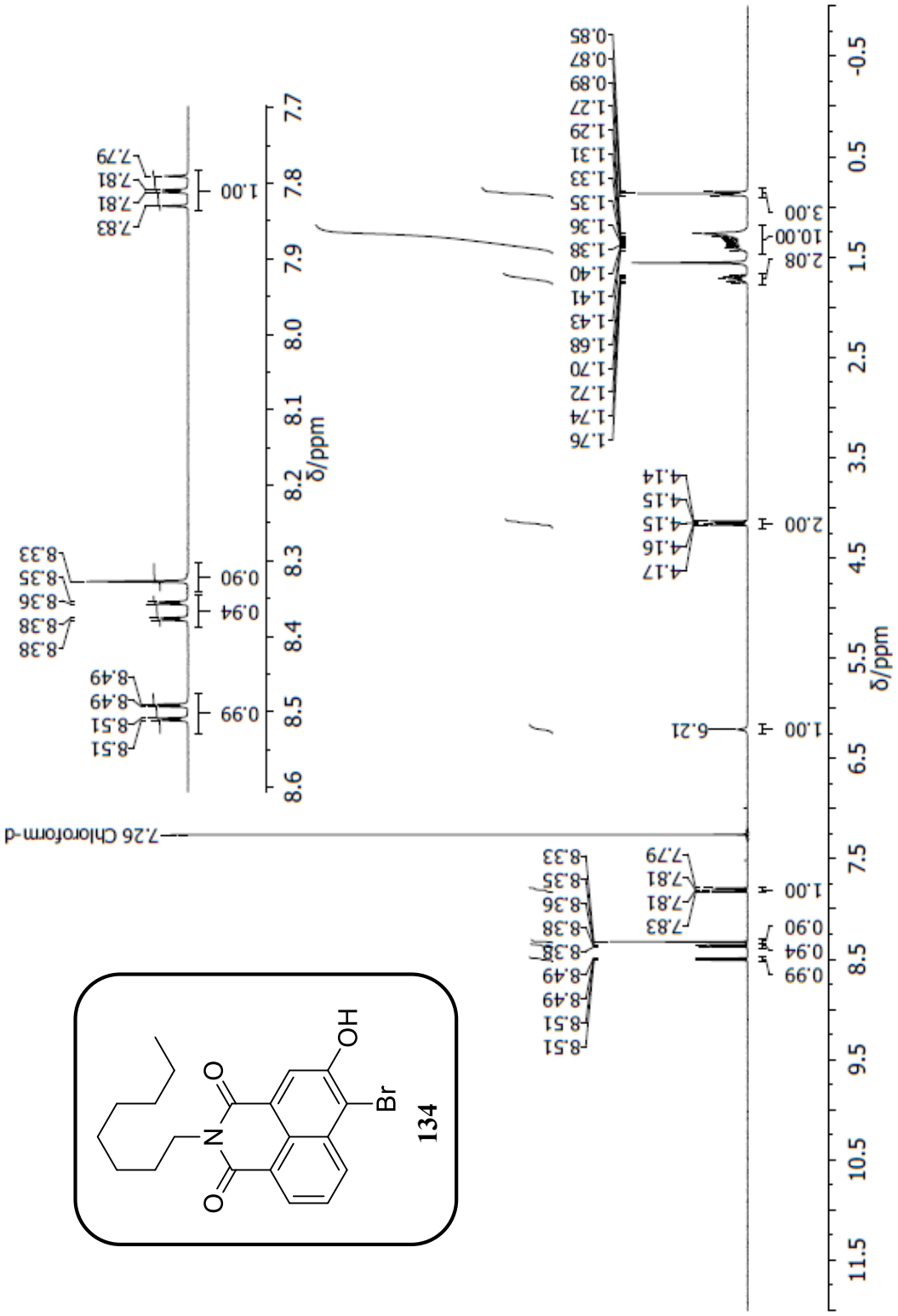

Figure 101: 400 MHz ^{1}H NMR spectrum of **134** in $CDCl_3$.

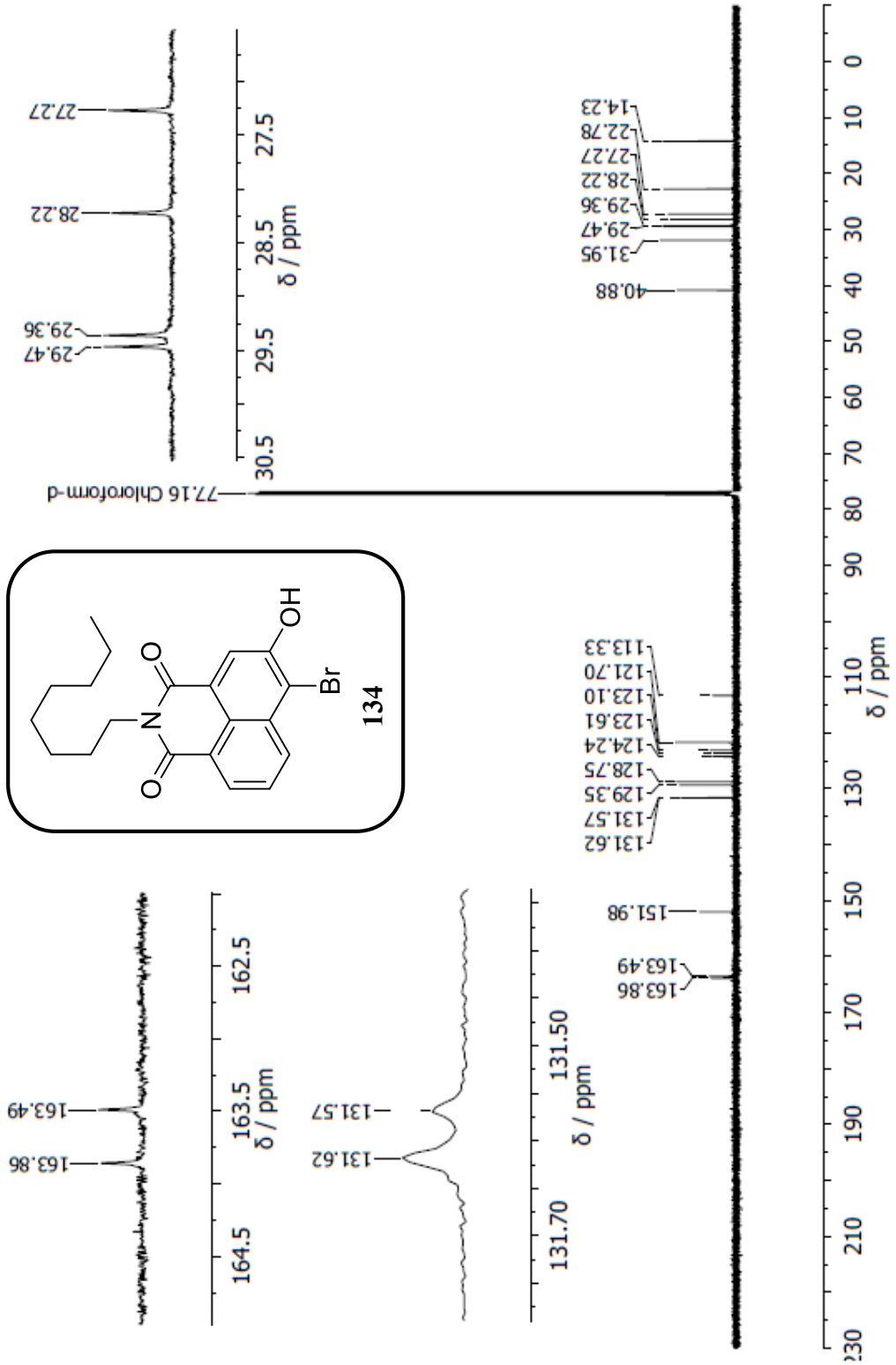

Figure 102: 126 MHz ^{13}C NMR spectrum of **134** in $CDCl_3$.

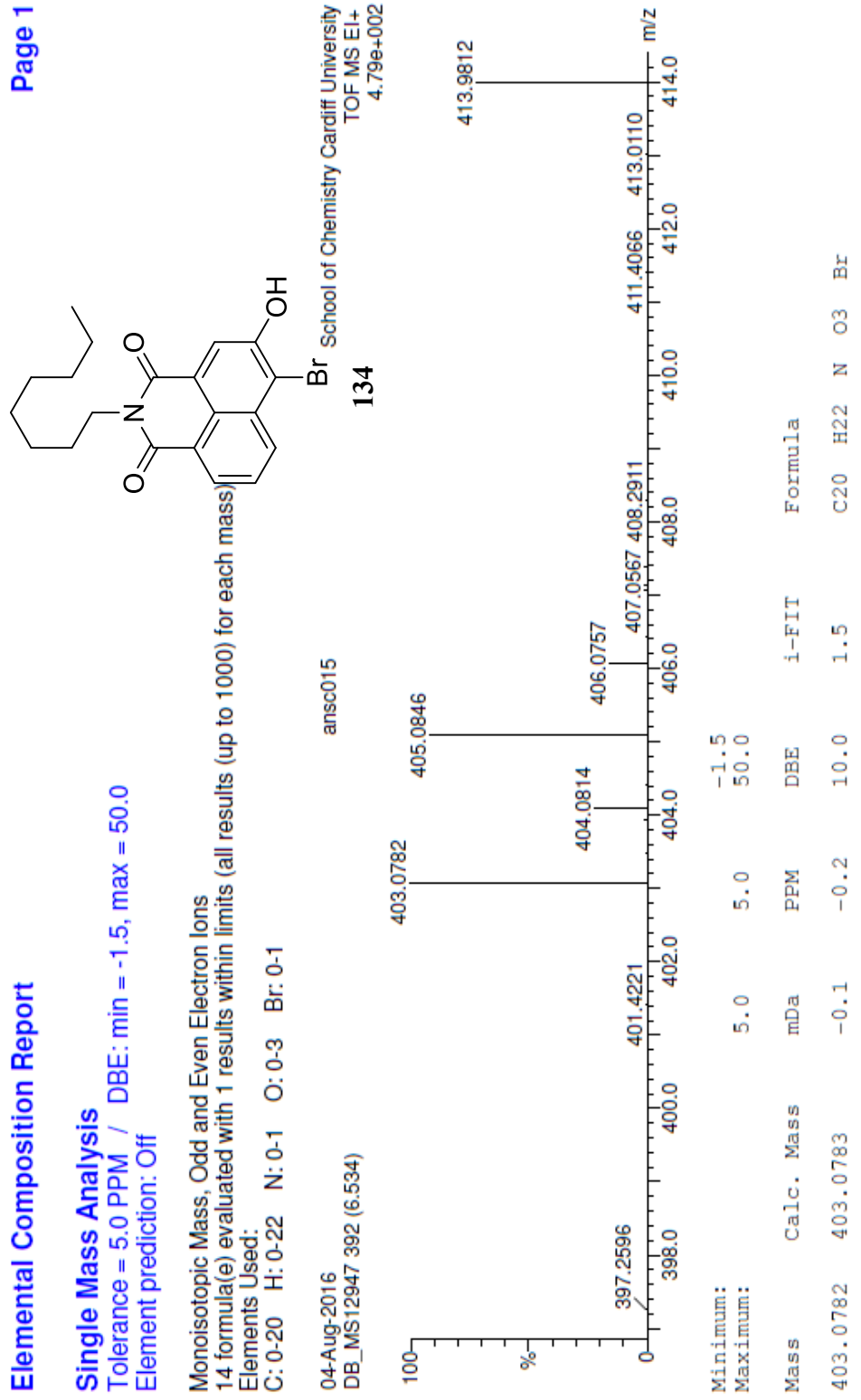

Figure 103: EI-HRSM spectrum of **134**.

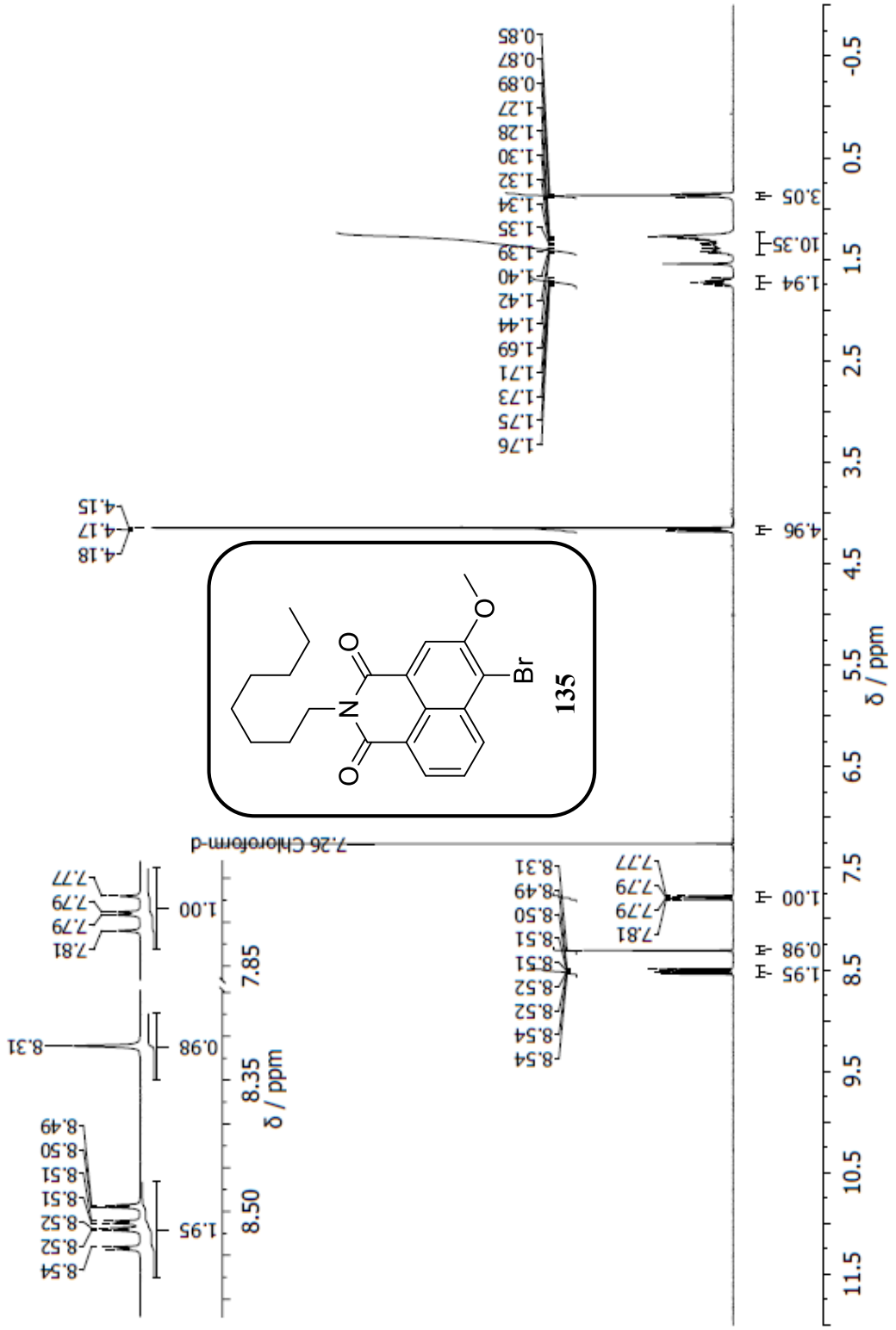

Figure 104: 400 MHz ^{1}H NMR spectrum of **135** in $CDCl_3$.

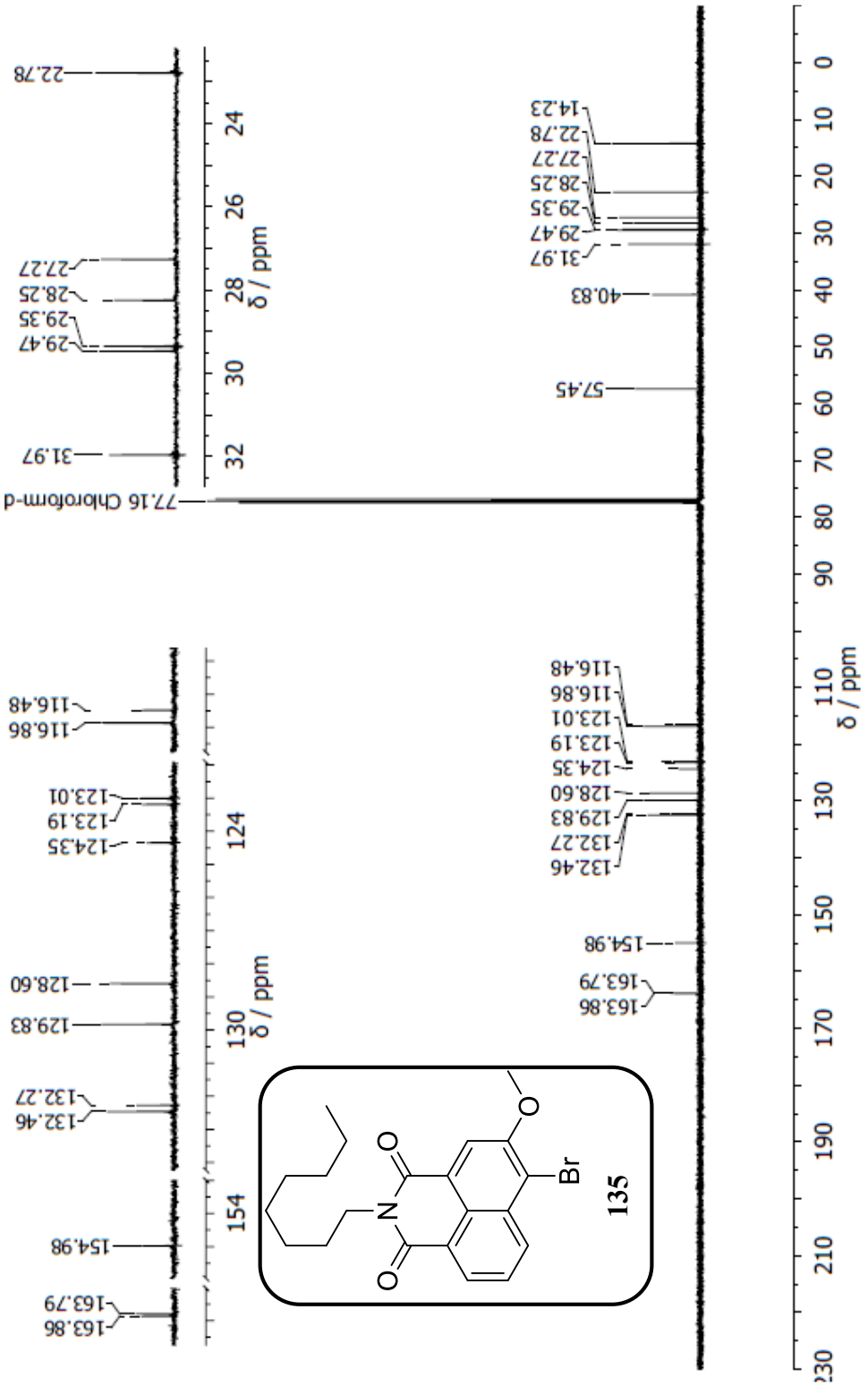

Figure 105: 126 MHz ^{13}C NMR spectrum of **135** in $CDCl_3$.

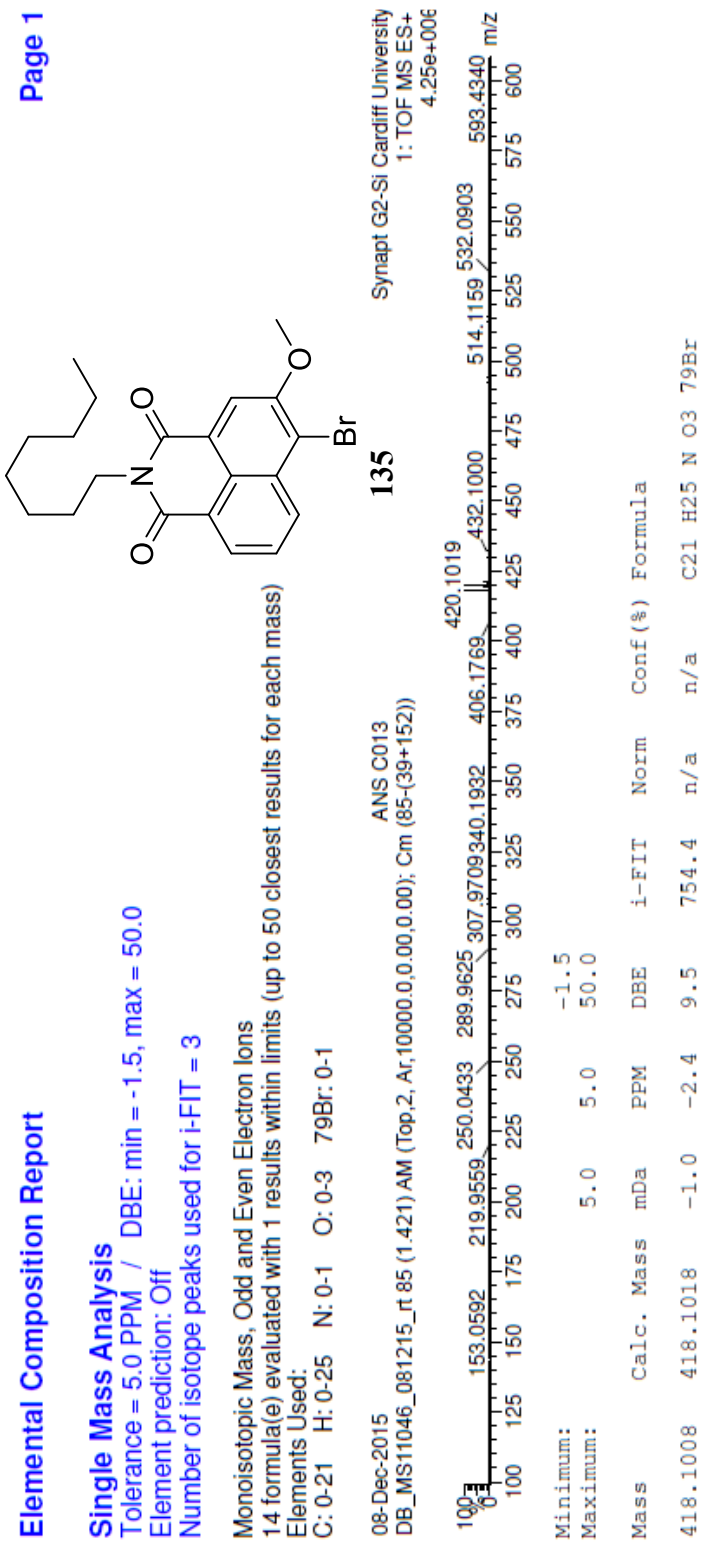

Figure 106: EI-HRSM spectrum of **135**.

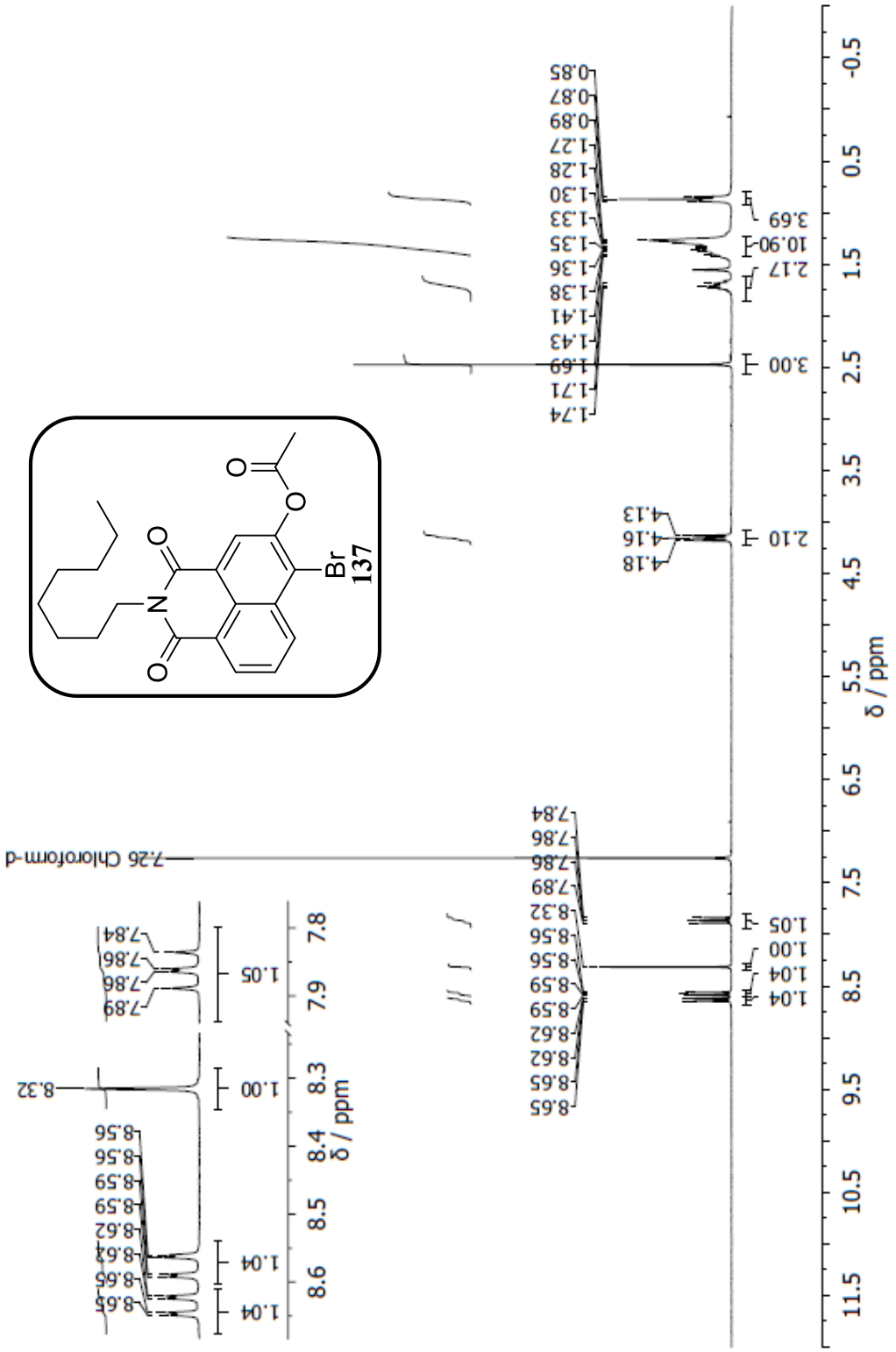

Figure 107: 300 MHz ^{1}H NMR spectrum of **137** in $CDCl_3$.

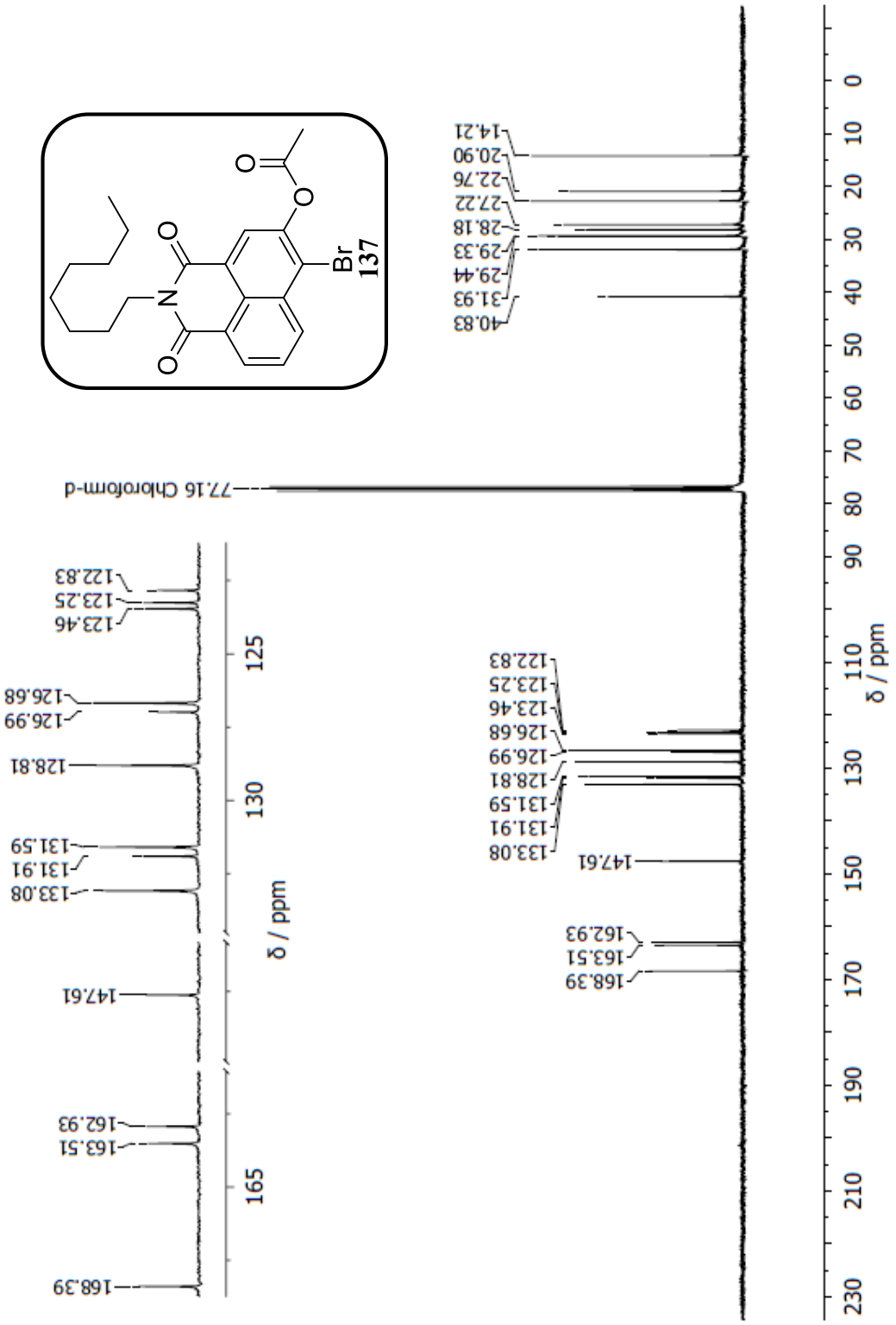

Figure 108: 75 MHz ^{13}C NMR spectrum of **137** in $CDCl_3$.

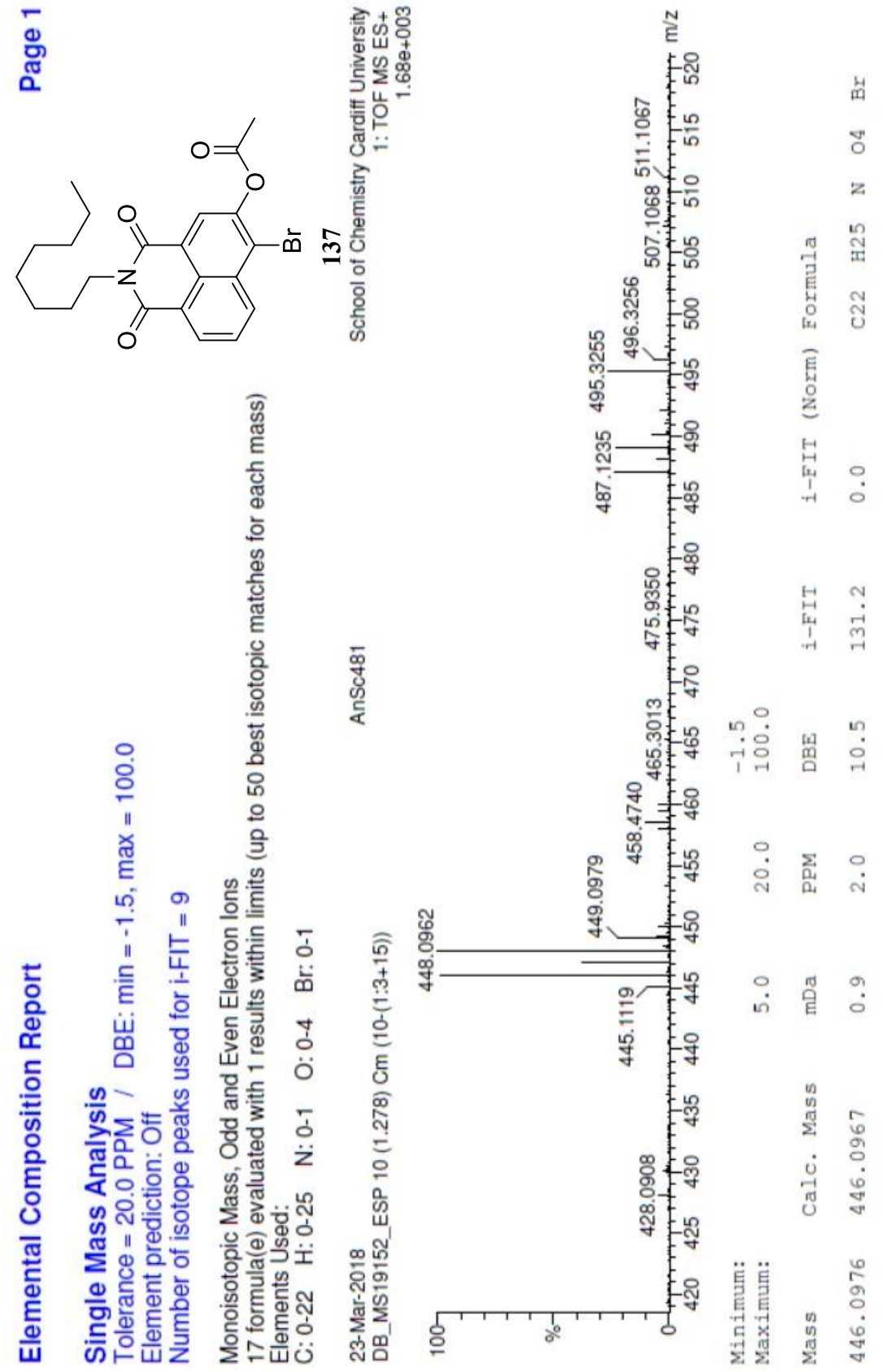

Figure 109: ESI-HRMS spectrum of **137**.

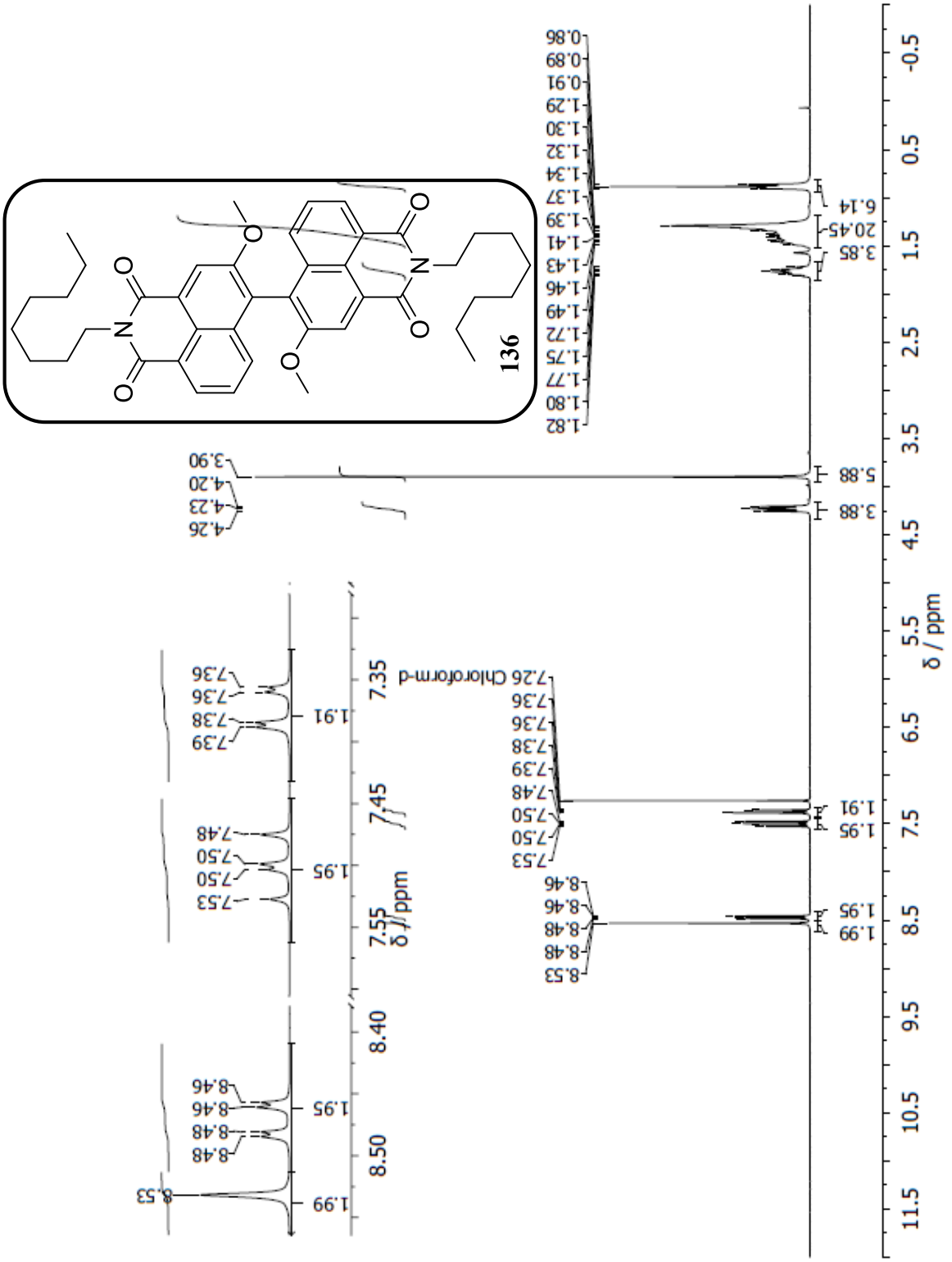

Figure 110: 300 MHz ^{1}H NMR spectrum of **136** in $CDCl_3$.

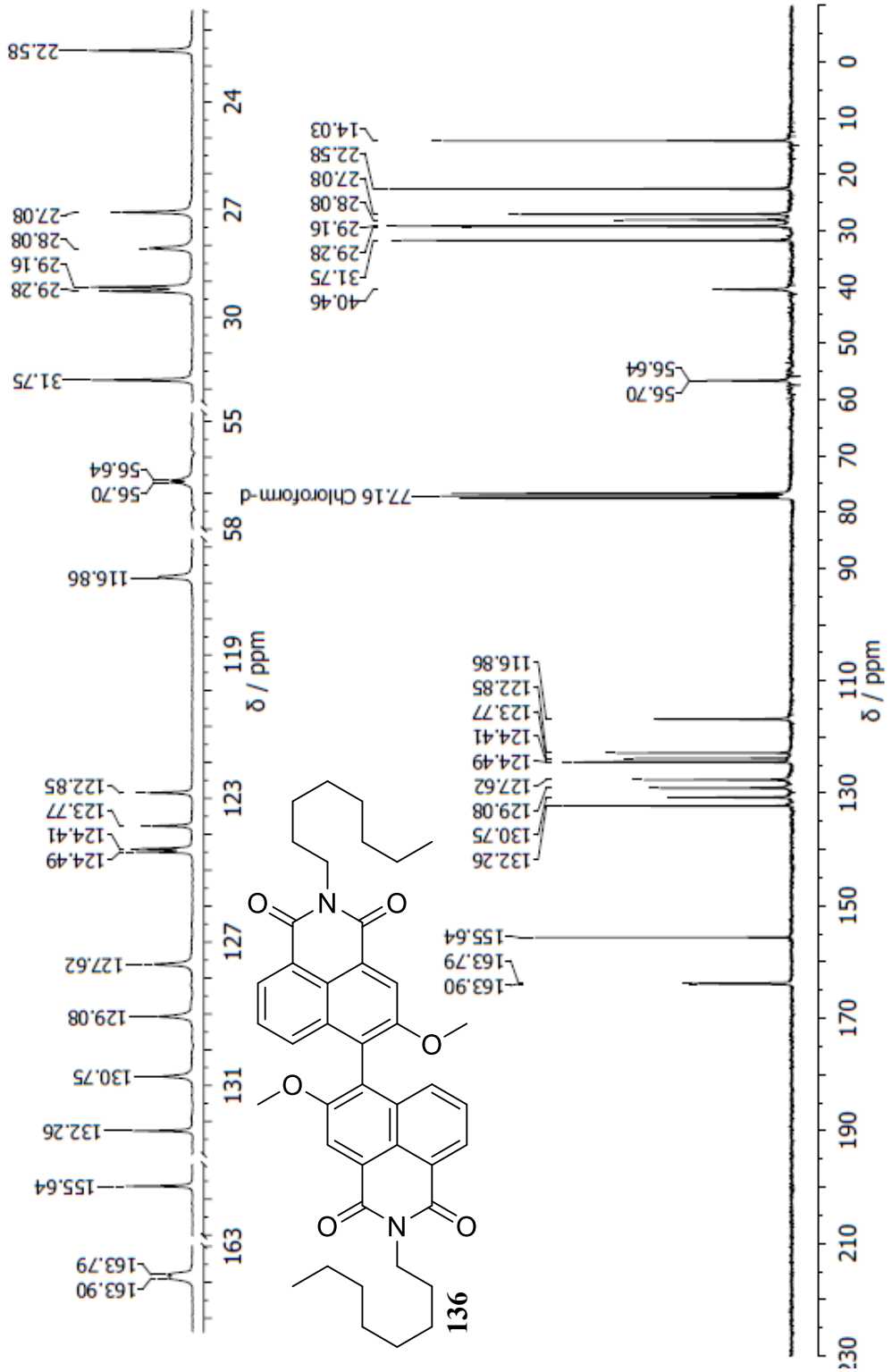

Figure 111: 75 MHz ^{13}C NMR spectrum of **136** in $CDCl_3$.

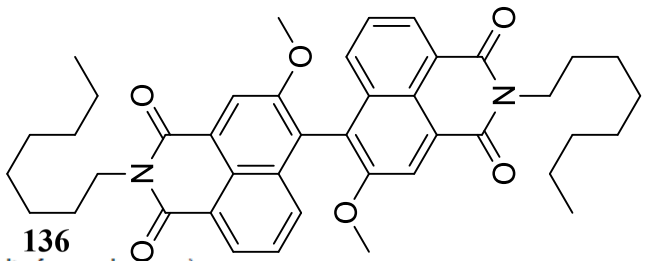

136

Elemental Composition Report

Single Mass Analysis

Tolerance = 5.0 PPM / DBE: min = -1.5, max = 100.0
Element prediction: Off
Number of isotope peaks used for i-FIT = 3

Monoisotopic Mass, Odd and Even Electron Ions
13 formula(e) evaluated with 1 results within limits (up to 50 closest results for each mass)
Elements Used:
C: 0-42 H: 0-49 N: 0-2 O: 0-6

12-Jan-2016 ANSC006 Synapt G2-Si Cardiff University
DB_MS11147 79 (1.365) AM2 (Ar,20000.0,1570.68,0.00); ABS; Cm (12:102) TOF MS LD+
6.26e+007

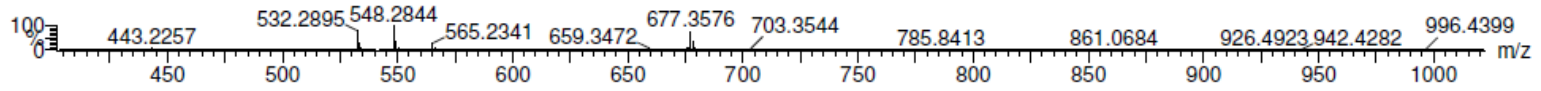

Minimum:				-1.5				
Maximum:		5.0	5.0	100.0				
Mass	Calc. Mass	mDa	PPM	DBE	i-FIT	Norm	Conf(%)	Formula
677.3576	677.3591	-1.5	-2.2	19.5	497.4	n/a	n/a	C42 H49 N2 O6

Figure 112: ESI-HRMS spectrum of **136**.

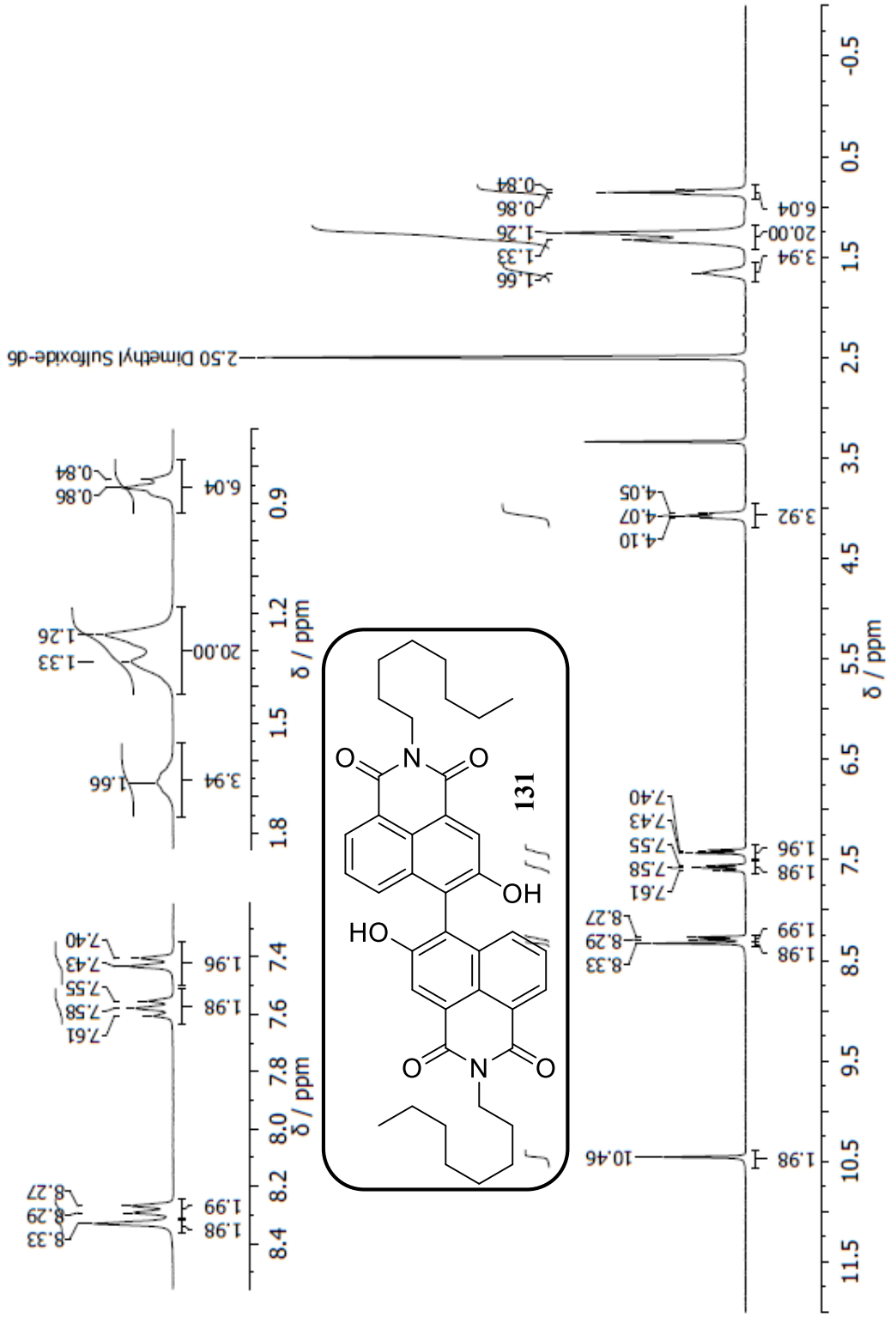

Figure 113: 300 MHz ^{1}H NMR spectrum of **131** in C_2D_6SO.

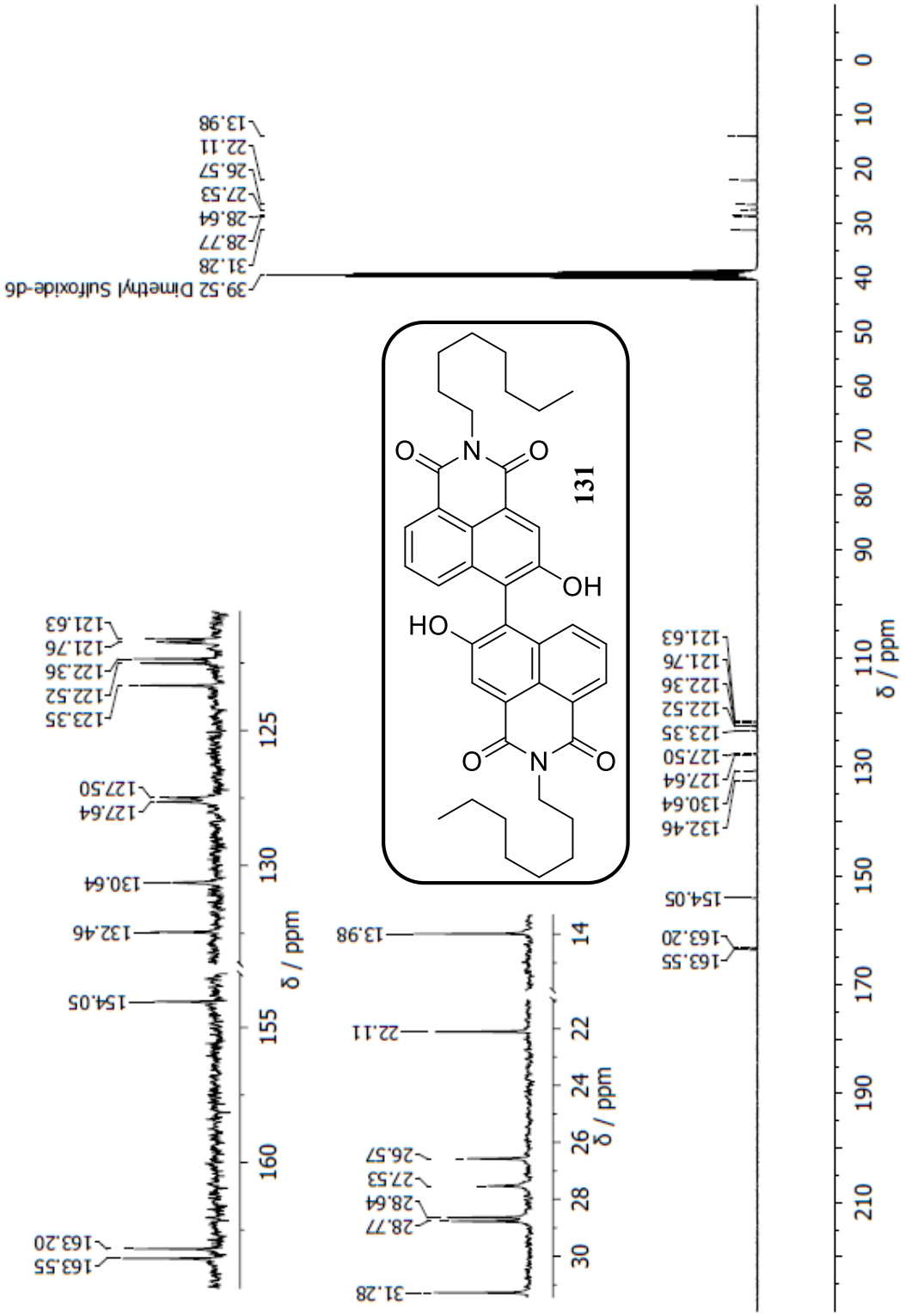

Figure 114: 75 MHz ^{13}C NMR spectrum of **131** in C_2D_6SO.

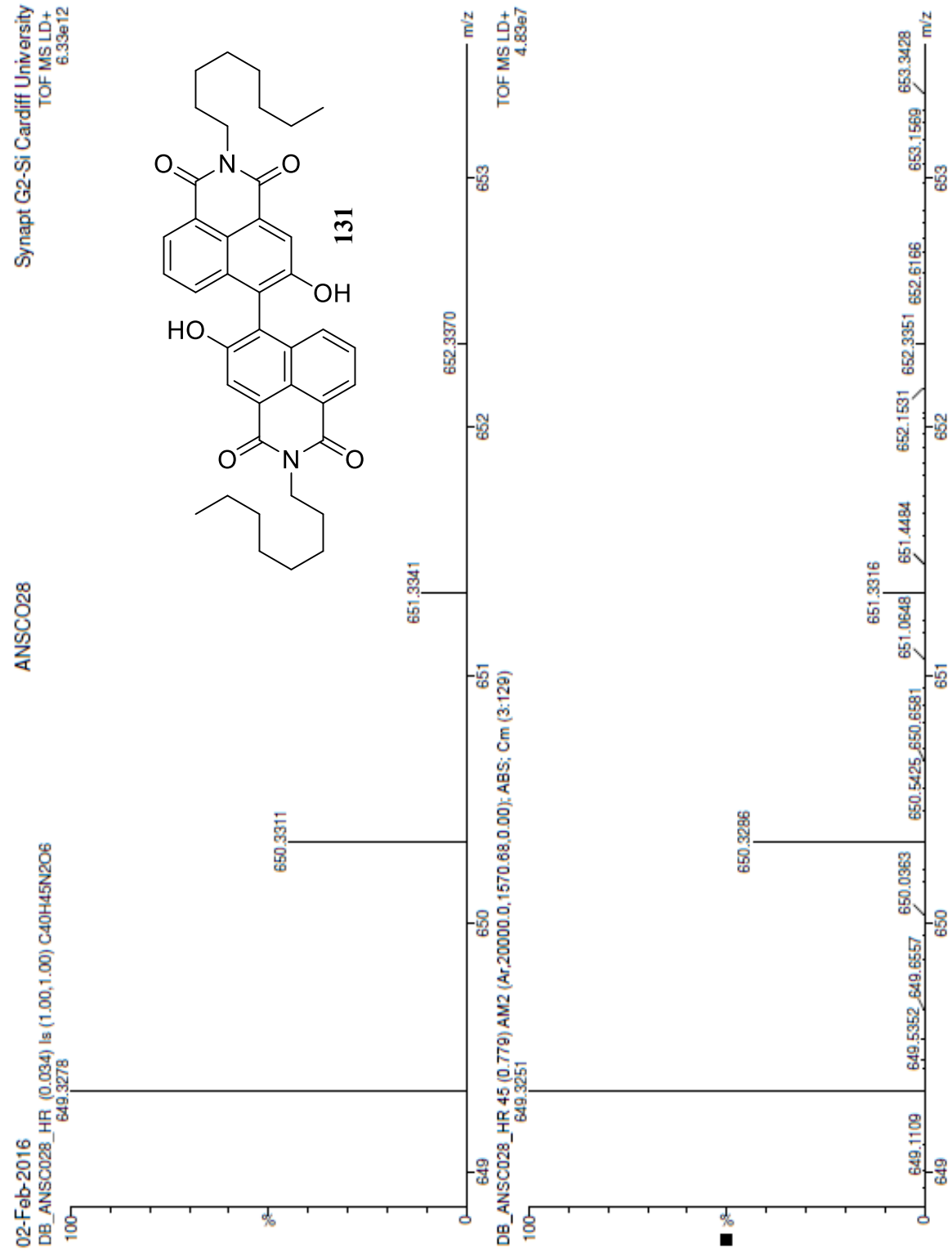

Figure 115: MALDI-HRMS spectrum of **131**.

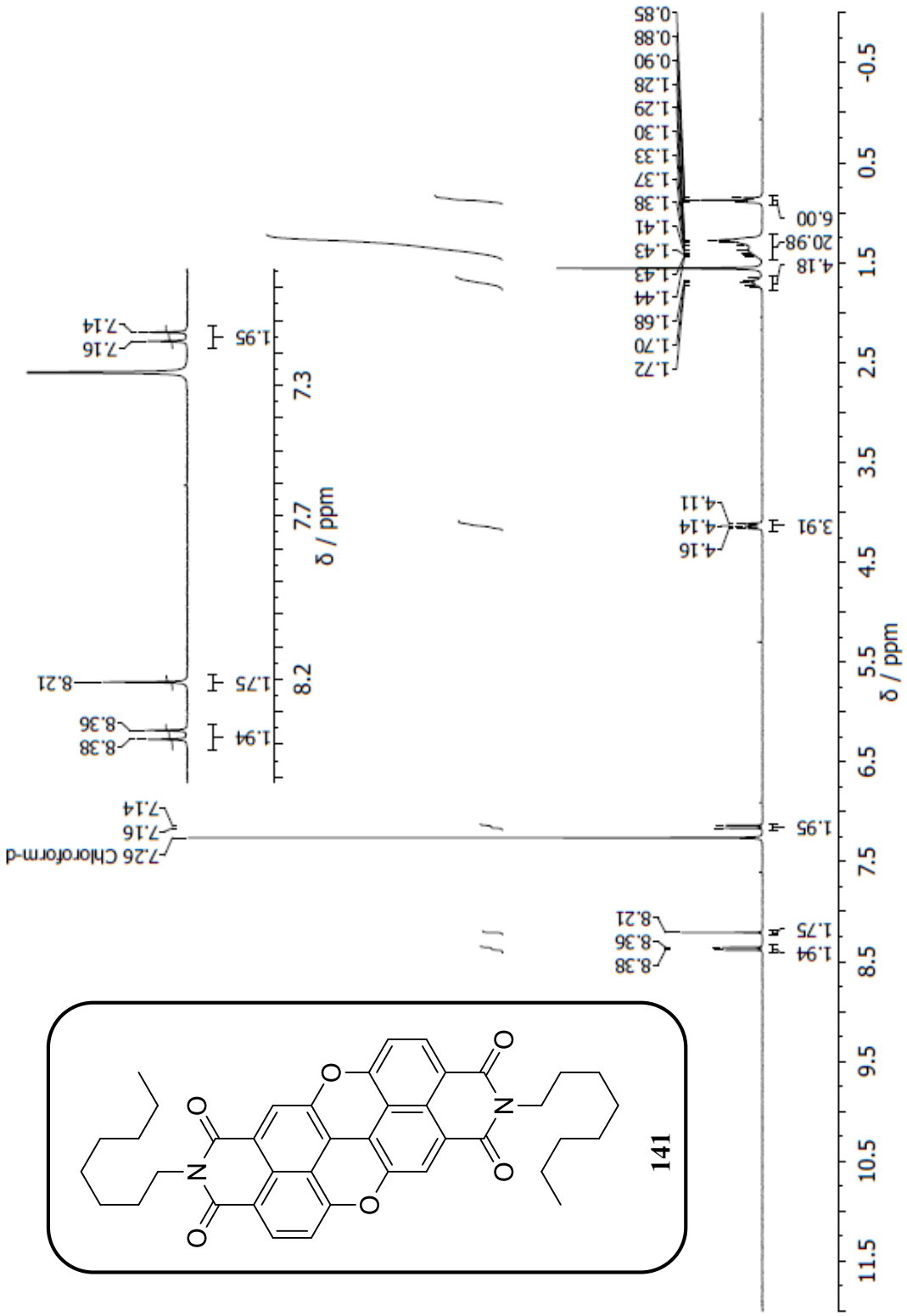

Figure 116: 300 MHz ^{1}H NMR spectrum of **141** in $CDCl_3$.

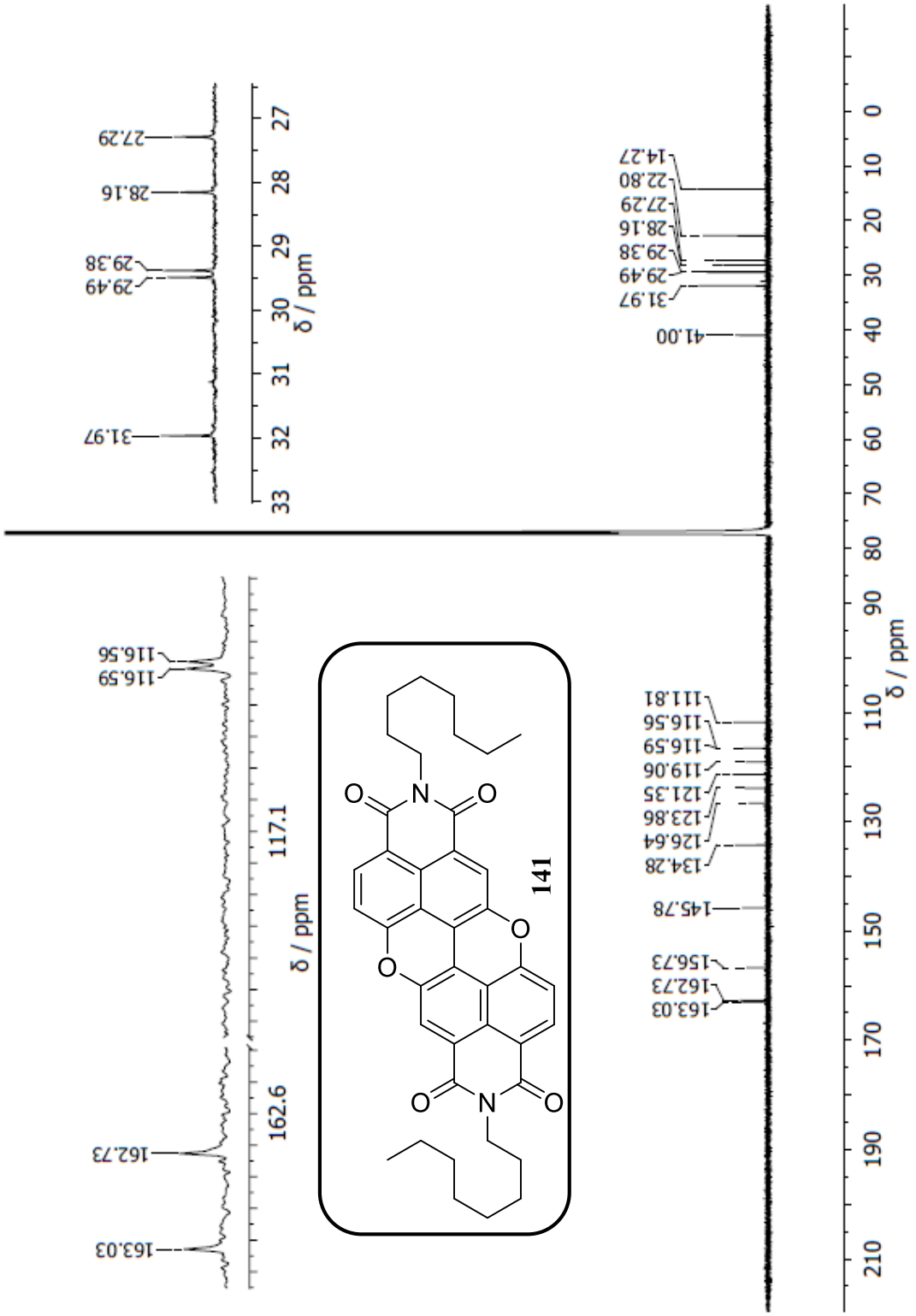

Figure 117: 151 MHz ^{13}C NMR spectrum of **141** in $CDCl_3$.

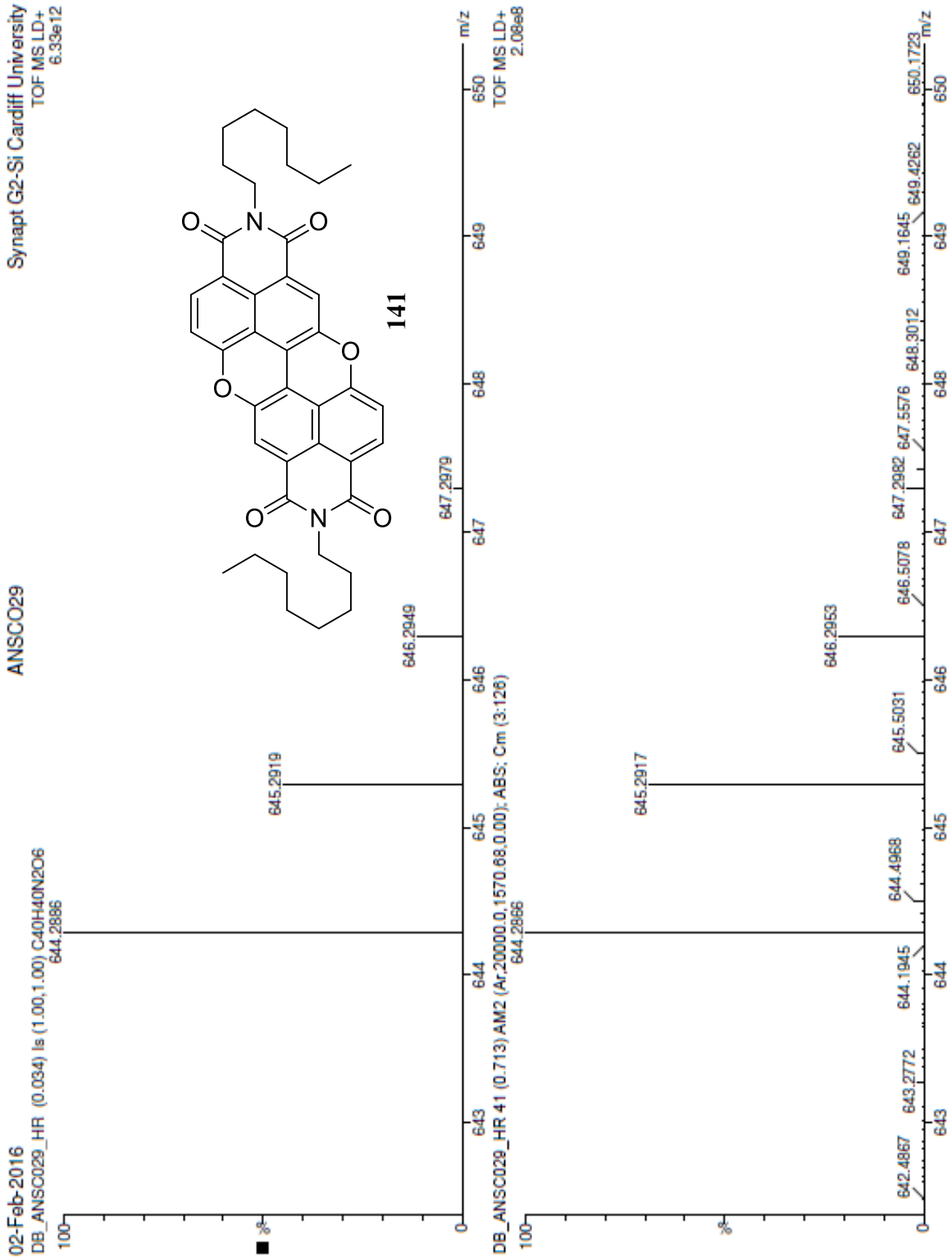

Figure 118: MALDI-HRMS spectrum of **141**.

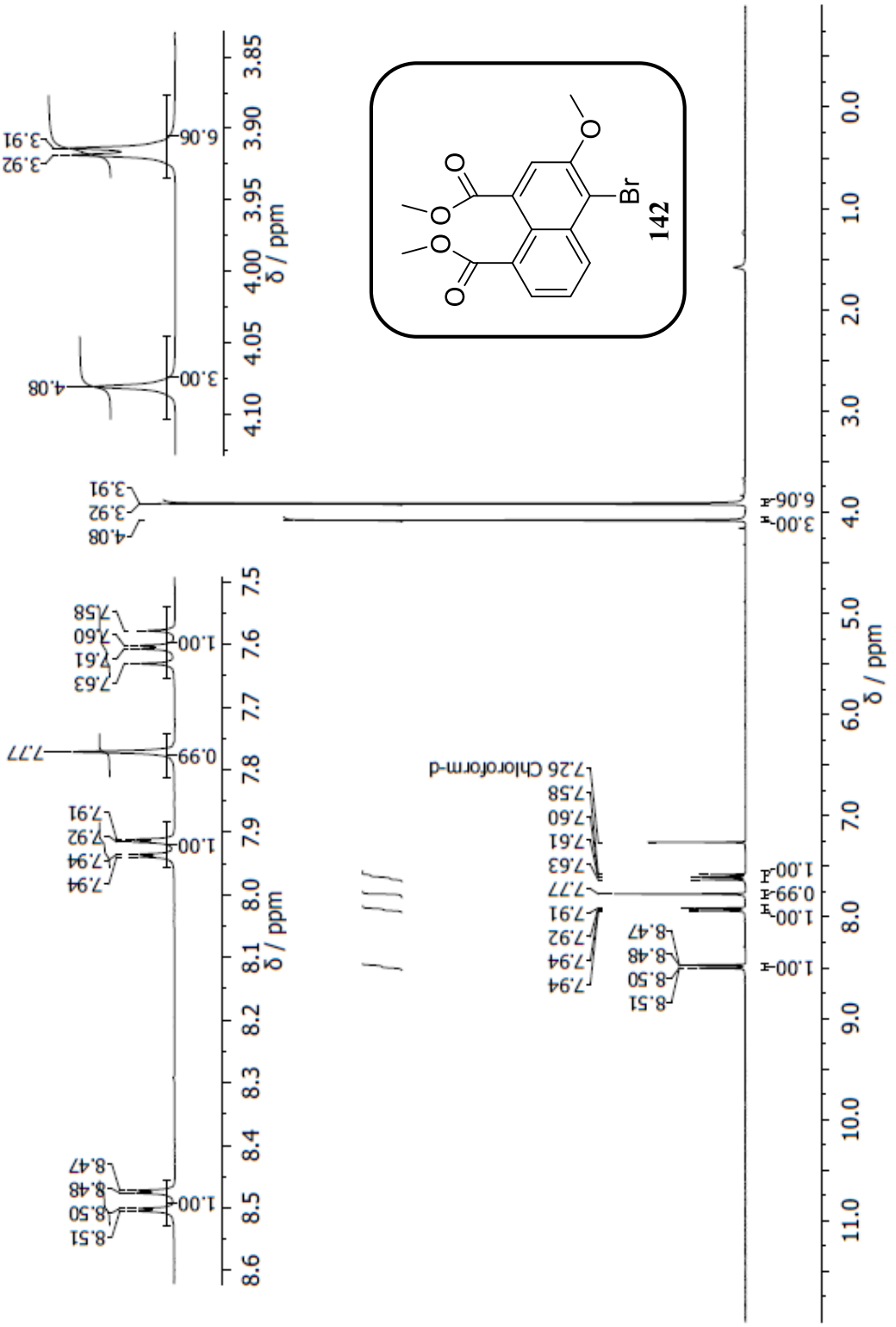

Figure 119: 300 MHz ^{1}H NMR spectrum of **142** in $CDCl_3$.

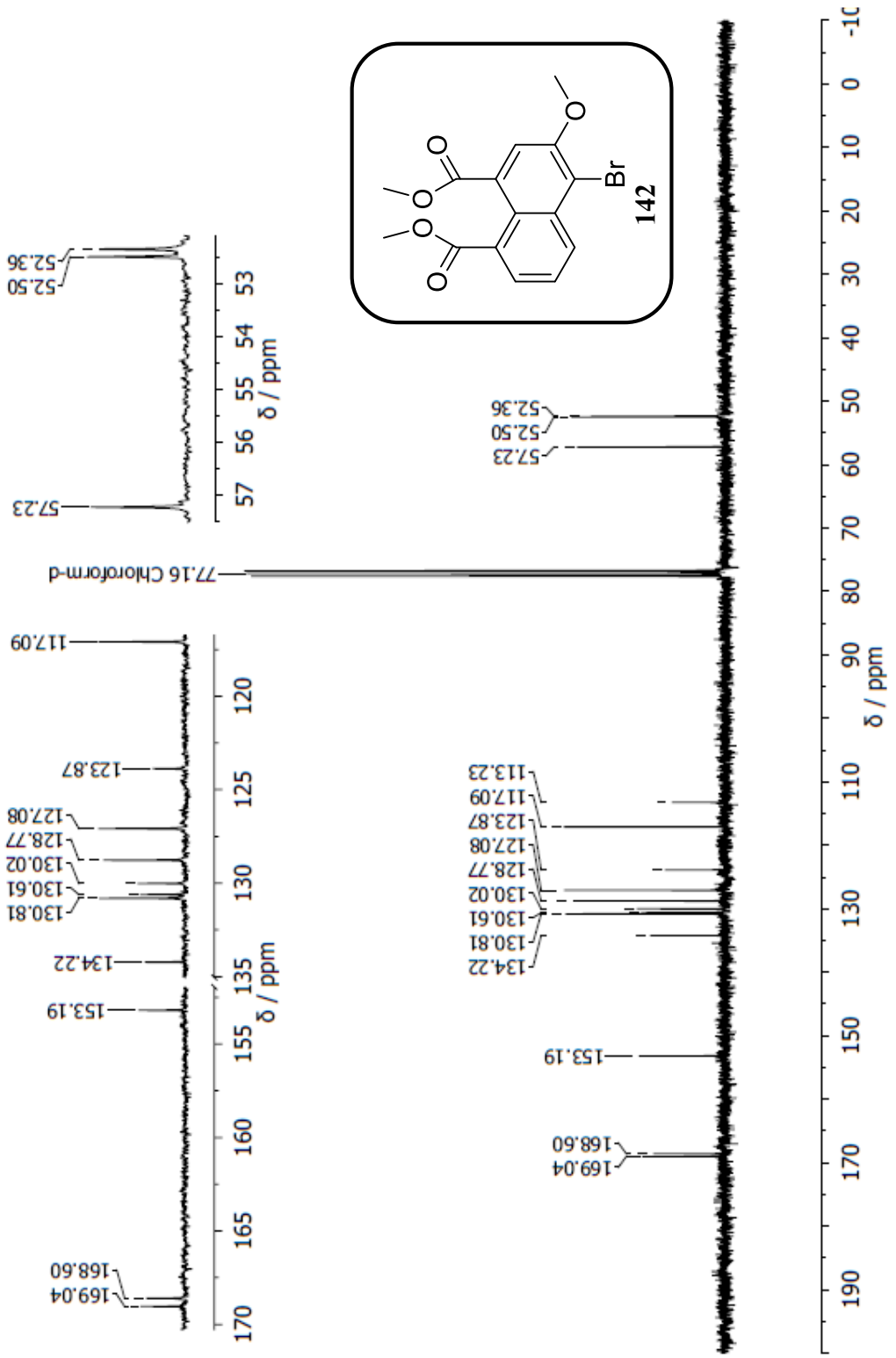

Figure 120: 75 MHz ^{13C} NMR spectrum of **142** in $CDCl_3$.

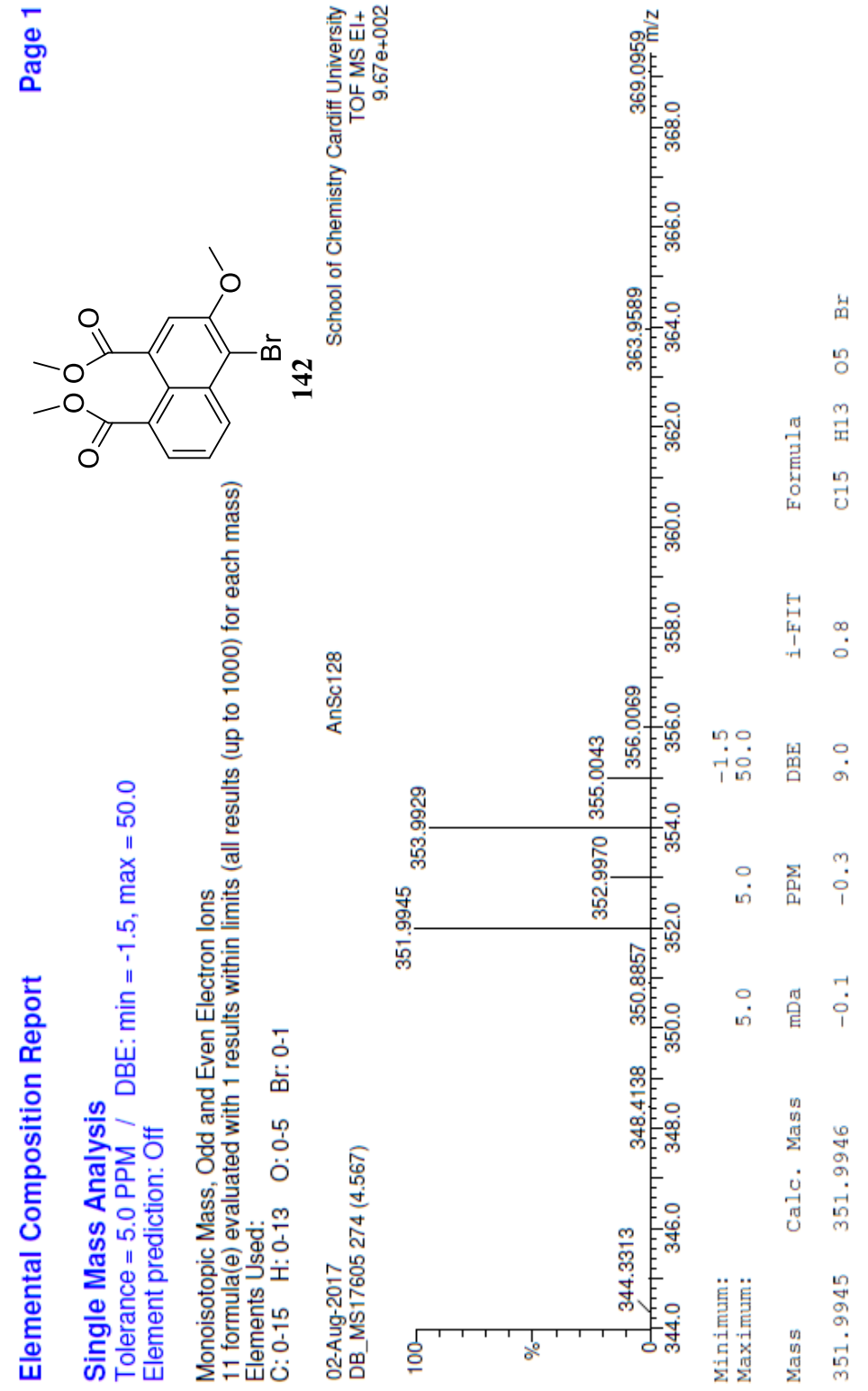

Figure 121: EI-HRMS spectrum of **142**.

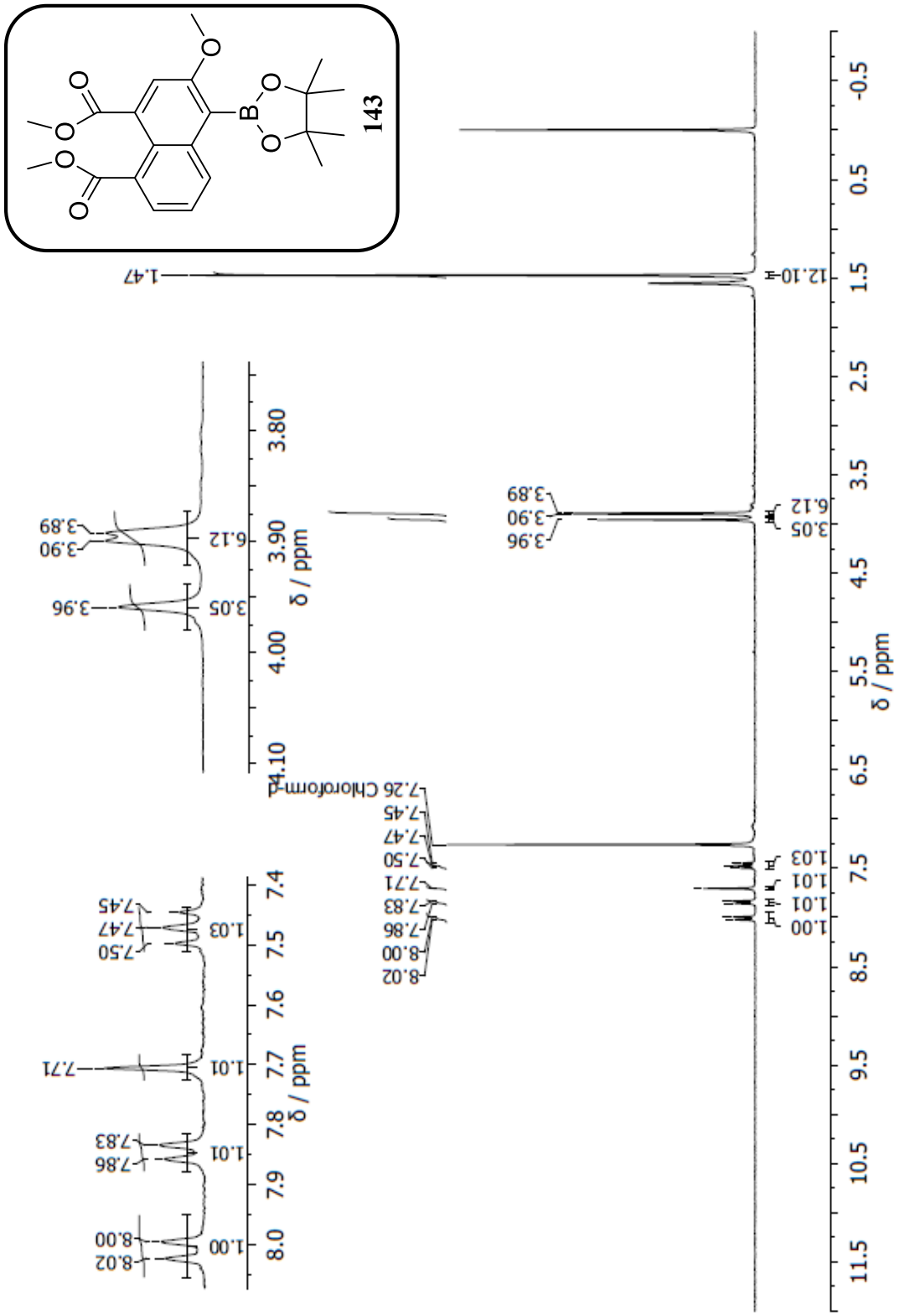

Figure 122: 300 MHz ^{1}H NMR spectrum of **143** in $CDCl_3$.

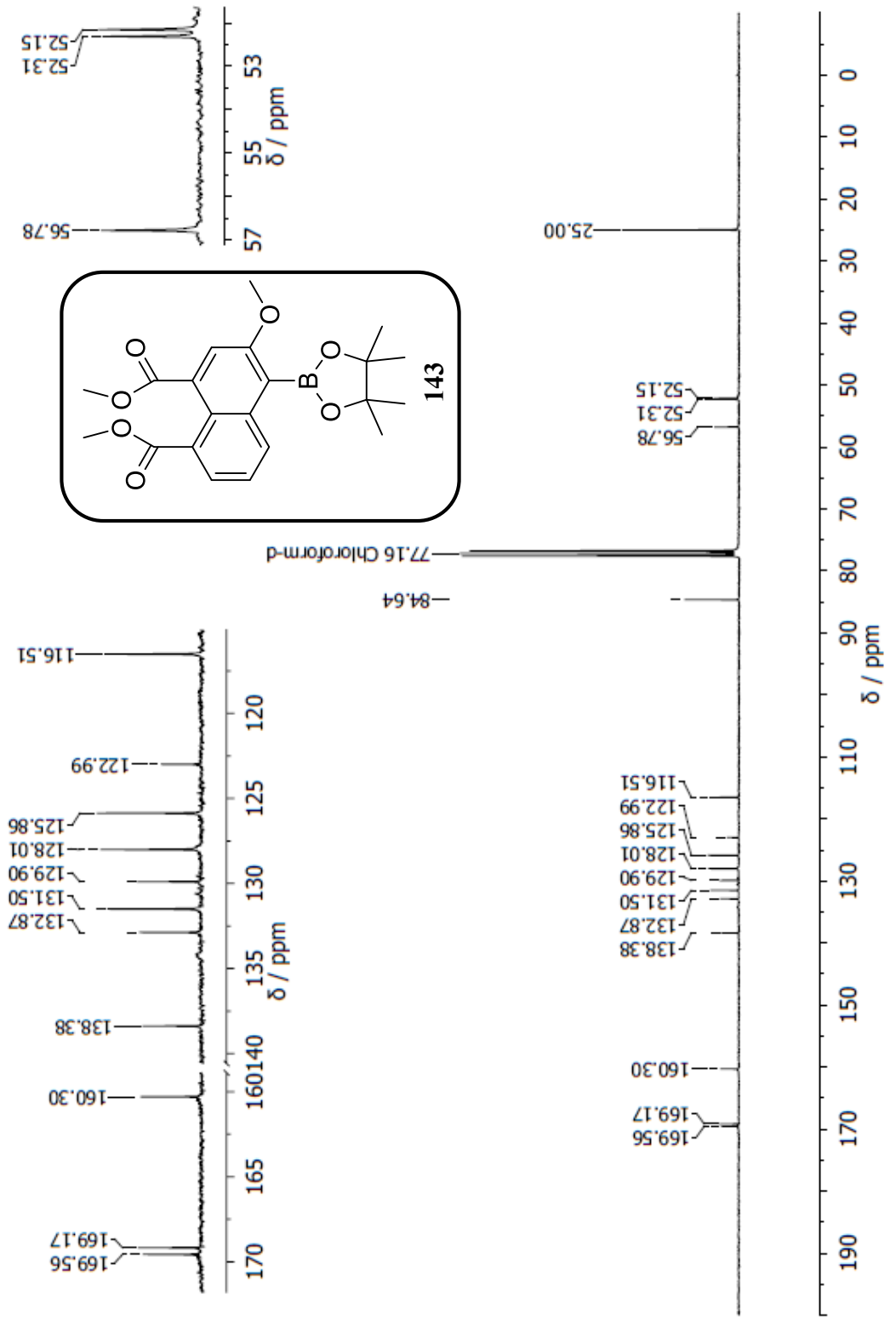

Figure 123: 75 MHz ^{13}C NMR spectrum of **143** in $CDCl_3$.

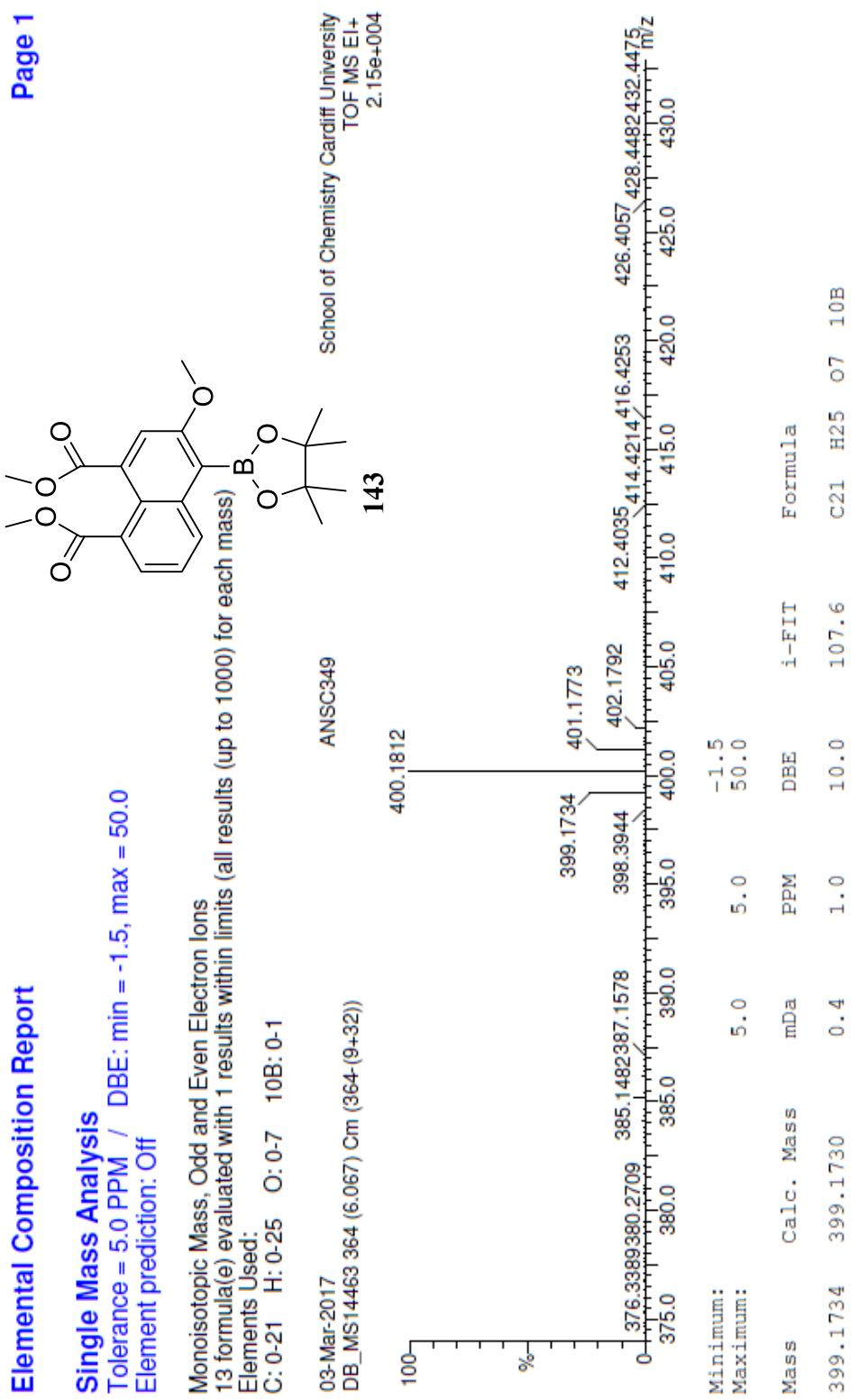

Figure 124: EI-HRMS spectrum of **143**.

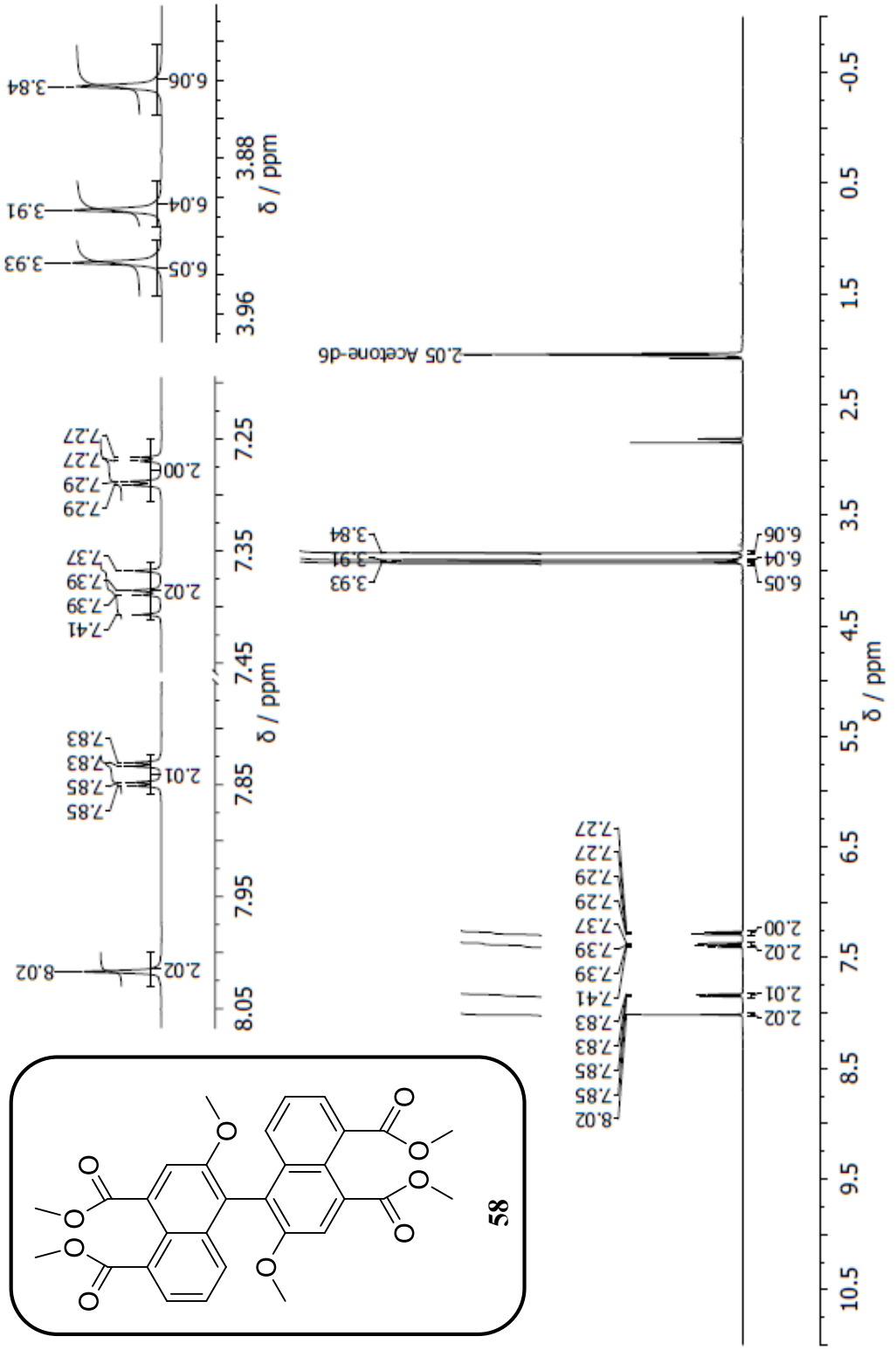

Figure 125: 400 MHz ^{1}H NMR spectrum of **58** in $(CD_3)_2CO$.

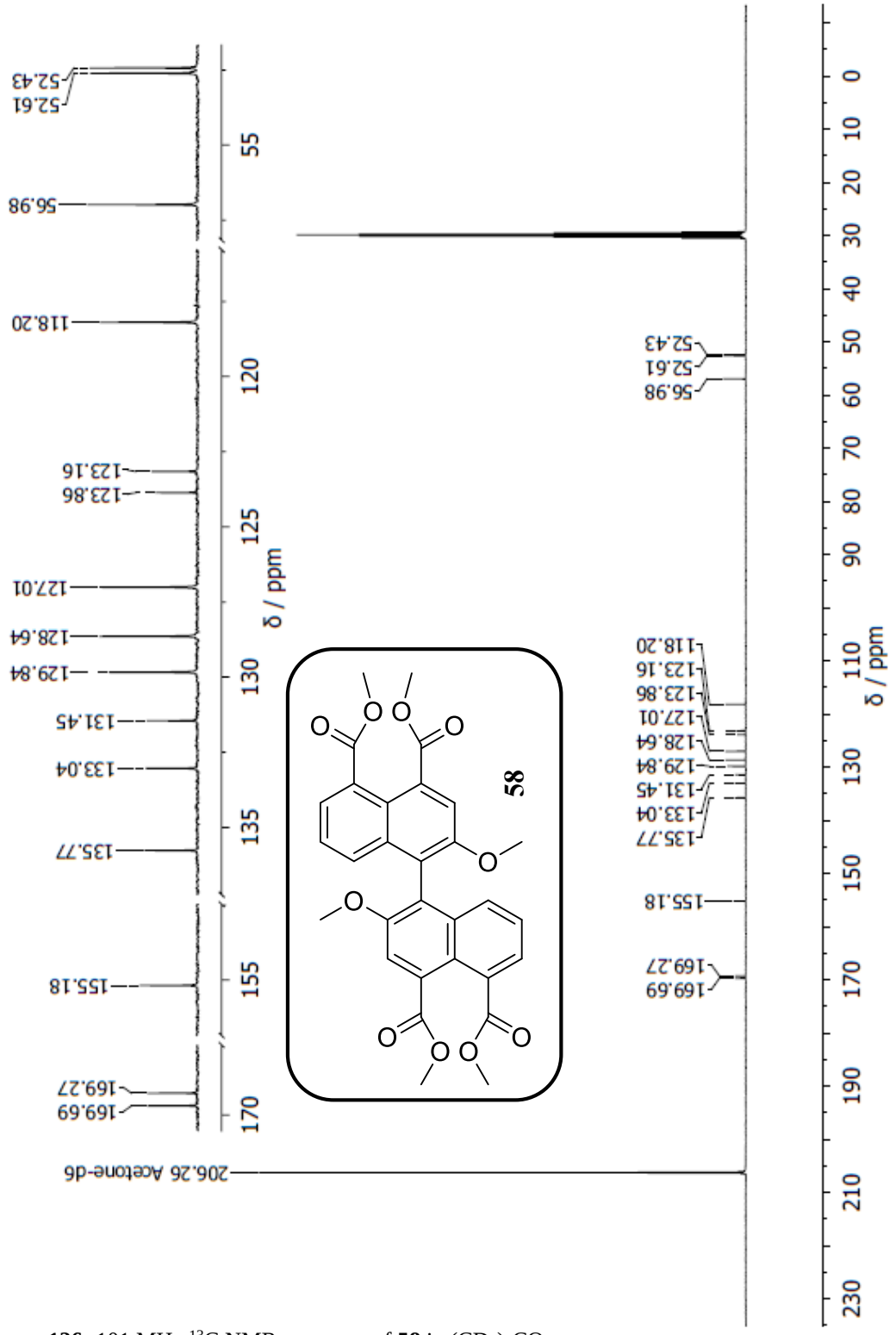

Figure 126: 101 MHz ^{13}C NMR spectrum of **58** in $(CD_3)_2CO$.

Figure 127: APCI-HRMS spectrum of **58**.

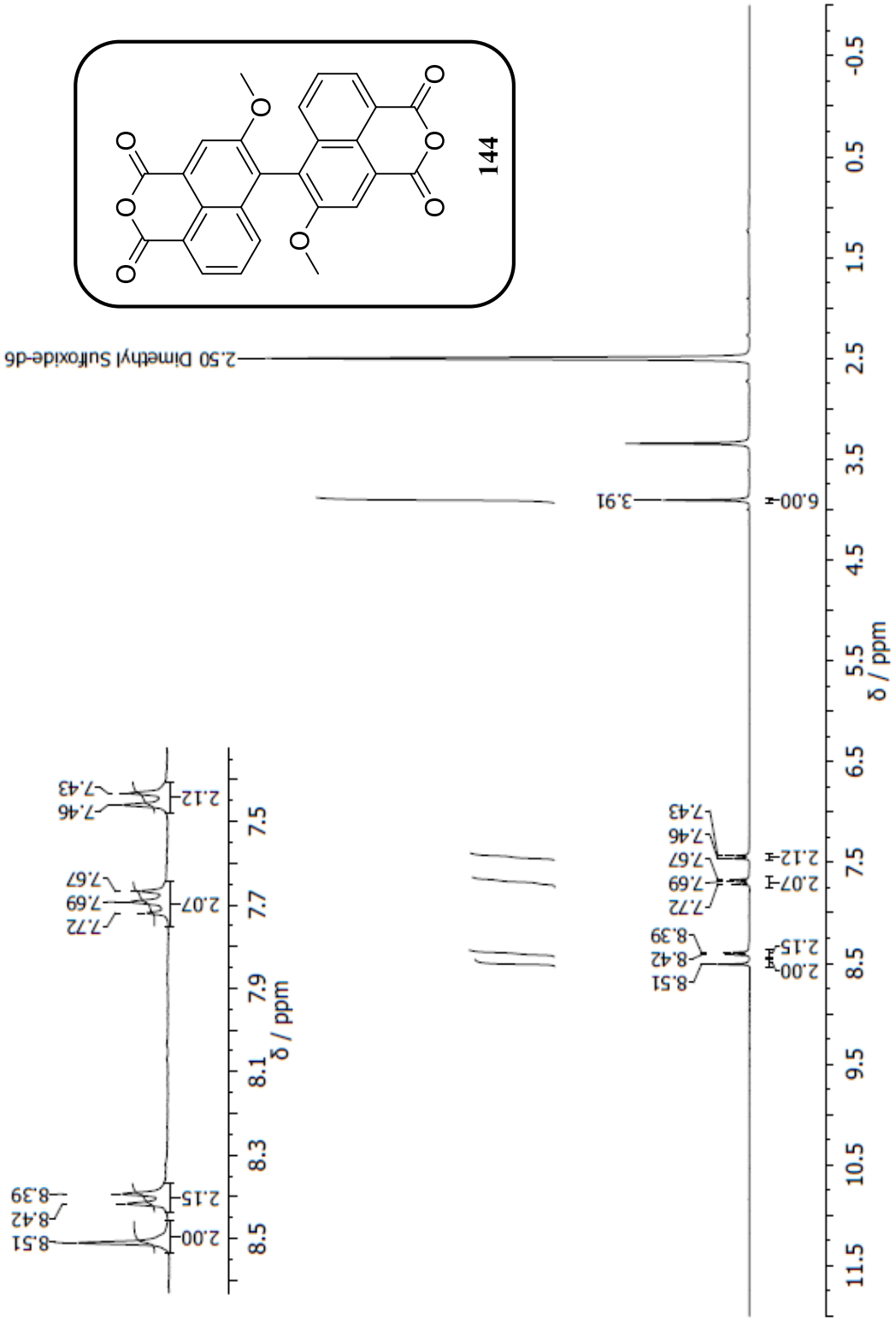

Figure 128: 300 MHz ^{1}H NMR spectrum of **144** in $(CD3)_2SO$.

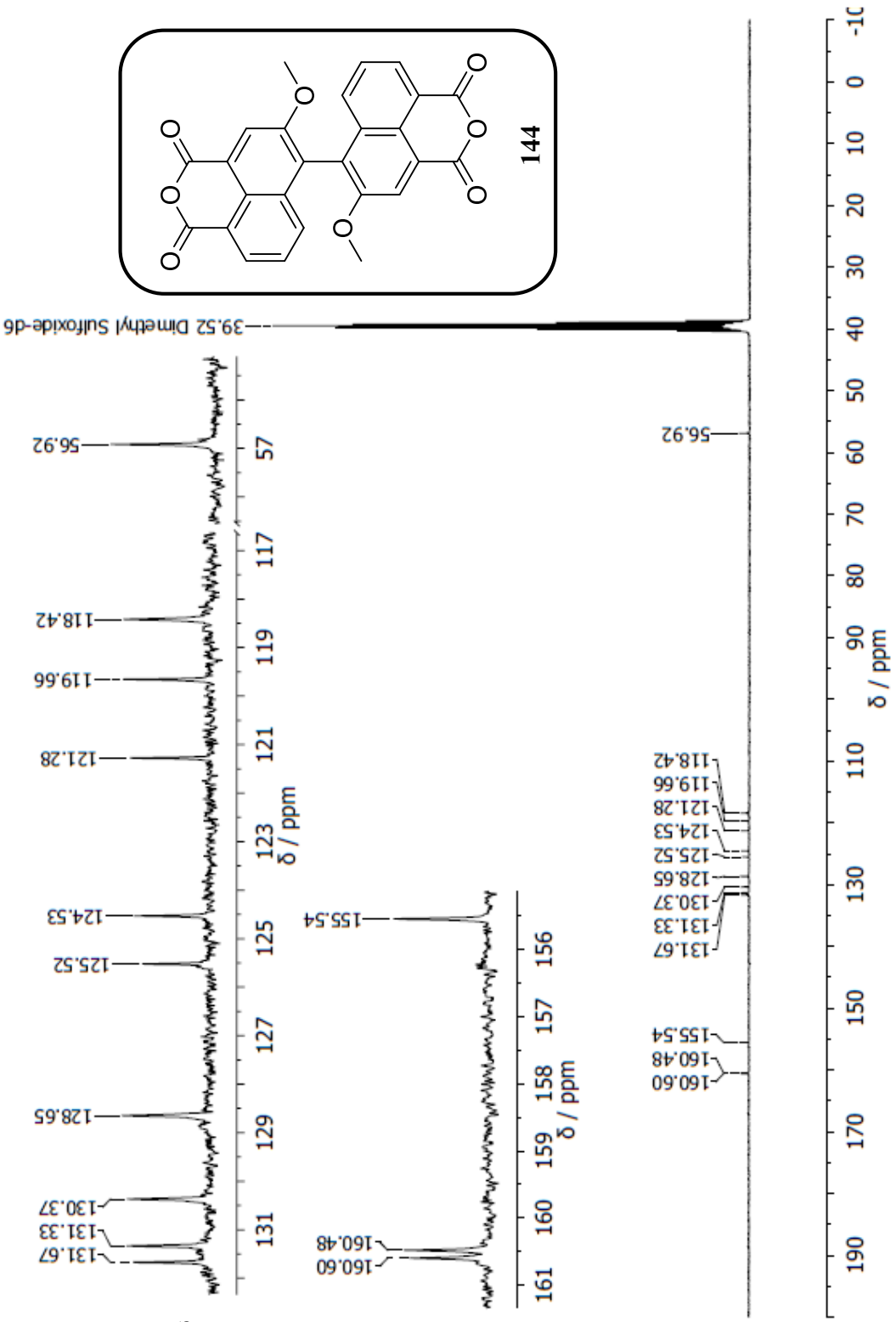

Figure 129: 75 MHz ^{13}C NMR spectrum of **144** in $(CD_3)_2SO$.

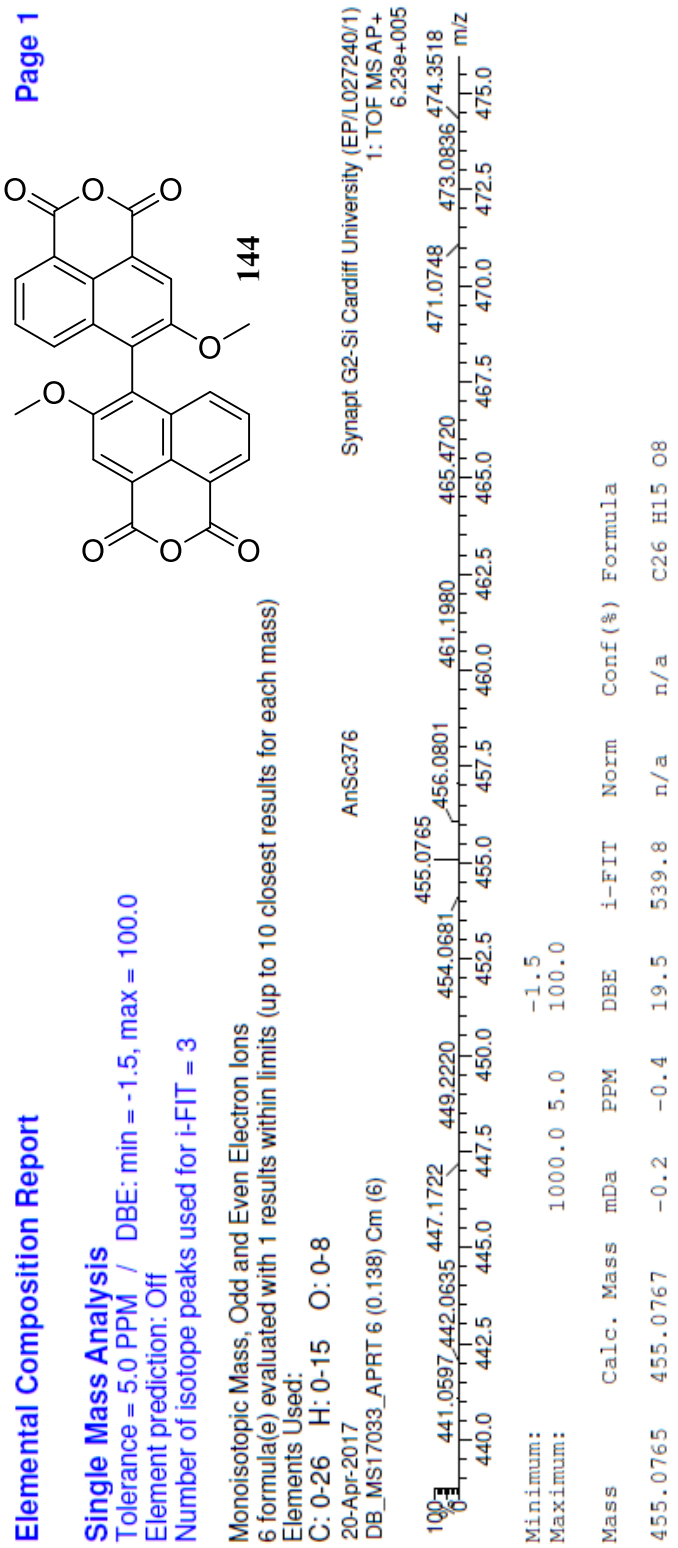

Figure 130: APCI-HRMS spectrum of **144**.

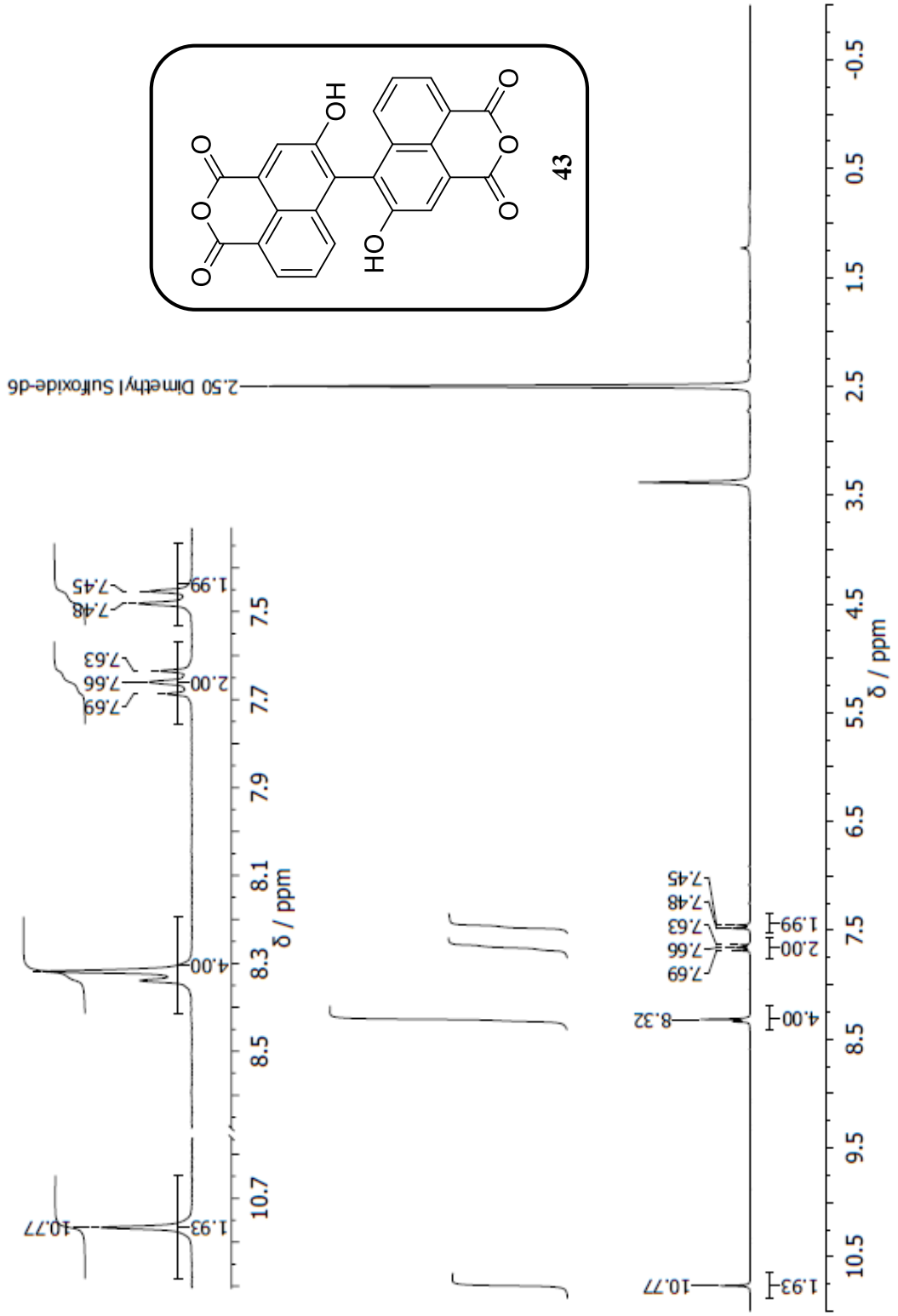

Figure 131: 300 MHz ^{1}H NMR spectrum of **43** in $(CD_3)_2SO$.

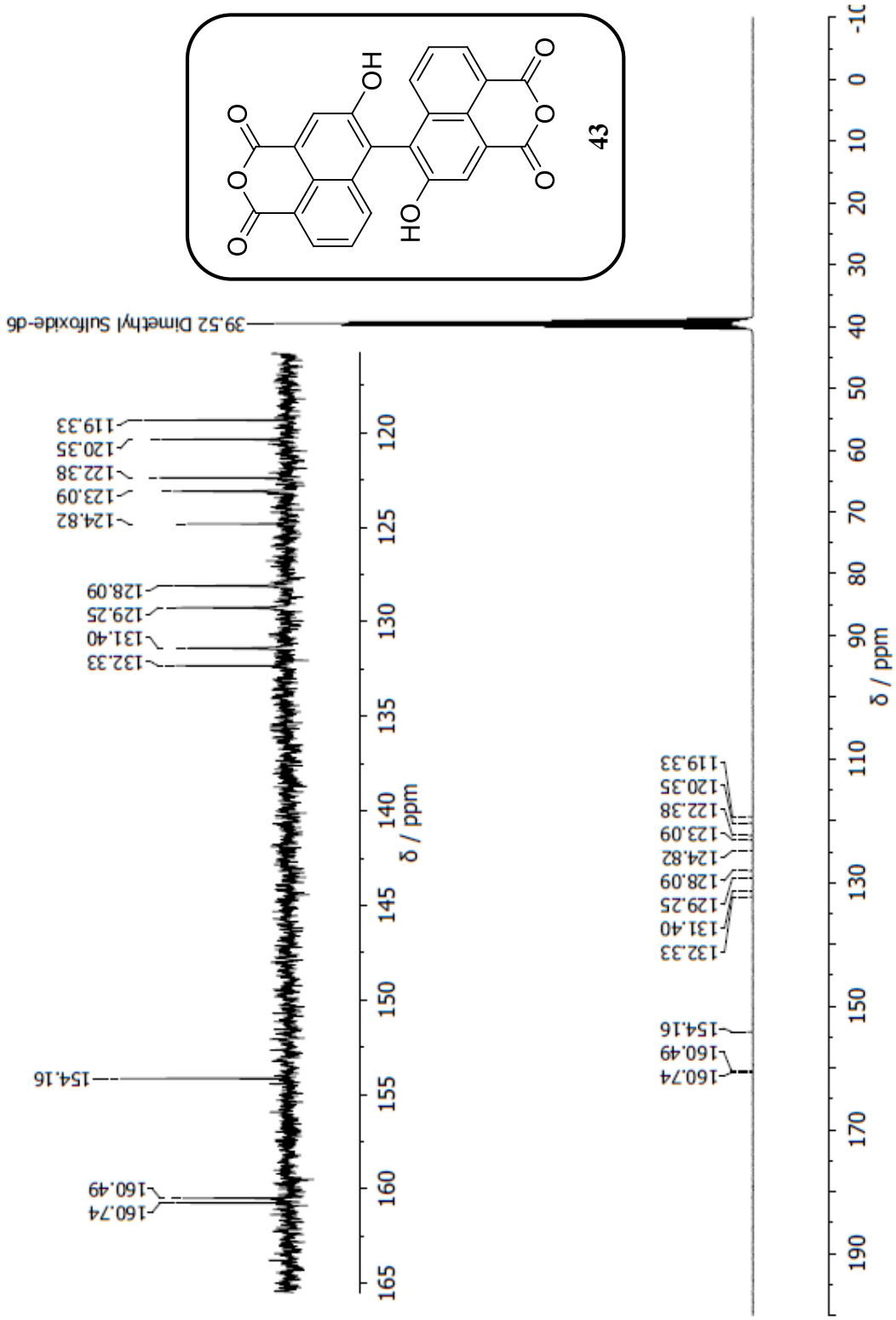

Figure 132: 75 MHz ^{13}C NMR spectrum of **43** in $(CD_3)_2SO$.

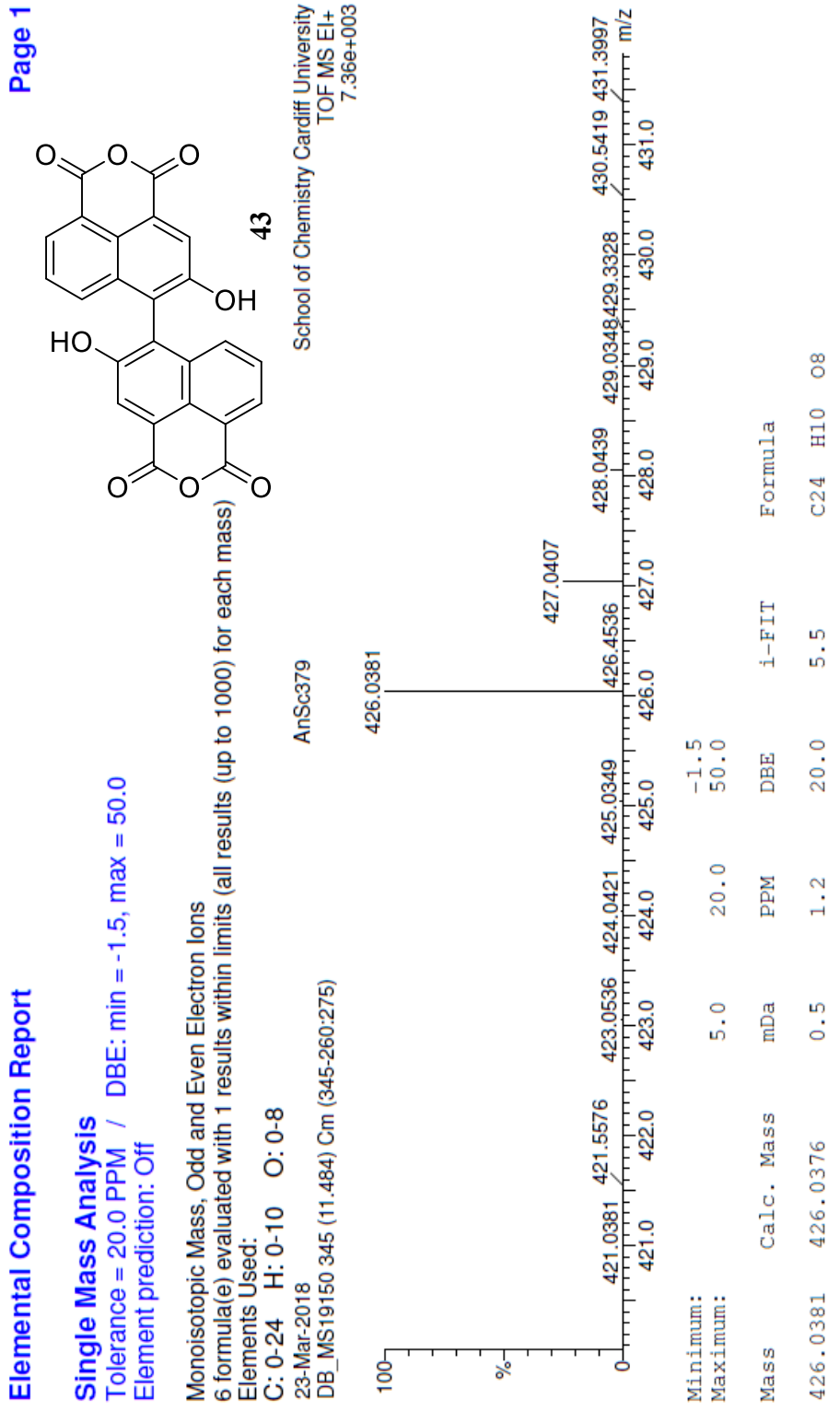

Figure 133: EI-HRMS spectrum of **43**.

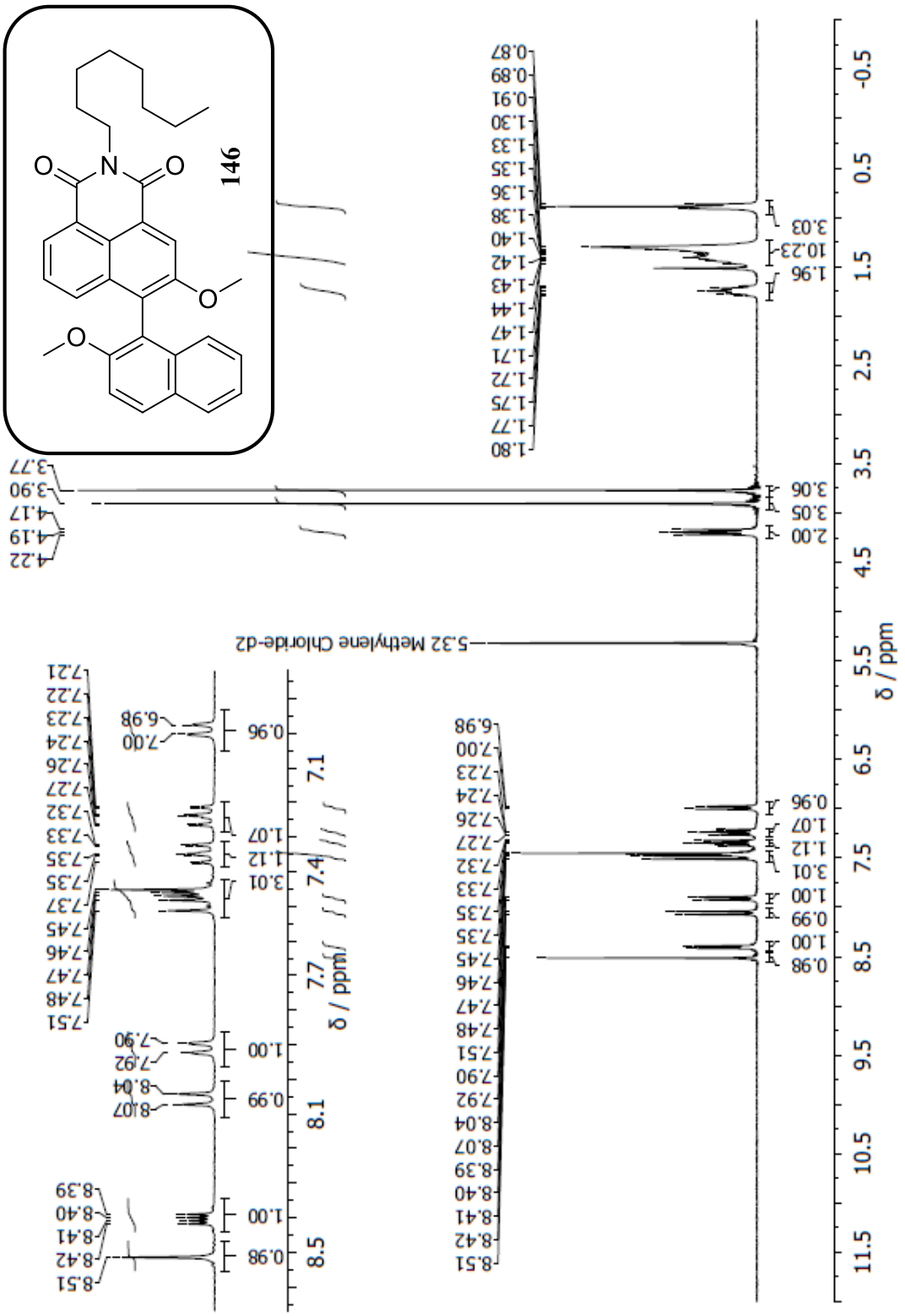

Figure 134: 300 ^{1}H NMR spectrum of **146** in CD_2Cl_2.

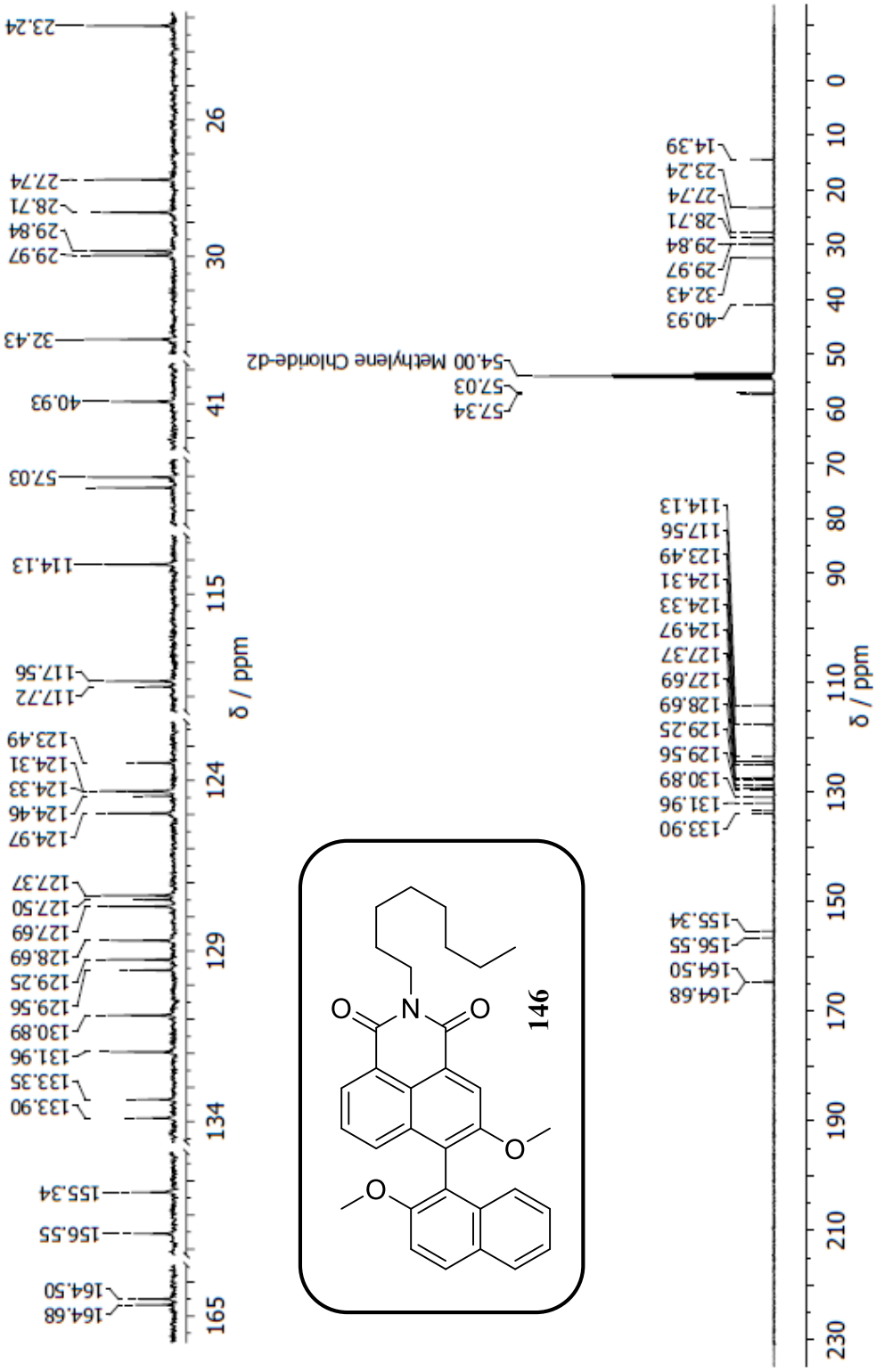

Figure 135: 101 ^{13}C NMR spectrum of **146** in CD_2Cl_2.

Figure 136: MALDI-HRMS spectrum of **146**.

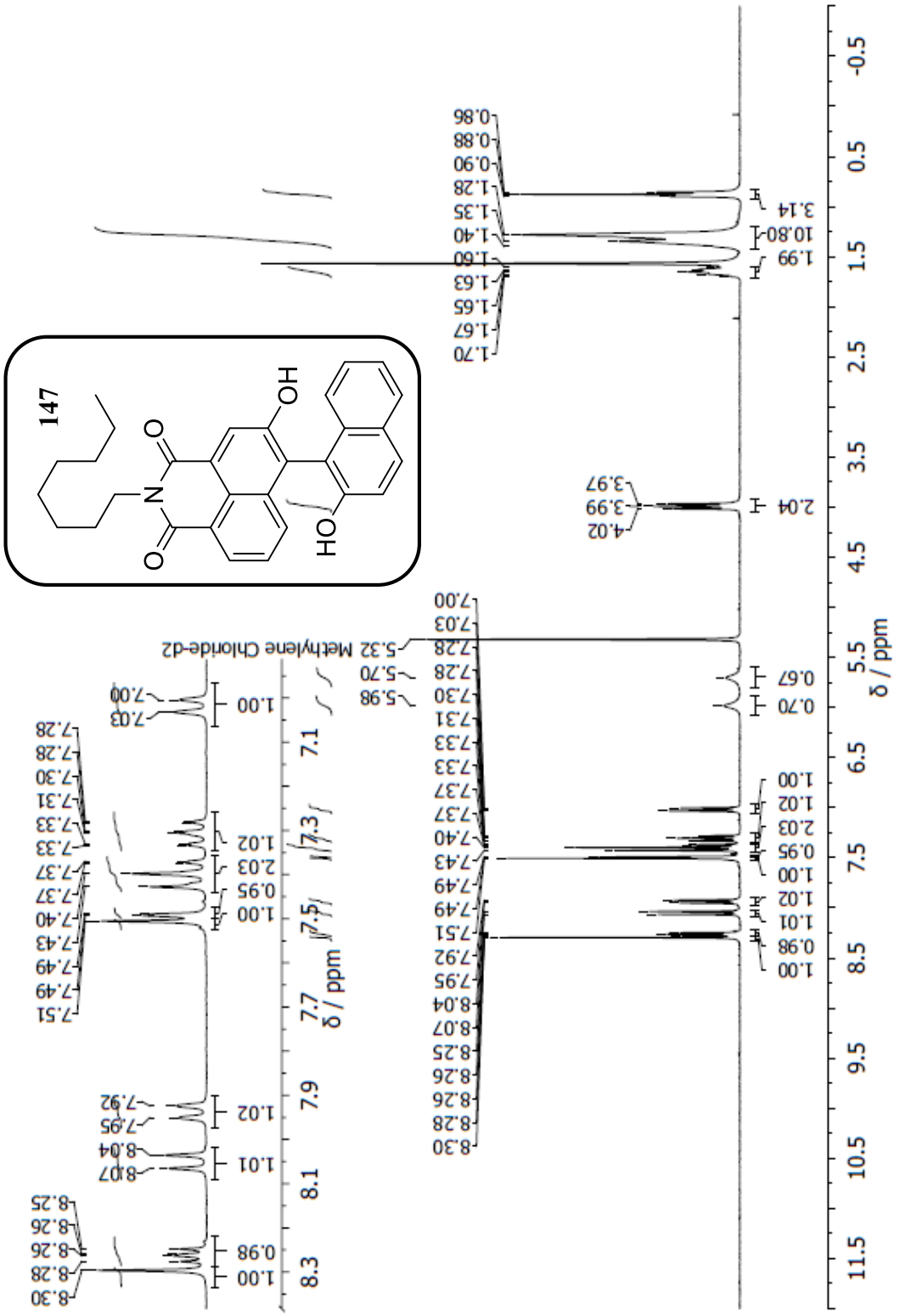

Figure 137: 300 ^{1}H NMR spectrum of **147** in CD_2Cl_2.

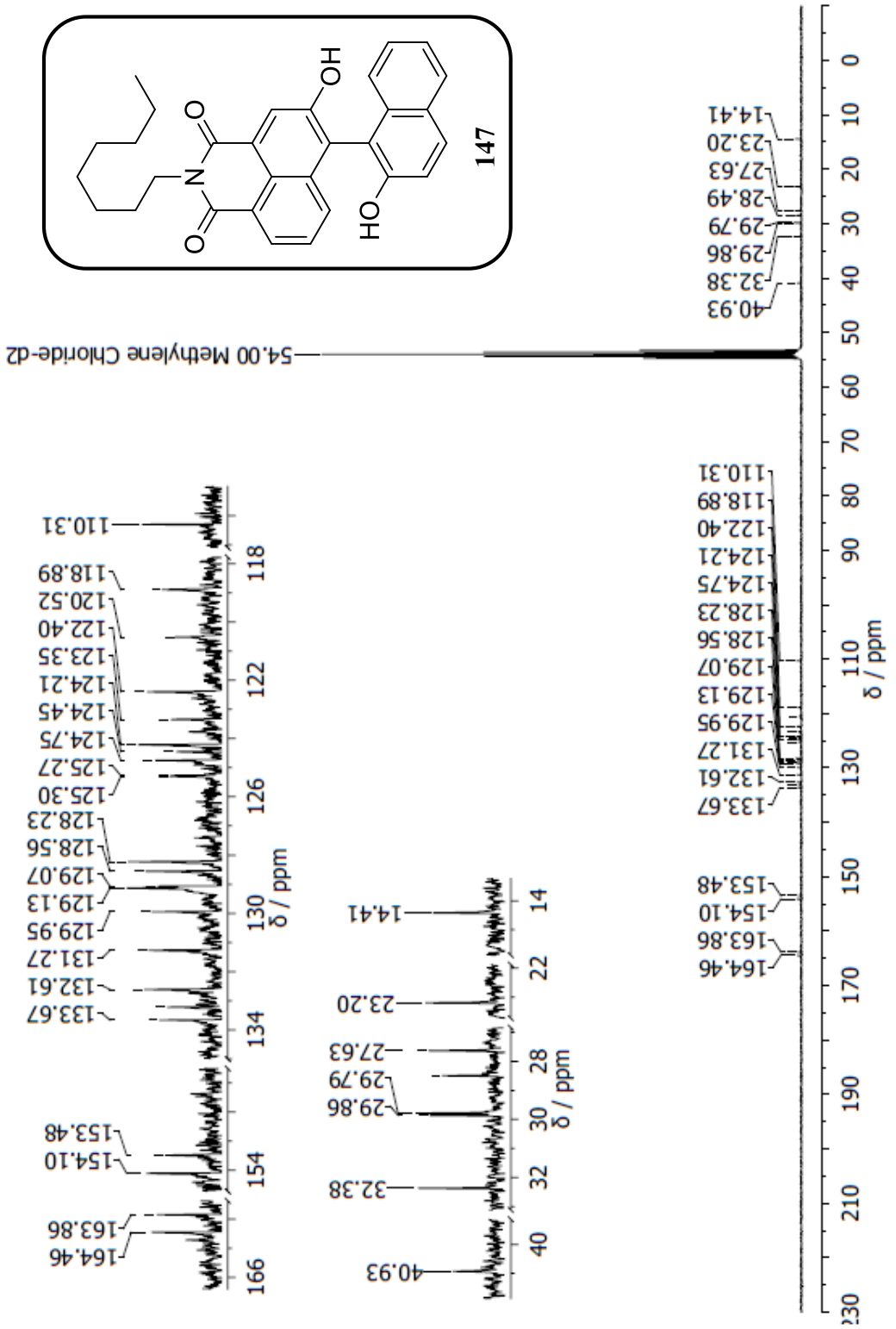

Figure 138: 75 ^{13}C NMR spectrum of **147** in CD_2Cl_2.

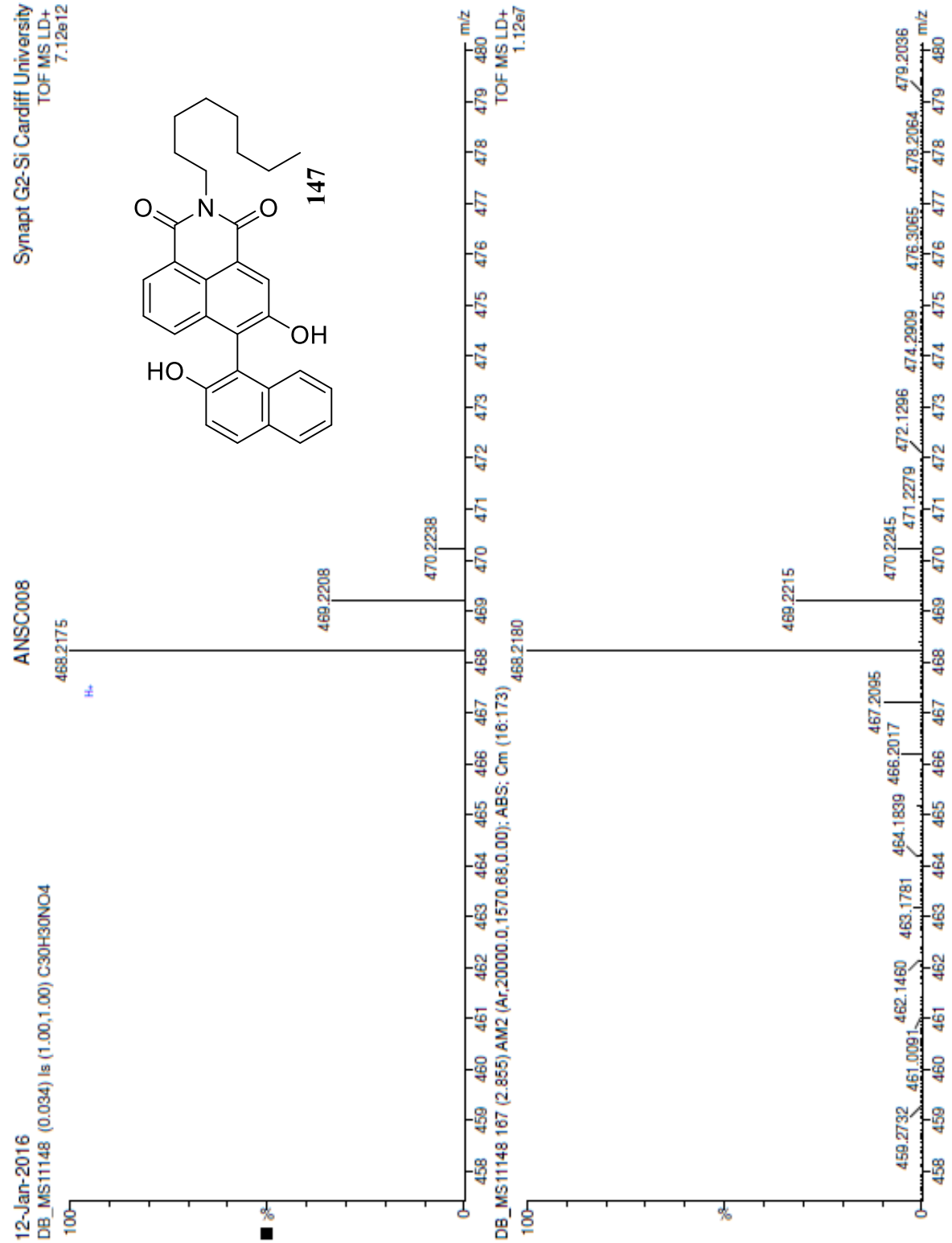

Figure 139: MALDI-HRMS spectrum of **147**.

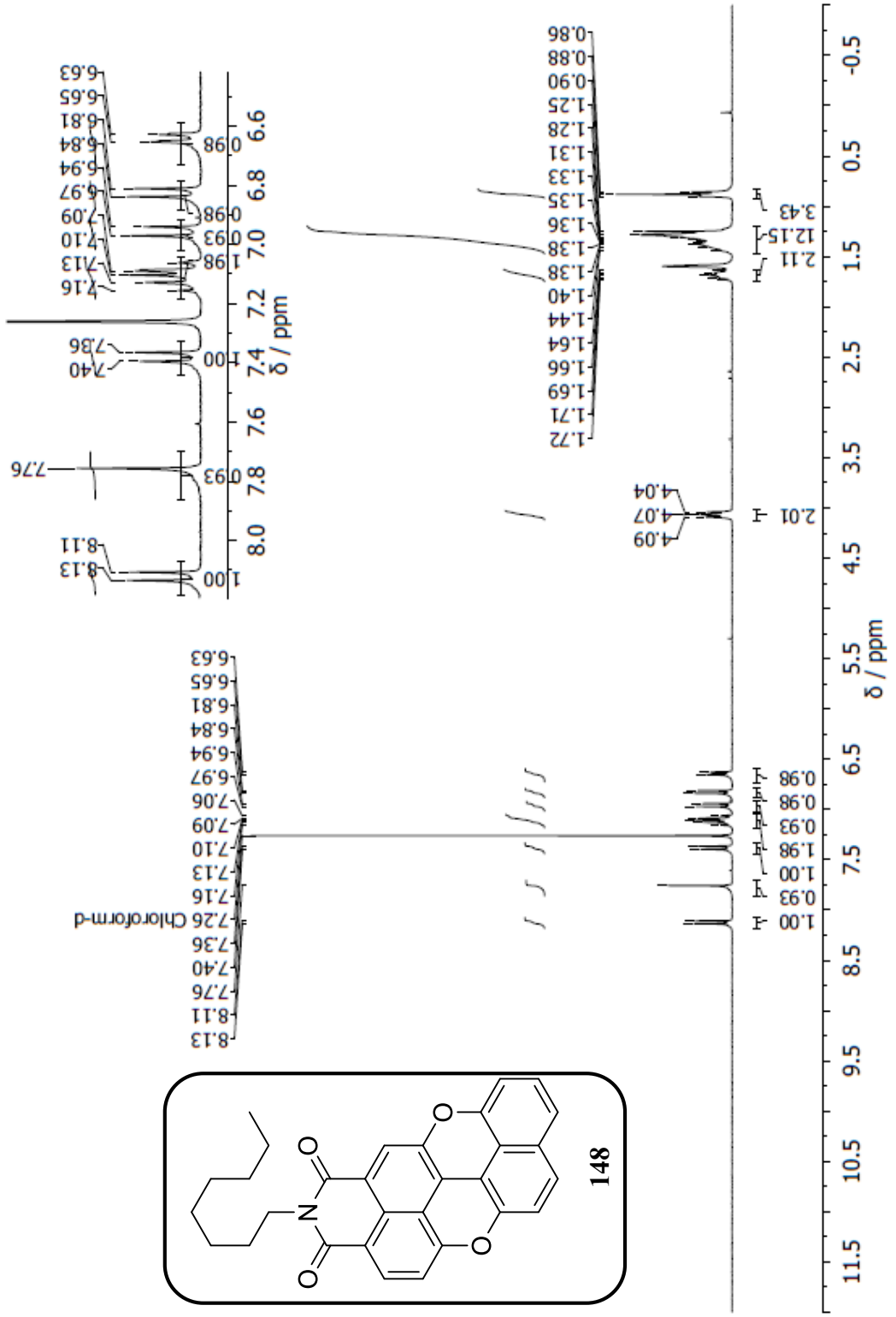

Figure 140: 300 MHz ^{1}H NMR spectrum of **148** in $CDCl_3$.

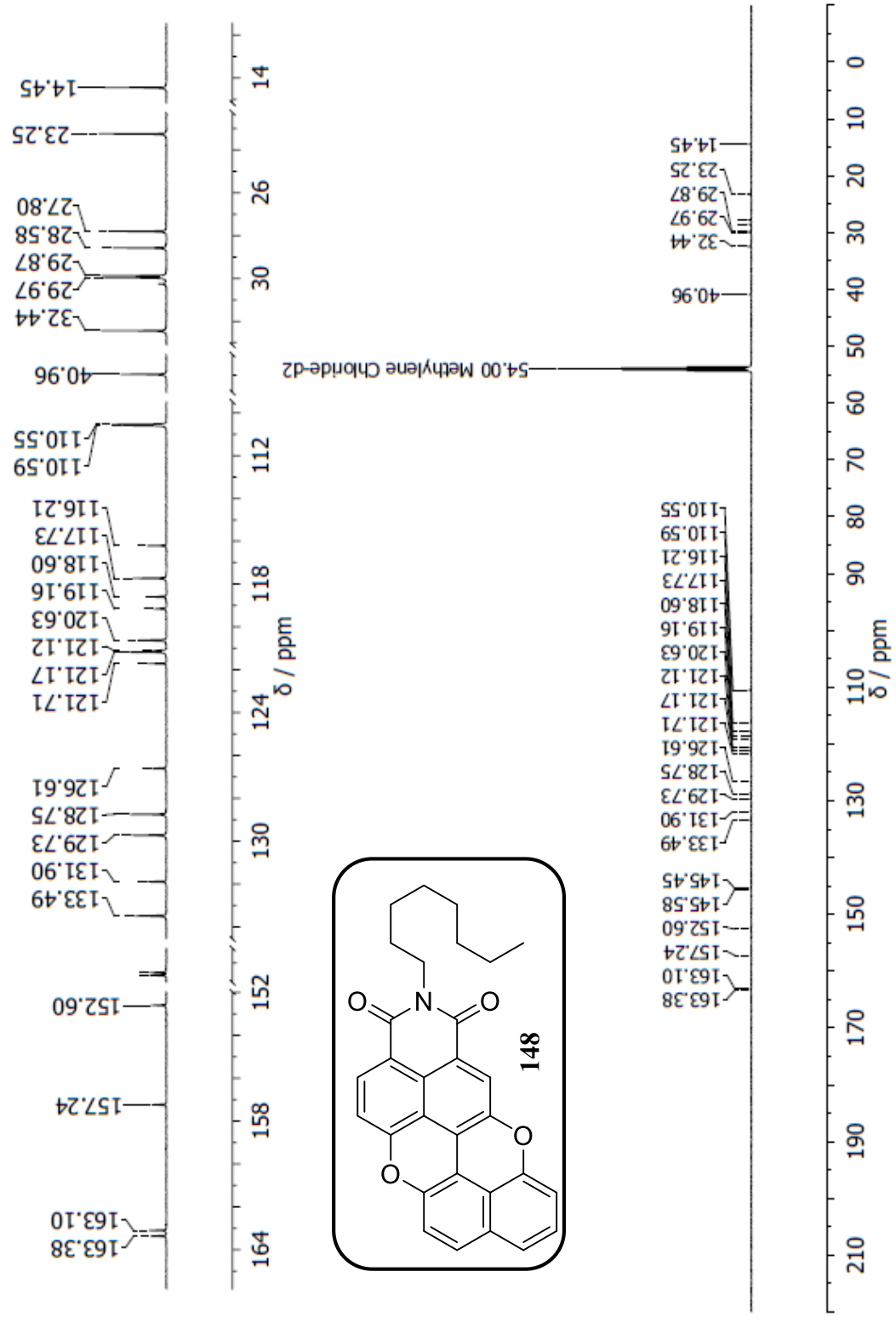

Figure 141: 151 MHz ^{13}C NMR spectrum of **148** in $CDCl_3$.

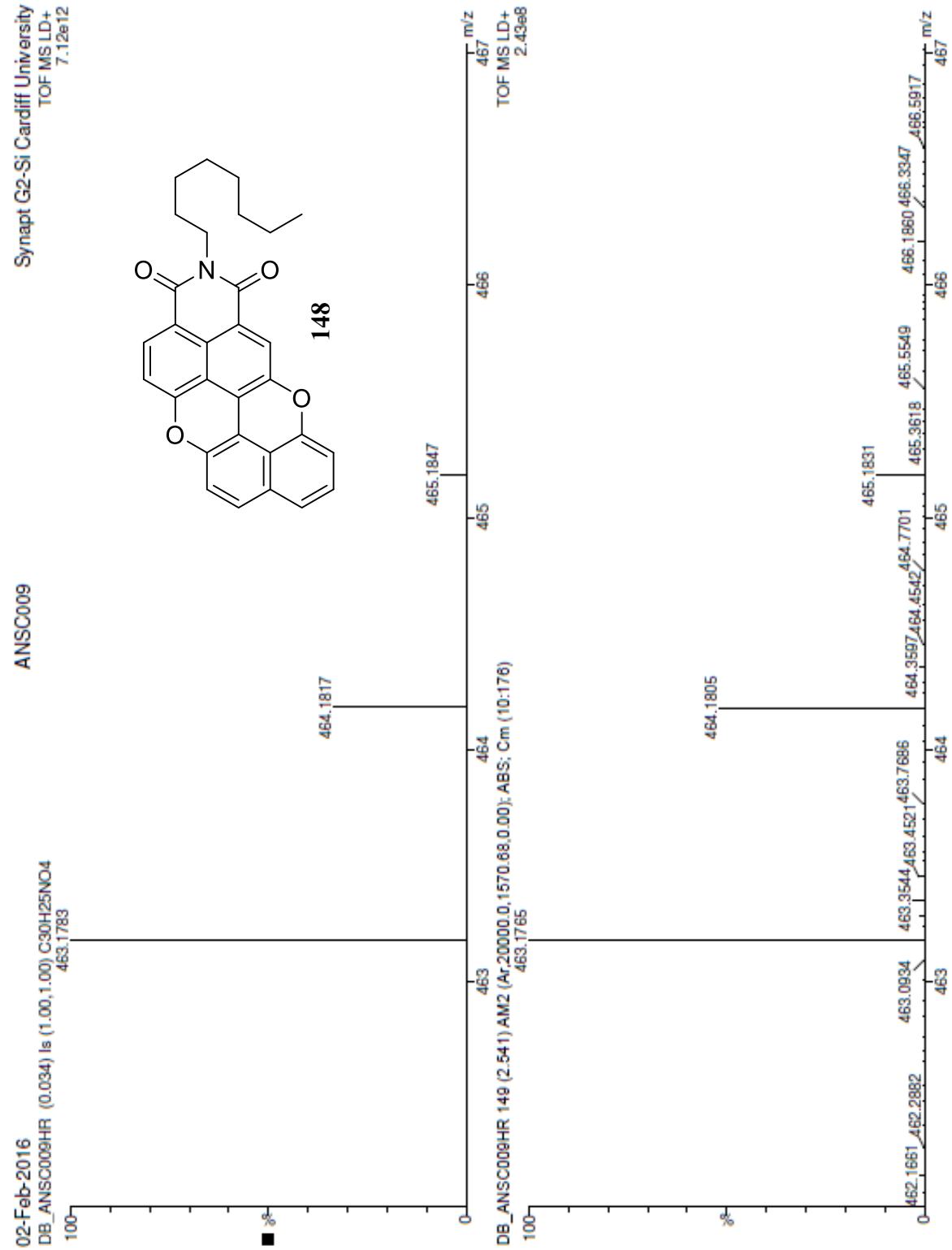

Figure 142: MALDI-HRMS spectrum of **148**.

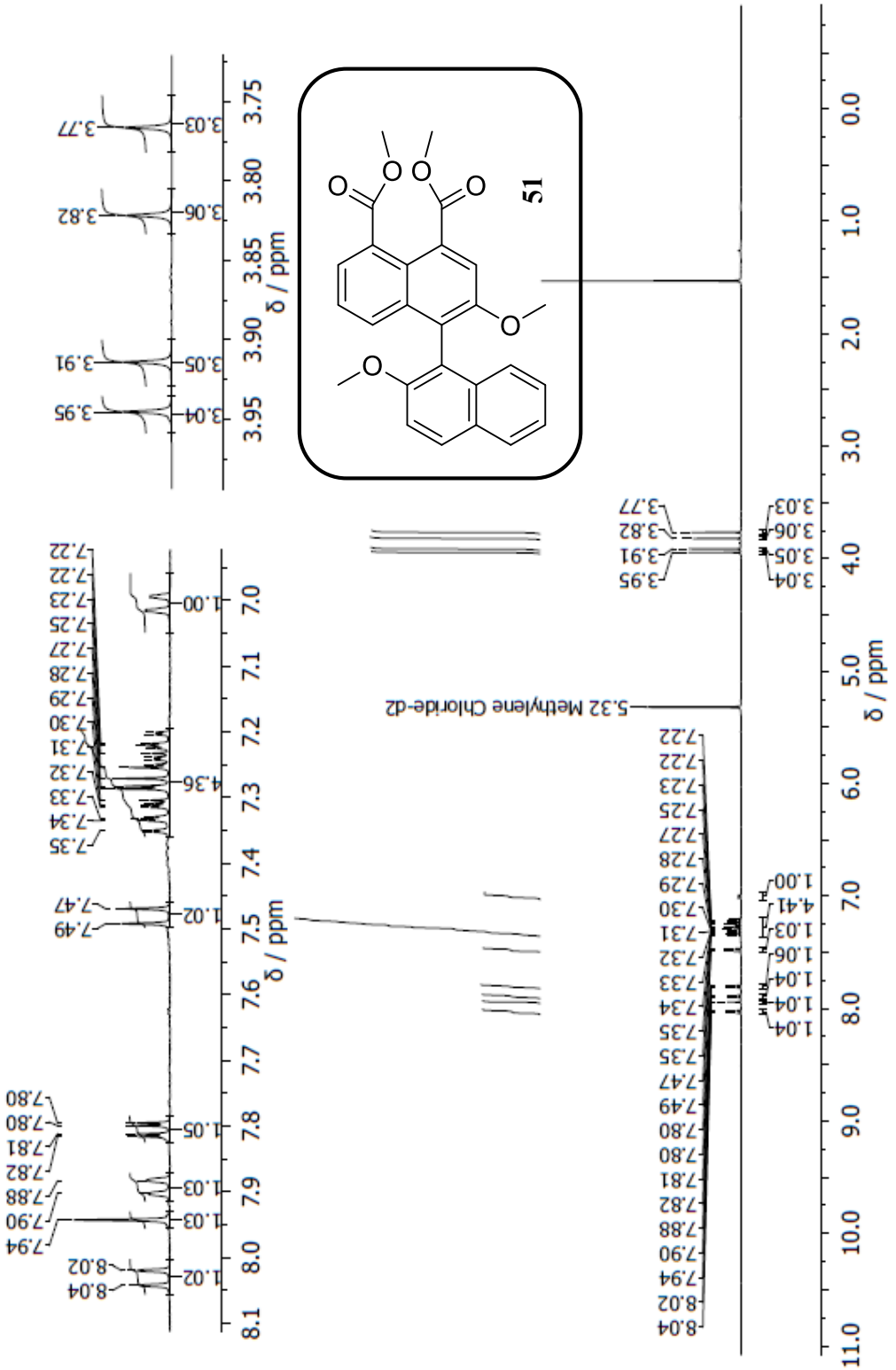

Figure 143: 300 MHz ^{1}H NMR spectrum of **51** in CD_2Cl_2.

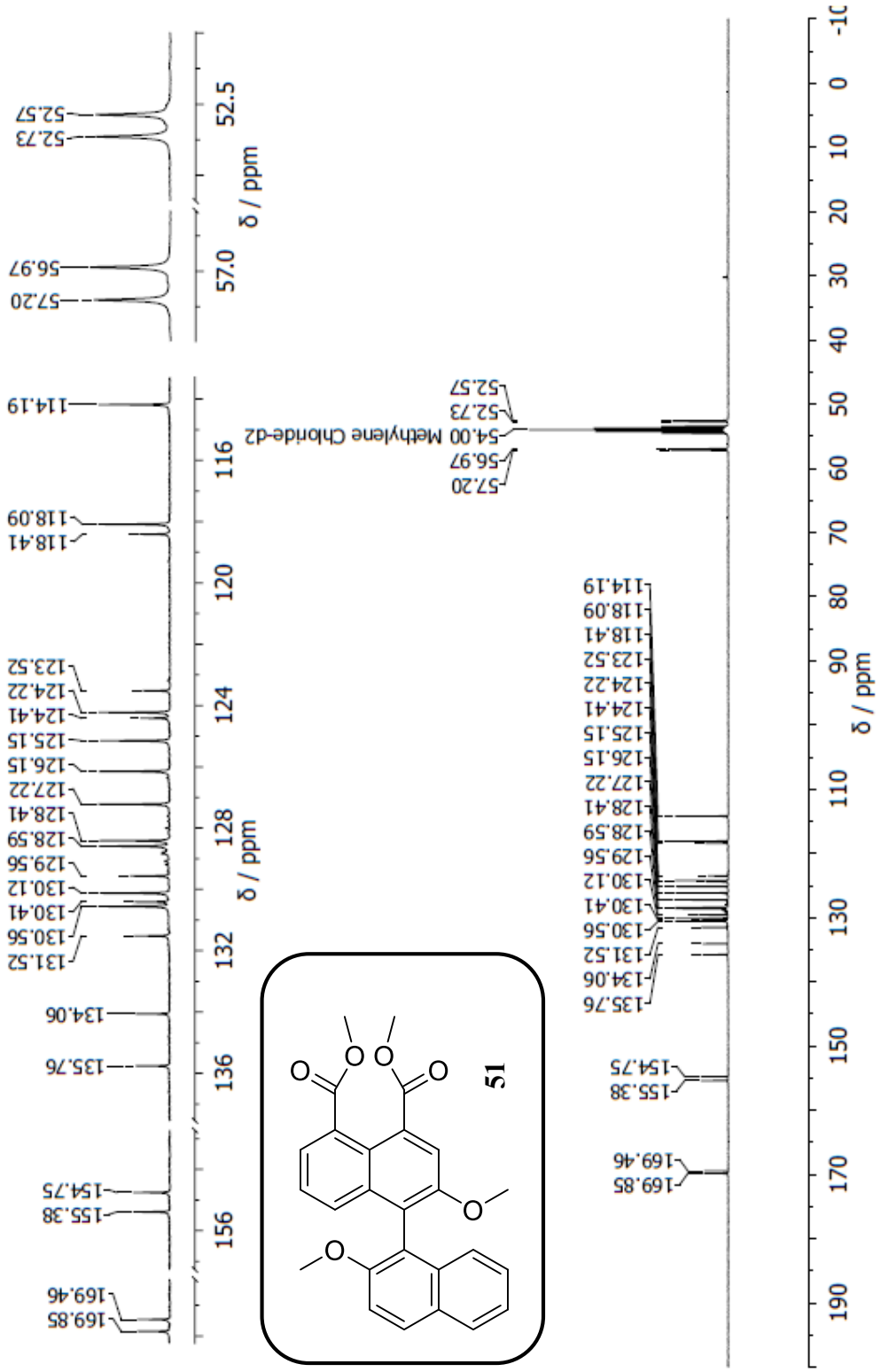

Figure 144: 101 MHz ^{13}C NMR spectrum of **51** in CD_2Cl_2.

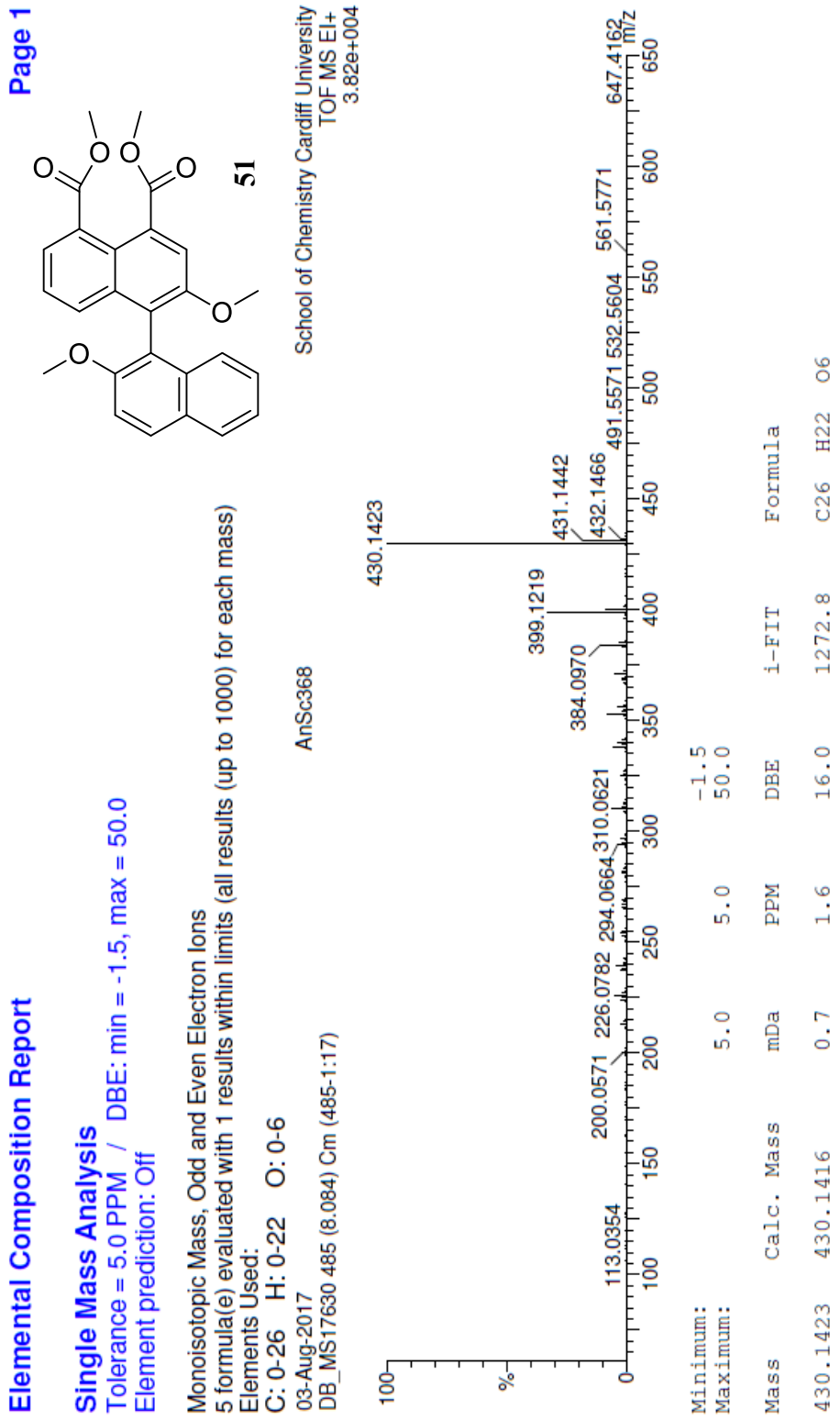

Figure 145: EI-HRMS spectrum of **51**.

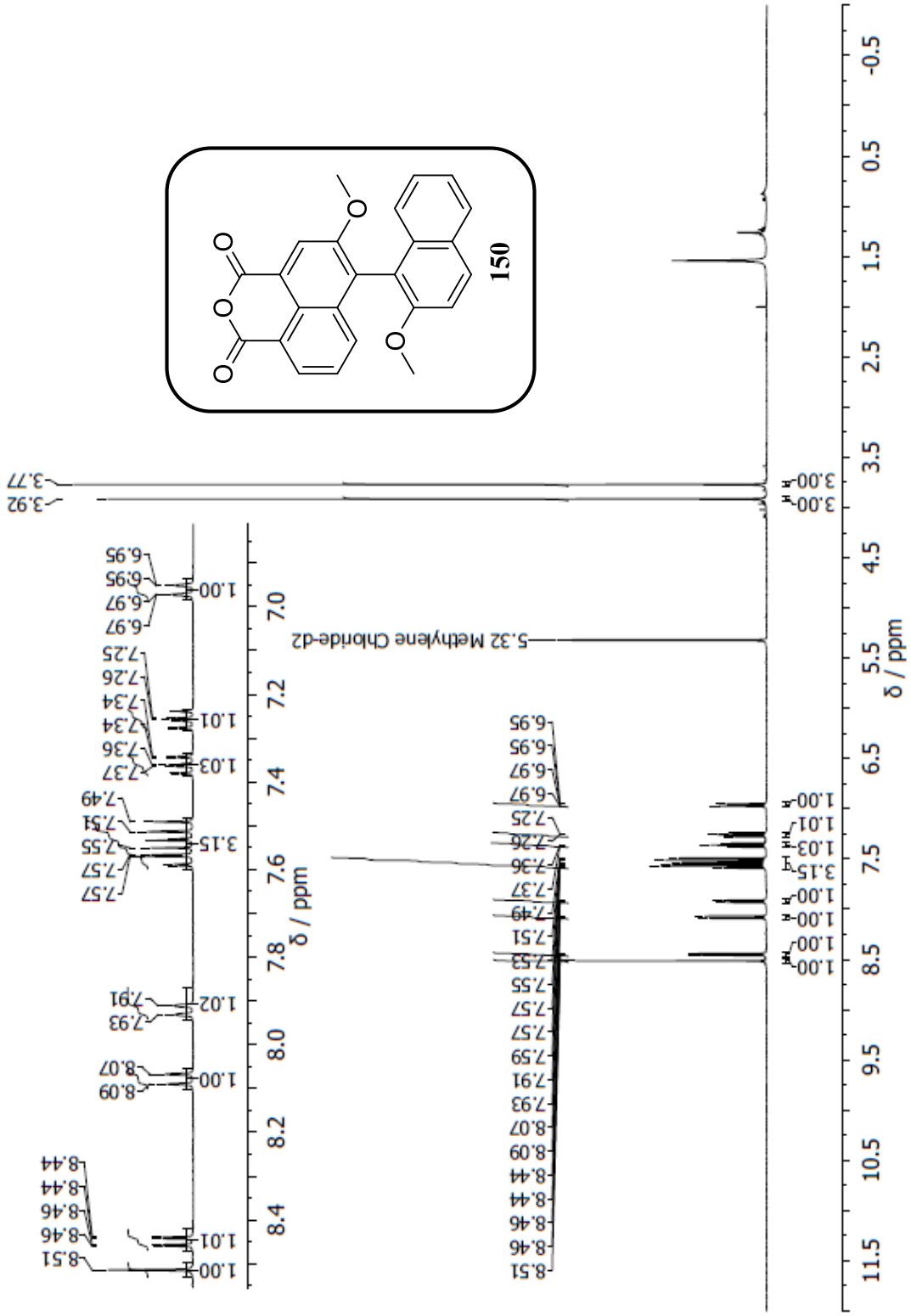

Figure 146: 400 MHz ^{1}H NMR spectrum of **150** in CD_2Cl_2.

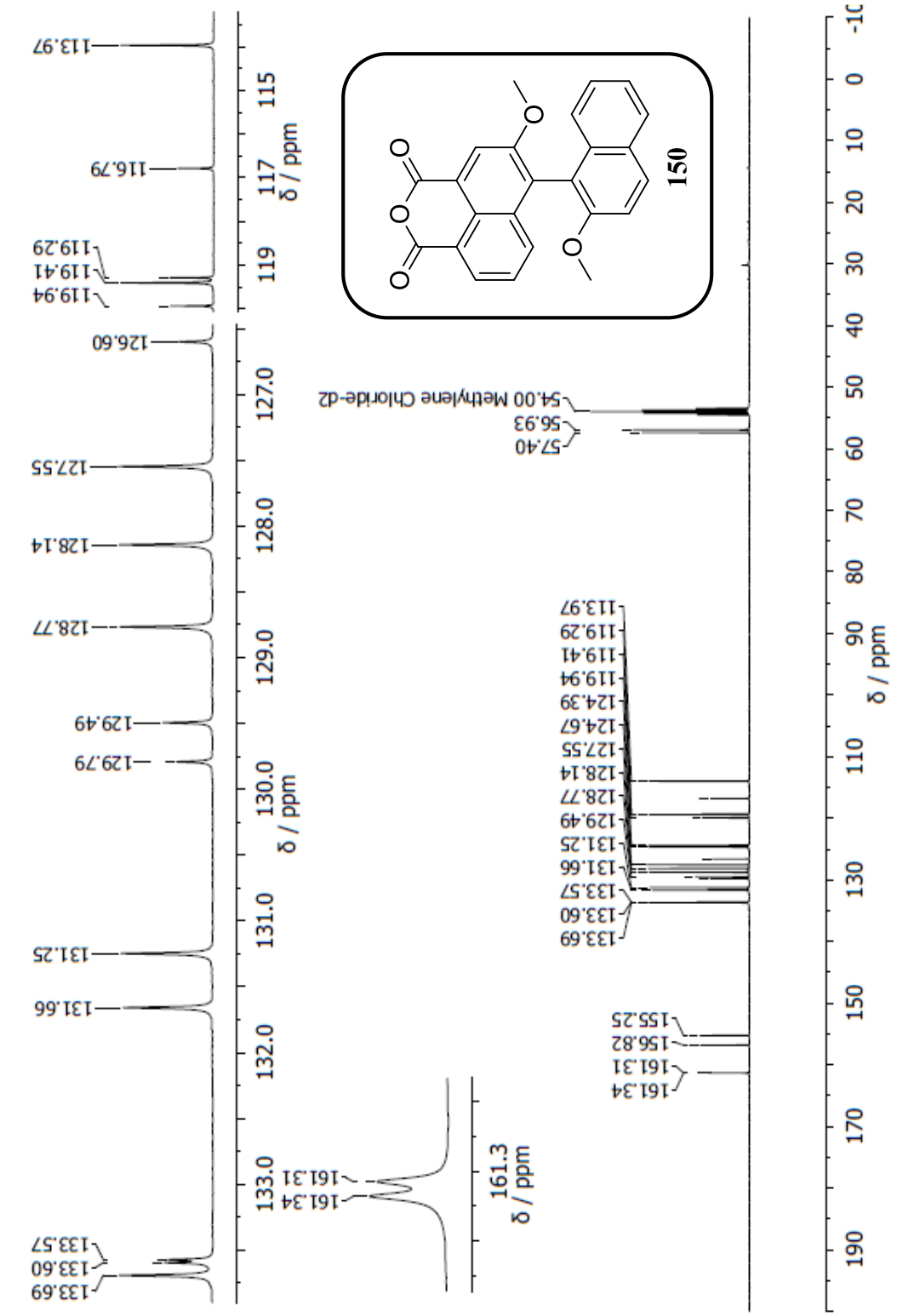

Figure 147: 101 MHz ^{13}C NMR spectrum of **150** in CD_2Cl_2.

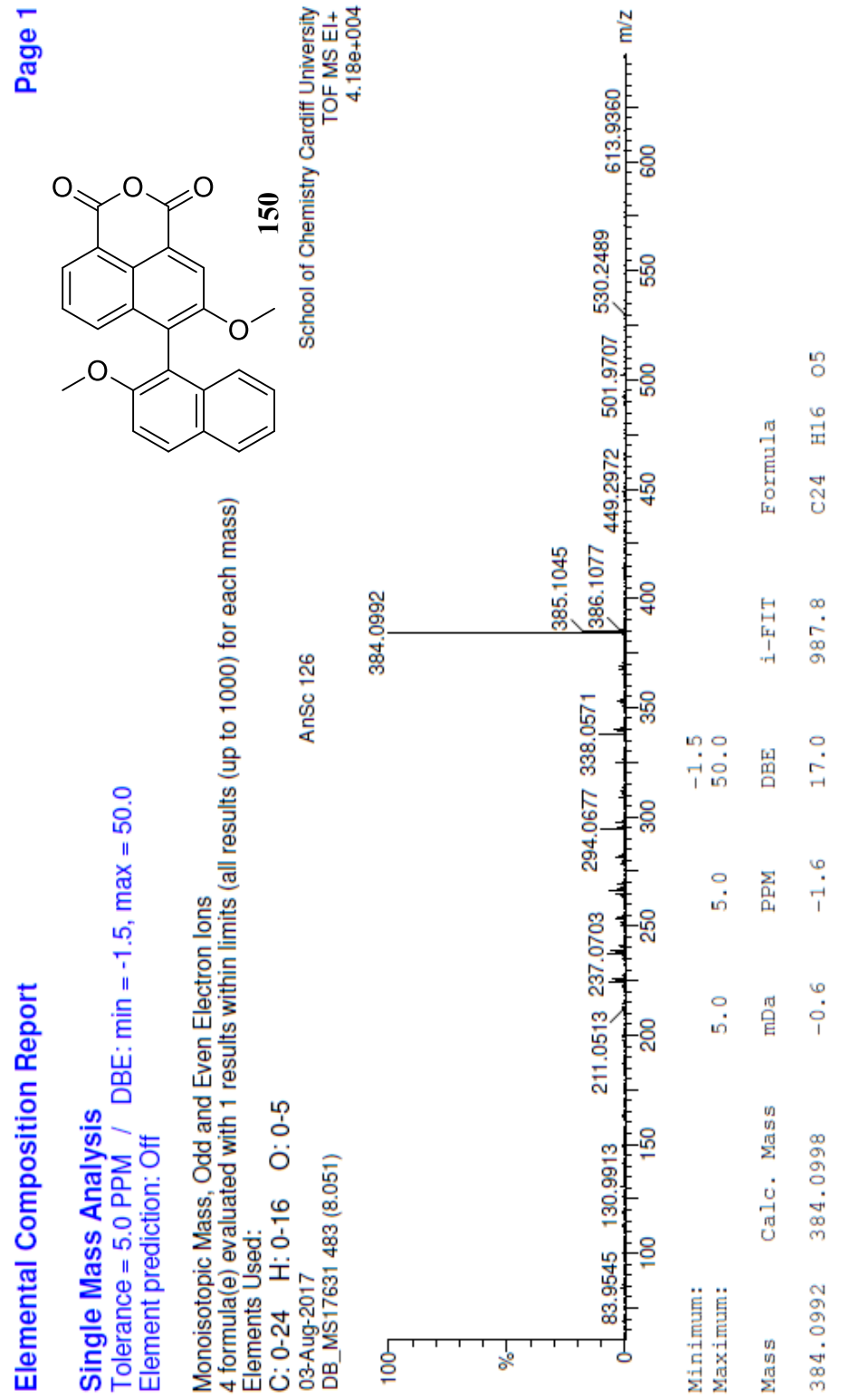

Figure 148: EI-HRMS spectrum of **150**.

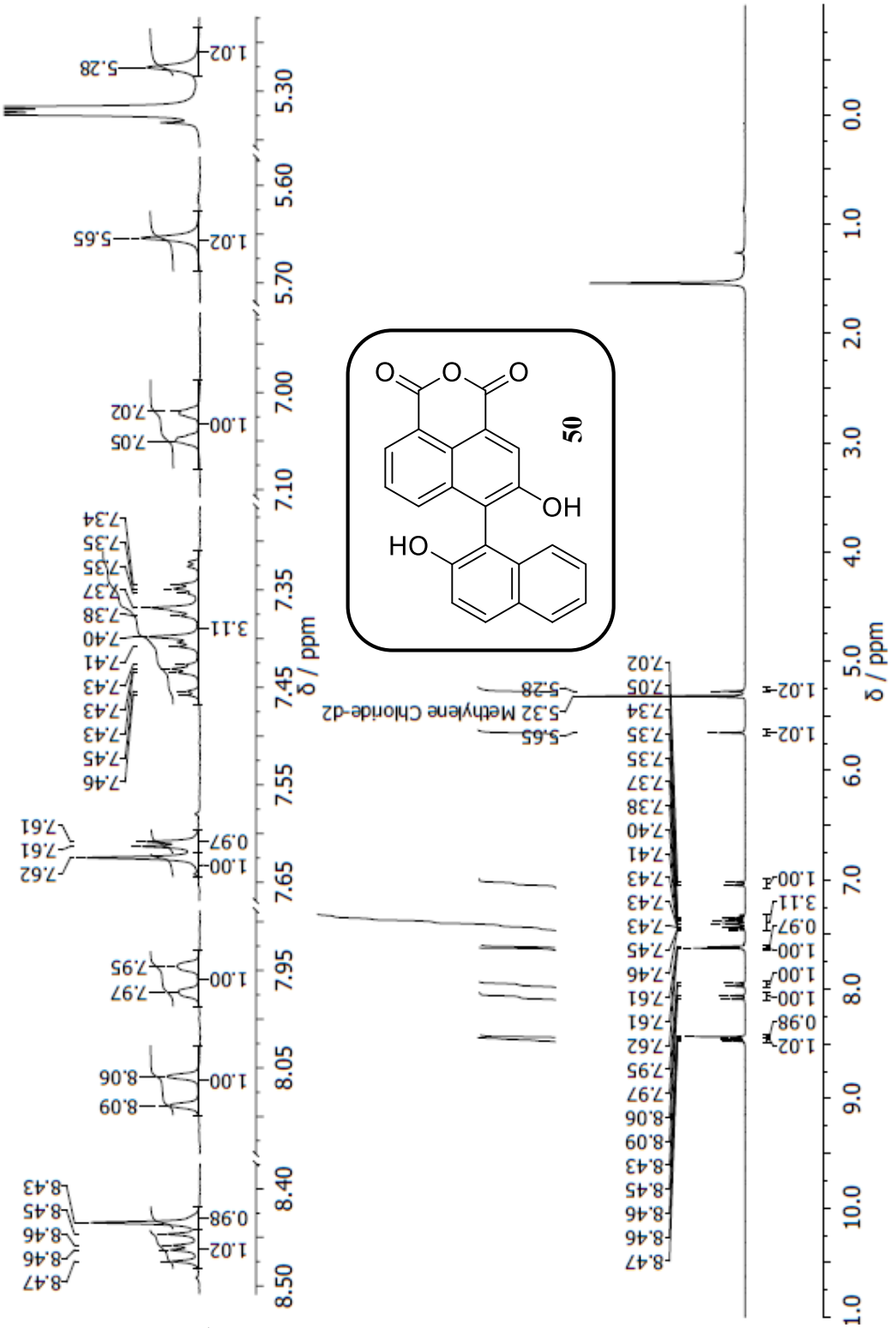

Figure 149: 400 MHz ^{1}H NMR spectrum of **50** in CD_2Cl_2.

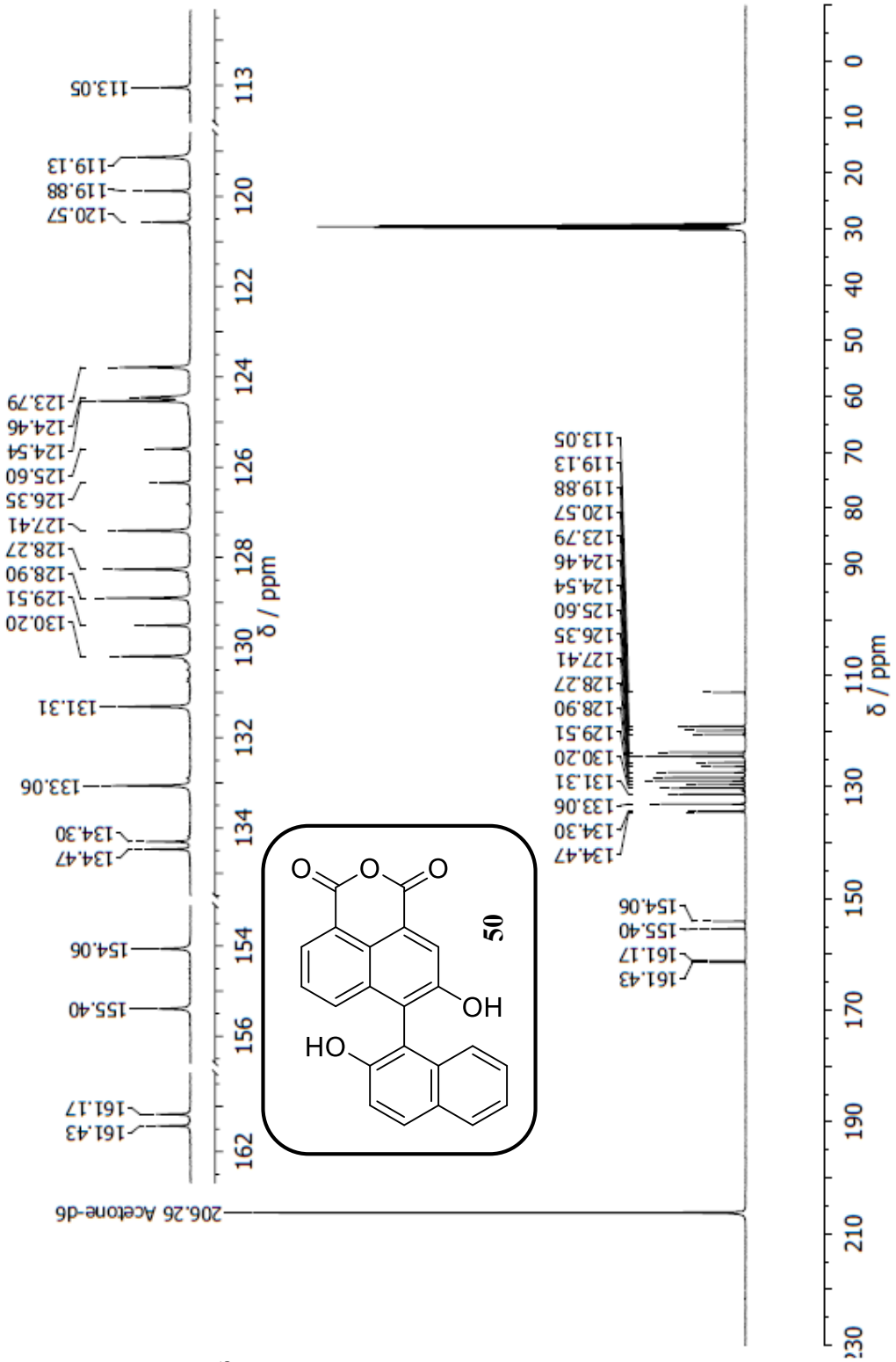

Figure 150: 101 MHz ^{13}C NMR spectrum of **50** in $(CD_3)_2CO$.

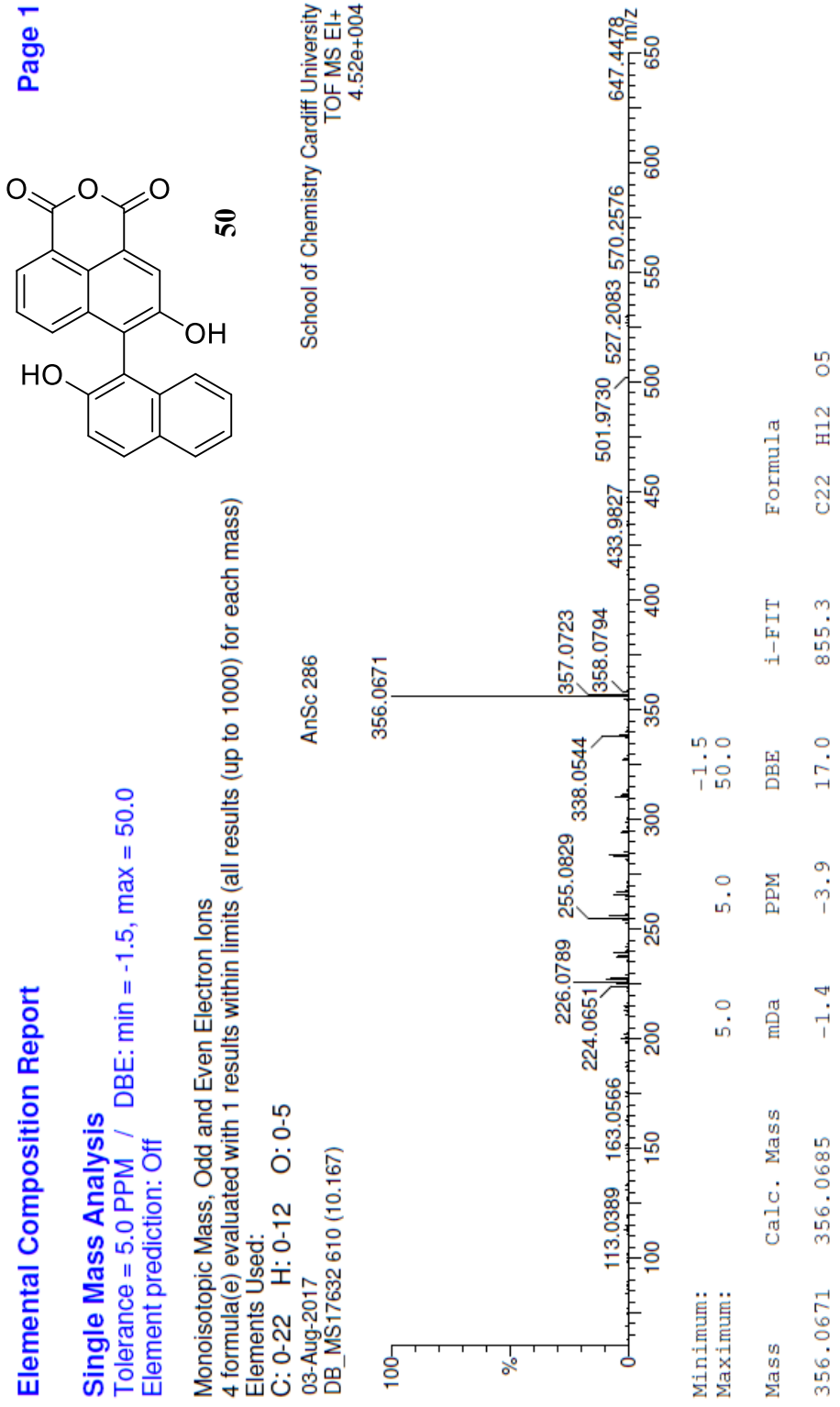

Figure 151: EI-HRMS spectrum of **50**.

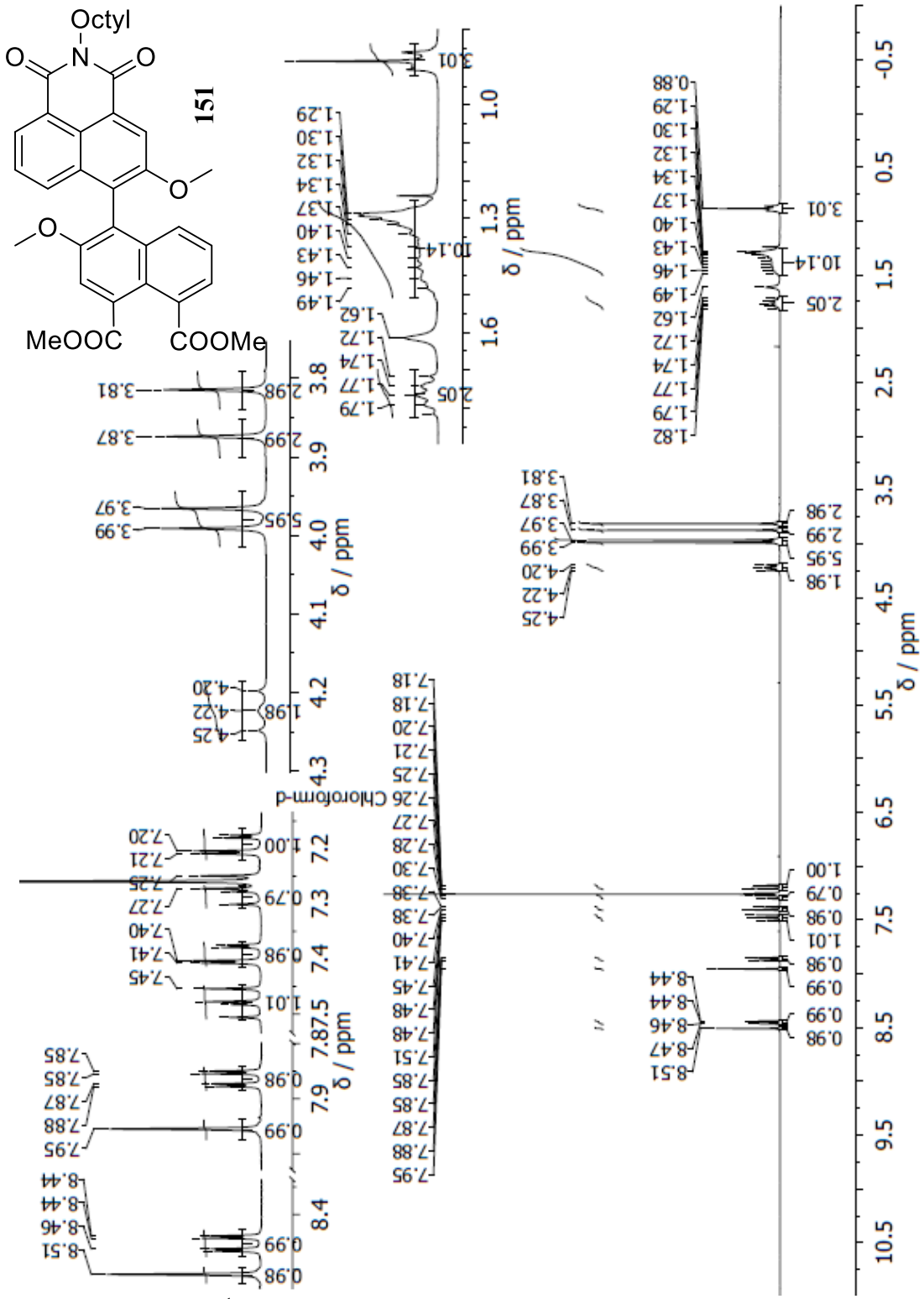

Figure 152: 300 MHz ^{1}H NMR of **151** in $CDCl_3$.

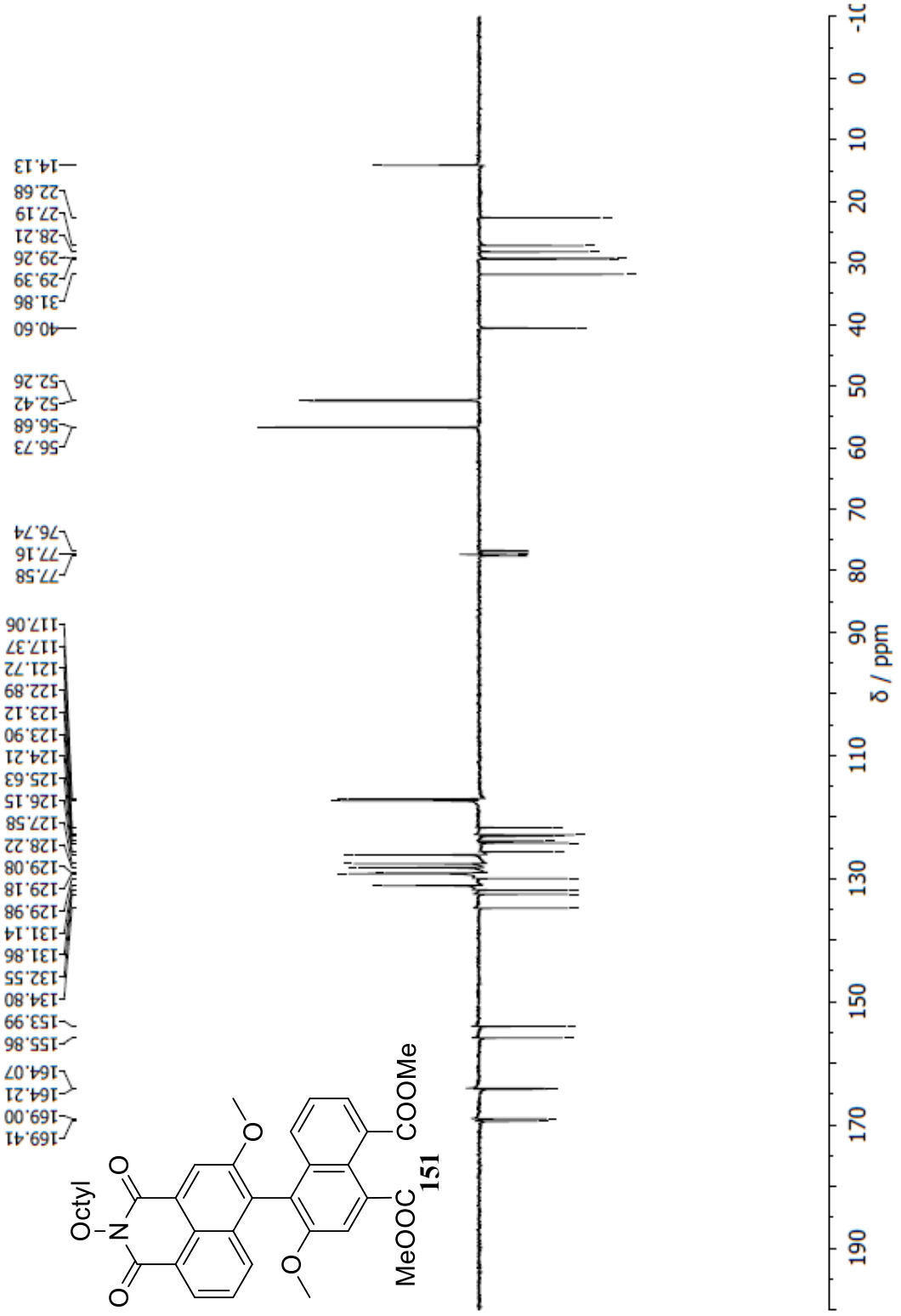

Figure 153: 75 MHz ^{13}C APT NMR of **151** in $CDCl_3$.

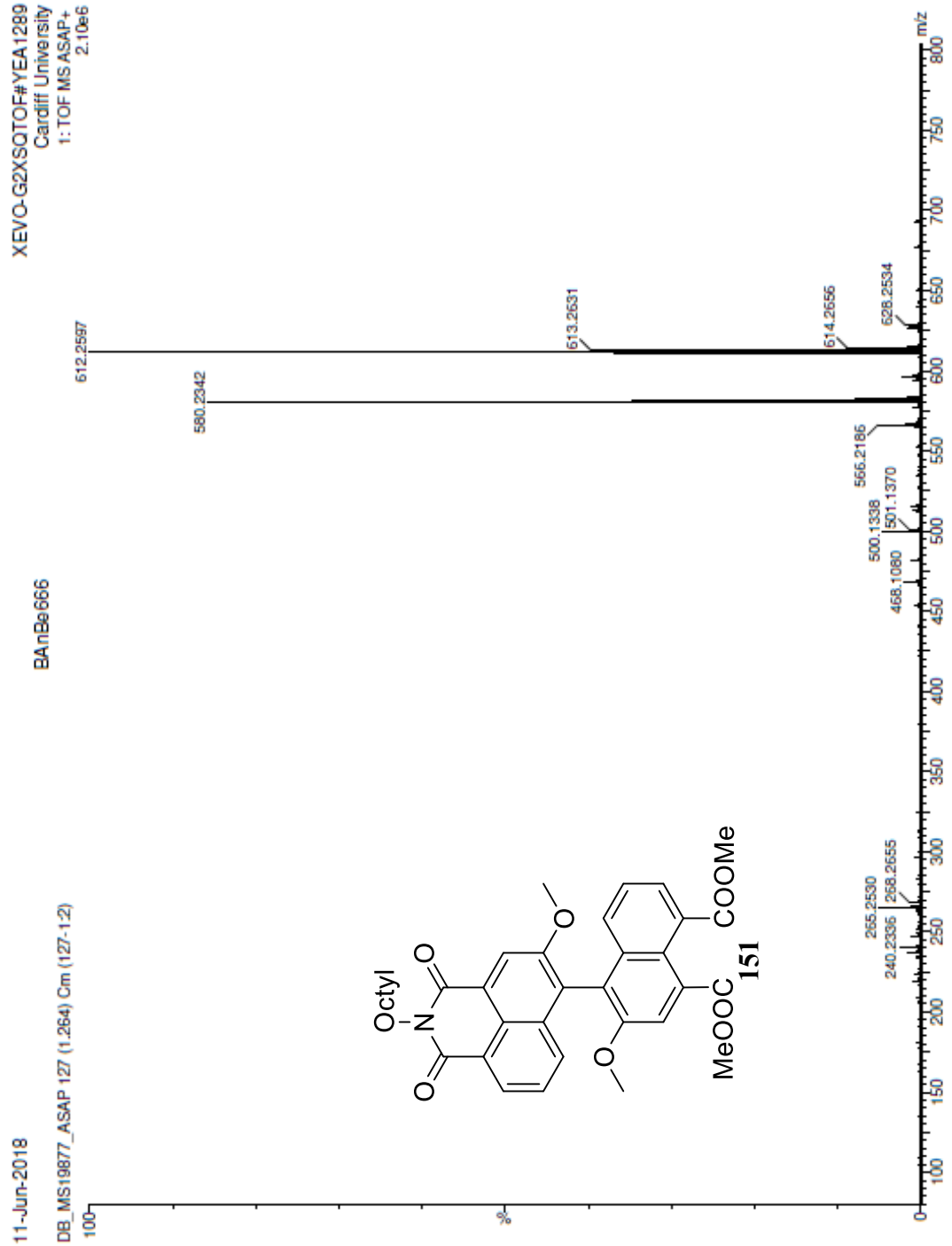

Figure 154: ASAP-HRMS spectrum of **151**.

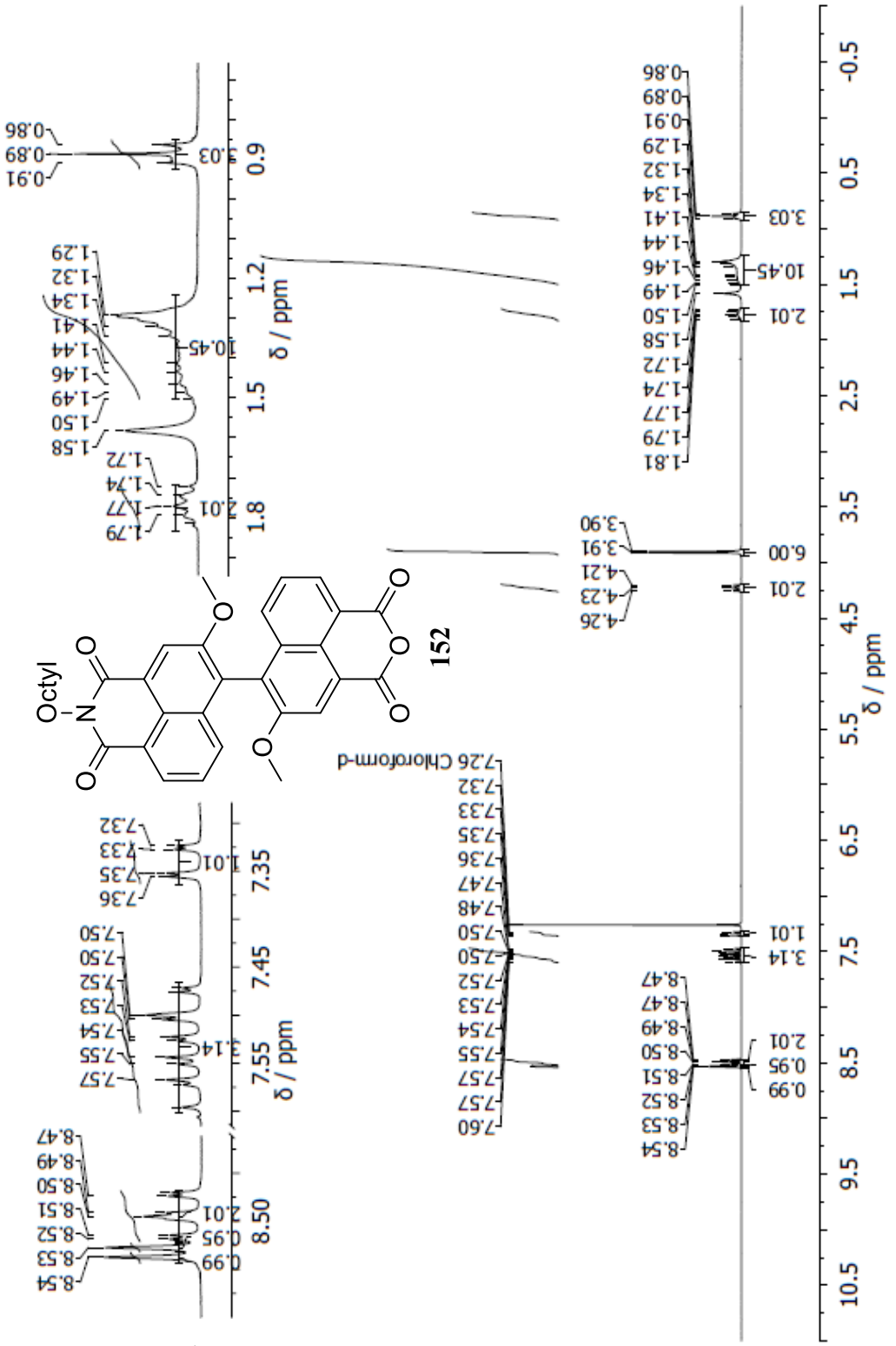

Figure 155: 300 MHz ^{1}H NMR spectrum of **152** in $CDCl_3$

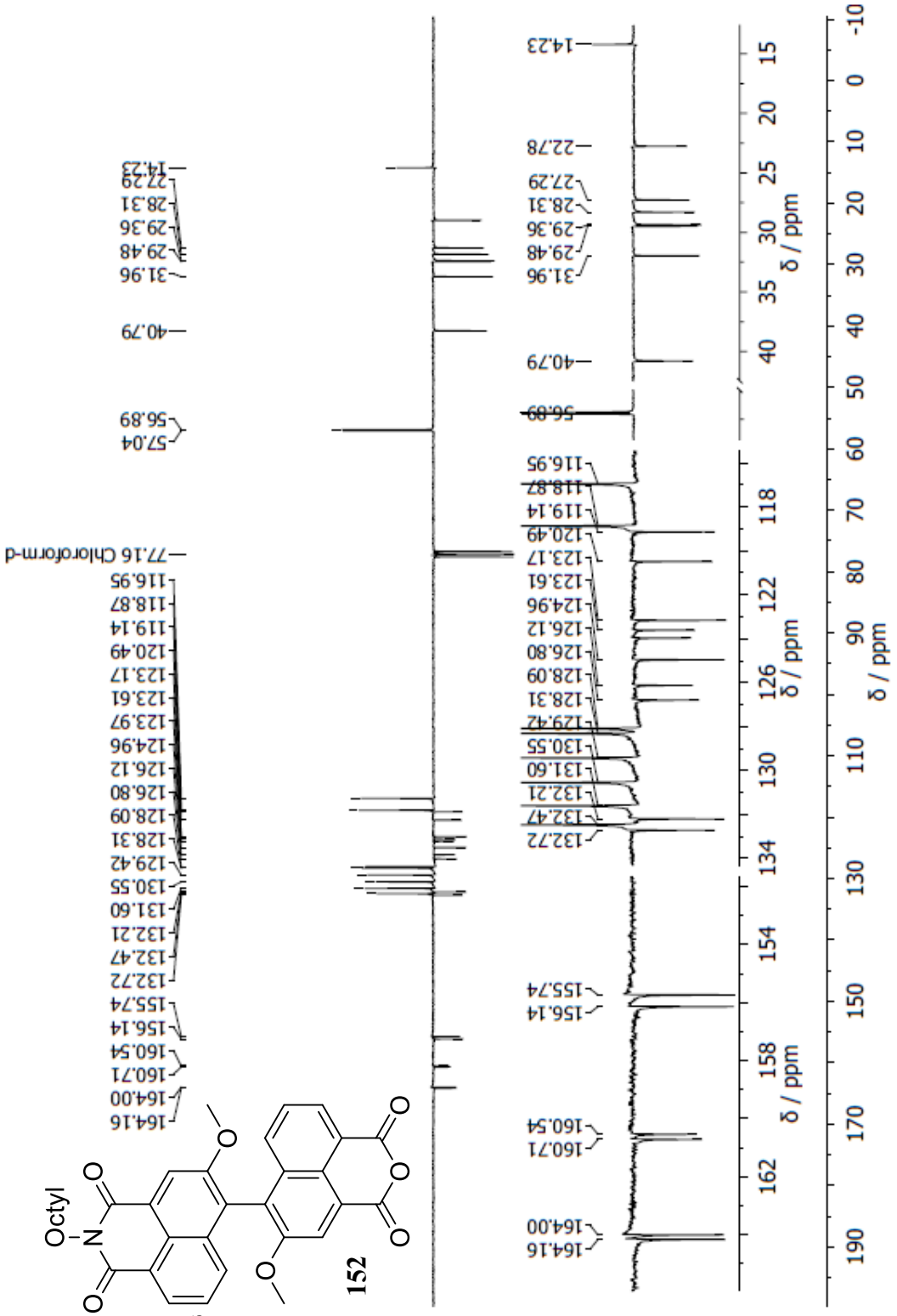

Figure 156: 75 MHz ^{13}C APT NMR of **152** in $CDCl_3$.

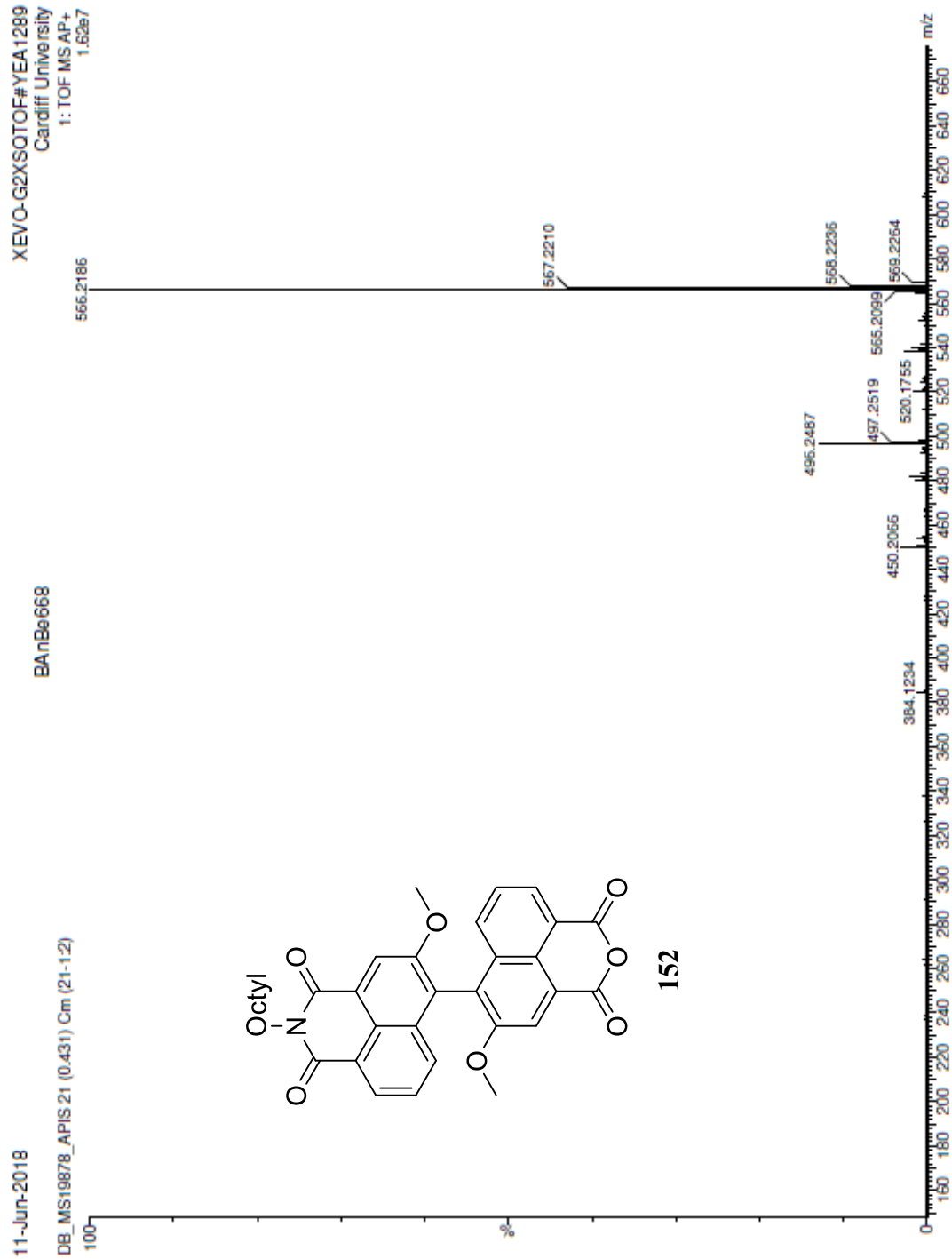

Figure 157:APCI-HRMS spectrum of **152**.

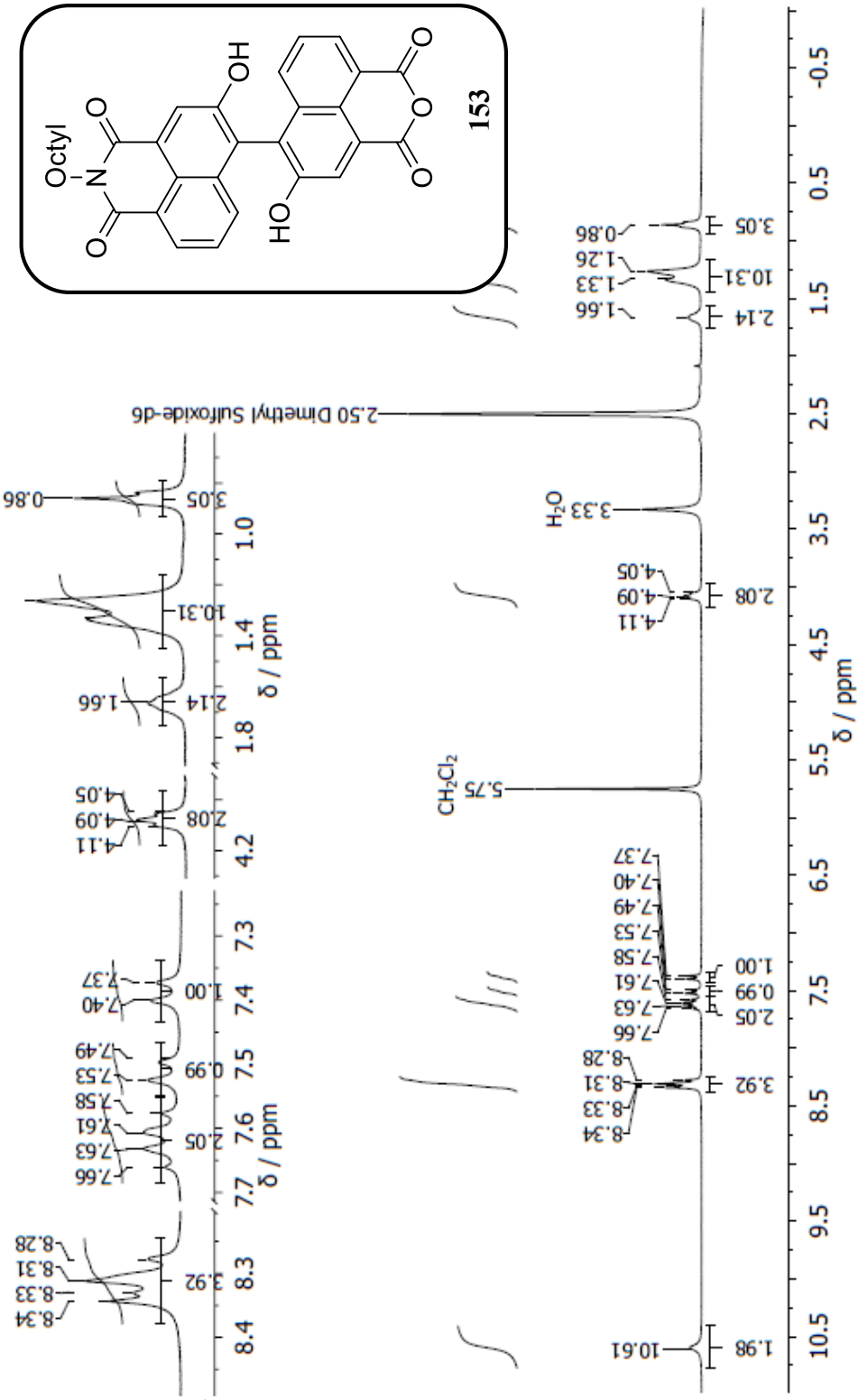

Figure 158: 300 MHz ^{1}H NMR spectrum of **153** in $(CD_3)_2SO$.

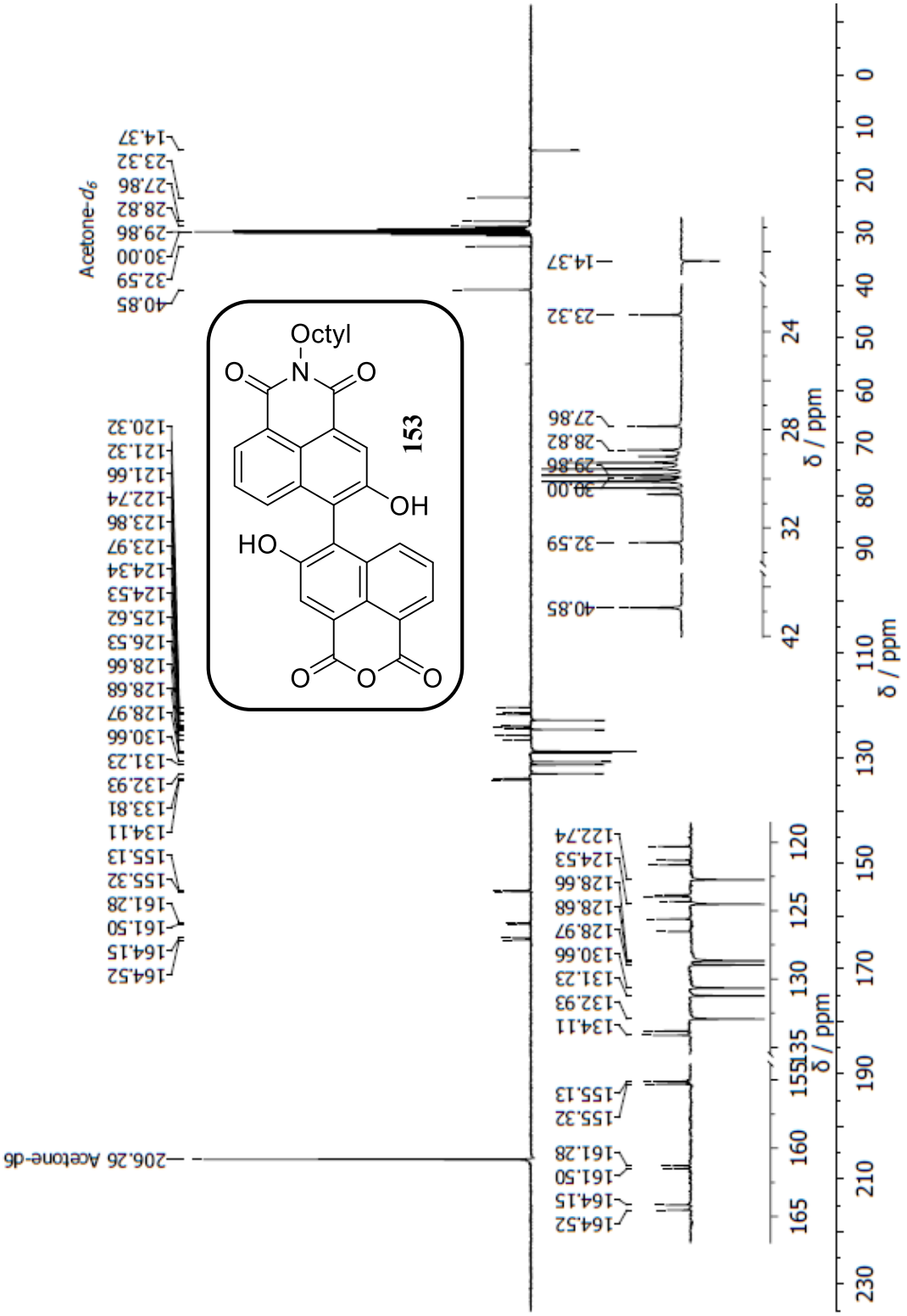

Figure 159: 75 MHz ^{13}C APT NMR of **153** in $(CD_3)_2CO$.

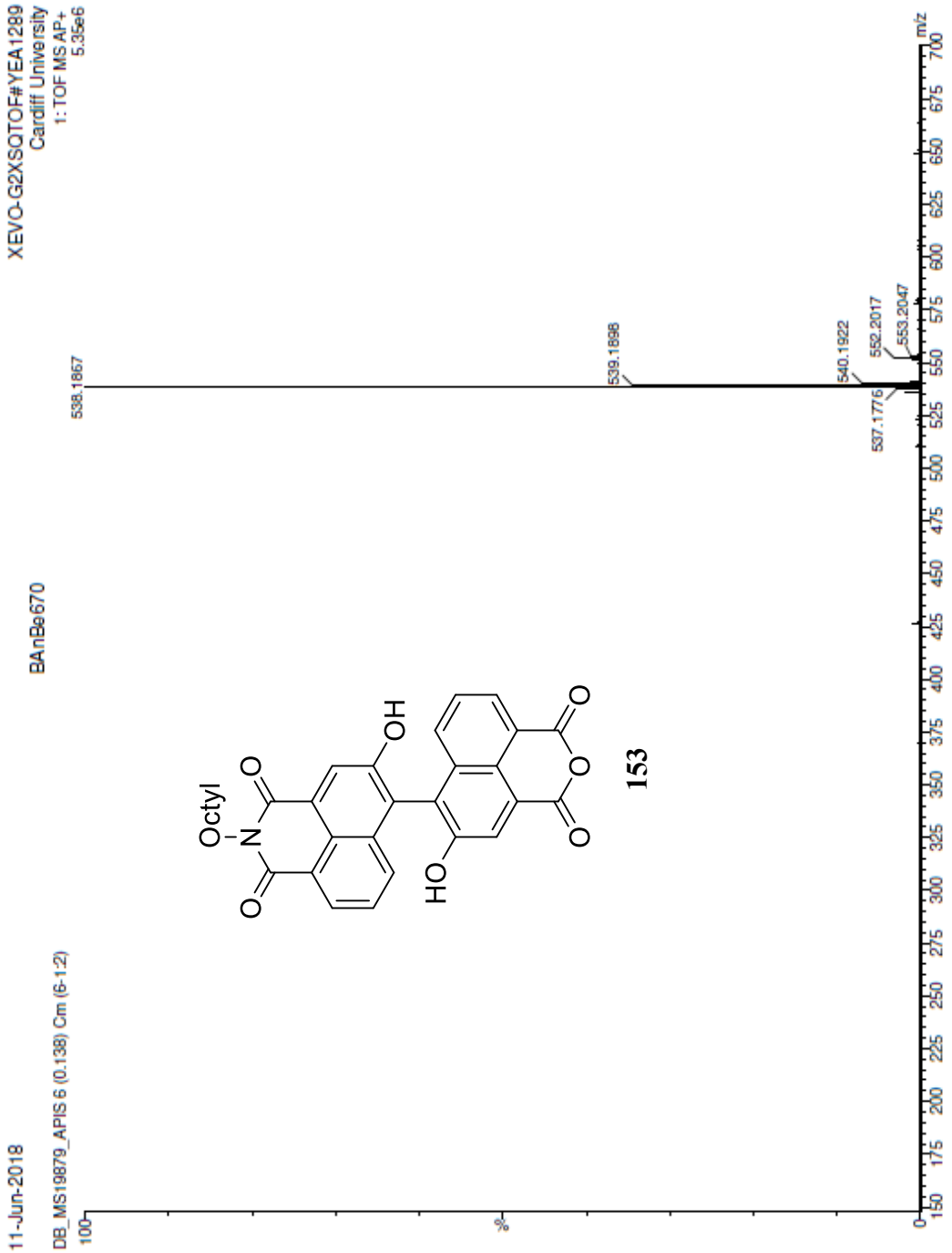

Figure 160: APCI-HRMS spectrum of **153**.

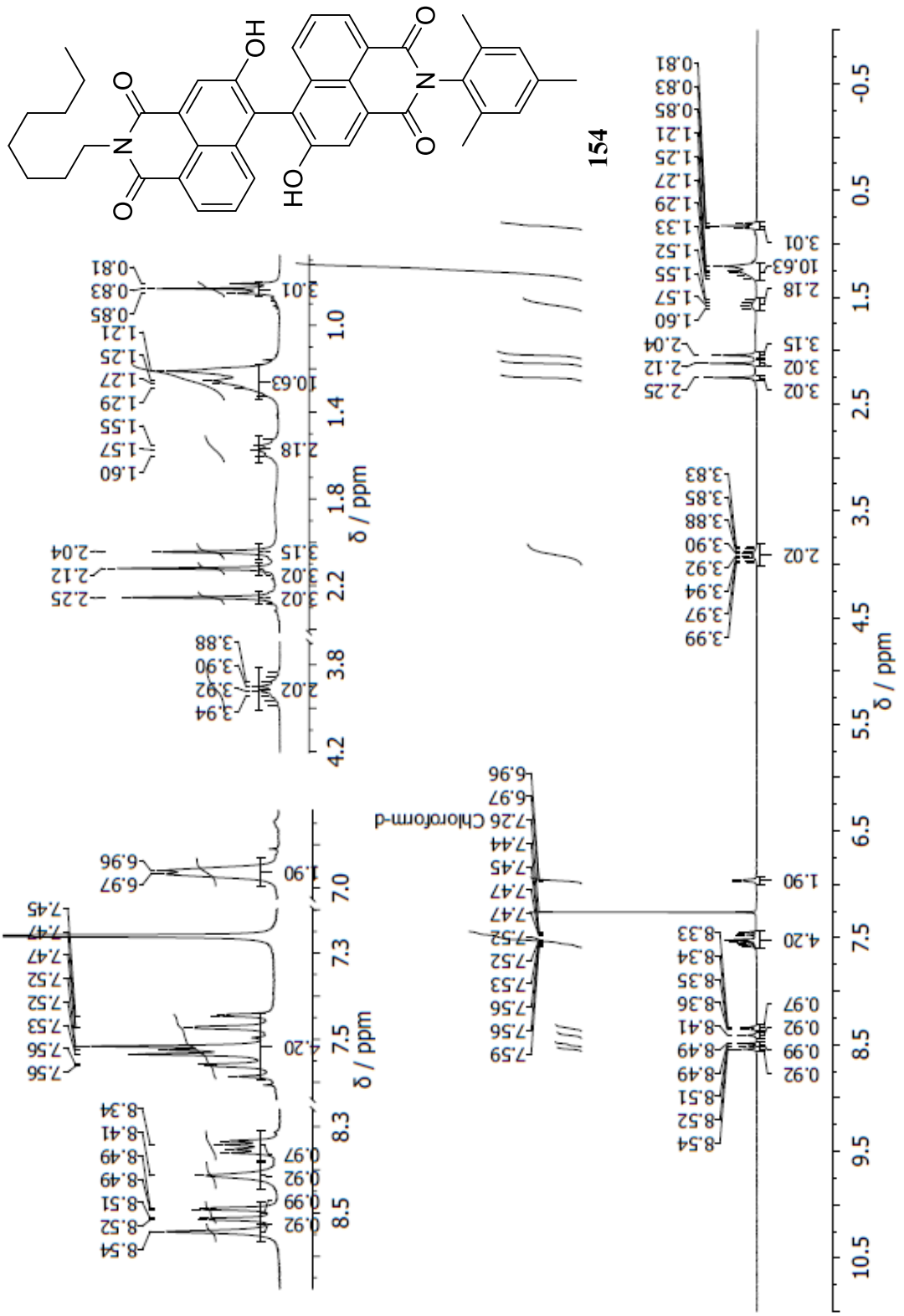

Figure 161: 300 MHz ^{1}H NMR spectrum of **154** in $CDCl_3$.

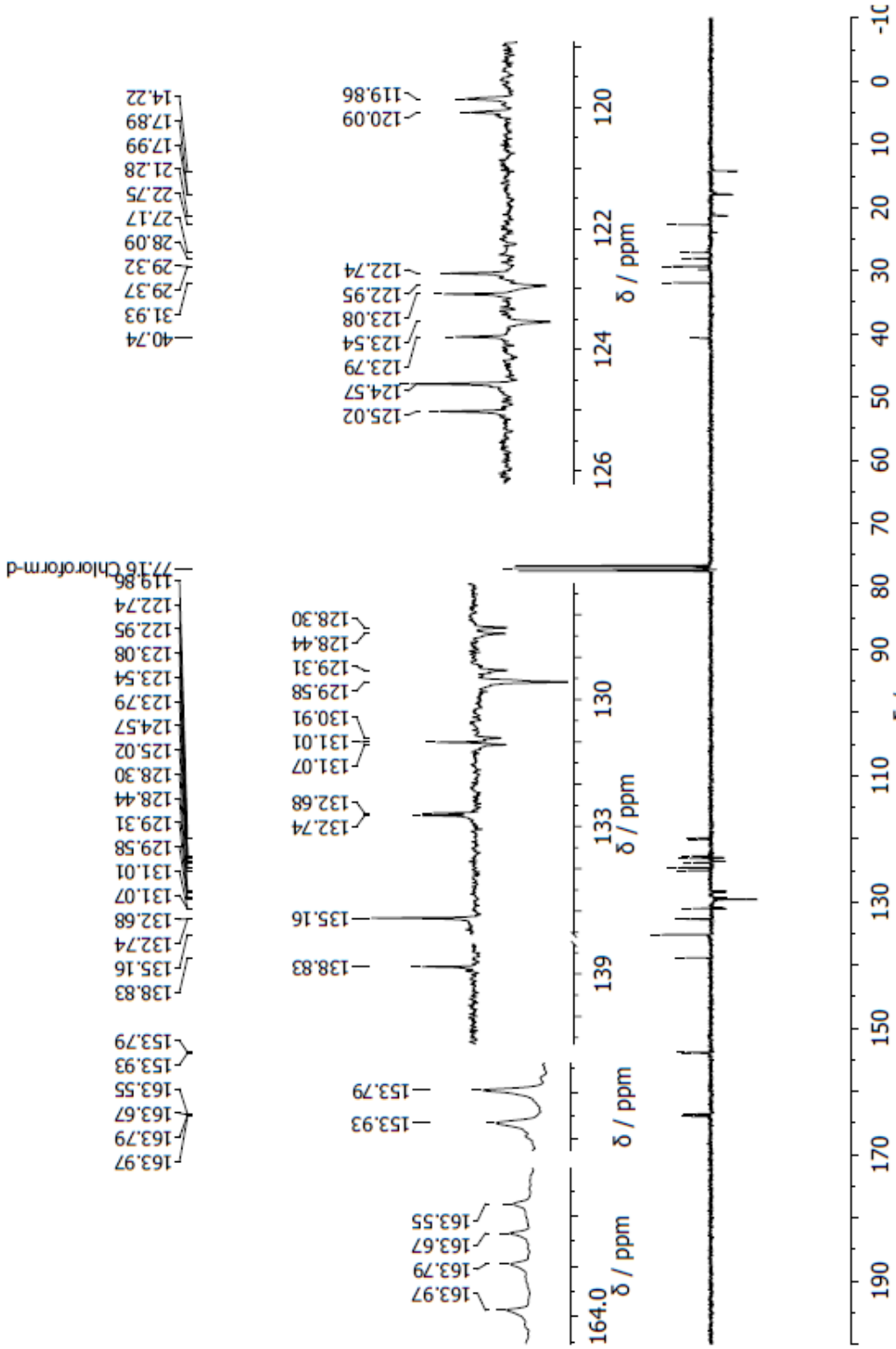

Figure 162: 75 MHz ^{13}C APT NMR of **154** in $CDCl_3$.

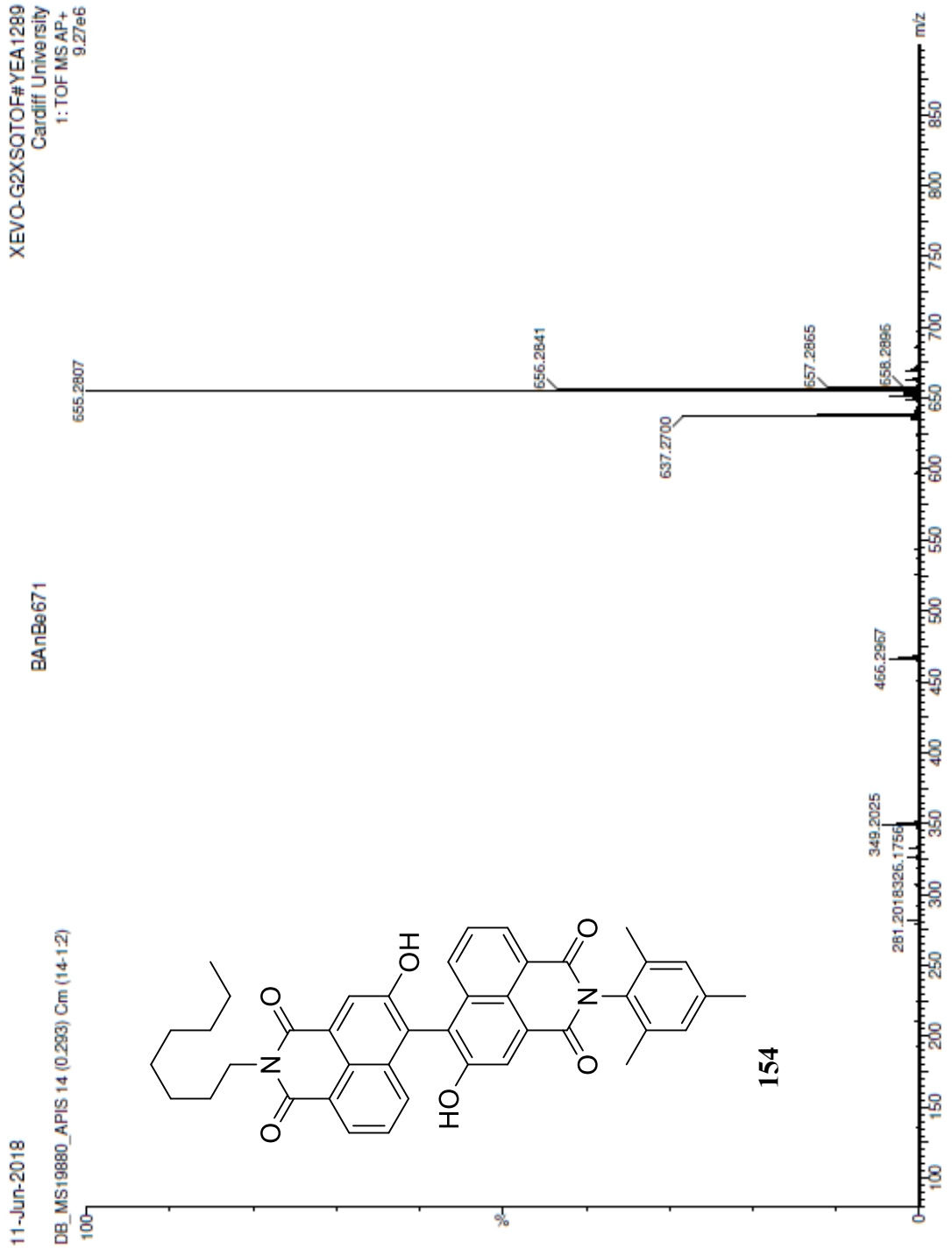

Figure 163: APCI-HRMS spectrum of **154**.

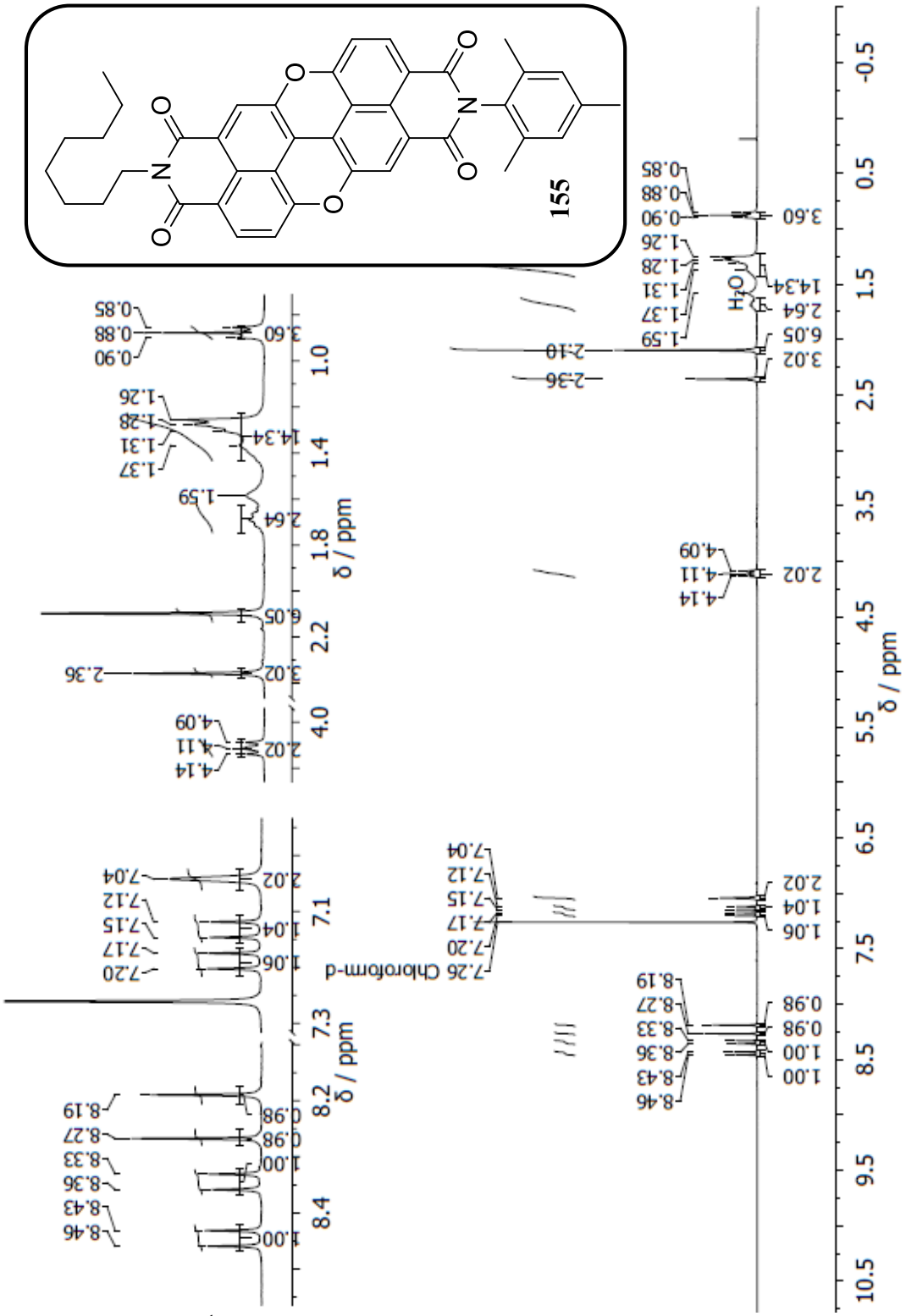

Figure 164: 300 MHz ^{1}H NMR spectrum of **155** in $CDCl_3$.

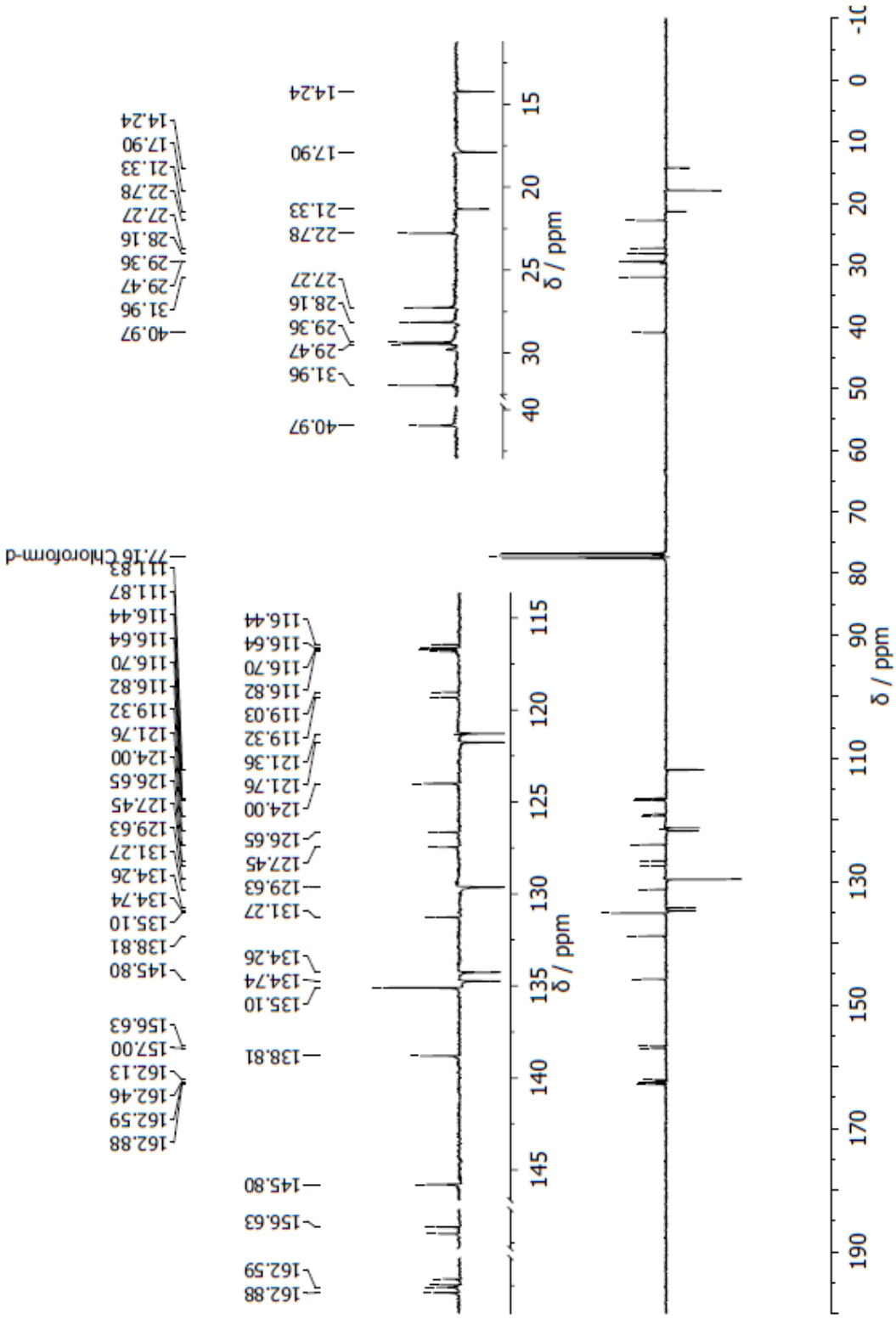

Figure 165: 75 MHz ^{13}C APT NMR of **155** in $CDCl_3$.

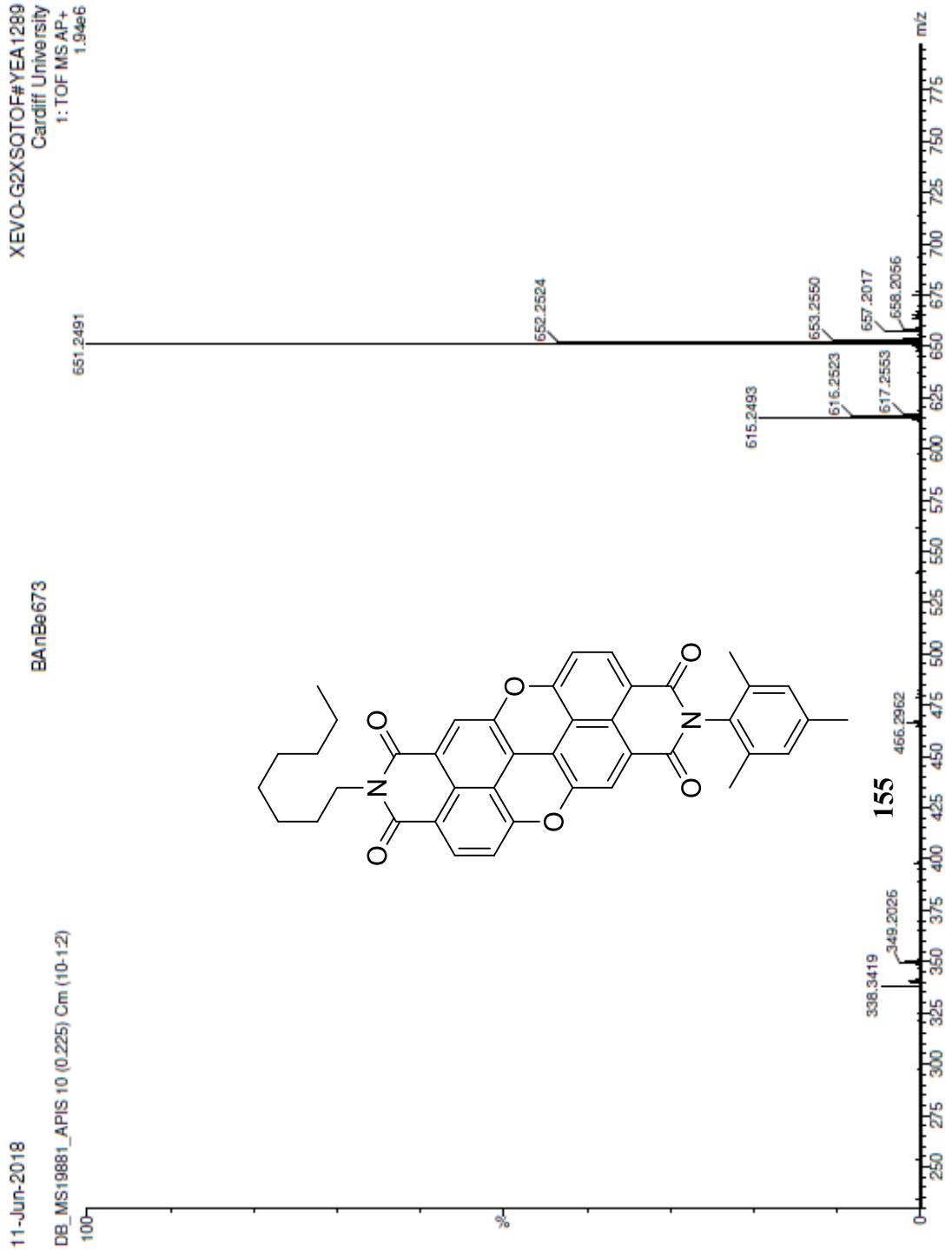

Figure 166: APCI-HRMS spectrum of **155**.